ADVANCES IN NUCLEAR PHYSICS

VOLUME 7

Contributors to This Volume

G. A. Bartholomew
Atomic Energy of Canada Limited
Chalk River Nuclear Laboratories
Chalk River, Canada

E. D. Earle
Atomic Energy of Canada Limited
Chalk River Nuclear Laboratories
Chalk River, Canada

A. J. Ferguson
Atomic Energy of Canada Limited
Chalk River Nuclear Laboratories
Chalk River, Canada

P. G. Hansen
European Organization for Nuclear Research
CERN, Geneva, Switzerland

J. W. Knowles
Atomic Energy of Canada Limited
Chalk River Nuclear Laboratories
Chalk River, Canada

A. M. Lane
Atomic Energy Research Establishment
Harwell, Berkshire, U. K.

M. A. Lone
Atomic Energy of Canada Limited
Chalk River Nuclear Laboratories
Chalk River, Canada

A. Z. Mekjian
Department of Physics
Rutgers University
New Brunswick, New Jersey, U.S.A.

A Continuation Order Plan is available for this series. A continuation order will bring delivery of each new volume immediately upon publication. Volumes are billed only upon actual shipment. For further information please contact the publisher.

ADVANCES IN NUCLEAR PHYSICS

Edited by

Michel Baranger

Center for Theoretical Physics
Massachusetts Institute of Technology
Cambridge, Massachusetts

Erich Vogt

Department of Physics
University of British Columbia
Vancouver, B.C., Canada

VOLUME 7

PLENUM PRESS • NEW YORK-LONDON

Library of Congress Catalog Card Number 67-29001

ISBN-13 : 978-1-4615-9046-0 e-ISBN-13 : 978-1-4615-9044-6
DOI : 10.1007/978-1-4615-9044-6

©1973 Plenum Press, New York
A Division of Plenum Publishing Corporation
227 West 17th Street, New York, N.Y. 10011

United Kingdom edition published by Plenum Press, London
A Division of Plenum Publishing Company, Ltd.
Davis House (4th Floor), 8 Scrubs Lane, Harlesden, London, NW10 6SE, England

All rights reserved

No part of this publication may be reproduced in any form
without written permission from the publisher

Softcover reprint of the hardcover 1st edition 1973

ARTICLES PUBLISHED IN EARLIER VOLUMES

Volume 1

The Reorientation Effect
J. de Boer and J. Eichler

The Nuclear SU_3 Model
M. Harvey

The Hartree–Fock Theory of Deformed Light Nuclei
G. Ripka

The Statistical Theory of Nuclear Reactions
E. Vogt

Three-Particle Scattering – A Review of Recent Work on the Nonrelativistic Theory
I. Duck

Volume 2

The Giant Dipole Resonance
B. M. Spicer

Polarization Phenomena in Nuclear Reactions
C. Glashausser and J. Thirion

The Pairing-Plus-Quadrupole Model
D. R. Bes and R. A. Sorensen

The Nuclear Potential
P. Signell

Muonic Atoms
S. Devons and I. Duerdoth

Volume 3

The Nuclear Three-Body Problem
A. N. Mitra

The Interaction of Pions with Nuclei
D. S. Koltun

Complex Spectroscopy
J. B. French, E.C. Halbert, J. B. McGrory, and S. S. M. Wong

Single Nucleon Transfer in Deformed Nuclei
B. Elbek and P. O. Tjøm

Isoscalar Transition Rates in Nuclei from the (α, α') Reaction
A. M. Bernstein

Volume 4

The Investigation of Hole States in Nuclei by Means of Knockout and Other Reactions
Daphne F. Jackson

High-Energy Scattering from Nuclei
Wiesław Czyż

Nucleosynthesis by Charged-Particle Reactions
C. A. Barnes

Nucleosynthesis and Neutron-Capture Cross Sections
B. J. Allen, J. H. Gibbons, and R. L. Macklin

Nuclear Structure Studies in the $Z = 50$ Region
Elizabeth Urey Baranger

An *s-d* Shell-Model Study for $A = 18$-22
E. C. Halbert, J. B. McGrory, B. H. Wildenthal, and S. P. Pandya

Volume 5

Variational Techniques in the Nuclear Three-Body Problem
L. M. Delves

Nuclear Matter Calculations
Donald W. L. Sprung

Clustering in Light Nuclei
Akito Arima, Hisashi Horiuchi, Kuniharu Kubodera, and Noboru Takigawa

Volume 6

Nuclear Fission
A. Michaudon

The Microscopic Theory of Nuclear Effective Interactions and Operators
Bruce R. Barrett and Michael W. Kirson

Two-Neutron Transfer Reactions and the Pairing Model
Ricardo Broglia, Ole Hansen, and Claus Riedel

ARTICLES PLANNED FOR FUTURE VOLUMES

Static Quadrupole Moments of Nuclear Excited States
Jack S. Greenberg and Allan Kleinfeld

Hypernuclei
A. Gal

Weak Interactions in Nuclei
H. Primakoff and C. W. Kim

One- and Two-Nucleon Transfer
S. Kahana and A. J. Baltz

Multinucleon Transfer
T. Fortune

PREFACE

As much by chance as by design, the present volume comes closer to having a single theme than any of our earlier volumes. That theme is the properties of nuclear strength functions or, alternatively, the problem of line spreading.

The line spreading or strength function concepts are essential for the nucleus because of its many degrees of freedom. The description of the nucleus is approached by using model wave functions—for example, the shell model or the collective model—in which one has truncated the number of degrees of freedom. The question then is how closely do the model wave functions correspond to the actual nuclear wave functions which enjoy all the degrees of freedom of the nuclear Hamiltonian? More precisely, one views the model wave functions as vectors in a Hilbert space and one views the actual wave functions as vectors spanning another, larger Hilbert space. Then the question is: how is a single-model wave function (or vector) spread among the vectors corresponding to the actual wave functions?

As an example we consider a model state which is a shell-model wave function with a single nucleon added to a closed shell. Such a model state is called a single-particle wave function. At the energy of the single-particle wave function one of the actual nuclear wave functions may resemble the single-particle wave function closely. If there are many actual wave functions in the energy neighborhood of the single-particle state (as is true for states lying well above the ground state) then it will be spread among many actual states. If we refer to the square of the overlap between the single-particle state and the actual states as the strength of the single-particle state then we know from much nuclear data that the strength is spread primarily in an energy interval of only a few MeV in the neighborhood of the original single-particle state. The function which describes the distribution of the strength is called the strength function. Not much is known about the shape of the strength function. Its spreading width is a measure of the validity of the shell model.

The concept of the strength function in nuclear physics originated with the study of single-particle states but the same concept is important for a variety of other nuclear problems. Many of the major ideas about nuclear strength functions are due to one of our present authors, Dr. A. M. Lane. In the first article of the present volume Mekjian employs it to describe the nature of doorway states and evidence for them. The doorway states are next, in order of complication, to the single-particle states: they correspond to the states generated when the single-particle has a single interaction with the other nucleons. The second article, by Lane and Mekjian, describes, in part, the mixing of nuclear states accomplished by the Coulomb interaction. This article uses some simple techniques to study, for example, the spreading of the isobaric analogue resonances. The third article, by Hansen, examines how the strength of beta transitions is spread. This is a very new field of study and promises to provide new information about pairing effects in nuclei. The final article, by Bartholomew, Earle, Ferguson, Knowles, and Lone, looks at the strength function for gamma rays. For two decades it has been known that the electric dipole transitions are dominated by the giant dipole resonance whose energy corresponds to gamma rays of more than 10 MeV. But the most commonly available gamma rays are those from neutron capture, and they have an energy of only a few MeV. Since they are not at the peak of the resonance of the dipole strength function the neutron capture gamma rays provide information about the distribution of strength away from the peak—in the wings of the resonance. The article by Bartholomew *et al.* clearly shows that the evidence about the shape of the strength function is still inconclusive.

It remains a challenge for all nuclear strength functions to discover more about their shape than is implied by one parameter, the spreading width. The assumption that the shape is Lorentzian runs through all past work, including that of the present volume. The Lorentzian shape underlies the nuclear optical model with local potentials. Other shapes of strength function might correspond to optical models not in present use. At present one gropes for the vestiges of nuclear models by trying to locate their resonance peaks and possibly their spreading widths. A great deal of interesting physics may be concealed in the reliance on Lorentzian shapes.

The editors are pleased at the continued cooperation and tolerance shown by all the authors in bringing the articles of this series into individual volumes.

July 31, 1973

M. Baranger
E. Vogt

PREFACE TO VOLUME 1

The aim of *Advances in Nuclear Physics* is to provide review papers which chart the field of nuclear physics with some regularity and completeness. We define the field of nuclear physics as that which deals with the structure and behavior of atomic nuclei. Although many good books and reviews on nuclear physics are available, none attempts to provide a coverage which is at the same time continuing and reasonably complete. Many people have felt the need for a new series to fill this gap and this is the ambition of *Advances in Nuclear Physics*. The articles will be aimed at a wide audience, from research students to active research workers. The selection of topics and their treatment will be varied but the basic viewpoint will be pedagogical.

In the past two decades the field of nuclear physics has achieved its own identity, occupying a central position between elementary particle physics on one side and atomic and solid state physics on the other. Nuclear physics is remarkable both by its unity, which it derives from its concise boundaries, and by its amazing diversity, which stems from the multiplicity of experimental approaches and from the complexity of the nucleon–nucleon force. Physicists specializing in one aspect of this strongly unified, yet very complex, field find it imperative to stay well-informed of the other aspects. This provides a strong motivation for a comprehensive series of reviews. Additional motivation arises from outside the community of nuclear physicists, through the inevitable occurrence of the nucleus as an accessory or as a tool in other fields of physics, and through its importance for terrestrial and stellar energy sources.

We hope to provide a varied selection of reviews in nuclear physics with a varied approach. The topics chosen will range over the field, the emphasis being on physics rather than on theoretical or experimental techniques. Some effort will be made to include regularly topics of great current interest which need to be made accessible by adequate reviews. Other reviews will attempt to bring older topics into clearer focus. The aim will be to attract the interest of both the active research worker and the research student. Authors will be asked to direct their article toward the maximum number of readers by separating clearly the technical material from the more basic

aspects of the subject and by adopting a pedagogical point of view rather than giving a simple recital of recent results.

Initially, the *Advances* are scheduled to appear about once a year with approximately six articles per volume. To ensure rapid publication of the papers, we shall use the "stream" technique, successfully employed for series in other fields. A considerable number of planned future articles constitute the source of the stream. The flow of articles from the source takes place primarily to suit the convenience of the authors, rather than to include any particular subset of articles in a given volume. Any attempt at a systematic classification of the reviews would result in considerable publication delays. Instead, each volume is published as soon as an appropriate number of articles have been completed; but some effort is made to achieve simultaneity, so that the spread in completion dates of the articles in a given volume is much less than the interval between volumes.

A list of articles planned for future volumes is given on page v. The prospective articles together with those in this first volume still fall far short of our long-range aims for coverage of the field of nuclear physics. In particular, we definitely intend to present more articles on experimental topics. We shall eagerly receive and discuss outside suggestions of topics for additional papers, and especially suggestions of suitable authors to write them.

The editors owe a great deal to the authors of the present volume for their cooperation in its rapid completion, and to many colleagues who have already given advice about the series. In embarking on this venture, we have had the support of Plenum Press, a relatively new publisher in the field of physics, and of its vice-president, Alan Liss, who has an almost unmatched background in physics publications.

M. Baranger
E. Vogt

October 15, 1967

CONTENTS

Chapter 1

NUCLEON–NUCLEUS COLLISIONS AND INTERMEDIATE STRUCTURE

Aram Mekjian

1. Introduction 1

2. A Simple Model of a Resonance Process 3
   - 2.1. The Model and Its Stationary State Solutions 3
   - 2.2. Time-Dependent Picture 6
   - 2.3. Applications of the Simple Model. 7
   - 2.4. Mixing Times in Nuclear Excitations 12

3. Nucleon–Nucleus Scattering and Intermediate Structure . . . 17
   - 3.1. Review of the Models of Nuclear Resonance Reactions. 17
   - 3.2. Physical Picture of Nucleon–Nucleus Scattering. 27
   - 3.3. The Optical-Model Strength Function as a Function of Mass Number 31
   - 3.4. Shell-Model Investigations of Doorway States 35
   - 3.5. Vibrations as Doorway States 40
   - 3.6. Doorway States and Isobaric Analog Resonances. . . . 43
   - 3.7. Electromagnetic Interactions and Intermediate Structure. . 51
   - 3.8. Intermediate Structure in Fission 57
   - 3.9. Doorway States and Partial Width Correlations 61
   - 3.10. Intermediate Structure and the High-Energy Neutron Tail in Neutron Evaporation Spectra 64
   - 3.11. Intermediate Structure and Statistical Fluctuations . . . 68
   - 3.12. Experimental Observations of Intermediate Structure in Total Neutron Cross Sections. 73

4. Theoretical Framework for Intermediate Resonances 77
4.1. Shell-Model Theory of Nuclear Reactions 77
4.2. Theory of Average Cross Sections 85
5. Summary 89
References 90

Chapter 2

COULOMB MIXING EFFECTS IN NUCLEI: A SURVEY BASED ON SUM RULES

A. M. Lane and A. Z. Mekjian

Abstract 97
1. Introduction 98
2. Sum-Rule Approach to Coulomb Mixing 101
3. Evaluation of Sum-Rule Quantities for Separate Isospins . . 104
3.1. Oscillator Shell Model 106
3.2. Shell Model with Correlations 106
3.3. Specification of $\bar{E}(T')$ 107
3.4. Specification of $N(T')$ 109
4. Total Isospin Impurities of States 110
4.1. Parent States 110
4.2. Analog States 112
5. Superallowed Fermi Transitions 113
6. Isobaric Mass Formula 115
6.1. First-Order Energy. 116
6.2. Second-Order Energy 117
6.3. Correlated Model 119
6.4. Configuration States 121
6.5. Observed Values 122
7. Analog States: General Remarks and Lowest-Order Effects. . 123
7.1. δE_c in Terms of Relative Coulomb Potential and Exact Parent State 123
7.2. δE_c in Terms of Coulomb Energy and Unperturbed Parent State 125
7.3. First-Order Shift Δ_1 and Pseudo-First-Order Shift Δ_1'. . 126

8. Analog States: Second-Order Shifts and Width 130
8.1. Estimate of $\delta E_c - \Delta_1' = -[\Delta(-+) + \Delta(+-)]$ 130
8.2. Estimate of $(\Delta_{2a} - \Delta_{2p})$ 133
8.3. Comparison of Δ_1 and Δ_1' 135
8.4. Implications for the Nolen–Schiffer Anomaly 135
8.5. Spreading Width 137

9. Second-Order Effects in Model Calculations 138
9.1. Coulomb Shift of Single-Particle States 139
9.2. Model Analog. 140
9.3. Analysis of Shift Calculated from the Model. 142
9.4. Analysis of Spreading Width Calculated from the Model 143

10. Conclusions 145

Acknowledgment 146

Appendix 1
Corrections from More Accurate Treatment of the Coulomb Potential 146

Appendix 2
Explicit Treatment of Effect of Correlations on Second-Order Coulomb Mixing 152

Appendix 3
Shell-Model Sum Rules for the One- and Two-Body Coulomb Forces 153

Appendix 4
Coulomb Mixing Properties of Oscillator Orbitals 155

References 156

Chapter 3

THE BETA STRENGTH FUNCTION

P. G. Hansen

1. Introduction 159

2. Beta-Transition Rates between Individual Nuclear Levels . . . 162
2.1. The Fermi Transitions 165
2.2. The Gamow–Teller Transitions 168
2.3. Forbidden Transitions 171

3. Expected Properties of the Beta Strength Function 172
3.1. The Shell Model and Effects of Pairing 173
3.2. The Correlations 176
3.3. Fluctuations 180

4. Experimental Results on Beta Strength 183
4.1. Nuclear Level Schemes 185
4.2. Total Absorption Spectrometry 188
4.3. The Systematics of Beta Halflives 195
4.4. Beta-Delayed Particle Emission 202
4.5. Muon-Capture and Electromagnetic Transitions 213

5. Concluding Remarks 219

Acknowledgments 220

References 221

Chapter 4

GAMMA-RAY STRENGTH FUNCTIONS

G. A. Bartholomew, E. D. Earle, A. J. Ferguson, J. W. Knowles, and M. A. Lone

1. Introduction 229

2. Theoretical Background 235
2.1. Nomenclature 235
2.2. Strength Functions. 237
2.3. Spectral Distributions 241

3. Experimental Methods 244
3.1. Photoexcitation Method 244
3.2. Spectrum Fitting Method. 253
3.3. Sequential Extraction Method. 259
3.4. High-Resolution Gamma-Ray Method 262
3.5. Comparison of Methods 268

4. Properties of Gamma-Ray Strength Functions 271
4.1. General Properties 272
4.2. Detailed Properties 289

5. Discussion 311
5.1. General 311

5.2. Compatibility of Strength Functions 312
5.3. $E1$ Strength Function 313
5.4. $M1$ Strength Function 316

6. Conclusion 317

Acknowledgments 317

References 318

Chapter 1

NUCLEON–NUCLEUS COLLISIONS AND INTERMEDIATE STRUCTURE

Aram Mekjian

Department of Physics
Rutgers University
New Brunswick, New Jersey

1. INTRODUCTION

This chapter is devoted to the topic of resonances in nuclear reactions and, in particular, to the topic of intermediate resonance structure in the energy dependence of the nuclear cross section (FKL 67, KRY 68). This latter topic is of considerable current interest, while the former topic has been discussed since the work of Breit and Wigner (BW 36) in the 1930's. The basis for the description of resonance reactions presented here will be that of the optical model plus residual interactions. Specifically, the reaction dynamics in a nucleon–nucleus scattering will be discussed from the viewpoint of an independent particle picture plus residual interactions. The "black box" description of the nuclear reaction amplitude in terms of resonance parameters will be abandoned in the hope that simple excitations of the target–incident-nucleon system are observable as some type of structure in the reaction amplitude. It is then hoped that the various parameters describing this structure can be calculated in terms of the interaction between the incident nucleon and the target nucleons. A likely candidate for

such a calculable structure is the experimental phenomenon called intermediate structure.

The expression intermediate structure refers to a property of the energy dependence of the cross section. By structure we mean resonance structure in the energy dependence of this cross section. Intermediate structure refers to variations in the cross section intermediate between the rapidly varying fine structure seen in experiments performed at very high resolution and the slowly varying gross structure seen in experiments performed with a beam of very poor resolution. Thus, intermediate structure, if it exists, will be seen with beams having resolution intermediate between these two extremes.

The observations of rapid variations of the cross section (resonances only eV apart in heavy nuclei bombarded with neutrons) were interpreted by Bohr (Boh 36, Boh 37) in terms of the concept of the compound nucleus. The high density of narrow resonances indicated the existence of long-lived states of high complexity in a many-particle system. In this picture, the total energy of the incident nucleon is immediately shared among all the nucleons in the target once the incident nucleon reaches the nuclear surface. On the other hand, the gross structure (resonances many MeV apart) in the slow variation of the average cross section with energy was interpreted in terms of the optical model of Feshbach, Porter, and Weisskopf (FPW 53, FPW 54). The existence of slow variations indicates the persistence of single-particle motion of the incident nucleon inside the nucleus. The giant resonance model of Lane, Thomas, and Wigner (LTW 56) was then introduced to account for the success of the optical model. The giant resonances corresponded to each of the single-particle states of the system when the residual interaction was neglected. Now, the interpretation of intermediate structure is in terms of the excitation of simple states of the nucleon–nucleus system. These states of simple structure have been called *doorway states*. They are, for example, the $2p$–$1h$ (2 particle–1 hole) states reached in the first collision, through two-body residual interactions of the incident nucleon on a $0p$–$0h$ closed-shell target. In such a picture, successive collisions produce a whole hierarchy of states; the more complicated states beyond the doorway states, e.g., $3p$–$2h$, $4p$–$3h$ states, have been called *hallway states* (FM 66); the giant resonance states are just the $1p$–$0h$ states.

This article will be primarily concerned with understanding the doorway concept and its relation to the existence of intermediate structure in the reaction amplitude. Experimental situations exhibiting intermediate structure will also be discussed.

2. A SIMPLE MODEL OF A RESONANCE PROCESS

2.1. The Model and Its Stationary State Solutions

Before discussing nucleon–nucleus scattering in general, it is helpful to consider a simple model which illustrates the characteristics of resonance structure. Consider a quantum mechanical system which can exist in an excited state or in its ground state. If this system is placed in its excited state, a mechanism exists for transferring the system to its ground state. For example, an excited atom or an excited nucleus will de-excite by emission of a photon. The emission of light by these excited states is a result of the fundamental coupling $e \rightarrow e + \gamma$ and $p \rightarrow p + \gamma$. The reverse processes, $\gamma + e \rightarrow e$ and $\gamma + p \rightarrow p$, also exist and correspond to light or photon absorption. Other processes described by the model will be discussed in Section 2.3.

For convenience, we will speak in the terminology of the atom–photon picture (WW 30a, WW 30b). The Hamiltonian of the system then consists of three parts: the Hamiltonian of an isolated atom H_{atom}, the Hamiltonian of an isolated photon H_{photon}, plus the Hamiltonian corresponding to the interaction of the atom and the electromagnetic field H_{int}. We therefore have

$$H = H_{\text{atom}} + H_{\text{photon}} + H_{\text{int}} \tag{1}$$

We desire a solution of the Schrödinger equation, and, in particular, we will consider solutions to the Schrödinger equation which are stationary in time:

$$H \mid \psi_{E_\nu}\rangle = E_\nu \mid \psi_{E_\nu}\rangle \tag{2}$$

The wavefunction $\mid \psi_{E_\nu}\rangle$ consists of two parts, one which describes the atom in an excited state and the vacuum for the photon, plus a second part describing the atom in its ground state and one photon emitted:

$$\mid \psi_{E_\nu}\rangle = a_0^\nu \mid \psi_{\text{ex}}\phi_{\text{vac}}\rangle + \sum_n b_n^\nu \mid \psi_g\phi_{n(1\gamma)}\rangle \tag{3}$$

We consider the photon states to be equally spaced around the energy of the excited state, which we define as the zero of energy. Here D is the level spacing and $\varrho = D^{-1}$ is the level density of one-photon states. The operation of the various components of H on the various components of ψ are given

as follows:

$$\begin{aligned} H_{\text{atom}}\psi_{\text{ex}} &= 0 \\ H_{\text{atom}}\psi_g &= E_g\psi_g \\ H_{\text{photon}}\phi_{\text{vac}} &= 0 \\ H_{\text{photon}}\phi_{n(1\gamma)} &= [|E_g| + nD]\phi_{n(1\gamma)} \\ \langle\psi_{\text{ex}}\phi_{\text{vac}} \mid H_{\text{int}} \mid \psi_g\phi_{n(1\gamma)}\rangle &= V \end{aligned} \tag{4}$$

The matrix element V is here taken to be independent of n. The justification for this is that the variation in the photon wavelength over the width of the resonance is small. Next, the solution to the Schrödinger equation

$$(H - E)\left[a_0^\nu \mid \psi_{\text{ex}}\phi_{\text{vac}}\rangle + \sum_n b_n^\nu \mid \psi_g\phi_{n(1\gamma)}\rangle\right] = 0 \tag{5}$$

is obtained by taking inner products with $\langle\psi_{\text{ex}}\phi_{\text{vac}} \mid$ and $\langle\psi_g\phi_{n(1\gamma)} \mid$ and solving a set of equations for the coefficients a, b, and the energy eigenvalues E_ν. Specifically, we have

$$V\sum_n b_n^\nu = E_\nu a_0^\nu \tag{6a}$$

$$Va_0^\nu + b_n^\nu nD = E_\nu b_n^\nu \tag{6b}$$

and from Eq. (6b) we obtain

$$b_n^\nu = \frac{Va_0^\nu}{E_\nu - nD} \tag{7}$$

Substituting this result into Eq. (1) gives the energy eigenvalue equation

$$E_\nu = \sum_n \frac{V^2}{E_\nu - nD} = \pi V^2 \varrho \cot[\pi\varrho E_\nu] \tag{8}$$

The solution to the eigenvalue equation can be obtained graphically as shown in Fig. 1. The eigenvalues are given by the intersection of the curves $y = E$ and $y = \sum V^2/(E - nD)$. From this figure we see that as $E \to \pm\infty$, $E_\nu \to \pm nD$, while those levels that are close to $E = 0$ are largely shifted from their unperturbed positions.

The square of the amplitude a_0^ν can be obtained from the normalization condition

$$(a_0^\nu)^2 + \sum_n (b_n^\nu)^2 = 1 = (a_0^\nu)^2\left[1 + V^2\sum_n \frac{1}{(E_n - nD)^2}\right] \tag{9}$$

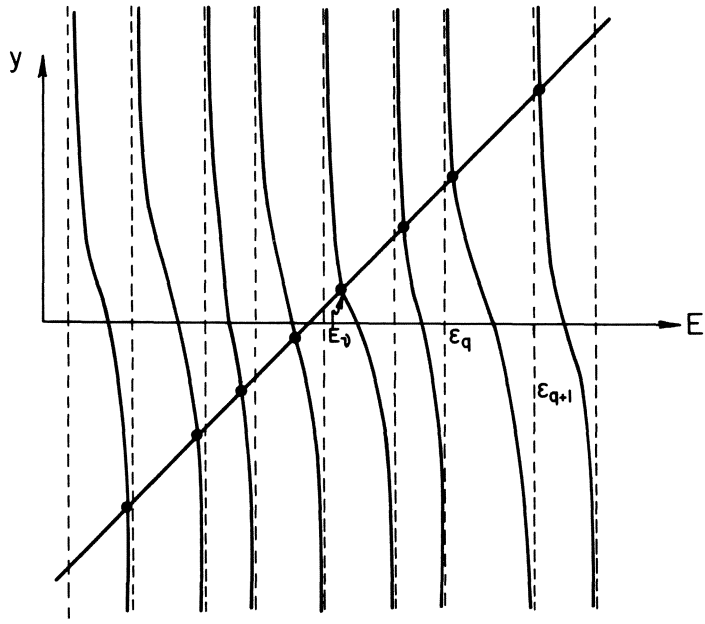

Fig. 1. Graphical solution of the eigenvalue equation. The eigenvalues are given by the intersection of the straight line $y = E$ with the curves $y = \Sigma\, V_n^2/(E - E_n)$. The situation of equally spaced levels $E_n = nD$ is considered in the text.

Noting that the quantity $\sum V^2/(E_\nu - nD)^2$ is the negative derivative with respect to E of the self-energy term $\sum V^2/(E - nD)$ evaluated at the energy E_ν:

$$\frac{\partial}{\partial E}\sum_n \frac{1}{E - nD} = -\sum \frac{1}{(E - nD)^2} = -\pi^2\varrho^2 \csc^2[\pi\varrho E] \tag{10}$$

and using the trigonometric relation $\csc^2[\pi\varrho E] = 1 + \cot^2[\pi\varrho E]$, we obtain

$$(a_0^\nu)^2 = \frac{1}{[1 + (\pi\varrho V)^2]\{1 + E_\nu^2/[V^2 + (\pi\varrho V^2)^2]\}} \tag{11}$$

Thus, the amplitude $(a_0^\nu)^2$ has a Lorentzian form with a half-width

$$\frac{\Gamma}{2} = \sqrt{V^2 + (\pi\varrho V^2)^2} \tag{12}$$

Using the fact that $(\pi\varrho V)^2 \gg 1$ and $(\pi\varrho V^2)^2 \gg V^2$, we simplify the amplitude $(a_0^\nu)^2$ to

$$\begin{aligned} (a_0^\nu)^2 &= \frac{\Gamma(D/2\pi)}{E_\nu^2 + (\Gamma/2)^2} \\ \Gamma &= 2\pi\varrho V^2 \end{aligned} \tag{13}$$

Recall that $(a_0^\nu)^2$ is the probability for finding the state $|\psi_{\text{ex}}\phi_{\text{vac}}\rangle$ in the state $|\psi_{E_\nu}\rangle$. Therefore, the distribution of this probability, considered as a continuous function of energy E, is a Lorentzian with a width given by the Fermi golden-rule expression $\Gamma = 2\pi\varrho V^2$.

2.2. Time-Dependent Picture

In the previous section, we considered the stationary state solutions of an excited atom interacting with its own radiation field. We now turn our attention to the time-dependent description of this system. Specifically, we consider the time evolution of a system which at $t = 0$ consists of only an excited atom and ask for the amplitude or probability of finding an excited atom at some other time. Initially, the state function describing the system is

$$|\psi(t{=}0)\rangle = |\psi_{\text{ex}}\phi_{\text{vac}}\rangle \tag{14}$$

We expand this state function in terms of the stationary state eigenfunction obtained in the previous section,

$$|\psi(t=0)\rangle = \sum C_\nu |\psi_{E_\nu}\rangle \tag{15}$$

where C_ν is the overlap of $|\psi\rangle$ with the eigenfunction $|\psi_{E_\nu}\rangle$ given by

$$|\psi_{E_\nu}\rangle = a_0^\nu |\psi_{\text{ex}}\phi_{\text{vac}}\rangle + \sum_n b_n^\nu |\psi_g\phi_{n(1\gamma)}\rangle \tag{16}$$

From these equations we immediately see that $a_0^\nu = C_\nu$. Now, since the stationary state eigenfunctions are not coupled to each other by the total Hamiltonian H, the state function describing our system at another time is given by

$$|\psi(t)\rangle = \sum_\nu C_\nu |\psi_{E_\nu}\rangle e^{-iE_\nu t} \tag{17}$$

This result can also be arrived at by applying the time translation operator $U(t, t{=}0) = \exp[-iHt]$ to the state $|\psi(t{=}0)\rangle$ to obtain the state $|\psi(t)\rangle = U(t, t{=}0)\,|\psi(t{=}0)\rangle$. The result of the above equation then follows immediately from the fact that the $|\psi_{E_\nu}\rangle$ is an eigenfunction of H, i.e., $H\,|\psi_{E_\nu}\rangle = E_\nu\,|\psi_{E_\nu}\rangle$. Next, using the fact that $C_\nu = a_0^\nu$, and expanding $|\psi_{E_\nu}\rangle$ in terms of $|\psi_{\text{ex}}\phi_{\text{vac}}\rangle$ and $|\psi_g\phi_{n(1\gamma)}\rangle$, we have

$$\psi(t) = \left[\sum_\nu e^{-iE_\nu t}(a_0^\nu)^2\right] |\psi_{\text{ex}}\phi_{\text{vac}}\rangle + \sum_n [\ \ ]\,|\psi_g\phi_{n(1\gamma)}\rangle \tag{18}$$

From this equation we obtain for the amplitude to find the atom excited at time t, $A(t)$, the expression

$$A(t) = \sum_{\nu} e^{-iE_\nu t}(a_0^\nu)^2 \tag{19}$$

Changing the discrete sum to a continuous integral, we have

$$A(t) = \int dE\varrho[a_0(E)]^2 e^{-iEt} \tag{20}$$

Then, using the expression for $(a_0^\nu)^2$ obtained in the previous section, we arrive at the result

$$A(t) = \varrho \int \frac{1}{(\pi\varrho V)^2} \frac{1}{1 + (E^2/\pi^2\varrho^2 V^4)} e^{-iEt}\, dE \tag{21}$$

This result can be rewritten, using the fact that $\Gamma = 2\pi\varrho V^2$, as

$$A(t) = \frac{\Gamma}{2\pi} \int \frac{e^{-iEt}\, dE}{E^2 + (\Gamma/2)^2} \tag{22}$$

The integral appearing in this equation is easily evaluated using contour integration. For $t > 0$ we continue the contour in the lower half of the E-plane and arrive at the result

$$A(t) = e^{-\Gamma t/2} \tag{23}$$

For $t < 0$, we continue the contour in the upper half of the complex E-plane and establish the result

$$A(t) = e^{\Gamma t/2} \tag{24}$$

The probability of finding the atom in an excited state is then

$$P(t) = |\, A(t)\, |^2 = e^{-\Gamma|t|} \tag{25}$$

and is thus given by the well-known exponential decay law. We note the cusp in $P(t)$ at $t = 0$ and the time-reversal invariance of $P(t)$. The lifetime of the state is given by $\tau = \Gamma^{-1}$, $(\hbar \equiv 1)$.

2.3. Applications of the Simple Model

In Section 2.1, we have solved the Schrödinger equation for the interaction of an atom (or nucleus) with the electromagnetic field. This model serves as a basis for a description of other processes. In general, if $|\, \psi_d\rangle$

is a particular type of state of a quantum mechanical system (e.g., $|\psi_{\text{ex}}\phi_{\text{vac}}\rangle$ of the atom–photon problem) and if $|\phi_q\rangle$ are a group of surrounding states of another type (e.g., $|\psi_g\phi_{q(1\gamma)}\rangle$) realized in the absence of couplings, then in the presence of a coupling between these types of states, new stationary states are generated which are given by

$$|\psi_{E_\nu}\rangle = a_d^\nu\,|\psi_d\rangle + \sum_q b_q^\nu\,|\phi_q\rangle \tag{26}$$

The amplitudes and eigenvalues E_ν are obtained from $[H - E]\,|\psi_{E_\nu}\rangle = 0$. The eigenvalues of this problem are solutions to

$$E_\nu - E_d = \sum \frac{V_q^2}{E_\nu - \varepsilon_q} \tag{27}$$

with E_d, ε_q the energy of the state ψ_d, ϕ_q, while the amplitude a_d^ν is given by

$$(a_d^\nu)^2 = \frac{1}{1 + \sum_q [V_q^2/(E_\nu - \varepsilon_q)^2]} \tag{28}$$

In the picket-fence-model limit of equal spacings D between the ϕ_q states and constant matrix elements $V = V_q$, the distribution of the $(a_d^\nu)^2$ has a Lorentzian envelope:

$$(a_d^\nu)^2 = \frac{\Gamma_f(D/2\pi)}{(E_\nu - E_d)^2 + (\Gamma/2)^2} \tag{29}$$

where $\Gamma^2 = 4V^2 + \Gamma_f^2$ and $\Gamma_f = 2\pi V^2/D$.

The model just described has applications to processes involving line broadening, some of which are summarized in Table I. The first process,

TABLE I

Some Physical Processes Describable by the Simple Model

Process	$\lvert\psi_d\rangle$	$\lvert\psi_q\rangle$
Photon emission	$\lvert\psi_{\text{ex}}\phi_{\text{vac}}\rangle$	$\lvert\psi_g\phi_{n(1\gamma)}\rangle$
Autoionization	$\lvert\psi_{\text{ex,ex}}\rangle$	$\lvert\psi_g\phi_{(1e)}\rangle$ $\lvert\psi_g\phi_{(1N)}\rangle$
Unstable particle in the Lee model	$\lvert\psi_{\text{V}}\rangle$	$\lvert\psi_N\phi_\theta\rangle$
Doorway state decay into the compound nucleus	$\lvert\psi_\alpha\rangle$	$\lvert\psi_{\text{comp}}\rangle$

photo de-excitation, has already been discussed. The possibility of autoionization (Fan 61) exists if an atom or nucleus consists of two excited electrons or nucleons. In an autoionization process one of the excited electrons can escape from the atom if it acquires enough energy from the second electron, which is de-excited in the process. That is, the interaction of the two electrons allows the emission of one by the de-excitation of the other—the reverse process produces resonances in the cross section for electron–atom or nucleon–nucleus scattering. The third process, the decay of the V particle (Lee 54) into the N and θ particles has been considered in detail by Glaser and Källén (GK 56). Finally, the decay of a doorway state into the compound nucleus will be the main concern of this subsection.

The model of Section 2.1 can also be used to describe the characteristics of the decay of a simple excitation of the nucleon–nucleus system (generated, for example, by the reversal of the autoionization process) into more complicated excitations which surround the simple excitation. These simple excitations are characterized by having a very large overlap or coupling matrix element with one of the observation channels. For example, such excitations are: single-particle states, analog states, dipole states, and doorway states such as the recently seen fission doorway states. The analog and dipole states can themselves be included in the doorway-state category (Fes 67). Because of this large coupling or overlap, such special states are easily seen in the reaction cross section as resonances. Next, the coupling between the special state and the background or surrounding ordinary states produces a spreading or fragmentation of the excitation strength of the special level. That is, the special state will no longer appear as a sharp line in the cross section, but instead, the line will be broadened.

A classic example is line broadening due to natural decay where the background states are the continuum. In this case, however, the broadened line will always be smooth, independent of the resolution of the beam. For the situation in which the background states are spaced at a distance D, improving the resolution to $I \sim D$ results in the appearance of a series of peaks or fine structure. In our doorway-state example, the background states are continuum states and more complex excitations. Situations can arise in which no complex excitation exist near the doorway state. For example, in light nuclei at low energies, the total energy in the compound system is not large enough to generate more complicated configurations, e.g., $3p$–$2h$ states. The states of the compound system will then be the simple excitations, the doorway states themselves, and resonances will be associated with them if these states are above particle emission thresholds. Such resonance structure in the cross section will have widths intermediate between

those of the gross structure arising from pure single-particle motion and those of the fine structure of complicated configurations of a many-particle system. However, in this case, increasing the resolution will show no fine structure.

The probability $(a_d^\nu)^2$ is the amount of the special state in the background state, and in particular, the amount of doorway state in the nearby compound nuclear states. The width of the distribution of the $(a_d^\nu)^2$ gives the region over which the doorway state distributes any of its characteristic properties. This width is written as $\Gamma_d^\downarrow$, and represents the decay width of the doorway state into the compound nucleus (the downward arrow signifies the decay of the doorway state away from the entrance channel and into the compound nucleus). Besides this width, the doorway state is strongly coupled to one or more of the observation channels c, and the corresponding width is $\Gamma_{d,c}^\uparrow$. The widths $\Gamma_d^\downarrow$ and $\Gamma_{d,c}^\uparrow$ characterize the decay properties of the doorway.

In the wings of the distribution of the $(a_d^\nu)^2$, the inequality $|E_\nu - E_d| \gg \Gamma_d^\downarrow$ holds, and the $(a_d^\nu)^2$ are given by the weak-mixing perturbation value result $V_q^2/(E_\nu - E_d)^2 \simeq V_q^2/(\varepsilon_q - E_d)^2$. For $|E_\nu - E_d| \ll \Gamma_d^\downarrow$ and $V_q \ll D$, this probability is

$$(a_d^\nu)^2 \sim \frac{D}{\hbar} \frac{\hbar}{\Gamma_d^\downarrow} \tag{30}$$

which reflects the uniform spreading or strong mixing of the simple state into the very nearby complicated states. The interpretation of this result is as follows. The factor $\hbar/\Gamma_d^\downarrow$ is the lifetime of the doorway state into the compound nucleus, while the factor $2\pi\hbar/D$ is the period of the compound nucleus (BW 66)—the time it takes the nucleus to go through all states of the compound nucleus consistent with the initial one. The probability of finding the simple excitation in the more complicated excitation is therefore given by the ratio of the time for decay of the simple excitation into the more complicated excitations to the time for the nucleus to travel through all possible configurations consistent with the initial condition. In Section 2.4 we will discuss weak and strong mixing in more detail.

The observability of intermediate structure depends on the extent of the spreading in $(a_d^\nu)^2$. As the width $\Gamma_d^\downarrow$ becomes large, the Lorentzian distribution of strength becomes broader. This means that more states receive about the same amount of doorway state so that the uniform spreading of the doorway extends over a larger interval. When the width $\Gamma_d^\downarrow$ becomes very large, the Bohr picture is realized. In this limit the lifetime of the state becomes very short and the concept of the persistence of single-particle motion and of simple excitations of the nucleus begins to lose its meaning.

We next consider the information obtainable from $(a_d^\nu)^2$. Since the complicated states are highly excited states of a many-body system, we expect the particle emission width of these states to a simple channel c to be small. This follows from the fact that it takes a long time for a single nucleon to acquire the necessary energy (shared among all other particles) to escape and leave the nucleus in a low energy state (simple channel). On the other hand, the doorway state is of simple structure and should therefore have a much shorter lifetime or much larger width. Thus, the width of the states near the doorway will be greatly enhanced (if $\Gamma_d^\downarrow$ is not very large) by the coupling to the doorway. The additional width acquired by the coupling to the doorway state should then be given by the amount of doorway state in the eigenstate multiplied by the decay width of the doorway state $\Gamma_{d,c}^\uparrow$ to the continuum:

$$2\pi \frac{\Gamma_{\nu,c}}{D} = \frac{\Gamma_{d,c}^\uparrow \Gamma_{d,f}^\downarrow}{(E_\nu - E_d)^2 + (\Gamma_d^\downarrow/2)^2} \tag{31}$$

From this equation we see that the distribution of widths in the picket-fence model is a Lorentzian with a width given by $\Gamma_d^\downarrow$.

This system has the classical analog of a number of oscillators coupled to a single central one which is being driven. The driving of one produces oscillations in the others, and the full range of normal modes of the system is excited.

It should also be noted that the eigenfrequencies E_ν and widths Γ_ν give the position of the poles and residues of the resonant part of the K-matrix (MM 67) (discussed in Section 4.1) and are not those of the S- or T-matrix:

$$K^{\text{res}} = V \frac{P_d}{E - H} V \tag{32}$$

The Hermitian K-matrix is related to the unitary S-matrix through the relationship $S = (1 - i\pi K)(1 + i\pi K)^{-1}$, while the S- and T-matrices are related by $S = 1 - 2\pi i T$.

The $V = H_{\text{int}}$ and P_d projects onto bound states. The matrix elements of K^{res} with a channel state $|\psi_c\rangle$ are

$$\langle \psi_c | K^{\text{res}} | \psi_c \rangle = \sum_\nu \frac{\Gamma_{\nu,c}}{E - E_\nu} \tag{33}$$

with $\Gamma_{\nu,c} = 2\pi |\langle \psi_c | V | \psi_\nu \rangle|^2$. An alternate form of the K-matrix elements can be obtained by inserting the states $|\psi_d\rangle$ and $|\phi_q\rangle$ and noting that

only the $|\psi_d\rangle$ state is coupled to the channel state. The resulting expression is

$$\langle\psi_c|K^{\text{res}}|\psi_c\rangle = \frac{\Gamma_{d,c}^{\uparrow}}{E - E_d - \sum_q [V_q^2/(E-\varepsilon_q)]} \tag{34}$$

with $\Gamma_{d,c}^{\uparrow} = 2\pi\,|\langle\psi_c|V|\psi_d\rangle|^2$.

2.4. Mixing Times in Nuclear Excitations

2.4.1. Bound States

The probability amplitude $(a_d^{\nu})^2$ gives the amount of the simple state in the fine-structure state due to mixing of the simple state with the background states. Considered as a continuous function of energy, the $[a_d(E)]^2$ has, as we have seen, a Lorentzian shape with a width given by $\Gamma_d^{\downarrow} = (4V^2 + \Gamma_{d,f}^{\downarrow})^{1/2}$, where $\Gamma_{d,f}^{\downarrow} = 2\pi V^2/D$. This distribution is not derived under any specific assumption about the magnitude of the coupling matrix element V compared to the level spacing D and therefore it applies to all degrees of mixing of the simple state with the background states.

Weak mixing between the simple state and the complicated states occurs when the shift of the eigenenergy E_ν from the associated unperturbed energy ε_n of the background state (see Fig. 1) is much less than the level distance D: $|E_\nu - \varepsilon_n| \ll D$. Then, the sum in the eigenvalue Eq. (8) will be dominated by the term with $E_\nu \approx \varepsilon_n$, so that

$$E_\nu - E_d \simeq \frac{V^2}{E_\nu - \varepsilon_n} \tag{35}$$

and the eigenfunction can be approximated by $|\psi_{E_\nu}\rangle = a_d^{\nu}|\psi_d\rangle + b_n^{\nu}|\phi_\varkappa\rangle$. The amplitude a_d^{ν} is then given by the weak-mixing perturbation value $(a_d^{\nu})^2 = V^2/(E_\nu - \varepsilon_n)^2$. From the above equation we see that the weak mixing condition will be met when

$$\frac{|E_\nu - \varepsilon_n|}{D} = \frac{V}{D}\,\frac{V}{|E_\nu - E_d|} = \frac{1}{2\pi}\,\frac{\Gamma_{d,f}^{\downarrow}}{|E_\nu - E_d|} \ll 1 \tag{36}$$

Thus, weak mixing will apply throughout the distribution when the inequality $|V| \ll D$ holds, or if $|V| \gg D$, when the inequality $|E_\nu - E_d| \gg V^2/D$ is met. For the latter situation, $|V| \gg D$, the simple state will mix thoroughly with the nearby states, until E_ν is such that the inequality $|E_\nu - E_d| > V^2/D$ is satisfied. Thereafter, weak mixing begins to apply.

The mixing time associated with the width $\Gamma_d^{\downarrow}$ is just $\tau^{\downarrow} = \hbar/\Gamma_d^{\downarrow}$. When weak mixing applies throughout, the mixing time is given by the perturbation value

$$\tau_{\text{weak}}^{\downarrow} = \frac{\hbar}{2\,|\,V\,|} \tag{37}$$

which, up to a factor of two, is the mixing time discussed by Morinaga (Mor 55), Wilkinson (Wil 56), and Lane and Thomas (LT 58). For a situation in which a thorough mixing occurs, that is, when $|\,V\,| \gg D$, the mixing time is

$$\tau_{\text{strong}}^{\downarrow} = \frac{\hbar}{2\pi V^2/D} = 4(\tau_{\text{weak}}^{\downarrow})^2 \frac{1}{\tau_{\text{period}}} \tag{38}$$

Thus, the mixing time in a strong-coupling situation is shortened from the weak-mixing situation by essentially the ratio of the weak-mixing time to the period of the nucleus $\tau_{\text{period}} = 2\pi\hbar/D$.

2.4.2. Unbound States

The solution of the eigenvalues and widths for the case when the simple state is unbound and therefore has a natural decay width can be approached from two viewpoints. On the one hand, the problem can be simplified initially by considering it to be a bound-state problem, the diagonalization being done neglecting the natural decay width of the simple state. The resulting real eigenvalues and widths are those obtained in Sections 2.3 and 2.4.1 and they are the poles and residues of the Hermitian K-matrix (or R-matrix),

$$\pi K_{cc} = \sum_{\nu} \frac{(a_d^{\nu})^2 \Gamma_{d,c}^{\uparrow}}{E - E_{\nu}} = \sum \frac{\Gamma_{\nu,c}}{E - E_{\nu}} \tag{39}$$

which will be discussed in detail in Section 4.1. The price that is paid for this initial simplification is that the K-matrix is related to the collision matrix through a nonlinear equation: $S \sim (1 - i\pi K)/(1 + i\pi K)$ and therefore involves a matrix inversion. The energies E_{ν} and widths $\Gamma_{\nu,c}$ will not, in general, be equal to those which appear in the pole expansion of the S- or T-matrix.

On the other hand, the effects of natural decay of the simple state can be included to obtain the poles and residues of the T-matrix:

$$T_{cc} = \sum_{\nu} \frac{(\tilde{a}_d^{\nu})^2 \Gamma_{d,c}^{\uparrow}}{E^{+} - \varepsilon_{\nu}} = \sum_{\nu} \frac{\tilde{\Gamma}_{\nu}}{E^{+} - \varepsilon_{\nu}} \tag{40}$$

The ε_ν and $\tilde{\Gamma}_\nu$ are now complex quantities. For the complex energy we write $\varepsilon_\nu = E_\nu - (i\Gamma_\nu/2)$ and state that in general $\Gamma_\nu \neq \tilde{\Gamma}_\nu$. The E_ν, Γ_ν, and $(\tilde{a}_d{}^\nu)^2$ are not equal to the corresponding quantities which appear in the pole expansion of the K-matrix; the change in the distribution of widths from that of the bound-state situation is produced by the natural decay width of the simple state as discussed by Rodberg (Rod 68), Mahaux and Weidenmuller (MW 67), and Lane (Lan 69). Specifically, if the simple state decays very quickly, the mixing forces have very little time to act and the simple state does not dissolve completely into the background states. To put this physical idea on a more quantitative footing, we investigate the distribution of poles and residues of the T-matrix.

The eigenvalue equation which gives the poles of the T-matrix is a simple generalization of Eq. (27). In fact, this equation is obtained from Eq. (27) by replacing the real energy E_d with complex energy $\varepsilon_d = E_d - (i\Gamma_d{}^\uparrow/2)$, where $\Gamma_d{}^\uparrow$ is the natural decay width of the simple state. The eigenvalues ε_ν will then be complex and satisfy the equation

$$\varepsilon_\nu - E_d + i\frac{\Gamma_d{}^\uparrow}{2} = \sum_q \frac{V^2}{\varepsilon_\nu - \varepsilon_q} = \tfrac{1}{2}\Gamma_{d,f}^\downarrow \cot\left(\pi \frac{\varepsilon_\nu}{D}\right) \tag{41}$$

The last equality follows from the assumption that the background states are equally spaced. Again, weak mixing will occur when the inequality $|\varepsilon_\nu - \varepsilon_q| \ll D$ is satisfied. This condition leads to the equation

$$\frac{(1/2\pi)\Gamma_d{}^\downarrow}{[(E_\nu - E_d)^2 + \frac{1}{4}(\Gamma_d{}^\uparrow - \Gamma_\nu)^2]^{1/2}} \approx \frac{(1/2\pi)\Gamma_d{}^\downarrow}{[(E_\nu - E_d)^2 + (\Gamma_d{}^\uparrow/2)^2]^{1/2}} \ll 1 \tag{42}$$

The presence of $\Gamma_d{}^\uparrow$ in the denominator shows the effect of natural decay in reducing the effective mixing. Weak mixing will apply throughout the distribution when the mixing parameter λ defined by Lane (Lan 69) as

$$\lambda \equiv \frac{(1/\pi)\Gamma_{d,f}^\downarrow}{[D^2 + \frac{1}{4}(\Gamma_d{}^\uparrow)^2]^{1/2}} \tag{43}$$

is much less than unity. This result also applies to the bound-state situation. Thus, a weak-mixing situation can arise through weak coupling or through rapid decay into continuum channels. The former source of weak mixing is just a static criterion which is met when the inequality $|V| \ll D$ is met, while the latter is a dynamic criterion and is met when the mixing time $\hbar/\Gamma_d{}^\downarrow$ is much greater than the natural decay time $\hbar/\Gamma_d{}^\uparrow$, so that the state decays before it mixes. We also note that a strong-coupling situation within the static criterion can be turned into a weak-mixing situation by

the dynamic criterion. This possibility is realized when the inequalities $\Gamma_d^{\uparrow} \gg \Gamma_{d,f}^{\downarrow} \gg D$ hold.

Using Eq. (41), the widths Γ_ν, which appear in the denominator of the pole expansion of the S-matrix, can be found to satisfy

$$\tanh\left(\pi \frac{\Gamma_\nu}{D}\right) = \frac{\frac{1}{2}\Gamma_{d,f}^{\downarrow}(\Gamma_d^{\uparrow} - \Gamma_\nu)}{(E_\nu - E_d)^2 + \frac{1}{4}(\Gamma_{d,f}^{\downarrow})^2 + \frac{1}{4}(\Gamma_d^{\uparrow} - \Gamma_\nu)^2} \tag{44}$$

The presence of the hyperbolic tangent function in the above equation is responsible for a qualitative change, under certain conditions, from the bound-state distribution of widths (Lan 69). In particular, this distribution does not have a Breit–Wigner or Lorentzian shape unless strong mixing applies. In the strong-mixing limit, $\Gamma_{d,f}^{\downarrow} \gg \Gamma_d^{\uparrow}$, $\Gamma_d^{\uparrow} \gg \Gamma_\nu$, and $\Gamma_\nu \ll D$, so that the distribution is again Lorentzian:

$$\pi \frac{\Gamma_\nu}{D} = \frac{\frac{1}{2}\Gamma_{d,f}^{\uparrow}\Gamma_d^{\downarrow}}{(E_\nu - E_d)^2 + \frac{1}{4}(\Gamma_{d,f}^{\downarrow})^2} \tag{45}$$

This distribution is identical with the strong-mixing limit of the bound-state distribution since the simple state thoroughly dissolves before it decays into the continuum channels. In the limit of weak mixing due to rapid decay, the distribution of widths will have one pronounced level with a width given by Γ_0, where Γ_0 can be obtained from the eigenvalue equation $\Gamma_d^{\uparrow} - \Gamma_0 = \Gamma_{d,f}^{\downarrow} \coth(\pi\Gamma_0/2D)$. When the situation applies $\Gamma_0 \gg D$, $\coth(\pi\Gamma_0/2D)$ is close to unity so that $\Gamma_0 = \Gamma_d^{\uparrow} - \Gamma_{d,f}^{\downarrow}$. Moreover, when the distribution is summed over the levels, the following sum rule is obtained:

$$\sum_\nu \Gamma_\nu \simeq \int_{-\infty}^{\infty} \frac{dE_\nu}{D} \Gamma(E_\nu) = \frac{\Gamma_{d,f}^{\downarrow}\Gamma_d^{\uparrow}}{\sqrt{(\Gamma_{d,f}^{\downarrow})^2 + (\Gamma_d^{\uparrow})^2}} \tag{46}$$

For the case $\Gamma_d^{\uparrow} \gg \Gamma_{d,f}^{\downarrow}$, the sum is just $\Gamma_{d,f}^{\downarrow}$, so that $\Gamma_0 = \Gamma_d^{\uparrow} - \sum_\nu \Gamma_\nu$. At the other extreme, that of strong mixing, $\Gamma_{d,f}^{\downarrow} \gg \Gamma_d^{\uparrow}$, and the sum of the fine-structure widths is just $\Gamma_d^{\uparrow}$, since the simple state thoroughly distributes its strength over the background levels.

The numerator widths of the T-matrix expansion can be obtained from the coefficient $(\tilde{a}_d^{\nu})^2 = \langle \psi_d \mid \psi_{E_\nu} \rangle^2$. In turn, the $(a_d^{\nu})^2$ can be obtained from Eq. (29) by simply replacing E_ν and E_d by the complex quantities ε_ν and ε_d. Thus, the complex quantity $(\tilde{a}_d^{\nu})^2$ is given by the equation

$$(\tilde{a}_d^{\nu})^2 = \frac{(D/2\pi)(\Gamma_{d,f}^{\downarrow})^2}{(\varepsilon_\nu - \varepsilon_d)^2 + (\Gamma_d^{\downarrow}/2)^2} \tag{47}$$

where $(\Gamma_d^{\uparrow})^2 = (\Gamma_{d,f}^{\downarrow})^2 + 4V^2$. In the strong-mixing limit, the quantity $(\tilde{a}_d^{\nu})^2\Gamma_d^{\uparrow}$ is

$$(\tilde{a}_d^{\nu})^2\Gamma_d^{\uparrow} = \frac{(D/2\pi)\Gamma_{d,f}^{\downarrow}\Gamma_d^{\uparrow}}{(E_\nu - E_d)^2 + (\Gamma_{d,f}^{\downarrow}/2)^2} = \Gamma_\nu \tag{48}$$

so that the numerator widths are real and equal to the denominator widths of the pole expansion of the T-matrix. When weak mixing due to rapid decay applies, the $(\tilde{a}_d^{\nu})^2$ are complex and they are obtained from the following equation:

$$(\tilde{a}_d^{\nu})^2 = \frac{(D/2\pi)\Gamma_{d,f}^{\downarrow}}{[E_\nu - E_d + i(\Gamma_d^{\uparrow}/2)]^2} \tag{49}$$

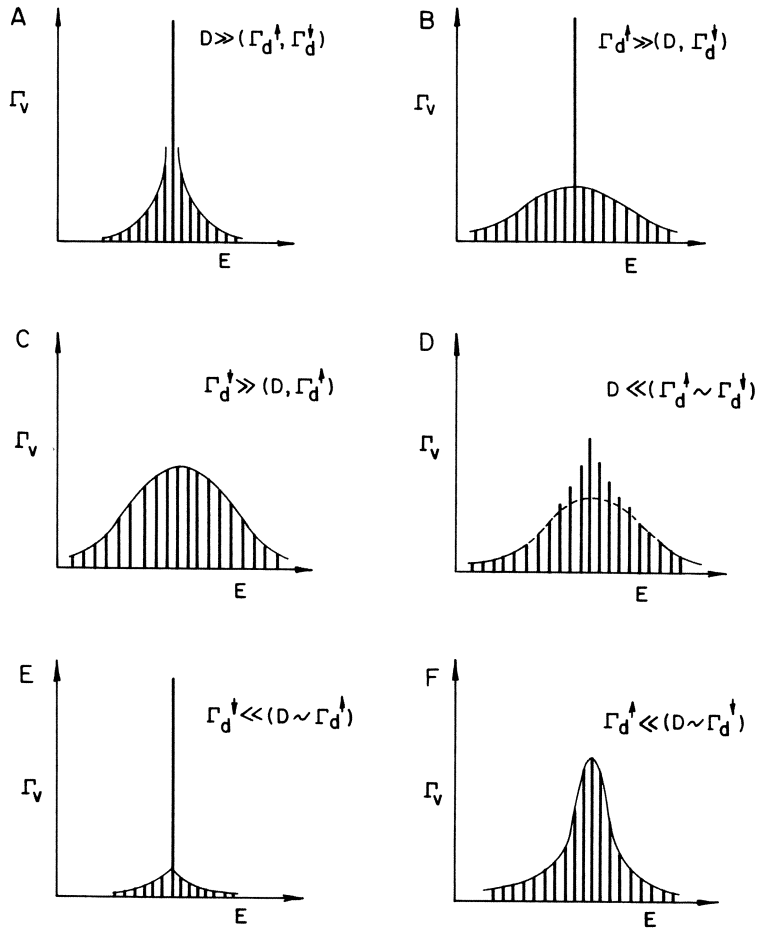

Fig. 2. Distribution of widths for various mixing situations. After Lane (La 69).

The phase angle χ_ν defined by $(\tilde{a}_d^\nu)^2 = |\tilde{a}_d^\nu|^2 \exp(2i\chi_\nu)$ satisfies the equation

$$\tan 2\chi_\nu = \frac{\Gamma_d^\uparrow(E_d - E_\nu)}{(E_\nu - E_d)^2 - (\Gamma_d^\uparrow/2)^2} \tag{50}$$

The distributions of Γ_ν for various mixing situations are shown in Fig. 2.

3. NUCLEON–NUCLEUS SCATTERING AND INTERMEDIATE STRUCTURE

3.1. Review of the Models of Nuclear Resonance Reactions

3.1.1. Potential Scattering Model

One of the earliest attempts at a description of nuclear reactions was due to Bethe (Bet 35), who described the scattering of a nucleon from a nucleus in terms of a simple real potential well [also consider by Bethe (Bet 35) was a square well with a large imaginary part]. In such a picture the target is left unchanged while the incident particle moves in a potential well which describes the effect the target, considered to be structureless, has on the incident nucleon. Within such a picture only two types of reactions are possible: elastic scattering and radiative phenomena. The former process dominates the cross section which shows slow, widely-spaced variations over energies of tens of MeV, which are characteristic of resonances due to single-particle motion in a well of nuclear dimensions. For example, the widths $\Gamma_{\text{s.p.}}$ and spacings $D_{\text{s.p.}}$ of such single-particle resonances in a square-well potential of radius R for $L = 0$ waves are

$$\begin{aligned} \Gamma_{\text{s.p.}} &= \frac{\hbar}{MR^2} 2kR \\ D_{\text{s.p.}} &= \frac{\hbar}{MR^2} \pi KR \end{aligned} \tag{51}$$

The K and k are the wavenumbers inside and outside the square well, respectively.

The potential scattering model predicted cross sections which varied from nuclear dimensions to much larger values at the single-particle resonance energies. While accounting for the large cross sections Fermi (Fer+34) found the model failed to account for the very rapid variations in the slow-neutron cross section (BW 35, FA 35, MT 35, FP 36) and also the large capture cross section. As an illustration, Fig. 3 shows a typical slow-neutron cross section.

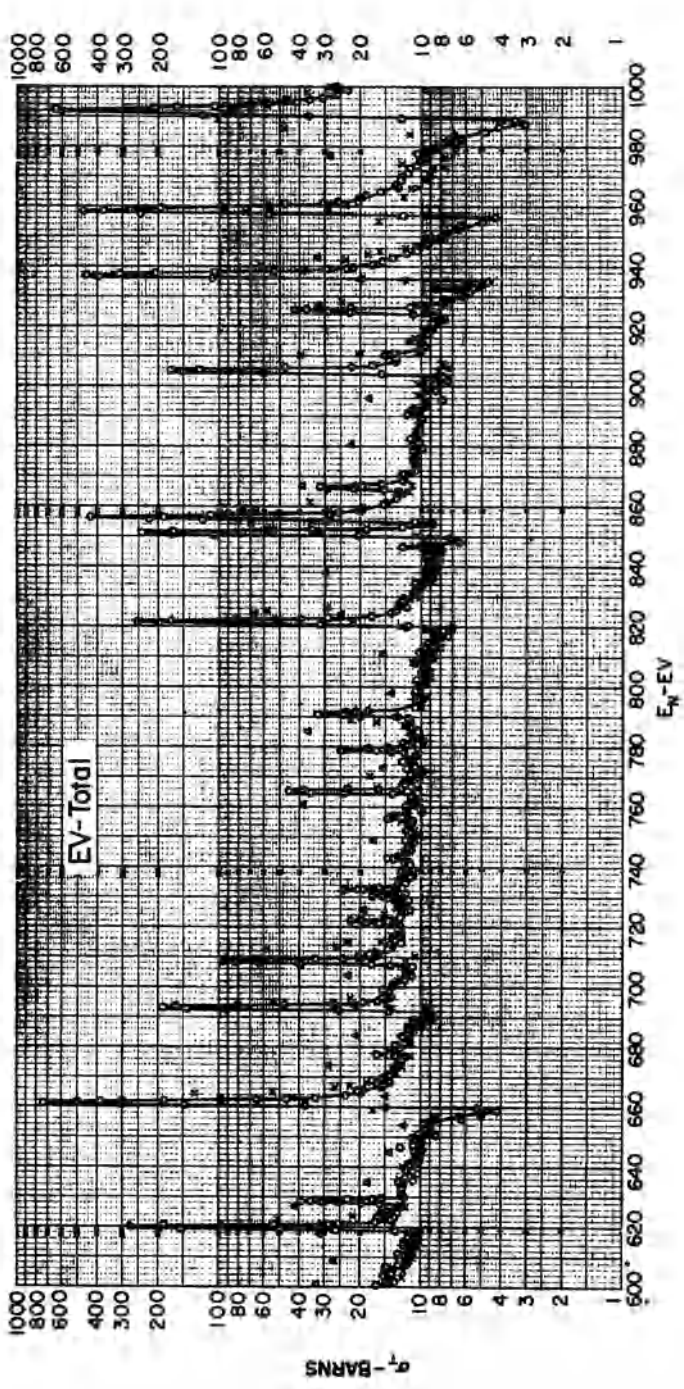

Fig. 3. Fine structure in a slow-neutron cross section for $n + U^{238}$. Data taken from the compilation: Neutron Cross Sections (BNL 1964).

3.1.2. Compound Nucleus Model and the Strong Absorption Model

To account for the narrow, closely-spaced resonances seen in high-resolution slow-neutron cross sections and the large capture probabilities, Bohr (Boh 36, Boh 37) and also Breit and Wigner (BW 36) introduced the compound nucleus. This scheme stood at the other extreme from Bethe's description of nucleon–nucleus scattering. In Bohr's picture, the incident nucleon, upon reaching the nuclear surface, strongly disturbs the state of the target nucleons by immediately coalescing with them to form a highly complex state of a many-particle system. In this state, the total energy of excitation is shared among many nucleons through the strong nuclear forces which exist between nucleons. An emission of a particle occurs when, during the course of the many collisions taking place, a statistical fluctuation occurs and a sizable fraction of the total energy is concentrated on one nucleon. Since such large statistical fluctuations are rare, the lifetime of the compound nucleus will be long and the resonance associated with the compound nuclear states will be narrow. Moreover, the close spacing of these resonances is a consequence of the large number of particles involved in the excitation of the compound nucleus.

Furthermore, because of the long lifetime of the compound state, the compound nucleus will have "forgotten" how it was formed by the time it decays. This result leads to Bohr's assumption that the decay of the compound nucleus is independent of the mode of formation. This independence hypothesis coupled with the picture of the immediate sharing of energy among all the nucleons formed the basis of a statistical description of nuclear cross sections in which thermodynamical concepts are introduced to describe the compound nucleus (Wei 37). In particular, the compound nucleus was considered to be a heated system with a characteristic temperature reflecting its state of excitation, and its subsequent decay was analogous to the evaporation of a molecule from a small drop of liquid. The predicted Maxwellian distribution for the energy of evaporating particles fitted fairly well the spectrum of neutrons and protons emitted from an excited nucleus (Gug 51).

While the compound-nucleus model qualitatively described the rapid variations seen in high-resolution cross sections, a more quantitative description of resonance phenomena was developed by Breit and Wigner (BW 36), and also by Kapur and Peierls (KP 38), which was later developed into a generalized description of nuclear reactions (WE 47, Tei 51). Next, to account for the energy dependence of the cross section appropriate for poor-resolution experiments, Feshbach, Peaslee, and Weisskopf (FPW 47)

introduced the strong-absorption or black-nucleus model, which was based on the compound nucleus description. Specifically, the basis for this model was Bohr's idea that a particle inside the nucleus interchanges energy very rapidly with other nucleons, so that any particle crossing the nuclear surface loses its energy and is absorbed. Then, if many channels are open these conditions imply that it is very unlikely that an incident projectile will reappear in the entrance channel. In turn, this allows the assumption of only incoming waves inside the nucleus so that the interior radial wave function for s-waves in a square well of wave number K is (FW 49)

$$u(r) \sim e^{-iKr} \tag{52}$$

and that the logarithmic derivative at the nuclear surface is

$$f = \left.\frac{ru'}{u}\right|_{r=R} = -iKR \tag{53}$$

The above results (easily extended to higher partial waves) are sufficient to calculate the cross section, since, once the interior wave function is known, the exterior wave function and phase shift are obtained by the continuity conditions on the wave function at the nuclear surface. The predicted average cross section of the black-nucleus model for compound nucleus formation is then (BW 66)

$$\langle\sigma\rangle = \pi(R + \lambda\!\!\!^{-})^2 \frac{4kK}{(k + K)^2} \tag{54}$$

and has a monotonically decreasing energy dependence.

3.1.3. Optical Model or Moderate Absorption Model

The compound nucleus model successfully accounted for narrow resonances and the small spacings of these resonances, and the statistical description of nuclear reactions gave a reasonable account of some of the important features of these reactions. Serious disagreements, however, appeared as data were accumulated on gross properties of the energy dependence of the total neutron cross section. In poor energy resolution, these cross sections (Bar 52, WB 54, Mil 52) show a variation with energy which has pronounced maxima and minima over intervals of several MeV, as shown in Fig. 4; that is, they reflected a behavior which was characteristic of the scattering of a nucleon off a potential well without the disturbance of the target. Nevertheless, looked at with high resolution, the cross section showed the closely-spaced narrow peaks of the compound

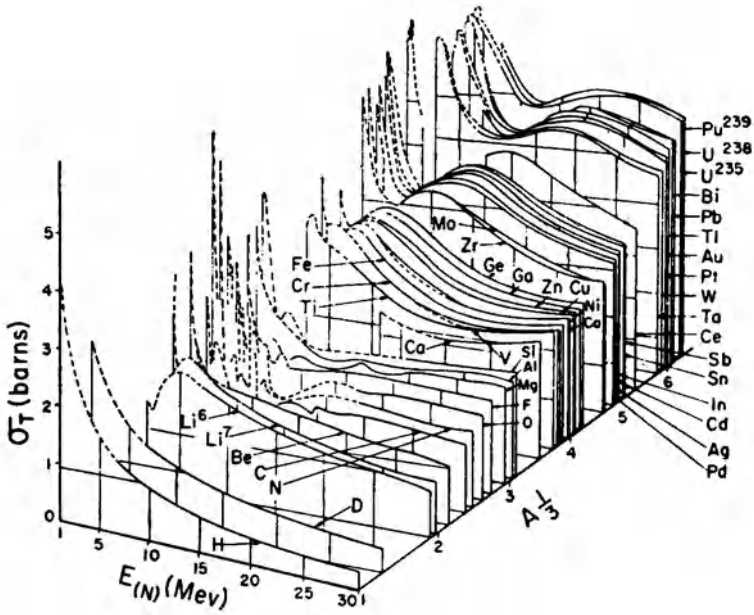

Fig. 4. Poor-resolution neutron total cross sections as a function of energy and atomic weight. For fixed A, the cross sections show periodic maxima and minima. Also seen is the result that the position of the cross-section maxima increase with increasing A and increasing E. This latter point is considered in more detail in Section 3.1.5. From Peterson (Pet 62).

nucleus. Thus, the observed high- and poor-resolution cross sections pointed to some combination of single-particle and compound motion.

Moreover, the success of the shell model in describing the properties of low-lying states of nuclei suggested a model in which a nucleon could move comparatively freely inside the nucleus. This result also contradicted the assumption of immediate formation which implied a vanishingly small mean free path for a nucleon which has entered the nucleus. Contrastingly, the success of the shell model meant that a nucleon could move in a well-defined single-particle orbit of a potential well arising from a structureless target. However, one knew from scattering data that there existed strong interactions among nucleons, in apparent contradiction to the weak-coupling picture implied by the shell model. The success of an independent-particle model was then explained by Brueckner and collaborators (BLM 54, BL 55, Bru 55, BEF 55) for the case of nuclear matter. The main reasons for the validity of the independent-particle model were found to be linked with the exclusion principle and the fact that the nuclear force just barely gave rise to a bound state (GWW 58).

Thus, the experimental situation again called for a new model, and the optical model (also known as the moderate-absorption model, complex-potential model, and cloudy crystal ball model) was introduced by Feshbach, Porter, and Weisskopf (FPW 54) to describe low-energy nucleon–nucleus scattering. A similar model had previously been introduced by Fernbach, Serber, and Taylor (FST 49) to describe nuclear scattering at high energies and also earlier by others (Ama+ 35, BH 35, PE 35) to explain the observed large neutron cross sections. This model, which superseded all previous models, combined both single-particle and compound nuclear aspects. The single-particle motion of an incident nucleon inside the nucleus was described in terms of a real potential $V_0(r)$ of the type used in shell-model calculations, while the compound nuclear aspects and, in particular, the absorption which is supposed to represent the formation of the compound nucleus, was accounted for by adding to the potential an imaginary part $iW_0(r)$. The total potential describing the interaction of the incident particle with a structureless target in this complex potential model is then

$$V(r) = V_0(r) + iW_0(r) \tag{55}$$

Because of the extreme simplicity of the potential, the optical model did not reproduce the compound nuclear resonances, but considered only the behavior of the cross section averaged over neighboring resonances.

One important implication of the complex-potential model was that the sum of the reduced widths γ_λ^2 of the compound nuclear levels λ per unit energy interval had a giant resonance dependence on the compound nuclear energies E_λ (FPW 54, Tho 55). The locations of the maxima in the strength function, γ_λ^2/D, were at the resonance energies of the real part of the optical potential while the widths of the giant resonances were just twice the imaginary part of this potential. This result holds for square wells and can be demonstrated by replacing E by $E - iW_0$ in the single-particle Breit–Wigner amplitude. A second important result of this model was the appearance of variations of the strength function which showed periodic maxima and minima with A, the atomic mass number. We first consider the former implication and return to a more detailed discussion of the latter phenomenon in Section 3.3.

3.1.4. Theoretical Attempts to Account for the Optical Model

Several attempts have been made to account for the complex-potential model. One attempt (Gol 48, LW 55, MMM 55) has been based on relating the real and imaginary parts of the optical potential to the observed prop-

erties of nucleon–nucleon scattering. This endeavor uses the optical analogy assumed in the complex-potential or cloudy crystal ball model, from which the following fundamental relation of the approach is obtained:

$$V_0 + iW_0 = \hbar v \varrho \left\langle \frac{2\pi}{k_{\text{rel}}} f(0) \right\rangle \tag{56}$$

The result is analogous to the relation between the index of refraction and the forward scattering amplitude of light. The average that appears in the above equation is over all relative wave numbers k_{rel} of the incident nucleon, moving with velocity v inside the nucleus, and target nucleons of density ϱ. The $f(0)$ is the forward scattering amplitude. From this equation, the imaginary part of the optical potential can be expressed in terms of the total cross section for two-particle scattering through the optical theorem which relates the total cross section σ_T to the imaginary part of the forward scattering amplitude. The resulting expression for W_0 is

$$W_0 = \frac{\hbar v \varrho}{2} \sigma_T \tag{57}$$

In evaluating σ_T the exclusion principle plays an important role by restricting the number of available states a nucleon can scatter into. This Pauli principle correction to the optical model, when expressed as a ratio of the nucleon–nucleon collision cross section in nuclear matter and in free space $P = \sigma/\sigma_F$, has been obtained by Goldberger (Gol 48) for a degenerate Fermi gas description of the target:

$$P(\eta) = \begin{cases} 1 - \frac{7}{5}\eta & \eta \leq \frac{1}{2} \\ 1 - \frac{7}{5}\eta + \frac{2}{5}\eta(2 - 1/\eta)^{5/2} & \eta \geq \frac{1}{2} \end{cases} \tag{58}$$

The $\eta = E_F/E_1$ is the ratio of the Fermi energy E_F to the kinetic energy E_1 of the incoming nucleon, measured from the bottom of the Fermi sea. The importance of the Pauli correction has also been discussed by others (LW 55, MMM 55, Ser 47, CV 55, Ste 57). The calculated imaginary part as obtained by Morrison *et al.* (MMM 57) is

$$W_0 \sim (3.0 + 0.35E) \text{ for neutrons}$$

and (59)

$$W_0 \sim (1.3 + 0.35E) \text{ for protons}$$

for $0 < E < 24$ MeV. The low values of W_0 obtained at low energies are a result of the exclusion principle. Ignoring the Pauli principle, Lane and Wandel (LW 55) find that W_0 is increased by about an order of magnitude at zero incident energy.

Although such a relationship between the optical model and nucleon–nucleon scattering is appealing, it is not valid at low energies because of multiple scattering corrections. This approach has therefore been referred to as the frivolous model. A second attempt (Blo 57a, Blo 57b, LTW 55, BD 57) is based on the R-matrix theory of nuclear reactions (WE 47, LT 58), which is a rigorous and general framework and should therefore, with appropriate approximations, account for the data which are described phenomenologically by the complex-potential model. In particular, Lane, Thomas, and Wigner (LTW 55) introduced the intermediate coupling model (not to be confused with intermediate structure) as an interpretation of the giant resonance behavior of the optical-model strength function. This model represents an in-between situation in which there is no coupling between an incident nucleon and the target nucleus [Bethe's picture (Bet 35)] and the case of strong coupling in which the single-particle states are completely dissolved [Bohr's picture (Boh 36, Boh 37)]. In terms of nuclear structure, the model stands between the independent-particle and uniform models (Wig 37). The essential idea behind the interpretation of the giant resonance behavior is that the single-particle states of the incident nucleon–target nucleus system spread their strength over the dense spectrum of states of the whole nucleus, with states far removed from the position of the simple states receiving only a small amplitude from this state and the nearby states receiving a much larger amount. The strength distribution obtained by Lane *et al.* (LTW 55) for the intermediate coupling situation has the form of Eq. (31) and is

$$\frac{\gamma_\lambda^2}{D} = \frac{(1/2\pi)\gamma_{\text{s.p.}}^2 W_p}{(E_\lambda - E_p)^2 + \frac{1}{4}W_p^2} \tag{60}$$

The $\gamma_{\text{s.p.}}^2$ is the single-particle reduced width and E_p the single-particle resonance energy. The W_p is the region over which the single-particle state spreads its strength and is $W_p = 2W_0$. For the case of a black nucleus, the strength function can be obtained by noting that, in this limit, the single-particle strength is uniformly distributed over the whole spectrum so that

$$\frac{\Gamma_{\text{s.p.}}}{D_{\text{s.p.}}} = \frac{\Gamma_\lambda}{D} = \frac{2}{\pi}\,\frac{k}{K} \tag{61}$$

from which we obtain

$$\frac{\gamma_\lambda^2}{D} = \frac{1}{\pi KR} \tag{62}$$

for the reduced-width strength function.

Lane *et al.* (LTW 55) also estimated the spreading width W_p by evaluating the second moment of the distribution for the probability amplitudes $a^2_{\lambda,\text{s.p.}}$ of the single-particle state (s.p.) over the compound nuclear states λ. This second moment is proportional to the expectation value of the square of the coupling potential which connects the single-particle state to the compound states:

$$M_2 \equiv \sum a^2_{\lambda,\text{s.p.}}(E_\lambda - E_{\text{s.p.}})^2 = (V^2)_{\text{s.p.,s.p.}} \tag{63}$$

For the square root of this second moment they obtain a value of 22.5 MeV when a Fermi gas is used for the target nucleons. This result is about an order of magnitude larger than the observed width of the giant resonance. Vogt (Vog 55, Vog 56), Vogt and Lascoux (VL 57) and Lane and Verlet (LV 55) have improved on the second-moment calculation by considering the correlations between the incident nucleon and target nucleons. These correlations are found to reduce the second moment to a more reasonable value.

Bloch (Blo 57) and Wigner (Wig 55b) have discussed situations in which the square root of the second moment will greatly overestimate the imaginary part of optical potential. Such situations will arise whenever the single-particle strength is well spread out, in which case, the second moment will give too much weight to the distant components of the strength distribution. For example, a Lorentzian distribution will have an infinite second moment because of the long tail of this distribution. In contrast, for a Gaussian distribution the second moment is $(1.12)^{-1}$ times the half-width at half-maximum.

3.1.5. The Nuclear Ramsauer Effect and Giant Resonances

The poor-resolution neutron cross sections show broad maxima as a function of energy for fixed A as can be seen in Fig. 4. An explanation of the phenomenon responsible for the appearance of these broad maxima has been given by Peterson (Pet 62) and McVoy (McV 67) in terms of the nuclear analog of the atomic Ramsauer effect (Ram 21, MM 50). Specifically, by examining optical-model calculations of the total cross section, they find that the maxima in these cross sections, except near zero energy, are not manifestations of the single-particle giant resonances of Lane *et al.* (LTW 55) which appear in the strength function; rather, they find that the broad maxima reflect constructive interference effects arising from that part of the beam which passes through the nucleus without delay and that part which passes around it. A similar picture was also employed by

Fernbach *et al.* (FST 49) and Lawson (Law 53) to interpret neutron scattering data at higher energies.

The key to the result that the broad maxima are not manifestations of single-particle resonances is in the dependence on energy E and mass number A of the position of the ridges and valleys that are present in Fig. 4. From this figure we note that the ridges move to higher A with increasing energy. This behavior is not characteristic of the position of single-particle resonances which decrease with increasing A. This latter conclusion follows from the observation that resonances arise from interference effects of the de Broglie wave produced by the reflections of the wave at the boundaries of the potential; they, thus, correspond to a large build up of the amplitude of the wave function inside the nucleus. A condition which determines the energy at which this occurs for s-waves is that the logarithmic derivative of the wave function at the nuclear boundary be zero. For s-waves in a square-well potential of depth V_0 and range R, this energy is obtained from the condition

$$KR = (n + \tfrac{1}{2})\pi \tag{64}$$

Here, the K is the wave number inside the well. Similar equations also apply to other partial waves. This condition therefore implies that if E increases, R and consequently A must decrease, a result which contradicts the experimental facts.

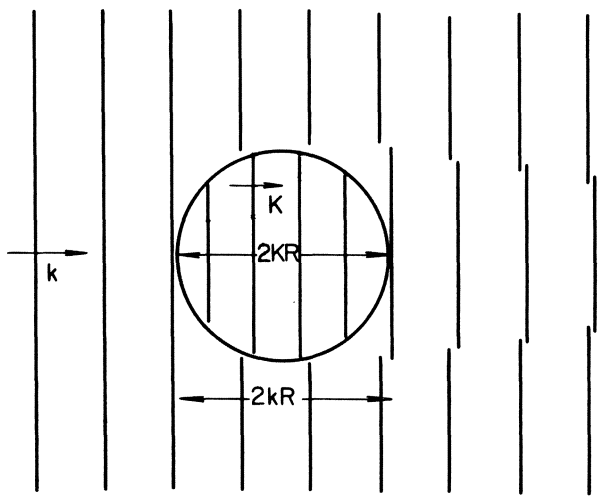

Fig. 5. Schematic illustration of the nuclear Ramsauer effect. Interferences are generated between the wave which passes through the nucleus and the wave which passes around it, resulting in oscillations in the cross section.

On the other hand, a description, as pictured in Fig. 5, of the maxima in terms of constructive interference of the wave which passes through the nucleus and that which goes around it will lead to the condition:

$$(K - k)R = (n + \tfrac{1}{2})\pi \tag{65}$$

This result gives the correct ridge behavior since $K - k$ decreases with increasing E, and thus R and A increase with increasing E. We also note that the phase shift $\delta = (K - k)R$ is a decreasing function of the energy so that the phase shift passes downward through $(n + \frac{1}{2})\pi$ at the maxima. As discussed by McVoy, such decreases of the phase shift can result from echoes of resonances since Levinson's theorem (Lev 49) states that $\delta_l(0) - \delta_l(\infty) = n_l\pi$, where n_l is the number of single-particle bound states of angular momentum l and the argument of δ is the energy. Thus, if there are m_l resonances, and if Levinson's theorem applies, there will be $n_l + m_l$ echoes where the phase shift will be decreasing through an odd multiple of $\pi/2$. Moreover, because of Wigner's (Wig 55a) limit on the rate of descent of the phase shift $d\delta/dk \geq -R$, the echo can be very broad.

Finally, we note that in the WKB approximation, δ_l is proportional to the chord length across the sphere at the impact parameter $b_l \sim l/k$, which is $2R$ for all $l \ll kR$. Consequently, if one partial wave l_1 with $l_1 \ll kR$ passes downward through $\pi/2$, all with $l < l_1$ will, and this accumulation of echoes in different partial waves results in broad interference maxima in the total cross section. McVoy then shows that the interfering nonresonant maxima wash out any resonant maxima in the total cross section, so that the effect of any giant resonances of the Lane–Thomas–Wigner type on the total cross section is very small and difficult to isolate, except near zero energy.

3.2. Physical Picture of Nucleon–Nucleus Scattering

3.2.1. Nucleon–Nucleus Collisions in an Independent-Particle Model with Residual Interactions

While the optical model is remarkably successful in fitting the experimental data on nuclear reactions, its shortcoming is that it gives information only on the total probability for absorption or elastic scattering. No information on the detailed mechanism of what happens when a particle enters the nucleus is supplied by the model. For this purpose, Weisskopf (Wei 61) has discussed a picture of nuclear reactions based on the independent-particle model. In this description, the nucleons in the target are considered to be in a finite well of the type used in conventional shell-model

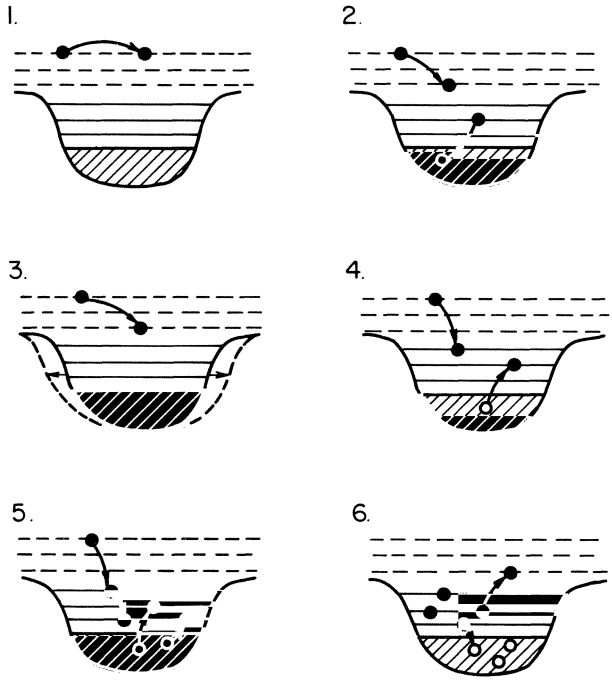

Fig. 6. The generation of the hierarchy of states through processes of multiple scattering in a shell-model description of nuclear reactions.

calculations, such as a Woods–Saxon well (WS 54) while the incident nucleon is in one of the positive energy continuum states of this well. This extended shell model can then be used to describe the mechanisms involved in different types of nuclear reactions.

First, in the absence of residual interactions between the incident nucleon and the nucleus, the only processes that can occur are potential scattering or radiative phenomena. Next, the residual nuclear interaction allows the incident nucleon to exchange energy with the target nucleons and the inclusion of this interaction leads to a whole series of different types of reactions, some of which are shown in Fig. 6. In this figure, the target is taken to be a closed shell, or $0p$–$0h$ state. The processes shown consist of:

1. Potential scattering—the incident nucleon scatters off the shape of the one-body potential without exchanging energy with one of the nucleons in the nucleus. The combined incident nucleon–target system is a $1p$–$0h$ state.

2. Direct inelastic scattering—the incident nucleon transfers energy to the target by exciting a nucleon into another bound state of the target, thereby exciting a $1p$–$1h$ state of the target. This process happens at the expense of some of the energy of the incident particle. If the incident energy is large enough, the nucleon will remain in a continuum state.
3. Direct inelastic scattering in which a collective motion of the nucleons in the target is excited. The excitation is still simple but involves many nucleons.
4. Precompound nucleus excitation, step 1—the incident nucleon loses a lot of energy and falls into a bound state; the released energy is taken up by a low-lying nucleon which also goes into a bound state so that the combined system is a $2p$–$1h$ state. This leads to an excited state of the nucleus from which no nucleon can escape. The total energy in such a state is positive with respect to the threshold for nucleon emission, so that these states are embedded in the continuum. Moreover, these simple states will lead to resonances in the cross section, a result which is one of the key consequences of this picture. The decay of such states by the emission of a particle is just the autoionization process we have already discussed. These simple states of the nucleon–nucleus system reached in the first collision of a nucleon with the nucleus act as doorway states into the compound nucleus.
5. Precompound nucleus excitation, step 2—the state formed in the first collision can also excite another particle into a bound state by losing additional energy, thereby creating a $3p$–$2h$ state. Further excitations by internal collisions will also occur, generating a whole hierarchy (Blo 66) of more complicated states, i.e., $4p$–$3h$, $5p$–$4h$, ..., states. After many such collisions, the compound nucleus is formed in which the average energy per particle is so small that no nucleon will escape.
6. Precompound nucleus emission—as a hierarchy of complex excitations are being passed through, a nucleon might acquire enough energy to escape before the compound nucleus is formed.

The first process, potential scattering, is accounted for in the optical potential by the real part V_0. All other processes outside of potential scattering are described in terms of the absorptive part, iW_0, of the optical potential. These include the remaining processes (2) to (6), which are lumped together and described in an average way in this complex-potential

model. In order to distinguish the process and investigate the reaction dynamics in a nucleon–nucleus collision the structure of the target must be included. The extended shell model offers a convenient basis for a microscopic description of the dynamics of the absorption of a particle described phenomenologically by the optical model.

3.2.2. Importance of the First Collision

The mean free path of a particle inside the nucleus is not zero in the optical-model description as it is in the strong-absorption picture of Bohr. The mean free path is related to the imaginary part, W_0, of this potential (FW 53) and is

$$L = \frac{1}{2} \frac{\hbar}{W_0} \left[\frac{2(E + V_0)}{m} \right]^{1/2} \tag{66}$$

The first factor is the absorption time while the second factor is the velocity of a particle with total energy E moving in a potential well of depth V_0. The reciprocal of the mean free path is the coalescence coefficient K discussed by Friedman and Weisskopf (FW 55). Using the values of V_0 and W_0 which best fit the experimental data for low-energy nucleon–nucleus scattering, $V_0 = 50$–55 MeV and $W_0 = 3$–5 MeV, we obtain for L the result $L = 5$ to $10\,f$. Thus the probability of absorption at low energies is about 50% for a nucleon making one trip across the nucleus. This long mean free path is a consequence of the exclusion principle which, at low energies,

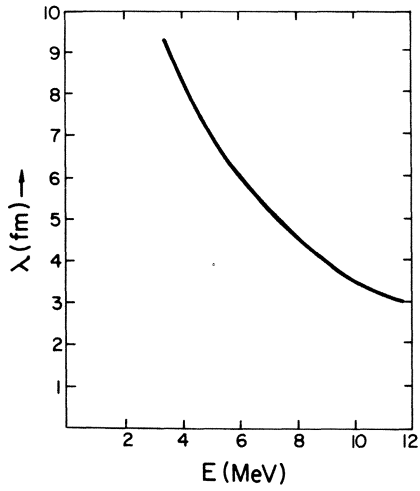

Fig. 7. Dependence of the mean free path on the energy of the incident nucleon. From Rodberg (Rod 61).

plays an important role in restricting the number of states a particle can scatter into. With increasing energy, the number of such states increases and with this increase, W_0 increases, thereby causing L to decrease. From the energy dependence of the imaginary potential, the dependence of the mean free path on the energy of the incident nucleon can be calculated and the result is shown in Fig. 7 (Rod 61).

The above results show that for energies less than, say, 5 MeV the incident nucleon has a mean free path of the order of the diameter of the nucleus and therefore has a good chance of escaping without making more than one collision. This result suggests the importance of the first collision, since if the nucleon is not captured into a doorway state in the first collision, it has a very good chance of escaping. Finally, the state reached in a first collision must be simple because of the two-body nature of the nucleon–nucleon force.

3.3. The Optical-Model Strength Function as a Function of Mass Number

3.3.1. Maxima in the Optical-Model Strength Function

The position of the maxima in the optical-model strength function is determined by the real part of the optical potential. As we have already mentioned, this term contributes only to potential scattering. However, it can lead to single-particle resonance in which a nucleon gets trapped in a well for a time longer than the transit time. These single-particle resonances arise from interference effects of the de Broglie wave produced from the reflections of this wave at the boundaries of the potential. A condition for the existence of an s-wave resonance in a square well of depth V_0 and radius R_0 is that the radius in units of the de Broglie wavelength $\lambda = \hbar/p$ is a half-integral multiple of π. We have

$$\frac{R_0}{\lambda} = R_0 \sqrt{\frac{2m(E + V_0)}{\hbar^2}} = (n + \tfrac{1}{2})\pi \tag{67}$$

This condition ensures that the logarithmic derivative of the interior wavefunction is zero. For $E \ll V_0$, we have a low-energy s-wave single-particle resonance when the radius of the nucleus is

$$R_0 = (n + \tfrac{1}{2})\pi\lambda_C \sqrt{\frac{mc^2}{2V_0}} \tag{68}$$

The λ_C is the Compton wavelength of the nucleon, $\lambda_C = \hbar/mc$. Taking V_0 to be 55 MeV and using the property of volume saturation of nuclei which can be written as $R_0 = r_0 A^{1/3}$, where $r_0 = 1.25f$, we have a low-energy resonance existing for $A = 50$ and 150 (FB 50, Ada 54, FPW 54). Here A is the atomic number. For nuclei with atomic numbers near 50 and 150 we therefore expect a larger s-wave absorption into the compound nucleus. Furthermore, this observation manifests itself in a larger excitation strength, measured by the strength function $\langle \gamma_\lambda^2/D \rangle$, near one of these single-particle resonances.

Figure 8 shows a plot of the experimentally determined values of the s-wave strength function as a function of A. The solid curve is the theoretical prediction of the spherical complex-potential model as obtained by Campbell *et al.* (Cam+ 60). The points are the experimentally determined values while the open circles are the results of a calculation discussed in Section 3.3.2. The dotted straight line is the prediction of the strong-absorption or black-nucleus model. From this figure we note several interesting char-

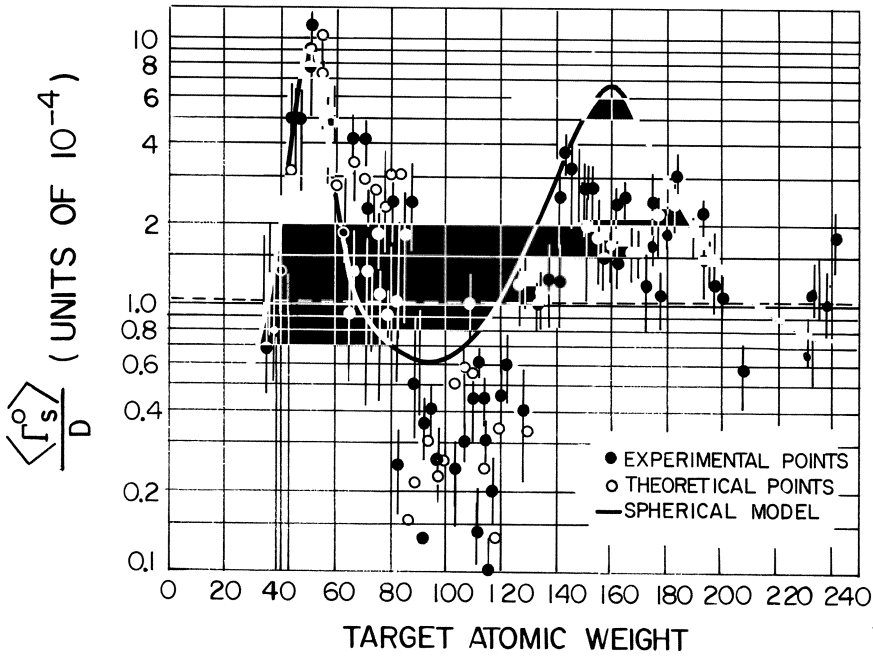

Fig. 8. The s-wave neutron strength function as a function of the atomic weight of the target. The theoretical points will be discussed in Section 3.3.2. After Block and Feshbach (BF 63).

acteristics of the strength function. First, we note the appearance of a maximum at $A = 55$ and an enhancement near $A = 160$. Secondly, the experimental points near the mass region $A = 160$ are suppressed below the value predicted by the spherical-potential model. Also we see the appearance of an anomalous dip at $A = 115$ and a rise at $A = 70$. Finally, the figure shows fluctuations in the strength function. We will consider the explanations of some of these features in the next section.

Similarly, p-wave maxima occur, as expected, when $(R_0/\lambda) = n\pi$, and with the above choices for V_0 and R_0, these occur at $A = 30$, 90, and 220. Recent data, reviewed by Newson (New 66), on p-wave resonances in low-energy neutron reactions show a maximum near $A = 90$.

3.3.2. *Doorway-State Interpretation of the Fluctuations in the Optical-Model Strength Function*

An interpretation of the anomalies of the neutron strength function in terms of doorway states was developed by Block and Feshbach (BF 63). Previously, Lane *et al.* (Lan+ 59) and Sugie (Sug 60) suggested that the anomalous dip at $A = 115$ is a consequence of the details of the shell structure and its effect on the imaginary part of the optical potential.

The Block–Feshbach description of these fluctuations evolved from remarks made by Weisskopf (Wei 61) about the importance of the first collision of an incident nucleon in a nucleus for the formation of the compound nucleus. The states reached in this first collision act as doorways into the compound nucleus. They couple the single-particle states to the compound nucleus and it is, thus, through these states that the compound nucleus is eventually reached through a series of scatterings. Therefore, Block and Feshbach have added another condition for the existence of a giant resonance, namely, that doorway states exist within their decay widths of the incident energy. Fluctuations in the strength function are then to be interpreted in terms of the number of such levels.

These authors write for the strength function, the equation

$$\left\langle \frac{\Gamma_\lambda}{D} \right\rangle \simeq \frac{4}{2\pi} \sum_d \frac{\Gamma_d^\uparrow}{\Gamma_d^\downarrow} \tag{69}$$

which is just Eq. (31) for $|E_\nu - E_d| \ll \Gamma_d^\downarrow$ and $V \gg D$. Here $\Gamma_d^\uparrow$ is the width for autoionization of the doorway and thus involves the coupling matrix element of the residual interaction V_r between the doorway state, a $2p$–$1h$ state in the shell model, and the continuum nucleon–target nucleus

state, a $1p$–$0h$ state in this model. Since the nucleon–nucleus wavefunction contains single-particle resonances this leads to a giant resonance behavior in $\langle \Gamma_\lambda/D \rangle$. Another feature contained in $\langle \Gamma_\lambda/D \rangle$ is the number of doorway states—the intermediate states which couple the single-particle scattering states to the compound nucleus. These states are classified by Block and Feshbach according to type arising from the properties of V_r. The V_r is next assumed to be a superposition of two-body potentials which are also assumed to be spin-independent. The potentials can then be expanded in purely spatial multipoles whose order is designated by l. Then, the expression for the strength function of Eq. (69) is decomposed into the various contributions of the different multipoles. For each l there will then be a number ν_l of doorways contributing. (Only those lying within $\Gamma_d^{\downarrow}$ of the energy are counted). The assumption is made that once the optical-model strength function $\langle \Gamma/D \rangle_{\text{opt}}$ is factored out and also the number of states ν_l of Eq. (69), the remainder is independent of the nucleus. Finally, only a minimal number of terms are kept in the multipole expansion and the expression

$$\left\langle \frac{\Gamma_\lambda}{D} \right\rangle \simeq (\nu_0 a^{(0)} + \nu_1 a^{(1)} + \nu_2 a^{(2)}) \left\langle \frac{\Gamma}{D} \right\rangle_{\text{opt}} \tag{70}$$

is written. The number ν_l was then counted for nuclei with A between 40 and 130, and the results are summarized in Table II. From this table we see a strong correlation between the number of doorways reached through the l'th multipole, the ν_l, and the properties of the strength function. In particular, we see that for A between 40 and 64 the $l = 0$ monopole is dominant for target neutron excitations. For A between 68 and 84, the table shows that there are many $l = 1$ and $l = 2$ excitations of target protons and target neutrons. Finally, at A from 88 to 130 only $l = 2$ transitions appear. Thus, the peak at $A = 50$ is correlated with the $l = 0$ monopole while the many large values of $\langle \Gamma_\lambda/D \rangle$ in the region between 70 to 88 are correlated with the large number of $l = 1$ and $l = 2$ transitions. Moreover, the dip from $A = 90$ to $A = 130$ is associated with the $l = 2$ multipole and suggests that $a^{(2)}$ is much less than $a^{(1)}$.

The parameters $a^{(0)}$, $a^{(1)}$, $a^{(2)}$, which are assumed independent of A, are determined empirically. The best fit was obtained for $a^{(0)} = 1.0$, $a^{(1)} = 0.15$, and $a^{(2)} = 0.05$, and $\Gamma^{\downarrow} = 2$ MeV. The results are shown by the open circles in Fig. 8. From this figure we see that the fluctuations in the number of doorways is strongly correlated with the fluctuations in the strength function. Also, the average behavior of $\langle \Gamma_\lambda/D \rangle$ is predicted.

TABLE II

Total Number of Proton and Neutron Target Excitations for Even–Even Nuclei

Target nucleus			Neutrons			Protons		
A	N	Z	$l=0$	$l=1$	$l=2$	$l=0$	$l=1$	$l=2$
40	20	20	1	0	0	0	0	0
44	24	20	1	0	0	0	0	0
50	26	24	1	0	0	0	0	0
54	28	26	1	0	0	0	0	0
54	30	24	1	3	0	0	0	0
58	30	28	1	1	0	0	0	0
60	32	28	1	0	0	0	0	0
64	36	28	1	0	0	0	0	0
68	38	30	1	4	5	0	4	5
70	40	30	1	5	4	0	2	6
74	42	32	1	6	3	0	5	5
78	44	34	1	5	3	0	6	4
80	44	36	1	8	5	0	12	9
84	48	36	1	8	5	0	13	4
88	50	38	0	0	2	0	0	5
90	50	40	0	0	2	0	0	7
94	54	40	0	0	6	0	0	4
98	56	42	0	0	3	0	0	4
100	56	44	0	0	4	0	0	4
104	60	44	0	0	8	0	0	7
108	62	46	0	0	7	0	0	9
110	62	48	0	0	7	0	0	8
114	66	48	0	0	2	0	0	4
118	68	50	0	0	0	0	0	3
120	70	50	0	0	3	0	0	3
130	76	54	0	0	3	0	0	1

3.4. Shell-Model Investigations of Doorway States

3.4.1. Widths and Spacings of Doorway States

The doorway-state concept will be a meaningful interpretation of intermediate structure if the total width of a doorway state, including its outward decay by particle emission and its downward decay into the compound nucleus, is smaller than the spacing of these states. Then, each

intermediate structure bump in the cross section can be interpreted in terms of a particular doorway state. Moreover, if the isolated doorway-state model applies, then the coupling matrix elements of a particular doorway state to various reaction channels will show a characteristic behavior which is determined by the structure of the doorway states. This will imply specific correlations in the excitation functions of various channels which are characteristic of the structure of the underlying state. If, on the other hand, doorway states overlap, then a bump in the cross section will result from the excitation of a group of doorway states, with no particular doorway state playing an essential role. Structure in the averaged cross section will result from statistical fluctuations in the density of doorway states and in the channel decay widths of these states (see Section 3.11). Furthermore, in the overlapping doorway case, there will be very little correlation in the excitation function of different channels (see Section 3.10).

The question of the magnitude of the widths of doorway states compared to their spacings was considered in detail by Payne (Pay 68) in the framework of the shell model. Only the case of simple $2p$–$1h$ states reached in a collision of an incident nucleon with a target nucleus, together taken as a $1p$–$0h$ state, was considered; the possibility of vibrational states as doorway states was not investigated. To illustrate Payne's calculation we consider a neutron incident on ^{40}Ca. The shell-model scheme for ^{40}Ca is illustrated in Fig. 9. We consider the type of $2p$–$1h$ states reached from an s-wave neutron. For example, the s-wave neutron can drop into a $2p_{3/2}$ bound orbital while exciting a $2s_{1/2}$ nucleon to the $2p_{3/2}$ level. Other transitions are also shown. In such transitions parity and angular momentum have to be conserved. To conserve energy the length of the downward arrow must equal the length of the upward arrow. This condition will approximately determine the resonance energy of the doorway state. Next, the particle emission width of the doorway state can be obtained by calculating the matrix elements of the residual interaction between the doorway state and the incident nucleon–target state. Finally, the $2p$–$1h$ state can decay into any surrounding $3p$–$2h$ state through one application of the two-body residual interaction.

Payne has performed the calculation outlined above for neutrons scattering off a series of target nuclei which include ^{28}Si, ^{32}S, ^{40}Ca, ^{54}Fe, ^{62}Ni, ^{92}Mo, ^{120}Sn, and ^{208}Pb. For the cases ^{28}Si, ^{32}S, ^{40}Ca, and ^{208}Pb, the density of more complicated configurations at low energies is small because of the large single-particle energy spacing, and therefore, $\Gamma_d^{\downarrow} \approx 0$. In these cases, the doorway states are the same as the compound states. For the remaining nuclei, ^{54}Fe, ^{62}Ni, ^{92}Mo, and ^{120}Sn, the density of more

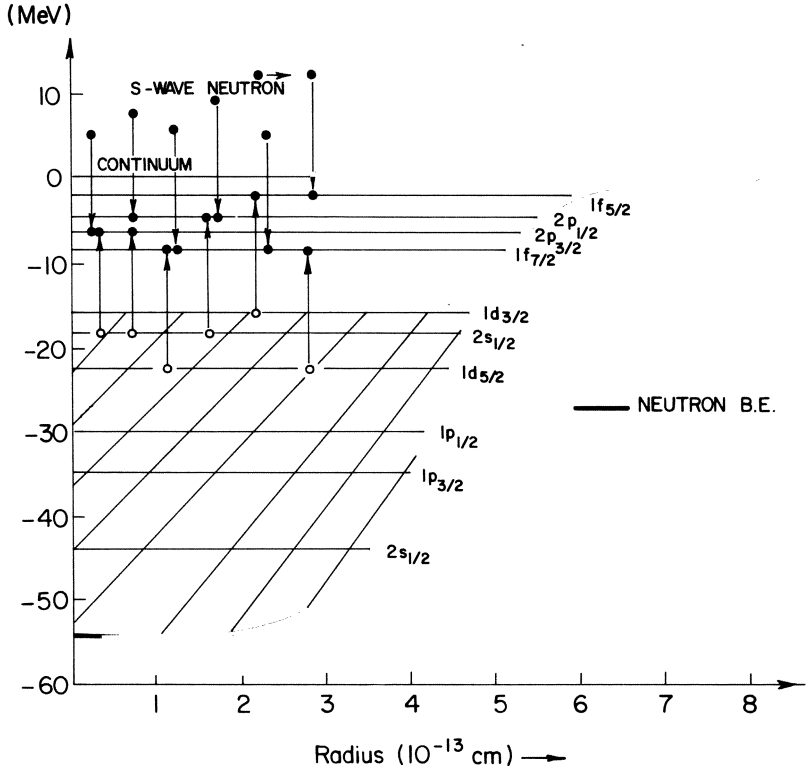

Fig. 9. Shell-model level scheme for ^{40}Ca and the type or $2p$-$1h$ states reached from an s-wave neutron.

complicated configurations is large and $\Gamma_d^{\downarrow} \gg \Gamma_d^{\uparrow}$. An exception occurs at ^{54}Fe for incident neutron energies 3 MeV for which $\Gamma_d^{\downarrow} \simeq \Gamma_d^{\uparrow}$.

Similar results on the number of $3p$–$2h$ states were obtained by Lande and Block (LB 64) who investigate even–even nuclei in the range $16 \leq A \leq 146$. They also found that, except for a few cases, these states do not exist at low energies for $A < 50$, while for $A > 60$ they are abundant. Also noted by them was the pronounced effect shell closing has on the density of these states.

The calculation (Pay 68) of the widths of the various possible doorway states was done using a δ-function two-body potential of the form used by Lemmer and Shakin (LS 64) in their calculation of widths for neutron emission from ^{16}N*:

$$v(\vec{r}_1 - \vec{r}_2) = -V_\delta[\pi_t + p\pi_s]\delta(\vec{r}_1 - \vec{r}_2) \tag{71}$$

The π_t and π_s are the triplet- and singlet-spin projection operators, respectively, and V_δ is chosen to give the correct pairing energy, while p is set equal to unity in this calculation. The emission widths of the two-particle–one hole states are found to vary from zero to several hundred keV. Since a delta-function force is used, a number of widths will turn out to be identically zero. This situation occurs when the space part of the wave function of the two nucleons involved in the transition is antisymmetric, i.e., two neutrons in a triplet spin state. For a two-body interaction of finite range, these matrix elements should be small. Thus, for those nuclei with $\Gamma_d^{\downarrow} \approx 0$ additional structure can arise from couplings to $2p$–$1h$ states with narrow widths. However, this substructure is not of the usual type described in doorway-state effects in which the doorway state spreads its strength over more complicated states to form a "microgiant" resonance (BS 64). As an example, the results of Paynes' calculation for the location and width of the different possible doorways in ^{40}Ca is shown in the Fig. 10. Also shown in this figure is an evaluation of the resonant cross section generated by these doorway states. From the figure we note that at low energies (below 3 MeV) the peaks in the cross section are correlated with individual $2p$–$1h$ states, while at higher energies peaks in the cross section arise from statistical effects, generated by fluctuations in widths and spacings of overlapping doorways. Based on the above nuclei, Payne concludes the following:

1. Not all $2p$–$1h$ states have appreciable width to the continuum. Consequently, in looking for doorway-state effects, a simple counting of the number of $2p$–$1h$ states is not complete and a calculation of the widths of these states must be done.
2. In light and doubly magic nuclei, the density of $3p$–$2h$ states is small at low energies (incident neutron energies 3 MeV) so that $\Gamma_d^{\downarrow}$ can be neglected compared to $\Gamma_d^{\uparrow}$. In this region, the isolated doorway condition, $\Gamma_d < D$, can be fulfilled and isolated resonances of intermediate width should be seen. Fine structure, if it is seen, will be due to $2p$–$1h$ states which are weakly coupled to the continuum.
3. For light nuclei at higher energies, the density of $2p$–$1h$ states is large so that the isolated doorway condition breaks down. Structure in the cross section is then produced by fluctuations in level width and level density.
4. For heavy nuclei ($A > 60$) with the exception of doubly magic ^{208}Pb, the density of $3p$–$2h$ states is large so that Γ_d is larger than the spacing of doorway states even at low energies. No isolated doorway effects should be seen at any energy.

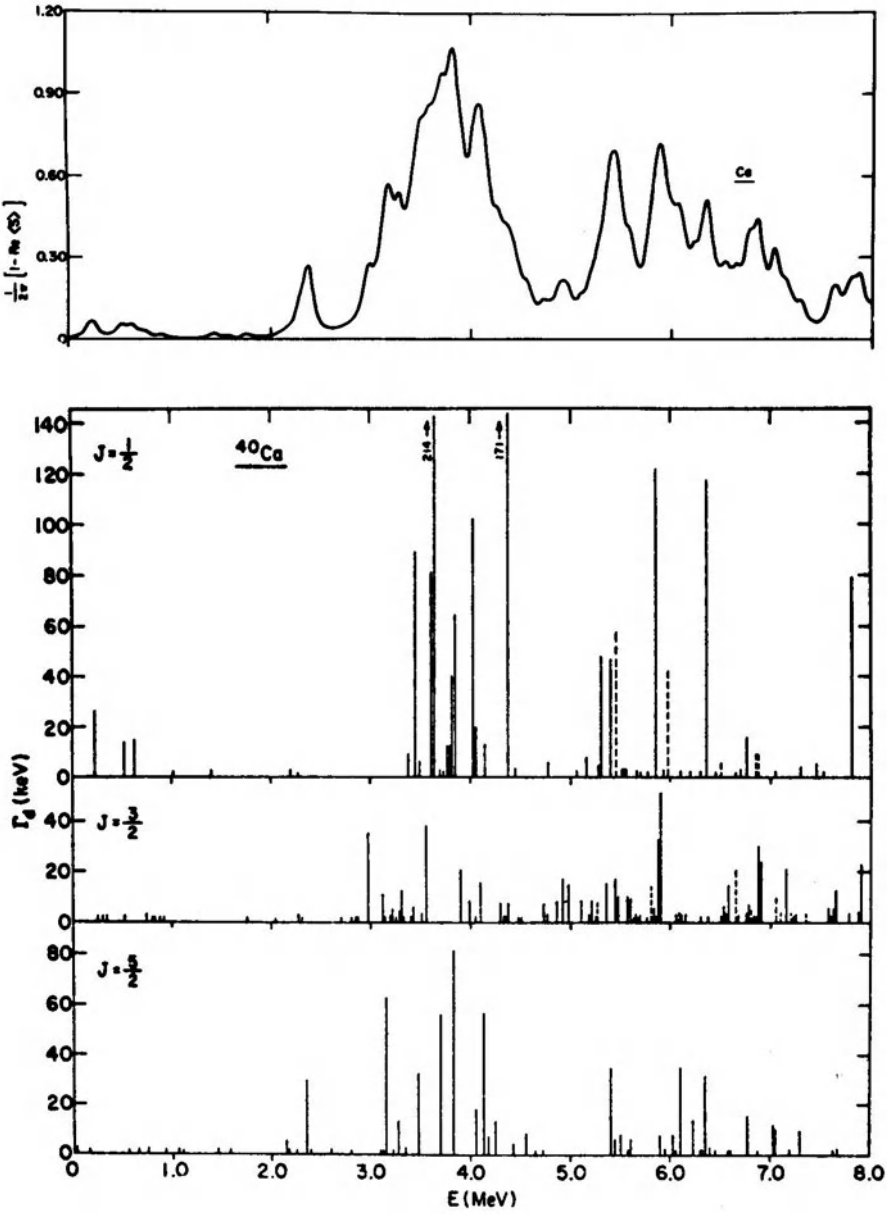

Fig. 10. Doorway-state energies and widths for ^{40}Ca and the corresponding cross section generated by these doorway states. After Payne (Pay 68).

5. For nuclei near ^{54}Fe and at low incident neutron energies $\Gamma_d^{\uparrow} \approx \Gamma_d^{\downarrow}$. In this region states with an average width of 75 keV and an average spacing of 130 keV were found. Thus, isolated doorway-state effects with fine structure due to more complicated states should be observable.

3.4.2. Situations in Which the First Excitation Is the Only Excitation

For the situation in which there are no states of higher complexity than those reached in the first collision, the simple states will be the compound nuclear states themselves. If we discuss the simple states in terms of the shell model, then these states are shell-model states of low particle–hole complexity. Such states, if above particle emission thresholds, will produce resonances in the cross section; but the resonances will lack fine-structure because of the absence of more complex states. Any structure, if it is present, will arise from other simple states which originally are weakly coupled to the continuum, and become enhanced by coupling to states strongly coupled to this continuum.

In the situation described above, a traditional shell-model diagonalization of the energy is performed on a restricted basis to locate the position and structure of the resulting states. Once this is done, an additional quantity is calculated, namely, the escape widths of these states. The cross section can also be calculated within the framework of some reaction theory. Calculations in this "extended" shell model have been performed by several groups, a discussion of which can be found in a review by Mahaux and Weidenmuller (MW 69).

3.5. Vibrations as Doorway States

3.5.1. Particle-Coupled-to-Vibration as a Doorway State

The picture of Kerman, Rodberg, and Young (KRY 68) and the calculations of Payne (Pay 68) and Block and Lande (BL 64) are concerned with $2p$–$1h$ states as doorway states. A picture stressed by Lande and Brown (LB 66, Lan 68) is the coupling of the incident nucleon to the vibrational states of the target core. We illustrate the two types of pictures in Fig. 11. In Fig. 11a, the incident nucleon excites a particle–hole pair which then decays into the original state. Figure 11b illustrates the particle–hole pair rescattering into another particle–hole excitation so that the incident nucleon is connected to a coherent sum of particle–hole excitations. As is

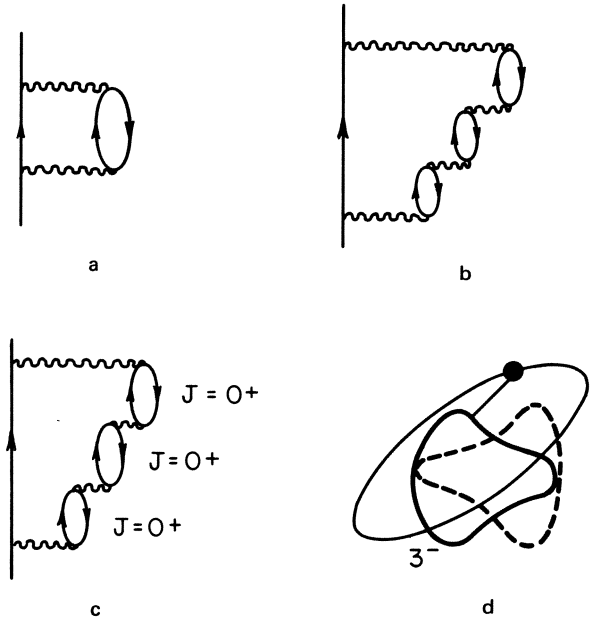

Fig. 11. Vibration as doorway states. In Fig. 11a, a simple $2p$-$1h$ state is generated; Fig. 11b shows the incident nucleon connected to a coherent sum of particle–hole excitations, while Fig. 11c illustrates the situation generated in isobaric analog resonances. In Fig. 11d, the incident nucleon is coupled to a 3^- surface vibration.

well known from dipole studies (BB 59, Bro 64), the rescattering produces large shifts in energies and leads to readjustments in strength distributions through coherences built up by the particle–hole interaction. In particular, the coherent state undergoes the largest shift and contains the total dipole strength.

This rescattering occurs because the particle–hole excitations are not the normal modes of the system. Rather, the coherent superposition together with the remaining incoherent mixtures act as normal modes. Such a coherent superposition is referred to as a vibration. Among the normal modes, the incident particle couples most strongly with it.

Thus, the Brown–Lande picture stresses the structure of doorway states as being an incident particle coupled to the vibrational states of target such as a 2^+ quadrupole vibration or a 3^- octupole vibration. The single-particle strength is then mainly split up among such vibrations, which in turn spread into the incoherent particle–hole excitations. For example, the best, although trivial, cases of intermediate structure are the

isobaric analog resonances (discussed in Section 3.6) which are monopole vibrations of the core as illustrated in Fig. 11c. Alternately, instead of discussing the vibration in terms of coherent states produced by the rescatterings, we can discuss it in terms of the oscillations of the deformation parameters $\alpha_{\lambda\mu}$ which appear in the expansion of the nuclear surface $R(\theta, \phi)$:

$$R(\theta, \phi) = R_0\left[1 + \sum_{\lambda=0}^{\infty} \sum_{\mu=-\lambda}^{1} \alpha_{\lambda\mu} y_\lambda{}^\mu(\theta, \phi)\right] \tag{72}$$

Moreover, the $\alpha_{\lambda\mu}$'s of this equation can be thought of as generalized coordinates, and for small deformations, the Hamiltonian associated with these coordinates is of the harmonic oscillator form. The eigenstates of this Hamiltonian can then be classified according to their phonon number. Figure 11d shows the incident nucleon coupled to a 3^- vibration of the target.

Brown and Lande examined the splitting of the single neutron strength in ^{59}Ni through the coupling of the incident neutron to 2^+ and 3^- phonons. They found approximately the same number of states per MeV with appreciable single-particle strength as found in the experiments of Fulmer *et al.* (Ful+ 64). However, because of the crudeness of the model, detailed agreement between the theoretical and experimental distribution of strength, as measured by the spectroscopic factors for ^{58}Ni$(d, p)^{59}$Ni stripping, was poor.

3.5.2. Vibrational Identification of the Doorway State Seen in Pb

Beres and Divadeenam (BD 70) have considered the particle-coupled-to-vibration picture in their investigation of the doorway states seen in the scattering of neutrons on ^{206}Pb and ^{208}Pb (Far+ 65). The high-resolution elastic scattering of neutrons from ^{206,207,208}Pb observed at Duke University shows the presence of a $\frac{1}{2}^+$ doorway state in the even isotopes. Specifically, the ^{209}Pb compound system gives rise to a single $\frac{1}{2}^+$ resonance at 500 keV with a neutron width of 58 keV. Moreover, the ^{207}Pb and ^{208}Pb compound systems show fine structure in the same region, with the ^{206}Pb$(n, n)^{206}$Pb excitation function having eleven $\frac{1}{2}^+$ resonances participating in an enhancement. The sum of the widths of these resonances is 60 keV while the centroid of the enhancement is at 470 keV and has a width $\Gamma_d^{\downarrow} \approx 190$ keV. The average spacing of the fine structure is 40 keV (LM 67).

With no free parameters in their calculation, Beres and Divadeenam show that the particle–vibration model accounts for the $\frac{1}{2}^+$ doorway state in ^{209}Pb. In particular, they find that the natural decay width and position of this resonance is accounted for by the presence of a doorway state with the

structure of a $2g_{9/2}$ neutron level coupled with the 4^+ vibration state at 4.31 MeV in ^{208}Pb (Sau+ 66). Moreover, Divadeenam and Beres (DB 72) have considered the extension of the particle-coupled-to-vibration model to all $\frac{1}{2}^+$ states in ^{209}Pb and ^{207}Pb. The particle–vibration states included are $4^+ \otimes 2g_{9/2}$, $6^+ \otimes 1i_{11/2}$, $2^+ \otimes 3d_{3/2}$, and $4^+ \otimes 2g_{7/2}$. The theoretical predictions of the natural decay widths and energies are found to be in very good agreement with the experimental results.

We end this section by noting that with an assumed configuration for a particular doorway state, the coupling matrix elements of this state to various channels can be calculated. The various calculated branching ratios can then be compared with the experimental results. If the structure of the doorway states is properly identified, the matrix elements of the doorway state to the various channels will show the same characteristic behavior as the experimental branching ratios. Thus, as a further check on an identification of a doorway, a comparison should also be made of such ratios.

3.6. Doorway States and Isobaric Analog Resonances

3.6.1. Isobaric Analog States as Doorway States

The cleanest and clearest example of intermediate structure in the energy dependence of the cross section is offered by the isobaric analog resonances. These resonances are observed in the elastic scattering of protons off neutron-rich targets. The states associated with such resonances are obtained from parent states in the neighboring isobar by application to them of the total isospin lower operator. Therefore, these states have the spin, parity, and isospin quantum number of the parent state. Moreover, isobaric analog resonances have isospin one unit higher than the compound nuclear states which surround them, which have the normal isospin $T = T_3$. Isobaric spin effects will prevent the decay width of the analog states into the compound nucleus from becoming very large. The total width of isobaric analog resonances range from several keV to several hundred keV, while the resonance energies of such states are Coulomb-shifted from the location of the parent configuration. The elastic proton decay width of an analog state is $(2T + 1)^{-1}$ times a single proton width. The spreading width or decay width of it into the compound nucleus is also much smaller (several hundred times smaller) than the spreading width of a single-proton state because analog states mix with the background only through the T-violating parts of the Hamiltonian, and in particular, through the Coulomb force. Even though the Coulomb force produces

large shifts in energy levels, its long-range character produces very little mixing, (because the mean square deviation of the Coulomb potential is much smaller than its average value) and therefore very little spreading. A second reduction arises from the neutron excess present in heavy nuclei which has pure isospin, thereby diluting any isospin impurities and reducing any mixings to states of different isospin.

Of the many analog resonances seen (FR 63, And+ 69, Wil 69), we will consider the one investigated in an experiment performed at Duke University (Key+ 66a, Key+ 66b) which involves scattering protons off Ar^{40}. The high-resolution nature of the experiment enables one to see

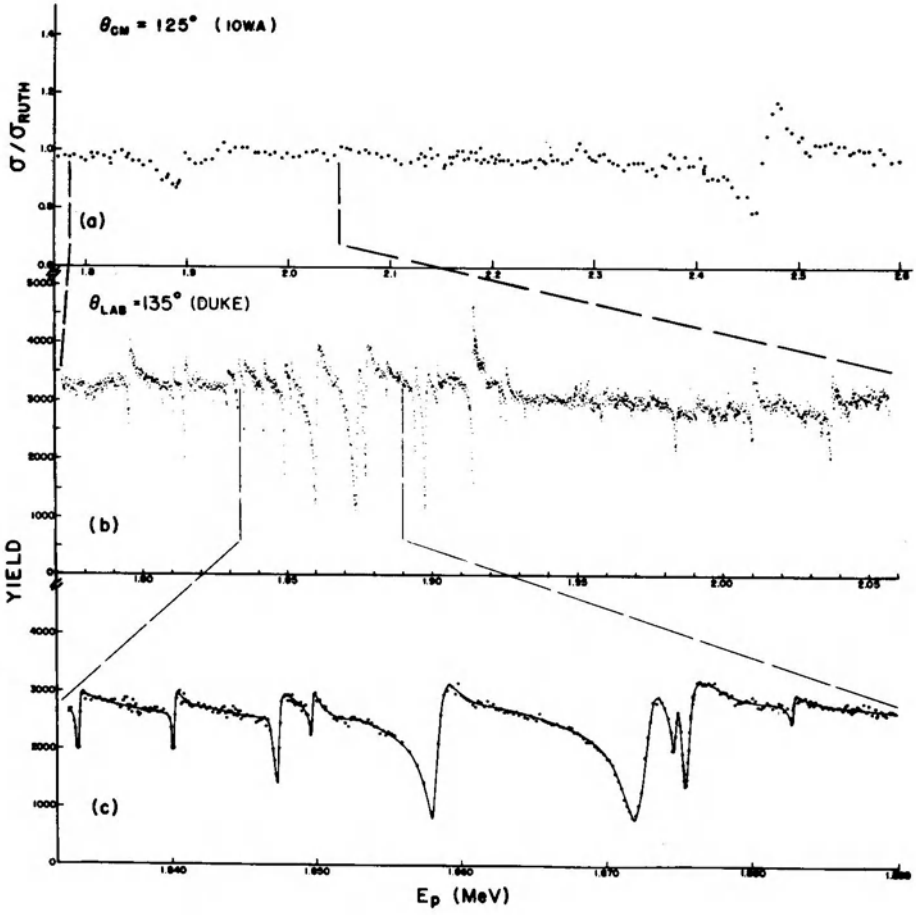

Fig. 12. High-resolution elastic proton yield from $^{40}Ar(p, p)^{40}Ar$. After Keyworth *et al.* (Key+ 66a).

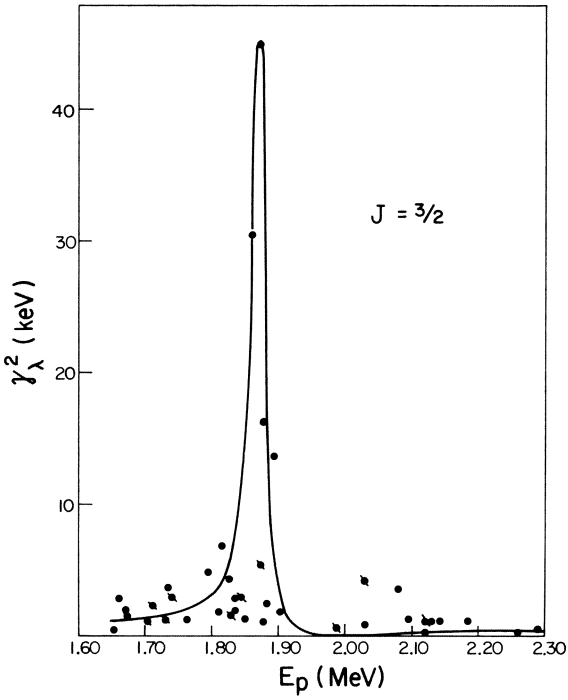

Fig. 13. Distribution of widths of the resonances seen in ^{40}Ar(p, p)^{40}Ar. After Mekjian and MacDonald (MM 67).

narrow resonances or fine structure in the cross section. The energy dependence in the elastic cross section is shown in Fig. 12. We note the following features in this energy dependence. First, the anomaly at 1.87 MeV shows pronounced structure. This structure is associated with the presence of the isobaric analog of the fourth excited state of Ar^{41}, with $J^\pi = \frac{3}{2}^-$, seen in (d, p) experiments (KHB 61). Secondly, away from the 1.87-MeV region, fine structure in the energy dependence of the cross section is seen. This fine structure is associated with the complicated states of the compound nucleus.

Each resonance in the cross section shown in Fig. 12 has associated with it a spin, parity, energy, and width. If the width of each $\frac{3}{2}^-$ resonance is plotted against the location at which it appears in the spectrum of K^{41}, a distribution of widths (MM 67) is obtained which is illustrated in Fig. 13. Now, the resulting distribution has itself several interesting features which are associated with three different regions. The three regions are separated according to their location with respect to the centroid E_a of the distribution.

They are (1) the near region— $|E - E_a| < 20$ keV, (2) the far region— $|E - E_a| > 200$ keV, and (3) the intermediate region—20 keV $< |E - E_a| < 200$ keV. In the near region, the widths have a characteristic enhancement. This enhancement is due to the presence of an analog state which acts a doorway state and couples the compound nucleus to the continuum. Since the amplitude of the analog state in the compound nuclear state is appreciable near the position of the analog state, the width of the compound nuclear state becomes greatly magnified. Specifically, the width near the center of the distribution is given by Eq. (31) and is

$$\Gamma_{\nu,p} = \Gamma_{a,p}^{\uparrow} \frac{(D/2\pi)\Gamma_{a,f}^{\downarrow}}{(E_a - E_\nu)^2 + (\Gamma_a^{\downarrow}/2)^2} \tag{73}$$

The values of the parameters are $D = 10$ keV, $\Gamma_{a,p}^{\uparrow} = 5$ keV, and $\Gamma_{a,f} = \Gamma_a^{\downarrow} = 20$ keV for this experiment. For $E_\nu - E_a = 0$, $\Gamma_{\nu,p}^{\uparrow}/\Gamma_{a,p}^{\uparrow} = \frac{1}{4}$, so that the state with the largest amount of analog component contains 25% of this state.

In the far region, narrow resonances with widths $\Gamma \simeq 15$ eV or about 1/2000 of a single particle width are seen. In this region, the presence of the analog state is not felt, so that the widths $\Gamma_{\nu,p}$ are just those characteristic of the compound nucleus in the absence of the analog state: $\Gamma_{\nu,p} = \Gamma_{f,p}$.

Finally, in the intermediate region, the original width of the complicated states and the width acquired by coupling to the analog state are comparable, so that

$$\Gamma_{\nu,p} = \left[\Gamma_{f,p}^{1/2} + \frac{V_{fa}}{E_\nu - E_a}(\Gamma_{a,p}^{\uparrow})^{1/2}\right]^2 \tag{74}$$

The V_{fa} is the coupling matrix element between the complicated state and the analog state. That we must add the amplitudes and square to obtain $\Gamma_{\nu,p}$ arises from the fact that both methods of decay, either directly or through the analog state, are available and cannot be distinguished. We illustrate the appropriate coupling schemes for the three regions in Fig. 14a.

An interesting feature of the intermediate region is the appearance of a minimum in the distribution of widths shown in Fig. 12. We note that the distribution of widths is slightly asymmetric about the centroid with the widths on the low-energy side of the centroid larger than the corresponding widths on the high-energy side. This minimum was first discussed by Robson (Rob 65) and has since been dealt with by several others (FF 65, MM 67, MM 68, TK 67, TK 68, Mel 67, MW 67, Lan 70). Returning to Eq. (75) we note that if $(\Gamma_{f,p})^{1/2}$ and V_{fa} are uncorrelated from one complicated state to the next, the distribution of $\Gamma_{\nu,p}$ will be quite random. On the high-

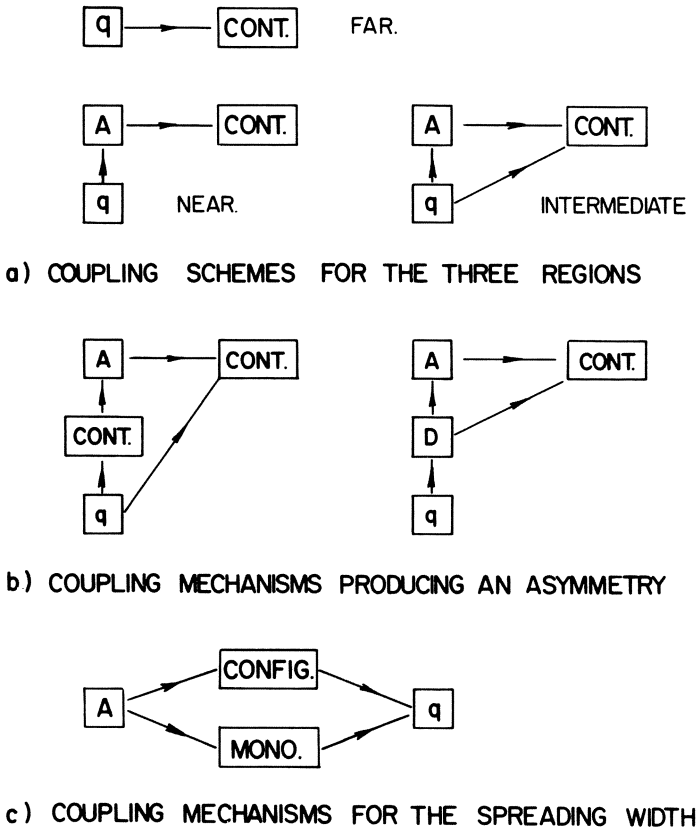

Fig. 14. Schematic illustration of the coupling mechanisms. Figures 14b,c are discussed in Section 3.6.2.

and low-energy side of the analog state, there will be as many terms in which $(\Gamma_{f,p})^{1/2}$ and $V_{fa}(\Gamma^{\uparrow}_{a,p})^{1/2}/(E_\nu - E_a)$ interfer constructively as destructively. At the other extreme is the possibility of a strong correlation between $(\Gamma_{f,p})^{1/2}$ and V_{fa}; that is, the possibility that the sign of the ratio $(\Gamma_{f,p})^{1/2}/M_{fa}$ is independent of f. If a strong correlation is present, the only change in sign over the distribution of widths between the first and second term of Eq. (75) occurs in the energy denominator $E_\nu - E_a$ when E_ν passes by the analog energy E_a. In this case the distribution of widths will be enhanced on one side of the analog state and suppressed on the other side.

Before discussing mechanisms for a possible explanation of the minimum, we note that a single expression for the averaged distribution of widths in the three regions which contains the characteristic features of

each region can be written (MM 68, Lan 70):

$$\pi \frac{\Gamma_{\nu,c}}{D} = \pi \frac{\Gamma_{f,c}}{D} \frac{(E - E_a + \Delta_{s,c})^2 + W_c^2}{(E - E_a)^2 + (\frac{1}{2}\Gamma_a^{\downarrow})^2} \tag{75}$$

In this expression c is the channel index, the energy shift $\Delta_{s,c}$ gives the position of the minimum while W_c^2 determines the depth of the minimum. For large E, the averaged distribution is simply the averaged distribution of the $\Gamma_{f,c}$'s. At $E = E_a$, the enhancement of the fine structure is

$$\frac{\Gamma_{\nu,c}/D}{\Gamma_{f,c}/D} = \frac{\Delta_{s,c}^2 + W_c^2}{(\Gamma_a^{\downarrow}/2)^2} \tag{76}$$

For the above experimental results, this ratio is of the order of 100.

3.6.2. The Effect of Nuclear Doorway States on the Distribution of Fine-Structure Widths

There are two situations in which an asymmetric fine-structure distribution with a complete suppression ($W_c^2 = 0$) will be observed. The first situation arises when the coupling between the analog state and the compound nuclear states is through one continuum channel (Rob 65). That is, since both states are coupled to the continuum, they are coupled to each other by the process of emission of a particle from one state and the subsequent absorption of the particle in the other state. Since these decay and absorption amplitudes are related to the widths of the states, the coupling matrix is then proportional to the geometric means of the decay probabilities of the two states: $V_{fa} = \lambda \Gamma_{f,c}^{1/2} (\Gamma_{a,c}^{\uparrow})^{1/2}$. From this expression we see that the decay amplitudes through direct decay $\Gamma_{f,c}^{1/2}$ and through analog-state decay $V_{fa}(\Gamma_{a,p}^{\uparrow})^{1/2}/(E_\nu - E_a)$ are correlated if $c = p$. This one-channel model has been criticized by Lane (Lan 70).

The second situation (FF 65, MM 68) in which the fine structure will show an asymmetry with a full suppression is that in which a single nuclear doorway (same isospin as the compound nuclear states) couples the compound nuclear states to the analog state and to the channels. This second doorway can be coupled either directly or through the continuum to the analog. The latter coupling has been discussed by Fallieros and Ferrell (FF 65). The correlation mechanisms are illustrated in Fig. 14b.

Next, let us consider the spreading width of an analog state (LS 62a, LS 62b, Tol+ 66, Wig 63, Mek 70). An interesting phenomenon becomes quite evident if we plot the spreading widths of analog states as a function

TABLE III

Experimental Values of the Spreading Width $\Gamma_A{}^{\downarrow}$

Analog	lJ^{π}	$\Gamma_A{}^{\downarrow}$(keV)	Reference
^{37}Cl + p	1 3^-	<50	(BV 66)
^{40}A + p	1 $3/2^-$	20	(Key+ 66b)
^{42}Ca + p	1 $1/2^-$	7	(Bro+ 68)
^{44}Ca + p	1 $3/2^-$	8	(Bro+ 68)
^{48}Ca + p	1 $3/2^-$	2	(Wil+ 69)
^{50}Ti + p	1 $1/2^-$	12	(GKN 68)
^{51}V + p	1	<14	(TF 66)
^{62}Ni + p	1 $3/2^-$	~10	(Bro+ 69)
^{64}Ni + p	1 $3/2^-$	~15	(Bro+ 69)
^{70}Zn + p		<20	(Mor 67a)
^{90}Zr + p	0 $1/2^+$	37	(Rob+ 65)
^{92}Mo + p	0 $1/2^+$	29	(Ric+ 64)
^{138}Ba + p	3 $7/2^-$	<40	(Wil+ 70)
^{207}Pb + p	1 0^+	<80	(LT 68)

of A, the mass number (Me 70). In particular, in Table III, the experimentally determined spreading widths of various analog states are listed. From this table we note that the spreading width decreases from Cl → Ar → Ca targets and then increases again. Thus, the spreading width as a function of mass number has a minimum in the calcium isotopes. A possible explanation of this minimum has been given by Mekjian (Me 70), which we briefly summarize. An evaluation of the sum of the squares of the off-diagonal Coulomb-coupling matrix elements shows the importance of the mixing of the analog state into two types of states. These states are the configuration states of Lane and Soper (LS 62a, LS 62b) with the same space configuration as the analog state (they are obtained from the same basis of particle–hole states as the analog state but have $T = T_3$) and a giant monopole vibration off the analog state. The latter state lies above the analog state and the former below it. Since the configuration and monopole states have normal isospin, they couple to other states of normal isospin by the nuclear force. Consequently, these states mix with the dense spectrum of such states near the analog, and it is just this latter damping which is believed to be responsible for the damping of the analog state. The

direct coupling of the analog to the surrounding normal isospin states ($T = T_3$) is small because of the complexity of these states. We illustrate the overall coupling mechanism in Fig. 14c and note that the configuration states and monopole vibration act as intermediate states coupling the analog state to the dense spectrum of compound nuclear states which surround it. If we next assume a giant resonance model type of mixing for the nuclear coupling, then the analog state lies between two peaks in the distribution of Coulomb mixing strength. Furthermore, it can be shown that the analog state moves from the lower peak to the upper peak with increasing A and $T_3 = (N - Z)/2$ due to symmetry forces. It is then this motion between the two peaks which gives the minimum in the spreading width.

3.6.3. Structure Seen within an Isobaric Analog Resonance

We end our discussion of isobaric analog states by noting an interesting result borne out by an experiment done at Rutgers University. Temmer *et al.* (Tem+ 71) report the appearance of significant substructure contained within a $J = \frac{1}{2}^+$ analog resonance in ^{71}As observed in elastic and inelastic scattering of protons on ^{70}Ge. We illustrate the experimental results in Fig. 15. From this figure we see that the width of the analog anomaly is about 63 keV, while substructure exists with widths of about 20 keV. The

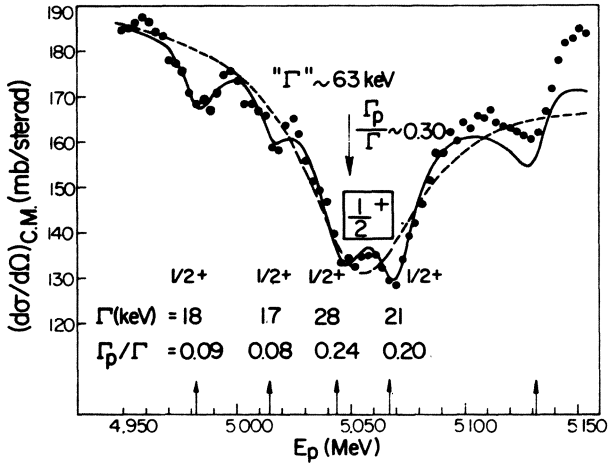

Fig. 15. Elastic-scattering excitation yield at $\theta_{lab} = 90°$ in ^{70}Ge(p, p)^{70}Ge. Dashed curve represents a fit with a single resonance, with parameters shown in figure and position indicated by downward-pointing arrow. Solid curve represents fit with four $l = 0$ resonances, the parameters and positions of which are shown in the bottom of the figure. From Temmer *et al.* (Tem+ 71).

ultimate fine structure of $J = \frac{1}{2}^+$ states is estimated to have a level spacing of one state per 300 eV and a level width of about 20 eV. From these results we can conclude that the substructure encompasses about 70 individual fine-structure states. It is then argued by these authors that the substructures do not arise from Ericson fluctuation because (a) $\Gamma \ll D$ for the fine structures; (b) the structure is correlated at several angles; (c) the structures have specific $L = 0$ signatures; and (d) the structures are correlated in several channels.

The experiment shows the existence of some form of substructure lying between the ultimate fine structure and the intermediate structure of the analog. A theoretical explanation of the substructure has not yet been given.

3.7. Electromagnetic Interactions and Intermediate Structure

3.7.1. Structure within Giant Dipole Excitations

The systematic features of dipole resonances, which occur in all nuclei and therefore constitute a general property of nuclei, are by now well known and discussed in detail in the reviews of Levinger (Lev 60), Brenig (Bre 65), Danos and Fuller (DF 65), and Spicer (Spi 69). The broad peak which appears in the γ-ray cross sections of nuclei occurs at an excitation energy which ranges from 25 MeV in light nuclei to 13 MeV in heavy nuclei. The width of the peak varies between 3 and 8 MeV, and is smallest for closed-shell nuclei. This width is partly due to nucleon emission or natural decay and partly due to the mixing of dipole state with more complicated states. In light nuclei the natural decay width and the spreading width, arising from the mixing to more complicated configurations, are comparable. In heavy nuclei, the spreading width account for most of the total width.

In high-resolution measurements, the photonuclear cross section shows considerable structure for light nuclei. As an example, the $^{27}Al(p, \gamma_0)^{28}Si$ measurement of Allas *et al.* (All+ 64, Sin 65) is shown in Fig. 16. The position of the giant dipole resonance in ^{28}Si is at an excitation energy of 20 MeV which corresponds to an energy of about 9 MeV in the $^{27}Al(p, \gamma)^{28}Si$. The peaks in the yield curve are about 50 keV wide and spaced approximately 100 keV apart. As the resolution is decreased, the corresponding cross section, also illustrated in the figure, shows structure of width intermediate between that of the fine structure (50 keV wide) and the gross structure (4 MeV wide). In particular, four peaks of intermediate width are seen. Moreover, the intermediate cross section is correlated with the $^{28}Si(\gamma, n)$ results of Caldwell *et al.* (Cal+ 63) which also show four peaks.

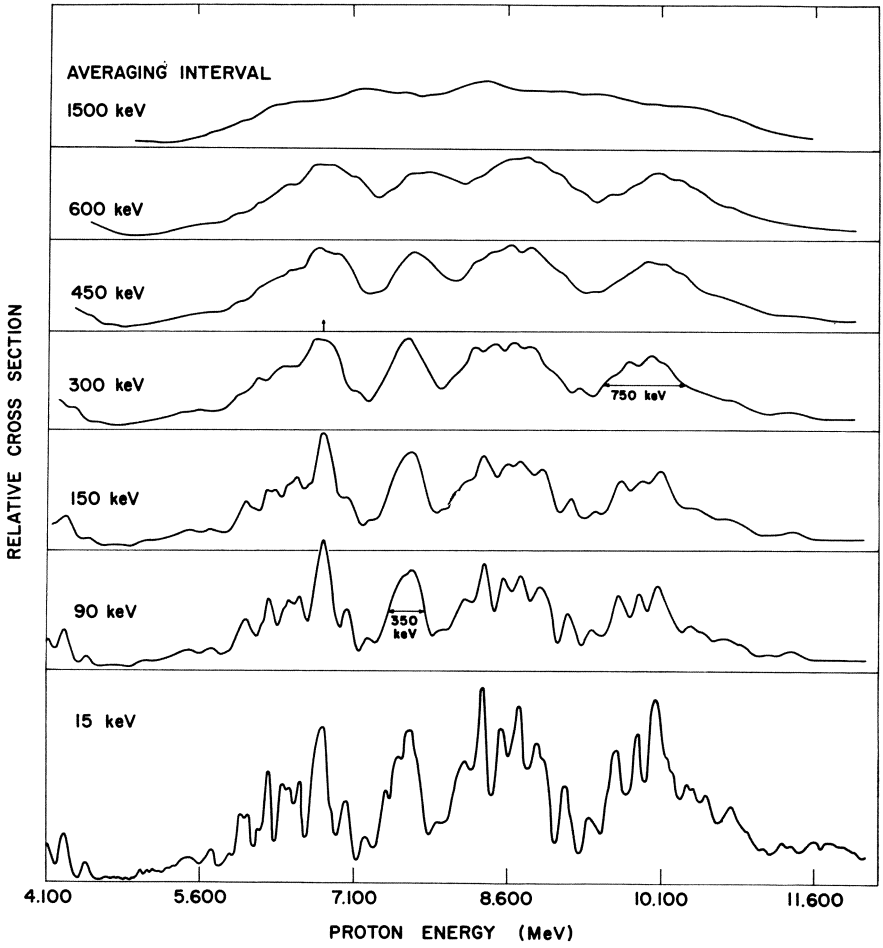

Fig. 16. The yield curve of $^{27}Al(p,\gamma_0)^{28}Si$ for various averaging intervals. From Allas *et al.* (All+ 64).

An unexpected feature of the proton-capture cross section in ^{27}Al is the invariance of the angular distribution of the outgoing photon throughout the energy region investigated. This invariance has been interpreted by Ferrell and MacDonald (FM 66) in terms of the doorway-state picture. Specifically, they suggest that the invariance in the yield is a consequence of the existence of a single doorway state which couples to the outside world other particle–hole states weakly coupled to the continuum and more complicated states which have no such direct coupling. The violent fluctuations or fine structure arise from the latter states, while the angular dis-

tribution is determined solely by the doorway state since this state completely determines the coupling to the outside world.

Similar structure is also seen in the proton capture reaction $^{19}F(p, \gamma)^{20}Ne$ reported by Segel *et al.* (Seg+ 67). The structure is correlated with the structure seen in the elastic neutron cross section $^{19}F(n, n)^{19}F$ (Elw+ 65) and with the structure in the giant photoresonance reaction $^{20}Ne(\gamma, n)^{19}Ne$ (Cal+ 63).

The giant dipole phenomenon has been interpreted in terms of a collective vibration of protons against neutrons by Goldhaber and Teller (GT 48), and in terms of the shell model. The earlier attempts at a shell-model description tried to account for the gross features of the dipole resonance in terms of $1p$–$1h$ excitations. Recently, more complicated configurations have been included in the calculations for light nuclei. For example, Gillet, Melkanoff, and Raynal (GMR 67) have suggested that the fine structure in the ^{16}O giant dipole resonance arises from coupling to many-particle–many-hole states. They show that the splitting of the 22-MeV peak of the ^{16}O giant dipole resonance can arise from the presence of a low-lying coherent $2p$–$2h$ state. However, unlike the splitting at 22 MeV, the $2p$–$2h$ mechanism could not account for the strong splitting of the 25-MeV peak. It was then suggested that $3p$–$3h$ and $4p$–$4h$ configurations should be present in the region of the giant dipole resonance and certain effects arising from them should be present. Along similar lines, Shakin and Wang (SW 71) have shown that the intermediate structure in the ^{16}O giant dipole could be accounted for by $3p$–$3h$ states. They obtain an impressive fit to the total cross section $^{16}O(\gamma, n)^{15}O$ in both magnitude and location of the structure using the interacting-boson approximation of Feshbach and Iachello (Fes 71).

For heavy nuclei, the damping width of the dipole state was first considered by Danos and Greiner (DG 65). This damping, in the first approximation, results from the scattering of the $1p$–$1h$ state into a $2p$–$2h$ states near the energy of the dipole state. Since the dipole is a coherent state it undergoes a large shift and ends at an energy where the density of $2p$–$2h$ states is large. For $A = 200$, there are several hundred such $2p$–$2h$ states near the dipole energy. The damping width of the dipole is given by the expression

$$\Gamma^{\downarrow}_{\text{dipole}} = 2\pi\overline{\langle 2p\text{–}2h \mid V \mid 1p\text{–}1h\rangle^2}\varrho_{2p-2h}(E_d) \tag{77}$$

For a delta-range interaction of strength V_0, the average squared matrix element was found to be $(V_0/4\pi R^3)^2 \times 0.085$. The value obtained for $\Gamma^{\downarrow}_{\text{dipole}}$ is $0.5\ \text{MeV} \leq \Gamma^{\downarrow}_{\text{dipole}} \leq 2.5\ \text{MeV}$ for $A = 200$. The uncertainty in the

damping width arises mostly from the uncertainty in the strength of the interaction. Along similar lines, Davidson (Dav 72) has recently calculated the spreading width of a 1^- state in ^{208}Pb and a 1^+ state in ^{208}Bi.

Finally, Bertsch (Ber 71) has discussed the connection between the spreading width of the giant dipole and that of a single particle. Even though the dipole state is described by a particle–hole wave function, the spreading width of this state is not the spreading width of the separate particle and hole components because of the coherence in the particle–hole components. That is, the spreading width of a coherent linear superposition of states may be different from the average spreading width of the separate states. This is a well-known phenomenon in the theory of the plasmon damping in an electron gas (Pin 63, Dub 59). For the dipole state, Bertsch finds $\Gamma^{\downarrow}_{\text{dipole}} = \frac{4}{9}\Gamma^{\downarrow}_{\text{single-particle}}$ for a Serber mixture. Dover, Hahne, and Lemmer (DHL 72), making a different set of assumptions than Bertsch, express the damping width of the dipole in terms of the damping widths of the particles and holes.

3.7.2. Structure in Photonuclear Reactions and in Radiative Capture

Local concentrations of γ-strength in the photoexcitation of levels in Fe and Pb near the neutron threshold energy has been reported by Bowman *et al.* (BBB 71). In the ^{207}Pb$(\gamma, n)^{206}$Pb reaction, they find an envelope of $E1$-radiation at the same position that an envelope exists for the $J^\pi = \frac{1}{2}^+$ levels excited in the reaction ^{206}Pb$(n, n)^{206}$Pb. However, Allen *et al.* (All+ 72) point out that the levels seen are not those enhanced in the ^{206}Pb(n, n) reaction. Also the ^{207}Pb$(\gamma, n)^{206}$Pb data (BBB 71) show an envelope in the distribution of γ-ray widths at $E_n = 125$ keV which corresponds to the $J^\pi = \frac{3}{2}^+$ levels excited by $E1$-radiation which decay by d-wave neutrons.

A local concentration of $M1$ strength is seen in the reaction ^{208}Pb(γ, n) ^{207}Pb at $E_n = 500$ keV (Bow+ 70). The seven levels excited in the energy range $0 < E_n < 1200$ keV are $J^\pi = 1^+$ which de-excite by emission of d-wave neutrons. The $M1$ strength arises from spin-flip transitions from the $i_{13/2}$ and $h_{11/2}$ orbits, whose transition strength is distributed among nearby levels. The seven levels are found to contain at least 50% of the total $M1$ transition strength for this nucleus.

For the ^{57}Fe$(\gamma, n)^{56}$Fe reaction, an envelope of $E1$ γ-ray widths is reported (BBB 71) at $E_n \sim 250$ keV which correspond to levels of $J^\pi = \frac{1}{2}^+$ in the compound system. The widths are not correlated with the enhancement of the neutron widths at $E_n \sim 360$ keV seen in the ^{56}Fe$(n, n)^{56}$Fe

reaction (EM 69). The $^{57}Fe(\gamma, n)^{56}Fe$ reaction for $0 < E_n < 700$ keV has also been measured by Jackson and Strait (JS 71). They assign a $J^\pi = \frac{3}{2}^-$ to two strong levels at $E_n \sim 220$ keV, which would then imply an $M1$ excitation and p-wave emission of these levels.

In the radiative processes $^{56}Fe(n, \gamma)^{57}Fe$, Ikegami and Emery (IE 64) have noted that the (n, γ) strength is anticorrelated with the single-particle $l = 1(d, p)$ stripping strength leading to the same final states. From this result it can be concluded that the radiative capture process is not through the direct capture mechanism of Lane and Lynn (LL 59) as this mechanism would produce a correlation between the (n, γ) and (d, p) reactions. To explain this anticorrelation behavior, Ikegami and Emery introduce a doorway-state mechanism. In this picture, the neutron is captured into a doorway state near zero energy which subsequently decays by γ-emission. Since the doorway state is not a single-particle state, the γ-ray transitions which proceed from it can go into regions where the single-particle stripping is small.

Another discrepancy with the predictions of the direct-capture model was found in the radiative capture reaction $^{142}Ce(p, \gamma)$ investigated by Daly *et al.* (DRH 64). In this case, the direct capture failed by an order of magnitude to fit the observed capture cross section below 20 MeV, where this cross section has a peak. To rectify this failure, Clement, Lane, and Rock (CLR 65), have extended the direct-capture model to include "collective" capture. In this latter description, the incident nucleon excites a collective state of the target nucleus while it itself falls into a bound state. This intermediate doorway state can then decay by emission of γ-radiation from the collective state. Moreover, the radiative decay from this intermediate state will be larger than usual because of the large decay rates of collective states. For $E1$ radiation, the collective state is taken to be the giant dipole resonance. The peak in the $^{142}Ce(p, \gamma)$ cross section at 15 MeV can then be understood in terms of the enhanced emission from the dipole resonance, which is located in the vicinity of the peak and broadened by decay into more complex configurations.

3.7.3. Doorway States and Inelastic Electron Scattering

We have stressed that if the doorway-state picture is valid, then the relevant doorway state completely determines the coupling of the compound nucleus to the outside world. For example, an isolated doorway state will solely determine the angular distribution of emitted particles from the compound nucleus and thereby produce an invariance in this distribution

despite rapid variations in the yield. Another interesting consequence of the doorway-state picture for the case of inelastic electron scattering has been investigated by Fallieros (Fal 71, KF 70).

In this case, Fallieros points out that when a particular doorway state dominates in the electroexcitation of nuclear levels, then the associated scattering form factors of these levels will have the same shape, which is determined by the form factor of the doorway state. Also, in this doorway-state model, the magnitude of the form factor in a particular state is a direct measure of the amount of doorway state present in this state. This result is expressed quantitatively as

$$F_{\lambda 0}(q) = F_{d0}(q) a_d^{\lambda} \tag{78}$$

for those levels λ whose electroexcitation properties are determined by the doorway d. The $F_{\lambda 0}(q)$ is the isoscalar monopole form factor

$$F_{\lambda 0}(q) = \left\langle \lambda \left| \frac{1}{2Z} \sum_{i=1}^{A} j_0(qr_i) \right| 0 \right\rangle \tag{79}$$

which describes the electroexcitation of the ground state $|0\rangle$ to the state $|\lambda\rangle$ at the momentum transfer q. The j_0 is the spherical Bessel function of order zero. The monopole matrix element $M_{\lambda 0} = \langle \lambda | \sum_{i=1}^{A} r_i^2/2 | 0 \rangle$ will also be determined by the doorway amplitude since $M_{\lambda 0} = M_{d0} a_d^{\lambda}$.

The form factor and matrix element satisfy the sum rules (Fal 71, KF 70)

$$\sum_{\lambda} (E_\lambda - E_0) M_{0\lambda} F_{\lambda 0}(q) = \frac{\hbar^2}{m} q^2 \frac{d}{d(q^2)} F_{\mathrm{el}}(q) \tag{80}$$

and

$$\sum_{\lambda} (E_\lambda - E_0) \, | M_{0\lambda} |^2 = \frac{\hbar^2}{m} Z \langle r^2 \rangle \tag{81}$$

with $F_{\mathrm{el}}(q) = F_{\infty}(q)$, the elastic scattering form factor. These sum rules are next interpreted in terms of a state $|C\rangle$, a collective monopole excitation, which contains the total strength of the sum rules. If the collective state is taken as the doorway state, a relation between the form factor and matrix element follows:

$$F_{\lambda 0}(q) = \frac{M_{\lambda 0}}{Z \langle r^2 \rangle} q^2 \frac{d}{d(q^2)} F_{\mathrm{el}}(q) \tag{82}$$

This equation then determines the inelastic scattering form factor of a particular level λ once the right-hand side is known for this level. Also, the transfer-momentum dependence of the form factor is uniquely de-

termined by the elastic scattering form factor. Fallieros compares this momentum dependence with the experimental results reported by Bergstrom *et al.* (Ber+ 70) of the first excited $J^{\pi} = 0^{+}$, $T = 0$ level of ^{16}O at 6.052 MeV and finds satisfactory agreement.

3.8. Intermediate Structure in Fission

In Fig. 17 we illustrate the measured high-resolution subthreshold fission cross section for neutrons incident on ^{240}Pu as obtained by Migneco and Theobald (MT 68). From this figure we note an interesting feature of the cross section, i.e., the appearance of groups of stronger resonances at intervals of ~650 eV. The mean fission width and spacing of the fine structure in the energy range between 450 eV and 4 keV was found to be $\langle \Gamma_f \rangle = 3.5$ MeV and $D = 14.9 \pm 0.8$ eV. The enhanced structures have widths about 10^4 times larger than the fine-structure widths. The grouping of the enhanced resonances indicates a new form of intermediate structure. Similar structure is observed by Weigman and Schmidt (WS 68) also for the reaction $^{240}Pu(n,f)$, while intermediate structure groups spaced at intervals of ~60 eV were reported by Fubini *et al.* (Fub+ 68) for the reaction $^{237}Np(n,f)$. The appearance of narrow structure in the average cross section of ^{241}Am was observed by Seeger *et al.* (SHD 67). A possible interpretation of such intermediate structure has been advanced by Lynn (Lyn 68) and Weigman (Wei 68) and involves the recent work of Strutinsky (Str 67), which we discuss briefly. A more comprehensive review by Michaudon (Mic 73) can be found in the preceding volume of this series.

Strutinsky has calculated the potential energy of deformation as a function of the deformation parameter β and found that in certain instances a second minimum appears in this potential in the region of the liquid-drop saddle point as shown in Fig. 18. This minimum arises from shell correction effects due to the appearance of gaps in the energies of the single-particle states in the deformed shell-model potential of Nilsson (Nil 55). For example, the appearance of such a gap at the deformation $\beta \sim 0.2$ is responsible for the permanent stable deformation appearing in the rare-earth region. The effect of gaps or bunching of levels in the independent-particle level spacing on the semiempirical liquid-drop mass formulas was first discussed by Swiatecki (Swi 64). Swiatecki formulated the correspondence between the liquid-drop and independent-particle models through the viewpoint that the liquid-drop model corresponds to an independent-particle model with a uniform level spacing. From this observation evolves a method of calculating shell corrections to the liquid-drop model of a

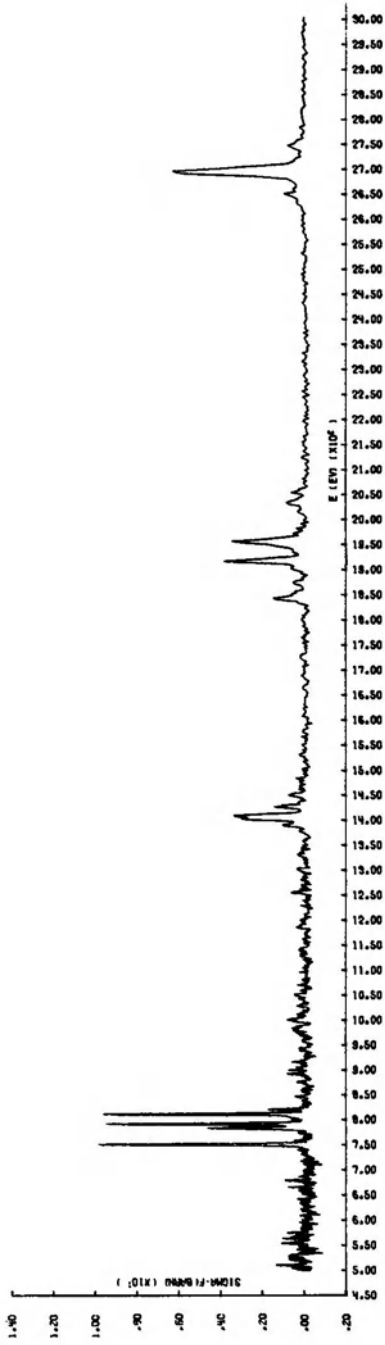

Fig. 17. High-resolution subthreshold fission cross section for $^{240}Pu(n, f)$. From Migneco and Theobald (MT 68).

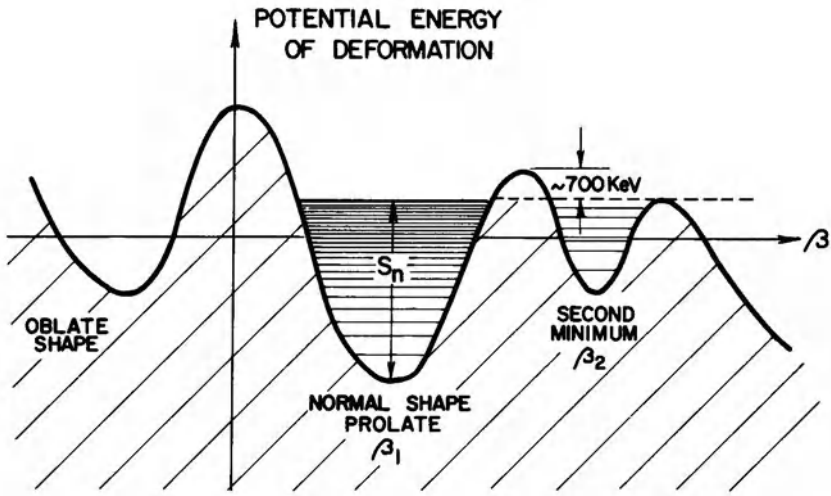

Fig. 18. Potential energy of deformation as a function of the deformation parameter β. The density of levels in each minimum are represented by the horizontal lines.

spherical nucleus when the independent-particle level density deviates from the uniform level spacing. Such deviations arise from the degeneracies which appear in a system with spherical symmetry. While Swiatecki assumed that these degeneracies would disappear with increasing departure from spherical symmetry, Strutinski recognized the fact that, while for small deformations this would be the case, for larger deformations the nucleonic levels would bunch together again. Such oscillations with increasing deformation are easily seen for the case of an anisotropic harmonic oscillator. In this case, Wong (Won 70) finds that shells appear at those deformations for which the axis lengths of the equipotential surfaces are reciprocally commensurate. It is just these oscillations which give rise to local minima in the potential energy of deformation.

Returning now to the intermediate structure phenomenon in fission, the interpretation advanced for this structure is that it represents the levels in the compound nucleus spectrum which are present in the second minimum at large deformations, i.e., at deformation β_2 of Fig. 18. The compound nucleus spectrum of the first minimum at β_1 gives rise to the fine-structure resonances. This result follows from the observation that the fission widths of the states of the first minimum, which are governed by the amplitude for the wavefunction to tunnel through both the saddle-point barrier and the intermediate maximum, will be much smaller than the fission widths of the states in the second barrier, whose wavefunctions must tunnel through only

the saddle-point barrier. Thus, each group of strongly fissioning resonances is located at the position of the compound states of the second minimum. Moreover, if one assumes that the potential minimum at deformation β_2 is higher than that at β_1, then for a given excitation energy E, the density of particle excitation levels at β_2 would be larger than at β_1. Specifically, the ^{240}Pu(n,f) data suggest that the average level spacing in the second minimum is 650 eV, while that of the first minimum is about 13 eV. Using Newton's (New 56) level-density formulas, Lynn estimates the potential energy difference to be 1.7 MeV, while for the Lang–Le Couteur (LC 60) formulas, the difference is increased to 1.9 MeV. For the ^{237}Np case, a similar calculation gives a potential energy difference of the order of 2.3 MeV.

The enhancement of the fine-structure widths (the group at 750 eV in ^{240}Pu contains five enhanced widths, that at 1400 eV, three enhanced widths, and that at 2000 eV, five enhancements) arises from the spreading of the intermediate compound state of the second minimum into the denser spectrum of fine-structure states of the first minimum. The small degree of spreading is a result of the poor overlap of the wave functions in the two minima due to the intermediate barrier. Using the expression

$$\Gamma_{\lambda f} = \frac{(D/2\pi)\Gamma_f^{\uparrow}\Gamma^{\downarrow}}{(E_\lambda - E)^2 + (\Gamma^{\downarrow}/2)^2} \tag{83}$$

Weigman (Wei 68) has obtained for $\Gamma^{\downarrow}$ the values 20 and 60 eV for the intermediate fission states in ^{240}Pu at 750 and 2000 eV, respectively.

We summarize the intermediate-state picture of fission with the description of Feshbach and Kerman (FK 68). First, the incident neutron is captured into a normal compound nuclear level. Then, the compound system penetrates the first fission barrier. There it undergoes oscillations in one of the fission modes of the well arising from the second minimum. Finally, the second barrier is penetrated and two separate fragments are quickly formed. This picture has the following consequence. Whenever the incident nucleon excites a compound nuclear level of the first minimum which is close in energy to a level in the second minimum, the probability of fission is increased. For those levels which are far away in energy from levels in the second minimum, the probability of fission is decreased. Thus, the fission cross section will show enhancements at the energies of states in the second minimum. The width of the states of the second minimum will be shared among the nearby levels of the first minimum. This picture can therefore account for the appearance of intermediate structure in fission.

3.9. Doorway States and Partial Width Correlations

3.9.1. Partial Width Correlations

Another interesting prediction of the doorway-state picture arises if a common doorway state couples the compound nuclear states to two different channels. As stressed by Chrein (Chr 69, Rim+ 69) and Bartholomew and collaborators (Bar 69, Bar+ 67) and investigated by Lane (Lan 71), the existence of isolated doorway states leads to strong correlations between partial widths and different channels.

Lane (Lan 71) has pointed out that the existence of such correlations is a remarkable feature of the data since these correlations run contrary to the predictions of the statistical model which is believed to apply in these experimental situations. In particular, since the observed neutron widths are only a very small fraction (about one-millionth) of the Wigner single-particle limit, and thus, the compound state is composed of a million or so complicated components, then such a high complexity of states would justify an extreme statistical picture. In such a picture, complete configuration mixing operates so that the components in the wave function representing simple motion of the nucleons is completely dissolved and any coherence or phase relation is washed out. In turn, this model can be used to make certain predictions, such as energy-independent transmission factors, a Maxwellian evaporation spectrum, Porter–Thomas distributions for partial widths, and negligible correlations among partial widths. Thus, the existence of such correlations contradicts the last implication of the model.

First, we establish that a common doorway for two channels c and c' leads to correlations. This can be seen easily from the observation that the decay amplitude of a state λ to channels c and c' is equal to the probability amplitude $\langle\lambda \mid d\rangle$ for finding the doorway state $\mid d\rangle$ in the compound state $\mid \lambda\rangle$ times the decay amplitude of the doorway state to the two channels c and c'. We write

$$\gamma_{\lambda c} = \langle\lambda \mid d\rangle\gamma_{dc} \tag{84}$$

for channel c, and

$$\gamma_{\lambda c'} = \langle\lambda \mid d\rangle\gamma_{dc'} \tag{85}$$

for channel c'. The $\gamma_{\lambda c}$, $\gamma_{\lambda c'}$, γ_{dc}, and $\gamma_{dc'}$, are decay amplitudes defined with penetrability factors removed. Now, upon taking the ratio of Eqs. (84) and (85), we arrive at a quantity which is independent of the probability amplitude $\langle\lambda \mid d\rangle$. Specifically, we obtain the result

$$\frac{\gamma_{\lambda c}}{\gamma_{\lambda c'}} = \frac{\gamma_{dc}}{\gamma_{dc'}} \tag{86}$$

Moreover, for every other state λ' coupled to the two channels through the same common doorway state, the ratio of the decay amplitudes to these two channels is given by the same equation, so that we have

$$\frac{\gamma_{\lambda,c}}{\gamma_{\lambda,c'}} = \frac{\gamma_{\lambda 2c}}{\gamma_{\lambda_2 c'}} = \cdots = \frac{\gamma_{\lambda nc}}{\gamma_{\lambda_n c'}} = \frac{\gamma_{dc}}{\gamma_{dc'}} \tag{87}$$

Equivalently, we could write

$$\frac{\gamma_{\lambda,c}\gamma_{\lambda,c'}}{\gamma^2_{\lambda,c'}} = \frac{\gamma_{\lambda 2c}\gamma_{\lambda 2c'}}{\gamma^2_{\lambda_2 c'}} = \cdots = \frac{\gamma_{\lambda nc}\gamma_{\lambda nc'}}{\gamma^2_{\lambda_n c'}} = \frac{\gamma_{dc}\gamma_{dc'}}{\gamma^2_{dc'}} \tag{88}$$

from which we can conclude that the isolated common doorway model predicts that $\gamma_{\lambda c}\gamma_{\lambda c'}$ should have the same phase, determined by the phase of $\gamma_{dc}\gamma_{dc'}$, for all λ, instead of fluctuating randomly. These results are just a statement of the existence of a strong correlation between the decay amplitudes to two different channels. Specifically, for the case of an isolated common doorway the results of the above expressions imply a value of unity for the reduced-width correlation coefficient

$$\varrho(\gamma_{\lambda c}, \gamma_{\lambda c'}) = \frac{\sum_\lambda \gamma_{\lambda c}\gamma_{\lambda c'}}{[\sum_\lambda \gamma^2_{\lambda c} \sum_\lambda \gamma^2_{\lambda c'}]^{1/2}} \tag{89}$$

and also a value of unity for

$$\varrho(\gamma^2_{\lambda c}, \gamma^2_{\lambda c'}) = \frac{\sum_\lambda (\gamma^2_{\lambda c} - \overline{\gamma^2_{\lambda c}})(\gamma^2_{\lambda c'} - \overline{\gamma^2_{\lambda c'}})}{[\sum_\lambda (\gamma^2_{\lambda c} - \overline{\gamma^2_{\lambda c}})^2 \sum_\lambda (\gamma^2_{\lambda c'} - \overline{\gamma^2_{\lambda c'}})^2]^{1/2}} \tag{90}$$

the latter being the product–moment correlation coefficient. The existence of several doorway states simultaneously coupling the compound states to the two different channels will reduce the value of these correlation coefficients from the maximum value of unity. For example, the opposite extreme of many overlapping doorways gives zero correlation. For the intermediate situation, Lane (Lan 71) shows that when $\varrho(\gamma^2_{\lambda c}, \gamma^2_{\lambda c'})$ has a typical value of 0.27, there is present a mean of four doorways but up to nine doorways could be operating with reasonable probability. In general, the mean value of $\varrho(\gamma^2_{\lambda c}, \gamma^2_{\lambda c'})$ is n^{-1} when n doorways are present and the γ_{dc}'s have random signs.

3.9.2. Pygmy Resonances as Possible Common Doorways

Having established the existence of large correlations when two channels have the same doorway state, we next consider whether such common doorways will exist in actual situations.

Lane (Lan 71) has proposed that a pygmy dipole resonance (KB 54, GD 57, BS 62) may be a prominent doorway for the neutron channel and for the photon channel. Specifically, a calculation of 1^- states in ^{208}Pb has shown the presence of an $E1$ doorway state at $E = 5.5$ MeV (Lan 71). These states are discussed in some detail by Bartholemew *et al.* in Chapter 4 in the present volume. This pygmy dipole resonance arises because certain $1p$–$1h$ states are uncoupled from the giant resonance. In fact, the $3p^{-1}4s$, $3p^{-1}3d$, and $2f^{-1}3d$ neutron states form a pygmy resonance lying below the giant dipole resonance and account for a few percent of the $E1$ sum rule. Moreover, the $3p^{-1}4s$ component also acts as a doorway for the neutron channel in the neutron threshold region. Thus, the pygmy resonance has features which make it a good candidate for a common doorway state. However, as Lane points out, the ^{208}Pb calculations are in serious disagreement with the experimental data since the elastic scattering of photons on ^{208}Pb shows no state in the appropriate region with any appreciable width. Consequently, until the discrepancy is resolved, the ^{208}Pb calculation only serves as an illustrative example of how common doorway effects can arise.

3.9.3. Experimental Results on Partial Width Correlations

Baglan *et al.* (BBB 71) investigated the reaction ^{207}Pb$(\gamma, n)^{206}$Pb using a photonuclear threshold technique to see if the doorway observed in the elastic scattering of neutrons off ^{206}Pb is also prominant in the photon channel. They find a similar envelope of γ-ray widths and a correlation between the neutron and γ-ray widths of the fine-structure resonances of the doorway state. The degree of correlation which exists between these two sets of widths, as measured by the product moment correlation coefficient, is claimed to be $\varrho = 0.45 \pm 0.1$.

Recently, however, Allen *et al.* (All+ 73) find that the capture resonances in ^{206}Pb(n, γ) are not the $s_{1/2}$ resonances of the Farrell *et al.* (Far+ 65), but rather small $p_{1/2}$ or $p_{3/2}$ resonances. Thus, Allen *et al.* find no correlation between the n and γ-ray widths. Other cases, ^{57}Fe and ^{53}Cr, were studied by Baglan *et al.* (BBB 71) and no correlation was found. Also, the Brookhaven experiment ^{175}Lu(n, γ) (WC 70) shows no correlation. However, this group finds partial width correlations in the reaction ^{169}Tm(n, γ) (Lon+ 68) with $\varrho_{j=1} = 0.274$, in ^{163}Dy(n, γ) with $\varrho_{j=3} = 0.35$, in ^{173}Yb with $\varrho_{j=3} = +0.43$, and in ^{92}Mo(n, γ) and ^{98}Mo(n, γ) (Chr 72a, Chr 72b). More recently, Thomas (Tho 72) reported no correlation for ^{169}Tm(n, γ) when more resonances are included and spins reassigned. A reinvestigation by the Brookhaven group (Chr 72a) also gave no evidence

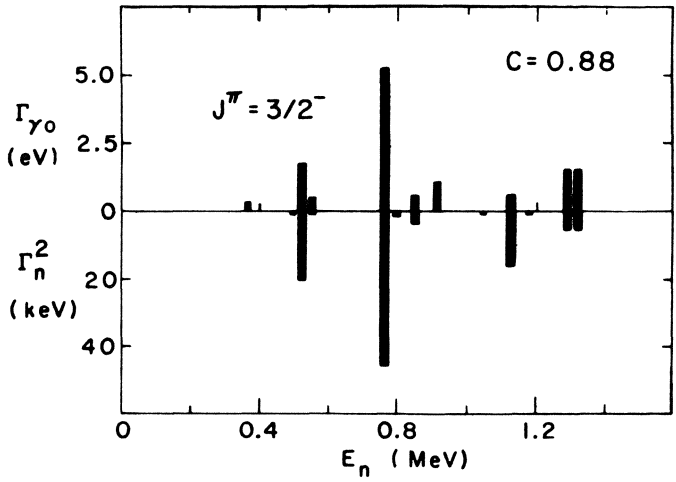

Fig. 19. Correlation between neutron and γ-ray widths in ^{29}Si(γ, n). From Jackson and Toohey (JT 72).

for width correlation in Tm, i.e., $\langle \varrho \rangle = +0.046 \pm 0.06$. Finally, Jackson and Toohey (JT 72) report a strong correlation in ^{29}Si(γ, n) with $\varrho = 0.8$, the results of which are shown in Fig. 19.

3.10. Intermediate Structure and the High-Energy Neutron Tail in Neutron Evaporation Spectra

3.10.1. Griffin's Model

J. J. Griffin (Gr 66) has applied the idea of a hierarchy of states implied in the intermediate structure model of nucleon–nucleus collisions to the question of the spectrum of emitted neutrons observed in (p, n) reactions. He proposes a model describing the formation and decay of compound nuclear states to explain the "high-energy" tail of neutrons emitted in such (p, n) reactions. The model is based on the assumption of weak two-body forces which produce transitions among the eigenstates of an independent-particle Hamiltonian. Successive operations of this weak two-body interaction takes the initial incident nucleon–nucleus system which is taken as a $1p$–$0h$ state, through states of higher particle–hole excitation. The system develops from the initial $1p$–$0h$ state into a $2p$–$1h$ doorway state, then a $3p$–$2h$ hallway state, etc., until after many collisions, the compound nucleus configuration, which is a complex linear combination of such particle–hole excitations, is reached. In his description, the independent-particle

model states are classified according to the number of particles and holes which are referred to as excitons. The assumption of two-body forces can then only cause transitions which change the exciton number by 0 or ± 2.

Previous calculations (Wei 37, BW 66) of the spectrum of emitted neutrons are based on processes occurring after the formation of the compound nucleus. These calculations predict a Maxwellian energy distribution of emitted particles similar to the distribution of particles evaporated from a surface at a given temperature. This evaporation spectrum fails to predict a "high-energy" tail in the energy distribution of emitted particles. Griffin explains the high-energy tail in terms of precompound decays. That is, in the evolution of the system from the initial $1p$–$0h$ state through the $2p$–$1h$, $3p$–$2h$, $4p$–$3h$, ... stages, to the final compound nucleus stage, there exist a small number of decays which can occur at each stage. A calculation of the spectrum of emitted neutrons from the precompound configuration proceeds as follows: The decay width of an n-exciton state to an n'-exciton state, where $n' = n, n \pm 2$, is given by Fermi's golden rule, which may be written $\Gamma = 2\pi M^2 \varrho_{n'}(E^*)$. As a starting point in the model, the interaction matrix element is taken to have a constant value unless it vanishes identically. The density of n-exciton states at an excitation energy E^* is given by (Gri 66)

$$\varrho_n(E^*) = g \frac{(gE^*)^{n-1}}{n!(n-1)!} \tag{91}$$

where g is the one-particle level spacing. For $n \ll \bar{n} = \sqrt{gE^*}$, the mean exciton number, the level densities are rapidly rising functions of n. Thus, for $n \ll \bar{n}$, a decay of an n-exciton state will be mainly to an $(n+2)$-exciton state; that is, the system will evolve toward more complex configurations. At each stage in this evolution to the compound state, there is a small but finite probability that one particle will have concentrated on it enough energy so that it can escape. This corresponds to a violent fluctuation away from the most probable distribution of energy in which the total energy is shared equally. Now, the probability of finding a particle with continuum energy E_0 in an n-exciton state is

$$\frac{\varrho_{n-1}(U)\varrho_c(E_0)\, dE_0}{\varrho_n(E^*)} \tag{92}$$

where $U = E^* - (E_0 + S)$, with S the separation energy of the emitted particle, while $\varrho_c(E_0) = 2\pi(2m/h^2)^{3/2}E_0^{1/2}$ is the density of one-particle continuum states. Summing over all exciton states then gives the precompound

emission probability:

$$W_p(E_0) = \sum_n \frac{\varrho_c(E_0)\varrho_{n-1}(U)}{\varrho_n(E^*)} \tag{93}$$

When the sum which appears in the above equation is evaluated, the following expression is obtained:

$$W_p(E_0) \propto \begin{cases} \dfrac{E_0^{1/2}}{E^*}\left[\dfrac{1+3r^2}{(1-r^2)^3} - 1\right] & \text{for } n \text{ even} \\ \dfrac{E_0^{1/2}}{E^*}\left[\dfrac{3r+r^3}{(1-r^2)^3} - 1\right] & \text{for } n \text{ odd} \end{cases} \tag{94}$$

where $r = U/E^*$.

Within the same framework, Griffin also calculated the compound emission probability. In the compound nuclear state, which is an equilibrium situation, the probability of finding an n'-exciton state is equal to $\varrho_{n'}(E^*)/\varrho(E^*)$, with $\varrho(E^*) = \sum_n \varrho_n(E^*)$. Such a state can scatter into an $(n-1)$-exciton state at energy U and a state with a particle in the continuum at energy E_0. Noting that this can happen from exciton states with $n' = n$, $n \pm 2$ and summing over all n, we obtain

$$W_c(E_0) = \sum_n \left(\frac{2\pi}{\hbar} \mid M \mid^2\right)\varrho_{n-1}(U)\varrho_c(E_0) \times \left[\frac{\varrho_{n-2}(E^*) + \varrho_n(E^*) + \varrho_{n+2}(E^*)}{\varrho(E^*)}\right] \tag{95}$$

for the compound emission probability. This equation results in the following expression for this probability:

$$W_c(E_0) \propto f(E^*, U) \exp[4(g^2E^*u)^{1/4}] \tag{96}$$

where

$$f(E^*, U) = E_0^{1/2}(E^*)^{19/8}U^{-11/8}[1 + r + r^2] \tag{97}$$

The $(UE^*)^{1/4}$ dependence results from assuming constant matrix elements $\mid M \mid$. [Blann (Bla 68) improves on this shortcoming as discussed in the next subsection.] This result should be compared with Weisskopf's (Wei 37, BW 66) for the spectrum of evaporated particles which reads:

$$W_c(E_0) = \text{const. } E_0\sigma_c(E_0) \exp\left[-\frac{E_0}{T(E)}\right] \tag{98}$$

The $\sigma_c(E_0)$ is the cross section and E is the kinetic energy in the outgoing channel. The $T(E)$ is interpreted in terms of a nuclear temperature with

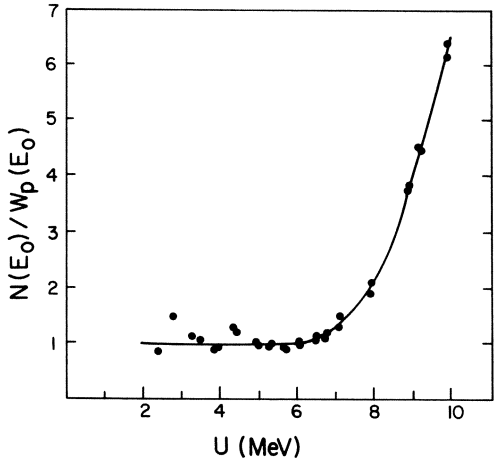

Fig. 20. The ratio of the experimentally determined neutron distribution for the reaction ^{117}Sn(p, n)^{117}Sb to the precompound distribution. From Griffin (Gri 66).

$T(E) = (E/a)^{1/2}$. The level density $\varrho(E)$ has the well-known exponential form $\varrho(E) = c \exp(2\sqrt{9E})$. As we shall see shortly, an improvement in the crude assumption of constant matrix elements leads to an expression similar to Weisskopf's.

From Griffin's results shown above, we see that the compound nuclear decays dominate the low-energy spectrum of emitted neutrons, while the precompound decays dominate the high-energy spectrum. In Fig. 20 we give the results of Griffin's calculation. This figure shows that for the reaction ^{117}Sn(p, n)^{117}Sb (HB 63, WBB 65), the number of decays $N(E_0)$ is accounted for by the precompound emissions for excitation energies in the residual nucleus of less than 6 MeV.

3.10.2. Blann's Extension of Griffin's Model

An extension of Griffin's statistical model to include charged-particle emission has been given by Blann (Bla 68) and applications of this extension have been considered by Cline and Blann (CB 71). In this extension, the interaction matrix elements are expressed in terms of the cross section $\sigma(v)$ for the scattering of two particles with relative velocity v. By noting that the decay probability $\omega = 2\pi h^{-1} \mid M \mid^2 \varrho_n(E^*)$ into an n-exciton state is also simply (Mor 53) $\omega = v\sigma(v)/\Omega$, where Ω is the volume, Blann obtains

$$\mid M \mid^2 = \frac{hv\sigma(v)}{12\pi\varrho_n(E^*)\Omega} \tag{99}$$

Thus the matrix elements decrease with increasing n, for $n \ll \bar{n}$. Using this connection, the resulting precompound probability is similar to Griffin's result, and is

$$W_p(E_0) \propto \frac{E_0\sigma(v)}{U^2} E^* \sum_n^{\bar{n}} r^n(n^2 - n) \tag{100}$$

whereas the equilibrium case is quite different from Griffin's result but similar to Weisskopf's expression, and is

$$W_c(E_0) \propto \frac{\sigma(v)\varrho(U)E_0}{\varrho(E^*)} [1 + r + r^{-1}] \tag{101}$$

The $r = U/E^*$. For $E^* \gg U$, and noting $\varrho(E) \propto E^{-1} \exp[2(gE)^{1/2}]$, Blann obtains

$$W_c(E_0) \propto \frac{E_0\sigma(v)U^{-3} \exp[2(gU)^{1/2}]}{(E^*)^{-3} \exp[2(gE^*)^{1/2}]} \tag{102}$$

Using the above results, one finds that emission from states of low exciton number ($n \ll \bar{n}$) give spectra with high-energy neutrons while emission from states with high exciton number ($n \gg \bar{n}$) have spectra with much lower kinetic energies than the equilibrium result.

3.11. Intermediate Structure and Statistical Fluctuations

3.11.1. Ericson Fluctuations and Intermediate Structure

In the case when doorway states overlap, bumps in the cross section of intermediate width can still be seen. An interpretation of such a phenomenon for the case of overlapping fine-structure states has been given by Ericson (Eri 60, Eri 63). Ericson argues that when compound nuclear states overlap, a nucleon incident on a target will excite all those states lying within their widths of the energy of the compound system. Moreover, correlations will be seen in the cross section measured at two different energies if the energies lie within the width of the compound nuclear states, since essentially the same states will be excited. On the other hand, if the two energies differ by more than the width of the compound nuclear states, a completely different set of states will be excited at each energy and the correlations should vanish. Ericson then shows that the correlation coefficient $C(\varepsilon)$, defined by the equation

$$C(\varepsilon) = \frac{\langle\sigma(E + \varepsilon)\sigma(E)\rangle - \langle\sigma(E + \varepsilon)\rangle\langle\sigma(E)\rangle}{\langle\sigma(E + \varepsilon)\rangle\langle\sigma(E)\rangle} \tag{103}$$

has the form

$$C(\varepsilon) = \frac{\Gamma^2}{\varepsilon^2 + \Gamma^2} \tag{104}$$

Similarly, when doorway states overlap, Ericson fluctuations of intermediate structure should be seen. Such overlapping doorways should give rise to fluctuation phenomena exactly like overlapping fine-structure states, and thus, a correlation coefficient $C(\varepsilon)$ should be measurable for this case also. Now, if we measure $C(\varepsilon)$ we should expect essentially two Γ's to appear. For small ε, correlations in the cross section at two different energies should be present because of overlapping fine-structure states, with Γ reflecting the width of the fine-structure states. For larger ε, longer-range correlations will be present owing to overlapping doorway states, with Γ reflecting the width of the doorway states. From these observations we can conclude that the presence of intermediate structure in the cross section does not guarantee that isolated doorways are present since overlapping doorways can give rise to intermediate bumps resulting from Ericson fluctuations.

3.11.2. Intermediate Structure Produced by Fluctuations in Level Spacing and Level Widths

While the signature of a doorway state is the presence of a resonance in the average cross section, the existence of a bump in the cross section can sometimes be accounted for by fluctuations in level density and level width. For the case of compound nuclear levels, Agodi and Pappalardo (AP 63) showed that such statistical fluctuation could account for the irregularly oscillating behavior of some neutron cross sections measured with energy resolution larger than the average level spacing (CPR 60, Cuz+ 60, Col+ 62). More recently, Singh *et al.* (SHL 66) and Baglan *et al.* (BBB 71) have considered the question of whether the origin of intermediate structure bumps can be accounted for by fluctuations in level spacing and level width. The former group considered the region of overlapping levels, $\langle\Gamma\rangle/D \gg 1$, while the latter group investigated the region $\langle\Gamma\rangle/D \ll 1$. In both cases, cross sections were generated from level-width and level-spacing parameters chosen in a random fashion from the Wigner distribution (Wig 56a):

$$P(Y) = \pi \frac{Y}{2D} e^{-\pi(Y^2/4)} \tag{105}$$

for the spacing of nearest levels, and from the Porter–Thomas distribution (PT 56),

$$P(X) = \frac{1}{\sqrt{2\pi X\langle\Gamma\rangle^2}}\, e^{-X/2} \tag{106}$$

for the level width. As shown by Blumberg and Porter (BP 58, Por 65), these distributions arise from ensembles of Hamiltonians (the eigenvalues of which are the energy levels of the compound nucleus) having random matrix elements with Gaussian distributions. In the above equations $Y = S/D$ is the distance S between nearest levels in units of the average level spacing D, and $X = \Gamma/\langle\Gamma\rangle$ is the level width Γ in units of the average width $\langle\Gamma\rangle$. Also, in both cases, structure of intermediate width resulted from the random fluctuations in resonance widths and level spacing. While Singh *et al.* found that such structure resulted from an accidental lumping of resonance contributions to the reaction amplitude, Moldauer (Mol 67b) has found that, in the strong-absorption cases, a statistical description of this amplitude contains such a broad distribution of widths that individual terms giving rise to intermediate structure occur quite frequently.

To illustrate the generation of intermediate structure from random fluctuations of spacings and widths, we consider the work of Baglan *et al.* (BBB 71) in further detail. In Fig. 21, we illustrate a sampling, over an

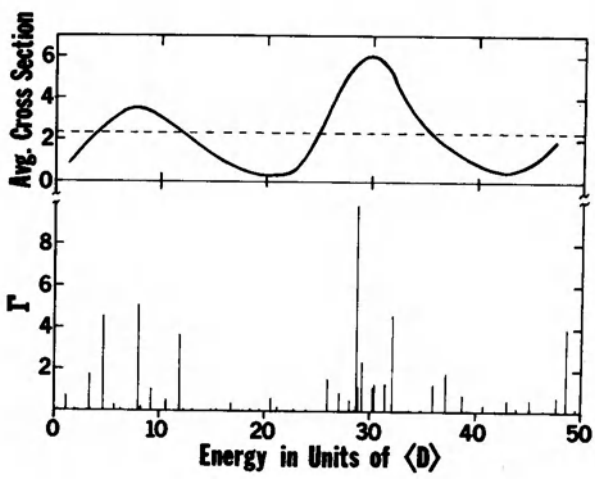

Fig. 21. A typical set of resonance widths and positions generated by a random choice of widths from a Porter–Thomas distribution and level spacings from a Wigner distribution. The upper part of the figure is the average cross section generated from these parameters. The dashed curve is the mean cross section.

interval $50D$, of resonance widths and energies chosen from the Porter–Thomas and Wigner distributions. Using these widths and energies, we can obtain the cross section and its average with various smoothing functions. The results for the mean cross section and average cross section for a square smoothing function of breadth $I = 8D$ is also shown in this figure. From the figure we see, first, the appearance of bumps of intermediate width and, secondly, the association of these bumps with the fluctuations of widths and spacings consistent with the Porter–Thomas and Wigner distributions. These results should be compared with those of Payne's calculation (Pay 68) shown in Fig. 9. One point to note is that, while the Wigner distribution has an absence of small level spacings due to level repulsion, the level-spacing distribution obtained from Fig. 9 will show no such behavior since the interaction of the doorways with each other are not considered in Payne's calculation. Also, the Porter–Thomas width distribution is based on a picture of complete configuration mixing interpreted in terms of random matrices which is the viewpoint opposite that of the shell model. We therefore expect the width distribution of Fig. 9 to contain a higher frequency of very large widths than that of the Porter–Thomas distribution.

Baglan *et al.* next proceed to calculate with what frequency these statistically generated intermediate structures occur. The criterion for such a structure were arbitrarily selected to be: (1) that its height be 1.5 times the mean cross section, and (2) that the structure contain at least ten contributing resonances. Then, within this framework, the frequency of statistically generated doorway states is one per every 67 resonances. Changing the number of contributing resonances changes the frequency of appearance of the structures. Specifically, raising this number decreases this frequency, and with a criterion of 14 contributing resonances, one statistically generated doorway exists per 100 resonances.

In the overlapping region, Singh *et al.* showed that due to fluctuations in widths and spacings there existed a 30% chance that in an internal $\Delta = 25\Gamma$ a structure of width 6Γ wide occurs with a peak in the cross section 1.4 times the average cross section. From this result, these authors conclude that widths alone are not reliable signatures of real intermediate structure.

3.11.3. Intermediate Fluctuations and the Experimentally Determined Neutron Cross Section

Carlson and Barschall (CB 67) have measured the total cross section for incident neutrons, with energies in the range 4.5 to 7.5 MeV, and with

energy spreads of 20 or 50 keV on a series of targets. The targets included the following 18 elements: Mg, Al, Si, S, Ti, Fe, Co, Zn, Y, Zr, Nb, Ag, Sn, Sb, Pr, Ta, Pb, and Bi. Their reported results showed no deviation from a smooth energy dependence in the cross section for the ten elements from Co to Ta. In the remaining elements, Mg, Al, Si, S, Ti, Fe, Pb, and Bi, fluctuations were observed with the last element having fluctuations barely outside the statistics. The amplitudes of the fluctuation were found to decrease with increasing energy. For these elements, the energy interval was extended until the cross section became flat.

An investigation of the cause of the fluctuations was then carried out. The following three possibilities were considered: (1) fluctuations in level spacings and level widths, (2) intermediate structure, (3) Ericson fluctuations. To investigate the first possibility Carlson and Barshall evaluated the unnormalized variance F of the cross section defined by

$$F = \langle(\sigma_n - \langle\sigma\rangle)^2\rangle \tag{107}$$

with σ_n the average cross section in an interval Δ_n. The σ_n will be different in different Δ_n due to fluctuations in widths and spacings. For spin-zero targets these authors find, following an approach similar to Agodi and Pappalardo's (AP 63), that

$$F = (\pi\lambda\!\!\!^{-2})^2 \sum_{J\pi} g^2(J) \frac{(T^J)^2}{\langle N^n_{J\pi}\rangle} [k_W + k_N] \tag{108}$$

The $g(J) = (2J + 1)/2$, the $T^J = 2\pi\langle\Gamma(J\pi)\rangle/D_{J\pi}$, the $N^n_{J\pi}$ is the number of compound nuclear levels of spin J and parity π in Δ_n, and the $k_N = V_{ar} \times [\Gamma(J\pi)]/\langle\Gamma(J\pi)\rangle^2$, while $k_N = V_{ar}N^n_{J\pi}/\langle N^n_{J\pi}\rangle$. For a Porter–Thomas distribution $k_N = 2.0$ and for a Wigner spacing distribution $k_N = 0.27$. The F was evaluated from the data, while the T^J was obtained from optical-model calculations; the $\langle N^n_{J\pi}\rangle$ was treated as an unknown which was compared to the value predicted by the Gilbert–Cameron expression (GC 65). In this comparison, satisfactory agreement resulted.

While fluctuations in density and width can account for fluctuations in the neutron cross section, it is also possible that true intermediate structure may also be present. This second possibility was tested for using the procedure of Pappalardo (Pap 64). In this analysis the correlation function $F(\varepsilon, \delta)$,

$$F(\varepsilon, \delta) = \frac{1}{N} \sum_{k=1}^{N} [\sigma_T(E_k) - \bar{\sigma}_{T\delta}(E_k)][\sigma_T(E_k + \varepsilon) - \bar{\sigma}_{T\delta}(E_k + \varepsilon)] \tag{109}$$

is used. The $\sigma_T(E)$ is the measured total cross section, the $\bar{\sigma}_{T\delta}(E)$ is the total cross section averaged over the range $E - \frac{1}{2}\delta$ to $E + \frac{1}{2}\delta$, and the N is the number of measurements. The $F(0, \delta)$ will be small for δ small compared to the fluctuations since the average curve $\bar{\sigma}_{T\delta}$ will follow the curve σ_T. With increasing δ the $F(0, \delta)$ will also increase until $\delta \gg \Gamma$ when $F(0, \delta)$ becomes independent of δ. Thus, when structure is present which is much broader than Γ, the $F(0, \delta)$ will increase again so that the $F(0, \delta)$ will have a secondary rise. The absence of a secondary rise is taken as evidence that intermediate structure is not present. For the elements considered, a secondary rise was not present.

The third possibility is analyzed for in a manner exactly analogous to the well-established Ericson theory of overlapping fine structure.

In summary, on the basis of their investigation, Carlson and Barschall concluded that the fluctuations and the transition to a smooth cross section could be accounted for by fluctuations in widths and spacings allowed within the Wigner and Porter–Thomas distributions and by the usually accepted level-density expression of Gilbert and Cameron. The assumption of intermediate structure was not necessary to account for any of the fluctuations. Finally, the Ericson theory, the conditions for the validity of which may not be satisfied at the low-energy end of the spectrum, was shown to account for any observed fluctuations at higher energies.

3.12. Experimental Observations of Intermediate Structure in Total Neutron Cross Sections

3.12.1. Clues and Criteria Relating to the Origin of Any Structure

The following clues can be used to qualitatively establish the existence of intermediate structure in the experimentally determined reaction cross section:

1. When performing an experiment with a beam having resolution $\Delta E \sim$ 10–100 keV, the existence of intermediate widths ($\Gamma \sim$ 10–100 keV) in the energy dependence of the cross section.
2. In high resolution, the presence of fine structure in the cross section with many levels undergoing a large enhancement.
3. The existence of correlations among different reaction channels.
4. The existence of angular distributions which can be associated with a unique angular momentum.

The first clue is normally regarded as the signature of a doorway state. However, as we have already discussed, the presence of intermediate structure can also arise from statistical and Ericson fluctuations, and therefore this clue does not guarantee the presence of an isolated underlying doorway state. Thus, further evidence is necessary to establish whether an isolated doorway state is responsible for an intermediate resonance. This evidence is supplied by (2), (3), and (4).

The above criteria are also just those used in standard resonance analysis. Thus, once the above criteria have been fulfilled, a quantitative analysis of the intermediate structure as observed intermediate resonances can be performed. The spin, parity, isotopic spin, the total and partial resonance widths, and the resonance energy can be extracted. A comparison can then be made with the theoretical predictions for these quantities based on some model for the structure of the underlying doorway state. For example, if a particular shell-model configuration is responsible for the intermediate resonance, then the matrix elements coupling the doorway state to various final states or reaction channels will reflect the shell-model configuration. Consequently, the branching ratios to these final states and the correlations among the different reaction channels should reflect the coupling matrix elements of the doorway state. Or, turning the problem around, the branching ratio should be a tool for determining the structure of the doorway state through a comparison of the experimentally determined ratios and theoretical predictions of it.

Apart from the above clues, Rodberg (Rod 68) has suggested the following rough criterion for analyzing the possible origin of structure in an excitation function. If the reaction cross sections are fitted with the standard Breit–Wigner form

$$\sigma_{\beta\alpha} = \frac{2J+1}{(2S_1+1)(2S_2+1)} \pi \lambda\!\!\!^{-}_{\alpha}{}^2 \frac{\Gamma_\beta \Gamma_\alpha}{(E-E_r)^2 + (\Gamma/2)^2} \tag{110}$$

the channel widths Γ_α and total width Γ can be extracted since the products $\Gamma_\alpha \Gamma_\beta$ can be obtained from the heights of σ in the different reaction channels while the Γ gives the width of the peak. From these extracted widths we can obtain the ratio $R = \sum_\alpha \Gamma_\alpha / \Gamma$ and then consider the three possibilities $R < 1$, $R = 1$, and $R > 1$. Rodberg's criteria are then:

1. If $R = 1$, then the peak corresponds to a true compound state.
2. If $R < 1$, it is an intermediate resonance with associated fine structure since the full width Γ contains $\Gamma^{\downarrow}$ as well as $\sum_\alpha \Gamma_\alpha$.

3. If $R > 1$, it is an Ericson fluctuation, since several overlapping resonances will usually increase the height more than the width.

The third possibility will never occur for a true compound state nor for an isolated doorway state. However, some fluctuations might satisfy the second possibility. Thus, condition (2) is then necessary, but not sufficient, for the existence of an isolated doorway with underlying fine structure. Criterion (1) also applies to simple excitations with no associated fine-structure, i.e., the compound nuclear levels are simple excitations, reached in the first collision, a situation realized in light nuclei and closed-shell nuclei at reasonably low excitation energies.

3.12.2. Systematic Studies

Structure in the energy dependence of the total neutron cross section has been reported by several groups, the results of which are summarized in Table IV. The interpretation of this structure, as listed in column four of the table, has been either in terms of fluctuations in level density and/or level width, in terms of "true" intermediate structure, and in terms of Ericson fluctuations.

The most convincing cases for intermediate structure are seen in ^{56}Fe$(n, n)^{56}$Fe (EM 69, ME 68), and ^{206}Pb$(n, n)^{206}$Pb (Far+ 65). In the former case, structure is seen at $E_n = 0.36$ MeV and $E_n = 0.7$ MeV. An analysis of the data (JM 69, ME 68) gives $J^\pi = \frac{1}{2}^+$, $\Gamma^\uparrow = 50$ keV, and $\Gamma^\downarrow = 95$ keV for the 0.36-MeV structure, and $J^\pi = \frac{1}{2}^+$, $\Gamma^\uparrow = 80$ keV, and $\Gamma^\downarrow = 95$ keV for the 0.7-MeV resonance. The spacing of the associated fine structure is $D \sim 25$ keV for both resonances. In the latter case, the ^{206}Pb$(n, n)^{206}$Pb has a resonance at $E = 0.4$ MeV with associated fine structure spaced at $D \sim 40$ keV. For this case, $J^\pi = \frac{1}{2}^+$, $\Gamma^\uparrow = 60$ keV, and $\Gamma^\downarrow = 190$ keV.

Apart from the above cases, the evidence for the existence of "true" intermediate structure in the neutron cross section is not conclusive and, therefore, we cannot say that true intermediate structure is a universal phenomenon systematically appearing in all nuclei. The detailed analysis of Carlson and Barshall (CB 67) showed that any structure in the energy interval $E_n = 4.5$ to 7.5 MeV could be accounted for in terms of fluctuations in level density and level width as discussed in Section 3.11.2. Similar interpretations of such structure were also reported by others and are quoted in Table IV. On the other hand, Kopsch and Cierjacks (KC 72) performed an analysis similar to that of Carlson and Barschall and found some evidence for intermediate structure. In particular, they found a second

TABLE IV

Experimental Investigations

In the fourth column (1) fluctuations in level density, (2) fluctuations in level width, (3) intermediate structure, (4) Ericson fluctuations.

Nuclei Studied	Energy range E (MeV)	Resolution I (keV)	Suggested interpretation	Reference
Na, Al, Mg, Si, P	2.5–5	20–50	1	(Cuz+ 60) (Cal+ 62) (Cal+ 63)
Si, P, S, Cl	3–5	20–50	1,2	(TT 63)
V, In, I, Bi	3.2–5.2		1	(Man 65)
F, Na, Al, P Ag, Pd, Rh, Mo, Nb	0.2–2.2	100–150	1,3	(Elw+ 64)
Zr, Y, Zn, Cu, Ti, Au Pt, Er, Gd, Nd, Sn, Cd Mg, Al, Si, S, Ti, Fe,	<0.65	8–10	3	(Set 65)
Ca, Zn, Y, Zr, Nb, Ag Sn, Sb, Pr, Ta, Pb, Bi	4.5–7.5	20,50	1,2	(CB 67)
Cu, Fe, Mg, Al	12–14	35–150	3,4	(AF 66)
F, Na, Al, Si, S, K, Ca V, Cr, Mn, Fe, Co, Ni	0.5–32	1–70	1,2,3	(KC 72)
Fe	0.36, 0.7		3	(ME 68) (EM 69)
PB	0.4		3	(Far+ 65)

rise in the correlation coefficient F of Eq. (109) and took this as evidence for the existence of intermediate structure. However, no interpretation in terms of a doorway state was tried. An investigation of the existence of correlations among different reaction channels is now being carried out by them. Seth (Set 65) and Elwyn *et al.* (Elw+ 64) have found structure in the low-energy spectrum of the neutron cross section and have suggested the possibility that they are examples of true intermediate structure. No analysis was given and it would therefore be interesting to know what an investigation of the type performed by Carlson and Barschall would yield for these lower-energy measurements.

4. THEORETICAL FRAMEWORK FOR INTERMEDIATE RESONANCES

There exist several suitable formalisms of nuclear reactions which can serve as a framework for a description of intermediate structure and in general line-broadening. The various formalisms have been used by different groups, which Lane (Lan 69) has summarized as:

1. Mahaux and Weidenmuller (MW 67a, 67b). The authors employ the reaction theory of Weidenmuller (Wei 66), which is a schematic version of the "shell-model theory of reactions" due to Bloch (Blo 66) and Fano (Fan 61).
2. MacDonald and Mekjian (MM 67a). The reaction theory used is a hybrid of the shell model theory of Bloch (Blo 66) and the "effective interaction theory of reactions" of MacDonald (Mac 64, Mac 66).
3. Feshbach, Kerman, and Lemmer (FKL 67) and Kerman and De Toledo Piza (TK 67, TK 68). The authors use the channel projection theory of Feshbach (Fes 58, Fes 62).
4. Lane and Robson (LR 67). This is based on a theory of reactions due to Kapur and Peierls (KP 38) and to Wigner and Eisenbud (WE 47).

Here, we will discuss intermediate resonances in the framework of the second group. However, the expressions developed for the cross section are formally equivalent to those obtained in the other formalisms. The difference in the results of the various frameworks lies in the prescription for calculating the various quantities which appear in a description of the cross section. These differences arise because the underlying dynamical pictures which form the foundation of the nuclear reaction theories vary.

4.1. Shell-Model Theory of Nuclear Reactions

4.1.1. Simplified Discussion

We begin with a simplified discussion of the properties of the cross section in the vicinity of a doorway state. In developing an expression for the cross section, we will follow Dirac's (Dir 58) theory of resonances. Similar procedures have also been given by Rice (Ric 33), Van Kampen (Van 51), and Fano (Fan 61). Consider the model discussed in Section 2.1. This model can be used to describe the effect of a doorway state on the scattering amplitude when the discrete sum which appears in Eqs. (5) and (6) is replaced by a continuous integral, representing the surrounding

continuum states. In particular, for the wave function we write

$$| \psi_E\rangle = a_E \, | \phi_d\rangle + \int d\varepsilon b_\varepsilon \, | \psi_g \phi_{\varepsilon(1\gamma)}\rangle \tag{111}$$

Then, the solution to the time-independent Schrödinger equation $(H - E) \times | \psi_E\rangle = 0$ is obtained from a solution of the coupled equations

$$(E_d - E)a_E + \int d\varepsilon \varrho M b_\varepsilon = 0 \tag{112a}$$

$$M a_E + b_\varepsilon(\varepsilon - E) = 0 \tag{112b}$$

These are just Eqs. (6a) and (6b) with the discrete sum replaced by a continuous integral and with the energy of the state $| \phi_d\rangle$ taken as E_d. The M is the matrix element coupling the discrete state to the continuum and $\varrho = D^{-1}$, the level density of the continuum (the limit $M \to 0$, $\varrho \to \infty$, with $M^2\varrho$ finite is to be taken). Now, Dirac's solution to the last equation is

$$b_\varepsilon = \left[P \frac{1}{E - \varepsilon} + Z(E)\delta(E - \varepsilon) \right] M a_E \tag{113}$$

which replaces Eq. (7). Here P means principal value integral, while $\delta(E - \varepsilon)$ is the Dirac delta-function in the argument $E - \varepsilon$. The $Z(E)$ is a function which we seek to determine. In fact, substituting Eq. (113) into the first expression which appears in Eq. (112a) results in

$$(E_d - E) + M^2 P \int \frac{1}{E - \varepsilon} d\varepsilon + Z(E) M \varrho^2 = 0 \tag{114}$$

Now, the principal value integral vanishes identically and we thus obtain the following simple expression for $Z(E)$:

$$Z(E) = \frac{E - E_d}{M^2 \varrho} \tag{115}$$

The way in which the function $Z(E)$ relates to the cross section follows from the asymptotic form of Eq. (111) in coordinate space. The first part of $| \psi(E)\rangle$ vanishes in the asymptotic region since it represents a localized wavefunction. The second part of $| \psi_E\rangle$ has the asymptotic form $\sin k_E r$ in coordinate space. Substituting Eq. (113) into the expression for $| \psi_E\rangle$ of Eq. (111), and then taking the asymptotic limit in the coordinate representation, we obtain

$$\psi_E(r \to \infty) = a_E \int d\varepsilon M \left[P \frac{1}{E - \varepsilon} + Z(E)\delta(E - \varepsilon) \right] \sin k_\varepsilon r \tag{116}$$

Next, using the results

$$\int P \frac{1}{E-\varepsilon} \sin k_\varepsilon r \, d\varepsilon = \pi \cos k_E r$$
$$\int \delta(E-\varepsilon) \sin k_\varepsilon r \, d\varepsilon = \sin k_E r \tag{117}$$

we arrive at the expression

$$\psi_E(r \to \infty) \propto [\pi \cos k_E r + Z(E) \sin k_E r] = \sin[k_E r + \delta(E)] \tag{118}$$

The phase shift δ_E is then given by

$$\cot \delta(E) = \frac{Z(E)}{\pi} = \frac{E - E_d}{\pi M^2 \varrho} = \frac{E - E_d}{\frac{1}{2}\Gamma_d^{\uparrow}} \tag{119}$$

where $\Gamma_d^{\uparrow} = 2\pi M^2 \varrho$. Thus, at $E = E_d$, the phase shift $\delta(E)$ is $\pi/2$. The phase shift $\delta(E)$ therefore represents an isolated resonance of width $\Gamma_d^{\uparrow}$. The cross section is obtainable from the well-known expression

$$\sigma(E) = \frac{4\pi}{k^2} \sin^2 \delta(E) \tag{120}$$

At resonance, $\sigma(E)$ attains its maximum value $4\pi k^{-2}$.

We must supplement the above theory of a resonance reaction so as to incorporate into it fine structure. Specifically, we add to the above model, a group of states which are not coupled to the continuum channel, but are coupled to the discrete state $|\phi_d\rangle$. These additional states are just the hallway states in the Ferrell–MacDonald (FM 66) picture.

Inclusion of these additional states then leads to the following set of coupled equations which replace Eq. (112):

$$(E_d - E)a_E + \int b_\varepsilon M \, d\varepsilon + \sum a_q V_q = 0 \tag{120a}$$

$$-a_q(E - E_q) + V_q a_E = 0 \tag{120b}$$

$$b_\varepsilon(\varepsilon - E) + M a_E = 0 \tag{120c}$$

Here, a_q is the amplitude of an arbitrary hallway state in the state $|\psi_E\rangle$, while ε_q and V_q are the energy and coupling matrix element of the hallway-state function. We can next solve the simple Eq. (120b) to obtain

$$a_q = \frac{V_q a_E}{E - \varepsilon_q} \tag{121}$$

set of coupled equations:

$$\left(E_d + \sum_q \frac{V_q^2}{E - \varepsilon_q} - E\right)a_E + \int b_\varepsilon M \, d\varepsilon = 0 \tag{122a}$$

$$(\varepsilon - E)b_\varepsilon + Ma_E = 0 \tag{122b}$$

Now, these two equations are identical with the two coupled equations which we wrote at the beginning of this section, except that E_d has been replaced by $E_d + \sum V_q^2/(E - \varepsilon_q)$. That is, the energy of the doorway state E_d has acquired a self-energy part from the coupling of this state with the more complicated hallway states. Consequently, the rest of the preceding development can be carried through with only the modification that E_d is to be replaced by $E_d + \sum V_q^2/(E - \varepsilon_q)$. Therefore, the expression for the phase shift of Eq. (119) now reads

$$\cot \delta(E) = \frac{E - E_d - \sum_q [V_q^2/(E - \varepsilon_q)]}{\frac{1}{2}\Gamma_d^\uparrow} \tag{123}$$

while the expression for the cross section becomes

$$\sigma(E) = \frac{\pi k^{-2}(\Gamma_d^\uparrow)^2}{\{E - E_d - \sum_q [V_q^2/(E - \varepsilon_q)]\}^2 + \frac{1}{4}(\Gamma_d^\uparrow)^2} \tag{124}$$

From this expression for the cross section, we first note that the cross section vanishes at the hallway energies ε_q since the self-energy operator $\sum V_q^2/(E - \varepsilon_q)$ is infinite at these energies. Secondly, at the energies E_ν which are solutions to the equation

$$E_\nu - E_d - \sum_q \frac{V_q^2}{E_\nu - \varepsilon_q} = 0 \tag{125}$$

the cross section reaches its unitary maximum value of $4\pi k^{-2}$. Moreover, from Section 2.3, Eq. (125) is just the equation which gives the eigenenergies of the hallway–doorway system. The graphical solution of the above equation is shown in Fig. 1. Thus, the cross section attains its maximum value at the eigenenergies of the hallway–doorway system and vanishes in between each of these energies, and in particular at the unperturbed hallway energies. Returning to Eq. (123), we obtain for $\tan \delta(E)$ the expression

$$\tan \delta(E) = \frac{\frac{1}{2}\Gamma_d^\uparrow}{E - E_d - \sum [V_q^2/(E - \varepsilon_q)]} \tag{126}$$

Our next point is that the zeroes of the denominator of this equation are

the resonance energies so that tan $\delta(E)$ can also be written as

$$\tan \delta(E) = \sum_{\nu} \frac{\frac{1}{2}\Gamma_{\nu}}{E - E_{\nu}} \tag{127}$$

where E_{ν} is determined by Eq. (125). Furthermore, the widths Γ_{ν} are determined by $\Gamma_{\nu} = a^2_{E_{\nu}}\Gamma_d^{\uparrow}$, where $a^2_{E_{\nu}}$ is given in Eq. (3). In particular, in the picket-fence model of equally spaced levels ε_q and constant matrix elements $V_q = V$, the distribution of widths Γ_{ν} is a Lorentzian with a width given by $\Gamma_d^{\downarrow} = 2\pi\varrho V^2$

$$\Gamma_{\nu} = \frac{(D/2\pi)\Gamma_d^{\uparrow}\Gamma_d^{\downarrow}}{(E_{\nu} - E_d)^2 + (\Gamma_d^{\downarrow}/2)^2} \tag{128}$$

4.1.2. The Shell-Model K-Matrix

In the previous subsection we considered a simplified model in which potential scattering, many channel effects, and direct reactions or continuum–continuum couplings were neglected. We now extend the model to include these effects. Our discussion will be based on the shell-model approach to nuclear reactions in a K-matrix formalism. A connection with the results of the previous section will follow from the observation that the function $Z(E)$ of Eq. (113) is just the reciprocal of the elastic channel K-matrix.

In a shell-model approach the total Hamiltonian for an A-particle system is broken up into two parts, an independent-particle Hamiltonian H_0, which includes a one-body finite well potential, and a residual interaction part V, representing the difference between the true two-body interaction and the one-body potential: $H = H_0 + V$. The bound and continuum single-particle eigenfunctions of H_0 can be used to construct wave functions of the many-particle system. We restrict ourselves to a limited subspace of these wave functions and consider only states in which all A-particles are bound and states in which only one particle is in the continuum and the other $A - 1$ particles bound.

The most general wave function that can be obtained from this limited subspace is then

$$|\psi\rangle = \sum_{\alpha} |\alpha\rangle\langle\alpha|\psi\rangle + \sum_{\beta jl} \int d\varepsilon\, |\beta; jl\varepsilon\rangle\langle\beta; jl\varepsilon|\psi\rangle \tag{129}$$

where

$$\begin{aligned} \langle\vec{r}_1\vec{r}_2 \ldots \vec{r}_A | \alpha\rangle &= \mathscr{A}\prod_i^A U_{\alpha_i}(\vec{r}_i) \\ \langle\vec{r}_1\vec{r}_2 \ldots \vec{r}_A | \beta; jl\varepsilon\rangle &= \mathscr{A}\prod_i^{A-1} U_{\alpha_i}(r_i)U_{jl\varepsilon}(\vec{r}_A) \end{aligned} \tag{130}$$

The $\mathscr{A}$ is an antisymmetrization operator, the $U_{\alpha_i}(\vec{r}_i)$ are the bound-state eigenfunctions of the shell-model Hamiltonian, while the $U_{jl\varepsilon}(\vec{r}_A)$ are the continuum eigenfunctions of this Hamiltonian normalized to delta-functions in energy: $\langle jl\varepsilon \mid j'l'\varepsilon'\rangle = \delta_{jj'}\delta_{ll'}\delta(\varepsilon - \varepsilon')$.

The solution of $(H_0 + V) \mid \psi\rangle = E \mid \psi\rangle$ is found by inserting the above expression for $\mid \psi\rangle$ into this equation and obtaining a set of coupled equations for the expansion coefficients. Following a procedure similar to that of the previous section (details can be found in MM 69), the elements of the K-matrix can be found and are

$$K_{cc'}(\varepsilon_c) = \langle c\varepsilon_c \mid V_e \mid c'\varepsilon_c'\rangle + \langle c\varepsilon_c \mid V_e P_d (E - H_s)^{-1} P_d V_e \mid c'\varepsilon_c'\rangle \tag{131}$$

Here we have split K into resonant and nonresonant parts. The P_d projects onto discrete states of the A-particle system. The channel states $\mid c\varepsilon_c\rangle = \mid \bar{\beta}; jl\varepsilon_c\rangle$, where $\mid \bar{\beta}\rangle$ are core target states of the $(A - 1)$-nucleon system which diagonalize the residual interaction. The V_e is obtained as follows: If V is the residual interaction and V_c is that part coupling continua to discrete states and to continua, then we define

$$V_e' = V_c + V_c(E - H_0 - V_r)^{-1} P_c V_e' \tag{132}$$

where V_r is that part of V coupling discrete states of $A - 1$ particles. The $V_e = V_e' + V_d$, with V_d that part of V coupling discrete states to discrete states. The $V = V_c + V_d$ and the $H_s = H_0 + P_d V_e P_d + V_r$.

The S-matrix is related to the K-matrix through the usual relation

$$S_{cc'} = e^{i\delta_c}[(1 + i\pi K)(1 - i\pi K)^{-1}]_{cc'} e^{i\delta_{c'}} \tag{133}$$

where δ_c is the potential phase shift of the single-particle continuum state for the shell-model central potential U.

4.1.3. Fine Structure

a. One Doorway–Hallway System. We define a doorway–hallway model by the following coupling matrix elements:

$$\begin{aligned}
\langle h_p \mid H_s \mid h_q\rangle &= \varepsilon_q \delta_{pq} \\
\langle h_p \mid V_e \mid c, \varepsilon\rangle &= 0 \\
\langle d \mid V_e \mid d\rangle &= E_d \\
\langle h_q \mid V_e \mid d\rangle &= V_q \\
\langle d \mid V_e \mid c\varepsilon_c\rangle &= (\Gamma^{\uparrow}_{d,c}/2\pi)^{1/2}
\end{aligned} \tag{134}$$

Then the resonant part of the K-matrix

$$K^R_{cc'} = \langle c\varepsilon_c \mid V_e P_d (E - H_s)^{-1} P_d V_e \mid c'\varepsilon_c' \rangle$$

is

$$\pi K^R_{cc'} = \frac{\Gamma^{1/2}_{d,c}\Gamma^{1/2}_{d,c'}/2}{E - E_d - \sum [V_q^2/(E - \varepsilon_q)]} \tag{135}$$

The S-matrix in the one-open-channel case is

$$S_{cc} = e^{2i\delta_c} \frac{E - E_d - \sum [V_q^2/(E - \varepsilon_q)] - \frac{1}{2}i\Gamma^{\uparrow}_{d,c}}{E - E_d - \sum [V_q^2/(E - \varepsilon_q)] + \frac{1}{2}i\Gamma^{\uparrow}_{d,c}} \tag{136}$$

From this equation a resonant phase shift δ_r can be defined and is

$$\tan \delta_r = \frac{\Gamma^{\uparrow}_{d,c}/2}{E - E_d - \sum [V_q^2/(E - \varepsilon_q)]} \tag{137}$$

The self-energy operator $\sum V_q^2/(E - \varepsilon_q)$ is a rapidly varying function of energy and produced rapid oscillations or fine structure in the cross section. If the matrix H_s is diagonalized on the discrete states, i.e.,

$$\begin{aligned} \mid \psi_\lambda \rangle &= \mid d \rangle \langle d \mid \psi_\lambda \rangle + \sum_q \mid h_q \rangle \langle h_q \mid \psi_\lambda \rangle \\ \langle \psi_\mu \mid H_s \mid \psi_\lambda \rangle &= E_\mu \delta_{\mu\lambda} \end{aligned} \tag{138}$$

then the K-matrix is also of the form

$$\pi K^R_{cc}(E) = \tfrac{1}{2} \sum_\lambda \frac{\Gamma_{\lambda c}}{E - E_\lambda} \tag{139}$$

which leads to an S-matrix of the form

$$S_{cc} = e^{2i\delta_c} \frac{1 - \frac{1}{2}i \sum_\lambda [\Gamma_{\lambda c}/(E - E_\lambda)]}{1 + \frac{1}{2}i \sum_\lambda [\Gamma_{\lambda c}/(E - E_\lambda)]} \tag{140}$$

For nonoverlapping levels λ we have

$$S_{cc} = e^{2i\delta_c}\left[1 - i \sum_\lambda \frac{\Gamma_{\lambda c}}{E - E_\lambda + (i/2)\Gamma_{\lambda c}}\right] \tag{141}$$

The

$$\Gamma_{\lambda c} = \langle c\varepsilon_c \mid \psi_\lambda \rangle^2 = \langle d \mid \psi_\lambda \rangle^2 \langle c\varepsilon_c \mid d \rangle^2$$

where the amplitudes $\langle d \mid \psi_\lambda \rangle^2$ are obtained from

$$\langle d \mid \psi_\lambda \rangle^2 = \frac{1}{1 + \sum_q V_q^2/(E_\lambda - \varepsilon_q)^2} \tag{142}$$

We note the following connections among the quantities:

$$\Gamma_{dc}^{\uparrow} = \sum \Gamma_{\nu c} \tag{143a}$$

$$E_\nu - E_d - \sum_q \frac{V_q^2}{E_\nu - \varepsilon_q} = 0 \tag{143b}$$

$$E_d + \sum_q \varepsilon_q = \sum_\nu E_\nu \tag{143c}$$

$$\sum_\nu \frac{\Gamma_{\nu c}}{\varepsilon_q - E_\nu} = 0 \tag{143d}$$

$$V_q^2 = \frac{\Gamma_{dc}^{\uparrow}}{\sum_\nu [\Gamma_{\nu c}/(E_\nu - \varepsilon_q)^2]} \tag{143e}$$

The first result follows from $\sum_\nu \langle d \mid \psi_\nu \rangle^2 = 1$; the second expression is just the eigenvalue equation; the third equation is obtained from the fact that the trace of H is invariant under orthogonal transformations; the fourth equality follows from equating the two equivalent expressions of the K-matrix and evaluating the resulting equation at $E = \varepsilon_q$; and the final formula is obtained by taking an energy derivative of the K-matrix and evaluating the resulting equation at $E = \varepsilon_q$. These expressions can be used to obtain the unperturbed quantities E_d, $\Gamma_{d,c}^{\uparrow}$ and the ε_q's and V_q's from the experimentally determined quantities—the E_ν's and $\Gamma_{\nu c}$'s.

b. Any Number of Doorways and Hallways. It is convenient to divide the matrix elements of H_s into a block corresponding to the doorway states, a block corresponding to the hallway states, and a block corresponding to the coupling between the doorway and hallway states:

$$H_s = \begin{bmatrix} D & H_{DH}^* \\ H_{DH} & H \end{bmatrix} \tag{144}$$

The resonant K-matrix is then

$$K_{cc'}^R = \sum_{i,j} \frac{\langle c\varepsilon_c \mid V_e \mid d_i \rangle M_{ji} \langle d_j \mid V_e \mid c'\varepsilon_c' \rangle}{\det(E - H_s)} \tag{145}$$

The M_{ij} is the cofactor of $(E - H_s)_{ij}$ in the matrix $E - H_s$. Again, if H_s is diagonalized on the set of doorway and hallway states, i.e.,

$$\begin{gathered} \mid \psi_\lambda \rangle = \sum_i \mid d_i \rangle \langle d_i \mid \psi_\lambda \rangle + \sum_q \mid h_q \rangle \langle h_q \mid \psi_\lambda \rangle \\ \langle \psi_\lambda \mid H_s \mid \psi_\mu \rangle = E_\lambda \delta_{\lambda\mu} \end{gathered} \tag{146}$$

the resonant K-matrix takes on the simpler form

$$\pi K_{cc'}^{R} = \tfrac{1}{2} \sum_{\lambda} \frac{\Gamma_{\lambda c}^{1/2} \Gamma_{\lambda c'}^{1/2}}{E - E_{\lambda}} \tag{147}$$

where

$$\Gamma_{\lambda c}^{1/2} = (2\pi)^{1/2} \sum_{j} \langle dj \mid \psi_{\lambda} \rangle^{*} \langle dj \mid V_{e} \mid c\varepsilon_{c} \rangle \tag{148}$$

4.2. Theory of Average Cross Sections

Having obtained an expression for the cross section for the scattering of a beam with infinite resolution, we now turn our attention to the averaged cross section. The averaged cross section is of interest because of the effect of finite energy resolution in determining the structure observed.

Consider a beam of particles with average energy E, having a spread in energies about this energy of width I. Let $\varrho_I(E, E')$ be the probability of finding particles with energy E' for the beam with average energy E and spread I. We define the average cross section to be

$$\sigma_I(E) = \int \varrho_I(E, E') \sigma_{I=0}(E')\, dE' \tag{149}$$

where $\sigma_{I=0}$ is the cross section with infinite resolution. This expression relates the cross section $\sigma_I(E)$ to the sum of the infinite resolution cross sections weighted by the factor $\varrho_I(E, E')$, the probability of finding the energy E' in the beam.

Two representations of ϱ used theoretically are the "box" weighting function,

$$\varrho_I(E, E') = \frac{1}{I} \begin{cases} 1 & \mid E - E' \mid \leq \tfrac{1}{2} I \\ 0 & \mid E - E' \mid > \tfrac{1}{2} I \end{cases} \tag{150}$$

and the Lorentzian weighting function,

$$\varrho_I(E, E') = \frac{I}{2\pi} \frac{1}{(E - E')^2 + I^2/4} \tag{151}$$

From Eqs. (149) and (150), we see that the "box" averaged cross section gives the mean value of the cross section over the interval I about the energy E. Now, narrow resonance levels will have smaller mean values than wider resonance levels for identical points on the associated Lorentzian curves

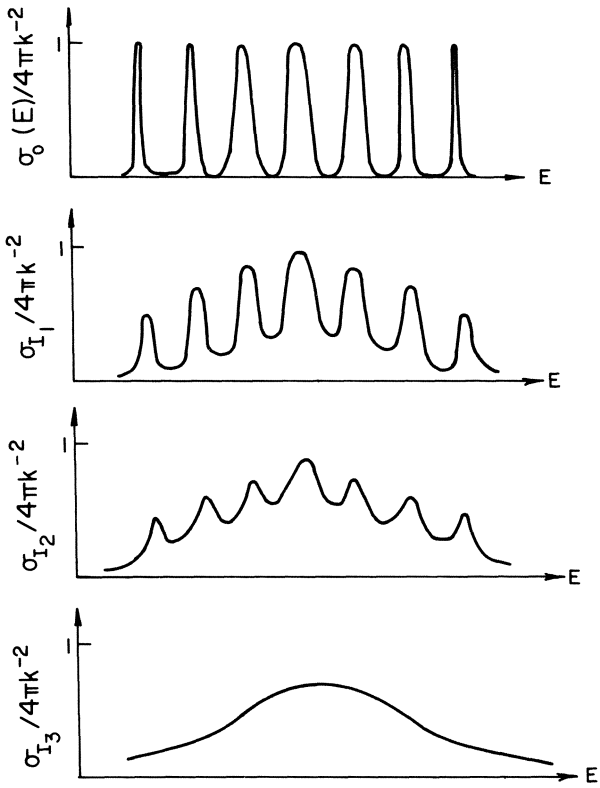

Fig. 22. Effect of averaging on the cross section for increasing values of the averaging interval. The infinite resolution cross section is given by σ_0. The averaged cross sections by σ_I, with $I_1 < I_2 < I_3$.

describing these resonances. In turn, this means that the height of the cross-sectional curve is suppressed for narrow resonances as compared to wider resonances. In infinite resolution, the maximum heights, apart from the factor $4\pi k^{-2}$ would be the same. In Fig. 22 we illustrate the effect of averaging for increasing values of I.

As we have already seen, the width of the fine structure of a one-doorway–hallway system is determined by the width of the doorway state into the continuum and the spreading width of this state into the compound nucleus. Since the height of the averaged cross section is determined by the underlying width of the fine structure and since the height of the averaged cross section as a function of energy determines the width of the averaged cross section, this width is therefore determined by the width of the doorway state into the continuum and into the compound nucleus. We thus expect

the width of the averaged cross section to be given by the relationship

$$\Gamma_d^{\downarrow} + \Gamma_d^{\uparrow} = \Gamma_d \tag{152}$$

We will now derive this result.

The average cross section is obtained by averaging $|1 - S|^2$ over an energy interval I which is greater than the hallway spacing but less than the width of the doorway state. Here, the S is the elastic channel S-matrix which is related to the phase shift defined in Eq. (123) by $S = \exp 2i\delta$. Now, from the unitarity of S for one channel, we have

$$\langle |1 - S|^2 \rangle = 2(1 - \text{Real}\langle S \rangle) \tag{153}$$

Next, since the poles of S lie in the lower half of the complex plane, an average of S for the Lorentzian weighting function can be found by an evaluation of the S-matrix at the complex energy $E + iI/2$

$$\langle S(E) \rangle = S\left(E + i\frac{I}{2}\right) \tag{154}$$

Our next observation is that the S-matrix can be written in terms of $\tan\delta$ as

$$S(E) = \frac{1 + i\tan\delta}{1 - i\tan\delta} \tag{155}$$

For the one-doorway–hallway system, $\tan\delta$ is given by

$$\tan\delta = \frac{\frac{1}{2}\Gamma_d^{\uparrow}}{E - E_d - \sum_q [V_q^2/(E - \varepsilon_q)]} \tag{156}$$

Evaluating this at the complex energy $E + iI/2$, we obtain

$$\langle \tan\delta \rangle = \frac{\frac{1}{2}\Gamma^{\uparrow}}{E - E_d + iI/2 - \sum [V_q^2/(E - \varepsilon_q + iI/2)]} \tag{157}$$

Then, using the equation

$$\sum \frac{V_q^2}{E - \varepsilon_q + iI/2} = \Delta_d - i\frac{\Gamma_d^{\downarrow}}{2} \tag{158}$$

we arrive at an expression for the averaged S-matrix element

$$\langle S(E) \rangle = \frac{E - E_d' - \frac{1}{2}i(\Gamma_d^{\uparrow} - \Gamma_d^{\downarrow} - I)}{E - E_d' + \frac{1}{2}i(\Gamma_d^{\uparrow} + \Gamma_d^{\downarrow} + I)} \tag{159}$$

where $E_d' = E_d + \Delta_d$. Also, the averaged cross section is given by

$$\sigma_I(E) = \frac{\Gamma_d^{\uparrow}(\Gamma_d + I)}{(E - E_d')^2 + \frac{1}{4}(\Gamma_d + I)^2} \frac{\pi}{k^2} \tag{160}$$

with $\Gamma_d = \Gamma_d^{\uparrow} + \Gamma_d^{\downarrow}$. At $E = E_d'$ the value of the cross section is

$$\sigma_I(E_d') = \frac{4\pi}{k_{E_d'}^2} \frac{\Gamma_d^{\uparrow}}{\Gamma_d + I} \tag{161}$$

Thus, the effect of the spreading width $\Gamma_d^{\downarrow}$ is to reduce the maximum cross section at the resonance energy and to increase the width. The effect of $\Gamma_d^{\downarrow}$ on the elastic scattering is precisely the same as if another channel had opened. Furthermore, we can write the total elastic scattering cross section as a sum of two incoherent parts. One part corresponds to shape elastic scattering and is given by

$$\sigma_{\text{S.E.}} = \frac{\pi}{k^2} \mid 1 - \langle S \rangle \mid^2 = \frac{\pi}{k^2} \frac{\Gamma_d^{\uparrow}\Gamma_d^{\uparrow}}{(E - E_d')^2 + \frac{1}{4}(\Gamma_d + I)^2} \tag{162}$$

while the second part corresponds to a compound elastic term and is given by

$$\sigma_{\text{C.E.}} = \frac{\pi}{k^2} (1 - \mid \langle S \rangle \mid^2) = \frac{\pi}{k^2} \frac{\Gamma_d^{\uparrow}(\Gamma_d^{\downarrow} + I)}{(E - E_d')^2 + \frac{1}{4}(\Gamma_d + I)^2} \tag{163}$$

The total elastic cross section is $\sigma = \sigma_{\text{C.E.}} + \sigma_{\text{S.E.}}$. These expressions suggest the interpretation of $\Gamma_d^{\downarrow}$ as the width to another channel.

The physical meaning of the division into compound elastic and shape elastic contributions has been given by Freidman and Weisskopf (FW 55). Consider a beam of particles prepared in an interval of time τ and, thus, having an uncertainty in energy $\hbar/\tau = I$ about a mean energy E. This beam of particles corresponds to a wave train of length $\langle v \rangle \tau$, where $\langle v \rangle = \sqrt{2E/m}$. The front part of this wave train will initiate reactions which can interfere with the rest of the wave train if the width of the states excited corresponds to a lifetime $\tau_R = \hbar/\Gamma$ which is less than the preparation interval $\tau = \hbar/I$. On the other hand, for those states with lifetimes longer than $\hbar/I$, the wave train will have passed by the time particles will be admitted from these states and no interference with the wave train will result. Thus, the shape elastic part corresponds to those particles which will be admitted from the nucleus within a period $\hbar/I$ after the arrival of the incident wave train. In contrast, the compound elastic part corresponds to particles emitted after the time interval $\hbar/I$; these particles spend more time inside the nucleus. We illustrate these remarks in Fig. 23.

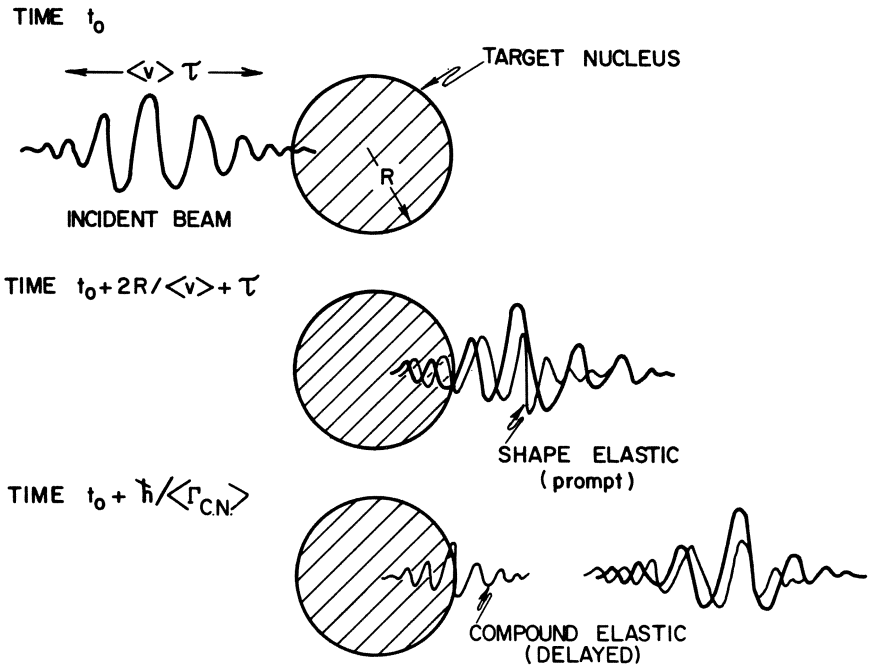

Fig. 23. Time sequence of a scattering process.

In the hallway–doorway picture we have been discussing, the incident beam can only excite the nucleus through the doorway state. For $\Gamma_d^{\uparrow} > I$, those particles which leave immediately through the doorway without decaying into the compound nucleus will give rise to shape elastic scattering. It is for this reason that the product $\Gamma_d^{\uparrow}\Gamma_d^{\uparrow}$ appears in the numerator of Eq. (162). Similarly, those particles which enter through the doorway and decay to the hallway states spend more time in the nucleus. Hence, they appear in the compound elastic term.

5. SUMMARY

The appearance of doorway states in neutron elastic scattering experiments has been far from a universal property of nuclei. The presence of intermediate structure in such experiments is quite widespread, but its interpretation in terms of doorway states is not conclusive, the structure being interpretable in terms of fluctuations of level spacings and level widths. In contrast, the presence of intermediate structure in the high-

resolution subthreshold fission cross section for neutrons has been convincingly interpreted in terms of the doorway-state picture. Intermediate structure has also been observed in photonuclear reactions and in proton-induced reactions. In the former, the dipole states act as doorway states while in the latter, the analog states do. Within the analog and dipole resonance, structure has also been observed which is not the ultimate fine structure of the compound nucleus. Intermediate structure in the expanding area of heavy-ion research (which we have not discussed here) has also been noted (MV 72). Thus, there exists a wealth of evidence for intermediate structure, some of which is evidence for the existence of doorway states. Such evidence must lead to a modification of the statistical theories of nuclear spectra so as to incorporate the accumulation of transition probabilities.

The doorway-state concept has also been a fruitful idea from a theoretical point of view. Its applications have accounted for the fluctuations of the optical-model strength function, for the properties of the distribution of enhanced fine-structure widths of isobaric analog resonances, for partial width correlations of different reaction channels, and for the high-energy tail in neutron evaporation spectra.

REFERENCES

Ada 54 R. K. Adair, *Phys. Rev.* **94**:737 (1954).

AF 66 J. C. Albergotti and J. M. Ferguson, *Nucl. Phys.* **82**:652 (1966).

All+ 64 R. G. Allas, S. S. Hanna, L. Meyer-Schützmeister, R. E. Segel, P. P. Singh, and Z. Vager, *Phys. Rev. Letters* **13**:628 (1964).

All+ 73 B. J. Allen, R. L. Macklin, C. Y. Fu, and R. R. Winters, to be published.

Ama+ 35 E. Amaldi, O. D'Agostina, E. Fermi, B. Pontecorvo, F. Rasetti, and E. Segre, *Proc. Roy. Soc. London* **A149**:522 (1935).

And+ 69 J. D. Anderson, S. D. Bloom, J. Cerny, and W. W. True (eds), *Nuclear Isospin*, Academic Press, New York (1969).

AP 63 A. Agodi and G. Pappalardo, *Nucl. Phys.* **47**:129 (1963).

Bar 52 H. H. Barschall, *Phys. Rev.* **86**:431 (1952).

Bar 69 G. A. Bartholomew, in: *Neutron Capture Gamma Ray Spectroscopy*, Proc. Studsvik Symposium, August 1969, I.A.E.A., Vienna (1969).

Bar+ 67 G. A. Nartholomew, E. C. Earle, A. J. Ferguson, and I. Berggviot, *Phys. Letters.* **B24**:47 (1967).

BB 59 M. Bolsterli and G. E. Brown, *Phys. Rev. Letters* **3**:472 (1959).

BBB 71 R. J. Baglan, C. D. Bowman, and B. L. Berman, *Phys. Rev.* **C3**:2475 (1971).

BD 57 G. E. Brown and C. T. deDominicus, *Proc. Phys. Soc. London* **A70**, 668, 681, (1957).

BD 70 W. P. Beres and M. Divadeenam, *Phys. Rev. Letters* **25**:596 (1970).

Ber+ 70 J. C. Bergstrom, W. Bertozzi, S. Kowalski, X. K. Maruyama, J. W. Lightbody, Jr., S. P. Firozinsky, and S. Penner, *Phys. Rev. Letters.* **24**:152 (1970).

Ber 71 G. Bertsch, *Phys. Letters* **37B**:470 (1971).

Bet 35 H. A. Bethe, *Phys. Rev.* **47**:747 (1935).

BEF 55 K. A. Brueckner, R. J. Eden, and N. C. Francis, *Phys. Rev.* **99**:76 (1955).

BF 63 B. Block and H. Feshbach, *Ann. Phys.* **23**:47 (1963).

BH 35 G. Beck and L. H. Horsley, *Phys. Rev.* **47**:510 (1935).

BL 55 K. A. Brueckner and C. A. Levinson, *Phys. Rev.* **97**:1344 (1955).

Blo 57a C. Bloch, *Nucl. Phys.* **3**:137 (1957).

Blo 57b C. Bloch, *Nucl. Phys.* **4**:503 (1957).

BL 64 B. Block and A. Lande, *Phys. Rev. Letters* **12**:344 (1964).

Blo 66 C. Bloch, in: *Proceedings of the International School of Physics, Enrico Fermi, VXXXVI* (C. Bloch, ed.), Academic Press, New York and London (1966).

Bla 68 M. Blann, *Phys. Rev. Letters* **21**:1357 (1968).

BLM 54 K. A. Brueckner, C. A. Levinson, and H. M. Mahmoud, *Phys. Rev.* **95**:217 (1954).

BNL 64 Brookhaven National Laboratory, Sigma Center, *Compilation of Neutron Cross Sections, BNL* 325, (1964).

Boh 36 N. Bohr, *Nature* **137**:344 (1936).

Boh 37 N. Bohr, *Science* **86**:161 (1937).

Bow+ 70 C. D. Bowman, R. J. Baglan, B. L. Berman, and T. W. Phillips, *Phys. Rev. Letters* **25**:1302 (1970).

BP 58 S. Blumberg and C. E. Porter, *Phys. Rev.* **110**:786 (1958).

Bre 65 W. Brenig, in: *Advances in Theoretical Physics*, Vol. 1 (K. A. Breuckner, ed.), Academic Press, New York and London (1965).

Bru 55 K. A. Brueckner, *Phys. Rev.* **100**:36 (1955).

Bro 64 G. E. Brown, *Unified Theory of Nuclear Models*, North-Holland Publishing Company, Amsterdam (1964).

Bro+ 68 J. C. Browne, G. A. Keyworth, D. P. Lindstrom, J. D. Moses, H. W. Newson, E. G. Bilpuch, and P. Wilhjelm, *Phys. Letters* **28B**:26 (1968).

Bro+ 69 J. C. Browne, D. P. Lindstrom, J. D. Moses, N. W. Newson, E. G. Bilpuch, and G. E. Mitchell, in: *Nuclear Isospin* (J. D. Anderson, S. D. Bloom, J. Cerny, and W. W. True, eds.), Academic Press, New York and London (1969).

BS 62 I. Bergqvist and N. Starfelt, *Nucl. Phys.* **39**:529 (1962).

BS 64 C. Bloch and J. P. Schiffer, *Phys. Letters* **12**:22 (1964).

BV 66 B. Bošnjaković and C. VanDerLeun, *Phys. Letters* **23**:687 (1966).

BW 35 T. Bjerge and C. H. Westcott, *Proc. Roy. Soc.* **A150**:709 (1935).

BW 36 G. Breit and E. P. Wigner, *Phys. Rev.*, **49**:519 (1936).

BW 66 J. M. Blatt and V. F. Weisskopf, *Theoretical Nuclear Physics*, John Wiley and Sons, Inc., New York (1966).

Cam+ 60 E. J. Campbell, H. Feshbach, C. E. Porter, and V. F. Weisskopf, Mass. Inst. Technol. Lab. Nucl. Sci., Tech. Rept. No. 73 1960 (unpublished).

Cal+ 62 G. Calvi, R. Potenza, R. Ricamo, and D. Vinciguerra, *Nucl. Phys.* **39**:621 (1962).

Cal+ 63 G. Calvi, R. Ricamo, A. Rubbino, and D. Zubke, *Nucl. Phys.* **48**:408 (1963).

Cal+ 63 J. T. Caldwell, R. R. Harvey, R. L. Bramblett, and S. C. Fultz, *Phys. Letters* **6**:213 (1963).

CB 67 A. D. Carlson and H. H. Barschall, *Phys. Rev.* **158**:1142 (1967).

CB 71 C. K. Cline and M. Blann, *Nucl. Phys.* **A172**:225 (1971).

Chr 69 R. E. Chrien, in: *Neutron Capture Gamma Ray Spectroscopy*, Proc. Studsvik Symposium, August 1969, I.A.E.A., Vienna (1969).

Chr 72a R. E. Chrien, in: *Statistical Properties of Nuclei* (J. B. Garg, ed.), Plenum Press, New York and London (1972).

Chr 72b R. E. Chrien, Lectures for the *International School on Nuclear Structure*, Alushta (Crimea), U.S.S.R. April 13-28, 1972.

CLR 65 C. F. Clement, A. M. Lane, J. R. Rook, *Nucl. Phys.* **66**:273 and 293 (1965).

Col+ 62 L. Colli, U. Facchini, I. Iori, G. M. Morcazzan, M. Milazzo, and F. Tonolini, *Phys. Letters* **1**:120 (1962).

CPR 60 P. Cuzzocrea, G. Pappalardo, and R. Ricamo, *Nuovo Cim.* **16**:450 (1960).

Cuz+ 60 P. Cuzzocrea, S. Notarrigo, R. Ricamo, and F. Vince, *Nuovo Cim.* **18**:671 (1960).

CV 55 E. Clementel and C. Villi, *Nuovo Cim.* **2**:176 (1955).

Dav 72 A. M. Davidson, *Nucl. Phys.* **A180**:208 (1972).

DB 62 W. R. Dodge and W. C. Barber, *Phys. Rev.* **127**:1746 (1962).

DB 72 M. Divadeenam and W. P. Beres, in: *Statistical Properties of Nuclei* (J. B. Garg, ed.), Plenum Press, New York and London (1972).

DF 65 M. Danos and E. G. Fuller, in: *Annual Review of Nuclear Science*, Vol. 15 (E. Segre, ed.) Annual Reviews, Inc. California (1965).

DG 65 M. Danos and W. Greiner, *Phys. Rev.* **138**:B876 (1965).

DHL 72 C. B. Dover, F. J. W. Hahne, and R. H. Lemmer, *Ann. Phys.* **70**:458 (1972).

Dir 58 P.A.M. Dirac, *The Principles of Quantum Mechanics* (4th ed.), Clarendon Press, Oxford and New York (1958).

DRH 64 P. J. Daly, J. R. Rook, and P. E. Hodgson, *Nucl. Phys.* **56**:331 (1964).

Dub 59 D. F. Dubois, *Ann. Phys.* **8**:24 (1959).

Elw+ 64 A. J. Elwyn, J. E. Monahan, R. O. Lane, and A. Langsdorf, Jr., *Nucl. Phys.* **59**:113 (1964).

Elw+ 65 A. J. Elwyn, J. E. Monahan, R. O. Lane, and F. P. Morring, Argonne National Laboratory Summer Report, ANL **7081**:24 (1965).

EM 69 A. J. Elwyn and J. E. Monahan, *Nucl. Phys.* **A123**:33 (1969).

Eri 60 T. Ericson, *Phys. Rev. Letters* **5**:430 (1960).

Eri 63 T. Ericson, *Ann. Phys.* **23**:390 (1963).

FA 35 E. Fermi and E. Amaldi, *Ric. Science* **A6**:544 (1935).

Fan 61 U. Fano, *Phys. Rev.* **124**:1866 (1961).

Far+ 65 J. A. Farell, G. J. Kyker, Dr., E. G. Bilpuch, and H. W. Newson, *Phys. Letters* **17**:286 (1965).

FA 71 S. Fallieros, in: *Statistical Properties of Nuclei* (J. B. Garg, ed.) Plenum Press, New York and London (1972).

FB 50 K. W. Ford and D. Bohm, *Phys. Rev.* **79**:745 (1950).

Fes 58 H. Feshbach, *Ann. Phys.* **5**:357 (1958).

Fes 62 H. Feshbach, *Ann. Phys.* **19**:287 (1962).

Fes 67 H. Feshbach, *Comments on Nuclear and Particle Physics* **1**:40 (1967).

Fes 71 H. Feshbach, *Bull. Am. Phys. Soc.*, HA3 Washington Meeting (April 1971) p. 591.

Fer+ 34 E. Fermi, E. Amaldi, B. Pontecorvo, F. Rasetti, E. Segré, *Ric. Science* **5**:282 (1934).

FF 65 S. Fallieros and R. Ferrell, *Phys. Rev.* **138**:B582 (1965).

FK 68 H. Feshbach and A. K. Kerman, *Comments on Nuclear and Particle Physics* **2**:125 (1968).

FKL 67 H. Feshbach, A. K. Kerman, and R. Lemmer, *Ann. Phys.* **41**:230 (1967).

FM 66 R. A. Ferrell and W. M. MacDonald, *Phys. Rev. Letters* **16**:187 (1966).
FP 36 O. R. Frisch and G. Placzek, *Nature* **137**:357 (1936).
FPW 47 H. Feshbach, D. C. Peaslee, and V. F. Weisskopf, *Phys. Rev.* **71**:145 (1947).
FPW 53 H. Feshbach, C. E. Porter, and V. F. Weisskopf, *Phys. Rev.* **90**:166 (1953).
FPW 54 H. Feshbach, C. Porter, and F. V. Weisskopf, *Phys. Rev.* **96**:448 (1954).
FR 63 *Isobaric Spin in Nuclear Physics* (J. D. Fox and D. Robson, eds.), Academic Press, New York (1963).
FST 49 S. Fernbach, R. Serber, and T. B. Taylor, *Phys. Rev.* **75**:1352 (1949).
Ful+ 64 R. H. Fulmer, A. L. McCarthy, B. L. Cohen, and R. Middleton, *Phys. Rev.* **133**:B955 (1964).
Fub+ 68 A. Fubini, J. Blons, A. Michaudon, and D. Paya, *Phys. Rev. Letters* **20**:1373 (1968).
FW 49 H. Feshbach and V. F. Weisskopf, *Phys. Rev.* **76**:1550 (1949).
FW 53 N. C. Francis and K. M. Watson, *Am. J. Phys.* **21**:659 (1953).
FW 55 F. L. Friedman and V. F. Weisskopf, in: *Niels Bohr and the Development of Physics*, Pergamon Press, London (1955).
GC 65 A. Gilbert and A. G. W. Cameron, *Can. J. Phys.* **43**:1446 (1965).
GD 57 L. V. Groshev and A. M. Demidov, *Atomaya Energy* **3**:91 (1957).
GK 56 V. Glaser and G. Källén, *Nucl. Phys.* **2**:706 (1956).
GKN 68 C. Gaarde, K. Kemp, and T. Nielsen, *Nucl. Phys.* **A118**:641 (1968).
GMR 67 V. Gillet, M. A. Melkanoff, and J. Raynal, *Nucl. Phys.* **A97**:631 (1967).
Gol 48 M. Goldberger, *Phys. Rev.* **74**:1269 (1948).
Gri 66 J. J. Griffin, *Phys. Rev. Letters* **17**:478 (1966).
GT 48 M. Goldhaber and E. Teller, *Phys. Rev.* **74**:1046 (1948).
GWW 58 L. C. Gomes, G. D. Walecka, and V. F. Weisskopf, *Ann. Phys.* **3**:241 (1958).
Gug 51 P. C. Gugelot, *Phys. Rev.* **81**:51 (1951).
HB 63 C. Holbrow and H. Barschall, *Nucl. Phys.* **42**:264 (1963).
IE 64 H. Ikegami and G. T. Emery, *Phys. Rev. Letters* **13**:26 (1964).
KB 54 B. B. Kinsey and G. A. Bartholomew, *Phys. Rev.* **93**:1260 (1954).
Key+ 66a G. A. Keyworth, G. C. Kyker, Jr., E. G. Bilpuch, and H. W. Newson, *Phys. Letters* **20**:281 (1966).
Key+ 66b G. A. Keyworth, G. C. Kyker, Jr., E. G. Bilpuch, and H. W. Newson, *Nucl. Phys.* **89**:590 (1966).
KC 72 D. Kopsch and S. Cierjacks, in: *Statistical Properties of Nuclei* (J. B. Garg, ed.), Plenum Press, New York and London (1972), p. 455.
KF 70 E. I. Kao and S. Fallieros, *Phys. Rev. Letters* **25**:827 (1970).
KHB 61 E. Kashy, A. M. Hoogenboom, and W. N. Buechner, *Phys. Rev.* **124**:1917 (1961).
KP 38 P. L. Kapur and R. E. Peierls, *Proc. Roy Soc. (London)* **A116**:277 (1938).
KRY 68 A. K. Kerman, L. Rodberg, and J. E. Young, *Phys. Rev. Letters* **11**:422 (1968).
JK 69 J. P. Jeukenne and C. Mahaux, *Nucl. Phys.* **A136**:49 (1969).
JT 72 H. E. Jackson and R. E. Toohey, *Phys. Rev. Letters* **29**:379 (1972).
JS 71 H. E. Jackson and E. N. Strait, *Phys. Rev. Letters* **27**:1654 (1971).
Law 53 J. D. Lawson, *Phil. Mag.* **44**:106 (1953).
Lan 68 A. Lande, in: *Intermediate Structure in Nuclear Reactions* (Hugh P. Kennedy and R. Schrils, eds.), University of Kentucky Press, Lexington, Kentucky (1968).
Lan 69 A. M. Lane, in: *Isospin in Nuclear Physics* (D. H. Wilkinson, ed.), North-

Lan 71 A. M. Lane, *Ann. Phys.* **63**:171 (1971).
Lon+ 68 M. A. Lone, R. E. Chrien, O. A. Wasson, M. Beer, M. R. Bhat, and H. R. Muether, *Phys. Rev.* **174**:1512 (1968).
Lan+ 59 A. M. Lane, J. E. Lynn, E. Melkonian, and E. R. Rae, *Phys. Rev. Letters* **2**:424 (1959).
LB 64 A. Lande and B. Block, *Phys. Rev. Letters* **12**:334 (1964).
LB 66 A. Lande and G. E. Brown, *Nucl. Phys.* **75**:344 (1966).
LC 60 D. W. Lang and K. J. Le Couteur, *Nucl. Phys.* **14**:21 (1960).
Lev 49 N. Levinson, *Kgl. Danske Videnskab. Selskab, Mat.-Fys. Medd* **25**, No. 9 (1949).
Lee 54 T. D. Lee, *Phys. Rev.* **95**:1329 (1954).
Lev 60 J. S. Levinger, *Nuclear Photo-Disintegration*, Oxford University Press, London and New York (1960).
LL 59 A. M. Lane and J. E. Lynn, *Nucl. Phys.* **11**:646 (1959).
LM 67 A. Lejeune and C. Mahaux, *Z. Phys.* **207**:35 (1967).
LR 67 A. M. Lane and D. Robson, *Phys. Rev.* **161**:982 (1967).
LS 62a A. M. Lane and J. M. Soper, *Nucl. Phys.* **37**:506 (1962).
LS 62b A. M. Lane and J. M. Soper, *Nucl. Phys.* **37**:663 (1962).
LS 64 R. H. Lemmer and C. M. Shakin, *Ann. Phys.* **27**:13 (1964).
LT 58 A. M. Lane and R. G. Thomas, *Rev. Mod. Phys.* **30**:257 (1958).
LT 68 G. H. Lenz and G. M. Temmer, *Nucl. Phys.* **A112**:625 (1968).
LTW 55 A. M. Lane, R. G. Thomas, and E. P. Wigner, *Phys. Rev.* **98**:693 (1955).
LV 55 A. M. Lane and L. Verlet, *Phys. Rev.* **100**:956 (1955).
LW 55 A. M. Lane and C. F. Wandel, *Phys. Rev.* **98**:693 (1955).
Lyn 68 E. Lynn, *Theory of Neutron Resonance Reactions*, Oxford University Press, London and New York (1968).
Mac 64 W. M. MacDonald, *Nucl. Phys.* **54**:393 (1964).
Man 65 F. Manero, *Nucl. Phys.* **65**:419 (1965).
Mac 66 W. M. MacDonald, *Nucl. Phys.* **56**:636 (1966).
McV 67 K. M. McVoy, *Ann. Phys.* **43**:91 (1967).
Mel 67 P. A. Mello, *Ann. Phys.* **45**:240 (1967).
ME 68 J. E. Monahan and A. J. Elwyn, *Phys. Rev. Letters* **20**:1119 (1968).
Mek 70 A. Z. Mekjian, *Phys. Rev. Letters* **25**:888 (1970).
Mic 73 A. Michaudon, in: *Advances in Nuclear Physics*, Vol. 6 (M. Baranger and E. Vogt, eds.), Plenum Press, New York (1973).
Mil+ 52 D. W. Miller, R. K. Adair, C. K. Bockelman, S. E. Darden, *Phys. Rev.* **88**: 83 (1952).
MM 50 N. F. Mott and H. S. Massey, *Theory of Atomic Collisions*, Clarendon Press, Oxford (1950), 2nd ed., p. 206.
MM 67a W. M. MacDonald and A. Z. Mekjian, *Phys. Rev.* **160**:730 (1967).
MM 67b A. Z. Mekjian and W. M. MacDonald, *Phys. Rev. Letters* **18**:706 (1967).
MM 68 A. Z. Mekjian and W. M. MacDonald, *Nucl. Phys.* **A121**:385 (1968).
MMM 55 G. C. Morrison, H. Muirhead and P. A. B. Murdock, *Phil. Mag.* **46**:795 (1955).
Mor 53 P. Morrison, in: *Experimental Nuclear Physics*, Vol. 2. (E. Segre, ed.), John Wiley and Sons, Inc., New York (1953).
Mor 55 H. Morinaga, *Phys. Rev.* **97**:444 (1955).
Mor. 67a G. Morrison, in: *Nuclear Research with Low Energy Accelerators* (J. B. Marion and D. M. Van Patter, eds.), Academic Press, New York and London (1967).

Mol 67b P. A. Moldauer, *Phys. Rev. Letters* **18**:249 (1967).
MT 35 P. B. Moon and J. R. Tillman, *Nature* **135**:904 (1935).
MT 68 E. Migneco and J. P. Theobald, *Nucl. Phys.* **A112**:603 (1968).
MV 72 G. J. Michaud and E. W. Vogt, *Phys. Rev.* **5C**:350 (1972).
MW 67a C. Mahaux and H. A. Weidenmuller, *Nucl. Phys.* **A91**:241 (1967).
MW 67b C. Mahaux and H. A. Weidenmuller, *Nucl. Phys.* **A94**:1 (1967).
MW 69 C. Mahaux and H. A. Weidenmuller, *Shell-Model Approach to Nuclear Reactions*, North-Holland, Amsterdam (1969).
New 56 T. D. Newton, *Can. J. Phys.* **34**:804 (1956).
New 66 H. W. Newson, in: *Nuclear Structure Studies with Neutrons* (M. N. de Mevergies, P. Von Assche, and J. Vervier, eds.), North Holland, Amsterdam (1966).
Nil 55 S. G. Nilsson, *K. Danske Vidensk. Selsk. Mat.-fys. Medd.* **29**:No. 16 (1955).
Pap 64 G. Pappalardo, *Phys. Letters* **13**:320 (1964).
Pay 68 G. L. Payne, *Phys. Rev.* **174**:1227 (1968).
PE 35 F. Perrin and W. M. Elasser, *Phys. Radium* **6**:194 (1935).
Pet 62 J. H. Peterson, *Phys. Rev.* **125**:955 (1962).
Pin 63 D. Pines, *Elementary Excitations in Solids*, C. Benjamin, New York (1963).
Por 65 C. E. Porter, Introduction in: *Statistical Theories of Spectra: Fluctuations* (C. E. Porter, ed.), Academic Press, New York (1965).
PT 56 C. E. Porter and R. G. Thomas, *Phys. Rev.* **104**:483 (1956).
Ram 21 C. Ramsauer, *Ann. Phys.* **66**:546 (1921).
Ric 33 O. K. Rice, *J. Chem. Phys.* **1**:375 (1935).
Ric+ 64 P. Richard, C. F. Moore, D. Robson, and J. D. Fox, *Phys. Rev. Letetrs* **13**: 343 (1964).
Rim+ 69 K. Rimawi, R. E. Chrien, J. B. Garg, M. R. Bhat, D. I. Garber, and O. A. Wasson, *Phys. Rev. Letters* **23**:1041 (1969).
Rob 65 D. Robson, *Phys. Rev.* **137B**:535 (1965).
Rob+ 65 D. Robson, J. F. Fox, P. Richard, and C. F. Moore, *Phys. Letters* **18**:86 (1965).
Rod 61 L. Rodberg, *Phys. Rev.* **124**:210 (1961).
Rod 68 L. S. Rodberg, in: *Intermediate Structure in Nuclear Reactions* (H. P. Kennedy and R. Schrils, eds.), University of Kentucky Press, Lexington, Kentucky (1968).
Sau+ 66 J. Saudinos, G. Vallois, O. Beer, M. Gendrot, and P. Lopato, *Phys. Letters* **22**:492 (1966).
Ser 47 R. Serber, *Phys. Rev.* **72**:1114 (1947).
Set 65 K. K. Seth, *Phys. Letters* **16**:306 (1965).
Seg+ 67 R. E. Segel, Z. Vager, L. Meyer-Schützmeister, P. P. Singh, and R. G. Allas, *Nucl. Phys.* **A93**:31 (1967).
SHD 67 P. A. Seeger, A. Hemmendinger, and B. C. Diven, *Nucl. Phys.* **A96**:605 (1967).
SHL 66 P. P. Singh, P. Hoffman-Pinther, and D. W. Lang, *Phys. Letters* **23**:255 (1966).
Sin+ 65 P. P. Singh, R. E. Segel, L. Meyer-Schützmeister, S. S. Hanna, and R. G. Allas, *Nucl. Phys.* **65**:577 (1965).
Spi 69 B. M. Spicer, in: *Advances in Nuclear Physics*, Vol. 2 (M. Baranger and E. Vogt, eds.), Plenum Press, New York (1969).
Ste 57 R. M. Sternheimer, *Phys. Rev.* **106**:1027 (1957).
Str 67 V. M. Strutinsky, *Nucl. Phys.* **A95**:420 (1967).
Sug 60 A. Sugie, *Phys. Rev. Letters* **4**:286 (1960).

Masses, Vienna, 1963 (W. H. Johnson, ed.), Springer-Verlag, Vienna and New York (1964).
SW 71 C. M. Shakin and W. L. Wang, *Phys. Rev. Letters* **26**:902 (1971).
Tei 51 T. Teichman, *Phys. Rev.* **77**:506 (1951).
Tem+ 71 G. M. Temmer, M. Maruyama, D. W. Mingay, M. Petrascu, and R. Van Bree, *Phys. Rev. Letters* **26**:1341 (1971).
TF 66 E. Teranishi and B. Furubayashi, in: *Isobaric Spin in Nuclear Physics* (J. D. Fox and D. Robson, eds.), Academic Press, New York and London (1966).
Tho 55 R. G. Thomas, *Phys. Rev.* **97**:224 (1955).
Tho 72 B. W. Thomas, in: *Statistical Properties of Nuclei* (J. B. Garg, ed.), Plenum Press, New York and London (1972).
TK 67 A. F. R. deToledo Piza and A. K. Kerman, *Ann. Phys.* **43**:363 (1967).
TK 68 A. F. R. deToledo Piza and A. K. Kerman, *Ann. Phys.* **48**:173 (1968).
Tol+ 66 A. F. R. deToledo Piza, A. K. Kerman, S. Fallieros, and R. H. Venter, *Nucl. Phys.* **89**:369 (1966).
TT 63 K. Tsudada and O. Tanaka, *J. Phys. Soc. Japan* **18**:610 (1963).
Van 51 N. V. Van Kampen, *K. Danske Videnskab. Selskab, Mat.-Fys. Medd.* **26**: No. 15 (1951).
VL 57 E. Vogt and J. Lascoux, *Phys. Rev.* **107**:1028 (1957).
Vog 55 E. Vogt, *Phys. Rev.* **100**:957 (1955).
Vog. 56 E. Vogt, *Phys. Rev.* **101**:1792 (1956).
WB 54 M. Walt and H. H. Barschall, *Phys. Rev.* **93**:1062 (1954).
WBB 65 R. Wood, R. Borchers, and H. Barschall, *Nucl. Phys.* **71**:529 (1965).
WC 70 O. A. Wasson and R. E. Chrien, *Phys. Rev.* **2**:675 (1970).
Wei 37 V. F. Weisskopf, *Phys. Rev.* **52**:295 (1937).
WE 47 E. P. Wigner and L. Eisenbud, *Phys. Rev.* **72**:29 (1947).
Wei 61 V. F. Weisskopf, *Physics Today* **14**:18 (1961).
Wei 66 H. A. Weidenmuller, *Nucl. Phys.* **75**:189 (1966).
Wei 68 H. Weigmann, *Z. Phys.* **214**:7 (1968).
Wig 37 E. P. Wigner, *Phys. Rev.* **51**:947 (1937).
Wig 55a E. P. Wigner, *Phys. Rev.* **98**:145 (1955).
Wig 55b E. P. Wigner, *Ann. Math.* **62**:548 (1955).
Wig 56a E. P. Wigner, *Proceedings Conference on Neutron Physics by Time-of-Flight*, Gattinburg, Tennessee, 1956; ORNL-2309 Report (1956).
Wig 63 E. P. Wigner, in: *Isobaric Spin in Nuclear Physics* (J. D. Fox and D. Robson, eds.), Academic Press, New York (1963).
Wil 56 D. H. Wilkinson, *Phil Mag.* **1**:379 (1956).
Wil 69 *Isospin in Nuclear Physics* (D. H. Wilkinson, ed.), North Holland, Amsterdam (1969).
Wil+ 69 P. Wilhjelm, G. A. Keyworth, J. C. Browne, W. P. Beres, M. Divadeenam, H. W. Newson, and E. G. Bilpuch, *Phys. Rev.* **177**:1553 (1969).
Wil+ 70 N. Williams, G. C. Morrison, J. A. Nolen, Jr., Z. Vager, and D. von Ehrenstein, *Phys. Rev.* **2c**:1539 (1970).
Won 70 C. Y. Wong, *Phys. Letters* **32B**:668 (1970).
WS 54 R. D. Woods and D. S. Saxon, *Phys. Rev.* **95**:577 (1954).
WS 68 H. Weigmann and H. Schmidt, *J. Nucl. Energy* **22**:317 (1968).
WW 30a V. Weisskopf and E. P. Wigner, *Z. Phys.* **63**:54 (1930).
WW 30b V. Weisskopf and E. P. Wigner, *Z. Phys.* **65**:18 (1930).

Chapter 2

COULOMB MIXING EFFECTS IN NUCLEI: A SURVEY BASED ON SUM RULES

A. M. Lane

Atomic Energy Research Establishment
Harwell, Berkshire, U. K.

and

A. Z. Mekjian

Physics Department, Rutgers University
New Brunswick, New Jersey, U.S.A.

ABSTRACT

We set up a systematic approach to Coulomb mixing based on two simplifications: (1) the two-body Coulomb force is replaced by the effective one-body force which is essentially the charge monopole operator, (2) the mixing effects of this operator are evaluated in terms of two sum rules of this operator. These yield the mean-square amplitude and mean energy of the charge monopole mode of oscillation. Contributions of different admixed isospins can be separated. Evaluations are made with two models, the shell model and an improved model taking two-body correlations into account. For the latter, we find it very useful to proceed by analogy with the well-known charge dipole problem. The bulk of the article is concerned with comparing experiment and theory for the different observed aspects of Coulomb mixing. An analysis is also made of the most complete calculation available of an analog state. Generally experiment and theory are

in accord, especially when the correlated model is used. When sum-rule evaluations are made with the shell model, no explanation is found of the Nolen–Schiffer anomaly; rather the opposite, viz., a large second-order shift (−2 MeV for ^{208}Pb) is found which *reduces* the estimated Coulomb displacement. However, when correlation effects are included, not only is this second-order shift less, but one finds evidence that correlations may increase the first-order term. These two effects are in the right direction but probably insufficient in magnitude to explain the anomaly.

1. INTRODUCTION

Coulomb mixing in nuclei has many different manifestations:

a. Isospin impurities[1–10] in low-lying nuclear states ($T = T_3$).
b. Departures from the simple isobaric relationship between wave functions of members of an isospin multiplet. These show themselves in changes of *ft*-values for the corresponding superallowed Fermi transitions.[1,8,11,12]
c. Modifications to the isobaric mass formula which gives the *relative* values of Coulomb shifts between members of a multiplet.[13–19] In the absence of mixing (i.e., of second-order Coulomb effects) this formula cuts off at T_3^2:

$$E(T, T_3) = a + bT_3 + cT_3^2$$

d. Second-order contributions[20–24] to the Coulomb displacement energy of an analog from its parent state. The evaluation of the leading (first-order) term from the observed proton density has recently been the subject of much discussion.[20–31] Before comparing with observed shifts, one needs estimates of the second-order corrections.
e. Spreading widths of analog states.[5,7,32–40]
f. Isospin impurities of analog states ($T = T_3 + 1$).[41–43]

These six items are characterized by the fact that they involve a single nuclear state or multiplet. This means that theoretical analysis involves diagonal matrix elements. In contrast, other items (transition probabilities), involve two states, so their discussion is more difficult, involving off-diagonal matrix elements.[44,45] There are several types of transitions:

g. Transitions involving initial and final states with $T = \pm T_3$ (i.e., their impurities are those of (a) above). These include: (1) $E1$ transitions between $T = 0$ states of nuclei with $T_3 = 0$; Fermi transitions.[46] Both of these are forbidden, so their occurrence reflects isospin mixing.

(2) Gamow–Teller mirror transitions,[47,48,49] especially ($T = 1, T_3 = \pm 1$) $\rightarrow$ ($T = 0$) and ($T = \frac{3}{2}, T_3 = \pm\frac{3}{2}$) $\rightarrow$ ($T = \frac{1}{2}$). In the absence of mixing, these are allowed and ft values for different T_3 are equal. Coulomb mixing makes them unequal. Unlike (1), this is an amplitude effect.

h. Transitions involving at least one state with $T = T_3 + 1$ (analog state). These include: (1) Neutron, deuteron, alpha transitions from $T = T_3 + 1$ compound states and proton transitions from $T = T_3 + 2$ compound states. For final low-lying states, these are all forbidden so their occurrence reflects mixing. This applies whether the analog state is "discrete" (as in light nuclei[50–53]) or "dissolved" (for heavier nuclei). In the latter case, recently reported studies include transitions of all types: ^{210}Po ($T = 23$) $\rightarrow$ ^{209}Bi$+p$ (see Miller[54]), ^{93}Nb ($T = 13/2$) $\rightarrow$ ^{92}Nb$+n$, ^{93}Nb ($T = 13/2$) $\rightarrow$ ^{89}Y$+\alpha$ (see Richter[55]), ^{209}Bi ($T = 45/2$) $\rightarrow d +$ ^{207}Pb (see Hambuger[56]). (2) Nucleon transitions[57–59] from ($T = 1$; $T_3 = 1, 0, -1$) states. These are simply related in the absence of mixing. Mixing causes changes in the relations. Unlike (1), this is an amplitude effect.

The present work is directed both at improving understanding of the separate items, and giving a unified view of the field as a whole. This requires a systematic approach in which we avoid consideration of special features and foibles of individual nuclear states, but concentrate on exposing general effects and trends.

This is more readily achieved if we use the effective one-body Coulomb force rather than the actual two-body force. These two are generally held to be almost equivalent, at least if used in conjunction with shell-model wave functions. We will indeed verify this, but we add a word of caution: the use of shell-model wave functions may tend to suppress the specifically two-body (e.g., isotensor $\Delta T = 2$) aspects of the Coulomb force, so that their effects may be more significant than this model suggests. Wave-function components of nonshell-model type (e.g., alpha clusters) may have rather different properties. With this reservation, we follow the conventional view that the two-body potential is adequately simulated by the one-body effective potential, $C = \sum_i (\frac{1}{2} - t_{3i}) V_c(r_i)$. In turn, the potential $V_c(r)$ is well-represented by the form, $a_0 - a_1 r^2$ for a given nucleus. For many purposes, the scalar part of the force is irrelevant since, by definition, it cannot give charge-dependent effects like isospin mixing. This leaves us with the vector part: $C_v = -\sum_i t_{3i}(a_0 - a_1 r_i^2)$ the essential part of which we recognize as the charge monopole operator: $\sum_i t_{3i} r_i^2$. Thus we see (as has been pointed out often before,[2,3,5,6] that, to a large extent, the problem

of Coulomb mixing in nuclei is equivalent to that of determining the parameters of the nuclear charge monopole mode of oscillation. This recognition leads to the second simplification to achieve our purpose of a systematic treatment, viz., we will use sum rules to estimate the parameters of the charge monopole mode in parallel to the familiar treatments of the charge dipole mode. In obvious notation, if we define

$$M = \sum_{n \neq 0} \langle n \mid C_v \mid 0 \rangle^2 = \langle 0 \mid C_v^2 \mid 0 \rangle^2 - \langle 0 \mid C_v \mid 0 \rangle^2$$

$$N = \sum_n (E_n - E_0) \langle n \mid C_v \mid 0 \rangle^2 = \tfrac{1}{2} \langle 0 \mid [C_v, [H, C_v]] \mid 0 \rangle$$

then the mean energy $\bar{E}$ of the mode is N/M. These sum rules can be separated into the three contributions of the different isospins of states n. Of the resulting six quantities, some are relatively model-independent and easy to evaluate. Others are more difficult; for these, we find great help in referring to the parallel charge dipole problem. Once the six quantities are evaluated, the sum-rule method enables one to predict all of the observed aspects of Coulomb mixing and to compare with the data.

The sum-rule method amounts to approximating the quantity $\sum_n \langle n \mid C_v \mid 0 \rangle^2 / (E_n - E_0)^p$ by M^{p+1}/N^p. For the second-order energy displacement $p = 1$; for the ground-state impurity admixture $p = 2$. For these low values of p, the method is reliable provided that the "line-shape" of the charge monopole mode is a single peak reasonably confined around its mean energy $\bar{E}$. Actually split peaks, or a main peak with outliers can be dealt with by extensions of the method if these are each confined in width and separated. The dipole case, where the line-shape (a single peak) is directly observed, is known to be accurately treated by the sum-rule method.

We prefer to use the sum-rule method rather than alternative ones (such as the hydrodynamical model[3] because we will need to bring out details like the charge-exchange contribution to N and to treat nuclei with $N \neq Z$. This is more satisfactorily done with the sum-rule method. [Recently a limited study[5] appeared using the method for M with shell-model wave functions, and applying it to items (a), (e), (f).]

In Section 2, we describe the sum-rule method, while Section 3 gives the details of the calculation of the six sum-rule quantities, both with the shell and correlated models. Sections 4 through 9 apply the results of the method to items (a) through (f) while Section 10 summarizes the successes and failures of the approach in explaining observed facts.

Besides attempting to understand the observed Coulomb mixing, we also give some attention to understanding the results of a theoretical cal-

culation[60] in which Coulomb forces are included, viz., the recent ambitious calculation of the properties of the analog of ^{208}Pb as revealed in ^{207}Pb $+ p$ scattering. This provides a very useful check on the methods and ideas that we use for observed Coulomb mixing.

We do not discuss the transition data, items (g) and (h), because, as mentioned above, these depend much more critically on details of the states involved, and so are not amenable to the systematic sum-rule approach.

2. SUM-RULE APPROACH TO COULOMB MIXING

In subsequent sections, various observed manifestations of isospin mixing due to Coulomb forces will be discussed. Our analysis of such data is based on three assumptions.

1. The two-body Coulomb force:

$$\mathscr{C} \equiv \tfrac{1}{2}\sum_{i,j} (\tfrac{1}{2} - t_{3i})(\tfrac{1}{2} - t_{3j}) \frac{e^2}{r_{ij}}$$

(with $i \neq j$) can be replaced by an effective one-body force

$$C \equiv \sum_i (\tfrac{1}{2} - t_{3i}) V_c(r_i)$$

where the radial factor $V_c(r_i)$ is a suitably chosen average in the nuclear state of interest:

$$V_c(r_i) \equiv \left\langle \sum_{j(\neq i)} (\tfrac{1}{2} - t_{3i}) \frac{e^2}{r_{ij}} \right\rangle$$

and which, ideally, takes space-exchange into account. One can see directly that this replacement is not to be used without qualification since even the diagonal values, $\langle \mathscr{C} \rangle$ and $\langle C \rangle$, are not equal ($\langle C \rangle \approx 2\langle \mathscr{C} \rangle$). However, this fault arises from the isoscalar parts of $\mathscr{C}$ and C, while the isospin mixing effects with which we are mostly concerned arise from the other parts. If we expand into terms of isoscalar, vector, and tensor parts,

$$\mathscr{C} = \mathscr{C}_s + \mathscr{C}_v + \mathscr{C}_t$$

$$C = C_s + C_v'$$

then our assumption is that $(\mathscr{C}_v + \mathscr{C}_t)$ can be replaced by C_v'. We will discuss this assumption further in Appendix 1.

2. *The radial factor $V_c(r_i)$ is to a good approximation quadratic in r_i^2:*

$$V_c(r_i) = a_0 - a_1 r_i^2$$

The constant term may be removed in the discussion of any given state $|\phi_0\rangle$ by working with

$$C_v \equiv -\sum_i t_{3i}(V_c(r_i) - \hat{V}_c)$$

where

$$\hat{V}_c \equiv \frac{1}{T_3}\langle\phi_0 \mid C_v' \mid \phi_0\rangle$$

and guarantees that $\langle\phi_0 \mid C_v \mid \phi_0\rangle = 0$. With the quadratic approximation

$$C_v = a_1 \sum_i t_{3i}\left(r_i^2 - \frac{1}{T_3}\langle\sum t_{3i} r_i^2\rangle\right)$$

The accuracy of the quadratic approximation and the evaluation of a_1 is discussed in Appendix 1.

3. *The charge monopole vibration of ϕ_0, viz.,*

$$|m\rangle \equiv \frac{C_v \mid \phi_0\rangle}{\langle\phi_0 \mid C_v^2 \mid \phi_0\rangle^{1/2}}$$

is reasonably localized in energy. More specifically, let us define the strength function for the spreading of the charge monopole state into eigenstates λ of the charge-independent Hamiltonian H (including the isoscalar $\mathscr{E}_s$):

$$s(E) \equiv [\langle\lambda \mid m\rangle^2]_E \varrho_\lambda(E)$$

where

$$H \mid \lambda\rangle = E_\lambda \mid \lambda\rangle$$

The square brackets signify average over states λ with E_λ near E, and $\varrho_\lambda(E)$ is their density. Generally,

$$s(E) = \frac{(1/2\pi)\Gamma}{(\bar{E} + \Delta - E)^2 + \frac{1}{4}\Gamma^2}$$

where

$$\bar{E} = \langle m \mid H \mid m\rangle$$

$$\Gamma(E) = 2\pi[\langle n \mid H \mid m\rangle^2]_E \varrho_n(E)$$

$$\Delta(E) = -P\int \frac{(1/2\pi)\Gamma(E')}{E' - E}\, dE$$

and $|n\rangle$ are eigenstates of QHQ, where $Q \equiv 1 - |m\rangle\langle m|$. A strength function satisfies

$$\int s(E)\, dE = 1$$

$$\int Es(E)\, dE = \bar{E}$$

The present assumption is that $s(E)$ is peaked at about $E = \bar{E}$ with a reasonably small width. The significance of this can be appreciated by anticipating the experimental quantities met in subsequent sections. These are like

$$\sum_\lambda \frac{\langle\lambda \mid C_v \mid \phi_0\rangle^2}{E_\lambda - E_0} = M \int \frac{s(E')}{E' - E_0}\, dE'$$

$$\sum_\lambda \frac{\langle\lambda \mid C_v \mid \phi_0\rangle^2}{(E_\lambda - E_0)^2} = M \int \frac{s(E')}{(E' - E_0)^2}\, dE'$$

$$\sum_\lambda \langle\lambda \mid C_v \mid \phi_0\rangle^2 \delta(E_\lambda - E_0) = Ms(E_0)$$

where

$$M \equiv \langle\phi_0 \mid C_v^2 \mid \phi_0\rangle$$

If the assumption is met so that $\Gamma < (\bar{E} - E_0)$ then these can be evaluated as $M/\bar{E}$, $M/\bar{E}^2$, and $M\Gamma/2\pi\bar{E}^2$. To evaluate the first two quantities requires values of $\bar{E}$ and M. We can obtain $\bar{E}$ by standard procedures for the energy of a collective state like $|m\rangle$ (e.g., Tamm–Dancoff diagonalization). If a shell-model wave function is used for ϕ_0, then M can be evaluated directly. If we wish to do better, however, the simplest method is to use

$$M = \frac{N}{\bar{E}}$$

where N is the energy-weighted sum

$$N \equiv \sum_\lambda (E_\lambda - E_0)\langle\lambda \mid C_v \mid \phi_0\rangle^2$$

$$= \tfrac{1}{2}\langle\phi_0 \mid [C_v[H, C_v]] \mid \phi_0\rangle$$

We can write $N = N(K) + N(U)$, where $H = K + U$ is the split of H into kinetic and potential terms. $N(K)$ is easily evaluated. Now the point is that the evaluation of M as $N/\bar{E}$ leads to an expression for M correct to first order in correlations U when $N(U)$ is evaluated with the shell-model state for ϕ_0. This important result has been proved in detail[61] for the charge dipole problem, and applies equally to the present monopole case. It means that the above quantities are evaluated as $N/\bar{E}^2$, $N/\bar{E}^3$, and $N\Gamma/2\pi\bar{E}^3$.

As an immediate generalization of the present assumption, we see that we can include cases where $s(E)$ has several peaks, provided that each of these is localized separately, and that the N and $\bar{E}$ quantities for the separate peaks can be evaluated. We will see below that the two or three classes of states λ of different isospin have different peaks; also we will see that the so-called "configuration states" form an outlying peak of the main peak in analog mixing.

In the absence of direct observation of $s(E)$, we cannot justify assumption (3) from data, but rather by analogy with the dipole case (where the peak is observed and the condition is satisfied very well), and also by reference to the situation of the oscillator shell model, where $s(E)$ is entirely localized at $(\bar{E} - E_0) = 2\hbar\omega$. Correlation effects will disperse $s(E)$ somewhat, but it seems reasonable that the dispersal will stop short of violating the assumption $\Gamma < (\bar{E} - E_0)$. In any case within our theory which is first-order in correlations, assumption (3) is unnecessary since the spreading of the peak is a second-order effect. Put otherwise, even if one knows the spreading width of state $|\, m\rangle$, one must ignore any effects from it in a consistent first-order treatment (Appendix 2).

3. EVALUATION OF SUM-RULE QUANTITIES FOR SEPARATE ISOSPINS

We can directly generalize the definition of the M and N sum rules to separate isospins $T' = (T-1), T, (T+1)$, where T is the isospin of $\phi_0 \equiv \phi_0(T, T_3)$:

$$M(T') = \sum_{\lambda(T')} \langle \lambda \mid C_v \mid \phi_0 \rangle^2$$

$$N(T') = \sum_{\lambda(T')} (E_\lambda - E_0) \langle \lambda \mid C_v \mid \phi_0 \rangle^2$$

These quantities, which depend on the T_3-value of ϕ_0, can be expressed in terms of reduced counterparts $M(\| T' \|)$ with no T_3-dependence:

$$M(T') = C^2(TT_3; 10 \mid T'T_3) M(\| T' \|)$$

and similarly for $N(T')$. Exactly as in the dipole problem,[61,62] we can now write these

$$M(\| T-1 \|) = \langle C_v^2 \rangle + \frac{T+1}{T}(M_1 - M_2) + 2\left(\frac{2T+1}{2T-1}\right) M_2$$

$$M(\| T \|) = \langle C_v^2 \rangle + \frac{1}{T}(M_1 - M_2)$$

$$M(\| T+1 \|) = \langle C_v^2 \rangle - (M_1 - M_2)$$

Also,

$$M \equiv \sum_{T'} M(T') = \langle C_v^2 \rangle + \frac{2(T^2 - T_3^2)}{T(2T-1)} M_2$$

Brackets $\langle\ \rangle$ without wave function indicate expectation value taken in the parent state, viz., $\phi_0(T, T_3) = \phi_0(T, T)$. The new quantities, M_1, M_2 are from the isovector and tensor parts of the operator $\mathbf{C}_v \times \mathbf{C}_v$:

$$M_1 \equiv -\sqrt{\tfrac{1}{2}} \langle (\mathbf{C}_v \times \mathbf{C}_v)_1 \rangle$$

$$M_2 \equiv -3\sqrt{\tfrac{1}{6}} \langle (\mathbf{C}_v \times \mathbf{C}_v)_2 \rangle$$

The corresponding isoscalar M_0,

$$M_0 \equiv -\sqrt{\tfrac{1}{3}} \langle (\mathbf{C}_v \times \mathbf{C}_v)_0 \rangle$$

is such that

$$\langle C_v^2 \rangle = M_0 - \tfrac{2}{3} M_2$$

The merit of these quantities is that they separate the relatively model-independent quantities, viz., those depending on one-body operators from those depending on two-body operators. M_0, M_2 are in the latter class while M_1 is in the former:

$$M_1 = \tfrac{1}{2} \left\langle \sum_i t_{3i} (V_c(r_i) - \hat{V}_c)^2 \right\rangle$$

$$= \frac{a_1^2}{4} \left[N\langle r^4 \rangle_N - Z\langle r^4 \rangle_P - \frac{(N\langle r^2 \rangle_N - Z\langle r^2 \rangle_P)^2}{N - Z} \right]$$

where $\langle\ \rangle_N$, $\langle\ \rangle_P$ signifies average over the neutron and proton densities.

Referring back to the equations for $M(T')$, $M(\| T' \|)$, and M, exactly similar relations apply to the N sum-rule quantities if $\mathbf{C}_v \times \mathbf{C}_v$ is replaced by $\tfrac{1}{2}[\mathbf{C}_v \times [H, \mathbf{C}_v]]$. In this case, on writing each of N_0, N_1, N_2 as a sum of kinetic and potential terms, we find that the model-independent ones are

$$N_0(K) = \frac{\hbar^2}{8m} \left\langle \sum_i (\nabla_i V_c)^2 \right\rangle$$

$$= \frac{\hbar^2 a_1^2 A}{2m} \langle r^2 \rangle$$

$$N_2(K) = 0$$

where $\langle\ \rangle$ signifies average over nucleon density. We also find the relation

$$N_2(U) = \frac{N-Z}{A} N_1(U)$$

In the following, we first evaluate the various model-dependent quantities with the oscillator shell model (without charge-exchange forces so $N(U) = 0$). Then we consider the effect of two-body correlations.

3.1. Oscillator Shell Model

As in the dipole problem, we can easily make evaluations for the oscillator shell model by exploiting the fact that, for most nuclear states of interest, $C_v \mid \phi_0\rangle$ contains only excitations whose energy relative to ϕ_0 is $2\hbar\omega$. Exceptions are the "configuration states" at zero energy when ϕ_0 is an analog. These account for a tiny part of $\langle C_v^2\rangle$ (see Sec. 9) and we ignore them here; then

$$N(\| T' \|, K) = 2\hbar\omega M(\| T' \|)$$

or, equivalently,

$$N_{\mathscr{T}}(K) = 2\hbar\omega M_{\mathscr{T}}$$

with $\mathscr{T} = 0, 1, 2$. Thus the quantities M_0, M_2, N_1 depending on two-body operators can be obtained from the known quantities M_1, $N_0(K)$, $N_2(K)$:

$$M_0 = \tfrac{1}{4} a_1^2 A b^2 \langle r^2\rangle$$

$$M_2 = 0$$

$$N_1(K) = (2\hbar\omega) M_1$$

where b is the oscillator size parameter; $\hbar^2/mb^2 = \hbar\omega$. Table I lists various relevant quantities for three representative nuclei ^{40}Ca, ^{90}Zr, ^{208}Pb. The quantity a_1 is evaluated as $(Z-1)e^2/2R^3$, the form appropriate to a uniform charge distribution inside radius R; then R^2 is taken as $(5/3)\langle r^2\rangle_P$. Appendix 1 indicates that self-consistency gives an increase in a_1^2 of 20%, at least for nuclei with $A \lesssim 50$; this is reproduced here if R is reduced by 0.15f.

3.2. Shell Model with Correlations

We have noted in Section 2 that, when correlations are present, the value of $\bar{E}$ obtained by a Tamm–Dancoff diagonalization is correct to first order in the correlations, while $N(K)$ is independent of correlations, and $N(U)$ is automatically correct to first order. Thus, when generalizing beyond

TABLE I

Evaluation of Sum-Rule Quantities with the Oscillator Shell Model

The entries are based on equal neutron and proton wells. Although this restriction implies $\langle r^2\rangle_N > \langle r^2\rangle_P$ for heavy nuclei conflicting with experimental evidence, it is needed to guarantee the isospin purity of the unmixed states, demanded by the present analysis. The entries for a_1^2 are obtained as $[(Z-1)e^2/2R^3]^2$ with $R = [(5/3)\langle r^2\rangle_P]^{1/2} - 0.15f$ (see text). Note that $M_0 = \langle C_v^2\rangle$ in shell-model evaluations like here.

	^{40}Ca	^{90}Zr	^{208}Pb
$\langle r^2\rangle_N/b^2$	3	41/10	693/126
$\langle r^2\rangle_P/b^2$	3	15/4	393/82
$\langle r^2\rangle/b^2$	3	71/18	1086/208
$\langle r^4\rangle_N/b^4$	—	91/4	10185/252
$\langle r^4\rangle_P/b^4$	—	39/2	5055/164
$M_0/\langle r^2\rangle_P{}^2a_1{}^2$	10/3	6.2	11.8
$M_1/\langle r^2\rangle_P{}^2a_1{}^2$	0	0.96	5.60
$N_0(K)\Big/\dfrac{\hbar^2}{m}\langle r^2\rangle_P a_1{}^2$	20	47	113
$N_1(K)\Big/\dfrac{\hbar^2}{m}\langle r^2\rangle_P a_1{}^2$	0	7.35	54.4
$a_1{}^2\langle r^2\rangle_P{}^3$ (in MeV$^2\cdot f^2$)	50	208	830
$\langle r^2\rangle_P^{1/2}$ (observed, in f)	3.53	4.2	5.52

the shell model, the natural quantities to use are $\bar{E}$ and N. The quantity M, if it is needed, can be obtained from $M = N/\bar{E}$. All of these remarks apply to the separate isospins, as well as to combined isospins.

3.3. Specification of $\bar{E}(T')$

In principle, this can be obtained for any given nucleus by a Tamm–Dancoff diagonalization. Since these calculations have rarely been done, there is a need for a plausible systematic formula. In the dipole case, such a formula has been set up by Fallieros and Akyuz,[63] and discussed by us elsewhere.[61] We expect that this formula applies to the monopole case as well:

$$\bar{E}(T') = 2\hbar\omega + \tfrac{1}{2}[T'(T'+1) - T(T+1) - 2]\frac{V_1}{A} + gM^{(0)}(\| T' \|)$$

where the superscript (0) denotes shell-model value. The second term represents the usual potential energy splitting of different isospin components of any given configuration or simple state, V_1 being the optical model coefficient for such splitting, $V_1 \approx 100$ MeV. The last term represents the collective shifts. From the expressions for $M(\| T' \|)$, plus the fact that the shell-model value of M_2 is zero, we can infer that the effect of the last term is to add a constant (Δ, say) to $2\hbar\omega$ and to reduce V_1:

$$\bar{E}(T') = (2\hbar\omega + \Delta) + \tfrac{1}{2}[T'(T'+1) - T(T+1) - 2]\frac{V_1'}{A}$$

The only Tamm–Dancoff calculation[5] that we are aware of gives a value $\Delta \approx 10$ MeV for various nuclei with $A \leq 56$, the two-body force having zero-range and being of a strength that fits the observed dipole shift. Noting that Δ in the dipole case is essentially independent of A (both experimentally and calculationally, if finite range forces are used), we will take $\Delta = 10$ MeV for all A in the monopole case. Turning to V_1', noting that $\Delta = gM_0^{(0)}$, $V_1' = V_1 - gAM_1^{(0)}/T$, we infer that

$$V_1' = V_1 - \Delta\left(\frac{A}{T}\right)\frac{M_1^{(0)}}{M_0^{(0)}}$$

The dipole case has a shift Δ of 6 MeV instead of the 10 MeV here. On the other hand, $M_1^{(0)}/M_0^{(0)}$ is about twice as large in the dipole case (at least for heavy nuclei, where the term in V_1' is most significant). Thus, to reasonable accuracy, we may use the same value of V_1' in both cases, viz., $V_1' \approx 0.5V_1 \approx 50$ MeV. Since we will frequently need values of $\bar{E}(T')$ in the following Sections, we list them for three nuclei in Table II.

TABLE II

Values of $E(T')$ Deduced from the Systematic Formula in the Text

Parameters: $\Delta = 10$ MeV, $V_1' = 50$ MeV; also $2\hbar\omega = 82A^{-1/3}$; all entries in MeV.

	^{42}Ca	^{90}Zr	^{208}Pb
$2\hbar\omega$	23	18	14
$\bar{E}(T-1)$	31	25	19
$\bar{E}(T)$	32	28	24
$\bar{E}(T+1)$	34	31	29

3.4. Specification of $N(T')$

Let us approach this problem in terms of N_0, N_1, N_2. We have noted in a related work[61] that the potential-energy contributions to $N_{\mathscr{T}}$ for the dipole and monopole problems are simply related, at least for large nuclei:

$$N_{\mathscr{T}}(U, \text{mon.}) = \frac{12R^2a_1^2}{5} N_{\mathscr{T}}(U, \text{dip})$$

We also have

$$N_{\mathscr{T}}(K, \text{mon.}) = 4\langle r^2\rangle a_1^2 N_{\mathscr{T}}(K, \text{dip})$$

Thus, if we set $R^2 = (3/5)\langle r^2\rangle$, the ratio of potential to kinetic contributions is the same in the two cases. In the dipole case, the observed value of the ratio for $\mathscr{T} = 0$ is 0.34. When we allow for finite-size effects and for R being somewhat less than suggested, the final result for the ratio in the monopole case is 0.23, i.e.,

$$N_0 = 1.23N_0(K)$$

In the dipole case, we have estimated $N_1(U) - N_2(U)$ for Rosenfeld and Hamada-Johnston forces, and find it to be $\lesssim 0.06N_0(K)$ for heavy nuclei and therefore negligible for our purposes. The same result applies here, so we drop $N_1(U)$, $N_2(U)$. The only unspecified term is now $N_1(K)$. In the dipole case, we inferred a value of this quantity from the data and found it to be about the same as the shell-model value. We will assume this to be correct in the present case also. (From Table I, we see that $N_1(K)$ is considerably less than $N_0(K)$ except for heavy nuclei, so that this assumption is not a critical one for subsequent results.) Summarizing, we will use the values

$$N_0 = 1.23N_0(K)$$
$$N_1 = N_1(K)$$
$$N_2 = 0$$

The only departure from the shell model in these values is in the 23% increase in N_0.

An important qualitative consequence[61] of these results is that M_2 is not zero in the correlated model but is simply related to M_1. The actual relation is

$$M_2 = \frac{V_1'}{A} \frac{(T - \frac{1}{2})}{\bar{E}(T)} M_1$$

The correlated-model estimate of $\langle C_v^2 \rangle$ is

$$\langle C_v^2 \rangle = \frac{N_0}{\bar{E}(T)} = 1.23 \frac{N_0(K)}{\bar{E}(T)}$$

4. TOTAL ISOSPIN IMPURITIES OF STATES

The formal perturbation expression of isospin impurity is

$$A = \sum_{T' \neq T} A(T')$$

where $A(T')$ is defined as

$$A(T') \equiv \sum_{\lambda(T')} \frac{\langle \lambda \mid \mathscr{C} \mid \phi_0 \rangle^2}{(E_\lambda - E_0)^2}$$

In general, four values of T' occur: $T' = T \pm 2$, $T \pm 1$. When $\mathscr{C}$ is replaced by the one-body form C, the values $T' = T \pm 2$ are suppressed. Actual calculations based on shell-model states[1] suggest that these values contribute very little to A. When a parent state $T = T_3$ is considered, T' is restricted to $(T + 1)$ only. Using our sum-rule method,

$$A(T') \approx \frac{M(T')}{(\bar{E}(T'))^2}$$

4.1. Parent States

For such states, $A = A(T + 1)$, where

$$A(T + 1) \approx \frac{M(\| T + 1 \|)}{(T + 1)(\bar{E}(T + 1))^2} = \frac{\langle C_v^2 \rangle - M_1 + M_2}{(T + 1)(\bar{E}(T + 1))^2}$$

To obtain values from the oscillator shell model, we set $\bar{E}(T + 1)$ equal to $2\hbar\omega$ listed in Table II, take $M_0 = \langle C_v^2 \rangle$, M_1 from Table I, and set $M_2 = 0$. To obtain the corresponding values in the presence of correlations, we use the results of Section 3, $\langle C_v^2 \rangle = 1.23 N_0(K)/\bar{E}(T)$, $M_2 = V_1' T M_1 / A\bar{E}(T)$, plus values of $N_0(K)$ and $M_1^{(0)}$ listed in Table I, plus $\bar{E}(T + 1)$ from Table II. This implies that the ratio of the two values of A is

$$\frac{(A(T + 1))_{\text{corr.}}}{(A(T + 1))_{\text{osc.}}} = \left(\frac{2\hbar\omega}{\bar{E}(T + 1)} \right)^2 \left(\frac{2\hbar\omega}{\bar{E}(T)} \right) \times \frac{1.23 M_0^{(0)} - (\bar{E}(T) - V_1' T/A) M_1^{(0)}/2\hbar\omega}{M_0^{(0)} - M_1^{(0)}}$$

TABLE III

Comparison of Evaluations of Isospin Impurity $A(T+1)$ by Different Models (Expressed in %)

Another Hartree–Fock calculation[65] gives an even smaller value (0.36) for ^{40}Ca, presumably due to smaller m^*/m, or stronger neutron–proton forces (see text).

	^{40}Ca	^{90}Zr	^{208}Pb
Oscillator shell model	2.4	3.2	3.7
Two-body correlations	0.91	0.80	0.61
Hydrodynamic model[3]	0.16	0.21	0.31
Hartree–Fock model[64]	0.60	0.40	0.28

Values of A calculated in the two schemes are given in Table III. We also give values from the hydrodynamic model:

$$A(T+1)_{\text{hyd.}} = (T+1)^{-1}5.55Z^{8/3}10^{-7}$$

These values are appreciably smaller than those for the correlated model. When one checks into this hydrodynamic model derivation for $T=0$ nuclei, one finds that it gives a formula of our sum-rule type above but with $N_0(U)=0$:

$$A(T+1) = \frac{N_0(K)}{(\bar{E}(T+1))^3}$$

The numerical value $N_0(K)$ is $1.4Z^{5/3}$ (MeV)^3. With our formula for $N_0(K)$, viz., $\hbar^2 A a_1^2 \langle r^2 \rangle / 2m$, and our choice of a_1, we get $2.3Z^{5/3}$, which is 60% larger. Finally, the hydrodynamic model sets $\bar{E}(T+1) = 4\hbar\omega$, which is larger than our value, except for heavy nuclei. The combination of these three differences all acting in the same direction, accounts for the difference between the two sets of values for $A(T+1)$.

It is instructive to compare our estimates of isospin impurity with another model, viz., the Hartree–Fock model[64] (corrected for spurious isospin mixing effects). The results are also listed in Table III. We see that the values are about one-half of our correlated-model values, and much less than the oscillator values. At first sight, it might seem that the Hartree–Fock results should be close to the oscillator results since they are both shell models. However, this is not so since, unlike the oscillator, the HF neutron potential is changed by the presence of Coulomb forces. Because

of neutron–proton attraction, the neutrons (and their potential) dilate along with the protons, and this reduces the impurity. From the relation between H–F functions with and without Coulomb forces, one can see that the H–F impurity is the same as that from the correlated model to first-order in the two-body forces U. Finally we note that the fact that the Hartree–Fock impurities in Table III are less than those of our model is probably due to the strongly expanded single-particle spectrum of the former, corresponding to an effective mass m^*/m of as small as 0.5.

4.2. Analog States

For such states, which have $T_3 = T - 1$, isospin impurities from $T' = T \pm 1$ can occur. Since the nearby states are those of $(T - 1)$, these dominate the analog mixing; in fact, in most analogs with $A > 30$, the analog is dissolved into such states, i.e., mixing is 100%. Nevertheless, for certain purposes[56] (see Sec. 8) it is useful to define mixing from distant states alone. This is the quantity provided automatically by the sum-rule method, which effectively sets all energy denominators equal to the mean separation $\bar{E}(T - 1)$ of the monopole mean energy from the analog:

$$A(T-1) = \frac{2T-1}{T(2T+1)} \frac{M(\| T-1 \|)}{(\bar{E}(T-1))^2}$$

For the shell-model evaluation of $A(T - 1)$, it is most convenient to use $M(\| T - 1 \|) = M_0 + (T + 1)M_1/T$ and Table I; for the correlated-model evaluation, we obtain $M(\| T - 1 \|)$ as $\langle C_v^2 \rangle + (T + 1)(M_1 - M_2)/T + 2(2T + 1)M_2/(2T - 1)$ and use results of Sec. 3 for $\langle C_v^2 \rangle$, M_2. Table IV gives the values thereby calculated. We see that the values of A for analogs in the correlated model are much larger than for parent states.

TABLE IV

Isospin Mixing $A(T - 1)$ for the Analogs of the Ground States of the Nuclei Listed

The values of $A(T + 1)$ are obtained from those in Table III, by multiplying them by $4T/(2T + 1)$ (values in %).

	^{90}Zr	^{208}Pb
Oscillator shell model	4.4	10.4
Two-body correlations	2.3	5.6

5. SUPERALLOWED FERMI TRANSITIONS

The matrix element for a Fermi transition between two states ψ_f, ψ_i of an isospin multiplet is

$$M_{if} = \langle \psi_f(T_3) \mid T_+ \mid \psi_i(T_3 - 1) \rangle$$

For a charge-independent Hamiltonian, the two states have pure isospin T (say) and

$$M_{if} = [(T - T_3)(T + T_3 + 1)]^{1/2}$$

With Coulomb forces present:

$$\psi_i = b_0{}^i \phi_0(T, T_3 - 1) + \sum_\lambda b_\lambda{}^i \phi_\lambda(T', T_3 - 1)$$

$$\psi_f = b_0{}^f \phi_0(T, T_3) + \sum_\lambda b_\lambda{}^f \phi_\lambda(T', T_3)$$

If we keep the one-body part of the Coulomb force, then T' runs over $T + 1, T, T - 1$ in ψ_i and over T, $(T + 1)$ in ψ_f. In the case $T = T_3$:

$$M_{if} = b_0{}^i b_0{}^f (2T)^{1/2} + \sum_{\lambda(T)} b_\lambda{}^i b_\lambda{}^f \, (2T)^{1/2} + \sum_{\lambda(T+1)} b_\lambda{}^i b_\lambda{}^f (2(2T + 1))^{1/2}$$

with the normalization conditions

$$(b_0{}^i)^2 + \sum_\lambda (b_\lambda{}^i)^2 = 1$$

$$(b_0{}^f)^2 + \sum_\lambda (b_\lambda{}^f)^2 = 1$$

The relative correction δ to the ft-value is such that

$$M_{if}^2 = 2T(1 - \delta)$$

$$\delta = \sum_{\lambda(T)} (b_\lambda{}^i - b_\lambda{}^f)^2 + \sum_{\lambda(T-1)} (b_\lambda{}^i)^2 - 2\left(\frac{2T + 1}{T}\right)^{1/2} \sum_{\lambda(T+1)} b_\lambda{}^i b_\lambda{}^f + \sum_{\lambda(T-1)} (b_\lambda{}^i)^2 + \sum_{\lambda(T+1)} (b_\lambda{}^f)^2$$

The perturbation expressions for the admixture amplitudes are

$$b_\lambda{}^i = \frac{\langle \phi_\lambda(T, T_3 - 1) \mid C_v \mid \phi_0(T, T_3 - 1) \rangle}{E_\lambda - E_0}$$

$$b_\lambda{}^f = \frac{\langle \phi_\lambda(T, T_3) \mid C_v \mid \phi_0(T, T_3) \rangle}{E_\lambda - E_0}$$

For $T = T_3$, using the relations and definitions of Sec. 3:

$$\delta = \frac{2T-1}{T(2T+1)} \frac{M(\| T-1 \|)}{\bar{E}^2(T-1)} + \frac{1}{T(T+1)} \frac{M(\| T \|)}{\bar{E}^2(T)} - \frac{2T+3}{(T+1)(2T+1)} \frac{M(\| T+1 \|)}{\bar{E}^2(T+1)}$$

If all three $\bar{E}(T')$ are equal, then, again using Sec. 3, we find

$$\delta = \frac{2}{T} \frac{M_1}{\bar{E}^2}$$

Evaluating with the shell model for ^{42}Ca ($T = 1$), we get

$$M_1 = \frac{a_1^2}{2} [\langle r^4 \rangle - \langle r^2 \rangle^2]$$

where the expectation values are in the $1f$ orbit. Using the oscillator results in

$$M_1 = \frac{9a_1^2 b^4}{4}$$

Taking a_1 from Table I and $\bar{E} = 2\hbar\omega$ from Table III, with $\hbar^2/mb^2 = \hbar\omega$, we get for the shell-model value of δ,

$$\delta = 0.003$$

The correlated model gives this value reduced by the ratio $(23/32)^2$ of the values of $\bar{E}^2$, viz, $\delta = 0.0015$. The smallness of this value comes from the cancelling out of the large term $\langle C_v^2 \rangle$ when all $\bar{E}(T')$ are equal. Let us now put in a splitting in accord with the formula given in Sec. 3. This gives the extra term

$$\frac{4V_1' \langle C_v^2 \rangle}{\bar{E}^3 A}$$

The ratio of this to the above term is

$$2 \frac{V_1' T}{A} \frac{1}{\bar{E}} \frac{\langle C_v^2 \rangle}{M_1} = 2 \frac{V_1' T}{A} \frac{1}{\bar{E}^2} \frac{N}{M_1}$$

Evaluating for ^{42}Ca, with $V_1' = 50$ MeV, $\bar{E} = 32$ MeV (Table II), $N = 1.23 N_0(K)$, and M_1 as above, we obtain for the ratio the value: 0.7.

Thus the final value of δ on the correlated model is $\delta = 0.0015 \times 1.7 = 0.0025$. This is less than the shell-model value, despite the contribution of the isosplitting term.

It is worth noting that any contributions from configuration states of $T' = (T - 1)$ will occur with small negative energy denominator, and could produce significant effects. However, in several of the nuclei where superallowed transitions are observed, the shell-model configuration of the states allows no "configuration states," e.g., in ^{42}Ca, there is no $J = 0$, $T = 0$ state of $(f_{7/2})^2$.

Before describing the data, we extend the prediction for $A = 42$, viz., $\delta = 0.0025$, to other nuclei. We find that this can be done to reasonable accuracy with $\delta \propto A^{4/3}$, which follows from the shell-model expressions.

Experimental Data. Recently[66] a plot has been given of fourteen *ft*-values for superallowed Fermi transitions. Of these, seven have much smaller errors ($\pm\frac{1}{2}\%$ or less) than the others ($\pm 2\%$). Considering only the cases with small errors, we see that the ^{14}O and ^{26}Al cases have particularly small errors ($\pm 0.1\%$) and agree with each other: $ft = 3090$. The others (^{34}Cl, ^{42}Sc, ^{46}V, ^{50}Mn, ^{54}Co) have larger values. The last four agree at $ft = 3130$ while, for ^{34}Cl, $ft = 3170$. On the face of it, the larger values for these five cases with higher *ft* might appear to be evidence for the Coulomb-mixing effects. However, recent[67] revised studies on ^{34}Cl taking hitherto unsuspected systematic errors into account, bring the *ft*-value for this case into accord with that for ^{14}O and ^{26}Al to within the errors. These errors are of the order of the effect we estimate, so there is consistency between experiment and theory. A more severe test will be provided by the planned re-study of ^{54}Co, where we predict that the *ft*-value will be larger than that of ^{14}O by 0.3%, or 10 units of *ft*-value.

6. ISOBARIC MASS FORMULA

Let us write the Coulomb energy of a state $\phi_0(TT_3)$ to all orders of perturbation as

$$E(T, T_3) = a + bT_3 + cT_3^2 + dT_3^3 + eT_3^4 + \cdots$$

Unlike most items of other sections, the present quantity involves a first-order Coulomb term. Since this is so much larger than the second-order term, we must evaluate it accurately; in particular one should use the two-body force $\mathscr{C}$.

6.1. First-Order Energy

In terms of the two-body Coulomb force $\mathscr{C} = \mathscr{C}_s + \mathscr{C}_v + \mathscr{C}_t$ the Coulomb energy of state $\phi_0(TT_3)$ to first order is

$$\begin{aligned} E_1(TT_3) &\equiv \langle \phi_0(TT_3) \mid \mathscr{C} \mid \phi_0(TT_3) \rangle \\ &= a_1 + b_1 T_3 + c_1 T_3^2 \end{aligned}$$

where

$$a_1 = \langle \mathscr{C} \rangle - \frac{T+1}{2T-1} \langle \mathscr{C}_t \rangle$$

$$b_1 = \frac{1}{T} \langle \mathscr{C}_v \rangle$$

$$c_1 = \frac{3}{T(2T-1)} \langle \mathscr{C}_t \rangle$$

and $\langle X \rangle$ denotes $\langle \phi_0(TT) \mid X \mid \phi_0(TT) \rangle$.

Ideally, a_1, b_1, c_1 should be evaluated exactly with a model like the shell model, including space-exchange effects. This has been done in some studies. (We mention the shell-model evaluation of the first-order term in Sec. 7.) Here we will use the uniform statistical model,[1,7,34] which is sufficient to bring out qualitative features. This gives

$$\langle \phi_0(TT) \mid \mathscr{C}_s \mid \phi_0(TT) \rangle = \tfrac{1}{8}\left[A(A-2) + \frac{4T}{3}(T+1) \right] \left\langle \frac{e^2}{r_{ij}} \right\rangle$$

$$\langle \phi_0(TT) \mid \mathscr{C}_v \mid \phi_0(TT) \rangle = \tfrac{1}{2} T(A-1) \left\langle \frac{e^2}{r_{ij}} \right\rangle$$

$$\langle \phi_0(TT) \mid \mathscr{C}_t \mid \phi_0(TT) \rangle = \frac{T}{6}(2T-1) \left\langle \frac{e^2}{r_{ij}} \right\rangle$$

whence

$$a_1 = \tfrac{1}{16} A(A-3) \left\langle \frac{e^2}{r_{ij}} \right\rangle$$

$$b_1 = -\tfrac{1}{2}(A-1) \left\langle \frac{e^2}{r_{ij}} \right\rangle$$

$$c_1 = \tfrac{1}{2} \left\langle \frac{e^2}{r_{ij}} \right\rangle$$

In light nuclei where $T \lesssim 1$, the quadratic term in $E_1(T, T_3)$ is smaller than the linear term by $O(1/A)$. In heavy nuclei, the contribution of the quadratic

term to the displacement,

$$E_1(T, T_3 - 1) - E_1(T, T_3)$$

is $-(2T_3 - 1)/(A - 1)$ times that of the linear term, i.e., about 20% and of opposite sign. Taking the two terms together, we get

$$E_1(T, T_3 - 1) - E_1(T, T_3) = Z\left\langle \frac{e^2}{r_{ij}} \right\rangle$$

as expected.

6.2. Second-Order Energy

The second-order Coulomb term in the energy of $\phi_0(T, T_3)$ will be evaluated with the one-body Coulomb force. The sum-rule method gives (see Appendix 3):

$$E_2(T, T_3) = -\left[\frac{M(T+1, C)}{\bar{E}(T+1)} + \frac{M(T, C)}{\bar{E}(T)} + \frac{M(T-1, C)}{\bar{E}(T-1)} \right]$$

where the $M(T', C)$ are the sum-rule quantities for the Coulomb force C. In the case of the oscillator shell model, $\bar{E}(T') = 2\hbar\omega$ and

$$E_2(T, T_3) = -\frac{M(C)}{2\hbar\omega}$$

$$\begin{aligned} M(C) &= b^2\langle r^2\rangle_P Z a_1^2 \\ &= b^2\langle r^2\rangle_P Z(Z-1)^2\left\langle \frac{e^2}{2R^3} \right\rangle^2 \end{aligned}$$

Equivalently,

$$E_2(T, T_3) = a_2 + b_2 T_3 + c_2 T_3^2 + d_2 T_3^3 + e_2 T_3^4$$

where

$$a_2 = -\left(\frac{A}{2}\right)^3 d_2$$

$$b_2 = 3\left(\frac{A}{2}\right)^2 d_2$$

$$c_2 = -3\left(\frac{A}{2}\right) d_2$$

$$d_2 = \frac{1}{2\hbar\omega} b^2\langle r^2\rangle_P \left(\frac{a_1}{Z}\right)^2$$

$$e_2 = 0$$

TABLE V

Table of Calculated Second-Order Values of Parameters in the Isobaric Mass Formula

(a) Shell-model values; (b) values from the correlated model. The shell-model value of e_2 is zero. (In the case of $A = 9$, the shell-model value of d_2 is increased[15] to 1.6 keV when the oscillator potential is replaced by a Saxon–Woods one).

	A	9	30	40
(a)	c_2 (keV)	-6	-8	-9
	d_2 (eV)	450	200	150
(b)	c_2 (keV)	3	7	11
	d_2 (eV)	-1.8	-1.0	-1.2
	e_2 (eV)	200	32	30

We have set $\bar{E}$ equal to its shell-model value $2\hbar\omega$. Since $\hbar\omega \propto A^{-1/3}$, $b^2 \propto A^{1/3}$, $\langle r^2\rangle_P \propto A^{2/3}$, and $(a_1/Z)^2 \propto A^{-2}$, d_2 decreases with A as $A^{-2/3}$, while c_2 increases as $A^{1/3}$. In Table V, we give values of these parameters based on the following parameters for $A \approx 40$: $2\hbar\omega = 23$ MeV, $a_1{}^2 = (50\,\text{MeV}^2 \cdot f^2)\langle r^2\rangle_P^{-3}$, $\langle r^2\rangle_P^{1/2} = 3.52f$. Note that $e_2 = 0$ and that c_2 has opposite sign to c_1. As might be expected, the shell-model values are sensitive to well-shape. The replacement of our choice of oscillator by the Saxon–Woods potential gives an increase of d_2 by a factor of 3 to 4, according to one study.[15]

Before passing to the correlated model, we should examine more closely the approximation of replacing the two-body force by the one-body force in the second-order terms. The validation of this approximation has two aspects: first, that the one- and two-body forces should agree on the value of $M(T+1)$, $M(T)$, $M(T-1)$; second, that $M(T+2)$ and $M(T-2)$ be negligible in the two-body case, since these terms have no counterpart in the one-body case. (Indeed if they were important, they would upset the whole theory, since the charge monopole state gives rise to no such terms). In Appendix 3, we give evidence that the first aspect is correct. We also show that $M \equiv \langle C^2\rangle$ is the same to $O(1/Z)$ for the one- and two-body problems, from which it follows that $M(T \pm 2)$ must be small. In the case of $M(T+2)$, this can be shown explicitly since the uniform statistical

model gives, to $O(1/Z)$:

$$M(\| T + 2 \|) = \frac{Z^2}{12}(J - 2I)$$

while

$$M(\| T + 1 \|) = \tfrac{1}{2}Z^2(ZI + \tfrac{1}{2}J)$$

On inserting vector coupling factors, and expanding $M(T+2)$ and $M(T+1)$ in powers of T_3 and dropping J-terms, we find that the coefficients in the former case are less than in the latter by factors of about $(2A)^{-1}$.

This is encouraging evidence for the equality of the one- and two-body results. However, there are two reservations that are worth bearing in mind:

1. We have dropped the J-terms; if we had included these, $M(T + 2)$ would have been much more important (since J is of order $30I$). However, this is not as crucial as it seems at first sight. The energy-weighted sum N associated with the J-terms is infinite, implying that the energy denominators in E_2 that are relevant for the J-terms are very large, thereby suppressing the effect of these terms.
2. When correlations are taken into account the difference between the forces may be larger. Trivially, if correlations hold pairs of protons close together, there will be a specifically two-body Coulomb effect. Since the two-body effects appear in the J-type terms, these would be enhanced.

6.3. Correlated Model

At this point, a small extension of the sum-rule method is needed since $M(T, C)$, with $C = C_s + C_v$, involves both the mass and charge monopole modes. We will define mean energy $\bar{E}'(T)$ for the mass mode; then the term C_s^2 contributes to $E_2(T, T_3)$ the amount

$$-\frac{\langle C_s^2 \rangle}{\bar{E}'(T)}$$

The cross-term may be treated similarly and gives, with mean energy $\bar{E}''(T)$,

$$\frac{2T_3}{T}\,\frac{\langle C_s C_v \rangle}{\bar{E}''(T)}$$

Inserting forms for the vector-coupling coefficients in $M(T', C)$, and taking

the factor a_1^2 in all sum rules to contain the factor $Z^2 = (A/2 - T_3)^2$, we find

$$a_2 = -\frac{A^2}{4} X$$

$$b_2 = \frac{A^2}{4} Y + AX$$

$$c_2 = \frac{A^2}{4} e_2 - AY - X$$

$$d_2 = -Ae_2 + Y$$

where

$$X \equiv \frac{\langle C_s^2 \rangle}{Z^2 \bar{E}'(T)} + \frac{1}{Z^2}\left[\frac{T+1}{2T+1}\,\frac{M(\| T+1 \|)}{\bar{E}(T+1)} + \frac{T}{2T+1}\,\frac{M(\| T-1 \|)}{\bar{E}(T-1)}\right]$$

$$Y = -\frac{2}{T}\,\frac{\langle C_s C_v \rangle}{Z^2 \bar{E}''(T)}$$

$$e_2 = \frac{1}{Z^2}\left[\frac{1}{(T+1)(2T+1)}\,\frac{M(\| T+1 \|)}{\bar{E}(T+1)} - \frac{1}{T(T+1)}\,\frac{M(\| T \|)}{\bar{E}(T)} + \frac{1}{T(2T+1)}\,\frac{M(\| T-1 \|)}{\bar{E}(T-1)}\right]$$

Allowing for the symmetry splitting of $\bar{E}(T')$ as described in Sec. 3, we get

$$X = \frac{\langle C_s^2 \rangle}{Z^2 \bar{E}'(T)} + \frac{1}{Z^2 \bar{E}(T)}\left[\langle C_v^2 \rangle + \frac{2T}{2T-1} M_2\right] + \frac{V_1'/A}{Z^2(\bar{E}(T))^2}(T+1)\left[M_1 + \frac{M_2}{2T-1}\right]$$

$$e_2 = \frac{1}{Z^2}\left[\frac{2}{T(2T-1)}\,\frac{M_2}{\bar{E}(T-1)} + \frac{(M_1 - M_2)V_1'A}{T(\bar{E}(T))^2}\right]$$

In Table V we give values for the various quantities, based on the following; (1) In e_2, use for M_2 the result mentioned in Sec. 3, viz., $M_2 = TV_1'M_1/A\bar{E}(T)$. For $T = \frac{3}{2}$, this means that the term in M_2 is $\bar{E}(T)/\bar{E}(T-1)$ times the term in M_1, i.e., it increases e_2 by more than a factor 2. (2) Use $\bar{E}(T) = (82A^{-1/3} + 10)$ MeV, $M_1 = (Ta_1^2/2)[\langle r^4 \rangle - \langle r^2 \rangle^2]$, where the latter factor is obtained from the relevant oscillator orbits in terms of $b = A^{1/6}f$;

also set $V_1' = 50$ MeV. (3) In X, take $\langle C_v^2 \rangle$ as $1.23N_0(K)/\bar{E}(T)$ and $\langle C_s^2 \rangle$ as $N_0(K)/\bar{E}'(T)$. Take $\bar{E}'(T) = (82A^{-1/3} - 6)$ MeV. Take M_1, M_2, V_1' as in (1) and (2). (4) Set $\langle C_s C_v \rangle$ and $Y = 0$. In the shell-model situation, $-(A/2T)\langle C_s C_v \rangle$ is large ($= \langle C_v^2 \rangle$) and the Y-term accounts for all of d_2. However, $\langle C_s C_v \rangle$ is expected to fall off with correlations because it is a measure of the extent to which the mass and charge monopole modes are not orthogonal. When correlations are present, and the two states $C_s \mid \phi_0 \rangle$ and $C_v \mid \phi_0 \rangle$ are split in energy, they are expected to be more nearly orthogonal. The values of d_2, arising from the term e_2, are several times the shell-model values arising from Y, and of the opposite sign. Thus the inclusion of terms Y will not qualitatively affect the estimates of d_2. In the case of c_2, the term AY contributes twice as much as the term X to c_2. The change in values of c_2 in Table V between the shell-model and correlated-model values comes from the neglect of term AY in the latter model and the presence of the e_2 term, which has opposite sign.

Note that the estimates are essentially independent of $T \geq \frac{3}{2}$, and that e_2 is nonzero.

6.4. Configuration States

There is a different sort of splitting that is important for lighter nuclei; viz., part of $M(T-1)$ arises from "configuration states," which have energy separations from ϕ_0 much less than that of the monopole state. In fact, they will tend to be on the opposite side of ϕ_0, and so make the energy denominator negative. For an orientation, suppose that a fraction y of $M(T-1)$ arises from configuration states at energy $\bar{E}(T-1) = -\mid e \mid$, and we ignore all other contributions; then,

$$e_2 \approx -y \frac{M(\| T-1 \|)}{\mid e \mid}$$

$$d_2 \approx -Ae_2$$

$$c_2 \approx \left(\frac{A^2}{4} - T^2\right) e_2$$

A detailed[16] calculation for $A = 30$, $T = \frac{3}{2}$ finds $c_2(\text{keV}) = -[20 \text{ MeV}/\mid e \mid]$; with the sum-rule method we find $c_2(\text{keV}) \approx [-2000 \text{ MeV}/\mid e \mid]$, implying $y \approx 0.01$, i.e., the configuration states account for only 1% of the sum rule $M(T-1)$. Taking $\mid e \mid$ as 4 MeV, we find $c_2 \approx -6$ keV, which is comparable with the magnitude that we estimate from the mono-

pole state in Table V, viz., $c_2 \approx 7$ keV. Thus, the configuration states are important despite the fact that they account for only 1% of the sum rule. Their relative contribution is several times larger than $0.01(\bar{E}/|e|)$; this is because of the large cancellation occurring in the contribution from the monopole state.

The relative values d_2/e_2 and c_2/d_2 in the quoted article are about twice those implied by the last formulas, presumably reflecting differences in details such as potential well and the use of two-body Coulomb forces. It is more puzzling that the article gives negative values to c, d, e while our formula makes d positive. We do not understand this.

6.5. Observed Values

First, we give a brief summary of the main facts about the larger coefficients, b and c. The value of b depends on m in $A \equiv 4n + m$ ($m = 0, 1, 2, 3$); $-b$ increases from 0.76 MeV for $A = 3$ to 7.61 MeV for $A = 42$. There is a staggering effect with the increases from $m = 1$ to 2 and $m = 2$ to 3 about three times larger than $m = 0$ to 1 and $m = 3$ to 0.

From $m = 2$, c decreases slowly from 330 keV at $A = 6$ to 280 keV at $A = 42$; for $m = 0$ it fluctuates between 350 and 150 keV; for $m = 1$, c decreases from 270 keV at $A = 9$ to 170 keV at $A = 37$. These values are of the order expected for $c_1 \approx (6/10)(e^2/R)$, which is 300 keV for $R = 2.8f$ ($A = 10$), 190 keV for $R = 4.5f$ ($A = 40$). (For more detailed comparison, see Auerbach *et al.*[17]).

The only experimental estimates for d_2 are for five $T = \frac{3}{2}$ quartets, viz.,

$$A = 9: \; d_2 = 8.0\ (\pm 3.7)\ \text{keV}$$

$$A = 13: d_2 = 0.8\ (\pm 3.4)\ \text{keV}$$

$$A = 17: d_2 = 4.8\ (\pm 9.2)\ \text{keV}$$

$$A = 25: d_2 = \left.\begin{array}{l} 1.9\ (\pm 2.9)\ \text{keV}\ (J = \frac{5}{2}) \\ 4.8\ (\pm 3.6)\ \text{keV}\ (J = \frac{3}{2}) \end{array}\right\} \text{Benenson } et\ al.^{68}$$

The most certain value is for $A = 9$; even here, the error is disconcertingly large. Our correlated-model evaluation of d_2 (Table V) gives a negative value, so there is disagreement in sign. A shell-model study[15] gives $d_2 = 1.6$ keV using a Woods–Saxon well, plus a further 2 keV from charge-dependent forces. Our results suggest that correlations drastically change the former, and convert it to a negative value.

7. ANALOG STATES: GENERAL REMARKS AND LOWEST-ORDER EFFECTS

There are two different ways of viewing and expressing the analog displacement energy (δE_c, say)—each with its advantages. (This has been noted before.[32]) It is instructive to keep both views in mind, so we discuss them in turn, then show their equivalence.

7.1. δE_c in Terms of Relative Coulomb Potential and Exact Parent State

In this approach, one bases the theory on the interpretation of the analog state as observed in cross sections.

Experimentally, an analog state in heavier nuclei shows up as a bump in a spectrum or excitation curve. We can assume that the reaction mechanism is such that the experiment creates the state $\psi_a' \equiv T_-\psi_p/\langle\psi_p \mid T_+T_- \mid \psi_p\rangle^{1/2}$, where ψ_p is the parent state. This would only be exactly true in the hypothetical case of an allowed Fermi transition from the parent state. It should be a very good approximation when the analog appears in the neutron spectrum of a (p, n) reaction. When it is a compound-state resonance, it is still very good. The main complication is that there is a background since the experiment excites the fine structure as well as ψ_a', and there is interference between the two. A reaction theory (like the R-matrix one) enables one to take account of this and to make explicit the relation between ψ_a' and the cross-section bump. (The fact that the energy agrees closely with that found in the (p, n) experiment shows that both studies are revealing the same object, viz., ψ_a').

The assumption that experiments reveal ψ_a' means that they reveal its strength function $s(E)$, where

$$s(E) = \frac{1}{\pi} \operatorname{Im} R(E^+)$$

$$R(E^+) = \frac{1}{\langle\psi_a' \mid H - HQ'[1/(Q'HQ' - E^+)]Q'H \mid \psi_a'\rangle - E^+}$$

Here, H is the total Hamiltonian $= H_0 + \mathscr{C}$, $E^+ \equiv E + i\varepsilon$, $Q' \equiv 1 - \mid \psi_a'\rangle\langle\psi_a' \mid$. The expectation value may be written, for E near $\langle\psi_a' \mid H \mid \psi_a'\rangle \equiv E_a'$ as

$$E_p + \delta E_c - \frac{i}{2}\Gamma^{\downarrow}$$

where $E_p \equiv \langle \psi_p \mid H \mid \psi_p \rangle$ and δE_c is the analog displacement

$$\delta E_c = E_a' - E_p - \left\langle \psi_a' \middle| H \frac{Q'}{Q'HQ' - E_a'} H \middle| \psi_a' \right\rangle$$
$$\equiv \Delta' - \Delta''$$

This is essentially exact. Since ψ_p is an eigenstate of H, the first term may be written

$$\Delta' \equiv E_a' - E_p$$
$$= \frac{-\langle \psi_p \mid T_+ \mathscr{C}^- \mid \psi_p \rangle}{\langle \psi_p \mid T_+ T_- \mid \psi_p \rangle}$$
$$= \frac{-[\langle \psi_p \mid [T_+, \mathscr{C}^-] \mid \psi_p \rangle + \langle \psi_p \mid \mathscr{C}^- T_+ \mid \psi_p \rangle]}{\langle \psi_p \mid T_+ T_- \mid \psi_p \rangle}$$

where $\mathscr{C}$ is the two-body Coulomb force, and

$$\mathscr{C}^- \equiv -[\mathscr{C}, T_-] = -\sum_{i,j} t_{i-}(\tfrac{1}{2} - t_{3j}) \frac{e^2}{r_{ij}}$$

We may develop this in powers of $\mathscr{C}$. We have

$$\psi_p = \phi_p - \frac{Q}{H_0 - E_0} \mathscr{C} \phi_p$$

where ϕ_p is the parent wave function in the absence of Coulomb forces, $H_0 \phi_p = E_0 \phi_p$ and $Q = 1 - \mid \phi_p \rangle \langle \phi_p \mid$. Since $T_+ T_- \mid \phi_p \rangle = 2T \mid \phi_p \rangle$ we find, to second order in $\mathscr{C}$:

$$\Delta' = \Delta_1' - \Delta(-+)$$

where

$$\Delta_1' = -\frac{1}{2T} \langle \psi_p \mid [T_+, \mathscr{C}^-] \mid \psi_p \rangle$$

$$\Delta(-+) = \frac{1}{2T} \langle \phi_p \mid \mathscr{C}^- \frac{Q}{H_0 - E_0} \mathscr{C}^+ \mid \phi_p \rangle$$

and

$$\mathscr{C}^+ \equiv [\mathscr{C}, T_+] = -\sum_{i,j} t_{i+}(\tfrac{1}{2} - t_{3j}) \frac{e^2}{r_{ij}}$$

The term Δ'' may be rewritten (using $Q' T_- \mid \psi_p \rangle = 0$):

$$\Delta'' = \frac{\langle \psi_p \mid \mathscr{C}^+ [Q'/(Q'HQ' - E_a')] \mathscr{C}^- \mid \psi_p \rangle}{\langle \psi_p \mid T_+ T_- \mid \psi_p \rangle}$$

To second order in $\mathscr{C}$, this is equal to

$$\Delta(+-) \equiv \frac{1}{2T} \langle \phi_p \mid \mathscr{C}^+ \frac{Q}{H_0 - E_0} \mathscr{C}^- \mid \phi_p \rangle$$

where we have replaced ψ_p by ϕ_p and $(Q'HQ' - E_a')$ by the zeroth-order form $(H_0 - E_0)$. Collecting formulas together, we have

$$\begin{aligned} \delta E_c &= \Delta' - \Delta'' \\ &= \Delta_1' - \Delta(-+) - \Delta(+-) \end{aligned}$$

to second order in $\mathscr{C}$.

7.2. δE_c in Terms of Coulomb Energy and Unperturbed Parent State

In this approach, we evaluate δE_c as $(E_a - E_p)$, where these are the exact energies of the analog and parent, and then evaluate each of these separately by perturbation theory. This gives, to second order in $\mathscr{C}$:

$$\delta E_c = \Delta_1 - (\Delta_{2a} - \Delta_{2p})$$

where

$$\begin{aligned} \Delta_1 &\equiv - \frac{\langle \phi_p \mid T_+ \mathscr{C}^- \mid \phi_p \rangle}{\langle \phi_p \mid T_+ T_- \mid \phi_p \rangle} \\ &= - \frac{1}{T} \langle \phi_p \mid \mathscr{C}_v + 3\mathscr{C}_t \mid \phi_p \rangle \end{aligned}$$

The two second-order terms are (with $x = a, p$):

$$\Delta_{2x} = \langle \phi_x \mid \mathscr{C} \frac{Q_x}{H_0 - E_0} \mathscr{C} \mid \phi_x \rangle$$

with

$$\begin{aligned} Q_x &= 1 - \mid \phi_x \rangle \langle \phi_x \mid \\ E_0 &= \langle \phi_a \mid H_0 \mid \phi_a \rangle = \langle \phi_p \mid H_0 \mid \phi_p \rangle \end{aligned}$$

One can show directly the equality of the two expressions of δE_c to second order by inserting

$$\psi_p = \phi_p - \frac{Q_p}{H_0 - E_0} \mathscr{C} \phi_p$$

in Δ_1' and suppressing Coulomb effects apart from the operator in Δ_2'

which becomes

$$\langle \phi_p \mid T_+T_- \mid \phi_p \rangle^{-1} \langle \phi_p \mid \mathscr{C}_v^+ \frac{Q_a \mathscr{C}_v^-}{H_0 - E_0} \mid \phi_p \rangle$$

On using $T_+Q_a = Q_pT_+$, the equality follows straightforwardly. The merit of the second expansion $\delta E_c = \Delta_1 - \Delta_2 \ldots$ is simply that it is a standard perturbation expansion in powers of the Coulomb energy. The merit of the first form $\delta E_c = \Delta' - \Delta''$ is twofold, both stemming from the common underlying feature that it is more physical. First (as we will use in Sec. 8) the imaginary counterpart, $\frac{1}{2}\Gamma^{\downarrow}$, of Δ'' is the analog spreading width, a physically observed quantity. Second, Δ_1' is more closely related to the numerical estimates that have been made of the displacement. We now discuss the quantities Δ_1 and Δ_1', and expose this feature.

7.3. First-Order Shift Δ_1 and Pseudo-First-Order Shift Δ_1'

Let us evaluate Δ_1 with a determinantal (i.e., closed shell) wave function. Straightforwardly,

$$\langle \mathscr{C}_s \rangle = \tfrac{1}{6}[I_{NN} + I_{PP} + I_{NP}]$$

$$\langle \mathscr{C}_v \rangle = -\tfrac{1}{4}[I_{NN} - I_{PP}]$$

$$\langle \mathscr{C}_t \rangle = \tfrac{1}{12}[I_{NN} + I_{PP} - 2I_{NP}]$$

where each $I = D - E$ and

$$D = \sum_{\alpha,\beta} \langle \alpha\beta \mid \frac{e^2}{r_{ij}} \mid \alpha\beta \rangle$$

$$E = \sum_{\alpha,\beta} \langle \alpha\beta \mid \frac{e^2}{r_{ij}} P_{ij}^{\sigma} P_{ij}^{x} \mid \alpha\beta \rangle = \sum_{\alpha,\beta} \langle \alpha\beta \mid \frac{e^2}{r_{ij}} \mid \beta\alpha \rangle$$

For instance, in $I_{NP} = D_{NP} - E_{NP}$, α, β runs over occupied neutron, proton states, respectively. Note that (i) pairs (α, β) of opposite intrinsic spin give zero contributions to E; (ii) any term in D_{PP} with $\alpha = \beta$ is cancelled by the corresponding term in E_{PP}. Similarly with D_{NN}, E_{NN}. The same applies to D_{NP}, E_{NP} if N, P orbits are the same; further, such terms will be the same in D_{NP}, E_{NP}, D_{PP}, E_{PP}. From the last form given for Δ_1:

$$\Delta_1 = -\frac{1}{2T}[I_{PP} - I_{NP}]$$

If we define a one-body Coulomb force:

$$V_c(i) = \sum_\alpha \langle \alpha(j) \mid \frac{e^2}{r_{ij}} (1 - P_{ij}^\sigma P_{ij}^x) \mid \alpha(j) \rangle$$

where α sums over all occupied proton orbits in the parent, then

$$\Delta_1 = \frac{1}{2T} [\langle V_c \rangle_N - \langle V_c \rangle_P]$$

where

$$\langle V_c \rangle = \sum_\beta \langle \beta \mid V_c \mid \beta \rangle$$

and β runs over neutron or proton orbits according to the subscript. While the space-exchange term is retained, $V_c(i)$ is nonlocal. If it is dropped, or replaced by a local average, then

$$\langle V_c \rangle = \int V_c(r) \varrho^0(r) \, \mathbf{dr}$$

where ϱ^0 is the neutron or proton density in the absence of Coulomb forces. Note that (i) the direct term in $V_c(i)$ is of order $Z\langle e^2/r_{ij} \rangle$, where Z is the parent charge; (ii) the exchange terms with $\alpha = \beta$ cancel between I_{PP} and I_{NP} (exactly, if N, P orbits are identical). Some aspects of these results have been derived before.[20] The most important qualitative feature is that when the wave function is determinantal, Δ_1 has the form of an integral over the one-body Coulomb force in the parent:

$$\Delta_1 = \frac{1}{2T} \int V_c(r) \big(\varrho_P{}^0(r) - \varrho_N{}^0(r)\big) \, \mathbf{dr}$$

where $V_c(r)$ includes the small effective local average of the nonlocal exchange effects $\alpha \neq \beta$. This derivation does not depend on neutron and proton orbits being the same (i.e., that the state has pure isospin).

Now let us discuss the quantity Δ_1'. We recognize that the operator in Δ_1' is just the same as in Δ_1. Thus, if we take ψ_p as a determinantal wave function, the first term in Δ_1' is like Δ_1 but with true densities ϱ in place of the zeroth-order densities ϱ^0:

$$\Delta_1' = \frac{1}{2T} \int V_c(r) (\varrho_N - \varrho_P) \, \mathbf{dr}$$

If ϕ_p is a determinant, and $\mathscr{E}$ is taken as a one-body Coulomb force, then it follows that ψ_p is also a determinant.

The difference between Δ_1' and Δ_1 is second order in $\mathscr{E}$. The most convenient expression of the difference for evaluation purposes is obtained from equating the two forms of δE_c, whence

$$\Delta_1' - \Delta_1 = \Delta(-+) + \Delta(+-) - \Delta_{2a} - \Delta_{2p}$$

Theoretical evaluations[20] of shifts have been mostly of the type Δ_1', characterized by being first order in $\mathscr{E}$ in the operator, but using the observed proton density. The neutron density is varied to fit the observed value of δE_c. When this is done, one finds that $\langle r^2 \rangle_N$ is much more nearly equal to $\langle r^2 \rangle_P$ than the shell model predicts (this is the Nolen–Schiffer[20] anomaly). This is true whether one includes a symmetry potential difference between neutron and proton potentials or not. It can be argued that one should not include this effect since it conflicts with the property that ϕ_p has pure isospin. However, it is not clear that this necessarily leads to a spurious estimate of Δ_1 or Δ_1'. If we start with a shell-model form for ϕ_p of pure isospin and introduce the effect of two-body correlations, these will modify $(\varrho_N - \varrho_P)$. Presumably a symmetry potential can reproduce the same change in $(\varrho_N - \varrho_P)$. If we now assume that the form of Δ_1 or Δ_1' as an integral on $(\varrho_N - \varrho_P)$ is not restricted to the shell model, then we see that the fact that the symmetry potential implies spurious isospin mixing does not invalidate its use for the evaluation of Δ_1 or Δ_1', since it enters only to provide the form of the factor $(\varrho_N - \varrho_P)$.

We now turn to the problem of the effect of correlations on Δ_1. Since the above derivation of the form for Δ_1 in terms of $(\varrho_N - \varrho_P)$ was based on the use of the shell model, it certainly is not exactly correct for correlated functions. However, it is possible that correlations are still covered by the formula to a good approximation, i.e., their main effect is to change $(\varrho_N - \varrho_P)$ rather than the structure of the formula for Δ_1. Obviously this cannot be generally true since it cannot cover all hypothetical cases such as that where pairs of protons are held close together by their nuclear attractive forces. To explore the problem further, let us simplify the discussion by applying the uniform statistical model to a state with $T = \frac{1}{2}$. For this the isotensor term vanishes and

$$\begin{aligned}\Delta_1 &= \left\langle \phi_p \left| \frac{1}{2} \sum_{i,j} (t_{3i} + t_{3j}) \frac{e^2}{r_{ij}} \right| \phi_p \right\rangle \\ &= \frac{Ze^2}{2} \left[(Z+1) \left\langle \frac{1}{r_{ij}} \right\rangle_{NN} - (Z-1) \left\langle \frac{1}{r_{ij}} \right\rangle_{PP} \right]\end{aligned}$$

where the averages are over the spatial wave functions of NN and PP pairs.

(Note that NP pairs do not contribute for this $T = \frac{1}{2}$ case). The two averages will be different in general because the neutron states include the valence orbital, which is more diffuse than the core orbits. However, for the exposure of correlation effects, we can ignore this, and exploit the fact that NN, PP pairs are necessarily $T = 1$ to write

$$\Delta_1 \approx Ze^2\left\langle \frac{1}{r_{ij}} \right\rangle_{T=1}$$

We see from this that Δ_1 is altered by correlations in proportion to the change caused in $\langle 1/r_{ij}\rangle_{T=1}$. Note that the spatial integral on r_{ij} involves a net factor r_{ij} (because of the volume element $r_{ij}^2\, dr_{ij}$) so that short-range correlation effects are somewhat weighted downward in value. This applies to both Pauli and dynamical correlations. The former reduces the relative wave functions for spin-parallel pairs. In the case of the shell model, detailed calculations[20] show that the reduction in $\Delta_1 = (1/2T)(D_{NP} - D_{PP})$ by the exchange term $(1/2T)(E_{NP} - E_{PP})$ is of order $(1/Z)\Delta_1$, so we can infer that $\langle 1/r_{ij}\rangle_{T=1}$ is reduced by a corresponding amount. The effect of dynamical correlations is not so easy to pinpoint. Some estimates[30,32] give very small values (usually, but not necessarily, increases) of order $(1/10Z)\Delta_1$. For a naive estimate, suppose that nucleons are held together in groups, as in alpha-particles. This will increase the total Coulomb energy if their mean separation is less than that of freely circulating nucleons. The value of the shift Δ_1 will not be affected if the last particle is a valence particle, but only if it is also involved in a cluster. For an alpha-cluster, the Coulomb energy shift is increased from $6Ze^2/5R$ by amount $6e^2(R - R_\alpha)/5RR_\alpha$, where R, R_α are the values of $(6/5)\langle 1/r_{ij}\rangle^{-1}$ for the nucleus and alpha-particle, respectively. If we estimate R^2 as $(5/3)\langle r^2\rangle$, and use the observed values of $\langle r^2\rangle$ the fractional increase for $A \approx 40$ will be by 6%. (Diffuseness effects correct the estimates of R, R_α downward by about 3%, 5%). Thus, under the most favorable assumptions (that the converted nucleon is involved in a cluster as close-packed as a free alpha-particle), the correlation correction to $\langle 1/r_{ij}\rangle_{T=1}$ is still significantly less than the 10% increase[20] in shift required for $A = 41$ to reconcile the observed shift with observed charge radii and corresponding shell-model neutron radii. Finally, we note that this still leaves the possibility that an appreciable correlation effect can arise from the change in $(\varrho_N - \varrho_P)$ from the shell-model form. In contrast to the effect just considered (that on $\langle 1/r_{ij}\rangle_{T=1}$), this does not depend on the specifically two-body aspect of the Coulomb force, but rather on the fact that the attractive N-P forces act to reduce any differences

between neutron and proton distributions. We will consider this effect in the next section. We find that it is appreciable, but is, unfortunately, partially neutralized by an appreciable second-order Coulomb shift in the opposite direction.

8. ANALOG STATES: SECOND-ORDER SHIFTS AND WIDTH

8.1. Estimate of $\delta E_c - \Delta_1' = -[\Delta(-+) + \Delta(+-)]$

First we consider the second-order corrections $-[\Delta(-+) + \Delta(+-)]$ when δE_c is expressed with leading term Δ_1'. There is a simplicity that does not apply to the other second-order terms, viz., that these depend on $\mathscr{C}^-$, $\mathscr{C}^+$, which means on $\mathscr{C}_v$, $\mathscr{C}_t$ rather than the full Coulomb force $\mathscr{C}$. For the small second-order effects, we proceed as usual by replacing the two-body force by the one-body force. This implies dropping the tensor term and replacing

$$\mathscr{C}_v^- \equiv -\sum_{i,j} t_{i-}(\tfrac{1}{2} - t_{3j}) \frac{e^2}{r_{ij}}$$

by

$$C_v^- \equiv -\sum_i t_{i-} V_c(r_i)$$

where

$$V_c(r_i) = \left\langle \sum_j (\tfrac{1}{2} - t_{3j}) \frac{e^2}{r_{ij}} \right\rangle$$

is the average over the parent nucleus. Note that: (i) this V_c involves the parent charge Z, i.e., it is the Coulomb potential appropriate to the analog; (ii) if we replace $\mathscr{C}$ in $\mathscr{C}_v^- \mid \phi_p\rangle = T_-\mathscr{C} \mid \phi_p\rangle - \mathscr{C}T_- \mid \phi_p\rangle$ by the parent and analog one-body Coulomb forces, we get $\mathscr{C}_v^- \mid \phi_p\rangle \approx 2C_v^- \mid \phi_p\rangle$, which is too large by a factor of 2. This is an example of how one must be careful to introduce the one-body potential correctly; (iii) the correctness of the replacement is exemplified by the near-equality of the sum rules:

$$\langle \phi_p \mid \mathscr{C}_+\mathscr{C}_- \mid \phi_p\rangle - \langle \phi_a \mid \mathscr{C}_- \mid \phi_p\rangle^2 = I(Z-1)[NZ+3(T^2 - T_3^2+T+T_3)] + J\text{-terms}$$

$$\langle \phi_p \mid C_v^+C_v^- \mid \phi_p\rangle = N[\langle V_c^2\rangle - \langle V_c\rangle^2]$$

(note that the definition of C_v is such that $\langle \phi_a \mid C_v^- \mid \phi_p\rangle = 0 = \langle \phi_p \mid C_v \mid \phi_p\rangle$). Since $[\langle V_c^2\rangle - \langle V_c\rangle^2] = Z^2I$, we see that the two are equal apart from the

J-terms and terms of relative order $6T/NZ$ ($\approx 1\%$ for ^{208}Pb). Thus it is reasonably accurate to replace $\mathscr{C}^-$ by C_v^-.

In order to use the sum-rule method, we must specify the amounts of the quantities $\Delta(+-)$ and $\Delta(-+)$ that come from intermediate states of different T'. First, let us consider $(1/2T)\langle\phi_p \mid C_v^+C_v^- \mid \phi_p\rangle$. This is the sum rule for mixing of the analog ψ_a'. Vector-coupling algebra gives the separate contributions:

$$\begin{aligned}\frac{1}{2T}\langle\phi_p \mid C_v^+C_v^- \mid \phi_p\rangle &= \langle\psi_a' \mid H^2 \mid \psi_a'\rangle - \langle\psi_a' \mid H \mid \psi_a'\rangle^2 \\ &= \frac{1}{T(2T+1)(T+1)}\,[M(\| T+1 \|) + (2T+1)M(\| T \|) \\ &\quad + (2T-1)(T+1)M(\| T-1 \|)] \\ &= \frac{1}{T}\,(\langle C_v^2\rangle + M_1 + M_2)\end{aligned}$$

Similarly,

$$\begin{aligned}\frac{1}{2T}\langle\phi_p \mid C_v^-C_v^+ \mid \phi_p\rangle &= \frac{1}{T}\,M(\| T+1 \|) \\ &= \frac{1}{T}\,(\langle C_v^2\rangle - M_1 + M_2)\end{aligned}$$

whence

$$\begin{aligned}\Delta(+-) + \Delta(-+) = \frac{1}{T(2T+1)(T+1)}\Bigg[&(2T^2+3T+2)\frac{M(\| T+1 \|)}{\bar{E}(T+1)} \\ &+ (2T+1)\frac{M(\| T \|)}{\bar{E}(T)} \\ &+ (2T-1)(T+1)\frac{M(\| T-1 \|)}{\bar{E}(T-1)}\Bigg]\end{aligned}$$

Allowing for a symmetry splitting of $\bar{E}(T')$ leads to

$$\begin{aligned}&\Delta(+-) + \Delta(-+) \\ &\quad = \frac{1}{T\bar{E}(T)}\left[2\langle C_v^2\rangle - \frac{2T+1}{(T+1)^2}\,(M_1 - M_2) + 2M_2\right] \\ &\qquad + \frac{2V_1'}{AT[\bar{E}(T)]^2}\left[-2\langle C_v^2\rangle + \frac{2T^2+T+2}{T+1}\,(M_1 - M_2) + 2TM_2\right]\end{aligned}$$

For the shell-model evaluation, we set $\bar{E}(T) = 2\hbar\omega$, $M_2 = 0$, and $V_1' = 0$,

TABLE VI

Values of Various Second-Order Shifts in MeV for Three Nuclei According to the Shell Model (a) and the Correlated Model (b)

The last two shifts (b) for ^{208}Pb depend on taking the energy of the mass-monopole mode at the value 8 MeV.

		^{42}Ca	^{90}Zr	^{208}Pb
$\Delta(+-)+\Delta(-+)$	(a)	1.17	1.59	2.02
	(b)	0.65	0.83	1.24
$\Delta_{2a}-\Delta_{2p}$	(a)	0.18	0.51	1.26
	(b)	0.13	0.56	1.75
$\Delta_1-\Delta_1'$	(a)	−0.99	−1.08	−0.76
	(b)	−0.52	−0.27	0.51

and take $\langle C_v^2\rangle$, M_1, $2\hbar\omega$ from Tables I and II. This gives the values in Table VI. For the correlated-model evaluation, we take $M_2 = V_1'TM_1/A\bar{E}(T)$, $\langle C_v^2\rangle = 1.23N_0(K)/\bar{E}(T)$, and values from Table II. The first term in $\Delta(+-)+\Delta(-+)$ increases from 0.74 to 0.96 MeV as A increases from 40 to 208, while the second term increases from −0.09 to 0.27 MeV. The total values are given in Table VI. These are about 60% of the shell-model values. Such large second-order shifts have a drastic effect on the analysis of Coulomb shifts. In the case of ^{208}Pb, the observed shift is

$$\delta E_c = \Delta_1' - [\Delta(+-)+\Delta(-+)]$$
$$\approx 18.9 \text{ MeV}$$

If we allow for an exchange shift of 0.3 MeV, and then exclude exchange effects from Δ_1', we find

$$\Delta_1' \approx 20.4 \text{ MeV}$$

When $\langle r^2\rangle_p^{1/2}$ is $5.51f$, the value (see Nolen[20]) 19.2 MeV for Δ_1' implies $\langle r^2\rangle_e^{1/2} = 5.95f$, where $\langle r^2\rangle_e^{1/2}$ is the rms radius of the neutron excess defined by

$$\langle r^2\rangle_e = \frac{1}{N-Z}\int r^2(\varrho_N - \varrho_P)\,\mathbf{dr}$$
$$= \frac{N\langle r^2\rangle_N - Z\langle r^2\rangle_P}{N-Z}$$

whence

$$\langle r^2\rangle_e - \langle r^2\rangle_P = \frac{N}{N-Z}\left(\langle r^2\rangle_N - \langle r^2\rangle_P\right)$$

It has been observed[20] that Δ_1' varies with $\langle r^2\rangle_e^{1/2}$ roughly as

$$\frac{\delta(\Delta_1')}{\Delta_1'} = -\tfrac{1}{2}\frac{\delta\langle r^2\rangle_e^{1/2}}{\langle r^2\rangle_e^{1/2}}$$

when $\langle r^2\rangle_P$ is fixed. This rule implies that increasing Δ_1' from 19.2 to 20.4 MeV decreases $\langle r^2\rangle_e^{1/2}$ from $5.95f$ to $5.26f$. The corresponding change in $\langle r^2\rangle_N^{1/2}$ is from $5.66f$ to $5.42f$. The shell model predicts $\langle r^2\rangle_e^{1/2} \approx 6.41f$, $\langle r^2\rangle_N^{1/2} \approx 5.85f$.

8.2. Estimate of $(\Delta_{2a} - \Delta_{2p})$

This is the second-order term occurring when δE_c is expanded as a perturbation series in $\mathscr{E}$. If all energy denominators in Δ_{2a} and Δ_{2p} are set equal to $2\hbar\omega$, we get

$$\Delta_{2a} = \frac{M_a(\mathscr{E})}{2\hbar\omega}$$

$$\Delta_{2p} = \frac{M_p(\mathscr{E})}{2\hbar\omega}$$

where

$$M_x(\mathscr{E}) \equiv \langle\phi_x \mid \mathscr{E}^2 \mid \phi_x\rangle - \langle\phi_x \mid \mathscr{E} \mid \phi_x\rangle^2$$

for $x = a, p$. From Appendix 3, the uniform statistical model gives

$$M_x(\mathscr{E}) = Z(Z-1)(Z-2)I$$

whence

$$\Delta_{2a} - \Delta_{2p} = \frac{3Z^2 I}{2\hbar\omega}$$

An equivalent result follows with the one-body potential C if we allow it to increase by a factor $(Z+1)/Z$ between parent and analog:

$$\Delta_{2a} - \Delta_{2p} = \frac{3}{2\hbar\omega}\left[\langle V_c^2\rangle - \langle V_c\rangle^2\right]$$

Using the sum-rule method with the one-body potential gives

$$\Delta_{2a} = \frac{\langle \phi_a \mid C_s^2 \mid \phi_a \rangle}{\bar{E}'(T)} + 2\frac{\langle \phi_a \mid C_s C_v \mid \phi_a \rangle}{\bar{E}''(T)}$$
$$+ \frac{4T}{(T+1)(2T+1)} \frac{M_a(\| T+1 \|)}{\bar{E}(T+1)} + \frac{(T-1)^2}{T(T+1)} \frac{M_a(\| T \|)}{\bar{E}(T)}$$
$$+ \frac{2T-1}{T(2T+1)} \frac{M_a(\| T-1 \|)}{\bar{E}(T-1)}$$

$$\Delta_{2p} = \frac{\langle \phi_p \mid C_s^2 \mid \phi_p \rangle}{\bar{E}'(T)} + 2\frac{\langle \phi_p \mid C_s C_v \mid \phi_p \rangle}{\bar{E}''(T)} + \frac{T}{T+1} \frac{M_p(\| T \|)}{\bar{E}(T)}$$
$$+ \frac{1}{T+1} \frac{M_p(\| T+1 \|)}{\bar{E}(T+1)}$$

Taking the difference, with the factor $(Z+1)/Z$ between C_s and C_v for the analog and parent and introducing a symmetry splitting of the energies $\bar{E}(T')$, we get

$$\Delta_{2a} - \Delta_{2p} = \frac{2}{Z} \frac{\langle C_s^2 \rangle}{\bar{E}'(T)} + 2\left(\frac{2}{Z} - \frac{1}{T}\right) \frac{\langle C_s C_v \rangle}{\bar{E}''(T)} + \frac{2}{T} \frac{M_2}{\bar{E}(T)}$$
$$+ \frac{V_1'}{A[\bar{E}(T)]^2} \left[\left(\frac{2T-1}{T}\right) M_1 + \frac{1}{T} M_2\right]$$
$$+ \frac{2}{Z} \frac{1}{\bar{E}(T)} \left[\langle C_v^2 \rangle + \frac{2M_2}{T}\right]$$
$$- \frac{2}{Z} \frac{V_1'}{A[\bar{E}(T)]^2} \left[\langle C_v^2 \rangle - \left(\frac{3T-1}{T}\right) M_1 + \left(\frac{T+1}{T}\right) M_2\right]$$

Checking on the shell-model result by setting $M_2 = 0$, $V_1' = 0$ and using Appendix 3 for $\langle C_s^2 \rangle$, $\langle C_s C_v \rangle$, $\langle C_v^2 \rangle$ we get

$$\Delta_{2a} - \Delta_{2p} = \frac{b^2 a_1^2}{2\hbar\omega} (2\langle r^2 \rangle + \langle r^2 \rangle_e)$$

agreeing with the result above when we replace the uniform-model quantity $\langle V_c^2 \rangle - \langle V_c \rangle^2$ by the corresponding shell-model quantity.

Let us now evaluate $\Delta_{2a} - \Delta_{2p}$ with the correlated model. In the previous expression, many terms are small for all nuclei. Retaining only larger terms and setting $M_2 = TV_1' M_1 / A\bar{E}(T)$, we get

$$\Delta_{2a} - \Delta_{2p} \approx \frac{2}{Z} \left[\frac{\langle C_s^2 \rangle}{\bar{E}'(T)} + \frac{\langle C_v^2 \rangle}{\bar{E}(T)}\right] + 2\left(\frac{2}{Z} - \frac{1}{T}\right) \frac{\langle C_s C_v \rangle}{\bar{E}''(T)}$$

With $\langle C_s^2 \rangle = N_0(K)/\bar{E}'(T)$, $\langle C_v^2 \rangle = 1.23 N_0(K)/\bar{E}(T)$ and $\bar{E}(T) = 2\hbar\omega + 10$ MeV, $\bar{E}'(T) = 2\hbar\omega - 6$ MeV, we find that the first two terms are larger than the shell-model values of $\Delta_{2a} - \Delta_{2p}$. Since the factor $[(2/Z) - (1/T)]$ is negative, and since $\langle C_s C_v \rangle$ is negative in the shell model and is expected to go quickly to zero with correlation effects, the last term in $(\Delta_{2a} - \Delta_{2p})$ is small and positive, and will serve only to slightly increase the quoted factors.

8.3. Comparison of Δ_1 and Δ_1'

Since

$$\Delta_1 - \Delta_1' = (\Delta_{2a} - \Delta_{2p}) - [\Delta(+-) + \Delta(-+)]$$

and we now have estimates of all the second-order quantities, we may now evaluate the difference between Δ_1 and Δ_1'. On inspecting Table VI, we see that the shell-model values for this difference are negative. At first glance, it may seem surprising, that any Coulomb expectation value is *increased* when Coulomb dilation of the wavefunctions is included. However, this is because the displacement energy Δ_1 involves the difference $(\varrho_N - \varrho_P)$. If ϱ_P is dilated without any change in ϱ_N (as happens in a shell model with a fixed, i.e., nonself-consistent, potential) then Δ_1' will be greater than Δ_1. At the other extreme, if the neutron–proton force is so strong that the neutron density dilates with the proton one, then Δ_1' will be less than Δ_1. We may expect that the actual situation is intermediate. From Table VI, we see that, in all nuclei, correlations reduce $(\Delta_1' - \Delta_1)$. In the heavier nuclei, they change the sign of $\Delta_1' - \Delta_1$ from positive to negative while, in light nuclei, $\Delta_1' - \Delta_1$ remains positive. Note that values for heavy nuclei are sensitive to the mass-monopole energy $\bar{E}'(T)$, which we have taken as 8 MeV for ^{208}Pb.

8.4. Implications for the Nolen–Schiffer Anomaly

The general conclusion from the last discussion is that correlations reduce $(\Delta_1' - \Delta_1)$ by the order of an MeV, so that one or both of these quantities change by an amount of this order. This means that the Nolen–Schiffer anomaly might be removed if correlations were taken into account, i.e., the value of Δ_1' may be increased by the effect of correlations on ϱ_N and ϱ_P. That this will actually happen is far from clear. We can illustrate this by referring to the oscillator model for ^{208}Pb. The effect of the Coulomb force on the protons is to increase $\langle r^2 \rangle_P$ from $0.875\langle r^2 \rangle_N$ to $1.045\langle r^2 \rangle_N$.

For small changes in radii, first-order shifts scale as[20]

$$\frac{\delta\Delta_1}{\Delta_1} = -\tfrac{1}{4}\left[\frac{\delta\langle r^2\rangle_e}{\langle r^2\rangle_e} + \frac{\delta\langle r^2\rangle_P}{\delta\langle r^2\rangle_P}\right]$$

Let us apply this to the change from Δ_1 to Δ_1', for which $\delta\langle r^2\rangle_N = 0$, so

$$\delta\langle r^2\rangle_e = \frac{-Z\delta\langle r^2\rangle_P}{N-Z}$$

Because the above dilation is so drastic, we get different answers, when we start from Δ_1 or Δ_1', viz., $|\,\delta\Delta_1\,| = 0.32, 0.93$ MeV. The value (0.76 MeV) in Table VII lies in between. Let us now apply the rule to the change in Δ_1 when correlations are included. Let us suppose that these correlations draw the neutrons and protons toward each other by equal and opposite changes in $\langle r^2\rangle_N$, $\langle r^2\rangle_P$, then Δ_1 is increased by

$$\frac{\delta\Delta_1}{\Delta_1} \approx 0.6\,\frac{\delta\langle r^2\rangle_P}{\langle r^2\rangle_P}$$

Applying the same picture to Δ_1', and recalling that protons are now outside the neutrons, we find that Δ_1' is decreased by

$$\frac{\delta\Delta_1'}{\Delta_1'} \approx -0.7\,\frac{|\,\delta\langle r^2\rangle_P\,|}{\delta\langle r^2\rangle}$$

Thus, in this illustration, we see that Δ_1' is decreased when correlations are included, i.e., the effect is in the wrong direction to explain the Nolen–Schiffer effect. The decrease in Δ_1' arises because of the oscillator feature that $\langle r^2\rangle_P > \langle r^2\rangle_N$ when Coulomb forces are present. This does not happen for a Saxon–Woods potential. (When the Coulomb force is present for ^{208}Pb, the neutron potential must be 7% less[20] than the proton one if $\langle r^2\rangle_N = \langle r^2\rangle_P$). Thus, the above decrease in Δ_1' from correlations is specific to the oscillator. A more realistic well will show an increase in Δ_1' as well as Δ_1, although less in Δ_1' than in Δ_1 since the shell-model neutron and proton densities overlap better when Coulomb forces are present, and therefore change less when correlations are included. If neutrons and protons move toward each other when correlations are included, the maximum increase in Δ_1 arises if the neutrons do all the moving, in which case

$$\delta\Delta_1 \approx 0.8 \text{ MeV}$$

If $\delta\Delta_1'$ is also positive and smaller, the decrease in $(\Delta_1' - \Delta_1)$ from correla-

tions is less than 0.8 MeV, which is less than the 1.2 MeV suggested by the above evaluation of $(\Delta_{2a} - \Delta_{2p}) - [\Delta(+-) + \Delta(-+)]$. Thus, apparently, the effect of the correlations implied in that evaluation is an overall contraction of neutrons and protons as well as movement toward each other. Note that, if this is a true diagnosis, and if the observed $\langle r^2 \rangle_P$ is used for the correlated system, this implies that the value of $\langle r^2 \rangle_P$ for the uncorrelated system is larger, so Δ_1' is even smaller than the Nolen–Schiffer shell-model estimate using the observed $\langle r^2 \rangle_P$. Thus the occurrence of a larger increase in Δ_1' when correlations are included does not help to fit the observed shift.

One can see directly that this is going to be very difficult by asking what value of $\langle r^2 \rangle_N$ is required if we force a fit of Δ_1' to the observed value (20.4 MeV, when corrected for second-order shift). As seen above, it requires that $\langle r^2 \rangle_N^{1/2}$ be appreciably *less* than $\langle r^2 \rangle_P^{1/2}$ ($5.42f$ rather than $5.52f$). At present, no theoretical model has this property. To this extent, the Nolen–Schiffer problem remains. Our studies here have not disposed of it, but rather indicate that, because of a large second-order shift, it is even more serious than previously believed.

8.5. Spreading Width

From Sec. 8, the spreading width of an analog state is given by

$$-\delta E_c + \frac{i}{2}\Gamma^{\downarrow} = \tfrac{1}{2}T\langle \phi_p \mid \mathscr{E}^+ \frac{Q}{H_0 - E_0^+} \mathscr{E}^- \mid \phi_p \rangle$$

Noting that the background states in the vicinity of the analog state are entirely of $T' = (T - 1)$, it follows that

$$\Gamma^{\downarrow} = 2\pi s(E_0)\left(\frac{2T-1}{2T+1}\right) M(\| T - 1 \|)$$

where $s(E)$ is the strength function describing the spreading of the $(T - 1)$ part of the charge monopole state by nuclear forces:

$$s(E) = \frac{(1/2\pi)\Gamma}{(E_M - E)^2 + \frac{1}{4}\Gamma^2}$$

Noting that $(E_M - E_0) = \bar{E}(T - 1)$, we have if $\Gamma < \bar{E}(T - 1)$

$$\Gamma^{\downarrow} \approx \frac{\Gamma}{T}\left(\frac{2T-1}{2T+1}\right)\frac{M(\| T - 1 \|)}{[\bar{E}(T-1)]^2} = \Gamma A(T - 1)$$

For ^{208}Pb, values of $A(T - 1)$ in Table IV lead to values of $\Gamma^{\downarrow}$ of 0.10Γ and 0.55Γ, respectively, for the shell and correlated models. To fit the

observed value $\Gamma^{\downarrow} \approx 100$ keV requires $\Gamma \approx 1$ MeV, 2 MeV, respectively (for ^{90}Zr, the observed value $\Gamma^{\downarrow} \approx 20$ keV requires $\Gamma \approx 0.5$, 1 MeV, respectively). Both of these are considerably less than one would have guessed if guided by values of Γ for single-particle states, where the optical-model absorption potential W indicates a value $\Gamma \sim 2W \sim 10$ MeV. However, there are three effects acting to reconcile these numbers:

1. The spreading width of a linear superposition of single-particle states (like the monopole state) may be less than the average width of the separate states. That this may occur theoretically for the dipole state has recently been shown by Bertsch,[69] who finds a factor $\frac{4}{9}$ for Serber forces. (However, Rosenfeld forces in his formulas give the opposite effect.)
2. The spreading width is not necessarily constant with energy, but may be different at energies distant from the center of the state (as in the present case). Again the dipole case provides evidence of this; the observed $E1$ strength function near the neutron threshold is considerably less than the value expected from extrapolating from a fit to the peak with a Breit–Wigner formula. In the monopole case, this means that the spreading width evaluated near the analog may be only a fraction of the width taken at the monopole state itself.
3. For a "volume" form of W, with central value $W = W_0$ the value of $\langle W \rangle$ taken in the analog state may be significantly less than W_0, because of the fact that an appreciable fraction of the analog state normalization is outside the region where W is significant. (Note that the physical analog is unbound, so that the normalization volume cannot be all space, but is confined to the region inside the channel turning-points). This effect may lead to a value of Γ that is 20–50% below $2W_0$. (Evidence for this effect comes from the shift[60] between the analog and configuration states in ^{208}Bi. The splitting between these is 12 MeV which is about 80% of the 15 MeV difference between neutron and proton nuclear potentials.)

9. SECOND-ORDER EFFECTS IN MODEL CALCULATIONS

So far we have compared estimates of second-order Coulomb effects with various items of data. It is instructive to apply the theory to certain model calculations that have been performed. These models are necessarily

restricted and omit various effects that occur in more realistic descriptions. Nevertheless, they provide valuable checks on our approach to Coulomb mixing.

We discuss two models; one is the simplest that can be done, while the other the most sophisticated that has been reported to date.

9.1. Coulomb Shift of Single-Particle States

Many calculations have been made of the exact displacement of a single-particle state by the Coulomb force. One can also evaluate the first-order displacement. The difference between the two (the so-called Thomas–Ehrman shift) is presumably dominated by the second-order term. Table VII shows values[60] for six orbitals in ^{208}Pb. The Saxon–Woods potential well has been chosen to make the binding energy in the absence of the Coulomb force equal to the observed energies of the hole states of ^{207}Pb relative to ^{208}Pb.

The first-order shifts are just as expected from an oscillator model, viz., all are roughly equal, except the $1i_{13/2}$ case where the reduction arises from the larger value of $\langle r^2 \rangle_{nl}$.

In contrast, the second-order effects of the last column are substantially affected by the proton orbitals being unbound, an effect which is not contained in the oscillator. This is clear because the oscillator gives a second-

TABLE VII

Coulomb Shifts for Six Single-Particle Orbitals in ^{208}Pb

All energies in MeV. The differences in the last column are presumably mainly second order in origin.

Orbital	First-order shift	Exact shift	Difference
$3p_{1/2}$	19.82	19.04	0.79
$3p_{3/2}$	19.90	19.15	0.75
$2f_{5/2}$	19.96	19.46	0.50
$2f_{7/2}$	19.92	19.59	0.38
$1i_{13/2}$	19.01	18.87	0.13
$1h_{9/2}$	20.09	19.96	0.14
$(2j+1)$ weighted mean	19.67	19.36	0.31

order shift for orbital nl proportional to $\langle r^2 \rangle_{nl}$ (Appendix 4). This is the same for all orbits (except $1i_{13/2}$) while the entries in the table vary widely.

In the oscillator model, one can check on the dominance of the second over higher-order terms since the exact corrected energy of an oscillator level $(N+\frac{1}{2})\hbar\omega$ when subject to $a_1 r^2$ is $(N+\frac{1}{2})\hbar\omega'$, where $\hbar\omega' = \hbar\omega(1-x)^{1/2}$, $x = 2a_1/m\omega^2$. In heavy nuclei, x is largest (≈ 0.30) and the third- and higher-order corrections are 23% of the second-order one (which is about 7% of the first-order one). (The second-order shift implied by this result is $\Delta(nl) = -(N+\frac{1}{2})a_1^2\hbar/2m^2\omega^3$, with $N \equiv (2n+l-1)$, agreeing with the direct derivation in Appendix 4.)

With a_1 from Table I and $\hbar\omega$ chosen to maximize overlap on the Saxon–Woods functions ($\hbar\omega = 7.75, 8.06, 8.81, 9.00$ MeV for the $3p$, $2f$, $1h$, $1i$ orbits), we obtain 0.45, 0.41, 0.28, 0.25 MeV respectively for the total (second-plus-higher-order) shifts. (The choice used in Table II, $\hbar\omega = 7$ MeV, gives 0.59, 0.68 MeV). These values center around those in Table VII and have the same trend, but their dispersion is less. The value of their $(2j+1)$-weighted mean, 0.33 MeV, is very close to that in Table VII.

If we assume that the shifts are dominated by the nearest neighbor orbitals of the same j (as exactly so in the oscillator):

$$\Delta(nl) = -\frac{1}{2\hbar\omega}\{M(n,l) - 2[M(n-1,l) + M(n-2,l)\ldots]\}$$

where the series has n terms. For the lowest orbital of given j, $n = 1$ and there is only one term. The energy denominators are assumed roughly equal to the oscillator value $2\hbar\omega$. $M(nl)$ is the sum rule for orbital nl:

$$M(nl) = a_1^2(\langle r^4 \rangle_{nl} - \langle r^2 \rangle_{nl}^2)$$

where $V_c(r)$ is taken as $a_0 - a_1 r^2$. Thus the variations in the table may be attributed to the $M(nl)$ or to the departure of the Coulomb force from the quadratic form.

9.2. Model Analog

The most complete calculation of an analog state is that[60] of the analog of ^{208}Pb. The basis of states $|(nlj)_N^{-1}(n'lj)_P\rangle$ is used, where (nlj) is one of the six excess neutron orbitals of ^{208}Pb. Instead of diagonalizing H in the infinite set of states $n' = 1, \ldots, \infty$, the problem is converted to the form of

six coupled differential equations (i.e., six coupled channels). Antisymmetry is imposed between the 44 excess nucleons but not between these and the 164 core nucleons. If the Coulomb force is suppressed, the analog is the bound state:

$$\phi_a = \frac{T_-\phi_p}{\langle \phi_p \mid T_+T_- \mid \phi_p \rangle^{1/2}}$$
$$= \frac{\sum_j (2j+1)^{1/2} \mid (nlj)_N^{-1}(nlj)_P\rangle}{[\sum_j (2j+1)]^{1/2}}$$

where ϕ_p is the closed-shell parent, ^{208}Pb. In the model calculation, since the core orbits are fixed, the Coulomb force between the converted proton and the core protons is allowed to excite the converted proton only; core excitation is suppressed.

In Sec. 7, we introduced two ways of expressing the Coulomb shift, δE_c, to second order:

$$\delta E_c = \Delta_1 - (\Delta_{2a} - \Delta_{2p}) = \Delta_1' - \Delta(+-) - \Delta(-+)$$

Within the present model, Δ_{2p} and $\Delta(-+)$ are zero, and the two expansions become identical; $\Delta_1 = \Delta_1'$ is the first-order shift, while $\Delta_{2a} = \Delta(+-)$ is the second-order one. The last equality can be seen directly since, in the absence of Coulomb excitation of core protons,

$$\langle n \mid C_v^- \mid \phi_p \rangle = \langle n \mid [C, T_-] \mid \phi_p \rangle = (2T)^{1/2} \langle n \mid C \mid \phi_a \rangle$$

for any state $n \neq \phi_a$, whence the total mixing is

$$\frac{1}{2T} \langle C_v^+ C_v^- \rangle = \langle \phi_a \mid C^2 \mid \phi_a \rangle - \langle \phi_a \mid C \mid \phi_a \rangle^2$$

Before evaluating this for the model, let us reconsider the normal shell-model evaluation of Sec. 8, and divide

$$\frac{1}{2T} \langle C_v^+ C_v^- \rangle = \frac{1}{T} (\langle C_v^2 \rangle + M_1 + M_2) = 18.2 a_1^2 b^4$$

into contributions from the excess and the core neutrons. We find by calculating individual matrix elements $\langle n \mid C_v^- \mid \phi_p \rangle$ and summing their squares (using Appendix 4), that upward excitations from the 44 excess neutrons contribute $810 a_1^2 b^4/88 = 9.2 a_1^2 b^4$ while upward excitations from the 82 core neutrons contribute $786 b a_1^2 b^4/88 = 8.95 a_1^2 b^4$. There is also a small contribution $105 a_1^2 b^4/484 = 0.22 a_1^2 b^4$ from mixing from the 44

excess neutrons to configuration states. Of the 82 core neutrons, only the highest 62 give rise to any contributions.

Returning to the model, we see that the absence of core excitation means that the core contribution is suppressed, thereby reducing $(1/2T) \times \langle C_v^+ C_v^- \rangle$ to 51% of its full shell-model value. In partial compensation of this, there is an extra contribution arising from the fact that *downward* excitations from the 44 excess orbits are allowed. This gives $210 a_1^2 b^4/88 = 2.4 a_1^2 b^4$, raising $(1/2T)\langle C_v^+ C_v^- \rangle$ to 64% of its shell-model value.

When we insert these results into the estimate of the shift $\Delta(+-)$, we must allow for the fact that the downward excitations have an energy denominator of opposite sign. The result is that both above effects reduce $\Delta(+-)$, the first to 51% and the second to 37.6% of the shell-model value. Thus the shell-model value $\Delta(+-) = -1.42$ MeV implied in Sec. 8 becomes a second-order shift of $\Delta = -0.53$ MeV when applied to the present model. There is a check on this result arising from the fact that the Coulomb shift of a shell-model state in any order is equal to the single-particle value (this is a special case of the result that the Pauli principle is irrelevant to the effect of a one-body operator on a state of noninteracting particles), i.e., the value of the second-order shift $\Delta = \Delta_{2a} = \Delta(+-)$ for the present model must equal the shell-model value of $(\Delta_{2a} - \Delta_{2p})$ of Sec. 8 since both must equal the single-particle value. For the analog containing several excess orbits, this is the $(2j+1)$ weighted mean $\sum_j (2j+1) \times \Delta(nlj)/\sum_j (2j+1)$, where $\sum_j (2j+1) = 2T$. Assigning oscillator values (mentioned above) to $\Delta(nlj)$ makes this quantity equal to -0.53 MeV, concluding the check.

9.3. Analysis of Shift Calculated from the Model

The coupled-channel calculation corresponding to the entries of Table VII gives an analog shift $\delta E_c = 18.88$ MeV agreeing with experiment. The calculation includes an exchange correction of 300 keV to the first-order term. From Table VII we see that the nonfirst-order shift emerging from the calculation is 0.18 MeV larger than the $(2j+1)$ weighted mean of the single-particle values, 0.31 MeV. A difference between the two values is not surprising since the energy denominators of the second-order shift that are implicit in the coupled-channels calculation are different to those of the separate single-particle problems. What is surprising is the direction of the difference. Since the shift is larger in the coupled-channel case, one infers that the energy denominators are less, i.e., the relevant part of the monopole state is at an excitation relative to the analog of $< 2\hbar\omega$. Recalling that

nearly all of $\langle C_v^+ C_v^- \rangle$ arises from states of $T' = (T - 1)$, the vital question is where this part of the monopole state occurs. In Table II, we give the value 19 MeV for $\bar{E}(T - 1)$; this is 5 MeV above the single-particle value $2\hbar\omega = 14$ MeV.

In the model calculation, the two-body force that is used implies a symmetry splitting term of energy levels of $(T - 1)$ and T of about 12 MeV. It is not clear what value of the $(T - 1)$ monopole shift $gM_0^{(0)}(1 + M_1^{(0)}/M_0^{(0)})$ is implied by the calculation. Let us fix the last factor at the value 1.47 implied by Table I, then the requirement of an energy denominator $< 2\hbar\omega$ implies that the mean shift $gM_0^{(0)}$ is < 8 MeV. To actually fit the increase in shift from 0.31 to 0.48 MeV requires that $gM_0^{(0)} \approx 6$ MeV. (We recall that we have used $gM_0^{(0)} = 10$ MeV in the present work, specifically in Table II.) It is difficult to give any direct evaluation of the monopole shift implicit in the model calculation. This calculation uses a zero-range force, $(a + bP^\sigma)V\delta(r)$, with $(a/2 + b)V$ fixed by the symmetry splitting at about 600 MeV $\cdot f^2$. With a Rosenfeld force mixture $a = 0.8$, $b = 0.2$, this means $V = 1000$ MeV $\cdot f^3$. In diagonalizations in the dipole problem this gives a shift of about 5 MeV for ^{208}Pb. Unfortunately, we do not have any corresponding results for the monopole case. We can only infer indirectly from the above analysis that it is of the order of 6 MeV.

It should be noted that the basis of the model calculation is insufficient to allow the construction of excited states of pure isospin $(T - 1)$ or T. (The analog and configuration states are exceptions.) States of $2p$–$2h$ type that are degenerate with the $1p$–$1h$ type in the basis are required for this construction. Thus the model monopole state does not split into its components $T - 1$, T, $T + 1$, but occurs in a constrained form at an energy determined by the major isospin in the basis. Although thirty states of the $2p$–$2h$ type are needed to supplement the six $1p$–$1h$ states of excitation $2\hbar\omega$ to construct 100% pure isospins, the six states have almost pure isospin $(T - 1)$. (They contain fraction $(T + 1)^{-1}$ of isospin T.) Thus this limitation in basis should not affect the above considerations since the monopole state will presumably be located at the energy relevant to the dominant $(T - 1)$ part.

9.4. Analysis of Spreading Width Calculated from the Model

We may start from the general expression for spreading width equivalent to that in Sec. 8:

$$\Gamma^{\downarrow} = 2\pi s(E_0) \frac{1}{2T} \langle C_v^+ C_v^- \rangle$$

When applying this to the model calculation, we must note the occurrence of the downward excitations (also of the configuration states, but these account for such a small fraction of $\langle C_v^+ C_v^- \rangle$, about 2%, that we will neglect these). We have seen above that, in the oscillator shell model, the downward excitations account for about 25% of the upward ones. Since each branch presumably has the same form of $s(E_0)$ and since each is roughly the same distance from the analog, we get, with $s(E_0) \approx \Gamma/2\pi[\bar{E}(T-1)]^2$:

$$\Gamma^{\downarrow} \approx \frac{5}{4} \frac{\Gamma}{\bar{E}(T-1)} \frac{(1/2T)\langle C_v^+ C_v^- \rangle_{\mathrm{up}}}{\bar{E}(T-1)}$$

where the subscript denotes upward excitations only. Strictly there should also be an interference term between the upward and downward excitations. Relative to the above term, this is approximately

$$\pm \frac{2}{\Gamma} \langle \phi_{\mathrm{up}} \mid W \mid \phi_{\mathrm{down}} \rangle$$

where $\phi_{\mathrm{up}}, \phi_{\mathrm{down}}$ are the normalized branches of the monopole state and W is the absorption potential in the model. This is such that

$$\Gamma \approx 2\langle W \rangle \equiv \frac{2\langle \phi_a \mid C_v^+ W C_v^- \mid \phi_a \rangle}{\langle \phi_a \mid C_v^+ C_v^- \mid \phi_a \rangle}$$

Since $\phi_{\mathrm{up}}, \phi_{\mathrm{down}}$ are orthogonal, we infer that the cross-term is small, and we will ignore it. In the formula for $\Gamma^{\downarrow}$, we may identify the last factor with the shift of the model, 0.6 MeV, and take $\bar{E}(T-1)$ to be the inferred value 11 MeV deduced above; then

$$\Gamma^{\downarrow} \approx 0.07\Gamma$$

Since the calculation fits the data, we may infer that it gives the observed value $\Gamma^{\downarrow} \approx 0.13$ MeV, whence $\Gamma \approx 2$ MeV, so $\langle W \rangle \approx 1$ MeV. The calculation uses two forms of $W(r)$:

(i) $$W_0(1+x)^{-1}, \quad W_0 = 2.5 \text{ MeV}$$

(ii) $$4W_s x(1+x)^{-2}, \quad W_s = 6.5 \text{ MeV}$$

where $x = \exp[(r-R)/a]$ and $R = 6.9f$, $a = 0.475f$. (The real potential used is of the form $V_0(1+x)^{-1}$.) If we estimate $\langle W \rangle$ as the average of $W(r)$ taken to the 10% point of $(1+x)^{-1}$, i.e., about $7.4f$, then $\langle W \rangle = 1.7$, 3.0 MeV in (i) and (ii). These values are too large by factors 1.7 and 3.

The mere fact that they give different values suggests that the recipe for $\langle W \rangle$ is poor.

In relation to this discrepancy, we note first that items (1) and (2) of Sec. 8 which may reduce $\Gamma^{\downarrow}$ for physical analog do not apply within the model. Item (3) does, and indeed is the only explanation that we have to offer, other than the possible (but improbable) importance of the neglected cross-term. Physically, it means that an appreciable fraction of the significant normalization of the analog lies outside 7.4*f*. For an unbound state like the analog, the effective normalization region is that inside the outer turning points.

10. CONCLUSIONS

We have based estimates of second-order Coulomb effects on the shell model and on an improved model that takes correlations into account by means of a sum-rule method.

The first three items examined (isospin impurities, departures from constant *ft* value of superallowed transitions, departures from quadratic form of the isobaric mass formula) are such that experiment mostly indicates upper limits to these effects rather than absolute values. The challenge to theory is mainly to see if estimates of Coulomb effects lie within these limits. This turns out to be true for the first two items, and would be true for the last except for the case of mass 9 where the cubic coefficient is 8.0 ($\pm$3.7) keV. This is larger than estimated ($\leq$ 1 keV). In view of the large quoted error, one cannot be too disturbed by this discrepancy at present, but the case must be reviewed when improved data are available. If the value survives, then charge-dependent nuclear forces[15] may be needed for an explanation.

Spreading widths and second-order shifts of analog states have been evaluated, both for physical analogs, and for a calculated-model analog. The comparison of estimates with true values is not entirely satisfactory but not sufficiently off-target to reveal any major discrepancy. The estimated widths are, at first essay, larger than observed by a serious factor ($\geq$ 5). However, there are three effects that will reduce this factor, and, therefore, while one cannot claim positive agreement, there is not an obvious disagreement. Unfortunately, the proper evaluation of these effects involves going considerably further than we have been able to go. (For instance, the distribution of $2p$–$2h$ states determining the energy dependence of the monopole-state strength function must be specified.) There is a smaller

but more clearcut disagreement in the case of the model analog[60] where the disagreement is less ($\sim$ factor 2), but two of the three effects do not occur. This may be due to the third effect [smallness of $\langle W \rangle$ arising from fraction of the analog normalization in the channels outside the range of $W(r)$], or possibly to the neglect of the upper–lower cross-term mentioned in the text. Since the estimate does not depend strongly the oscillator model, but rather relates the spreading width to the shift and uses the true value of the latter, the discrepancy is probably not due to shortcomings of the oscillator model. Further study is needed since clearly one must understand calculations before one can hope to understand physical analogs.

Finally there are the second-order shifts of analog states. We have found large second-order effects (order of an MeV), which reduce the calculated shift. Thus the Nolen–Schiffer problem that the first-order shell-model shift is smaller than the observed shift[20] is made more acute by including second-order effects within the shell model. There is a strong overall discrepancy of the order of 2 MeV. When correlations are included, the second-order shift is less, but it is not clear that the first-order shift will be increased (through the change in ϱ_P, ϱ_N) sufficiently to remove the discrepancy. It seems unlikely, and, to that extent, the problem remains.

ACKNOWLEDGMENT

We have received valuable help and advice from many colleagues, especially Drs. L. Zamick, D. Wilmore, J. P. Schiffer, J. A. Nolen, Y. Waghmare, L. C. Biedenharn, S. Kahana, N. van Giai, and N. Auerbach.

APPENDIX 1

Corrections from More Accurate Treatment of the Coulomb Potential

We have approximated the Coulomb potential of the nucleus in two ways (1) we have suppressed specifically two-body effects, and have worked with the effective one-body force $V_c(r)$, (2) we have restricted $V_c(r)$ to the form $a_0 - a_1 r^2$. This applies to the interior of a uniform distribution. For more realistic distributions $V_c(r)$ is rather different, although this difference is less than would be the case if the Coulomb force were of shorter range. We consider these two approximations and their effect on our estimates.

Corrections from Two-Body Coulomb Forces

The two-body force is

$$\mathscr{C} = \tfrac{1}{2}\sum_i (\tfrac{1}{2} - t_{3i}) \sum_{j\neq i} (\tfrac{1}{2} - t_{3j}) \frac{e^2}{r_{ij}}$$

When operating on a given determinantal state $|\Phi_0\rangle$, this can be separated into three parts corresponding to zero-particle, one-particle, and two-particle excitation, viz., $\mathscr{C} = \mathscr{C}^{(0)} + \mathscr{C}^{(1)} + \mathscr{C}^{(2)}$; $\mathscr{C}^{(0)}$ is simply the number $\langle\phi_0 | \mathscr{C} | \phi_0\rangle$; $\mathscr{C}^{(1)}$ has the form

$$\mathscr{C}^{(1)} = \sum_i (\tfrac{1}{2} - t_{3i}) f_i$$

and is defined such that it reproduces the single-particle excitation matrix elements of

$$\langle ph | \mathscr{C}^{(1)} | \Phi_0\rangle = \langle ph | \mathscr{C} | \Phi_0\rangle$$

It follows that

$$\langle p | f | h\rangle = \langle p | V_c | h\rangle - \langle p | V_c' | h\rangle$$

where V_c is the local potential

$$V_c(r_i) \equiv \int \mathbf{d}\mathbf{r}_j \varrho_P(r_j) \frac{1}{r_{ij}}$$

in terms of proton density $\varrho_P(r_j)$, and V_c' is the nonlocal part:

$$\langle \mathbf{r} | V_c' | \mathbf{r}'\rangle = \sum_{h'} u_{h'}(\mathbf{r}) u_{h'}(\mathbf{r}') \frac{1}{|\mathbf{r} - \mathbf{r}'|}$$

where $u_{h'}(\mathbf{r})$ are the proton-occupied states (satisfying $\varrho_P(r) = \sum_{h'} |u_{h'}(\mathbf{r})|^2$. Note that the contributions to $\langle p | f | h\rangle$ from the terms $h' = h$ in V_c and V_c' cancel, so these terms may be omitted if desired. This means that ϱ_P in V_c is replaced by $\varrho_P - |u_h(\mathbf{r})|^2$, which is approximately $(Z - 1)\varrho_P/Z$. $\mathscr{C}^{(2)}$ is obtained from the difference $(\mathscr{C} - \mathscr{C}^{(0)} - \mathscr{C}^{(1)})$. The scalar part of $\mathscr{C}^{(1)}$ is irrelevant for most of the discussions of isospin mixing; the more interesting part is the vector part:

$$\mathscr{C}_v^{(1)} = -\sum_i t_{3i}[V_c(r_i) - \langle\Phi_0 | V_c(r_i) | \Phi_0\rangle]$$

and this is identical to the one-body force C_v that we have been using. The following considers the role of the specifically two-body force $\mathscr{C}^{(2)}$ relative

to $\mathscr{C}_v$. More precisely, since the scalar parts of both are irrelevant for mixing, we are really studying the role of $\mathscr{C}_v^{(2)} + \mathscr{C}_t^{(2)}$ relative to $\mathscr{C}_v^{(1)}$. We do this by evaluating the fractional change in the sum rules $M(T')$ when $\mathscr{C}^{(1)}$ is replaced by the full* Coulomb force (or, equivalently, by $\mathscr{C} - \mathscr{C}^{(0)} = \mathscr{C}^{(1)} + \mathscr{C}^{(2)}$). Consider a parent state $\phi_0(T = T_3)$. From the uniform statistical model[7] which assumes that all spatial orbits can be replaced by a common orbit and ignores space-exchange terms:

$$M(T+1) + M(T+2) = \frac{1}{2T+2} Z(Z-1)[(Z-3)I + J]e^4$$

where I, J are spatial averages in ϕ_0:

$$I \equiv \left\langle \frac{1}{r_{12}r_{13}} \right\rangle - \left\langle \frac{1}{r_{12}} \right\rangle^2$$

$$J \equiv \left\langle \frac{1}{r_{12}^2} \right\rangle - \left\langle \frac{1}{r_{12}} \right\rangle^2$$

Note that $M(T+1) + M(T+2)$ depends on $(\mathscr{C}_v + \mathscr{C}_t)$ only.

With the one-body force of the present paper, using the results of Sec. 3 and noting that $M(T+2) = 0$ for a one-body force, we get, with the same uniform statistical model as used above:

$$M(T+1) + M(T+2) = \frac{1}{T+1} (\langle C_v^2 \rangle - M_1)$$

$$\langle C_v^2 \rangle = \tfrac{1}{4}A(\langle V_c^2 \rangle - \langle V_c \rangle^2)$$

$$M_1 = \tfrac{1}{4}(N-Z)(\langle V_c^2 \rangle - \langle V_c \rangle^2)$$

whence,

$$M(T+1) + M(T+2) = \frac{1}{2T+2} (Z-1)^2 ZIe^4$$

where we have used

$$\langle V_c^2 \rangle - \langle V_c \rangle^2 = (Z-1)^2 I$$

This is essentially equal to the first term of the above expression. Thus

* In the papers of Mekjian,[34] a hybrid force is used, viz., $\mathscr{C}_v = \mathscr{C}_v^{(1)} + \mathscr{C}_v^{(2)}$, i.e., this includes the two-body vector force but ignores the two-body tensor force. The corresponding sum rules are essentially equal to those for the full Coulomb force increased by factor $(A/2Z)^2$ implying destructive interference of the tensor and vector parts when the full force is used. Further the J-terms is increased relative to the I-term by A/Z.

the two expressions differ just in the J-term, which, as expected, is a specifically two-body effect (the quantity $1/r_{12}^2$ has no one-body counterpart).

For another comparison, consider the total mixing of an analog state by the relative Coulomb force. As we see in Sec. 8, this mixing arises from $[\mathscr{C}, T_-]$ so that the scalar part of $\mathscr{C}$ is irrelevant, and the comparison is between $\mathscr{C}_v^{(1)}$ and $(\mathscr{C}_v + \mathscr{C}_t)$. Lane and Soper[7] give

$$\langle [T_+, \mathscr{C}][\mathscr{C}, T_-] \rangle = (Z-1)Ie^4\left[\frac{N(Z-3)}{2T} + 3\right] + Je^4\left[\frac{N(Z-1)}{2T} + 1\right]$$

for the two-body force, the uniform statistical model gives for the one-body force,

$$\langle [T_+, C_v][C_v, T_-] \rangle = \frac{1}{2T} N(Z-1)^2 Ie^4$$

As before, we see that the one-body result is essentially equal to the I-part of the two-body force; also the J-part gives a positive correction by a factor $(1 + J/ZI)$. The uniform model gives $J/I \approx 50$, so the correction is appreciable: $(1 + J/ZI) = 3.5, 1.6$ for $Z = 20, 80$.

When the energy-weighted sum rules are evaluated, one again finds a correspondence between the one-body result and certain terms (the I-like terms) of the two-body case. The remaining (J-type) terms give an infinite value for the kinetic energy part. This is interpreted as evidence that $\mathscr{C}^{(2)}$ is responsible for much higher excitations than $\mathscr{C}^{(1)}$ so that, for purposes of estimating quantities with energy denominators (like isospin admixtures and second-order shifts), $\mathscr{C}^{(2)}$ can be ignored. This means that the J-terms should be dropped. In this sense, when using sum rules for the study of Coulomb effects involving energy denominators, the use of the true two-body Coulomb force is less suitable than the effective one-body force.

Corrections from Consistency of the One-Body Coulomb Force and Proton Density

The local part of the one-body force (as derived above with term $h' = h$ cancelled and $\varrho_P - |u_h(r)|^2$ replaced by $(Z-1)\varrho_P/Z$) is

$$V_c(r_i) = \left(\frac{Z-1}{Z}\right)e^2 \int \frac{1}{r_{ij}} \varrho_P(r_j)\, \mathbf{dr}_j$$

where $\varrho_P(r)$ is total proton density, normalized to Z.

Clearly $V_c(r_i)$ depends or ϱ_P, so that our discussion has been approximate when guided by the uniform-density model to put $V_c = a_0 - a_1 r^2$ with

$a_1 = (Z-1)e^2/2R^3$, where $R^2 = (5/3)\langle r^2\rangle$. We now consider the effect of nonuniform distributions on $V_c(r)$, and on the sum rules.

First we consider the value of $V_c(r)$ in the center of the nucleus:

$$V_c(0) = \left(\frac{Z-1}{Z}\right)4\pi e^2 \int \varrho(r) r\, dr$$

where the number of particles and the rms radius are fixed:

$$4\pi \int \varrho(r) r^2\, dr = Z$$

$$4\pi \int \varrho(r) r^4\, dr = Z\langle r^2\rangle \equiv Z\tfrac{3}{5}R^2$$

For the uniform distribution of radius R:

$$V_c(0) = \left(\frac{Z-1}{Z}\right)e^2 \frac{3}{2R}$$

For a Saxon–Woods distribution of midway radius c and surface thickness parameter a:

$$\varrho(r) = \varrho_0\left[1 + \exp\left(\frac{r-c}{a}\right)\right]^{-1}$$

we have, using

$$\int r^n \varrho(r)\, dr = (n+1)^{-1}c^{n+1}\left(1 + \frac{n(n+1)}{6}\pi^2\frac{a^2}{c^2}\right)$$

$$\varrho_0 = Z\left[\tfrac{4}{3}\pi c^3\left(1 + \pi^2\frac{a^2}{c^2}\right)\right]^{-1}$$

$$\tfrac{3}{5}R^2 = \langle r^2\rangle = \frac{4\pi}{5}c^5\varrho_0\left(1 + \frac{10}{3}\pi^2\frac{a^2}{c^2}\right)$$

$$\approx \tfrac{3}{5}c^2\left(1 + \tfrac{7}{3}\pi^2\frac{a^2}{c^2}\right)$$

$$\left(\frac{Z}{Z-1}\right)V_c(0) = \frac{4\pi e^2}{2}c^2\varrho_0^2\left(1 + \tfrac{1}{3}\pi^2\frac{a^2}{c^2}\right)$$

$$\approx \frac{3Ze^2}{c}\left(1 - \frac{2\pi^2}{3}\frac{a^2}{c^2}\right)$$

$$\approx \frac{3Ze^2}{R}\left(1 + \tfrac{1}{2}\pi^2\frac{a^2}{R^2}\right)$$

TABLE A-I

	$(V_c)^2/(Z-1)^2$	$D = \langle (V_c - \bar{V}_c)^2 \rangle/(Z-1)^2$
^{4}He	0.64	0.03
^{16}O	0.40	0.013
^{40}Ca	0.30	0.0095

Thus, with $a = 0.6f$, $R = 7.1f$, the finite surface thickness increases $V_c(0)$ by about $3\frac{1}{2}\%$ for a system with fixed $\langle r^2 \rangle \equiv (3/5)R^2$. Since the potential outside the region of proton density is Ze^2/r, independent of a, and since $V_c(r)$ decreases with increasing a in the outer surface region r, this increase implies a steeper slope of $V_c(r)$ with r inside the nuclear region. This in turn implies a larger value for $D \equiv 4\pi \int_0^\infty (V_c - \bar{V}_c)^2 \varrho r^2\, dr$, the leading term in M. If we fit the correct $V_c(r)$ to the form $a_0 - a_1 r^2$, then a_1 is increased by an amount comparable to $V_c(0)$, so that we can estimate that the increase in the integral is $\lesssim 10\%$. Thus the consistency corrections do not change our results qualitatively in a heavy nucleus. For lighter nuclei, the effect is larger, 15% in $V_c(0)$ and a_1, or of the order of 30% in the integral.

For lighter nuclei, one can infer the correction by using earlier results obtained with the oscillator model. Starting from two-body Coulomb forces, and ignoring exchange and J-terms, one finds[34] the results shown in Table A-I. The units are e^4/b^2. From Appendix 4, we find when V_c is replaced by $a_0 - a_1 r^2$ with $a_1 = (Z-1)e^2/2R^3$, $R^2 = (3/5)\langle r^2 \rangle$, we get the figures shown in Table A-II.

From the values of the last two columns, in Table A-II, (Db^2/e^4) is 0.024, 0.0115, 0.0075. These are about 20% less than the values in the previous table. This confirms the existence of an appreciable increase in M for lighter nuclei arising from the consistency condition on V_c. Nevertheless, it does not change the qualitative picture. In fact, it shows that the identifica-

TABLE A-II[a]

	$D - d$	D	$\langle r^2 \rangle/b^2$
^{4}He	3/2	3/2	3/2
^{16}O	9/4	39/16	9/4
^{40}Ca	33/10	15/4	3

[a] Entries $D - d$, D are in units $a_1^2 b^4$.

tion of R in $a_1 = (E - 1)e^2/2R^3$ with the quantity $[(5/3)\langle r^2\rangle]^{1/2}$ is quite good. Noting that M depends on R as R^{-6}, better values would be obtained with values of R smaller by about 3%. In contrast, if R were taken as the mean radius or the half-density radius, both of which are considerably smaller, then M would be much too large, especially in lighter nuclei.

APPENDIX 2

Explicit Treatment of Effect of Correlations on Second-Order Coulomb Mixing

We are interested in quantities like

$$I_n(\phi) \equiv \langle \phi \mid C_v G^n C_v \mid \phi \rangle$$

where $G \equiv Q(H - E)^{-1}$, $Q = 1 - \mid \phi\rangle\langle\phi \mid$ and $n = 1$ or 2. If Φ is the shell-model version of ϕ, then

$$\phi = \Phi - GH'\Phi$$

To first order in correlations, $H' \equiv H - H_0$, we have

$$I_n(\Phi) - I_n(\phi) = \langle h' G_0 C_v G_0{}^n C_v\rangle + \langle C_v G_0{}^n C_v G_0 h'\rangle + \langle C_v G_0{}^n h' G_0 G_v\rangle + \langle C_v G_0 h' G_0{}^n C_v\rangle$$

where $G_0 \equiv (H_0 - E_0)^{-1}$, $Q_0 = 1 - \mid \Phi\rangle\langle\Phi \mid$, $h' = H' - \langle H'\rangle$, and $\langle\ \rangle$ denotes expectation value in Φ. If we take H_0 to include interaction between degenerate states then $C_v\Phi$, $Q_0 C_v{}^2\Phi$ are eigenstates of H_0 of excitation energies $\bar{E}$, $2\bar{E}$ to a good approximation, where $\bar{E}$ is $2\hbar\omega$ plus the collective shift Δ. One finds

$$I_n(\Phi_0) - I_n(\phi_0) = \frac{\langle H' Q C_v{}^2\rangle}{\bar{E}^{(n+1)}} = \frac{N - N(TD)}{\bar{E}^{(n+1)}}$$

where

$$N \equiv \langle C_v H C_v\rangle - \langle C_v{}^2 H\rangle$$

$$N(TD) \equiv \langle C_v H C_v\rangle - \langle C_v{}^2\rangle\langle H\rangle$$

The latter quantity is the Tamm–Dancoff evaluation of the sum rule N. Since the mean energy of such a calculation is $\bar{E}$ to first order, we have $I_n(\Phi) = N(TD)/\bar{E}^{(n+1)}$, whence

$$I_n(\phi) = \frac{N}{\bar{E}^{n+1}}$$

i.e., the value of I_n corrected for first-order correlations can be obtained as $N/\bar{E}^{n+1}$. Considerations of the spreading profile of $C_v \mid \phi\rangle$ do not affect the result since the spreading is a second-order effect.

APPENDIX 3

Shell-Model Sum Rules for the One- and Two-Body Coulomb Forces

One-Body Coulomb Force

Since states of isospin $T' \neq T$ are excited from the state $\phi_0(TT_3)$ by C_v, not C_s, the effect of passing from C_v to $(C_s + C_v)$ is to leave $M(T')$ unchanged for $T' \neq T$, but to change $M(T)$; denoting the sum rules for the full Coulomb force by argument C

$$M(T \pm 1, C) = M(T \pm 1) = C^2(TT_3\colon 10 \mid (T \pm 1)T_3)M(\| T \pm 1 \|)$$

$$\begin{aligned} M(T, C) - M(T) &= M(C) - M \\ &= \langle \phi_0(TT_3) \mid (C_s + C_v)^2 - C_v^2 \mid \phi_0(TT_3)\rangle \\ &= \langle C_s^2\rangle + 2\frac{T_3}{T}\langle C_s C_v\rangle \end{aligned}$$

where a constant is included with C_s to make $\langle C_s\rangle = 0$ and brackets signify expectation value in the parent state.

Shell-Model Evaluation

Using the shell model, as in Sec. 3, we find (with $N - Z = 2T$, not $2T_3$):

$$\langle C_s^2\rangle = \langle C_v^2\rangle = \frac{N_0(K)}{2\hbar\omega} = \tfrac{1}{4}b^2 a_1^2 A\langle r^2\rangle$$

$$\langle C_s C_v\rangle = \frac{\frac{1}{2}\langle [C_s, [H, C_v]]\rangle}{2\hbar\omega} = \frac{-b^2}{4}a_1^2(N\langle r^2\rangle_N - Z\langle r^2\rangle_P)$$

$$M(\| T + 1 \|) = \langle C_v^2\rangle - M_1$$

$$M(\| T - 1 \|) = \langle C_v^2\rangle + \frac{T+1}{T}M_1$$

$$M(\| T \|) = \langle C_v^2\rangle + \frac{1}{T}M_1$$

$$M_1 = \tfrac{1}{2}\left\langle \sum_i t_{3i}(V_c - \hat{V}_c)^2 \right\rangle$$

$$M(C) = b^2 a_1^2 Z\langle r^2\rangle_P$$

Uniform Statistical Model[7]

This model neglects space-exchange and sets all spatial integrals equal. The resulting expressions are of the same form as those of the shell model, but with $b^2a_1^2\langle r^2\rangle$ replaced by $[\langle V_c^2\rangle - \langle V_c\rangle^2]$. If $V_c = a_0 - a_1r^2$, this quantity is $(4/21)\langle r^2\rangle^2a_1^2$ so the two quantities are roughly equal in heavy nuclei where $\langle r^2\rangle \approx 5b^2$. In lighter nuclei, the shell-model values are larger.

Two-Body Coulomb Force

If we use the uniform statistical model for this, we may check whether the one- and two-body Coulomb forces are equivalent. We have

$$M(\mathscr{C}) \equiv \langle \mathscr{C}^2\rangle - \langle \mathscr{C}\rangle^2 = Z(Z-1)(Z-2)I$$

where I is the spatial integral of Appendix 1. (We suppress the J-integrals here since we know that they have no counterpart in the one-body case.) This agrees with the statistical model form of $M(C)$, to $0(1/Z)$, when we use the relation

$$\langle V_c^2\rangle - \langle V_c\rangle^2 = (Z-1)^2I.$$

Other relations are

$$M(T-1, \mathscr{C}_v) = C^2(TT_3; 10 \mid (T-1)T_3)\tfrac{1}{2}\left(\frac{A}{2} + T + 1\right)\frac{(A-2)(A-4)}{4}I$$

$$M(T+1, \mathscr{C}_v) = C^2(TT_3; 10 \mid (T+1)T_3)\tfrac{1}{2}\left(\frac{A}{2} - T\right)\frac{(A-2)(A-4)}{4}I$$

$$M(T, \mathscr{C}_v) = C^2(TT_3; 10 \mid TT_3)\tfrac{1}{2}\left(\frac{A}{2} + 1\right)\frac{(A-2)(A-4)}{4}I$$

$$M(\mathscr{C}_v) = \left[\tfrac{1}{4}A\frac{(A-2)(A-4)}{4} + \tfrac{3}{4}(A-2)T_3^2\right]I$$

These agree with the one-body expressions except that they are larger by a factor $(A/2Z)^2$, as already noted in Appendix 1. Since $\langle \mathscr{C}_v^2\rangle$ is unchanged when neutrons and protons are exchanged, these quantities cannot involve odd powers of T_3, so cannot be expected to be exactly equal to their one-body counterparts which involve $Z^2 = (A/2 - T_3)^2$. We assume that the inclusion of $\mathscr{C}_t$ with $\mathscr{C}_v$ would lead to agreement with the one-body results. In general, it is tedious to check this assumption, but it is easy to do in the special case of $M(T+1)$ for a parent state ($T_3 = T$). For the full Coulomb

force,

$$M(T+1, \mathscr{C}) + M(T+2, \mathscr{C}) = \frac{1}{2T+2} Z(Z-1)(Z-3)I$$

$$M(T+2, \mathscr{C}) = -\frac{Z^2}{(T+2)(2T+3)} I$$

(The positive definite quantity $M(T+2, \mathscr{C})$ actually involves $(I - \frac{1}{2}J)$ in place of I, but we are neglecting J-terms). Thus $M(T+1, \mathscr{C})$ equals $(2T+2)^{-1}Z^3I$ (plus corrections of order $1/Z$), showing that the inclusion of $\mathscr{C}_t$ with $\mathscr{C}_v$ restores the equality with the one-body result $M(T+1, C) = (2T+2)^{-1}Z[\langle V_c^2\rangle - \langle V_c\rangle^2]$.

We will not give all of $\langle \mathscr{C}_s^2\rangle$, $\langle \mathscr{C}_t^2\rangle$ and the three cross-terms, but use $\langle \mathscr{C}_s^2\rangle$ as an example:

$$\langle \mathscr{C}_s^2\rangle - \langle \mathscr{C}_s\rangle^2 = \tfrac{1}{16}I\left[A^3 + \frac{25}{9}AT^2 + \cdots\right]$$

where omitted terms are quadratic and linear in A, T. Comparing with the one-body form, we see that the leading terms agree when we expand in powers of T/A. The agreement cannot apply beyond the first term since the one-body form involves a term in A^2T_3, which cannot arise for scalar $\mathscr{C}_s$.

APPENDIX 4

Coulomb Mixing Properties of Oscillator Orbitals

Using the oscillator results:

$$\langle r^2\rangle_{nl} \equiv \langle nl \mid r^2 \mid nl\rangle = b^2\left(\frac{4n+2l-1}{2}\right)$$

$$\langle (n+1)l \mid r^2 \mid nl\rangle = b^2\left(\frac{n(2n+2l+1)}{2}\right)^{1/2}$$

it follows that the second-order energy shift of level nl due to the perturbation $V_c = a_0 - a_1r^2$ is

$$\Delta(nl) = \frac{a_1^2}{2\hbar\omega}(\langle (n+1)l \mid r^2 \mid nl\rangle^2 - \langle (n-1)l \mid r^2 \mid nl\rangle^2)$$

$$= -\frac{a_1^2b^4}{4\hbar\omega}(4n+2l-1) = \frac{-a_1^2b^2}{2\hbar\omega}\langle r^2\rangle_{nl}$$

$$= \frac{-Z^2e^4m}{16\hbar^2}\left(\frac{b}{R}\right)^6(4n+2l-1)$$

using $a_1 = Ze^2/2R^3$, $\hbar\omega = \hbar^2/mb^2$. (This result applies to the case $n = 1$ despite there being no state $|(n-1)l\rangle$). The last form shows that, once b/R is given, there is no dependence of Δ on the absolute value of nuclear size; b/R may be fixed by demanding that the rms value of all the protons equal $(3R^2/5)^{1/2}$. The same formulas also give

$$\begin{aligned} M(nl) &= a_1^2(\langle r^4\rangle_{nl} - \langle r^2\rangle_{nl}^2) \\ &= a_1^2(\langle (n+1)l \mid r^2 \mid nl\rangle^2 + \langle (n-1)l \mid r^2 \mid nl\rangle^2) \\ &= \frac{a_1^2 b^4}{2}\,[N^2 + N + 1 - l^2 - l] \end{aligned}$$

where $N = 2n + l - 1$ is the oscillator level of energy $(N + \frac{1}{2})\hbar\omega$. Thus for states in the same level, $M(nl)$ strongly decreases as l increases, e.g., for the $3p$, $2f$, $1\hbar$ states of $N = 6$, M has relative values 41:31:13. Since Δ is the same for all such states, and since the formula $\Delta = M/2\hbar\omega$ is correct for the $1h$ state, this formula gives gross overestimates (by 31/13, 41/13) for the $2f$, $3p$ states.

REFERENCES

1. W. M. MacDonald, *Phys. Rev.* **100**:51 (1955); **101**:271 (1956); **110**:1420 (1959); *Isotopic Spin Selection Rules*, in: *Nuclear Spectroscopy B* (F. Ajzenberg-Selore, ed.), Academic Press, New York, p. 932.
2. J. M. Soper, *Isospin in Nuclear Physics* (D. H. Wilkinson, ed.), North-Holland, Amsterdam (1969), p. 229.
3. A. Bohr, J. Damgaard, and B. R. Mottelson, *Nuclear Structure* (A. Hossain, ed.), North-Holland, Amsterdam (1967), p. 1.
4. R. Mohan, M. Danos, and L. C. Biedenharn, *Phys. Rev.* **C3**:1740 (1971); **C3**:468 (1971).
5. N. Auerbach, *Nucl. Phys.* **A182**:247 (1972).
6. J. V. Noble, *Phys. Lett.* **35B**:140 (1971).
7. A. M. Lane, and J. M. Soper, *Nucl. Phys.* **37**:663 (1962).
8. S. B. Khadkikar and C. S. Warke, *Phys. Rev.* **A130**, 577 (1969).
9. L. A. Sliv and Y. I. Kharitonov, *Phys. Lett.* **16**:176 (1965).
10. L. A. Radicati, *Proc. Phys. Soc.* **66A**:139 (1953), **67A**:39 (1953).
11. R. J. Blin Stoyle, *Isospin in Nuclear β Decay*, in: *Isospin in Nuclear Physics* (D. H. Wilkinson, ed.), North-Holland, Amsterdam (1969), p. 115.
12. S. A. Fayans, *Phys. Lett.* **37B**:155 (1971).
13. D. H. Wilkinson, *Phys. Lett.* **11**:243 (1964).
14. J. Janecke, *Nucl. Phys.* **A128**:632 (1969); *Systematics of Coulomb Energies and Excitation Energies of Isobaric Analogue States*, in: *Isospin in Nuclear Physics* (D. H. Wilkinson, ed.), North-Holland, Amsterdam (1969), p. 297.
15. G. Bertsch and S. Kahana, *Phys. Lett.* **33B**:193 (1970)

16. N. Auerbach and A. Lev, *Nucl. Phys.* **A180**:651 (1972).
17. N. Auerbach, A. Lev, and E. Kashy, *Phys. Lett.* **36B**:453 (1971).
18. K. T. Hecht, *Nucl. Phys.* **A114**:280 (1968).
19. C. E. Lacy, *Ann. Phys.* **65**:87 (1971).
20. J. A. Nolen and J. P. Schiffer, *Ann. Rev. Nucl. Sci.* **19**:471 (1969).
21. N. Auerbach, J. Hufner, A. K. Kerman, and C. M. Shakin, *Phys. Rev. Lett.* **23**:484 (1969).
22. N. Van Giai, D. Vautherin, M. Veneroni, and D. M. Brink, *Phys. Lett.* **35B**:135 (1971).
23. E. Friedman and B. Mandelbaum, *Nucl. Phys.* **A135**:472 (1969).
24. S. Ramavataram, *Phys. Lett.* **32B**:239 (1970).
25. N. Auerbach, *Phys. Lett.* **36B**:293 (1971).
26. E. H. Auerbach, S. Kahana, and J. Weneser, *Phys. Rev. Lett.* **23**:1253 (1969).
27. J. Damgaard, C. K. Scott, and E. Osnes, *Nucl. Phys.* **A154**:12 (1970).
28. J. Janecke, *Nucl. Phys.* **A181**:49 (1972).
29. E. Friedman, *Phys. Lett.* **35B**:543 (1971).
30. J. W. Negcle, *Nucl. Phys.* **A165**:305 (1971).
31. C. W. Wong, *Nucl. Phys.* **A151**:323 (1971).
32. N. Auerbach, J. Hufner, A. K. Kerman, and C. M. Shakin, *Rev. Mod. Phys.* **44**: 481 (1972).
33. D. Robson, *Phys. Rev.* **137**:535 (1965); **A157**:32 (1970).
34. A. Z. Mekjian, *Phys. Lett.* **29B**:461 (1969); *Nucl. Phys.* **A146**:288 (1970); *Phys. Rev. Lett.* **25**:888 (1970); *Phys. Rev.* **184**:1031 (1969).
35. F. de Toledo Piza and A. K. Kerman, *Ann. Phys.* **43**:363 (1967); **48**:173 (1968).
36. A. Z. Mekjian and W. M. MacDonald, *Nucl. Phys.* **A121**:385 (1968).
37. A. M. Lane, *Phys. Lett.* **29B**:263 (1969).
38. M. di Toro, *Nucl. Phys.* **A155**:385 (1970).
39. A. F. de Toledo Piza, A. K. Kerman, S. Fallieros, and R. H. Ventner, *Nucl. Phys.* **89**:369 (1966).
40. C. Mahaux and H. A. Weidenmuller, *Nucl. Phys.* **A130**:481 (1969); *Shell Model Approach to Nuclear Reactions*, North-Holland, Amsterdam (1969).
41. C. Mahaux and H. A. Weidenmuller, *Nucl. Phys.* **89**:33 (1966); **94**:1 (1967); *Zeit. fur Physik* **202**:97 (1967).
42. C. Mahaux and C. A. Wiedner, *Nucl. Phys.* **A93**:327 (1967).
43. D. Robson, *Isobaric Spin in Nuclear Physics*, Academic Press, New York and London (1966), p. 411.
44. D. H. Wilkinson, *Analysis of Gamma-Ray Data*, in: *Nuclear Spectroscopy B* (F. Ajzenberg-Selove, ed.), Academic Press, New York (1960).
45. E. K. Warburton and J. Weneser, *The Role of Isospin in Electromagnetic Transition*, in: *Isospin in Nuclear Physics* (D. H. Wilkinson, ed.), North-Holland, Amsterdam (1969).
46. J. I. Fujita and K. Ikeda, *Prog. Theor. Phys.* **36**:530 (1966).
47. D. H. Wilkinson, *Phys. Rev. Lett.* **27**:1018 (1971).
48. R. J. Blin-Stoyle, J. A. Evans, and A. M. Khan, *Phys. Lett.* **36B**:202 (1971).
49. A. Laverne and G. Do Dang, *Nucl. Phys.* **A177**:665 (1971).
50. J. B. Woods and D. H. Wilkinson, *Nucl. Phys.* **61**:661 (1965).
51. G. M. Temmer, *Isobaric Analogue Resonances in Nuclear Spectroscopy*, in: *Isospin in Nuclear Physics* (D. H. Wilkinson, ed.), North-Holland, Amsterdam (1969).

52. A. Arima and S. Yoshida, *Nucl. Phys.* **161**:492 (1971).
53. N. Auerbach and A. Lev, *Phys. Lett.* **34B**:13 (1971).
54. G. A. Miller and A. K. Kerman, *Phys. Rev. Lett.* **28**:373 (1972).
55. A. Richter, E. Grosse, J. Hufner, and H. A. Weidenmuller, *Phys. Lett.* **38B**:349 (1972).
56. E. W. Hamburger, *Phys. Rev. Lett.* **19**:36 (1967).
57. F. C. Barker, *Nucl. Phys.* **83**:418 (1966).
58. R. E. Segel, *Isobaric Spin in Nuclear Physics* (J. D. Fox and D. Robson, eds.), Academic Press, New York (1966), p. 194.
59. J. B. Marion, *Phys. Lett.* **14**:315 (1965); *Nuclear Research with Low Energy Accelerators* (J. B. Marion and D. M. Van Patten, eds.), Academic Press, New York (1967).
60. D. J. Edens, S. Ramavataram, and D. Wilmore, *Nucl. Phys.* (to be published).
61. A. M. Lane and A. Z. Mekjian, submitted for publication.
62. S. Fallieros and B. Goulard, *Nucl. Phys.* **147**:593 (1970).
63. S. Fallieros and R. O. Akyuz, *Phys. Rev. Lett.* **27**:1016 (1971).
64. N. Van Giai, thesis, Orsay 1972.
65. H. C. Lee and R. Y. Cusson, *Ann. Phys.* **72**:353 (1972).
66. J. C. Hardy, H. Schmeing, J. S. Geiger, R. L. Graham, and I. S. Towner, *Phys. Rev. Letters* **29**:1027 (1972).
67. J. S. Ryder, G. J. Clark, J. E. Draper, J. M. Freeman, W. E. Burcham, and G. T. A. Squier, *Phys. Lett.* **43B**, 30 (1973).
68. W. Benenson, E. Kashy, and I. D. Proctor, *Phys. Rev.* **C7**, 1143 (1973).
69. G. F. Bertsch, *Phys. Lett.* **37B**:470 (1971).

Chapter 3

THE BETA STRENGTH FUNCTION

P. G. Hansen*

European Organization for Nuclear Research
CERN, Geneva, Switzerland

1. INTRODUCTION

In recent years, it has become possible to study experimentally the properties of many nuclei with a neutron number differing greatly from that of stable nuclei [see, e.g., (FHR 67), (Ley 70)]. The present survey deals with the information about nuclear structure that may be gained from the investigation of the beta-decay properties of nuclei far away from beta stability, where the energy available for beta decay is very large. The decay can therefore proceed to a very large number of excited levels of the kind that are observed as resonance or final states in the neutron-capture process. Because of the large number and density of final states it becomes expedient to deal with high-energy beta decay in the language of the statistical model [for general reviews, see Lynn (Lyn 68) and Vogt (Vog 68)], and to discuss the beta-decay rate in terms of a strength function.

The concept of a strength function in beta decay is a natural generalization of strength functions employed in other areas of nuclear physics. In each case the strength function refers to the behavior of the squares of overlap integrals, $\gamma_{\lambda c}^2$, between two sets of nuclear wave functions: the one set, labeled λ, represents various states of excitation (classified by energy, spin, and parity and, occasionally, also by isospin) of a given

* On leave from the Institute of Physics, University of Aarhus, Denmark.

nucleus; the other set, labeled c, refers to the different reaction channels into which the nucleus can decay. One may also choose to let c represent the reaction channels through which the states λ are formed; the theorem of reciprocity makes the two descriptions equivalent. In either case c labels the kind of particles in the channel (e.g., neutron plus residual nucleus), the internal excitation of the particles, and the relative angular momentum of the pair, as well as other quantum numbers when necessary. The overlap integrals $\gamma_{\lambda c}^2$ are not directly observable but they are factors of observed partial widths, $\Gamma_{\lambda c} = 2P_c\gamma_{\lambda c}^2$ (Vog 68a), where the other factor, $2P_c$, refers to barrier penetration in the channel. Hence, the $\gamma_{\lambda c}^2$ are called reduced widths because they are obtained from observed widths by removal of the penetration factors which are not directly relevant to nuclear structure. Alternatively, the overlap integrals are deduced from transition amplitudes in direct reactions and they are then called spectroscopic factors.

The individual spacings between the states λ as well as the reduced widths show pronounced fluctuations [see, e.g., (Lyn 68)]. It is therefore convenient to deal only with averages over many levels. An especially useful quantity is the strength function, which is defined as the total value of $\gamma_{\lambda c}^2$ per unit energy interval of λ:

$$S_{\lambda c} = \langle \gamma_{\lambda c}^2 \rangle \varrho_\lambda \tag{1}$$

where ϱ_λ is the density of levels λ. The strength function S_λ is a function of the energy, but the concept is most useful if one may assume that S_λ varies slowly with energy, i.e., that the variation occurs over energy intervals much larger than ϱ_λ^{-1}. An especially instructive model of strength-function phenomena has been discussed by Bohr and Mottelson (BM 69a,a), who also give examples of commonly used strength functions such as the single-particle strength function as studied by single-particle transfer reactions, the s-wave neutron strength function, and the strength function associated with deeply bound nucleons as studied in high-energy $(p, 2p)$ reactions. The various multipole strength functions for photons are discussed by Bartholomew *et al.* (Bar 72) in Chapter 4 of this volume.

It is often convenient to define the strength function [Eq. (1)] to involve a summation over some of the quantum numbers included in λ and c in order to define a quantity which is experimentally observable. (An example is the nucleon p-wave strength function which usually includes both $p_{1/2}$ and $p_{3/2}$). For beta decay most of the experiments (Section 4) can distinguish neither allowed and forbidden strength nor the multipolarities 0 and 1. This is taken into account in the definition given below, although we shall

occasionally use a terminology which implies that the total beta strength may be split according to multipolarity, parity, and spin of the final state $S_\beta(E) = \sum_{\lambda\pi I_i} S_\beta^{\lambda\pi I_i}(E)$.

The reduced beta-transition probability is normally quoted in terms of the reciprocal *ft*-values, where $f(Z, Q)$ is the statistical rate function for allowed beta decay (see Section 2) and t is the partial halflife. Thus f is the analog of the penetration factors removed from nucleon widths to obtain reduced widths. It is convenient to define (Duk+ 70) the beta strength function $S_\beta(E)$ as a reciprocal *ft*-value calculated per MeV of final levels at the excitation energy E in the daughter nucleus

$$S_\beta(E) \equiv \frac{b(E)}{f(Z, Q - E) \cdot T_{1/2}} \tag{2}$$

where $b(E)$ is the absolute beta intensity per MeV of levels at the energy E, and Q is the total energy available. As traditionally f is in absolute units while $T_{1/2}$ is in seconds, the unit of S_β is $\text{sec}^{-1}\ \text{MeV}^{-1}$. Defined in this way, the beta strength function incorporates both allowed and forbidden beta transitions. If one calculates the reduced beta-transition probability $B_{i\nu}(E)$ measured in units of $g_V^2/4\pi$ (BM 69a) to levels at energy E with the spin and parity $I_i^{\pi_i}$ and labeled by the running index ν, one may express the strength theoretically as

$$\begin{aligned} S_\beta(E) &\cong D^{-1} \frac{d[\overline{\sum_i \sum_\nu B_{i\nu}(E)}]}{dE} \\ &= D^{-1} \sum_i \varrho_i(E)\overline{B_i(E)} \end{aligned} \tag{3}$$

where $\varrho_i(E)$ is the density of levels $I_i^{\pi_i}$ and the constant D takes the value 6260 ± 60 sec (see Section 2). The average sign in Eq. (3) denotes smoothing of the summed quantity as a function of energy.

Beta strength is associated with the disappearance of a neutron (or proton) and the appearance of a proton (or neutron) where the quantum states of the two particles obey certain selection rules. At higher excitation energies the corresponding particle–hole final states seem to be distributed over a large number of levels, so that one observes a slowly varying strength function $S_\beta(E)$. Furthermore, at these energies, the major part of the strength originates in the paired system of the nucleus, while the contribution from any unpaired nucleons present in the mother nucleus typically is small; consequently, it becomes an acceptable first approximation to regard the beta strength function as a slowly varying function of the neutron and

proton number (Section 4.3). The muon-capture strength function behaves similarly (Section 4.5).

There is a great similarity between the beta strength functions on one side and proton and neutron strength functions on the other side because both involve overlap integrals between initial and final states as described above (Lyn 68), (Hod 71); both are slowly varying functions of E, Z, N, and both can be understood qualitatively in terms of the shell-model states involved. Quantitatively there are, however, large differences. The single-particle models (shell model, optical model) account well for all major features of the proton and neutron strength functions. The beta strength function, on the other hand, depends on the coordinates of two particles (or a hole and a particle), and such excitations may jointly give rise to collective states. The corresponding collective beta transitions in turn modify the beta strength function in a significant way. A complete analogy exists here to the electromagnetic transition probabilities, which also depend on the coordinates of two particles and for which the collective effects also bring about striking changes in the distribution of the strength as compared with a single-particle model. Examples may be found in the companion paper by Bartholomew *et al.* (Bar +72), and in other references given in Section 4.5.

The main theme of the present review is then the use of beta strength functions as an experimental tool for learning about hole–particle excitations in nuclei. Much of the original thinking about this subject originates in studies of absolute beta-transition probabilities to low-lying levels, and for this reason Section 2 gives a short summary of ideas and results in this area. Following this, Section 3 deals with the main features of the beta strength function as an introduction to a detailed survey (Section 4) of experimental methods and results.

2. BETA-TRANSITION RATES BETWEEN INDIVIDUAL NUCLEAR LEVELS

The experimental and theoretical study of the beta strength function was initiated by progress during the last decade in the understanding of absolute beta-transition probabilities between individual low-lying levels. Though the beta-decay process furnishes many excellent examples of the selection rules predicted by the single-particle model of the nucleus, it is nevertheless clear from experiments that these models overestimate the transition probabilities in the heavier nuclei by sizable factors. This effect

was finally explained as the result of (normally unobserved) collective beta transitions which hold a large fraction of the shell-model strength and also renormalize the coupling constants. A discussion from a theoretical point of view may be found in a recent and rather complete review by some of the physicists (Mor+ 71) who have contributed most to the understanding of absolute beta-transition rates; this paper should be referred to for a survey of the relevant theory. The following is a summary of the main experimental findings and the ideas behind their interpretation.

The microscopic theory of nuclear collective motion [see, e.g., (Bro 71)] explains the collective states as the result of residual interactions acting upon basis states of particle–hole nature. The transition matrix elements of operators corresponding to the generators of the collective state are particularly large ("collective") to the collective states, and correspondingly the small collective admixtures in the wave functions of the "simple" states will normally lead to important reductions in the transition probabilities to those. For beta decay this effect is frequently discussed in terms of "effective coupling constants"; for static and dynamic electromagnetic nuclear moments one has a completely analogous renormalization of the matrix elements ("core polarization," "effective charges"). These phenomena have been discussed together in a very illuminating way by Mottelson (Mot 67).

The theory of nuclear beta decay has been reviewed in several books (BM 69a,bc, Kon 66, Sch 66, WM 66). We recall here just a few important facts. The wavelength associated with the lepton emission in nuclear beta decay is much larger than the nuclear radius. This permits a rapidly converging series expansion which leads to a grouping of the matrix elements into "allowed," "first-forbidden," "second-forbidden," *etc.* Allowed beta transitions (no change in the parity) have, in the general case, contributions from two nuclear matrix elements, which differ in their dependence on the nucleon spin. The one, first proposed by Fermi, corresponds to an operator of multipole order zero, which is essentially a sum over all nucleons of isospin raising and lowering operators $T_\pm = \sum_{i=1}^{A} t_\pm{}^i$, where t_+ is the operator that transforms a proton into a neutron. The other operator, first proposed by Gamow and Teller, acts on the nucleon spin coordinates $\mathbf{Y}_\pm = \sum_{i=1}^{A} \boldsymbol{\sigma}^i t_\pm{}^i$, so that the selection rules permit a spin change of unity or zero (but not $0 \rightarrow 0$). The allowed transitions have "allowed" or "statistical" shape, and there are no angular correlations between the emitted beta particles and any subsequent gamma decays of the nucleus. The total transition probability in beta decays per second may be expressed in terms of the reduced transition probabilities B_F and B_{GT} (BM 69a,bc) measured

in units of the coupling constant $g_V^2/4\pi$ for the beta interaction

$$t^{-1} \ln 2 = \ln 2 f(Z, Q_\beta) \frac{B_F + B_{GT}}{D} \tag{4}$$

where t is the partial halflife, Z is the atomic number, and Q_β the total beta energy. The constant D, which determines the Fermi coupling constant g_V^2, takes the value 6260 ± 60 sec (Fre+ 66). The statistical rate function $f(Z, Q_\beta)$ for $\beta^\pm$ emission may be written

$$f_\pm(Z, Q_\beta) = \int_1^{Q_\beta} F(\mp Z, E_\beta)(Q_\beta - E_\beta)^2 p E_\beta \, dE_\beta \tag{5}$$

where the positron (electron) energy E_β and momentum p are measured in absolute units, and the Fermi function F is unity in the limit of small Z. For electron capture, one has the statistical rate function

$$f_{EC} = \sum_x \frac{\pi}{2} G_x^2 (Q_\beta - E_\beta - B_x)^2$$

where the product of the bound electron wave function $(\pi/2)G_x^2$ and the neutrino phase-space factor are summed over all electron shells x. Here, B_x denotes the electron binding energy. In the following we normally use the symbol $f(Z, Q_\beta)$ to denote either f_- or the sum $(f_+ + f_{EC})$ as appropriate. Equation (4) includes in B_{GT} the strength of the Gamow–Teller interaction relative to that of the Fermi interaction; this ratio has been determined from the decay rate of the free neutron (Chr+ 67, Chr+ 71) as $(g_A/g_V)^2 = 1.54 \pm 0.03$. It is normal practice to quote reduced beta-transition probabilities in terms of the product ft [Eq. (4)], and it was to facilitate comparison that the beta strength function was defined (Section 1) to correspond to a reciprocal ft value per MeV of final levels.

First-forbidden beta transitions involve a change in parity and have, in the general case, contributions from six nuclear matrix elements, two of which are of multipolarity zero, and three of which are of multipolarity one. Only one first-forbidden matrix element (denoted $\int B_{ij}$) carries two units of angular momentum, so that for the case of a spin change of two units this matrix element alone contributes ("unique first-forbidden transition"). An important simplification occurs for most nonunique first-forbidden transitions in the heavier nuclei. Owing to the large Coulomb energy of the electron inside the nucleus, it becomes permissible to neglect certain energy-dependent terms in the transition probability which then may be expressed by Eq. (4), provided that B_F and B_{GT} are replaced by

appropriate linear combinations of first-forbidden matrix elements with multipolarities 0 and 1, respectively. This approximation (ξ-approximation) holds if the quantity $\xi = Ze^2/2R \cong 0.6ZA^{-1/3}$ MeV is much greater than the Q-value (see, e.g., BM 69a,c), and if the main matrix elements are large and show no cancellations. The cases where the ξ-approximation fails are attractive experimentally because they allow more measurements (deviation of the shape from the allowed one, β–γ angular correlations); the theoretical analysis, however, is often sensitive to small impurities in the wave function and it becomes difficult to extract nuclear structure information. With the famous case of "RaE" (^{210}Bi) and other cases near ^{208}Pb (see Section 2.3) as happy exceptions, it seems that for both allowed and forbidden transitions, the major part of the nuclear-structure information (even in forbidden decays) is contained in one number—the transition probability for a given multipole order—and that the safest conclusions may be drawn when the transition probability is close to its maximum value. This is similar to the situation for electromagnetic transitions where refinements such as anomalous internal conversion coefficients and structure-dependent particle parameters occur for very hindered transitions and rarely contribute to the structure information.

We consider now the hindrance phenomena. In this connection it is instructive (see, e.g., Mor+ 71) to consider the sum rule for the strength associated with the transition operator Ω which gives rise to transitions from the initial state $|i\rangle$ to a complete set of final states $|f\rangle$:

$$\sum_f |\langle f|\Omega|i\rangle|^2 = \sum_f \langle i|\Omega^+|f\rangle\langle f|\Omega|i\rangle = \langle i|\Omega^+\Omega|i\rangle$$
$$= \left|\frac{\langle i|\Omega^+}{\langle i|\Omega^+\Omega|i\rangle^{1/2}}\Omega|i\rangle\right|^2 \tag{6}$$

which implies that if the normalized state $\Omega|i\rangle/\langle i|\Omega^+\Omega|i\rangle^{1/2}$ belongs to the complete set of final states $|f\rangle$, the sum-rule strength is exhausted by the transition to this state.

We consider in the following section the Fermi transitions as a particularly good example of this sum rule.

2.1. The Fermi Transitions

The discovery (AWM 62) in 1962 of the existence of isobaric analog states in the heavier nuclei (here defined as nuclei with $N > Z$) had a profound effect upon the understanding of Fermi-transition rates. It was pointed out by Lane and Soper (LS 62) that it is an immediate consequence

that isospin remains a reasonably pure (and in their terminology "useless") quantum number in heavy nuclei. Since the (unnormalized) generating operator for the isobaric analog state $T_- = \sum_{i=1}^{A} t_-^i$ is identical to the Fermi-transition operator for β^- decay (see above), one obtains immediately from the sum rule (6) that the (normally unobservable) β^- transition to the isobaric analog state exhausts the Fermi sum rule $\sum B_F = 2T$, where T is the isospin of the mother nucleus in β^- decay. Beta transitions to low-lying levels can therefore only proceed through small admixtures of the analog (AlF 61). This is borne out experimentally in the study of isospin-forbidden beta transitions ($\Delta T = 1$), either from the determination of the mixing ratio in mixed F/GT transitions or from the rates of $0^+ \rightarrow 0^+$ transitions which must be pure Fermi (see the discussion in BM 69a,d). Table I shows as an example the beta transitions from the decay of ^{156}Eu. It is interesting to note that it has been possible in suitable cases (Dam 66) to account for the rates of isospin-forbidden transitions by taking into account the perturbations caused by the Coulomb force which breaks down the isospin symmetry.

Although the isospin selection rule is sufficient explanation for the smallness of observed Fermi matrix elements such as those given in Table I, it may still be instructive to ask the questions: How do we explain the effect in the language of a single-particle model? Why does a single-particle transition $(lj) \rightarrow (lj)$ where the spatial overlap seems perfect come out with a vanishingly small B_F? An illuminating example given by Damgaard (Dam 67) is shown in Fig. 1. At first sight the decay of the $p_{3/2}$ neutron in ^{49}Ca to the 3.1-MeV $p_{3/2}$ proton level would appear to be favored with a Fermi matrix element of 1 corresponding to that of the free neutron. Isospin

TABLE I

Pure Fermi Beta Transitions in the Decay of $^{156}_{63}$Eu ($I^\pi = 0^+$)

Final 0^+ level in ^{156}Gd (keV)	T	E_β max (MeV)	ft (sec)	B_F ($g_V^2/4\pi$)	Reference
0	14	2.44	$(6.5 \pm 0.7) \times 10^9$	1.0×10^{-6}	(Wil+ 65)
1,050	14	1.39	$(14.5 \pm 2.4) \times 10^9$	0.43×10^{-6}	(HNW 67)
1,168	14	1.27	$(3.9 \pm 0.4) \times 10^9$	1.6×10^{-6}	(Nil+ 69)
17,600	15	—	2.1×10^2	30	[a]

[a] Theoretical values for the isobaric analog state. Note that this state is in a continuum of $T = 14$ states.

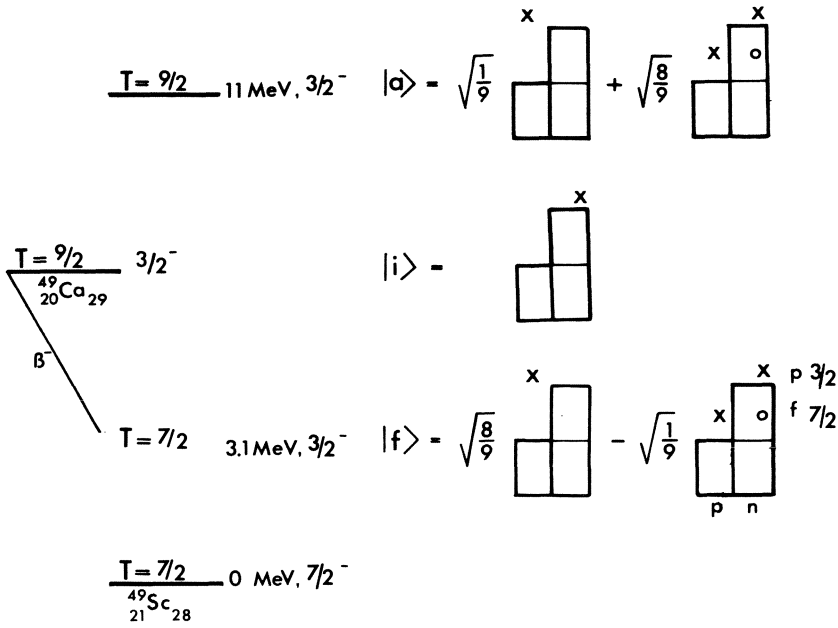

Fig. 1. Schematic decay scheme and wave functions according to Damgaard (Dam 67) for the $3/2^-$ levels in the decay of $^{49}_{20}Ca_{29}$ to $^{49}_{21}Sc_{28}$. The wave functions are written symbolically in terms of filling diagrams indicating the double-closed shell ^{40}Ca and eight neutrons in the $f_{7/2}$ shell. The crosses denote single-particle excitations outside of the closed shells and the circles denote single-hole excitations of the $f_{7/2}$ neutron shell. The combination *xo* represents the antisymmetrized contribution from the eight $f_{7/2}$ neutrons with the hole and the particle coupled to 0^+. The nucleus ^{49}Ca (denoted $|\, i\rangle$) has one neutron in the $p^n_{3/2}$ state and has isospin 9/2. The basic $3/2^-$ configurations in ^{49}Sc are *either* a $p_{3/2}$ proton coupled to the ^{48}Ca core ($T = 4$) *or* the 0^+ neutron–hole–proton excitation of the $f_{7/2}$ shell of ^{49}Ca. Neither of these two configurations are states of pure isospin; the proper linear combinations corresponding to $T = 9/2$ (the isobaric analog state $|\, a\rangle$) and $T = 7/2$ (the anti-analog state, $|\, f\rangle$) are given in the figure. Both have isospin projection $T_Z = 7/2$. The Fermi decay of the single $p_{3/2}$ neutron has a matrix element M_F ($= B_F^{1/2}$) of 1, while the hole–particle excitation of the closed $f_{7/2}$ shell has the collective matrix element $8^{1/2}$. With the wave functions given in the graph, one then calculates

$$\langle a \,|\, T_- \,|\, i\rangle = 9^{-1/2} \cdot 1 + (8/9)^{1/2}\, 8^{1/2} = 9^{1/2}$$
$$\langle f \,|\, T_- \,|\, i\rangle = (8/9)^{1/2} \cdot 1 - 9^{-1/2}\, 8^{1/2} = 0$$

conservation, however, requires that the 3.1-MeV level is only 89% pure with an 11% admixture of hole–particle excitations. These give rise to a collective contribution to the Fermi matrix element which causes a complete cancellation. This is, of course, no coincidence but another way of expressing the forbiddenness due to the selection rule $\Delta T = 0$. Note also

that the transition to the isobaric analog state has the full sum-rule strength $B_F = 9$.

This agrees qualitatively with the experimental finding by Mann and Bloom (MB 70) that $B_F \leq 10^{-4}$. A more detailed consideration must take into account the mixing of the states $|a\rangle$ and $|f\rangle$ caused by the Coulomb interaction as well as more detailed properties of the shell-model wave functions (MB 70, Dam 67, BD 66).

2.2. The Gamow–Teller Transitions

It has long been known that normal allowed beta transitions are typically of order 20 times slower than the superallowed ones, although the single-particle models would predict for both types of transitions a $\log ft$ of about 3.5. Many references to theoretical papers dealing with this problem can be found in the survey by Morita *et al.* (Mor+ 71), who also summarize the historical development. Here only the newer developments are mentioned.

The first applications of pairing theory to beta decay (Sol 63, MP 63) showed that pairing corrections (see Section 3.1) could explain the A-dependence of the beta-transition rates within a given group. The corrections were not large enough, however, to give quantitative agreement; thus for the deformed rare earths the experimental transition probabilities were found (Zyl+ 67) to be about a factor of 8 slower than calculated from the Nilsson model with pairing corrections included.

An explanation was first suggested by Ikeda *et al.* (IFF 63) as shown in a qualitative way in Fig. 2. Corresponding to the Gamow–Teller operator, one has a broad collective state situated near the isobaric analog state. This collective state, which seems to be directly observable in light nuclei (see Fig. 22) exhausts a large fraction of the Gamow–Teller strength and causes the reduction in the GT transition probabilities. Symbolically the mechanism illustrated for Fermi transitions in Fig. 1 still applies if it is understood that the hole–particle excitations ("nuclear core polarization") now couple to spin and parity 1^+. [The GT decay of ^{49}Ca is discussed in (BD 66).]

Fujita *et al.* point out (IFF 63, FI 65) that one may view the GT transition rates as evidence for a badly broken but persistent Wigner supermultiplet structure (Wig 37). Such a structure would ideally exist if nuclear forces were not only charge-independent but also spin-independent. An isospin multiplet then becomes a supermultiplet because of the assumed degeneracy with respect to changes in the projected value of the nucleon

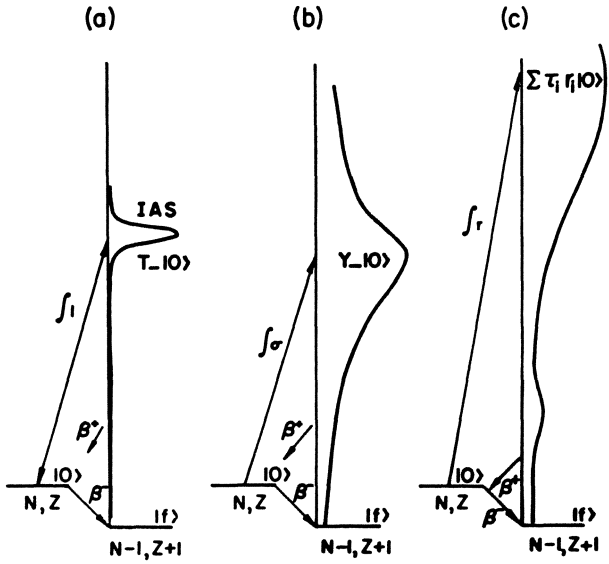

Fig. 2. Beta strength distributions (schematic) corresponding to $\beta^{\pm}$ transitions of the types Fermi, Gamow–Teller, and first-forbidden of the type $\int \mathbf{r}t_-$. [From (Eji 68). The abbreviations $T_- = \Sigma_i t_-^i$ and $Y_- = \Sigma_i t_-^i \sigma^i$ have been used.] The giant-resonance structures are assumed to be responsible for the retardation of transitions between low-lying levels. Compare with Table I, which also gives the resonance energy for a nucleus with $A \sim 150$.

spin (within the limits imposed by the Pauli principle). The spin-flip components of the supermultiplet would then exhaust the Gamow–Teller strength, and the *GT* resonance would coincide with the isobaric analog state. This high degeneracy is lifted by the spin-dependence of the nuclear forces and the *GT* strength presumably is spread over some MeV.

A number of calculations of Gamow–Teller transition rates have been carried out which take nuclear core polarization into account (FFI 64, FI 65, HS 67, BO 67, FFI 68). The "allowed-unhindered" beta transitions which are encountered systematically in the deformed rare earths are especially well suited for a test of a theory of Gamow–Teller rates because the single-particle (Nilsson) wave functions are known to be very precise. The example shown in Fig. 3 is taken from the work of Bochnacki and Ogaza (BO 67).

The polarization effects are due to neutron–hole proton excitations and therefore place β^- and β^+ decay on a completely different footing (see Fig. 2) as the relevant admixtures in the two cases are in the daughter levels and in the initial level, respectively. It seems plausible that the sys-

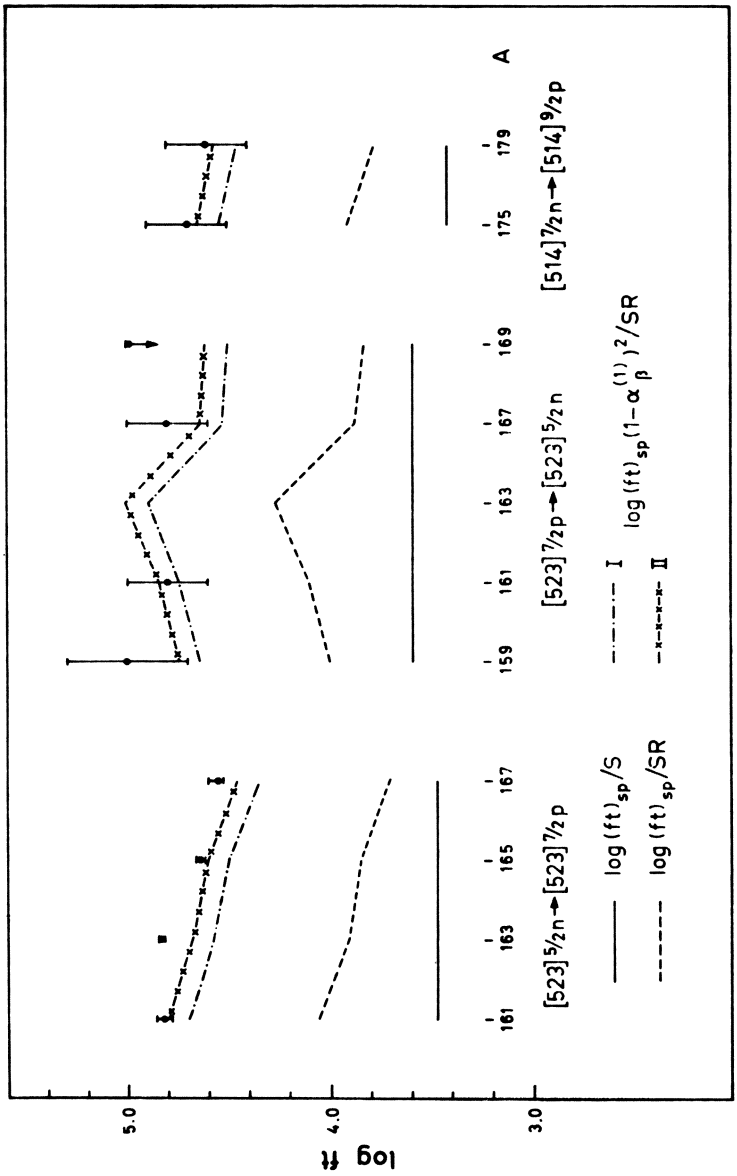

Fig. 3. Absolute beta-transition rates for "allowed-unhindered" beta transitions in rare-earth nuclei. The transitions are characterized by their Nilsson quantum numbers $[Nn_z\Lambda]\Omega$, where Ω corresponds to the projection of angular momentum upon the nuclear symmetry axis (MN 59). The experimental results are compared with a theoretical calculation by Bochnacki and Ogaza (BO 67), who include a statistical factor (S) and a pairing correction (R) together with two estimates (I and II) of the polarization correction. It is interesting to note that the strength of the spin–isospin dependent force, which gives rise to the correction, was chosen to correspond to the strength used by the same authors (BO 65, BO 66) for a calculation of longitudinal and transverse spin polarization in deformed nuclei.

tematic enhancement of β^+ transitions relative to β^- transitions found by Ejiri (Eji 67) for $1^+(\beta^\pm)0^+$ transitions reflects this asymmetry. The effect appears, however, in a more clear-cut way when one considers the energy dependence of the strength functions in β^+, *EC*, and β^- decay (Section 4).

2.3. Forbidden Transitions

The influence of collective effects upon the rates of forbidden transitions was first investigated by Ejiri *et al.* (EIF 68), who pointed out that the forbidden beta transitions have analogous electromagnetic transitions, and that knowledge of the $E1$ giant resonance may be used to calculate one of the first-forbidden beta matrix elements (denoted $\int \mathbf{r}t_\pm$, see Fig. 2). They estimated the theoretical hindrance factor to be approximately 4.

A comparison with experimental data is simplest for unique transitions for which only one matrix element contributes. A general survey (EIF 68) of the data for first-forbidden unique transitions in spherical nuclei gave a hindrance of order 10 relative to the shell model with pairing corrections, while for deformed nuclei Sharma *et al.* (SNH 70) found hindrance factors ranging from 0.9 to 11. First-forbidden transitions in the $A = 90$ region have been considered by Vergados (Ver 71) and by Ejiri (Eji 72), who find evidence for hindrance factors of order 3. Unique-forbidden transitions of higher forbiddenness than first are encountered mainly in the light nuclei; this problem was considered in the theoretical analysis by Warburton *et al.* (WGT 70), who give some evidence for collective suppression of the matrix elements of second- and third-forbidden unique beta transitions.

Much greater difficulties are encountered for nonunique transitions. The most complete information on hindrance factors for nonunique first-forbidden transitions comes from nuclei near ^{208}Pb (DW 64, DBR 69, BM 69a,b, RS 71, RG 71, GS 72, Ast 72). For the $s_{1/2} \rightarrow p_{1/2}$ transition the analysis by Damgaard shows (DW 64, DBR 69) that the dominant contribution corresponds to multipolarity one. This finds support in an experiment by Ehnholm *et al.* (Ehn+ 70), who find 7 ± 1 for the ratio of multipolarity one to multipolarity zero for the case of the $\frac{1}{2}^+ \rightarrow \frac{1}{2}^-$ beta transition in ^{197}Pt. Damgaard *et al.* further find that the hindrance in the case of the decay of ^{207}Tl is approximately 3, and that although the data are consistent with equal renormalizations of the vector and axial-vector terms, the precise ratio cannot be determined (see also the summary in BM 69a,b). The hindrance factor of 13 found (GS 72) for the $p_{1/2} \rightarrow s_{1/2}$ transition from ^{208}Tl (5^+) to the 3.20-MeV level (5^-) of ^{208}Pb probably incorporates contributions from configuration mixing.

The nonunique beta transitions in the rare-earth region have been studied by Bogdan (Bog 65), who finds that the experimental transition probabilities are systematically lower than the theoretical ones calculated from the Nilsson model with pairing corrections included. The beta decay of ^{141}Ce ($\frac{7}{2}^- \rightarrow \frac{5}{2}^+$) is hindered approximately 100 times compared with the single-particle estimate. Ejiri *et al.* (Eji+ 69) have used a measurement of the ($\frac{7}{2}^- \rightarrow \frac{5}{2}^+$) $E1$ matrix element from the isobaric analog state of ^{141}Ce to analyze the beta matrix elements. They account for the retardation of the beta transition as resulting partly from a cancellation in the beta matrix elements and partly from the collective reduction of the matrix element $\int \mathbf{r}$. Another experimental technique has been developed by Shoda *et al.* (Sho+ 71), who determined $\int \mathbf{r}$ from the cross section of the $(e, e'p)$ reaction through the isobaric analog state.

For the very light nuclei the ξ approximation does not hold, and there is no immediate reason to expect that the first-forbidden transitions should have allowed shape. A theoretical study by Towner and Hardy (TH 72) shows that one encounters collective suppressions of the forbidden matrix elements also in the light nuclei, and that the collective effects there may serve to restore the statistical shape of the beta spectrum. They quote as an example the decay of ^{15}C ($\frac{1}{2}^+ \rightarrow \frac{1}{2}^-$) for which Alburger *et al.* (AGW 59) measured allowed shape.

3. EXPECTED PROPERTIES OF THE BETA STRENGTH FUNCTION

As described in the previous section the absolute beta transition rates between individual nuclear levels were explained theoretically in terms of an individual-particle model modified by the introduction of (usually unobserved) strongly collective beta transitions. This posed the question of the general behavior of the beta strength function. Although the existing theories of beta strength are still of a semiquantitative nature they provide a useful basis for discussing the experimental evidence (Section 4). The present section outlines some of the expected main features; for a discussion of assumptions and of theoretical techniques the reader is referred to the papers cited.

3.1. The Shell Model and Effects of Pairing

For Gamow–Teller as well as for first-forbidden transitions it is expected that (in spite of the renormalization effects discussed in Section 2) the shell model will provide at least a rough first estimate of the origins and energy dependence of the beta strength. Figure 4 shows in a schematic fashion the transitions believed to be of importance for electron-capture beta decay of nuclei in the Xe and Hg regions. Note that in the Hg case the neutron excess, which amounts to almost one shell, leads to a predominance

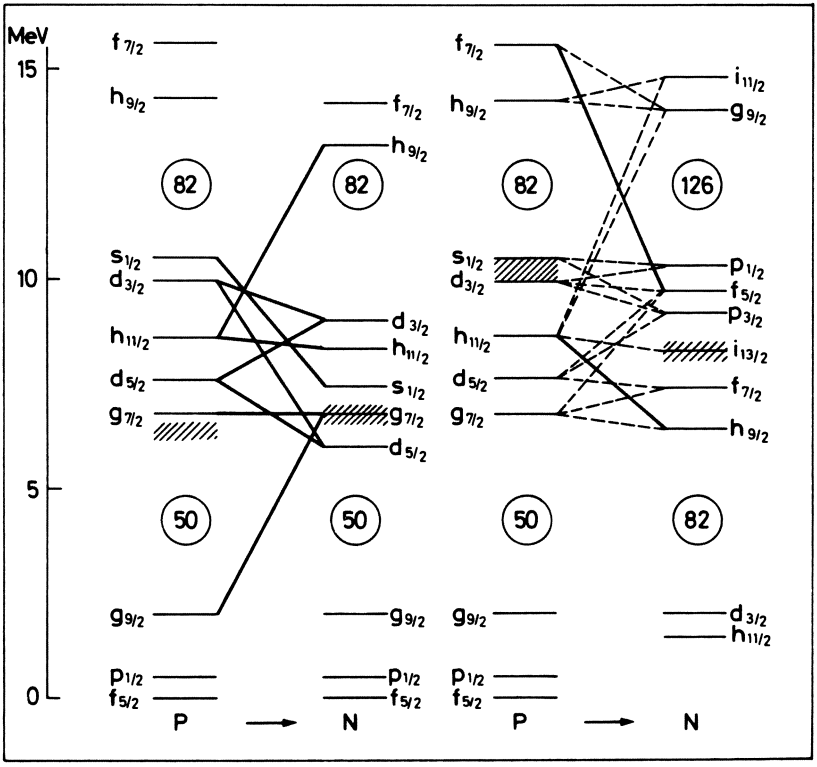

Fig. 4. Shell-model level schemes corresponding to the electron-capture beta decay for $A \simeq 115$ (left) and for $A \simeq 185$ (right). The (approximate) level spacings were taken from (MR 72, BW 68). Allowed transitions are represented by full-drawn lines, while first-forbidden transitions are represented by dashed lines. The hatched areas indicate the approximate position of the Fermi surface for the cases of ^{115}Xe (see also Figs. 5, 17, 19, and 28) and ^{185}Hg (see Figs. 16 and 21). Because of the pairing corrections $u_n^2 v_p^2$ to the shell-model matrix elements (see text) the dominant transitions are those that originate near or below the proton Fermi surface and go to neutron levels near or above the neutron Fermi surface.

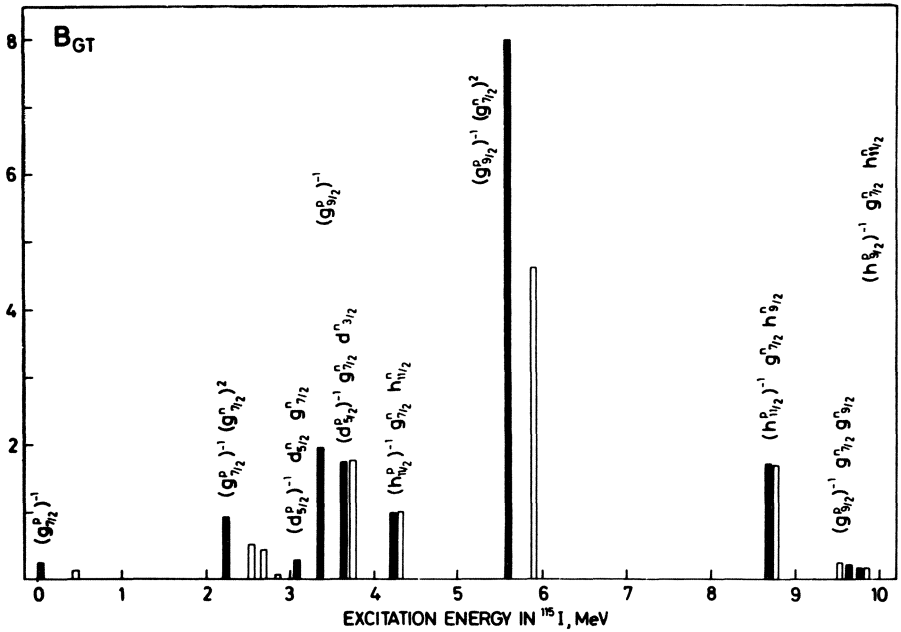

Fig. 5. Distribution of reduced β-transition probabilities for ^{115}Xe as obtained by Martinsen and Randrup (MR 72, Ran 72) in a shell-model calculation with pairing included. The full lines assume the single-particle levels shown to the left in Fig. 4; the distribution in the unfilled lines was obtained by inverting the $d_{5/2}$ and $g_{7/2}$ neutron levels. This inversion leads for ^{115}Xe to the ground-state spin 5/2, which from delayed-proton experiments (Hor+ 72c, d) seems the most probable value. The gap parameter from pairing theory was assumed to be $\Delta = 12\, A^{-1/2}$ MeV for both neutrons and protons. Note that, e.g., the state between 5.5 and 6 MeV has three spin parity values ($5/2^+$, $7/2^+$, $9/2^+$ for the full-drawn lines), which in the calculation were assumed degenerate. The notation used in labeling the states arbitrarily lists the proton state as a "hole" and unpaired neutrons as "particles."

of forbidden transitions, while the strength in the lighter nuclei is predominantly allowed.

Martinsen and Randrup (MR 72, Ran 72) have performed calculations of beta strength functions for isotopes in the Xe region (left-hand diagram in Fig. 4). Figure 5 shows their results for ^{115}Xe with the single-particle shell model with pairing included (see below). The main contribution to the beta strength comes from the $(g^p_{9/2})^{-1} g^n_{7/2}$ hole–particle excitation coupling to the unpaired neutron ($g_{7/2}$ or $d_{5/2}$) in ^{115}Xe. The contribution from the one-quasiparticle strength is considerably weaker but not negligible. The calculation explains the peak which is encountered in the ^{115}Xe strength func-

tion (Figs. 17 and 28) as (mainly) the $(g^p_{9/2})^{-1}g^n_{7/2}$ structure, but it exaggerates the absolute strength by a factor of the order of 10 (Fig. 17 and Hor+ 72a). This is clearly the effect of the correlations discussed in Section 2.2, and to which we shall return in Section 3.2. In the absence of collective effects, the peak from $(g^p_{9/2})^{-1}g^n_{7/2}$ would have of the order of 10 single-particle units. Because of the collective effects one often speaks of such a peak as a "pygmy" resonance. There are, as yet, no shell-model calculations of beta strength functions in the heavier region where forbidden transitions dominate.

The pair-correlation theory for nuclei (BMP 58) entails important corrections to the single-particle beta-decay rates. In this theory (see, e.g., NN 65) the nucleons in paired states have a diffuse Fermi surface characterized for each state by emptiness and fullness coefficients u^2 and v^2, where $u^2 + v^2 = 1$. For the electron-capture beta decay of an even–even nucleus, for example, the shell-model transition probability $(j \to j_1)$ is modified by the factor $v^2_{p,j}u^2_{n,j_1}$. Corrections of this type have been included in the estimates quoted in Section 2 and in Fig. 5. The diffuseness of the Fermi surface is given by the gap parameter $\Delta(\simeq 12A^{-1/2}$ MeV); the quantity 2Δ is the smallest energy required for breaking a pair. In this picture the single-particle states have both hole and particle character: the accepted jargon therefore refers to "quasiparticle states."

Because of the large number of nucleons in paired orbits the main beta strength involves the breaking of a pair: consequently, another effect of pairing is to push the onset of the main strength above the gap energy 2Δ (Duk+ 70). Figure 5 shows an example of this cutoff effect, which in general leads to a pronounced difference in the appearance of the beta strength function for even–even, odd–mass, and odd–odd nuclei, which have cutoff values of 0, 2Δ, and 4Δ, respectively. This phenomenon, which is illustrated schematically in Fig. 6, is well documented experimentally and plays an important role in the systematics of beta halflives (Section 4). An analogous effect should occur in the strength functions for muon capture and for electromagnetic transitions, which for all heavier nuclei should increase markedly at the gap energy. This feature of the gamma-ray strength function has not yet been observed in nuclear physics. A corresponding effect was demonstrated in solid-state physics by Richards and Tinkham (RT 60), who measured the absorption spectrum of superconducting materials at wavelengths in the far-infrared region. They found that there was no absorption until the frequency corresponding to the gap energy was reached.

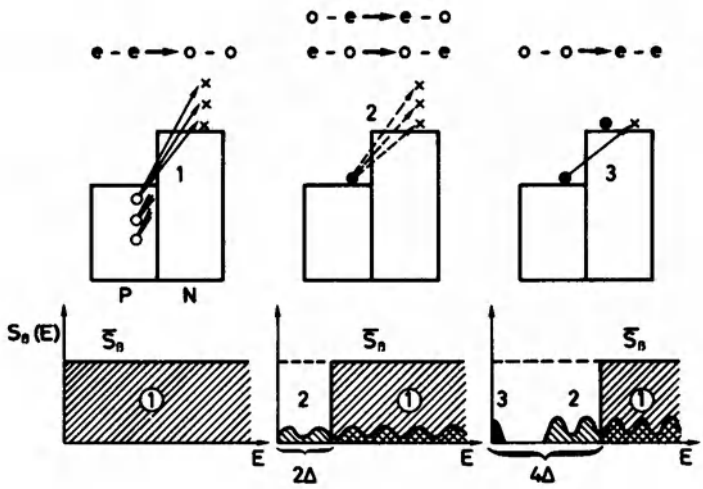

Fig. 6. Schematic filling diagrams (top) and model beta strength functions (Han 69) for the high-energy beta decay of (left to right) even–even, odd-mass, and odd–odd nuclei. It is instructive to classify the transitions with respect to the seniority v ($\equiv$ the number of particles in unpaired states). Owing to the large number of particles in paired states, the transitions of the type $\Delta v = +2$ (labeled 1) dominate in all three cases. Odd-mass and odd–odd mother nuclei have smaller contributions from $\Delta v = 0$ transitions (labeled 2). The odd–odd nuclei (right) have one $\Delta v = -2$ transition. For the three types of nuclei the beta strength functions therefore have the appearance shown schematically in the bottom diagrams. These "caricature" strength functions are characterized by a cutoff energy and by their average value $\bar{S}_\beta$. Such model strength functions have been used in the systematics of beta halflives (Figs. 19-21) and for calculations of delayed-proton intensities Table II).

3.2. The Correlations

Although it is possible to take the correlation effects discussed in Sections 2.1–2.3 into account on the basis of the shell model, we shall begin here with the most sweeping attempt to understand the main features of beta decay with high Q-values. A "gross theory" of beta decay was first proposed by Yamada in 1965 (Yam 65) and has since been developed by him, Takahashi and others (TY 69, KTY 70, Tak 71, Tak 72a). This theory starts with a single-particle model and assumes that there are sufficiently many final levels to permit a continuous approximation, and it presupposes the existence of correlations which enter in the form of a single-particle strength function. We shall outline this theory as applied to Gamow–Teller transitions (Yam 65, TY 69) and leave out further refinements.

Denote the total energy of the decaying nucleon by ε, and let the number density of particles of this kind be $dn_1/d\varepsilon$. Let the total energy release be $\mathscr{E}$ measured from the ground state of the decaying nucleus so that in the notation used in this paper [Eq. (2)] one has $\mathscr{E} = E - Q$. Yamada and co-workers then write the strength function for decay of the type Ω (here denoting Gamow–Teller):

$$6260 S_\beta^\Omega(E)\ \mathrm{MeV}^{-1} \simeq |\, M_\Omega(\mathscr{E})\,|^2 \cdot \frac{3g_A^2}{g_V^2}$$
$$= \frac{3g_A^2}{g_V^2} \int_{\varepsilon_{\min}}^{\varepsilon_{\max}} D_\Omega(\mathscr{E}, \varepsilon) W(\mathscr{E}, \varepsilon) \frac{dn_1}{d\varepsilon} \cdot d\varepsilon \tag{7}$$

where $D_\Omega(\mathscr{E}, \varepsilon)$ is the single-particle strength function and $W(\mathscr{E}, \varepsilon)$ is a weight function which takes the Pauli principle into account. Yamada and co-workers then go on to approximate $dn_1/d\varepsilon$ by the Fermi gas expression* for a nuclear volume V and an effective nucleon mass m

$$\frac{dn_1}{d\varepsilon} = \pi^{-2} V (2m^3\varepsilon)^{1/2} \tag{8}$$

They approximate the function W by 1 for nucleons with $\varepsilon - \varepsilon_F > -Q - \mathscr{E}$, i.e., that are not deeper below the Fermi surface than the energy available for the transition to $\mathscr{E}$, and they let W take the value 0 elsewhere, so that the Pauli principle effectively is taken care of in the limits of integration. Finally, the single-nucleon strength function is included as a trial function, which is assumed independent of ε and which is centered around the Coulomb shift $\Delta_C = \pm(1.44 Z_< A^{-1/3} - 0.78)$ MeV for $\beta^\mp$ decay. The trial function may take a Gaussian shape

$$D_{GT} = 2^{-1/2}\pi^{-1/2}\sigma_{GT}^{-1} \exp\left[\frac{-(\mathscr{E} - \Delta_C)^2}{2\sigma_{GT}^2}\right] \tag{9}$$

where a comparison (TY 69) with experimental data on halflives and strength functions (see Section 4) shows the spreading width σ_{GT} of the GT resonance to be of order 5 MeV. Other types of trial functions (e.g., Lorenzian) have also been used.

With the assumption [Eq. (9)] that D_{GT} is independent of the single-particle energy, the integral (7) simplifies to a product of D_{GT} and the integral over (8), which for energies that are small in comparison with

* Without the inclusion of correlations, the beta decay of a Fermi gas corresponds to complete supermultiplet structure.

the Fermi energy is proportional to the excitation energy $E(= Q + \mathscr{E})$. This second term simply represents the density of one-particle–one-hole excitations. Because of the correlation term (9) the gross theory predicts a different energy dependence of the GT strength functions for β^- and for β^+, EC decays. This appears to have been observed experimentally, as will be discussed in Section 4.

The gross theory has been refined to take into account the effects of pairing (TY 69), and it has been extended to include Fermi transitions (KTY 70) and first-forbidden transitions (Tak 71). The qualitative behavior of the strength functions in the gross theory is shown in Fig. 7. A comparison with experiment is given in Section 4, see especially Fig. 16.

The correlation effects which are the essence of the gross theory should manifest themselves also in a dependence of the strength, at a given excitation energy, upon the Q-value. This effect is illustrated in the calculated curves in Fig. 8, which agree well with the overall trend in the measured strength functions (Section 4). The deviations (e.g., Xe) probably reflect shell effects as well as uncertainties in the experimental definition of average strength.

It seems clear that a detailed discussion of the beta strength function

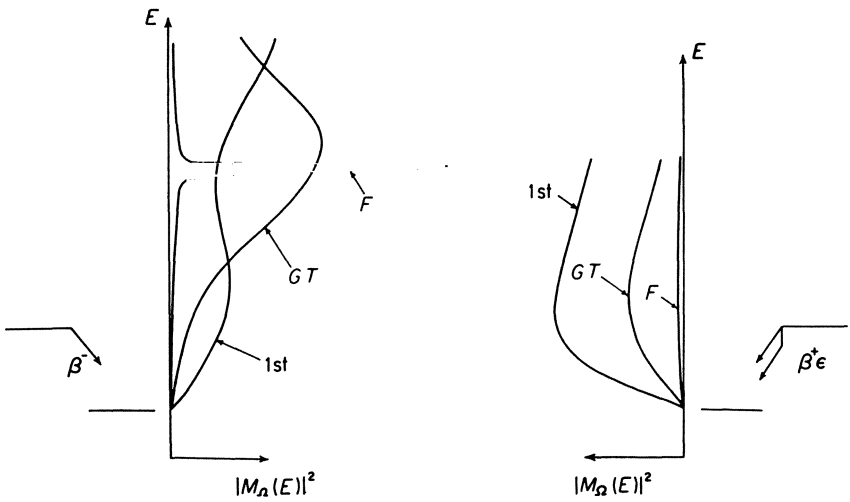

Fig. 7. Schematic illustration of beta strength functions for $A \simeq 200$ in the gross theory of beta decay (from Mor+ 71). The left diagram represents β^- decay, right diagram β^+, EC decay. Note that in this mass region the first-forbidden strength (labeled 1st) dominates over the Gamow–Teller (GT) strength. The Fermi (F) contribution is negligible. For the left diagram (β^- decay) the energy difference between the resonance "F" and the initial state corresponds to the Coulomb energy, i.e., $\sim$15 MeV (see Table I).

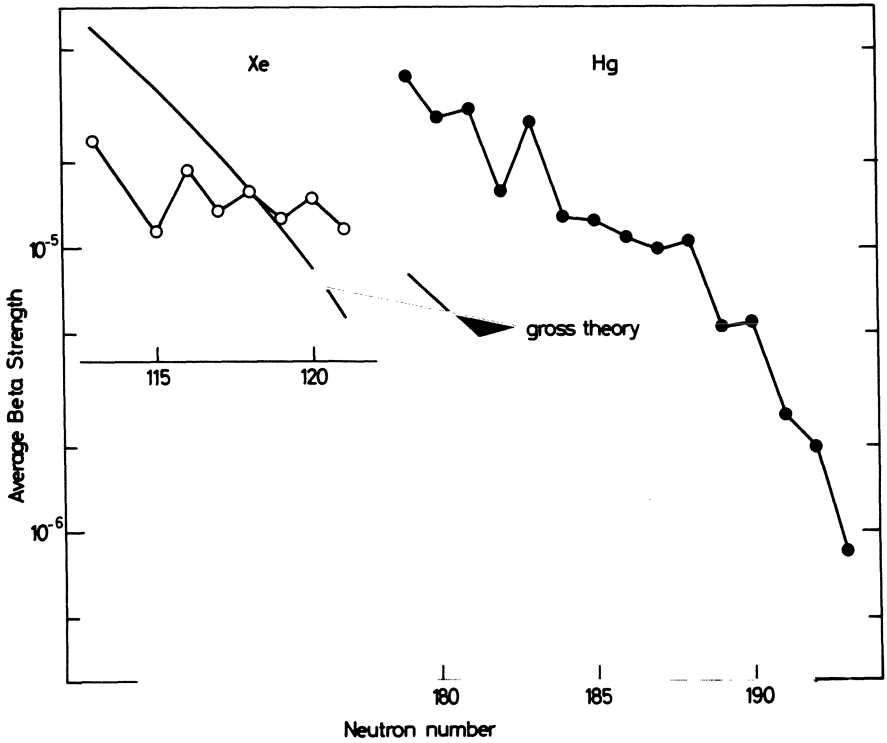

Fig. 8. Average beta strength for isotopes of Xe and Hg. The experimental points are from Fig. 19 and (Duk+ 70). The curves represent the prediction of the gross theory (Gaussian distribution, no pairing) for the Gamow–Teller strength at 2 MeV excitation energy. The apparent mass dependence is effectively a dependence upon the Q-value. The large difference for the case of Hg is due to first-forbidden contributions, which were neglected in the estimate given here. When this is taken into account (Tak 71) the agreement with experiment is very good.

will have to incorporate nuclear-structure effects (shells and deformations) as well as correlation effects, but no general theory is yet in sight. Gabrakov *et al.* (GP 71, GKP 71a) used a semimicroscopical theory to calculate beta strength functions for 0^+ and 1^+ states in deformed nuclei. They obtained strongly collectivized Fermi and *GT* resonances in good agreement with the Fujita–Ikeda theory (Section 3.2) and with the gross theory. Their results cannot be directly compared with experiment because of the large contribution from forbidden transitions, which were not considered. The spherical shell model together with a residual force of the Gamow–Teller type was used to calculate β^+ strength functions in the region of the Xe isotopes (MR 72, Ran 72).

3.3. Fluctuations

In Eq. (2) the beta strength function was defined as an average over many final levels (or, in the language of the statistical model, resonances) at the given excitation energy. This section deals with fluctuations arising from the finite number of resonances contributing to the average. There are two reasons why an investigation of this phenomenon is of interest. The first is that the expected magnitude of the fluctuations provides the natural basis for evaluating the significance of any fine-structure that may be encountered experimentally in the beta strength function. Secondly, the fluctuations provide an experimental tool for measuring level densities and other microscopic parameters. For both applications it is important to note that the delayed-particle experiments (Section 4.4) seem to show that beta strength in the heavier nuclei varies relatively slowly with energy. The gross-structures that are encountered seem to have a typical width of the order of 1 MeV (compare Figs. 26 and 28), so that fluctuations are observable as a much more rapidly varying component.

The statistical properties of ensembles of closely spaced nuclear levels have been studied for a long time, especially by means of neutron reactions. Very useful summaries may be found in the reprint collection edited by Porter (Por 65), in the book by Lynn (Lyn 68), and in the proceedings of the Albany conference (Gar 72). There exists today a well-established statistical theory on the basis of which it is possible to predict the main statistical behavior of high-energy beta decay.

For most cases of interest for beta decay, the spacings between the resonances will be much larger than their natural widths.* One may then for a given spin–parity group consider separately fluctuations in the spacings and fluctuations in the partial (and total) level widths, especially as there seem to be no correlations between spacings and widths.

The nearest-neighbor spacing follows the Wigner law according to which the probability density is

$$p_W(x) = \tfrac{1}{2}\pi x \exp\left(\frac{-\pi x^2}{4}\right) \tag{10}$$

where x is the ratio, $D/\bar{D}$, of the spacing to its mean value. This distribution has a variance of 0.27 and is thus relatively narrow. Furthermore, there are long-range correlations in the spacings so that the variance on the nth-

* This condition simplifies the discussion but is not essential. It should, in principle, be possible to incorporate fluctuation phenomena in which interference between resonances plays a role; see, e.g., the review (BMC 70) of Ericson fluctuations.

order spacing D_n decreases more rapidly (Lyn 68,a) than n^{-1}. In all experiments where the detector halfwidth is large enough to include (on the average) a few resonances, it therefore seems permissible to neglect the fluctuations in the level density in comparison with the fluctuations in the level widths.

The distribution of the reduced partial width x (in units of its average value) for a given reaction channel is given by the Porter–Thomas law

$$p_{PT}(x) = (2\pi x)^{-1/2} \exp\left(\frac{-x}{2}\right) \tag{11}$$

This expression has been verified experimentally for reduced neutron and gamma widths, and it may be derived from the very general assumption (PT 56) that the reaction amplitude has a normal distribution with zero mean. It is therefore natural to assume that the law will also apply to the reduced beta-transition probabilities to individual resonances. It is characteristic of this distribution (illustrated in Fig. 9) that it diverges for zero width and that it has a variance as large as 2. The contributions from the widths will therefore dominate the fluctuations in an unresolved spectrum.

Experimentally it is difficult to observe the beta strength function directly with sufficient resolution for a study of fluctuations (see Section 4), and the best possibility seems to be the observation of secondary processes such as the emission of high-energy gamma rays, or of delayed particles (Section 4.4). Let the observed quantity be of the type a, where a stands for a gamma ray, proton, etc. The intensity of a line corresponding to a particular resonance is then

$$R_a^{if\nu} = \frac{R_\beta^{i\nu}\Gamma_a^{if\nu}}{\Gamma_{\text{total}}^{i\nu}} \tag{12}$$

i.e., proportional to the beta feed $R_\beta^{i\nu}$ to the νth resonance with spin and parity $I_i^{\pi_i}$. The fluctuation law for such a quantity is relatively complicated, but it is instructive to consider two limiting cases. If the exit channel corresponding to the emission of a dominates, one has $\Gamma_a^{if\nu} = \Gamma_{\text{total}}^{i\nu}$, and the result is simply the Porter–Thomas law

$$(\overline{R_a^{if}})^{-2} \operatorname{Var} R_a^{if} \equiv \alpha_a^{if} = 2 \tag{13}$$

Another useful limit is obtained if Γ_{total} is dominated by the total gamma width which may be regarded as a constant because of the many partial gamma widths which constitute the total width (Lyn 68). Under the as-

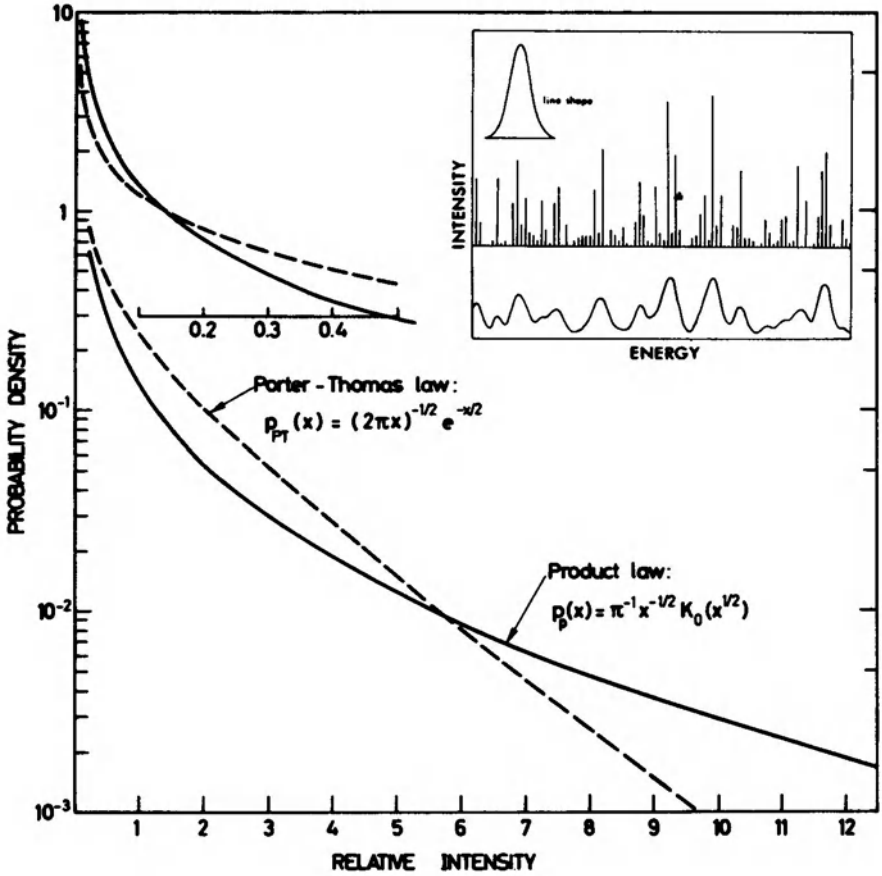

Fig. 9. Probability density corresponding to the Porter–Thomas law [Eq. (11)] and to the product distribution [Eq. (14)] as a function of the reduced width x measured in units of the mean value, so that $\bar{x} = 1$ for both distributions. The inset shows (as equally spaced vertical bars) a sequence of Porter–Thomas distributed random numbers and the corresponding spectrum for a detector with the indicated Gaussian response function. (Compare with the experimental spectra of delayed particles, Figs. 24–27).

sumption of no correlations between the beta channel and the exit channel a, the distribution is (HHJ 72f) the product distribution of two Porter–Thomas distributed variables

$$p_p(x) = \pi^{-1} x^{-1/2} K_0(x^{1/2}) \tag{14}$$

where $x = R_a^{if}/\overline{R_a^{if}}$, and K_0 is the modified Bessel function. For this distribution the variance α_a^{if} takes the value 8. Figure 9 compares the product distribution with the Porter–Thomas distribution.

It should be possible experimentally to find cases where the individual resonances can be resolved, but until now the experimental line width in the delayed-particle spectra appears to have been comparable to or greater than the average level spacing. The experiments then record gross fluctuations* as illustrated in the inset of Fig. 9. In the simple case where the half-width $W_{1/2}$ for the detector is much greater than the average level spacing, one may use the central limit theorem to obtain (HHJ 72, Han 72) the variance on the total intensity of particles of type a:

$$\mathrm{Var}\, I_a = (2 \ln 2)^{1/2} \pi^{-1/2} W_{1/2}^{-1} \sum_f \sum_i \frac{(I_a^{if})^2 \alpha_a^{if}}{\varrho_i} \tag{15}$$

where a Gaussian line width was assumed. The quantity α_a^{if} is numerically of the order of 2 to 8,† and was defined by the left part of Eq. (13). The quantity ϱ_i is the density of levels $I_i^{\pi i}$ This expression has been applied to delayed-proton spectra (Section 4.4). In principle it should not be difficult to perform calculations also for cases where the condition $\varrho_i W_{1/2} \gg 1$ is not fulfilled.

4. EXPERIMENTAL RESULTS ON BETA STRENGTH

The experimental study of the beta strength function involves nuclei with very large Q-values for beta decay, as illustrated for ^{181}Hg in Fig. 10. Although interesting information may be obtained from the simpler cases where at least reasonably complete decay schemes are available (Section 4.1), it has been necessary to develop experimental techniques (Sections 4.2–4.4) that measure only some of the main features of the beta-decay pattern. It is interesting to compare (Section 4.5) the results with those obtained in the study of muon-capture and electromagnetic decays.

The experimental difficulties in the study of beta strength functions are, however, not only associated with the absence of suitable and direct high-resolution methods. In connection with experiments on nuclei with a considerable excess or deficit of neutrons (nuclei far off the beta stability line), there are a number of more general problems which have been discussed at the Lysekil and Leysin conferences (FHR 67, Ley 70) as well as in a recent review by Klapisch (Kla 72), to which the reader is referred for

* Fluctuations arising from unresolved resonances were first discussed by Egelstaff (Ege 58) in connection with average neutron cross sections.

† Values higher than 8 are theoretically possible but are without great practical interest.

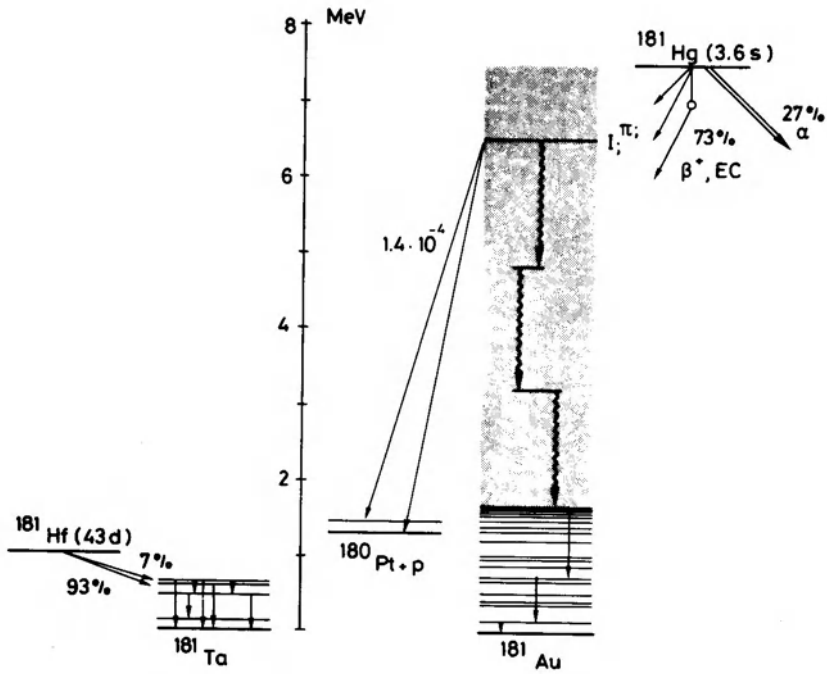

Fig. 10. Schematic decay schemes of 43*d* ^{181}Hf and 3.6 sec ^{181}Hg. In the former case the Q-value is approximately 1 MeV and the β^- decay populates two levels in ^{181}Ta (LHP 67). The decay of ^{181}Hg (Han+ 70) has, in addition to a 27% alpha branch, a beta decay with a calculated Q_{EC} of 7.5 MeV (MS 65); one estimates that of the order of 10^5 levels are populated directly in the beta decay, and that the average level spacing in the top part of the spectrum is about 10 eV. The odd proton in ^{181}Au is only bound by $\sim$ 1.3 MeV (MS 65) so that beta-delayed proton emission occurs with an intensity of 1.4×10^{-4} proton/dis (Hor+ 71a). Proton emission is inhibited by the Coulomb barrier which has a height of about 15 MeV for ^{180}Pt + p. The proton spectrum may be used to obtain information about the beta strength function. One must expect the ^{181}Hg gamma-ray spectrum to be very complex: tne evaporation cascade of $\sim$ 2 MeV gamma rays leads into a sequence of individual gamma rays near the ground state.

a more detailed discussion and references. Here we point only to the main experimental difficulties: (1) *Production cross sections.* For neutron-rich light nuclei spectacular results have been obtained in fragmentation reactions with 25-GeV protons (Cha 69, Kla+ 72a) to give sodium isotopes up to ^{33}Na, and in multinucleon transfer reactions with heavy ions (Art+ 71). For heavier nuclei the main production method for neutron-rich nuclei is fission; many regions, however, are not accessible and the cross sections become vanishingly small long before the ground states become unstable

with respect to neutron emission ("the neutron drip line"). For neutron-deficient isotopes the main production methods involve bombardment with heavy ions or high-energy protons. In both cases the predominance of proton evaporation at small proton binding energies seems to lead again to extremely small cross sections (SLD 71, WGB 72) long before one reaches nuclei which are proton-unbound by an energy corresponding to the Coulomb barrier. (2) *Complex reaction mixtures.* The reactions leading to nuclei far from stability tend to give rise to very complex mixtures of isotopes. The most interesting experiments are often those that deal with products that have very small cross sections [see (1)], and therefore highly selective detection and/or separation techniques are required. Many of the experiments discussed in the following have been based on on-line mass separation, which provides a separation according to both Z and A. (3) *Short halflives.* The products with high Q-values have short halflives, and only small delays can be tolerated between production and detection.

According to Eq. (2), the experimental determination of the beta strength function requires knowledge of $T_{1/2}$, Q, and $b(E)$. Although the measurement of the first two parameters is far from trivial, we shall not discuss this more general problem here, but concentrate on the third parameter $b(E)$, the beta feeding per MeV of final levels.

4.1. Nuclear Level Schemes

The study of beta transition rates over many years has contributed to the understanding of the structure of low-lying nuclear levels. This body of information also provides the starting point for understanding the beta transition rates to more complicated levels. The dominant transitions are those corresponding to large admixtures in the wave function of "simple" excitations with large beta-transition probabilities.

The beta transitions in the region of ^{208}Pb provide an especially instructive example. One expects (see the right part of Fig. 4) that the dominant transitions are first-forbidden of the types $g_{9/2} \rightarrow h_{9/2}$, $p_{1/2} \rightarrow s_{1/2}$, and $p_{3/2} \rightarrow s_{1/2}$, which were discussed briefly in Section 2.3, where further references may be found. In the decay of ^{208}Tl (5^+) the strength concentrates on the 4^- and 5^- levels at 3–4-MeV excitation energy [see the discussion by Gupta and Sastry (GS 72)]. For the recently discovered isotope 2.9 min ^{207}Hg (Nie 72), the beta-decay pattern is almost the same (see Fig. 11), leading in this case to two-hole–one-particle configurations $(s^p_{1/2})^{-1}(p^n_{1/2})^{-1}g^n_{9/2}$ and $(s^p_{1/2})^{-2}h^p_{9/2}$. Only a more detailed analysis aided by further experiments could determine the details of the makeup of the ^{208}Pb and ^{207}Tl levels as

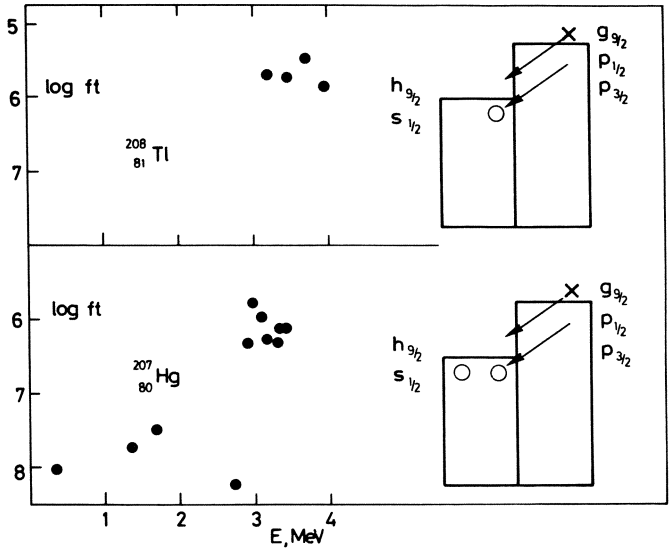

Fig. 11. The log *ft* values in the β^- decays of $^{208}_{81}$Tl (LHP 67) and $^{207}_{80}$Hg (Nie 72) as a function of excitation energy. The main strength is found near 3 MeV in both cases with total values of 1.9×10^{-5} sec^{-1} and 1.2×10^{-5} sec^{-1}, respectively. The analysis shows (see Fig. 4) that the strength originates in the $p^n_{1/2} \rightarrow s^p_{1/2}$ and $g^n_{9/2} \rightarrow h^p_{9/2}$ transitions, which in both nuclei lead to final excitations of the types $h^p_{9/2}\,(s^n_{1/2})^{-1}$ and $g^n_{9/2}\,(p^n_{1/2})^{-1}$, i.e., to excitations across the closed shells. For protons as well as for neutrons such an excitation requires about 3 MeV (BW 68). The same transitions dominate the electron-capture beta decay of $^{210}_{85}$At to $^{210}_{84}$Po; in this case (not shown here) the main beta feed goes to levels at 2910 keV (71%) and 3026 keV (19%) (JPH 72). In the decay scheme of $^{210}_{86}$Rn (Jon+ 72) the first beta transition with appreciable strength is the first-forbidden decay to a 2.28-MeV level with spin-parity 0^- or 1^-.

well as the extent to which they have vibrational character. Further examples of the forbidden strength in this region may be found in the papers of Alpsten, Appelqvist, Astner, and Jonson (AAA 71, Ast 72, Jon+ 71, Jon+ 72), who also discuss the allowed strength in neutron-deficient nuclei just above ^{208}Pb. They point out that the weak allowed transitions must originate in the $f^p_{7/2} \rightarrow f^n_{5/2}$ transition (Fig. 4), which because of pairing corrections is slowed down by a factor of the order of 100.

For nuclei in which the neutrons and the protons are filling different shells, one encounters prominent allowed transitions between the spin-orbit partners. In the deformed rare-earth region there is a family of "allowed-unhindered" transitions between Nilsson states that differ only in the spin projection quantum number (see Fig. 3). These transitions have played an important role in identifying unambiguously certain three-quasiparticle

components in highly excited levels. Many such examples can be found in the review by Bunker and Reich (BR 71).

McHarris *et al.* (McH 70, BKM 69) have drawn attention to the allowed beta decays of neutron-deficient odd-mass isotopes with N equal to 79 and 81. As an example, Fig. 12 shows the decay scheme of 5.5h $^{139}_{60}$Nd. The $\frac{11}{2}^-$ isomer ($h_{11/2}$) cannot decay to the $\frac{11}{2}^-$ neutron state which is full at $N = 80$. Allowed beta decay in this region is carried by the $d^p_{5/2} \rightarrow d^n_{3/2}$ transition which presumably is responsible for the strength in the region 1.6–2.2 MeV, where six levels are fed with $\log ft$ values from 5.6 to 6.3.

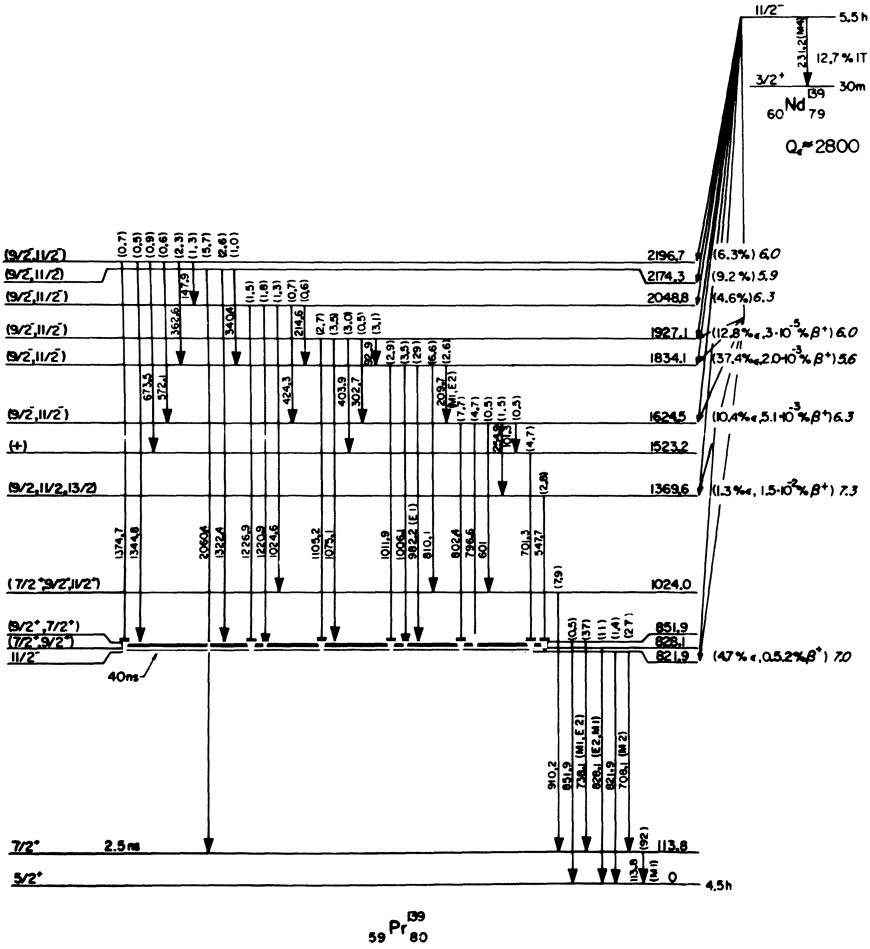

Fig. 12. The decay scheme of $^{139m}_{60}$Nd according to McHarris *et al.* (McH + 70, BKM 69). In their interpretation the allowed beta strength in the region 1.6–2.2 MeV is associated with three-quasiparticle excitations of the type $(d^p_{5/2})^{-1}\, d^n_{3/2}\, h^n_{11/2}$.

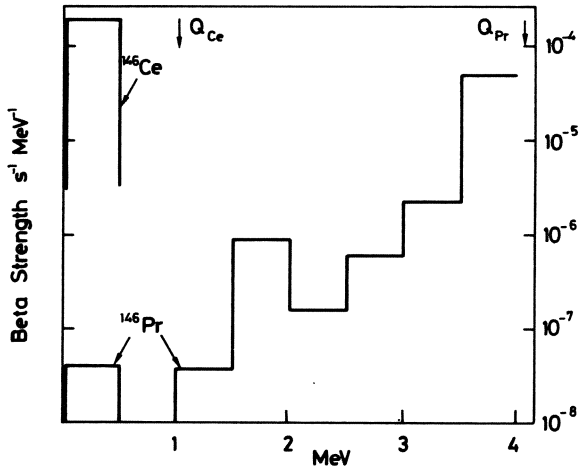

Fig. 13. Beta strength shown as a histogram with 0.5-MeV bins for the β^- decay of ^{146}Ce and ^{146}Pr. The Q-values of the two decays have been marked by arrows in the top part of the diagram. Only one transition (to 315 keV) has been observed in the ^{146}Ce decay (HMD 67), but transitions to levels between 0.5 and 1 MeV would have been difficult to detect experimentally in this case. For the decay of the odd–odd ^{146}Pr (Mar 67), the beta strength sets in close to the expected cutoff energy: $4\Delta \simeq 4 \times 12 \times 146^{-1/2} = 4.0$ MeV. In both nuclei the beta strength is expected to originate in the $(h^n_{9/2})^{-1}$ $(h^p_{11/2})$ state (HMD 67)

The onset of beta strength near 2 MeV in ^{139}Pr (Fig. 12) is characteristic of the cutoff effect associated with pairing (Section 3.1). Systematic evidence for this effect may be found in the decay schemes available in the literature, as illustrated in Fig. 13 which shows the beta strength functions calculated from the decay schemes of ^{146}Ce and ^{146}Pr (Mar 67, HMD 67) It is seen that whereas the even–even decay displays no cutoff, one encounters the main strength in the ^{146}Pr decay at an energy corresponding to approximately twice the gap energy. Other evidence for the cutoff (nuclear Richards–Tinkham effect, Section 3.1) comes from total absorption spectrometry and the systematics of beta halflives (Duk+ 70). We consider in the following these and other methods that may serve to give information about the beta strength function in the case when complete information (the "decay scheme") is not available.

4.2. Total Absorption Spectrometry

In order to determine the beta strength function [Eq. (2)], it is necessary to measure the intensity $b(E)$ of beta decays to levels (resonances) at the energy E. Such a measurement may be performed with a large NaI(Tl)

spectrometer in a 4π geometry. In the ideal case, this instrument sums the contributions from all gamma rays in the evaporation cascade (Fig. 10), and a single output pulse appears corresponding to the energy E of the initial level. In the early years of NaI spectrometry the total absorption technique often helped (NB 65) in the construction of nuclear-level schemes; here we consider primarily the case where many levels contribute within the experimental resolution.

The first application (Duk+ 70) of this technique was to the electron-capture decay of nuclei in the Os–Rn region, where the positron branches are known to be weak. It seemed safe to neglect the X-rays following the beta decays as well as gamma energy lost through highly converted gamma transitions, because the energies involved are typically considerably smaller than the experimental energy resolution. Furthermore, isomeric transitions were neglected as being both relatively rare and normally of low energy. These effects will not be discussed any further, as they seem insignificant in comparison with one to be discussed later in this section—the correction for the efficiency of the total absorption spectrometer.

The total absorption technique cannot be applied directly to decays where there is a substantial contribution from $\beta^{\pm}$ radiation because the NaI(Tl) detectors are sensitive to electrons of high energy and also because of contributions from bremsstrahlung and annihilation radiation. A modified technique suitable for β^- decay has been introduced by Johansen *et al.* (JBR 72). Their apparatus (shown in Fig. 14) uses a coincidence demand to select events in which the electron has left the volume between the two NaI(Tl) detectors.

The same technique is applicable to β^+, EC decays, but as the electron-capture part favors the high-lying levels (the transition probability is quadratic in Q–E, whereas the positron part approaches a 5th-power law) it seems advantageous to select the electron-capture events. This can be done by means of veto pulses from a 4π beta counter placed between the two NaI crystals (Hor+ 72a).

The measurement of beta strength functions by total-absorption spectrometry is best carried out with mass-separated samples (Duk+ 70, JBR 72). The data are recorded as a function of time in order to allow the calculation of the spectra for the various elements in an isobaric chain. The spectra have to be normalized with respect to the source strength; in the EC, β^+ experiment this was obtained (Duk+ 70) as the integral count rate above a bias set below the energy of the K X-ray; in the β^- experiment (JBR 72) the singles β^- count rate was used. The most important correction, however, originates in the finite size of the NaI crystals to be considered next.

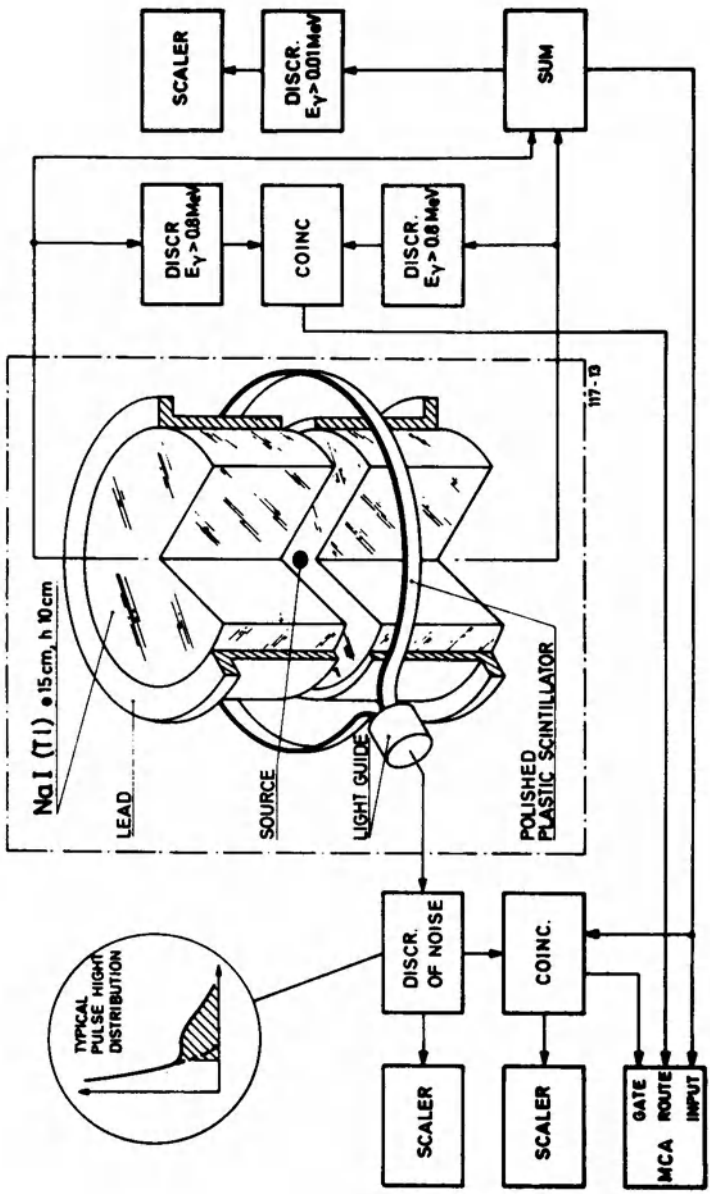

Fig. 14. Total-absorption spectrometer (schematic) used by Johansen *et al.* (JBR 72) for measuring strength functions from β^- decay. The output pulses from two 15 cm diameter $\times$10 cm height NaI(Tl) crystals are summed and taken to the input of the multichannel analyzer (MCA). A coincidence gate selects events corresponding to the simultaneous detection of gamma rays and of beta particles in the ring-shaped plastic scintillator. A lead shield prevents secondary radiations produced in this counter from re-entering the NaI spectrometer. A second coincidence arrangement permits separate recording of events where appreciable energy ($>$ 0.8 MeV) is deposited in both crystals; this information makes it possible to estimate the multiplicity of the gamma cascade.

For a spectrometer such as that shown in Fig. 14 the detection efficiency (both crystals together) for a 1- to 2-MeV gamma ray is only 60–70%, and only one-third of this falls in the full-energy peak. Therefore, for a cascade of gamma rays only a small fraction of the response falls at the full energy. The problem is, then, from a measured spectrum $g(W)$ to calculate the true beta intensity distribution $b(E)$. If it is permissible to assume a response function $L(W, E)$ for cascades starting at the energy E, the relation is simply

$$g(W) = \int_0^\infty L(W, E)b(E)\,dE$$
$$= \int_W^Q L(W, E)b(E)\,dE \tag{16}$$

Fortunately it seems to be a good approximation to assume a single response function $L(W, E)$, at least for each nuclide, and furthermore $L(W, E)$ seems to vary relatively slowly with Z and N. There are two reasons for this: (1) At high energies (Fig. 10) one is very far from a "decay scheme" situation. The evaporation cascade of gamma rays develops with very many final levels available, and as the gamma strength function varies slowly with energy one expects an average over many cascades to show a very slow dependence* on Z and N and to vary smoothly with the excitation energy E. (2) the total absorption spectrometer has a response that depends relatively little upon the energy split and multiplicity of the cascade (this is, of course, the very reason for choosing this instrument).

Calculations of the function $L(W, E, Z, N)$ have been performed by Erdal and Rudstam (ER 72). They have approximated the integration over all possible cascades by two methods, a Monte-Carlo simulation and a recursion analysis, which agree in their main features. The most accurate seems to be the Monte-Carlo calculation, of which Fig. 15 gives an example. The calculation assumes that the (unnormalized) probability density for having a gamma ray of energy E_γ from a level with effective excitation energy U_i is (BW 52)

$$p(E_\gamma) = NE_\gamma{}^3\varrho(U_i - E_\gamma) \tag{17}$$

where ϱ is the level density, and the parameter N is independent of energy if one assumes a constant gamma strength function. It has been found by Bollinger (Bol 68, see also the discussion in Bar+ 72) that near ^{195}Pt it is

* The familiar near-constancy of total gamma widths (Lyn 68) is another manifestation of the same phenomenon.

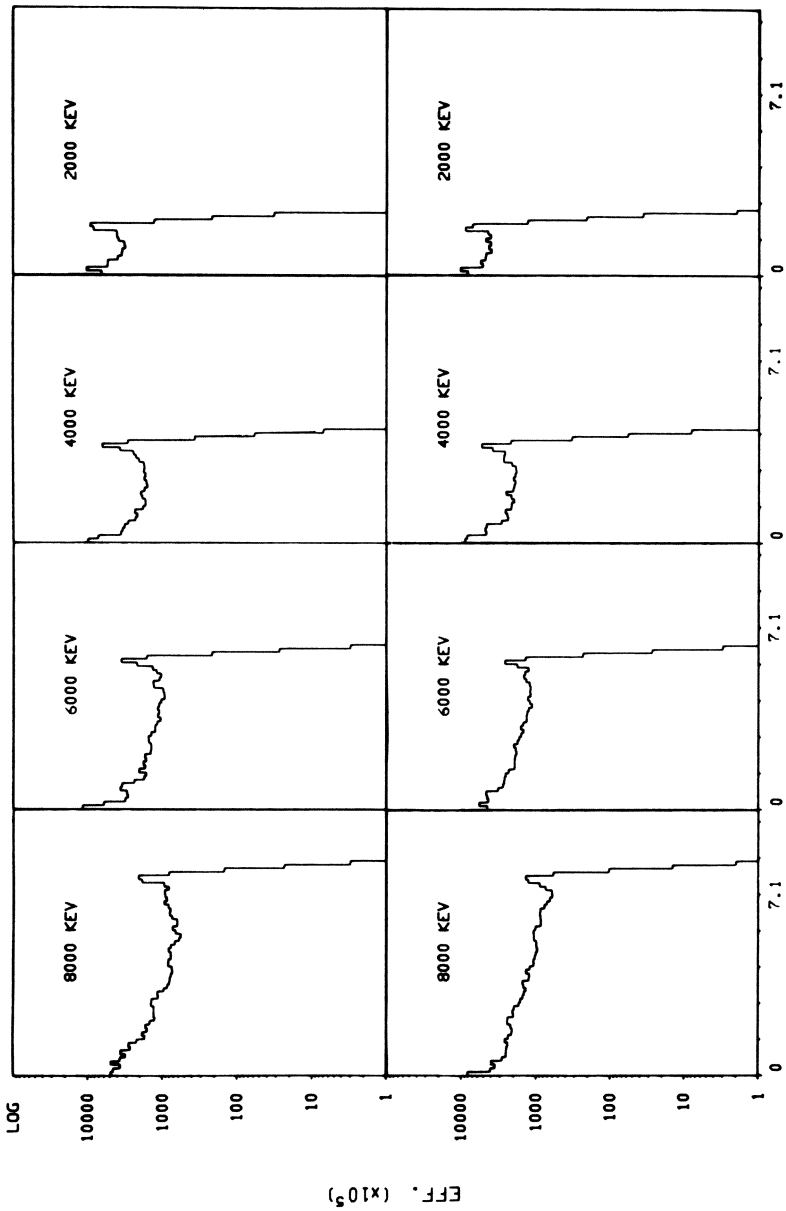

Fig. 15. Response functions obtained in a Monte-Carlo calculation by Erdal and Rudstam (ER 72). The functions are for a total-absorption spectrometer with two 15 cm diameter $\times$10 cm height NaI(Tl) crystals for the isotope ^{198}Au and for total cascade energies of 2, 4, 6, and 8 MeV. The lower diagrams assume a constant gamma strength function [Eq. (17)] while the upper ones assume a quadratic energy dependence of the gamma strength function. The efficiency scale gives the fraction of the response (in units of 10^5) within an interval of one channel.

better to assume a quadratic energy dependence of the gamma strength function ($N = N_1 E_\gamma^2$); this prescription was also tried by Erdal and Rudstam (ER 72) (see Fig. 15). The gamma cascade was terminated by a ground-state transition when the effective excitation energy U_i came below 0.5 MeV (for odd–odd/odd-mass/even–even nuclei, U_i is measured from $0/\Delta/2\Delta$ above the ground state). The response corresponding to one cascade was calculated by folding the measured response functions for single gamma rays; only about 20 cascades were required to obtain convergence. Figure 15 shows that for odd–odd ^{186}Au, it makes only a rather small difference if the gamma strength function is assumed to depend on energy. The Monte-Carlo calculations give as a byproduct the average number of gamma rays per cascade (the multiplicity) which at 6 MeV is about four for ^{118}I and about three for ^{186}Au. (These numbers, of course, do not include low-energy gamma rays originating near the ground state.) This agrees with measurements* (Mue 50, Deg+ 72, Duk+ 70), and also with calculations by von Egidy (Egi 69).

Total absorption spectrometry has until now been used to measure beta strength functions in approximately 90 cases (Duk+ 70, JBR 72, Hor+ 72a). Examples of the results are shown in Figs. 16 and 18. The main conclusions from an investigation of the Os–Rn region (Duk+ 70, Fig. 16) were:

1. The existence of a cutoff in $S_\beta(E)$ for odd-mass and odd–odd nuclei; this implies (see Section 3.2) that the main beta strength is associated with transitions that originate in the paired system.
2. Peaks were observed in the Hg–Au region. These presumably correspond to the remaining allowed strength ($h^p_{11/2} \rightarrow h^n_{9/2}$), while the strength closer to ^{208}Pb is forbidden (see Figs. 4 and 11).
3. Above the cutoff the beta strength varies slowly with energy as well as with Z and N (this is the basis for the concept of an average beta strength function used in Section 4.3). The overall behavior is in agreement with Takahashi's "gross theory" of forbidden beta decay (Tak 71), although discrepancies due to shell effects remain.

In the lighter nuclei the allowed strength dominates (Section 3.1) and a comparison with theory is easier. Figure 17 compares data for two Xe isotopes with the shell-model calculation discussed in Section 3.1. The renormalization factor of about 20 is similar to the values quoted in Section 2.2.

* The subject of gamma-ray multiplicities falls outside of the scope of this review. Apart from the special case of compound levels with very high angular momentum, very little has been done in this field until quite recently.

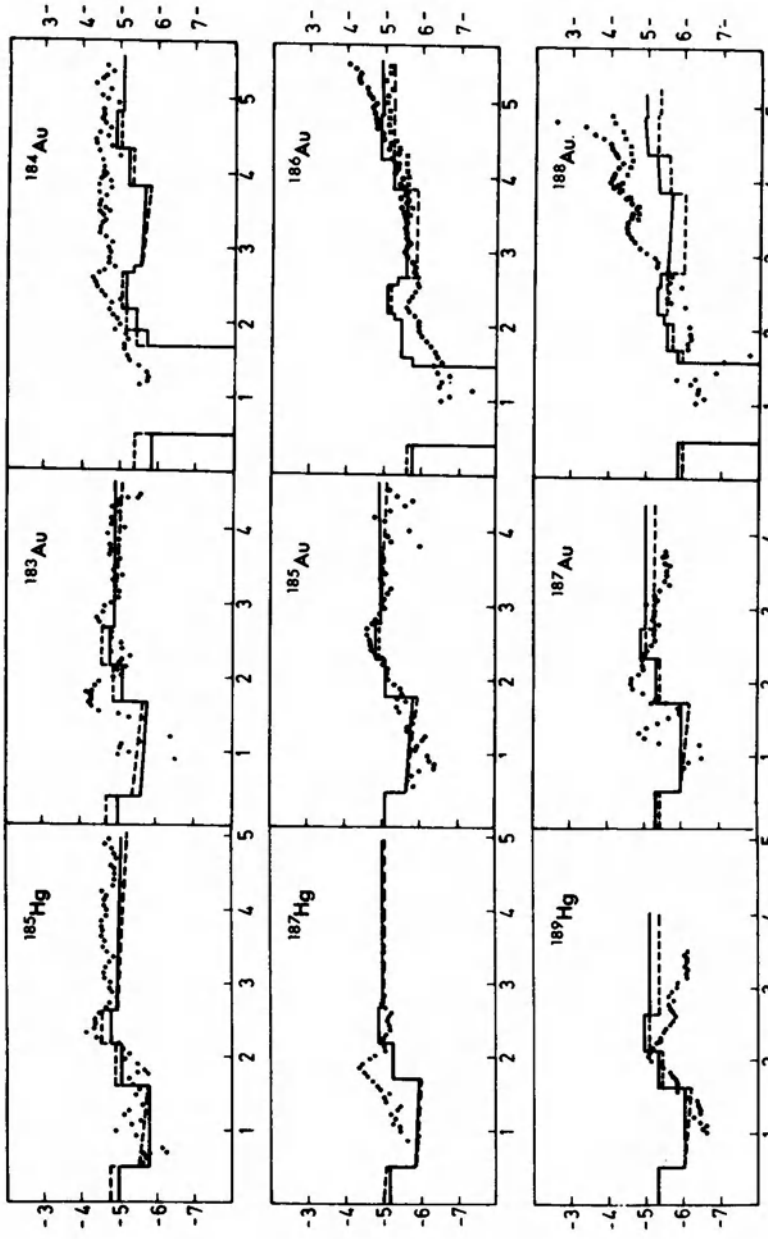

Fig. 16. Measured and calculated beta strength functions for Au and Hg isotopes (Duk+ 70, Tak 71). The diagrams show log $S_\beta(E)$ as a function of the excitation energy E (in MeV). The data were calculated with less sophisticated response functions than later work, but the main features are independent of these assumptions. A comparison is made with Takahashi's (Tak 71) theoretical estimates based on the gross theory (Section 3.2), which included both allowed and first-forbidden contributions. The calculations used two trial functions, Gaussian (solid line) and modified Lorenzian (dashed line).

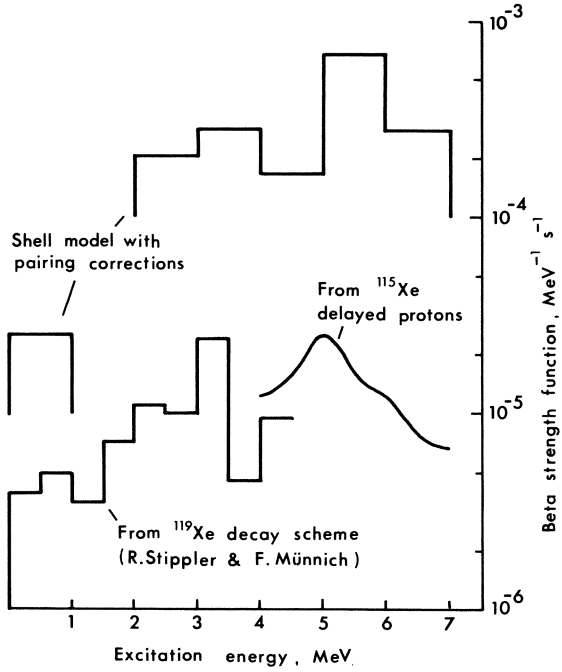

Fig. 17. Beta strength functions for ^{119,115}Xe. Functions obtained from the decay scheme (SM 72) and from a re-analysis of the ^{115}Xe delayed-proton spectrum (Fig. 28), respectively. The shell-model calculation (MR 72) with pairing corrections is for ^{115}Xe. It gives the peak (Fig. 5) in the right place, but overestimates the strength by roughly a factor of 20.

The experiments by Johansen *et al.* (JBR 72, Figs. 14 and 18) show that the β^- strength function above the cutoff increases markedly with energy. The same conclusion has been obtained indirectly from analysis of delayed-neutron intensities to be discussed in Section 4.4 (it is for historical reasons, associated with delayed-neutron emission, that Johansen *et al.* point out that the increase roughly follows the increase in level density). The β^- and EC, β^+ strength functions are thus very different; this is in support of the theories (Section 3.2) which predict such a behavior as a result of the Coulomb displacement. Shell effects also appear and add to the complexity of the data.

4.3. The Systematics of Beta Halflives

If it is possible to express the beta strength function $S_\beta(E)$ as a one-parameter function of the energy, then the knowledge of the halflife, the beta branching ratio, and the Q-value will suffice to determine the free

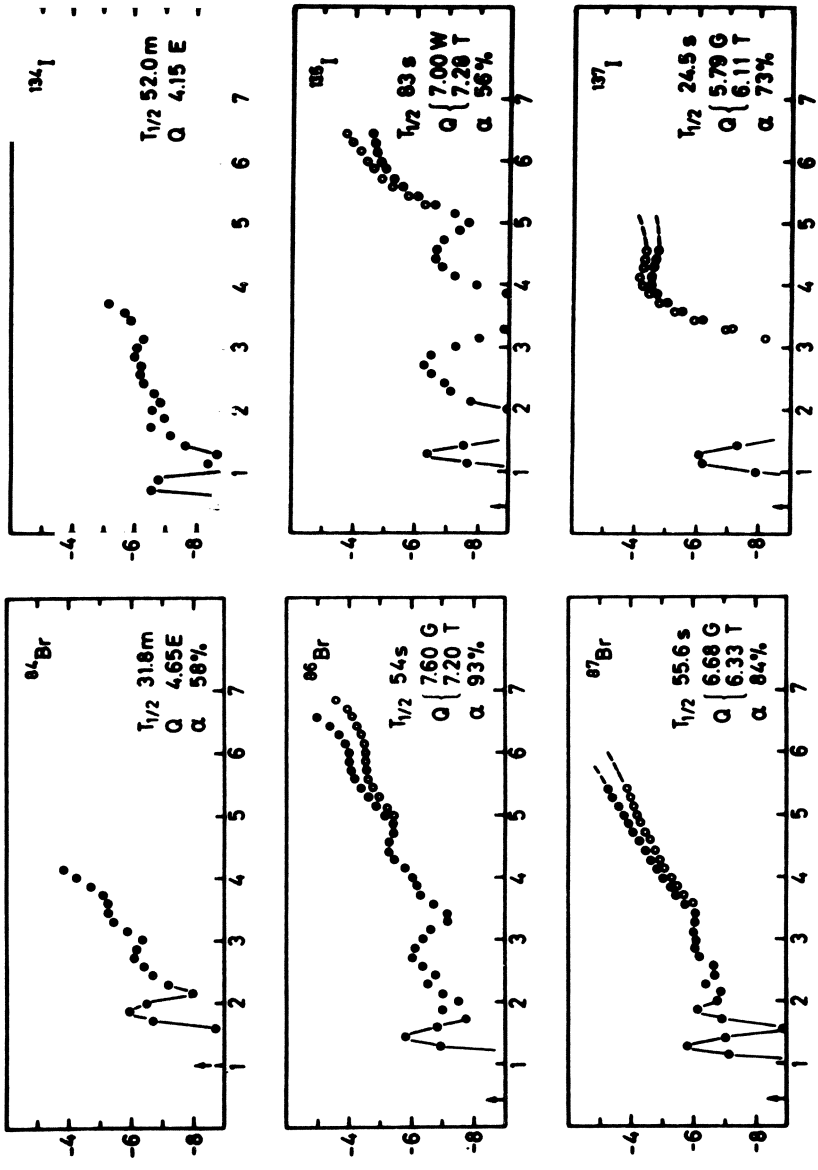

Fig. 18. Strength functions for the β^- decay of ^{84,86,87}Br and of ^{134,136,137}I (from JBR 72). The halflives and Q-values (those which have been experimentally determined are denoted E) are given as inserts together with the parameter α which indicates the fraction of the beta decay which proceeds to levels at energies above 0.5 MeV (above 1 MeV for ^{84}Br). Note that the use of a higher Q-value leads to a more slowly increasing strength function.

parameter. The model strength function introduced by Duke *et al.* (Duk+ 70) and illustrated in Fig. 6 is a good approximation for the case of electron capture. Below a cutoff energy C (different for odd–odd, odd-mass, and even–even nuclei) the strength is assumed to be zero; above C it takes the constant value $\overline{S_\beta}$ called the average beta strength. By integrating Eq. (2) one obtains the expression

$$\overline{S_\beta} = (1 - b_a)\left[T_{1/2} \int_C^Q f(Z, Q - E)\, dE\right]^{-1} \tag{18}$$

where b_a is the total branching ratio for other decay modes (e.g., α, IT) competing with beta decay and $T_{1/2}$ is the physical halflife. The quantity b_a could also be defined to include beta branches to low-lying levels in order to correct for this (often troublesome) source of systematic errors.

The estimate Eq. (18) does not depend very sensitively upon Q, which in the majority of cases must be taken from a mass table. For beta decays of odd–odd and odd–mass nuclei, however, the transitions with $\Delta v = -2$ and $\Delta v = 0$ (see Fig. 6) to low-lying levels may affect the halflife considerably because of the strong energy dependence of the f-function. It is therefore to be expected that misleading (high) values of $\overline{S_\beta}$ will be obtained in certain cases, e.g., for 1^+ odd–odd nuclei where the proton and the neutron have the same orbital angular momentum. Most often, however, the transitions to low-lying levels are forbidden or strongly hindered, and Eq. (18) is a good estimate. Experimentally it was found for the Os–Rn region (Duk+ 70) that the average beta strength functions calculated from Eq. (18) agree well with the values found from total absorption spectrometry, and that the best results were obtained if the cutoff values were fixed at 60% of the values predicted by pairing theory. The reason for the latter finding is clear: if the full gap energies were to be used, the calculated $\overline{S_\beta}$ would systematically be larger than the true value.

Figures 19 through 21 give a general survey of average beta strength functions for neutron-deficient nuclei in the region $50 < N < 126$. (For lighter nuclei not enough halflife values are known; for heavier nuclei there is normally little or no information about the α/EC branching rates.) The following main features seem to emerge from these figures.

The average strength tends to vary smoothly with Z and N. This is in support of the assumption that beta strength at the higher energies originates in the paired system of the nucleus and it demonstrates the applicability of a statistical approach to high-energy beta decay. Toward the closed shells $N = 82$ and $N = 126$ the strength decreases strongly.

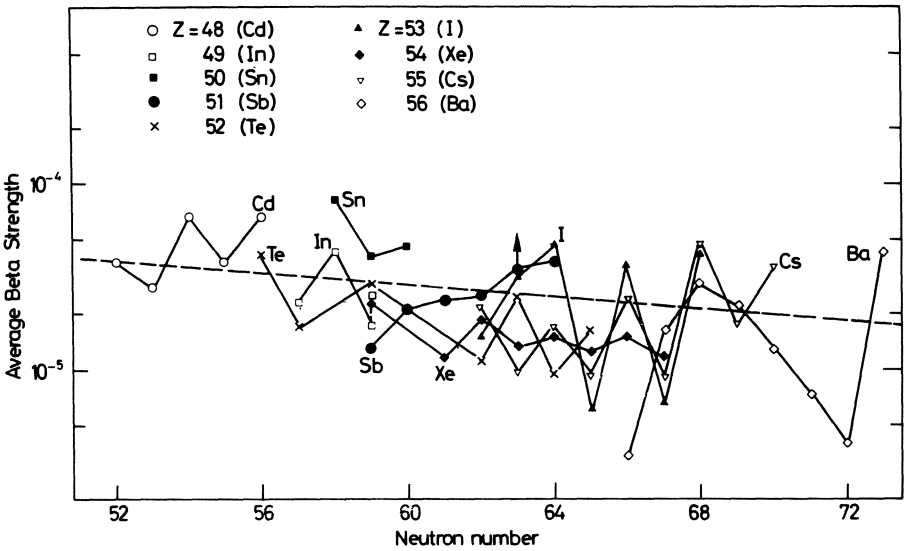

Fig. 19. Average beta strength functions for β^+, EC beta decay in the region $52 \leq N \leq 73$. The halflives have been taken from: Nuclear Data Sheets, Nuclear Data: Recent References, and, for the Xe and Cs isotopes, from (RSW 72 and Hag 72). In the cases where more than one isomer is known, only the one with the longest beta halflife has been included in the systematics. The Q-values are from (MS 65). The cutoff values C [Eq. (18)] have been taken to be 0.6 times the three- and four-quasiparticle gap energies: 24 $A^{-1/2}$ MeV (odd-mass nuclei) and 48 $A^{-1/2}$ MeV (even–even daughter nuclei). The parameter C is zero for odd–odd daughter nuclei. Cases where Q exceeds C by less than 1 MeV have been excluded from the systematics. The dashed line gives the overall A-dependence according to Takahashi and Yamada's gross theory of allowed beta decay for an assumed Q-value of 6 MeV and an excitation energy of 2 MeV. The inclusion of the theoretical Q-value dependence would lead to an improved fit (see text and also Fig. 8).

Although part of this decrease clearly must be an effect of the correlations (see Fig. 8), there is also a shell effect. The effects of the major shells are most easily understood if the spin-orbit interactions are neglected, in which case the transition strength from the Nth proton shell into the $(N+1)$st, neutron shell is first-forbidden. Once the neutron shell is full, there is (in this approximation) no strength left. The spin-orbit interaction relaxes this selection rule, but at relatively low excitation energies the effect still remains, partly because the next orbitals that can contribute are separated by the shell gap. In the lighter nuclei the strength is mainly allowed, thus for the Sn–Cs region a major contribution is the $g^p_{9/2} \rightarrow g^n_{7/2}$ together with $g^p_{7/2} \rightarrow g^n_{7/2}$ and $d^p_{5/2} \rightarrow d^n_{5/2}$ (see the discussion in Sections 3.1 and 4.4 and also Figs. 4 and 5). Other regions where strong allowed transitions appear are

discussed in the captions to Figs. 19 through 21. Note also that certain configurations give rise to strong ground-state transitions, and that the corresponding short halflives lead to an overestimate of the average beta strength. It seems clear, for example, that ^{165}Yb and ^{169}Hf must have a ground-state configuration characterized by the Nilsson quantum numbers

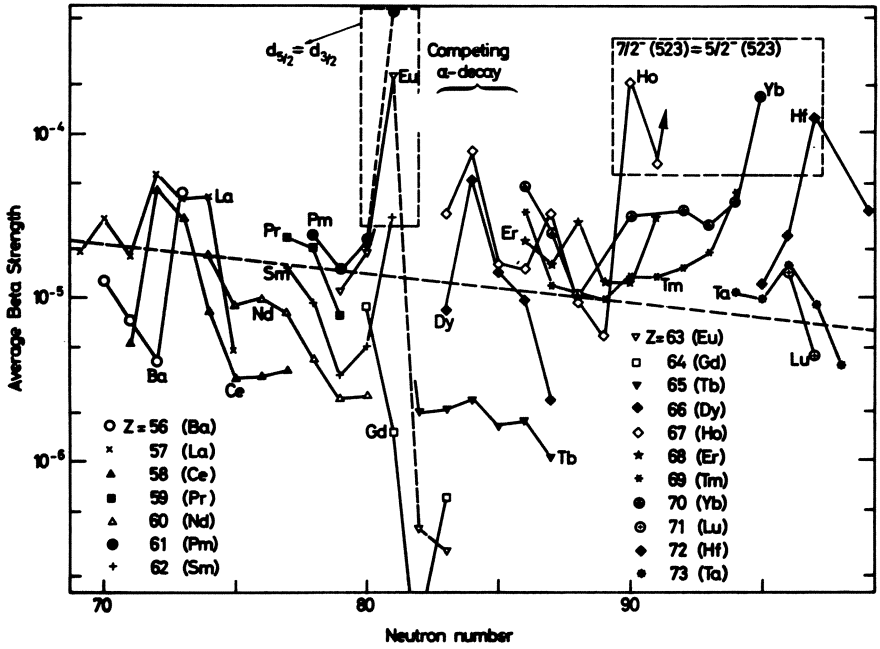

Fig. 20. Average beta strength functions in the region $69 < N \leq 99$. See caption to Fig. 19 with the following additional remarks. The points have been corrected for alpha branching according to the review by Eskola (Esk 67). The corrections applied for ^{150}Dy and ^{151}Ho (84 neutrons) correspond to 18% and 25% alpha decay, respectively. Isotopes (of Tm, Yb, Lu, Hf) for which alpha decay clearly dominates have been left out. The Eu and Gd isotopes show a strongly decreasing average strength at the magic number $N = 82$; the increase (for Pm, Eu, Sm) for $N = 80$, 81 seems to be associated with a $d^p_{5/2} \rightarrow d^n_{3/2}$ transition (see Fig. 12 and the corresponding discussion in the text). The onset of strength above $N = 82$ is presumably associated with the appearance of the $h_{9/2}$ neutron level at an excitation energy where the $h_{11/2} \rightarrow h_{9/2}$ transition begins to contribute strongly to the average strength function. This transition contributes throughout the region (to approximately $N = 110$). In the deformed region the high points (deviations from the systematics) are associated with ground-state transitions involving the "allowed-unhindered" transition $[523]_p\ 7/2^- \rightarrow [523]_n\ 5/2^-$ (see MN 59). (See caption to Fig. 3). Evidently the [523] $7/2^-$ proton becomes the ground state for the Ho isotopes for $N \geq 90$ (the onset of deformation), while for ^{165}Yb and ^{169}Hf, the [523] $5/2^-$ neutron is the ground state. This extends the systematics for Nilsson orbitals given by Bunker and Reich (BR 71).

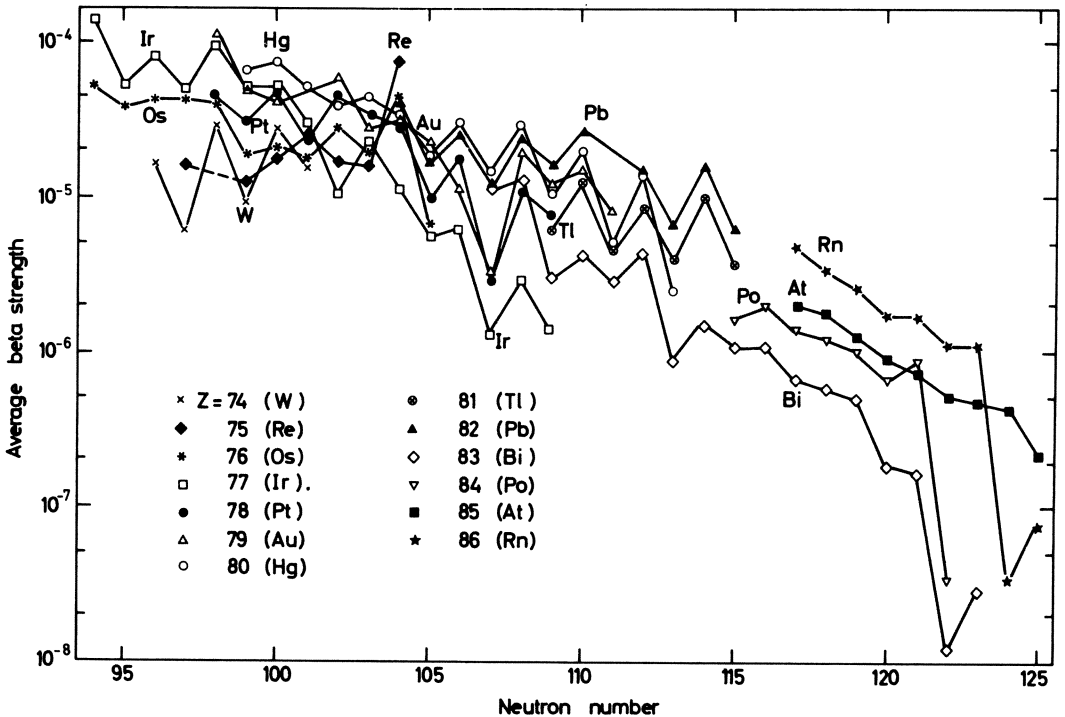

Fig. 21. Average beta strength functions in the regions $94 \leq N \leq 125$. See caption to Fig. 19 with the following additional remarks. Many of the points emerge from alpha measurements (Esk 67, Han+ 70, Han+ 71, Hor+ 71b, BH 71, Tot+ 72) and have been corrected for α competition. Note the overall decrease in beta strength as the magic number $N = 126$ is approached; this, presumably, is associated with the filling up of the $p_{1/2}$, $p_{3/2}$, $i_{13/2}$, $f_{5/2}$ final levels which give rise to the (forbidden) beta strength; note also that above $Z = 82$ (Bi, Po, At, Rn) strength comes back in again, presumably because of the $h^p_{9/2} \rightarrow g^n_{9/2}$ transition. A previous version of this figure (Duk+ 70) was based upon the Zeldes mass formula (ZGS 67). A comparison will show that the main features of the systematics of $\bar{S}_\beta$ are not influenced by the choice of mass formula. The evidence for a submagic number $N = 108$, however, is less pronounced, *cf.* (Nil+ 69) and the discussion by Jasztrebski (Jas 72) and also the irregularities in two-neutron separation energies and pairing energies observed by Duckworth *et al.* (Duc+ 69).

$[523]\frac{5}{2}^-$ in extension of (and in agreement with) the systematics presented by Bunker and Reich (BR 71).

The overall behavior of $\overline{S_\beta}$ as a function of the neutron number is well described by the gross theory of beta decay (dashed line in Figs. 19 and 20). The agreement would be even better if the Q-value-dependent correlations were also taken into account (see Fig. 8 and Section 3.2): the average beta strength as defined here is not only structure-dependent but also Q-value-dependent.

It is now clear that the β^- strength function depends more strongly on energy than the β^+, EC strength function (see Sections 4.2 and 4.4). For this reason Eq. (18) is not a very useful definition of an average value of the β^- strength, and the systematics given by Damkjaer *et al.* (Dam+ 70) should be viewed with some suspicion. It appears, though, that the β^- strength increases strongly for neutron numbers just above $N = 50$ and 82. This was interpreted (Dam+ 70) as being due to the onset of contributions from the beta transitions $g^n_{7/2} \rightarrow g^p_{9/2}$ and $h^n_{9/2} \rightarrow h^p_{11/2}$, respectively.

The concept of an average beta strength function serves to provide a preview of the systematics before more complete data become available. Further precision could perhaps be gained by a redefinition along the lines of the gross theory of Takahashi and Yamada in order to take the correlations into account. For isotopes decaying by EC, β^+ emission it is possible to improve the estimate of $\overline{S_\beta}$ by determining experimentally the partial electron-capture halflife. Preliminary results of such measurements were reported by Damkjaer *et al.* (Dam+ 70, Dam 71), but there is not yet enough information available to allow any significant corrections to Figs. 19-21. It would probably also be possible in relatively simple experiments to correct the branching ratios for dominant transitions to low-lying levels.

The regular behavior of the halflife systematics given in Figs. 19-21 has several practical implications. By extrapolating the data for each element one may, with rather good precision, predict the halflives of unobserved beta-emitters. (The extrapolation of $\overline{S_\beta}$ rather than of $T_{1/2,\beta}$ eliminates a large part of the Q-value dependence, and allows even–even, odd–odd, and odd-mass nuclei to be incorporated in the same systematics.) This technique has been used for estimating the α branching ratio of alpha-radioactive isotopes (Han+ 71, Hor+ 71b). A further practical consequence is that isomer pairs far from stability will have nearly the same beta halflives, and that for this reason many such pairs are likely to have remained unobserved. (The argument relates to cases where the "core-type" beta decay dominates.)

Particular interest attaches to the prediction of the β^- halflives of extremely neutron-rich nuclei, because of applications to r-process calculations. In this process (Bur 57), rapid neutron captures lead to extremely neutron-rich nuclei under conditions where (n, γ) and (γ, n) processes reach a steady state. The waiting times in the "reservoirs" are therefore determined by the beta halflives, which affect the predicted abundances in a very direct way. The assumptions made by Seeger *et al.* (SFC 65) correspond to assuming that the β^- strength function is independent of energy and of Z and N. The review by Cameron *et al.* (CDT 70) points to the need for an improved treatment of the beta halflives relevant to the r-process. A step in this direction has been taken by Boleu *et al.* (Bol+ 72) who incorporated beta halflives from the Yamada–Takahashi gross theory (Section 3.2) in their calculation of the possible r-process synthesis of superheavy elements.

4.4. Beta-Delayed Particle Emission

As yet there is no direct method for measuring the beta strength function with good energy resolution, but related information may be obtained by measuring the energy spectra of particles (p, n, and α) emitted from resonances populated in high-energy beta decay. Formally this method is analogous to the photoneutron method, in which one uses a gamma-ray continuum to excite resonance levels above the neutron threshold (BST 63, see also references given in two recent papers JS 72 and BBB 72), so that the energies can be measured from the time-of-flight spectrum of the outgoing neutrons.

The emission of particles from excited nuclear levels populated in beta decay was first observed in the form of "long-range α-particles" (RCE 30) from ^{212,214}Bi. Following the discovery of nuclear fission, a large number of delayed-neutron emitters were found [see, e.g., reviews by Amiel (Ami 69) and by Tomlinson (Tom 72)], and the corresponding process of beta-delayed proton emission has now been known for about 10 years (KTS 62, Bar+ 63). There is evidence for the existence of beta-delayed fission (KSF 66). Hardy (Har 72a) has given a comprehensive review of delayed-particle emission and a summary (Har 72b) of all decays leading to proton and alpha emission. This paper is referred to for all general features; here we shall concentrate on the information related to the beta strength function.

Light nuclei play a special role, because it appears that it is only for nuclei with $Z > N$ that the collective modes in beta decay (see Section 2.2) can be excited. The heaviest proton-rich nucleus observed until now is

^{53}Co (Jac+ 70) with isospin projection $T_z = -\frac{1}{2}$. The isotopes with $T_z = -\frac{3}{2}$, which have been observed from ^{9}C to ^{49}Fe, are all beta-delayed proton emitters in which one observes the collective beta transition to the isobaric analog state, typically together with other strong transitions believed to represent the (fractionated) Gamow–Teller strength. An analysis of the beta strength functions in the decay of ^{17}N and ^{33}Ar (Har+ 71) has been given by Hardy (Har 71), who points out (see Fig. 22) that the ~1-MeV wide composite peak above the isobaric analog state of ^{33}Ar presumably represents Fujita's *GT* resonance (Section 2.2). One notes that this peak contains about $\frac{2}{3}$ of the strength in the Fermi peak, and that the transitions to levels below 1 MeV, which in all likelihood also are of *GT* type, represent $\frac{1}{6}$ of the strength in the *GT* resonance.

It is only in special cases that one has knowledge of the multipolarity (or multipolarities) for a given beta transition. A new technique developed by Macfarlane *et al.* (MON 71) permits the determination of *F*/*GT* ratios from an analysis of line-shapes in delayed-particle emission. These line-shapes are determined by the recoil spectrum, and thus indirectly reflect

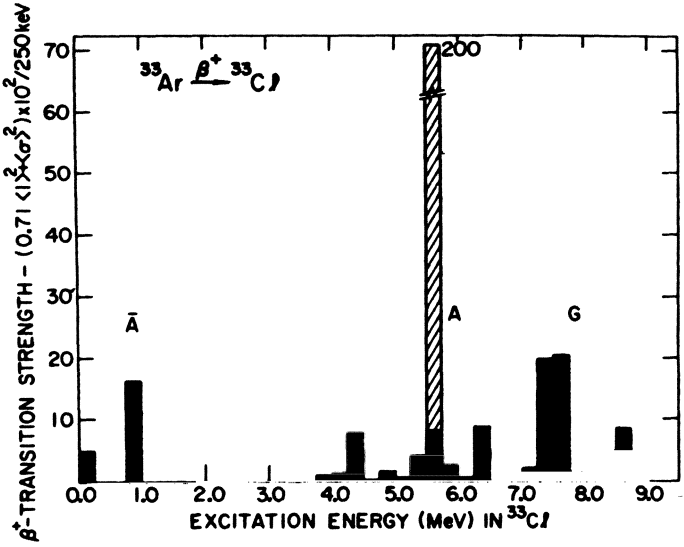

Fig. 22. Distribution of the beta-transition strength (in units of $4.10 \times 10^5/ft$ summed over 250-keV intervals) for the β^+ decay of ^{33}Ar according to Hardy (Har 71, Har 72a). The Fermi decay to the analog state is labeled *A*; the Gamow–Teller decay presumably proceeds to low-lying configurations (here labeled $\bar{A}$ for "antianalog") and to a 1-MeV broad cluster of levels near 8 MeV which presumably represents the Gamow–Teller resonance (G).

the β–ν angular correlation. In the first application (Fig. 23) it was found that the alpha lines in ^{20}Na were much broader than the experimental energy resolution because of recoil effects, and that the shape could be used for deducing the ratio of multipolarity 1 to multipolarity 0. It seems conceivable (MON 71) that the method could be applied also to the weaker delayed-alpha branches in ^{20}Na so that the spreading of the isobaric analog state (associated with multipolarity 0) could be directly measured.

The remainder of this section considers delayed-neutron and delayed-proton emission in the heavier nuclei ($A > 50$) where the collective beta-decay modes are not directly observable.

Although many delayed-neutron emitters have been identified and characterized by their (beta) halflife and neutron branching ratio P_n (Ami 69), it is only recently that the first measurements of spectral shapes for

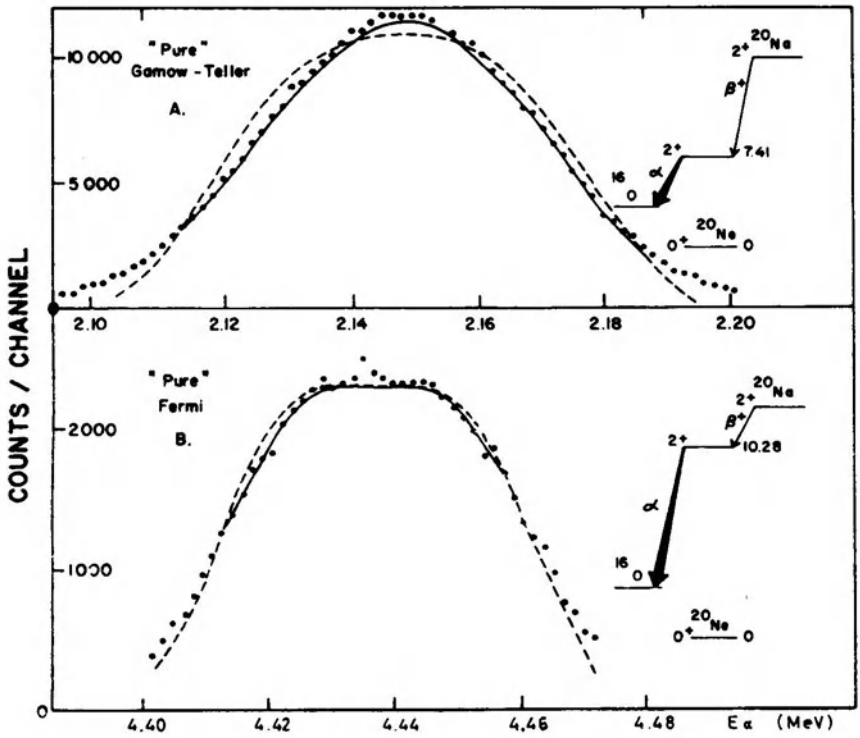

Fig. 23. Line shapes (MON 71) for the alpha decay of resonances in ^{20}Ne following the β^+ decay of ^{20}Na. The $\beta^+\nu$ correlation determines the recoil spectrum and hence the energy spectrum of the alpha particle. According to the analysis by Macfarlane *et al.* (MON 71) the 4.44-MeV line is 84 ± 7% Fermi while the 2.15-MeV line is 2 ± 2% Fermi.

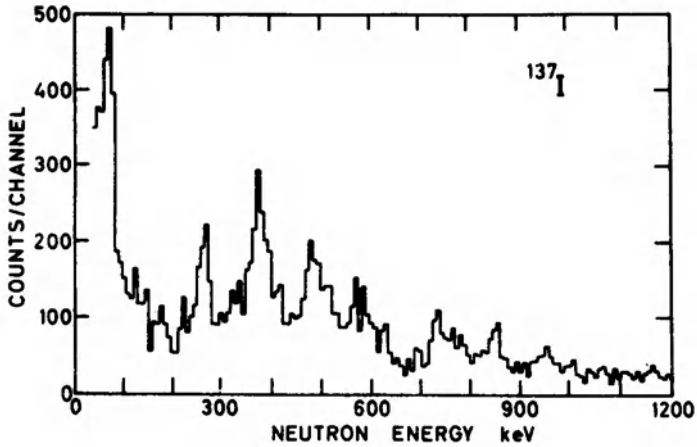

Fig. 24. The delayed neutron spectrum of ^{137}I measured with a high-pressure ^{3}He ion chamber on mass-separated samples (SR 72). The figure is from (SR 71). The fine-structure presumably reflects fluctuations, cf. Section 3.3 and the comment in (SR 72).

beta-delayed neutrons have become available (Fra+ 72, SR 72). An example taken from the work of Shalev and Rudstam (SR 71, SR 72) is shown in Fig. 24.

All delayed-proton emitters found in nuclei with $A > 50$ are listed in Table II from which it will be seen that very detailed information on branching and coincidence relationships are available for several delayed-proton emitters. Examples of the spectral shapes are given in Figs. 25 through 28 from which the immediate conclusion is that the beta strength in heavier nuclei is distributed over a wide energy range. We shall now outline how one can understand these spectra in terms of a compound nucleus theory.

The levels that give rise to delayed-particle emission from the heavier nuclei are, in general, at so high an energy that one expects the compound-nucleus structure to prevail. The only relevant quantum numbers are then E, I^{π} and a statistical calculation should be a good first approximation, although one certainly also expects nonstatistical phenomena to play a role.

All calculations of delayed-particle spectra contain roughly the following ingredients (see Hor+ 72d). Consider a beta decay with the total energy Q. If the beta strength function is assumed to be $S_\beta(E)$, one may calculate the total beta intensity per MeV of final levels at the energy E:

$$b(E) = \frac{S_\beta(E) f(Z, Q - E)}{\int_0^Q S_\beta(E) F(Z, Q - E)\, dE} \tag{19}$$

TABLE II

Delayed-Proton Emitters in Nuclei with $A > 50$

Isotope	$T_{1/2}$ (sec)	Final levels[a] MeV (%)	Experimental proton intensity p/β decay	Calculated proton intensity[b] P_p	References
^{73}Kr	34 ± 4	0.0 (65%) 0.862 (35%)	$(6.8 \pm 1.2) \times 10^{-3}$	5×10^{-3}	(Hor+ 72b)
	25.9 ± 0.6				(DG 73)
^{109}Te	$\left.\begin{matrix}4.2\\5.4\end{matrix}\right\} \pm 0.2$	[c]	[c]	3.4×10^{-2}	(BKP 72) (Mac 67)
^{111}Te	19.0 ± 0.7	[c]	[c]	1.2×10^{-3}	(Mac 67) (KT 67) (Bog+ 67)
^{113}Xe	2.8 ± 0.2	[c]	[c]	4.2×10^{-2}	(Hor+ 71c) (Hag+ 72)
^{115}Xe	19 ± 5	0.0 (42%) 0.709 (58%) 1.484 (<2%)	$(3.4 \pm 0.6) \times 10^{-3}$	2.3×10^{-3}	(Hor+ 71a, Hor+ 72c)
^{117}Xe	65 ± 6	0.0 (86%) 0.679 (14%)	$(2.9 \pm 0.6) \times 10^{-5}$	2.0×10^{-5}	

^{116}Cs	3.5	[c]	[d]	1.9×10^{-2}	(RSW 72) (Hag 73)
^{118}Cs	16 ± 1	γ 0.115 (14%) γ 0.160 (8%) γ 0.220 (13%) γ 0.305 (3%)	$(4.2 \pm 0.6) \times 10^{-4}$	1.3×10^{-3}	(RSW 72, Hor+ 72e)
^{120}Cs	61.3 ± 1.4	[c]	$d, \leq 5 \times 10^{-8}$	6×10^{-6}	(RSW 72, Cha+ 69)
^{119}Ba	~5	[c]	[c]	—	[e]
^{179}Hg	1.09 ± 0.04	[c]	$\sim 2.8 \times 10^{-3}$	6.1×10^{-3}	(Hor+ 71a, Hor+ 72c)
^{181}Hg	3.6 ± 0.3	0.0 (50%) 0.158 (50%)	$(1.8 \pm 0.5) \times 10^{-4}$	5.5×10^{-4}	
^{183}Hg	8.8 ± 0.5	[c]	$(3.1 \pm 0.7) \times 10^{-6}$	9.5×10^{-6}	

[a] From proton–gamma coincidence experiments (Hor+72b, Hor+72c, Hor+72e).
[b] From (Hor+72d) and private communication. Masses from (MS 65).
[c] Not measured.
[d] Assignment tentative.
[e] V. A. Karnaukhov, quoted in (Har 72b).

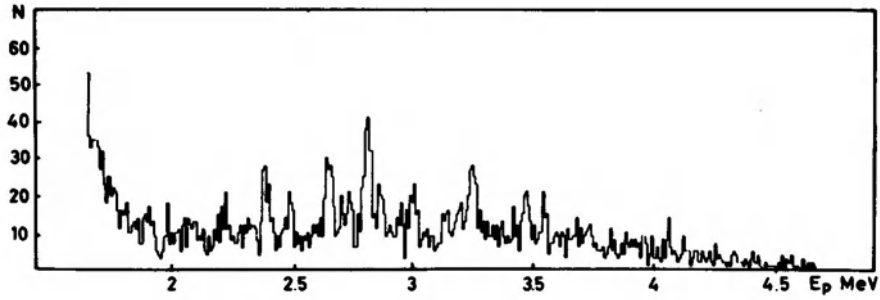

Fig. 25. Delayed-proton spectrum of ^{111}Te measured by Bogdanov *et al.* (Bog+ 67, KT 67) The fine structure may be viewed as fluctuations (Kar 69) (see also Section 3.3).

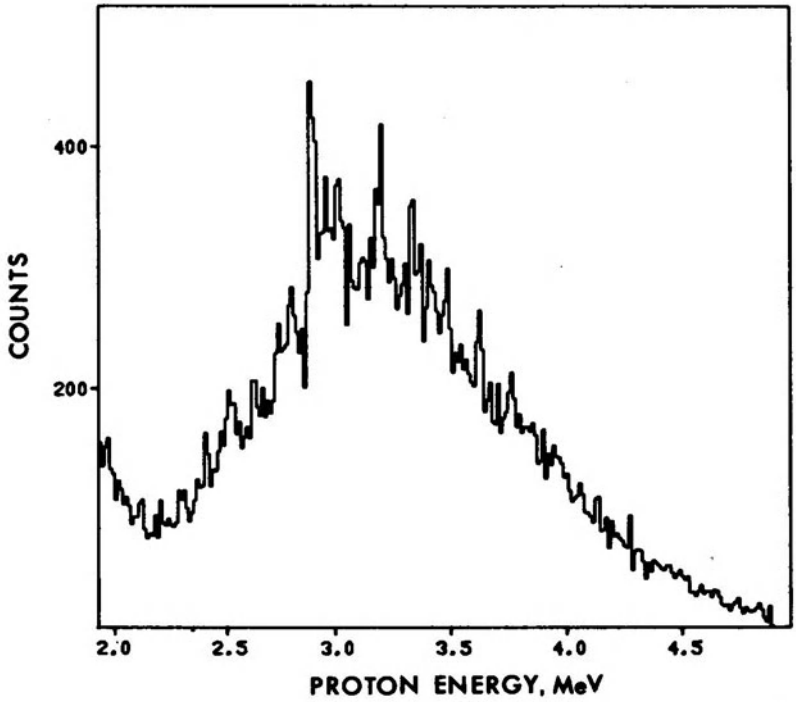

Fig. 26. Delayed-proton spectrum of ^{115}Xe measured (Hor+ 72c) with a single counter with 15-keV energy resolution. The tail at low energies is due to positrons; it disappears when the protons are counted with a counter telescope, as may be seen from Fig. 28. The fine structure may be viewed as fluctuations (see Section 3.3) and the text.

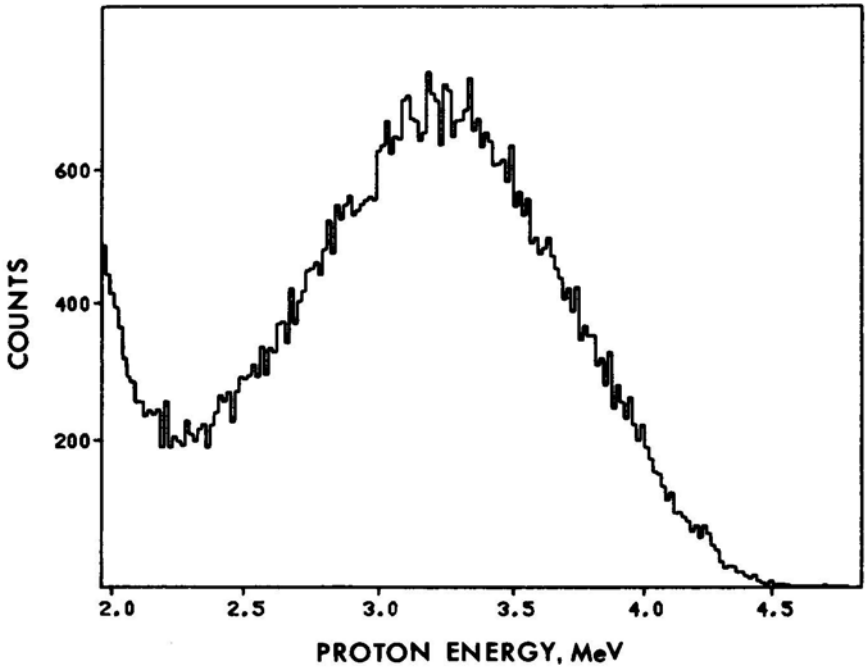

Fig. 27. Delayed-proton spectrum of ^{118}Cs measured (Hor + 72e) with a single Si counter with 15-keV energy resolution. The tail at low energies is due to positrons. The fluctuations are very weak but still real.

The initial nucleus with spin and parity I^{π} will at the excitation energy E populate levels $I_i^{\pi_i}$ in a fraction* $\omega(I, I_i)$. The intensity of the particle emission to final levels f is then given by the usual compound nucleus expression

$$I_p^{if}(E_p) = \frac{\omega(I, I_i)b(E)\Gamma_p^{if}(E_p)}{\Gamma^i} \tag{20}$$

where it has been assumed for simplicity that only one kind of particle (labeled p) is emitted, and the total width is the sum of the total gamma

* The distribution with respect to spin and parity of beta strength at high energies is experimentally an almost completely open question. The approximation used in the calculation outlined here is $\omega(I, I_i) = (2I_i + 1)/3(2I + 1)$ corresponding to the statistical weight for excitations of the paired system. The calculation (Hor 72d) assumed first-forbidden strength for the Hg region and allowed strength for the Xe region. The results are not very sensitive to the parity.

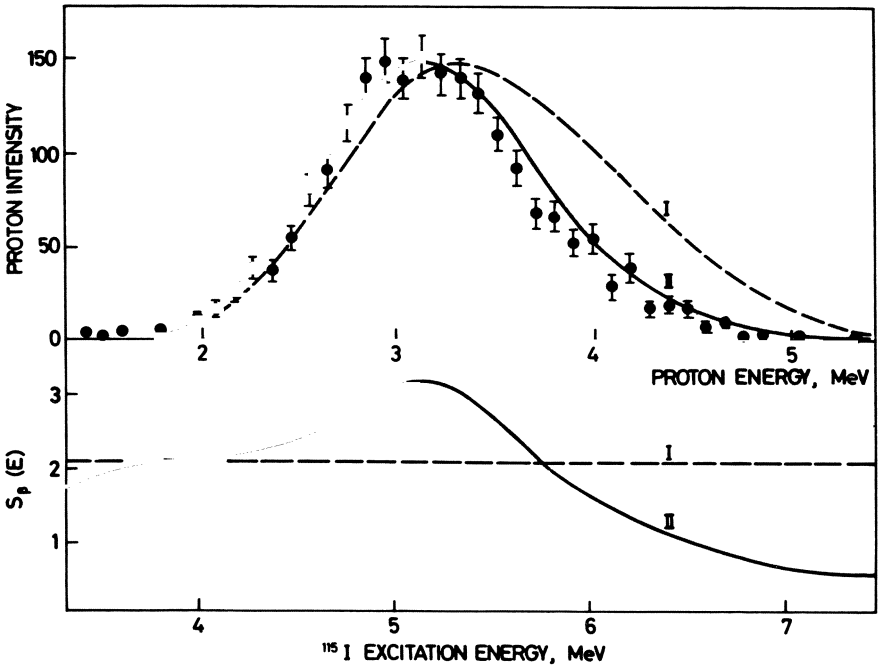

Fig. 28. The delayed-proton spectrum (upper graph) of ^{115}Xe measured with a counter telescope (Hor+ 71a). (Compare with Fig. 26.) Two theoretical calculations (Hor+ 72d) are shown; they differ in the assumed shape of the beta strength functions (lower graph). The greatly improved fit for the strength function labeled "II" is strong evidence for a "pygmy" resonance at about 5 MeV, corresponding mainly to the $(g^p_{9/2})^{-1}\, g^n_{7/2}$ excitation (see the discussion, Section 3.1). Note that as pointed out by Jonson (Jon 72), the proton width dominates above 3 MeV, for which reason the calculation is not very sensitive to the assumed values for transmission coefficients, level densities, and gamma widths. This has permitted the calculation of absolute values of the ^{115}Xe beta strength (Fig. 17). The intensities calculated in the two cases shown here (for $I^\pi = 5/2^+$) are 2.3×10^{-3} (S_β = constant) and 4.3×10^{-3} (varying S_β). The experimental value is $(3.4 \pm 0.6) \times 10^{-3}$ (see Table II). Curve II corresponds to the diagram Fig. 5 (filled lines) folded with a 1-MeV-wide Gaussian. The main peak has been shifted down to 5.2 MeV.

width and the partial widths of all open particle channels:

$$\Gamma^i = \Gamma_\gamma^{\,i} + \sum_{f'} \Gamma_p^{if'}(E_p') \tag{21}$$

The total intensity of particles with energy E_p is

$$I_p(E_p) = \sum_f \sum_i I_p^{if}(E_p) \tag{22}$$

and the number of particles per beta decay is

$$P_p = \int_0^{E_{p,\max}} I_p(E_p)\, dE_p \tag{23}$$

The partial particle width $\Gamma_p^{if}(E_p)$ may be calculated from transmission coefficients T_{lj} obtained in an optical-model calculation

$$\Gamma_p^{if}(E_p) = \frac{\sum_{j\pi_i\pi_f} T_{lj}(E_p)}{2\pi\varrho_i(E)} \tag{24}$$

where $\varrho_i(E)$ is the density of final levels with spin-parity $I_i\pi_i$.

The most complete set of experimental data for comparison with theoretical calculations is available for the delayed-proton emitters: spectral shapes, proton–gamma coincidences identifying the final levels, and measured absolute intensities. Furthermore, the experimental data for beta strength functions of neutron-deficient nuclei provide (Section 4.2) a model strength function to substitute for $S_\beta(E)$ in Eq. (19). The results of a calculation (Hor+ 72d) which incorporates an optical-model calculation of the proton widths is given in Column 5 of Table II. It will be seen that the agreement between theoretical and experimental values of P_p is very satisfactory. It is further found (Hor+ 72d) that if reasonable spin values are assumed, the calculations reproduce the measured proton branching ratios (Hor 72c) to the final levels well.* The assumption of constant beta strength also reproduces the gross spectral shape, as had been noted already by Bogdanov *et al.* (Bog+ 67). However, for a more detailed fit it is necessary to consider the energy dependence of the beta strength function: the analysis by (Hor 72d) shows that the ^{115}Xe proton spectrum reflects a $(g_{9/2}^p)^{-1}g_{7/2}^n$ "pygmy" resonance in the beta strength function (Figs. 17 and 28). Such a structure also seems to manifest itself in the proton decay of ^{109}Te (BKP 72), and it is expected from the shell-model calculation (see Fig. 5).

The calculation of delayed-neutron spectra is an older problem, and, as it seems, also a more difficult one. Two recent papers, by Pappas and Sverdrup (PSP 72) and by Takahashi (TAK 72), now find that the solution lies in the strong energy dependence of the β^- strength function. Earlier papers (cited in PS 72, Tak 72a) normally assumed a "constant beta matrix element" corresponding to a beta strength function varying proportionally

* Measurements of proton branching ratios provide one possibility for learning about the spin weight factor $\omega(I, I_i)$ for the compound levels.

TABLE III

Beta-Delayed Neutron Emitters. Comparison of Experimental and Calculated Neutron Fractions P_n

Isotope	P_n in %				
	Experiment[a]	$S_\beta \sim \varrho$[b]	$S_\beta = \text{const}$[c]	Gross theory[d]	Exp. $S_\beta(E)$[e]
^{85}As	18 ± 4	63	2	24	
^{87}Br	2.4 ± 0.3	2	0.01	6.9	2–8
^{89}Br	8.9 ± 0.9	33	0.5	9.8	
^{93}Rb	1.63 ± 0.23	6	0.04	0.17	
^{95}Rb	7.1 ± 0.9	42	0.8	0.42	
^{135}Sb	8 ± 2	78	3	12	
^{137}I	5.5 ± 1.3	12	0.09	5.6	0.8–3
^{139}I	14 ± 5	55	1.1	3.2	

[a] (Tom 72).
[b] (PS 72), Zeldes mass formula (ZGS 67), "constant beta-matrix element."
[c] (PS 72), Zeldes mass formula, "constant beta strength."
[d] (Tak 72a), Myers–Swiatecki mass formula (MS 65), "gross theory of beta decay."
[e] (JBR 72), experimental $S_\beta(E)$ (see Fig. 18). Myers–Swiatecki mass formula. The range given corresponds to estimated error limits incorporating among other effects the uncertainty in Q and B_n.

to the level density. By comparing this model with one with constant strength it is found (PS 72) that the experimental data tend to lie between the two assumptions although closest to the level-density expression. A cutoff does not seem applicable. The gross theory of beta decay (which for β^--decay gives an increasing beta strength function), yields the best results to date for the neutron intensities (Tak 72). In Table III selected results from the two calculations are given and compared (for the cases ^{87}Br and ^{137}I) with the estimates based on the measured β^- strength function.

The delayed-particle spectra offer a possibility of studying the statistical properties of the beta strength function. This problem was first considered by Karnaukhov (Kar 69), who attributed the structure in the ^{111}Te proton spectrum to fluctuations in the level density, and who on this basis gave an estimate of the number of contributing transitions. Although an accurate analysis of the fluctuation phenomena will have to include also the density fluctuations (especially at low level densities), it now seems clear (Section 3.3) that the fluctuations originate predominantly in the partial widths,

which are distributed according to the Porter–Thomas law [Eq. (11)]. Any attempt to account for the experimental spectra must therefore take into account the preponderance of very small reduced widths implied by this relationship (see the inset Fig. 9), a problem which, of course, is analogous to the problem of correcting for unobserved weak resonances in neutron resonance spectroscopy. In the experimental situation where the product law* [Eq. (14)] applies, the distribution becomes even wider than a Porter–Thomas distribution.

The delayed-particle spectra chosen as illustrations to this section all show evidence of fluctuations (Figs. 24-27) although the amplitudes differ widely. For the cases ^{111}Te and ^{115}Xe a preliminary analysis of the fluctuation amplitudes has been carried out by Hornshøj *et al.* (HHJ 72), who conclude that with the Newton level-density law (New 56) with Cameron's parameters (Cam 56) one obtains good agreement for the case of ^{111}Te, whereas a fit to the ^{115}Xe fluctuation amplitudes requires an increase in level density of about a factor of 4. A similar analysis has recently been performed by Karnaukhov (Kar 73). Much work remains to be done on fluctuation phenomena; it would be especially valuable if the analysis was supported by cases where the individual resonances had been resolved so that the distribution laws could be tested directly.

4.5. Muon-Capture and Electromagnetic Transitions

The capture of a negative muon from an atomic orbit is completely analogous to electron-capture beta decay, and it is governed by essentially the same interaction (Kon 66, Sch 66, WM 66). It therefore seems natural to summarize briefly what is known at present about the muon-capture strength function.

The capture process

$$^{A}Z + \mu^{-} \rightarrow {}^{A}(Z-1)^{*} + \nu_{\mu} \tag{25}$$

occurs in competition with the beta decay of the muon, over which process it dominates for all nuclei with $Z > 12$. The large rest mass of the muon makes the process (25) very different from the capture of electrons. First of all, a wider spectrum of excited levels are populated in the daughter nucleus,

* The product law assumes that there are no correlations between the beta and particle channels. It is easy to imagine a situation where this does not hold true so that one observes a "doorway" for delayed particle emission.

and most of these will be particle-unbound, so that muon capture is normally followed by particle emission as well as by gamma-ray emission. Secondly, the large momentum transfer in muon capture implies that the series expansion which in nuclear beta decay leads to allowed transitions, first-forbidden transitions, etc., in the case of muons converges much more slowly, so that the "forbidden" terms are relatively of much greater importance. Consider, as an example, the level schemes in Fig. 4 which, if taken to represent muon capture, show less blocking due to the Pauli principle than for the case of electron capture. For the same reasons one would expect direct muon capture (i.e., capture to the ground state of the daughter) to be quite unimportant for the heavier nuclei. In the following we discuss some aspects of muon capture: (1) the energy spectrum of the final states; (2) the reaction mechanism for the emission of neutrons; and (3) the absolute capture rates.

If a muon is captured by a free proton, the recoil energy imparted to the outgoing neutron is about 5 MeV. For a proton inside a nucleus the average excitation energy following muon capture is greater, partly because of the Fermi motion of the nucleons and partly because of collective effects. The Fermi motion was taken into account in the calculation by Singer (Sin 62), who used Brueckner theory to obtain the spectrum of excited states. He found a rather broad distribution extending from 0 to 30 MeV; it seems clear from a comparison with the experimental data (see below) that this theory greatly overestimates the population of the lowest part of the spectrum. This is to a certain extent due to the cutoff effect (known from the beta strength function, see Section 3.1) arising because the major part of the transforming protons will initially be in paired states, but much more important are the collective effects. It was pointed out by Foldy and Walecka (FW 64) that as the allowed muon capture is strongly suppressed by the Pauli principle (see, e.g., Fig. 4), the dominant process would involve first-forbidden capture leading to members of the Wigner supermultiplet built on the electric dipole state [see also (Ube 66)]. The role of this type of excitation seems to be less in nuclei with a large neutron excess (BM 71), and other types of collective excitations presumably take over (BM 69b). Takahashi has recently attempted to extend the gross theory of beta decay to muon capture (Tak 72b). Shell-model calculations of muon capture rates have been carried out by Bunatyan (Bun 65), who found that for heavy nuclei such as ^{208}Pb the dominating contribution to the capture rate comes from the multipole order $L = 2$ (50%) with smaller contributions from the L-values 0, 1, and 3. Similar results have been obtained by Joseph *et al.* (JLG 72). For ^{208}Pb Bunatyan's calculation overestimates the capture

rate by a factor of 3.5, while the agreement is somewhat better for ^{16}O and ^{40}Ca.

There are no direct techniques available for measuring the energy distribution of the final states in muon capture, so most of our knowledge comes from the study of particle multiplicities, i.e., the relative probabilities of processes where 0, 1, 2, etc., neutrons are emitted and also where, more rarely, protons are emitted. In the lighter nuclei the zero-neutron process has appreciable probability as may be seen from the radioactivation experiments of Bunatyan *et al.* (Bun+ 69, Bun+ 70), who found 28 $\pm$ 4% for ^{28}Si and 16.0 $\pm$ 2.5% for ^{56}Fe leading to ^{28}Al and ^{56}Mn via the (μ^-, ν) process. For ^{28}Si, proton emission amounts to 15 $\pm$ 2% with a proton spectrum that peaks at 2.5 MeV and has a long tail toward higher energies (SW 68). A more general survey of neutron multiplicities has been carried out by Macdonald *et al.* (Mac+ 65), who used a large liquid-scintillation counter for determining the number of neutrons emitted per muon stopped in the target. The data given in this paper are *experimental* multiplicities referred to the experimental arrangement used by the authors, *cf.* the comment (Kap 70). It may be deduced that their data correspond to 36 $\pm$ 6% for the no-neutron probability in ^{28}Si; this presumably should be compared with roughly the sum 43% of the (μ^-, ν) and $(\mu^-, \nu p)$ probabilities mentioned above. The experiment yields smaller no-neutron probabilities for heavier elements: I (4$\pm$3)%, Au (11$\pm$2)%, and Pb (0$\pm$3)% (Kap 70). This finding is qualitatively confirmed (Bac+ 71, Pet+ 71) in measurements of nuclear gamma rays following muon capture. In this method one takes advantage of the de-excitation mechanism following particle emission: the probability of direct gamma-ray emission from an excited level to the nuclear ground state is expected to be small, and the normal path will be via an evaporation cascade of gamma rays of 1–3 MeV. This cascade will eventually excite known levels near the nuclear ground state, and the resulting transitions will unambiguously identify the end-product. The sum of the identified ground-state intensities directly gives the yield, which may be put to an absolute scale from the measured intensities of muonic X-rays (Bac+ 71) or from the number of muon stops (Pet+ 71). An example is given in Fig. 29. Typically 70–80% of the total capture rate is detected in these experiments, presumably because of weak transitions missed in the gamma spectra. [It is tempting to speculate that a correction to the estimates could be obtained by comparison with the much more detailed spectra from (n, γ) reactions.] The main conclusion from measurements of particle multiplicities is, however, clear: the average excitation energy following muon capture is of the order of 15 MeV (Mac+ 65)

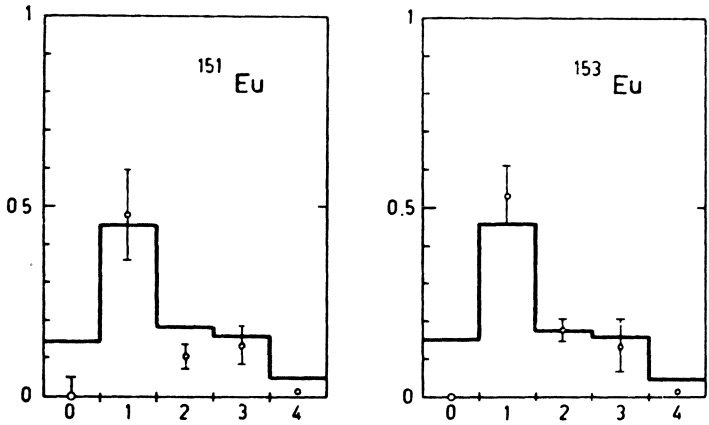

Fig. 29. Experimental neutron multiplicities following muon capture calculated from the yields of gamma rays (Pet+ 71). The total observed transition intensity is 75% for ^{151}Eu and 87.5% for ^{153}Eu. The lines represent the theoretical expectations according to the model of Singer (Sin 62), who did not incorporate collective effects.

and varies only slowly with Z. Up to about 8 MeV the strength is small (Bac+ 71, Pet+ 71), which is in support of the giant-resonance picture of the muon-capture process.

The emission of neutrons following muon capture is formally completely analogous to the process of delayed-particle emission following beta decay, which was discussed in Section 4.4. While the latter process can be calculated rather well in a compound-nucleus theory, it seems clear that other reaction mechanisms contribute in the (μ, xn) reaction. The newest results come from the time-of-flight measurements by Schröder *et al.* (Sch 71, Jah+ 72, Sch+ 72), which indicate that in addition to the (dominant) evaporation spectrum of neutrons there is a high-energy tail, which for the heavier elements accounts for about 10% of the neutrons. This is taken to be evidence for a direct-emission mechanism. The low-energy part of the spectrum shows fine-structure, which is especially pronounced for calcium (Jah+ 72).

The measurement of the lifetime of a captured muon directly gives the disappearance rate, which is the sum of the capture rate and the rate of the muon decay. The lifetimes are in a range conveniently accessible by delayed-coincidence techniques, but as rather large samples are needed for these measurements little is known about the behavior of the individual isotopes of even-Z elements. The systematics of muon capture rates have normally been discussed in terms of the Primakoff formula (Pri 59) accord-

ing to which the capture rate for the isotope Z, A is

$$\lambda_c(Z, A) = Z_{\text{eff}}^4 \gamma \lambda_c(1, 1)\left[1 - \delta \frac{(A - Z)}{2A}\right] \tag{26}$$

where γ measures the phase space available to the neutrino, Z_{eff} measures the overlap of the muon wavefunction with the nucleus, and the last term corrects for the effect of the Pauli principle, which forbids the transforming proton from final states that are already occupied by neutrons. The main term is thus, in the limit of low Z, a product of the muon density at the nucleus (proportional to Z^3) times the number of decaying protons Z. A number of investigations (Sen 59, Cra+ 62, Tel 62, Bob+ 66, Pov+ 70, and Pet+ 71), have compared experimental muon-capture rates with the Primakoff expression; as an example, Fig. 30 reproduces the systematics given by Bobrov *et al.* (Bob+ 66). While the earlier investigations emphasized the essential correctness of the Primakoff expression, it is now clear that effects of nuclear structure are observable. Locally such effects

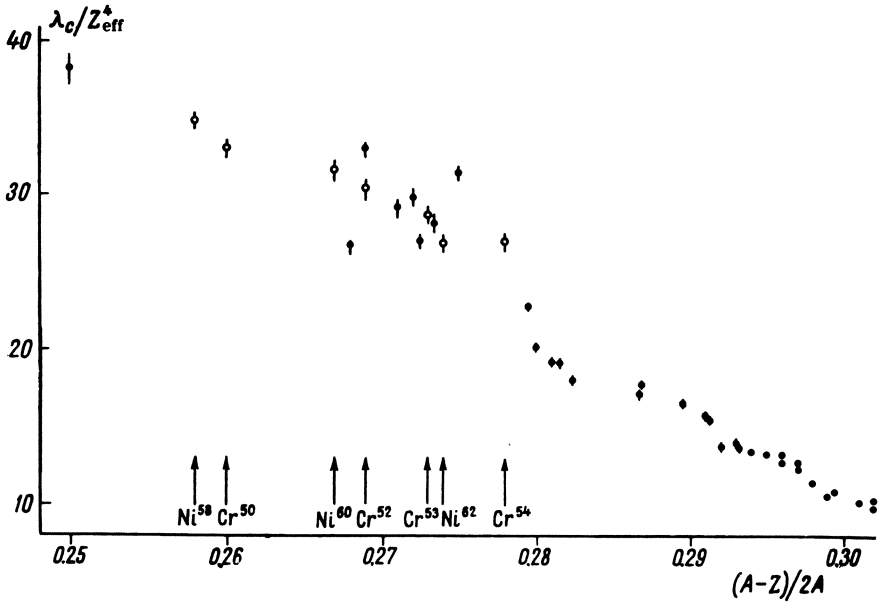

Fig. 30. The systematics of reduced muon-capture rates (Primakoff plot) showing $\lambda_c/Z_{\text{eff}}^4$ as a function of the neutron excess in units of $(A - Z)/2A$ (from Bob+ 66). A straight line is a good overall approximation to the data, but the scatter in the middle of the diagram is clearly evidence for individual structure effects. Compare with the systematics of average beta strength functions shown in Figs. 19 through 21.

have been detected in measurements of ratios of capture rates for isotopes of the same element For ^{151,153}Eu the ratio agrees (Pet+ 71) with the Primakoff formula, while for ^{79,81}Br Povel *et al.* (Pov+ 70) found that the addition of two neutrons increases the capture rate by $8 \pm 8\%$ while a decrease of 14% was expected. Such discrepancies are not surprising; already in 1964 Bell and Løvseth (BL 64) discussed the theory of muon-capture rates in heavy nuclei and concluded that "the excellence of the agreement with experiment of the present crude theory can only be accidental." The fine-structure in the systematics of muon-capture rates should be expected to convey nuclear-structure information in the same way as do the total beta-decay rates discussed in Section 4.3.

For a survey of gamma-ray strength functions the reader is referred to the paper of Bartholomew et al. (Bar+ 72), which deals especially with energies near the nucleon threshold. Here we shall only bring out two points that are of special relevance to the subject of beta strength functions.

The study of gamma-ray strength functions has, over a period of many years, provided a large body of experimental facts and theoretical ideas which together provide a firm basis for the discussion of related phenomena such as beta decay and muon capture. Suffice it here to mention the electric dipole giant resonance state (see, e.g., Fir 70), which has become the parent of a whole family of related phenomena, and to mention the statistical laws, which, elucidated in gamma-ray and neutron experiments, have taught us how to interpret a situation where nuclear structure and fluctuations are encountered together. Instructive examples may be found in the papers by Axel and by Bollinger (Axe 68, Bol 68, BT 70).

The formal analogy between beta- and gamma-transition probabilities has been referred to a number of times above. The connection is, however, especially intimate if it is possible to compare the beta decay of a certain initial state $|i\rangle$ (see Fig. 1) with analogous electromagnetic transitions originating in the isobaric analog $|a\rangle$. The $E1$ transitions from the isobaric analog state (Section 2.1) may aid in the analysis of the matrix elements of first-forbidden transitions. For allowed beta transitions one may analogously exploit the relation between the Gamow–Teller beta decay and the spin part of the corresponding magnetic dipole decay of the isobaric analog state (see, e.g., Gaa+ 70, Hir 70, SBG 70). This technique gives interesting information about $M1$ strength-function phenomena in the lighter nuclei. Gaarde *et al.* (Gaa+ 70) find that the gamma rays from the isobaric analog of the ^{51}Ti ground state show a clustering of the $M1$ strength to a $\sim$1 MeV broad group of states at about 5 MeV in ^{51}V (i.e., about 5 MeV below the analog). This structure is believed to carry a significant part of the GT strength.

5. CONCLUDING REMARKS

At this point it only remains to sum up what has been learned from the study of strength functions in nuclear beta decay and to point to some of the hopes that one may have for future research in this area. It maybe is useful to keep in mind that the field is still a young one. The experiments have until now been carried out by relatively primitive methods, and the interpretation has, so far, aimed at an overall understanding. The interaction with other areas of nuclear-structure research will probably become stronger as more sophisticated experimental and theoretical techniques are developed.

Beta decay involves the transformation of a proton into a neutron or vice versa. The transition rates, however, are not what one calculates in an individual-particle picture, but are strongly affected by interactions with other nucleons ("effective coupling constants"). This effect is a general one for two-particle or particle–hole strength functions, and it is encountered also in muon capture and in electromagnetic transitions ("effective charges"). In the allowed beta-decay process the collective states involved are, in the picture by Fujita *et al.* (see Sections 2.1 and 2.2), the components of the Wigner supermultiplet, so that the supermultiplet symmetry, although badly broken, persists and influences the transition rates strongly. These ideas have been incorporated in the semiempirical theory of beta-decay rates proposed by Yamada and Takahashi (Section 3.3). Experiments on beta strength functions provide support for this approach. Especially noteworthy is the different energy dependence found for β^- and for β^+ strength functions.

The delayed-particle experiments demonstrate that the beta strength function varies slowly with excitation energy, even at rather low energies. In fact, the observable fine-structure seems to be consistent with the fluctuations expected on the basis of a compound-nucleus picture. The gross structure has in certain cases been explained on the basis of the shell model; an example is provided by the beta strength functions in the neutron-deficient Xe isotopes, where a broad "pygmy" resonance exists at about 5-MeV excitation energy. As discussed in more detail by Bartholomew *et al.* in Chapter 4 of this volume, similar phenomena appear also in the gamma strength functions.

A novel feature brought out in work on beta strength is the existence of a low-energy cutoff corresponding to the pairing gap. The explanation for this phenomenon is that beta strength originates predominantly in the paired system of the nucleus, as may be seen also from the smooth behavior of the average beta strength as a function of Z and N. A cutoff should also

exist in the gamma-ray and muon-capture strength functions, but the effect has not been observed for obvious technical reasons. The solid state analog is well known (RT 60).

Much more experimental work is clearly needed, not the least of it being on the neutron-rich side, where still relatively little is known about the β^- strength function, which plays an important role in the astrophysical calculations of the *r*-process for the production of heavy elements by neutron addition in a rapid time scale. Improved techniques for the study of the delayed-particle emitters should also give interesting information on level densities and strength functions for nuclei very far from stability. Experiments on the fluctuation phenomena seem promising, but the intensity problem has to be solved. One may also hope to use beta decay for studying the spreading widths of the simple two-particle levels as a function of the excitation energy.

The experimental study of beta strength is technically too difficult to make it a very general tool, and does not possess the richness of the neutron and gamma-ray experiments which for such a long time have remained our most important source of information about the resonance region. The study of beta strength can, however, serve as a supplement because of special features that are best brought out by this technique. The cutoff effect due to pairing was mentioned above as an example. Another is provided by the very exclusive selection rules for allowed beta decay which allow us to look very selectively for special components of the nuclear wave function: admixtures of the isobaric analog state or the 1^+ Gamow–Teller excitation. For nuclei far from stability, beta decay becomes one of the dominant techniques for studying the structure, and it offers the advantage of bridging, in an almost continuous fashion, the gap between the low-lying levels, to which we ascribe structure quantum numbers, and the resonance levels, which we characterize only by average values and by fluctuations around the average. Studies in the intermediate region where the structure quantum numbers have begun to dissolve should be very fruitful.

ACKNOWLEDGMENTS

It is a pleasure to thank Drs. G. Backenstoss, B. Jonson, O. Kofoed-Hansen, A. C. Pappas, and K. Takahashi for discussions and helpful comments. The author is especially grateful to Dr. E. Vogt for numerous suggestions for improvements of the manuscript. The help of Mrs. R. Mohr in the preparation of the manuscript is greatly appreciated.

REFERENCES

AAA 71 M. Alpsten, Å. Appelqvist, and G. Astner, *Physica Scripta* **4**:137 (1971).

AF 61 W. P. Alford and J. B. French, *Phys. Rev. Letters* **6**:119 (1961).

AGW 59 D. E. Alburger, A. Gallmann, and D. H. Wilkinson, *Phys. Rev.* **116**:939 (1959).

Ami 69 S. Amiel, in: *Proceedings of the Second Sympsoium on the Physics and Chemistry of Fission*, Vienna, 1969, IAEA, Vienna (1969), p. 569.

Art+ 71 A. G. Artukh, V. V. Avdeichikov, G. F. Gridnev, V. L. Mikheev, V. V. Volkov, and J. Wilczynski, *Nucl. Phys.* **A176**:284 (1971).

Ast 72 G. Astner, "Nuclear Structure Studies in the Lead Region Using Mass-Separated Radioactive Sources," Dissertation, Stockholm 1972, p. 12, and references therein.

AWM 62 J. D. Anderson, C. Wong, and J. W. McClure, *Phys. Rev.* **126**:2170 (1962).

Axe 68 P. Axel, in: *Proceedings of the International Symposium on Nuclear Structure*, Dubna, July 4-11, 1968, IAEA, Vienna, 1968, p. 299.

Bac+ 71 G. Backenstoss, S. Charalambus, H. Daniel, W. D. Hamilton, U. Lynen, Ch. von der Malsburg, G. Poelz and H. P. Povel, *Nucl. Phys.* **A162**:541 (1971).

Bar+ 63 R. Barton, R. McPherson, R. E. Bell, W. R. Frisken, W. T. Link, and R. B. Moore, *Can. J. Phys.* **41**:2007 (1963).

Bar+ 72 G. A. Bartholomew, E. D. Earle, A. J. Ferguson, J. W. Knowles, and M. A. Lone, Gamma-Ray Strength Functions, in: *Advances in Nuclear Physics*, Vol. 7 (M. Baranger and E. Vogt, eds.) Plenum Press, New York (1973), p. 229.

BBB 72 B. L. Berman, C. D. Bowman, and R. J. Baglan, in: *Statistical Properties of Nuclei* (J. B. Garg, ed.), Plenum Press, New York (1972), p. 611.

BD 66 G. F. Bertsch and J. Damgaard, *Phys. Letters* **23**:342 (1966).

BH 71 J. Borggren and E. K. Hyde, *Nucl. Phys.* **A162**:407 (1971).

BKM 69 D. B. Beery, W. H. Kelly, and Wm. C. McHarris, *Phys. Rev.* **188**:1851 (1969).

BKP 72 D. D. Bogdanov, V. A. Karnaukhov, and L. A. Petrov, JINR-P7-6604 (1972).

BL 64 J. S. Bell and J. Løvseth, *Nuovo Cimento* **32**:433 (1964).

BMC 70 M. G. Braga-Marcazzan and L. M. Colli, *Progr. Nucl. Phys.* **10**:145 (1970).

BM 69a A. Bohr and B. R. Mottelson, *Nuclear Structure*, Benjamin Inc., New York (1969) Vol. I, (a) p. 302, (b) p. 345, (c) p. 395, (d) p. 53.

BM 69b A. Bohr and B. R. Mottelson, in: *Neutron Capture Gamma-Ray Spectroscopy*, IAEA, Vienna (1969), p. 3.

BM 71 T. Bressani and A. Molinari, *Phys. Letters* **36B**:297 (1971).

BMP 58 A. Bohr, B. R. Mottelson, and D. Pines, *Phys. Rev.* **110**:936 (1958).

Bob+ 66 V. Bobrov, V. Varlamov, Yu. Grashin, B. Dolgoshein, V. Kirillov-Ugryumov, Yu. Nikitin, V. Roganov, A. Samoilov, and S. Somov, *Yadernaya Fiz.* **4**:75 (1966) [English translation: *Soviet J. Nucl. Phys.* **4**:53 (1967)].

BO 65 Z. Bochnacki and S. Ogaza, *Nucl. Phys.* **69**:186 (1965).

BO 66 Z. Bochnacki and S. Ogaza, *Nucl. Phys.* **83**:619 (1966).

BO 67 Z. Bochnacki and S. Ogaza, *Nucl. Phys.* **A102**:529 (1967).

Bog 65 D. Bogdan, *Nucl. Phys.* **61**:241 (1965).

Bog+ 67 D. Bogdanov, S. Daroczy, V. A. Karnaukhov, L. A. Petrov, and G. M. Ter-Akopyan, *Yadernaya Fiz.* **6**:893 (1967).

Bol 68 L. M. Bollinger, in: *Nuclear Structure*, Dubna Symposium, 1968, IAEA, Vienna (1968), p. 317.

Bol+ 72 R. Boleu, S. G. Nilsson, R. K. Sheline, and K. Takahashi, *Phys. Letters* **40B**:517 (1972).

BR 71 M. E. Bunker and C. W. Reich, *Revs. Mod. Phys.* **43**:348 (1971).

Bro 71 G. E. Brown, *Unified Theory of Nuclear Models and Forces*, North-Holland Publ. Co., Amsterdam (1971).

BST 63 W. Bertozzi, C. P. Sargent, and W. Turchinetz, *Phys. Letters* **6**:108 (1963).

BT 70 L. M. Bollinger and G. E. Thomas, *Phys. Rev.* **C2**:1951 (1970).

Bun 65 G. G. Bunatyan, *Yadernaya Fiz.* **2**:862 (1965) [English translation: *Soviet J. Nucl. Phys.* **2**:619 (1966)].

Bun+ 69 G. G. Bunatyan, V. S. Evseev, L. N. Nikityak, A. A. Nikolina, V. N. Pokrovskii, V. S. Roganov, L. M. Smirnova, and I. A. Yutlandov, *Yadernaya Fiz.*, **9**:783 (1969) [English translation: *Soviet J. Nucl. Phys.* **9**:457 (1969)].

Bun+ 70 G. G. Bunatyan, V. S. Evseev, L. N. Nikityak, V. N. Pokrovskii, V. N. Rybakov, and I. A. Yutlandov, *Yadernaya Fiz.* **11**:795 (1970) [English translation: *Soviet J. Nucl. Phys.* **11**:444 (1970)].

Bur+ 57 E. M. Burbidge, G. R. Burbidge, W. A. Fowler, and F. Hoyle, *Revs. Mod. Phys.* **29**:547 (1957).

BW 52 J. M. Blatt and V. F. Weisskopf, *Theoretical Nuclear Physics*, J. Wiley and Sons, New York (1952), p. 647-651.

BW 68 D. A. Bromley and J. Weneser, *Comm. Nuclear Particle Physics* **11**:151 (1968).

Cam 56 A. G. W. Cameron, *Can. J. Phys.* **35**:666 (1957).

CDT 70 A. G. W. Cameron, M. D. Delano, and J. W. Truran, in: Ley-70, p. 735.

Cha+ 69 J. Chaumont, E. Roeckl, Y. Nir-El, C. Thibault-Phillippe, R. Klapisch, and R. Bernas, *Phys. Letters* **29B**:562 (1969).

Chr+ 67 C. J. Christensen, A. Nielsen, B .Bahnsen, W. K. Brown, and B. M. Rustad *Phys. Letters* **26B**:11 (1967); *Phys. Rev.* **D5**:1628 (1972).

Chr+ 71 C. J. Christensen, A. Nielsen, A. Bahnsen, W. K. Brown, and B. M. Rustad, Risö Report No. 226 (1971).

Cra+ 62 W. A. Cramer, V. L. Telegdi, R. Winston, and R. A. Lundby, *Nuovo Cimento* **24**:546 (1962).

Dam 66 J. Damgaard, *Nucl. Phys.* **79**:374 (1966).

Dam 67 J. Damgaard, in: *Symposium on Beta Decay and Weak Interactions* (B. Eman and D. Tadić, eds.) Zagreb, 1967, p. 151.

Dam+ 70 A. Damkjaer, C. L. Duke, P. Hornshøj, K. Wilsky, P. G. Hansen, B. Jonson, O. B. Nielsen, and G. Rudstam, in: Proceedings International Conference on the Properties of Nuclei Far from the Region of Beta Stability, Leysin, 1970, CERN 70–30 (1970), p. 421.

Dam 71 A. Damkjaer, Cand. Scient. thesis, University of Aarhus (1971) (in Danish, unpublished).

DBR 69 J. Damgaard, R. Broglia, and C. Riedel, *Nucl. Phys.* **A135**:310 (1969).

Deg+ 72 J. Degnan, B. L. Cohen, R. C. Petty, C. L. Fink, G. R. Rao, and R. Balsubramanian, *Phys. Rev.* **C5**:836 (1972).

DG 73 C. N. Davids and D. R. Goosman, *Phys. Rev. C,* May 1973.

Duc+ 69 H. E. Duckworth, R. C. Barber, P. van Rookhuysen, J. C. Macdougall, W. McLatchie, S. Whineray, R. L. Bishop, J. O. Meredith, P. Williams, G. Southon, W. Wong, B. G. Hogg and M. E. Kettner, *Phys. Rev. Letters* **23**: 592 (1969).

Duk+ 70 C. L. Duke, P. G. Hansen, O. B. Nielsen, and G. Rudstam, *Nuclear Phys.* **A151**:609 (1970).
DW 64 J. Damgaard and A. Winther, *Nuclear Phys.* **54**:615 (1964).
Ege 58 P. A. Egelstaff, *Proc. Phys. Soc.* **71**:910 (1958).
Egi 69 T. von Egidy, in: *Neutron Capture Gamma-Ray Spectroscopy* IAEA, Vienna (1969), p. 541.
Ehn+ 70 G. J. Ehnholm. T. E. Katila, O. V. Lounasmaa, P. Reivari, and G. M. Kalvius, *Phys. Rev.* **C1**:2109 (1970).
EIF 68 H. Ejiri, K. Ikeda, and J.-I. Fujita, *Phys. Rev.* **176**:1277 (1968).
Eji 67 H. Ejiri, J. *Phys. Soc. Japan* **22**:360 (1967).
Eji+ 69 H. Ejiri, P. Richard, S. Ferguson, R. Heffner, and D. Perry, *Nucl. Phys.* **A128**:388 (1969).
Eji 72 H. Ejiri, *Nucl. Phys.* **A178**:350 (1972).
ER 72 B. R. Erdal and G. Rudstam, *Nucl. Instrum. Methods* **104**:263 (1972).
Esk 67 P. Eskola, *Ark. Fys.* **36**:477 (1967).
FFI 64 J. I. Fujita, S. Fujii, and K. Ikeda, *Phys. Rev.* **133**:B549 (1964).
FFI 68 J. I. Fujita, Y. Futami, and I. Ikeda, *Proceedings International Conference on Nuclear Structure*, Tokyo (1967); *J. Phys. Soc., Japan, Suppl.* **24**:437 (1968).
FHR 67 W. Forsling, C. J. Herrlander, and H. Ryde, eds., *Nuclides Far Off the Stability Line*, Almqvist and Wiksell, Stockholm (1967); also published as *Ark. Fys.* **36**.
FI 65 J. I. Fujita and K. Ikeda, *Nucl. Phys.* **67**:145 (1965).
Fir 70 F. W. K. Firk, *Ann. Rev. Nucl. Sci.* **20**:39 (1970).
Fra+ 72 H. Franz, G. Herrmann, J. V. Kratz, and K. L. Kratz, *European Conference on Nuclear Physics*, Aix-en-Provence 26 June–1 July 1972, Communications p. 31, and private communication.
Fre+ 66 J. M. Freeman, J. G. Jenkin, G. Murray, and W. E. Burcham, *Phys. Rev. Letters* **16**:959 (1966).
FW 64 L. L. Foldy and J. D. Walecka, *Nuovo Cimento* **34**:1206 (1964).
Gaa+ 70 C. Gaarde, K. Kemp, Y. V. Naumov, and P. R. Amundsen, *Nucl. Phys.* **A143**:497 (1970).
Gar 72 J. B. Garg, ed., *Statistical Properties of Nuclei*, Plenum Press, New York (1972).
GKP 71 S. I. Gabrakov, A. A. Kuliev and N. I. Pyatov, *Physics Letters* **36B**:275 (1971).
GP 71 S. I. Gabrakov and N. I. Pyatov, *Symposium on Nuclear and Weak Interactions*, Zagreb (July 1971).
GS 72 N. K. Gupta and K. S. R. Sastry, in: *Radioactivity in Nuclear Spectroscopy* (J. H. Hamilton and J. C. Manthuruthil, eds.), Gordon and Breach, New York (1972), p. 1279.
Hag 72 E. Hagberg, P. G. Hansen, B. Jonson, B. G. G. Jørgensen, E. Kugler, and T. Mowinckel, to be published in *Nucl. Phys.*
Hag 73 E. Hagberg *et al.*, to be published.
Han 69 P. G. Hansen, *Proceedings of the International Conference on the Properties of Nuclear States*, Montreal (M. Harvey, ed.), Presses de l'Université de Montréal, Montreal (1969), p. 189.
Han+ 70 P. G. Hansen, H. L. Nielsen, K. Wilsky, M. Alpsten, M. Finger, A. Lindahl, R. A. Naumann, and O. B. Nielsen, *Nucl. Phys.* **A148**:249 (1970).
Han+ 71 P. G. Hansen, B. Jonson, J. Żylicz, M. Alpsten, Å. L. Appelqvist, and G. Nyman, *Nucl. Phys.* **A160**:445 (1971).

Han 72 P. G. Hansen, in: *Nuclear Structure* (V. G. Soloviev, ed.), Proceedings of the International School on Nuclear Structure, Alushta, USSR (1972) JINR-D-6465 (1972), p. 365-397.

Har+ 71 J. C. Hardy, J. E. Esterl, R. B. Sextro, and J. Cerny, *Phys. Rev.* **C3**:700 (1971).

Har 71 J. C. Hardy, in: *Proceedings of the International Conference on Heavy-Ion Physics*, Dubna, 1971, Dubna report D7-5769 (1971), p. 261.

Har 72a J. C. Hardy, in: *Nuclear Spectroscopy* (J. Cerny, ed.), to be published by Academic Press, New York.

Har 72b J. C. Hardy, *Nuclear Data Tables* **11**:327 (1972).

HHJ 72 P. Hornshøj, P. G. Hansen, and B. Jonson, to be published.

Hir 70 M. Hirata, *Phys. Letters* **32B**:656 (1970).

HMD 67 D. C. Hoffmann, O. B. Michelsen, and W. R. Daniels, *Ark. Fys.* **36**:211 (1967).

HNW 67 P. G. Hansen, H. L. Nielsen, and K. Wilsky, *Izv. Akad. Nauk SSSR Ser. Fiz.* **31**:68 (1967).

Hod 71 P. E. Hodgson, *Nuclear Reactions and Nuclear Structure*, Clarendon Press, Oxford (1971).

Hor+ 71a P. Hornshøj, K. Wilsky, P. G. Hansen, B. Jonson, M. Alpsten, G. Andersson, Å. Appelqvist, B. Bengtsson, and O. B. Nielsen, *Phys. Letters* **34B**:591 (1971).

Hor+ 71b P. Hornshøj, K. Wilsky, P. G. Hansen, A. Lindahl, and O. B. Nielsen, *Nucl. Phys.* **A163**:277 (1971).

Hor+ 71c P. Hornshøj, K. Wilsky, P. G. Hansen, B. Jonson, and O. B. Nielsen, in: *Proceedings of the International Conference on Heavy-Ion Physics*, Dubna, 1971, JINR D7-5769 (1971), p. 249.

Hor+ 72a P. Hornshøj, K. Wilsky, B. Erdal, P. G. Hansen, B. Jonson, K. A. Johansson, and G. Nyman, to be published.

Hor+ 72b P. Hornshøj, K. Wilsky, P. G. Hansen, and B. Jonson, *Nucl. Phys.* **A187**:637 (1972).

Hor+ 72c P. Hornshøj, K. Wilsky, P. G. Hansen, B. Jonson, and O. B. Nielsen, *Nucl. Phys.* **A187**:599 (1972).

Hor+ 72d P. Hornshøj, K. Wilsky, P. G. Hansen, B. Jonson, and O. B. Nielsen, *Nucl. Phys.* **A187**:609 (1972).

Hor+ 72e P. Hornshøj *et al.*, to be published.

HS 67 J. A. Halbleib and R. A. Sorensen, *Nucl. Phys.* **A98**:542 (1967).

IFF 63 K. Ikeda, S. Fujii, and J. I. Fujita, *Phys. Letters* **3**:271 (1963).

Jac+ 70 K. P. Jackson, C. U. Cardinal, H. C. Evans, N. A. Jelley, and J. Cerny, *Phys. Letters* **33B**:281 (1970); J. Cerny, J. E. Esterl, R. A. Gough, and R. G. Sextro, *Phys. Letters* **33B**:284 (1970).

Jah+ 72 U. Jahnke, K. H. Lindenberger, G. Röschert, W. U. Schröder, H. Backe, R. Engfer, E. Kankeleit, H. Schneuwly, J. L. Vuilleumier, and H. K. Walter, *Helv. Phys. Act.* **45**:49 (1972).

Jas 72 J. Jastrzebski, *Acta Phys. Polon.* **B3**:397 (1972).

JBR 72 K. H. Johansen, K. Bonde Nielsen, and G. Rudstam, *Nucl. Phys.* **A203** (1973) 481.

JLG 72 J. Joseph, F. Ledoyen, and B. Goulard, *Phys. Rev.* **6**:1742 (1972).

Jon+ 71 B. Jonson, M. Alpsten, Å. Appelqvist, and G. Astner, *Nucl. Phys.* **A174**: 225 (1971).

Jon 72 B. Jonson, Tech. Dr. Thesis, Department of Physics, Chalmers University of Technology, Gothenburg (1972).

Jon+ 72 B. Jonson, M. Alpsten, Å. Appelqvist, B. Bengtsson, and K. A. Johansson, to be published in *Physica Scripta.*

JPH 72 L. J. Jardine, S. G. Prussin, and J. M. Hollander, LBL-666 (1972), p. 29, and to be published in *Nuclear Physics.*

JS 72 H. E. Jackson and E. N. Strait, in: *Statistical Properties of Nuclei* (J. B. Garg, ed.), Plenum Press, New York (1972).

Kap 70 S. N. Kaplan, in: *High-Energy Physics and Nuclear Structure* (S. Devons, ed.), Plenum Press, New York (1970), p. 143.

Kar 69 V. A. Karnaukhov, *Yadernaya Fiz.* **10**:450 (1969).
V. A. Karnaukhov, *Nucl. Phys.* **A206**:583 (1973).

Kla 72 R. Klapisch, "On-line mass separation," in: *Nuclear Spectroscopy* (J. Cerny, ed.), to be published by Academic Press, New York.

Kla+ 72 R. Klapisch, C. Thibault, A. M. Poskanzer, R. Prieels, C. Rigaud, and E. Roeckl, *Phys. Rev. Letters* **29**:1254 (1972).

Kon 66 E. J. Konopinski, *The Theory of Beta Radioactivity*, Clarendon Press, Oxford (1966).

KSF 66 V. I. Kuznetsov, N. K. Skobelev, and G. N. Flerov, *Yadernaya Fiz.* **4**:279 (1966); N. K. Skobelev, JINR Report P7-5584 (1971).

KT 67 V. A. Karnaukhov and G. M. Ter-Akopyan, *Ark. Fys.* **36**:419 (1967).

KTS 62 V. A. Karnaukhov, G. M. Ter-Akopyan, and V. G. Subbotin, JINR Report P-1072 (1962).

KTY 70 S. I. Koyama, K. Takahashi, and M. Yamada, *Progr. Theor. Phys.* **44**:663 (1970).

LS 62 A. M. Lane and J. M. Soper, *Nucl. Phys.* **37**:663 (1962).

LHP 67 C. M. Lederer, J. M. Hollander, and I. Perlman, *Table of Isotopes*, John Wiley and Sons, New York (1967).

Ley 70 Proceedings International Conference on the Properties of Nuclei Far from the Region of Beta Stability, Leysin, 1970, CERN 70-30 (1970), Vols. I and II.

Lyn 68 J. E. Lynn, *The Theory of Neutron Resonance Reactions*, Clarendon Press, Oxford (1968), (a) p. 201-206.

Mac+ 65 B. Macdonald, J. A. Diaz, S. N. Kaplan, and R. V. Pyle, *Phys. Rev.* **139**: B1253 (1965).

Mac 67 R. D. Macfarlane, *Ark. Fys.* **36**:431 (1967).

Mar 67 M. J. Martin, *Nucl. Data* **B2**, No. 4 (1967).

MB 70 L. G. Mann and S. D. Bloom, *Nucl. Phys.* **A140**:598 (1970).

McH+ 70 Wm. C. McHarris, R. E. Eppley, R. A. Warner, R. R. Todd, and W. H. Kelly, in: Proceedings International Conference on the Properties of Nuclei Far from the Region of Beta Stability, Leysin, 1970, CERN 70–30 (1970), p. 435.

MN 59 B. R. Mottelson and S. G. Nilsson, K. *Danske Vidensk. Selsk. Mat.-Fys. Skr.* **1**, No. 8 (1959).

MON 71 R. D. Macfarlane, N. S. Oakey, and R. J. Nickles, *Phys. Letters* **34B**:133 (1971).

Mor+ 71 M. Morita, M. Yamada, J. I. Fujita, A. Fujii, H. Ohtsubo, R. Morita, K. Ikeda, Y. Yokoo, M. Hiro-Oka, and K. Takahashi, *Suppl. Progr. Theor. Phys.* **48**:41 (1971).

Mot 67 B. R. Mottelson, Lecture Notes from the Nikko Summer School (1967), NORDITA publication No. 288.

MP 63 A. F. de Miranda and M. A. Preston, *Nucl. Phys.* **44**:529 (1963).

MR 72 P. Martinsen and J. Randrup, *Nucl. Phys.* **A195**:26-32 (1972).

MS 65 W. D. Myers and W. I. Swiatecki, UCRL-11980 (1965).

Mue 50 C. O. Muehlhause, *Phys. Rev.* **79**:277 (1950).

NB 65 J. H. Neiler and P. R. Bell, *Alpha-, Beta-, and Gamma-Ray Spectroscopy* (K. Siegbahn, ed.), North-Holland Publishing Co., Amsterdam (1965), p. 245.

New 56 T. D. Newton, *Canad. J. Phys.* **34**:804 (1956).

Nie 72 O. B. Nielsen *et al.*, private communication (1972).

Nil+ 69 S. G. Nilsson, Chin Fu Tsang, A. Sobiczewski, Z. Szymanski, S. Wychech, C. Gustafson, I. L. Lamm, P. Möller, and B. Nilsson, *Nucl. Phys.* **A131**:1 (1969).

NN 65 O. Nathan and S. G. Nilsson, in: *Alpha-, Beta-, and Gamma-Ray Spectroscopy* (K. Siegbahn, ed.), North-Holland Publishing Co., Amsterdam (1965), p. 601.

NRW 69 H. L. Nielsen, N. Rud, and K. Wilsky, *Phys. Letters* **30B**:169 (1969).

Pet+ 71 C. Petitjean, H. Backe, R. Engfer, U. Jahnke, K. H. Lindenberger, H. Schneuwly, W. U. Schröder, and H. K. Walter, *Nucl. Phys.* **A178**:193 (1971).

Por 65 C. E. Porter, ed., *Statistical Theories of Spectra: Fluctuations*, Academic Press, New York (1965).

Pov+ 70 H. Povel, H. Koch, W. D. Hamilton, S. Charalambus, and G. Backenstoss, *Phys. Letters* **33B**:620 (1970).

Pri 59 H. Primakoff, *Rev. Mod. Phys.* **31**:802 (1959).

PT 56 C. E. Porter and R. G. Thomas, *Phys. Rev.* **104**:483 (1956).

PS 72 A. C. Pappas and T. Sverdrup, *Nucl. Phys.* **A188**:48 (1972).

Ran 72 J. Randrup, Theoretical Study of *GT* Strength Functions Within the Framework of the Spherical Shell Model with Particular Attention to the Effect of a *GT*-Type Residual Force (Lic. scient. thesis, University of Aarhus, 1972).

RCE 30 E. Rutherford, J. Chadwick, and C. D. Ellis, *Radiations from Radioactive Substances*, Cambridge University Press (1930), p. 94.

RG 71 D. V. Rao and W. J. Gerace, *Nucl. Phys.* **A175**:405 (1971).

RS 71 D. V. Rao and K. S. R. Sastry, *Nucl. Phys.* **A175**:396 (1971).

RSW 72 H. L. Ravn, S. Sundell, and L. Westgaard, *Phys. Letters* **39B**:327 (1972).

RT 60 P. L. Richards and M. Tinkham, *Phys. Rev.* **119**:575 (1960).

SBG 70 M. Sakai, R. Bertini, and C. Gehringer, INS-141 (1970).

Sch 66 H. F. Schopper, *Weak Interactions and Nuclear Beta Decay*, North-Holland Publishing Co., Amsterdam (1966).

Sch 71 W.-U. Schröder, Dissertation, Institut für Technische Kernphysik der Technischen Hochschule Darmstadt (1971).

Sch+ 72 W.-U. Schröder, U. Jahnke, K. H. Lindenberger, G. Röschert, J. L. Villeumier, H. Backe, R. Engfer, E. Kankeleit, H. Schneuwly, and H. K. Walter, to be published in *Nuclear Physics*.

Sen 59 J. C. Sens, *Phys. Rev.* **113**:679 (1959).

SFC 65 P. A. Seeger, W. A. Fowler, and D. D. Clayton, *Astrophys. J. Suppl.* **11**, No. 97:121 (1965).

Sho+ 71 K. Shoda, A. Suzuku, M. Sugawara, T. Saito, H. Miyase, and S. Oikawa, *Phys. Rev.* **C3**:1999 and 2006 (1971).

Sin 62 P. Singer, *Nuovo Cimento* **23**:669 (1962).

SLD 71 F. S. Stephens, J. R. Leigh, and R. M. Diamond, *Nucl. Phys.* **A170**:321 (1971).

SM 72 R. Stippler and F. Münnich, to be published.

SNH 70 R. P. Sharma, H. L. Nielsen, and P. G. Hansen, *Nucl. Phys.* **A152**:225 (1970).

Sol 63 V. G. Soloviev, *K. Danske Vidensk. Selsk. Mat.-Fys. Medd.* **27**, No. 16 (1963).

SR 71 S. Shalev and G. Rudstam, *Amer. Nucl. Soc. Transactions* **14**:373 (1971).

SR 72 S. Shalev and G. Rudstam, *Phys. Rev. Letters* **28**:687 (1972).

SW 68 S. E. Sobottka and E. L. Wills, *Phys. Rev. Letters* **20**:596 (1968).

Tak 71 K. Takahashi, *Progr. Theor. Phys.* **45**:1466 (1971).

Tak 72a K. Takahashi, *Progr. Theor. Phys.* **47**:1500 (1972).

Tak 72b K. Takahashi, private communication (1972).

Tel 62 V. L. Telegdi, *Phys. Rev. Letters* **8**:327 (1962).

TH 72 I. S. Towner and J. C. Hardy, *Phys. Rev.* **A179**:482 (1972).

Tom 72 L. Tomlinson, Delayed Neutrons from Fission, AERE R-6993 (1972).

Tot+ 72 K. S. Toth, R. L. Hahn, M. A. Ijaz, and R. F. Walker, *Phys. Rev.* **C5**:2060 (1972).

TY 69 K. Takahashi and M. Yamada, *Progr. Theor. Phys.* **41**:1470 (1969).

Ube 66 H. Überall, *Suppl. Nuovo Cimento* **4**:781 (1966).

Ver 71 J. D. Vergados, *Nucl. Phys.* **A166**:285 (1971).

Vog 68a E. Vogt, The Statistical Theory of Nuclear Reactions, in: *Advances in Nuclear Physics, Vol. 1* (M. Baranger and E. Vogt, eds.), Plenum Press, New York (1968), pp. 261–342, (a) p. 290.

WGT 70 E. K. Warburton, G. T. Garvey and I. S. Towner, *Ann. Phys.* (USA) **57**:174 (1970).

WGB 72 W. G. Winn, H. H. Gutbrod and M. Blann, *Nucl. Phys.* **A188**:423 (1972).

Wig 37 E. P. Wigner, *Phys. Rev.* **51**:106 (1937); *Phys. Rev.* **56**:519 (1939).

Wil+ 65 E. T. Williams, P. G. Hansen, J. Lippert, H. L. Nielsen, and K. Wilsky, *Phys. Letters* **15**:143 (1965).

WM 66 C. S. Wu and S. A. Moszkowsky, *Beta Decay*, Interscience, New York (1966).

Yam 65 M. Yamada, *Bull. Sci. Eng. Research Lab.*, Waseda University, No. 31–32: 146 (1965).

ZGS 67 N. Zeldes, A. Grill, and A. Simievic, *K. Danske Vidensk. Selsk. Mat.-Fys. Skr.* **3**, No. 5 (1967).

Zyl+ 67 J. Żylicz, P. G. Hansen, H. L. Nielsen, and K. Wilsky, *Ark. Fys.* **36**:643 (1967).

Chapter 4

GAMMA-RAY STRENGTH FUNCTIONS

G. A. Bartholomew, E. D. Earle,
A. J. Ferguson, J. W. Knowles,
and M. A. Lone

Atomic Energy of Canada Limited
Chalk River Nuclear Laboratories
Chalk River, Canada

1. INTRODUCTION

The study of the energy dependence of multipole transition probabilities is a broad subject in which certain subfields have progressed much more rapidly than others. Thus for gamma rays $\lesssim 2$ MeV, $E1$, $M1$, and $E2$ transition probabilities have been well studied (Per 66, SHR 66, SG 65), and at higher energies, $\gtrsim 10$ MeV, the absorption cross section and other properties of the $E1$ giant resonance are well known (Fir 70), but between these energies there are large gaps in our knowledge. In the present review we are concerned with the distribution of reduced radiation width, particularly for $E1$ and $M1$ radiation, in the less well-known "tail region" well below the peak of the $E1$ giant resonance. We will concentrate on elements with mass number $A \gtrsim 90$, where a statistical description of radiative processes is appropriate, and on γ-ray energies above ~ 2 MeV.

The gamma-ray strength function as used herein is the distribution, as a function of γ-ray energy, of the average reduced width for transitions of a particular multipole type. Specifically, for transitions of energy E_γ and multipole type XL (X is either E (electric) or M (magnetic) and L

is the multipolarity), between states of energies E_i and E_λ ($E_i < E_\lambda$), the strength function is

$$f^J_{i\lambda XL}(E_\gamma) = \frac{\bar{\Gamma}^J_{\gamma i\lambda XL}}{E_\gamma^{2L+1}} \varrho_J(E_\lambda) \tag{1.1}$$

where $\bar{\Gamma}^J_{\gamma i\lambda XL}$ is the γ-ray partial width averaged over states λ of a given spin and parity (denoted together by J) in the neighborhood of E_λ, $\varrho_J(E_\lambda)$ is the average level density for such states and E_γ^{2L+1} is the energy dependence for multipolarity L. The factor E_γ^{2L+1} is analogous to the penetration factor which is removed from nucleon widths to obtain nucleon reduced widths or strength functions.

The γ-ray strength function is thus an average quantity like the nuclear-level density. Regions where it is appropriate to discuss level densities instead of single levels are also regions where it is useful to think in terms of γ-ray strength functions instead of individual radiation widths. In some experiments in thermal neutron capture and γ-ray resonance scattering, radiation widths of a few individual γ-rays from a particular excitation region are all that can be extracted from any one nucleus. This type of data have been surveyed by Bartholomew (Bar 61, Bar 62) Demidov and Shadiev (DS 68), and Bollinger (Bol 68) for (n, γ) reactions and by Ben David, Moreh, and others (Ben+ 66, MSW 70) for (γ, γ) reactions. Because of Porter–Thomas fluctuations (PT 56), these individual transition widths have limited usefulness as indicators of average strength and, apart from a brief historical treatment in this section, we will have only occasional recourse to such data in this review. Average data may be obtained more directly from photoabsorption or inelastic scattering cross-section measurements with a photon beam with energy spread large compared to the spacing $D_J(E_\lambda)$ or by neutron capture or other reactions in which many resonances near the energy E_λ are excited and resonance-averaged radiation is detected.

The surveys of individual γ-rays from thermal neutron capture (Bar 61, Bar 62, DS 68) shed light on the relative strength of various multipoles, the level-spacing dependence, and also on the A-dependence of γ-ray reduced widths. All such studies were limited to a narrow range of E_γ near the neutron separation energy because it was only in this range that multipolarities could be established from the known spins and parities of the initial and final states. For each γ-ray, a "strength"

$$k_{E1} = \frac{\Gamma_{\gamma E1}}{E_\gamma{}^3 D_J A^{2/3}} \tag{1.2}$$

or

$$k_{M1} = \frac{\Gamma_{\gamma M1}}{E_\gamma{}^3 D_J} \tag{1.3}$$

was evaluated and average values $\bar{k}_{E1}$ and $\bar{k}_{M1}$, averaged over both E_γ and A, were obtained. Here the $E1$ strength contained an $A^{2/3}$ dependence as suggested by the single-particle formula (BW 52). These strengths were found, on the average, to compare reasonably well in absolute magnitude with the single-particle estimates (BW 52) when certain plausible values were assumed for a level-spacing parameter appearing in the theory. Because of the small energy range covered, these data provided no definitive test of the energy dependence of $E1$ or $M1$ radiation widths predicted by the single-particle formula. That the single-particle estimates, which imply constant strength functions, were inadequate in this regard was evident from the failure to obtain realistic estimates of total radiation width of neutron resonances (Cam 59) with the same $\bar{k}_{E1}$ as found for the high-energy transitions (Bar 61). However, the true significance of that discrepancy was somewhat obscured because the energy dependence of level densities also entering the calculations was poorly known experimentally and had to be taken from semiempirical formulas (New 56, Cam 59).

It was pointed out by Brink (Bri 55) and emphasized by Axel (Axe 62, Axe 63) that a more realistic energy dependence of the $E1$ transition probability is provided by the energy dependence of the $E1$ photoabsorption cross section. As shown in Sec. 2.2 the strength function for $E1$ photoexcitation from the ground state may then be written

$$\vec{f}_{0\lambda E1} = K \frac{\Gamma_G E_\gamma}{(E_\gamma{}^2 - E_G{}^2)^2 + \Gamma_G{}^2 E_\gamma{}^2} \tag{1.4}$$

where the arrow is used to distinguish photoexcitation strength functions from strength functions determined in decay processes, K is constant for any particular nucleus, and the quotient, involving the width Γ_G and energy E_G of the electric giant dipole resonance, is derived from the classical Lorentz line. The application of this strength function to γ-ray transitions from highly excited states to the ground state is straightforward, but its application generally to describe γ-decay to states other than the ground state requires an additional assumption. This assumption, usually referred to as the Brink hypothesis, states that an excited state has built on it a giant resonance similar to that for the ground state but shifted upward in energy by the energy of the excited state. With the strength function thus determined by the photoabsorption cross section, both the energy-dependence and A

dependence of the transition probability for $E1$ radiation vary more rapidly than in the Weisskopf estimate. Axel (Axe 62) showed from Eq. (1.4) that radiative widths should vary approximately as E_γ^5 and $A^{8/3}$ in the region of 7 MeV. Support for this A-dependence was first obtained by Carpenter (Car 62) who analyzed data from photonuclear reactions and thermal and resonance-averaged neutron-capture data. Support for the E_γ^5 dependence has been found by Bollinger and co-workers (Bol 68, BT 70) in several elements but examples where high powers of E_γ fit the observations better have been reported in other examples (e.g., Bol 70, Smi+ 72).

Evidence that subthreshold strength functions may have local irregularities or fine structure was early noted by Axel and co-workers (Axe+ 63). Of course the demonstrable fact that such irregularities are present in the giant resonance itself in light elements and at closed shells in heavy elements (FH 62b, Bow+ 70) makes it scarcely surprising that irregularities are present to some degree in the giant resonance tail in nuclei where the statistical model is more secure. The important questions are really: in what nuclei does this substructure occur, how important is it relative to the smooth statistical background, i.e., how does it modify or modulate the general Lorentz-like dependence, and to what nuclear structure is it related?

An important manifestation of irregular behavior of the strength function is the so-called 5.5-MeV "anomalous" bump appearing in various γ-ray spectra, particularly those following neutron-transfer reactions near closed shells. It was first noticed by Kinsey and co-workers (JK 51, K in 55) that the spectral distribution of high-energy γ-rays in elements near closed shells contained too much radiation to be easily accounted for by an E_γ^3 energy dependence for the transition probability and an exponential level-density energy dependence. The same effect was emphasized by Groshev and co-workers (Gro+ 58) and a quantitative demonstration of the effect in terms of the fraction of the total available energy (separation energy) radiated in γ-rays in the top half of the spectrum was given by Groshev (Gro 55). It was early pointed out by Bartholomew and co-workers (Bar+ 57), (Bar 62) that while this radiation near the top of the spectrum indeed had an anomalous *intensity* it did not appear to result from anomalously large *radiation widths*; i.e., strengths for the γ-rays concerned when compared to γ-rays from neighboring nuclei that did not exhibit the effect. Alternative explanations involving level-density effects were considered (Bar 62) but the crucial experiments identifying the effect not with irregularities in level density but in strength function were carried out by Bergqvist, Lundberg, and Starfelt (BS 62, LS 65) in fast-neutron capture. They showed that since

the 5.5-MeV γ-ray bump remained at $\sim$5.5 MeV regardless of neutron bombarding energy from thermal energies to $\sim$4 MeV it could not be accounted for by level-density effects. They also showed that neither a simple E_γ^3 law, nor the more rapid energy dependence derived from the Lorentz line, was sufficient to account for the observed spectral distribution and postulated instead that the true strength function be represented by a smooth giant resonance tail with a "pigmy resonance" superimposed on it at 5.5 MeV.* This work was shortly followed by evidence that the γ-rays in the bump were predominantly $E1$ (BGE 67). A similar γ-ray bump was found for excitation below the neutron threshold in studies of the $(d, p\gamma)$ reaction (Bar+ 70) and while strength functions extracted in that work in Au and neighboring nuclei showed departures from a smoothly varying energy dependence, it was again noted that the absolute strengths of γ-rays at 5.5 MeV were nevertheless little greater than those in Ta where no γ-ray bump was found. It became apparent that the 5.5-MeV radiation might, at least in some nuclei, be caused as much, or more, by a deficit of strength below 5.5 MeV than by a "resonance" at 5.5 MeV (Bar 69). Recent demonstrations by Loper and coworkers (LBT 72) that the strengths of γ-rays in the 5.5-MeV region in Au were not greater than those of γ-rays of the same energy in Ta further confirm this view. Recently, careful fitting of available capture γ-ray spectra with trial strength functions and recalculation of the strength functions extracted from $(d, p\gamma)$ reactions, both carried out with more realistic level densities (LBE 72, Lon+ 73) has led to a consolidation of previously conflicting data.

Evidence for the 5.5-MeV bump radiation has been found also in (γ, γ') (MW 69) and (p, γ) (Brz+ 71) reactions. However, it was early reported (Ber+ 66a) that no such radiation appears in the $(n, n'\gamma)$ reaction in elements where it is seen strongly in the (n, γ) reaction. Subsequent experiments showed that it was also absent in $(\mu^-, xn\gamma)$ reactions (EB 71) and in $(p, p'\gamma)$ reactions (Lon+ 72). An exception is ^{207}Pb$(p, p'\gamma)^{207}$Pb where a γ-ray spectrum very similar to that from ^{206}Pb$(d, p\gamma)^{207}$Pb was found (Bar 69).

* It is important not to confuse the bump in the γ-ray spectrum with the pigmy resonance in the strength function. The γ-ray bump is an experimental fact. The pigmy resonance, as originally presented, was primarily an analytical device introduced by analogy with the giant resonance in order to explain the bump. As we shall show, the bump can be generated with little or no pigmy resonance in the strength function. The adjective "anomalous" has also caused confusion. It applied only to the bump, not to features of the strength function, and reflected the difficulty of accounting for the bump with the aid of a smoothly varying strength function.

Recent information on individual $M1$ γ-ray strengths has been tabulated by Bollinger (Bol 68). It was found that, for γ-rays near 7 MeV in elements with $A > 90$, the average γ-ray width for $M1$ radiation is closer to that for $E1$ radiation than was deduced earlier from more limited data (Bar 61). Furthermore, exceptionally strong $M1$ transitions have been reported near closed shells in (n, γ) reactions (HSM 65, UVL 66) and local concentrations of strength have been observed in photonuclear (Bow+ 70, TJ 72, Wol+ 72) and electron scattering (PW 71) reactions. The energy dependence of $M1$ strength in the region between 5 and 8 MeV approximately has been studied in a few elements (Bol 68, BT 70, LEB 70). Although the above information taken together is fragmentary, support for the neutron spin flip mechanism (Mot 60, Bri 63) and for predicted peaks in the $M1$ strength function below 9 MeV approximately (SE 69) appears to be accumulating.

Recent reviews stressing the determination of radiation strengths for individual γ-rays, mostly by the resonance-average technique, have been given by Bollinger (Bol 68, BT 70). A review of experimental and theoretical work concerning the reaction mechanism of neutron capture has been published by Bergqvist and Starfelt (BS 70a). A general review of radiative properties following resonant neutron capture has been provided by Chrien (Chr 72). Axel (Axe 68) has discussed the significance of the γ-ray strength function in relation to intermediate structure and the spreading of single-particle strength. Lane (Lan 71, Lan 72) has reviewed the theoretical implications of the 5.5-MeV anomalous radiation in the broader context of partial width correlations and common doorway states. In the present paper we study the functional form and other properties of the gamma-ray strength function as determined experimentally in photoexcitation, neutron transfer, and other reactions in heavy elements. This review supersedes an earlier survey (Bar 69) that covered some of this material. The subject of beta strength functions is reviewed in the companion paper by Hansen (Han 73).

In Sec. 2, a brief review is given of the theoretical concepts and expressions needed for subsequent discussion. In Sec. 3 we review critically the several methods for measuring and extracting strength function information. In Sec. 4 we compare the strength functions from these various methods, discuss their accuracy and reliability, and review the evidence for gross substructure. In Sec. 5 we summarize the present experimental picture in photon strength functions and attempt to relate this to theoretical notions in current use.

2. THEORETICAL BACKGROUND

The theory of radiative process in nuclei has been discussed by many authors (see for example BW 52, LL 60, dST 63, Lyn 68, BM 69). Since this review is concerned mainly with determinations from experiment of the energy dependence of strengths of various multipoles in a restricted energy range in heavy elements, no attempt is made to provide a comprehensive summary of the theory. In this section we merely establish nomenclature and outline concepts based on statistical models needed for the ensuing presentation and discussion of results.

2.1. Nomenclature

In discussing radiative processes we shall use the convention illustrated in Fig. 1. In order to identify the γ-ray transitions between states, two indices will be used. The index λ for the upper state or group of states (hereafter, for the sake of clarity, referred to as *levels*) and the index i for the lower state or group of states ($E_i < E_\lambda$) involved in the transitions of interest. Both λ and i are running indices. For brevity we use J as short for J_λ^π to indicate a specific spin and parity of the upper level or group of levels, λ. Symbols are defined in Table I.

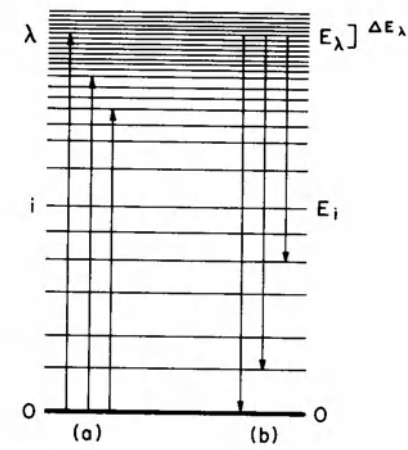

Fig. 1. Nomenclature. The index λ denotes the upper level or group of levels of the same J_λ^π and the index i the lower state or group of states. Radiation width distributions (a) for photoabsorption to a range of levels, λ, and (b) for γ-decay from a localized interval of levels, λ, to a range of lower states, i, are illustrated.

TABLE I

Nomenclature

Symbol	Abbreviation	Definition
B_{XL}		Reduced transition rate for multipole XL
C_{XL}		Energy weighted sum of the reduced matrix elements for multipole XL
$D_J(E)$	D_J	Spacing of levels of spin J at excitation E
E_B		Neutron separation energy
E_G		Giant resonance peak energy
E_γ		Gamma-ray energy
E_n		Neutron bombarding energy
E_t		Energy below which discrete levels are adopted for spectra calculations
$\vec{f}^J_{i\lambda XL}$	$\vec{f}$	Strength function for photoexcitation, from the initial state at excitation E_i, of levels of single spin J within unit energy interval at $E_\lambda = E_\gamma + E_i$ by radiation of type X and multipolarity L. Normally the initial state is the ground state ($i = 0$). The arrow implies that the target state i is fixed and the excited level λ is variable.
$\overleftarrow{f}^J_{i\lambda XL}$	$\overleftarrow{f}$	Strength function for decay of levels of single spin J within unit energy interval at E_λ to a state at energy E_i by emission of radiation of multiple XL. The arrow indicates that the initial level λ is fixed and the final state i is variable.
g_J	g	Statistical factor $(2J + 1)/(2J_0 + 1)$
$\Gamma^J_{\gamma i\lambda XL}$	$\Gamma_{\gamma i\lambda}$	Partial radiative width for the transition between level λ of spin J and state i. ($E_\lambda > E_i$)
$\Gamma^J_{\gamma T\lambda}$	$\Gamma_{\gamma T\lambda}$	Total radiative width of a spin-J level at excitation energy E_λ.
$\Gamma^J_{T\lambda}$	$\Gamma_{T\lambda}$	Total width of the spin-J level at excitation energy E_λ.
Γ_G		Width of the giant resonance
I_γ		Individual γ-ray intensity
J, J_0		J and J_0 represent spin of the compound and target state respectively.
k_{E1}		Individual electric dipole γ-ray strength $\Gamma_{\gamma i\lambda E1}/[E_\gamma{}^3 D_J(E_\lambda)A^{2/3}]$
k_{M1}		Individual magnetic dipole γ-ray strength $\Gamma_{\gamma i\lambda M1}/[E_\gamma{}^3 D_J(E_\lambda)]$
$\nu^J_{i\lambda XL}$	$\nu_{i\lambda}$	Average γ-ray spectral distribution per unit γ-ray energy interval of primary γ-radiation of multiple XL from a level at an excitation E_λ with unit population to states at excitation E_i.

TABLE I (*continued*)

Simbol	Abbreviation	Definition
$\nu_{t\lambda XL}$	$\nu_{t\lambda}$, ν	Average γ-ray spectral distribution per unit γ-ray energy interval of primary plus secondary and subsequent γ-radiations of multipole XL per γ-ray energy interval from a level at excitation E_λ with unit population.
P_λ		Population of level λ
$P(E_\gamma)$		Pulse-height distribution
$\varrho_J(E)$	ϱ_J, ϱ	Level density of spin-J states at excitation E
S		Statistical fluctuation factor $\overline{\Gamma_i\Gamma_j}/\bar{\Gamma}_i\bar{\Gamma}_j$
σ_{OG}		Peak giant dipole resonance cross section
σ		Spin-cutoff parameter
$\bar{\sigma}^J_{\gamma aXL}(E_\gamma)$	$\bar{\sigma}_{\gamma a}$	Average photoabsorption cross section for γ-rays of type X and multipolarity L and excitation of compound level of spin J at energy E_γ. The symbols $\bar{\sigma}_{\gamma\gamma}$, $\bar{\sigma}_{\gamma\gamma'}$, $\bar{\sigma}_{\gamma n}$, $\bar{\sigma}_{\gamma f}$, and $\bar{\sigma}_{\gamma p}$ are used for (γ, γ), (γ, γ'), (γ, n), (γ, f), and (γ, p) reactions respectively. The total cross section $\sum_{\gamma'} \bar{\sigma}_{\gamma\gamma'}$ is indicated by $\bar{\sigma}_{\gamma T}$.
XL		X represents the multipole type, electric (E) or magnetic (M), and L the multipolarity.

2.2. Strength Functions

Experimentally one encounters two types of radiation width distribution with respect to γ-ray energy; the distribution for photoabsorption from a low energy state, usually the ground state, to a range of excited levels and the distribution for γ-decay from a localized interval of excited levels to a range of lower states. These are illustrated by the arrows in Fig. 1. We use $\vec{f}$ and $\overleftarrow{f}$ to differentiate between the corresponding photoexcitation and γ-decay strength functions.

The strength function for photoexcitation from the ground state of levels of spin J within unit energy interval at E_λ by radiation of type X and multipolarity L is

$$\vec{f}^J_{0\lambda XL}(E_\gamma) = \frac{\bar{\Gamma}^J_{\gamma 0\lambda XL}\, \varrho_J(E_\lambda)}{E_\gamma^{2L+1}} \tag{2.1}$$

where $E_\gamma = E_\lambda$ and other symbols are defined in Table I. The strength function is proportional to the amount of reduced matrix element squared, $(2J + 1)\, B_{XL}$ (BM 69, p. 382) per unit excitation energy interval.

The strength function for decay of levels of spin J within unit energy interval at E_λ to a state at energy E_i by emission of radiation of multipole XL is

$$\overleftarrow{f}^J_{i\lambda XL}(E_\gamma) = \frac{\bar{\Gamma}^J_{\gamma i\lambda XL}\, \varrho_J(E_\lambda)}{E_\gamma^{2L+1}} \tag{2.2}$$

where $E_\gamma = E_\lambda - E_i$. In this process E_λ is fixed and E_i is a variable. It is understood that the averages in Eqs. (2.1) and (2.2) are over large numbers of levels of the same spin and parity, at E_λ.

At high excitation energies the wavefunctions of the physical states contain a large number of configurations. These give rise to a broad distribution of the individual reduced widths. There is now much evidence (Bol 70) that, for γ-rays, this distribution is a χ^2 distribution with one degree of freedom or the Porter–Thomas (PT 56) distribution

$$P\left(\frac{\Gamma_\gamma}{\bar{\Gamma}_\gamma}\right) = \left(\frac{2\pi\Gamma_\gamma}{\bar{\Gamma}_\gamma}\right)^{-1/2} e^{-\Gamma_\gamma/2\bar{\Gamma}_\gamma} \tag{2.3}$$

With this distribution the uncertainty in the strength function for a sample of m states is

$$\Delta f = f\sqrt{2/m} \tag{2.4}$$

Predictions of the energy dependence of the gamma-ray strength function vary with the model used. On the extreme statistical assumption, that the single-particle strength is distributed equally among the physical states of the nucleus, Blatt and Weisskopf (BW 52) predicted that the strength function for any multipole is independent of energy. In this model there is no distinction between $\vec{f}$ and $\overleftarrow{f}$. The absolute magnitudes of the strength function depend on the values of the nuclear radius and the spacing between single-particle shells. These estimates have been discussed by several authors (e.g., Bar 61, Bol 70). As discussed in Sec. 1 these single-particle estimates are too crude to explain the observed energy dependence of the $E1$ strength function or to give accurately the relative strengths of various multipoles (see Sec. 4).

A more refined estimate of the strength function $\vec{f}$ is obtained from the photoabsorption cross section (Axe 68):

$$\vec{f}^J_{0\lambda XL}(E_\gamma) = 26 \cdot 10^{-8}\, \frac{\bar{\sigma}^J_{\gamma aXL}(E_\gamma)}{g_J E_\gamma^{2L-1}}\ (\mathrm{MeV})^{-(2L+1)} \tag{2.5}$$

where g_J is the statistical factor $(2J+1)/(2J_0+1)$, $\bar{\sigma}^J_{\gamma aXL}$ (mb) is the average absorption cross section of a nucleus in the ground state of spin J_0 for excitation of levels of spin J at energy $E_\lambda = E_\gamma$ (MeV).

On a classical damped simple harmonic oscillator model, the energy dependence of the average absorption cross section summed over all allowed J's is given by the Lorentz line shape (Bri 55, Bri 63, DG 65)

$$\begin{aligned}\bar{\sigma}_{\gamma aXL}(E_\gamma) &= \sum_J \bar{\sigma}^J_{\gamma aXL}(E_\gamma) \\ &= C_{XL} \frac{\Gamma_G E_\gamma^{\,2}}{(E_\gamma^{\,2} - E_G^{\,2})^2 + \Gamma_G^{\,2} E_\gamma^{\,2}}\end{aligned} \tag{2.6}$$

where the quantity C_{XL} depends on the multipolarity and can in principle be obtained from sum rules (Jac 67). For electric dipole radiation the sum rule is independent of nuclear models; however, there is an uncertainty of up to a factor of two due to the lack of precise knowledge of the magnitude of exchange terms in nuclear forces (LB 50). For other multipoles (electric or magnetic) the sum rule depends on specific nuclear models and details of two-body forces.

From the electric dipole sum rule we obtain (Hay 65)

$$\bar{\sigma}_{\gamma aE1}(E_\gamma) = 38 \frac{NZ}{A} (1 + 0.8x) \frac{\Gamma_G E_\gamma^{\,2}}{(E_\gamma^{\,2} - E_G^{\,2})^2 + \Gamma_G^{\,2} E_\gamma^{\,2}} \text{ mb} \tag{2.7}$$

where x is the fraction of exchange forces present in the nuclear forces (LB 50) and all energies are in MeV.

Brink (Bri 55) has shown that a modified energy-weighted sum of squares of the reduced matrix elements for any multipole moment (summed over levels with a particular total angular momentum J) is also independent of J. Then assuming that the energy dependence of the photoexcitation cross section for any spin states is given by the Lorentzian, the cross section for spin J states is

$$\bar{\sigma}^J_{\gamma aE1} = \frac{g_J}{3} \bar{\sigma}_{\gamma aE1} \tag{2.8}$$

Because of the nuclear-model dependence of the sum rules it is not practical to write a general expression for cross section for other multipoles. Estimates of the strength functions from specific nuclear models have been discussed by several authors, for example for $E1$ in ^{208}Pb (KH 73, Lan 71, Per 70, KBB 70, GGS 66), for $M1$ (HKW 72, SE 69) and valence model for $E1$ and $M1$ (Lyn 68). In this paper we first present the experimental strength function without invoking specific nuclear models, using the Lorentz line shape for comparison. In Sec. 5 we discuss deviations of the empirical strength function from the Lorentzian shape in the light of some recent models.

Both the extreme statistical model (BW 52, page 645) and the classical damped simple harmonic oscillator model [see Eqs. (2.5), (2.7) and (2.8)] predict that the strength function is independent of J. In both cases the arguments are, in principle, based on the assumption that the wave functions of the highly excited levels contain a large number of configurations. Lynn shows that even in the valency capture model (see Lyn 68, page 329) if the number of configurations (one for each valency transition) contributing to the partial width are large, then the strength function has little dependence on the spins of the levels. The broad distribution of the observed individual reduced widths, i.e., the Porter–Thomas distribution, indicates that these transitions are from complicated levels. Therefore we shall assume J-independence of the strength function and henceforth drop the J superscript. However, it should be borne in mind that the strength function as used in this paper refers to a single J for the states λ.

It is not immediately obvious (except in the case of the extreme statistical model) that $\vec{f}$ should be identical to $\overleftarrow{f}$. For electric dipole radiation equating $\vec{f}_{0\lambda E1}(E_\gamma) = \vec{f}_{i\lambda' E1}(E_\gamma) = \overleftarrow{f}_{i\lambda' E1}(E_\gamma)$ is tantamount to assuming, following Brink (Bri 55), that the energy dependence of the photoeffect is independent of the detailed structure of the initial state, so that if it were possible to perform the photoeffect on an excited state, the cross section for absorption would have the same energy dependence as for the ground state. Rosensweig has presented plausibility arguments in support of this hypothesis (Ros 68). A thorough experimental verification has yet to be made.

In practice, it is possible to measure $\vec{f}_{0\lambda XL}$ for all E_λ's but exceedingly difficult if not impossible to obtain $\vec{f}_{i\lambda XL}$ ($i > 0$). On the other hand, one may, in principle, determine all $\overleftarrow{f}_{i\lambda XL}$. For E_λ above a particle threshold one can obtain $\vec{f}_{i\lambda XL}$ by detailed balance from the corresponding capture reaction. With this method Allas *et al.* (All+ 64) have shown that in ^{12}C the γ-ray strength functions based on the ground state and the first excited state are similar and depend only on the γ-ray energy. Below the particle threshold one can use the (γ, γ') reaction to obtain $\vec{f}_{i\lambda XL}$ for i near the ground state by measuring the elastic to inelastic scattering ratio as a function of E_λ. However, no such attempt has been made. Confirmation of the compatibility of $\vec{f}_{0\lambda E1}$ with $\overleftarrow{f}_{i\lambda' E1}$ for the restricted case where E_λ represents the excitation energy interval at the neutron separation energy and $E_i < 4$ MeV, is obtained from the spectrum average technique discussed in Sec. 3.4. One can, in principle, determine all $\overleftarrow{f}_{i\lambda XL}$ by the sequential extraction method described in Sec. 3.3. It yields the functional form (energy dependence) of the $\overleftarrow{f}_{i\lambda XL}$ but not their absolute normalization. However, for

the purpose of testing the Brink hypothesis one need only show that the functional forms of $\overleftarrow{f}_{i\lambda XL}$ for all λ and of $\overrightarrow{f}_{0\lambda XL}$ in the energy range $0 \leq E_\gamma \leq E_\lambda$ are the same. Unfortunately, as will be discussed in Sec. 5 these conditions have as yet not been achieved in any one nuclide.

In the absence of a rigorous proof of this hypothesis, it would be admissible to proceed by assuming that it is true, and subsequently to examine the consequences of having made the assumption. However, in this review we will find it convenient in presenting strength functions derived from experiment to maintain the distinction between $\overrightarrow{f}$ and $\overleftarrow{f}$. But, guided by experimental results discussed in Sec. 3.3, we shall assume that the functional form of $\overleftarrow{f}_{i\lambda XL}$ is independent of the levels involved. For simplicity we write $\overrightarrow{f}_{XL}$, in referring to photoexcitation from the ground state to levels λ, and $\overleftarrow{f}_{XL}$ in referring to decay transitions from a fixed level λ to final states i.

In Eq. (2.5) the strength function is expressed in terms of the photoabsorption cross section. Because of the competition from other processes it is impractical to measure the photoabsorption cross section below the particle threshold. Instead the elastic or, more often, the quasielastic scattering cross section is usually measured. This can be related to the photoabsorption cross section by

$$\bar{\sigma}^J_{\gamma\gamma' XL}(E_\gamma) = \bar{\sigma}^J_{\gamma a XL}(E_\gamma) \frac{\bar{\Gamma}^J_{\gamma i\lambda XL}}{\bar{\Gamma}^J_{\gamma T\lambda}} S \tag{2.9}$$

where the statistical fluctuation factor $S = \overline{\Gamma_{\gamma i\lambda}\Gamma_{\gamma 0\lambda}}/(\bar{\Gamma}_{\gamma i\lambda}\bar{\Gamma}_{\gamma 0\lambda})$ depends on the statistical distribution of the partial widths and the size of the sample. For a sample size, $n_\lambda > 100$, and with a Porter–Thomas distribution of the partial widths, S is 3. It decreases with sample size, becoming unity for $n_\lambda = 1$. The branching ratio $\bar{\Gamma}^J_{\gamma i\lambda XL}/\bar{\Gamma}^J_{\gamma T\lambda}$ can be calculated as discussed in Secs. 2.3 and 3.1.

2.3. Spectral Distributions

The average spectral distribution $\nu^J_{i\lambda XL}(E_\gamma)$ per unit γ-ray energy of primary γ-rays of type X and multipolarity L from an excited level of spin J at an excitation energy E_λ with unit initial population is

$$\begin{aligned} \nu^J_{i\lambda XL}(E_\gamma) &= \frac{\bar{\Gamma}^J_{\gamma i\lambda XL}}{\bar{\Gamma}^J_{T\lambda}} \sum_{I=J-L}^{J+L} \varrho_I(E_i) \\ &= E_\gamma^{2L+1} \frac{\overleftarrow{f}_{XL}(E_\gamma)}{\bar{\Gamma}^J_{T\lambda}} \frac{\sum_{I=J-L}^{J+L} \varrho_I(E_\lambda - E_\gamma)}{\varrho_J(E_\lambda)} \end{aligned} \tag{2.10}$$

where $\bar{\Gamma}^J_{T\lambda}$ is the average total width, and $\varrho_I(E_i)$ is the density of states, at an excitation $E_i = E_\lambda - E_\gamma$, which combine with levels of spin J for emission of radiation of multipole XL.

The average total radiative width is given by

$$\bar{\Gamma}^J_{\gamma T\lambda} = \sum_{XL} \int_0^{E_\lambda} \bar{\Gamma}^J_{\gamma i\lambda XL} \sum_{I=J-L}^{J+L} \varrho_I(E_i)\, dE_i$$

$$= \sum_{XL} \int_0^{E_\lambda} E_\gamma^{2L+1} \overleftarrow{f}_{XL}(E_\gamma) \frac{\sum_{I=J-L}^{J+L} \varrho_I(E_\lambda - E_\gamma)}{\varrho_J(E_\lambda)}\, dE_\gamma \qquad (2.11)$$

For levels above the particle threshold, $\bar{\Gamma}^J_{T\lambda}$ in Eq. (2.10) includes the total radiative width and the widths for all particle channels.

Information on the level-density distributions needed for these calculations must be obtained from other sources. Excellent recent summaries of the theoretical and experimental situations have been provided by Block (Blo 72), French and Chang (FC 72) and Huizenga (Hui 72). However, none of the theoretical level-density formulas are adequate near closed shells and at low excitation energies. There have been several attempts to calculate the level densities with combinatorial methods (e.g., HG 69) using shell-model states. Although somewhat more realistic than the free Fermi gas model, these methods suffer from uncertainties in the numbers and energies of the shell-model states included in the calculation.

The J-dependence of the level density is usually assumed to be given by (Bet 36, Blo 72)

$$\varrho_J(E) = \varrho_0(E)(2J + 1)e^{-(J+1/2)^2/2\sigma^2} \qquad (2.12)$$

where ϱ_0 denotes the density of levels with $J = 0$ and σ is the spin-cutoff factor. This formula is applicable to both parities and is based on the assumption that the nuclear system can be represented by a system of independent Fermi particles. The derived level density is then a well-defined function of the single-particle level density, which can be defined by means of Laplace transforms. The functional form of $\varrho_0(E)$ and the spin-cutoff factor σ depend on the models used for the single-particle level density and the method used for inverting the Laplace transform (Blo 72). The factorization of ϱ_J into spin-dependent and spin-independent parts depends, in principle, on the assumption that a large number of particles are excited (Eri 60). However, this assumption breaks down, and therefore Eq. (2.12) may not be valid, for energies near the ground state. Even at higher excitation energies the validity of Eq. (2.12) has not been fully investigated. This factorization of the level-density formula into spin-

and energy-dependent terms is extremely useful provided σ is independent of energy. Then for dipole radiation for excitation energies below all particle thresholds, Eq. (2.10) reduces to

$$\nu_{i\lambda X1}(E_\gamma) = 3\,\frac{E_\gamma{}^3 \overleftarrow{f}_{X1}(E_\gamma)}{\bar{\Gamma}_{\gamma T\lambda}}\,\frac{\varrho_0(E_\lambda - E_\gamma)}{\varrho_0(E_\lambda)} \tag{2.13}$$

which implies that the spectral distribution is independent of the spins of the states involved. The nondependence of $\bar{\Gamma}_{\gamma T\lambda}$ on J follows from Eq. (2.11). The observed total radiation widths of neutron resonances ($E_\lambda \simeq 6$ MeV) show no significant dependence on the spins, $J_0 - \frac{1}{2}$ and $J_0 + \frac{1}{2}$, of s-wave neutron resonances in target nuclei with spin J_0 ranging from 0 to $\frac{7}{2}$ (Lyn 68). This observation provides confirmation that $\overleftarrow{f}$ is independent of J and to some extent supports the validity of Eq. (2.12), although it sheds but little light on the energy dependence of σ, since the spins involved are low.

If we assume that the spin-cutoff factor is energy-dependent then Eq. (2.13) is not valid and both $\bar{\Gamma}_{\gamma T\lambda}$ and $\nu_{i\lambda XL}$ depend on the spin of the states at E_λ. Gilbert and Cameron (GC 65) show that for a free Fermi gas model, $\sigma \propto (E)^{1/4}$. Combinatorial calculations (HG 69) also show that at low excitation energies, in general, low spin levels predominate. Again this can be simulated by making σ energy-dependent. Under these circumstances one must use Eq. (2.10) for the calculation of spectral distributions.

In the theoretical level-density formulas the functional form of ϱ_0 depends on the theoretical model assumed. In this paper, for the analysis in Sec. 3 we need level densities near closed shells and for excitation energies from the ground state to $\sim$8 MeV. This is the region where these models are found to be inadequate. From a review of the data available to 1965, Gilbert and Cameron (GC 65) showed that an expression of the type $\varrho_0 \propto e^{2\sqrt{aE}}$ could not be valid simultaneously for the lower levels and for the neutron and proton resonances. On the other hand, they found that a formula of the type $\varrho_0 \propto e^{E/T}$ gave a good fit to the experimental data over the first few MeV of excitation energy. A review of the data shows that the functional forms $\varrho_0 \propto (E - E_0)^{-2} e^{2\sqrt{a(E-\Delta)}}$ or $\varrho_0 \propto e^{E/T}$ can be fitted to the known level densities (Gol+ 66, Gro+ 68, 69) up to an excitation energy of $\sim$8 MeV. Similar conclusions were drawn by Maruyama (Mar 69), who investigated the functional forms of the level densities needed to fit the neutron yields from the (n, n') reactions in several nuclei. In even–even nuclei the concept of the statistical level density has no validity at an excitation energy below the pairing gap. Therefore in this paper, for excitation energies E above a lower limit E_t approximately equal to the pairing

gap, we adopt the level-density formula Eq. (2.12), for both parities, with

$$\varrho_0 = Ae^{E/T} \tag{2.14}$$

where the constants A and T are determined empirically from the known level densities (normalized to zero spin) 1–2 MeV above the ground state and at the neutron threshold. Below E_t the known discrete levels are adopted with their appropriate spins and parities.

3. EXPERIMENTAL METHODS

Four experimental methods for the determination of γ-ray strength functions will be considered. The first, involving *photoexcitation techniques*, leads to determinations of $\vec{f}$; the other three to determinations of $\overleftarrow{f}$. In the second method, herein called the *spectrum fitting method*, $\overleftarrow{f}$ is found by trial fitting of various forms of strength function in a calculation reproducing the total γ-decay spectral distribution. In the third method, *sequential extraction*, the primary γ-ray spectral distribution is extracted from the data thereby enabling a unique $\overleftarrow{f}$ to be deduced by Eq. (2.13). In the fourth method, called the *high-resolution γ-ray method*, $\overleftarrow{f}$ is found by applying Eq. (2.2) to high-energy γ-rays known, or presumed to be, primaries.

In this section each of the four methods is discussed in turn with attention to its underlying assumptions and inherent experimental limitations. Some of the assumptions are supported by direct experimental evidence but discussion of those experiments is deferred to later sections. At the end of this section we compare the advantages and disadvantages of the various methods.

3.1. Photoexcitation Method

The photoexcitation strength function $\vec{f}$ may be extracted from photoexcitation experiments in which the energy spread of the incident γ-radiation is greater than the level spacing $D(E_\gamma)$ so that averages over the initial states λ are obtained, as it were, automatically. If available, variable energy incident beams of resolution high enough to resolve individual levels could also be used to obtain radiation widths of such levels from which average values could then be derived to determine the strength function. So far, because of inadequate resolution of variable-energy beams, few experiments have fallen into this category. However, much the same thing is accomplished in several experiments in which high-resolution detectors are used, thereby permitting individual resonances to be examined in spite of poor beam resolution.

In this section the various photoexcitation techniques are described and the extraction of $\vec{f}$ from the measurements is discussed in some detail. Inelastic scattering experiments at individual resonances from which the γ-decay strength function $\vec{f}$ may be determined are also discussed briefly.

Determinations of $\vec{f}$ require that one first obtain $\bar{\sigma}_{\gamma a}$, from which the strength function is deduced with the aid of Eq. (2.5) or related expressions, or that one obtain $\Gamma_{\gamma 0\lambda}$ for individual transitions and then, after averaging over several resonances near E_λ, obtain $\vec{f}$ from Eq. (2.1). In practice, transmission measurements yielding $\bar{\sigma}_{\gamma a}$ directly are usually not feasible because of the much larger cross sections for competing atomic absorption processes and hence one must resort to indirect estimation of $\bar{\sigma}_{\gamma a}$ from measurements of other cross sections such as $\bar{\sigma}_{\gamma n}$, $\bar{\sigma}_{\gamma f}$, $\bar{\sigma}_{\gamma\gamma}$, and $\bar{\sigma}_{\gamma\gamma'}$, various combinations of which dominate $\bar{\sigma}_{\gamma a}$ depending on the nucleus and the energy regime in question.

3.1.1. Measurements above the Neutron Threshold

In nonfissionable heavy nuclei, in the energy range from a few hundred keV above the neutron separation energy to the energy, usually 1–3 MeV higher, where charged particle emission becomes important one has, to a good approximation, $\Gamma_n \gg \Gamma_\gamma$ and hence $\bar{\sigma}_{\gamma a} \simeq \bar{\sigma}_{\gamma n}$. If dominance of dipole radiation is assumed, Eq. (2.5) can then be written

$$\vec{f}_{X1} = \frac{26 \cdot 10^{-8} \bar{\sigma}_{\gamma n}\,(\text{mb})}{g E_\gamma\,(\text{MeV})} \tag{3.1}$$

where it is understood that $\bar{\sigma}_{\gamma n}$ is averaged over all levels of appropriate J and $\vec{f}$ is in MeV^{-3} units.

The photoneutron cross section has been measured for most heavy natural element targets (see photonuclear review (FGC 70). Early measurements (NH 54, FH 56) were made with a broad bremsstrahlung beam and differential analysis was used to extract $\bar{\sigma}_{\gamma n}$ from neutron yields measured with a 4π "Halpern-type" BF_3 counter (GF 67). More recently incident photon beams with energy spreads of 100–200 keV, from positron annihilation in flight (Ful+ 69, Bei+ 69) have resulted in much improved data. Examples of $\bar{\sigma}_{\gamma n}$ data obtained by these methods (FH 62b, Bei+ 69) for targets of ^{206}Pb, ^{208}Pb, and ^{209}Bi are shown in Fig. 2.

In fissionable nuclei above the neutron separation energy the photoabsorption cross section is given to good approximation by

$$\bar{\sigma}_{\gamma a} = \bar{\sigma}_{\gamma n} + \bar{\sigma}_{\gamma f} \tag{3.2}$$

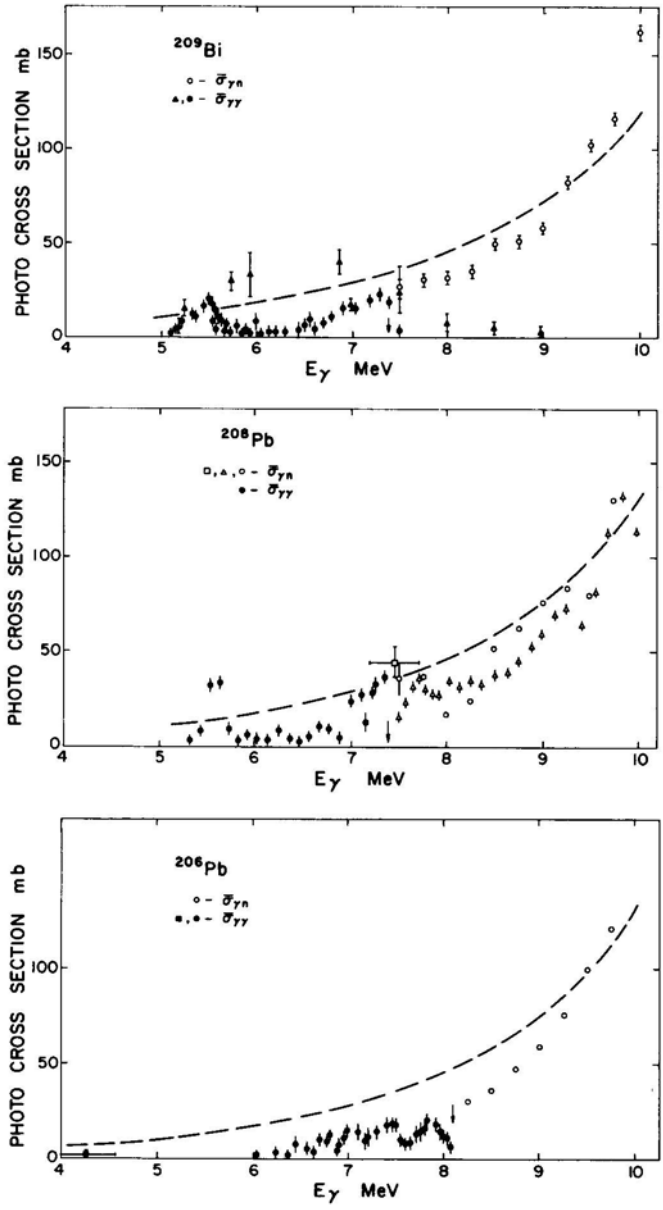

Fig. 2. The photo cross section for Bi and Pb isotopes. The photoneutron cross sections $\bar{\sigma}_{\gamma n}$ of ^{209}Bi, ^{208}Pb, and ^{206}Pb, above the neutron threshold (indicated by the vertical arrow) are indicated by ○ (FH 62b), △ (Bei+ 69) and □ (Bow+ 70). The photoelastic cross sections $\bar{\sigma}_{\gamma\gamma}$ are indicated by ▲ (FH 62a), ■ (Swa 73a), and ● (Axe+ 63) in ^{209}Bi and ^{206}Pb and (KK 67) in ^{208}Pb. The broken line shows the Lorentzian fitted to the giant dipole resonance with constants given in Table V.

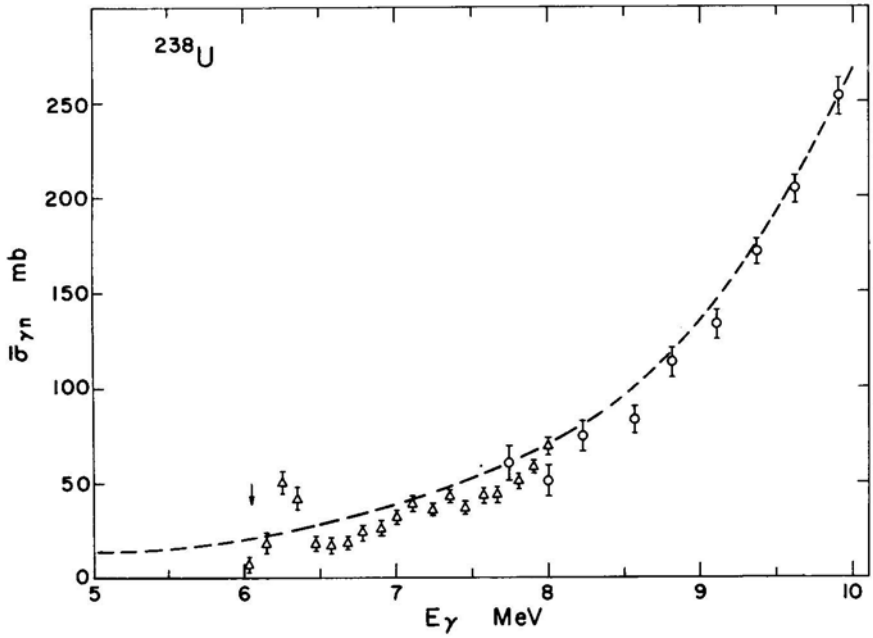

Fig. 3. The photoabsorption cross section $\bar{\sigma}_{\gamma a}$ of ^{238}U from references; Δ, (KM 73) and O, (Ber+ 72). For other details see Fig. 2.

The energy dependence of $\bar{\sigma}_{\gamma a}$ for ^{238}U given in Fig. 3 was obtained from the photoneutron and photofission measurements of Bergère *et al.* (Ber+ 72) and Knowles and Mafra (KM 73) shown by circles and triangles, respectively.

The γ-ray beam used by Knowles and Mafra (KM 73) was produced by the Compton-monochromator facility (KA 66) at Chalk River Nuclear Laboratories. This device provides a variable-energy γ-ray beam between 3 and 8.3 MeV with energy spread of $\sim$2.5%. The source of radiation is an intense line spectrum of maximum energy 8.99 MeV from the ^{58}Ni(n, γ)^{59}Ni reaction produced by a nickel plate located in a region of high flux in a reactor beam tube. Any energy between 3 and 8.3 MeV may be selected by Compton scattering from a wide, curved, aluminum scatter-plate. The geometry is such that γ-radiation impinging on the target, following scattering of a particular source γ-ray from all parts of the scatterer, is monoenergetic and may be varied by changing the position of the target relative to source and scatterer.

In a related high-resolution experiment, (Kno 70) the unscattered nickel γ-rays, Doppler-broadened by thermal motion in source and target

to an effective beam width of 10–18 eV at 5–9 MeV, were allowed to impinge on a ^{238}U target. At energies above about 7 MeV, the level densities in ^{238}U are high enough that more than one $J = 1$ state would be expected to be excited by such a beam, and $\vec{f}$ and fluctuations of $\vec{f}$ could be measured (Kno 70). Below 7 MeV in ^{238}U, and higher energies in lighter nuclei, photoexcitation by a high-resolution beam occurs only through chance overlap between the beam energy and a level energy. Experiments of this type have been most extensively exploited by Israeli workers (Ben+ 66, MSW 70). While they provide useful information on the widths and other parameters of isolated levels they do not provide much information on the average behavior of γ-ray strength functions.

A powerful method of studying photoexcitation with high-resolution detectors in a restricted energy range above the neutron separation energy is the so-called threshold photonuclear technique. In this method, which was first used by Bertozzi *et al.* (BST 63) and later developed by others (BSB 66, JS 71), 5–10 MeV electrons from a linac are used to produce bremsstrahlung which is incident on the target under study. The energy of the electrons is adjusted so that the highest-energy bremsstrahlung just exceeds the (γ, n) threshold and hence only neutron transitions to the ground state of the product nucleus are energetically possible. The neutron energy, determined by time-of-flight techniques, can be found very precisely and resonances in the compound nucleus can therefore be observed with good resolution as peaks in the ground-state neutron spectrum. In measurements on isotopes of lead, Bowman *et al.* (Bow+ 70) and Toohey and Jackson (TJ 72) have studied the shapes and thus the widths of individual resonances from 0 to 1 MeV above the neutron separation energy. The results of Toohey and Jackson (TJ 72) (Fig. 4) are typical of this technique. By the same methods, the average level spacing between resonances can be determined and the spin and parity of the compound nucleus and hence information on the multipolarity of the absorbed radiation can be obtained by measuring the neutron angular distributions. This, then, is a valuable method for studying properties of individual resonances and for obtaining $\vec{f}$ [with the aid of Eq. (2.5)] in a restricted range above the neutron separation energy.

3.1.2. Measurements below the Neutron Threshold

Below the neutron separation energy and fission threshold, $\bar{\sigma}_{\gamma a}$ is given by

$$\bar{\sigma}_{\gamma a} = \bar{\sigma}_{\gamma\gamma} + \sum_{\gamma'} \bar{\sigma}_{\gamma\gamma'} \tag{3.3}$$

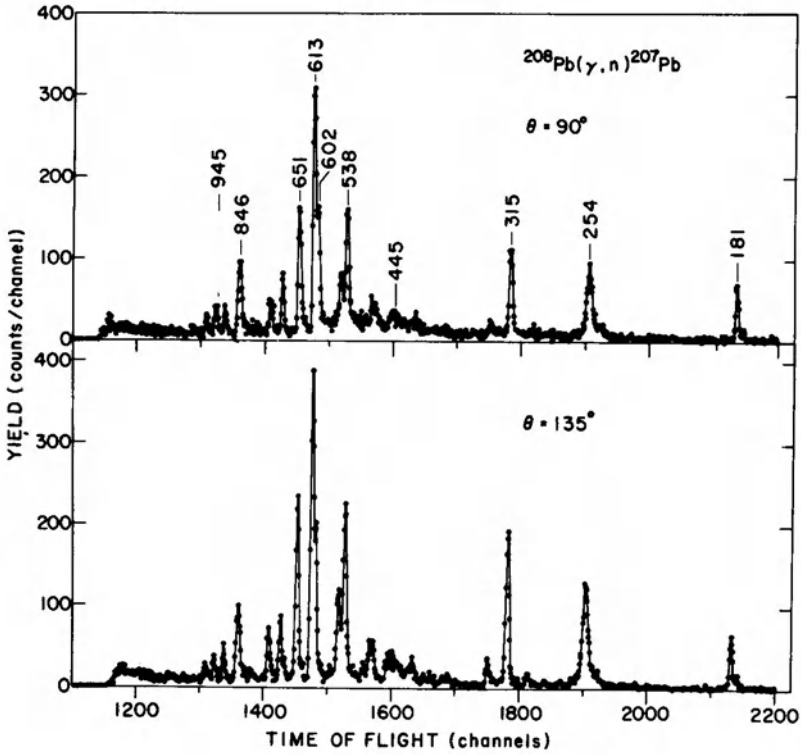

Fig. 4. The threshold photoneutron yield in ^{208}Pb(γ, n)^{207}Pb measured at 90 and 135° (TJ 72) plotted as a function of the neutron time-of-flight. Peaks are labeled with the neutron energy in keV.

and determinations of $\bar{\sigma}_{\gamma a}$ and hence $\vec{f}$ require measurements of the elastics $\bar{\sigma}_{\gamma\gamma}$, and total inelastic scattering cross sections or, alternatively, what in effect amounts to a measurement of $\bar{\sigma}_{\gamma\gamma}$ plus a measurement, or judicious estimate, of the ground-state branching ratio.

For the more common experimental situation in heavy nuclei where the energy spread of the incident γ-ray beam spans many resonances so that the complexity of the inelastic spectrum precludes an accurate measurement of the branching ratio, one may still determine $\vec{f}$ by measuring $\bar{\sigma}_{\gamma\gamma}$ and combining this with an assumed or estimated branching ratio. In the more crude determinations of this kind, the branching ratio has been assumed to be unity but a more realistic value can be derived from the strength function $\overleftarrow{f}$.

The relationship giving $\vec{f}$ in terms of $\bar{\sigma}_{\gamma\gamma}$ and $\overleftarrow{f}$, obtained by combining

Eqs. (2.5), (2.8), (2.9), and (2.11), is

$$\vec{f}^2(E_\gamma) = \frac{78 \cdot 10^{-8}}{SE_\gamma^4} \bar{\sigma}_{\gamma\gamma} \int_0^{E_\gamma} E_{\gamma'}^3 \overleftarrow{f}(E_{\gamma'}) \varrho_0(E_\gamma - E_{\gamma'})\, dE_{\gamma'} \qquad (3.4)$$

where $\bar{\sigma}_{\gamma\gamma}$ is in mb and E_γ is in MeV. In solving for $\vec{f}$ in any particular case, $\overleftarrow{f}$ may be known from γ-decay experiments in the same nucleus or may be adopted from an adjacent nucleus. Alternatively, $\vec{f}$ can be substituted for $\overleftarrow{f}$, assuming the Brink hypothesis; Eq. (3.4) then becomes an integral equation solvable for $\vec{f}$. If $\bar{\sigma}_{\gamma\gamma}$ is not known below a certain energy, $E_{\min}$, Eq. (3.4) can still be solved above that energy provided some estimate of $\overleftarrow{f}$ below $E_{\min}$ is available.

Experiments giving information on $\vec{f}$ below the neutron threshold are listed in Table II. Of these, those using recoil broadening of 7-MeV γ-rays from the $^{19}F(p, \alpha\gamma)^{16}O$ reaction (RM 60, Swa 73b, and Hui+ 62) give values of the strength function at isolated γ-ray energies only. The other three methods yield the elastic scattering cross section over a range of E_γ from which, in principle, one can determine $\vec{f}$ with the aid of Eq. (3.4).

One of the more powerful tools for this type of measurement is the bremsstrahlung monochromator (OTA 62) used by Axel *et al.* (Axe+ 63, AMS 70). In this instrument electrons from a betatron are incident on a thin copper foil in which they produce bremsstrahlung with wide energy spread but limited to a narrow forward cone. This beam is directed at the target. Photons in a narrow energy band of the bremsstrahlung spectrum are tagged by observing coincidences between γ-radiation scattered from the target and electrons from the copper foil selected by a wide-angle magnetic spectrometer. The energy resolution of the spectrometer and hence also of the tagged bremsstrahlung radiation is about 100 keV. This device has been used to measure the elastic scattering cross sections of natural lead, radiolead, bismuth, tin, and zirconium (Axe+ 63, AMS 70).

Another effective instrument for subthreshold γ-ray scattering measurements is the Compton monochromator (KA 66) described in Sec. 3.1.1. This facility has been used for elastic scattering measurements on targets of ^{197}Au, ^{205}Tl, natural lead, radiolead (88% ^{206}Pb, 9% ^{207}Pb, 3% ^{208}Pb) and lead enriched to 78% in ^{208}Pb and for self-absorption measurements on natural and radiolead. The scattered radiation is conveniently measured with a NaI detector but measurements are also possible with large volume Ge(Li) detectors. Similar measurements of elastic scattering and self-absorption are in progress at Saclay (Luc+ 72).

Elastic scattering cross sections for ^{206}Pb, ^{208}Pb, and ^{209}Bi, shown by solid points in Fig. 2, are examples of the data that can be obtained by these

TABLE II

Photoexcitation Experiments Below the Neutron Separation Energy

Geometry	Energy range, MeV	Resolution keV	Detector	Target		References
				Scattering	Self-absorption	
1) Recoil broadening	6–7	130	NaI(Tl)	31 elements	5 elements	(RM 60)
	6–7	6.8	Ge(Li)	^{207,208}Pb, ^{209}Bi		(Swa 73b)
	6–7	130	Ge(Li)	^{232}Th, $^{233-238}$U, ^{237}Np		(Hui+ 62)
2) Bremsstrahlung differential analysis	6–20	10%	NaI(Tl)	^{206,207,208}Pb	^{206,207,208}Pb, ^{209}Bi	(FH 62a)
	3–5	6.8	Ge(Li)	^{206,207,208}Pb, ^{209}Bi		(Swa 73a)
3) Bremsstrahlung monochromator	5–19	100	NaI(Tl)	^{90}Zr, Nat-Sn, Nat-Pb, Radio-Pb, ^{209}Bi		(AMS 70) (Axe+ 63)
4) Compton monochromator	3–8.3	200	NaI(Tl)	^{205}Tl, ^{197}Au, Radio-Pb	Nat-Pb	(Ear+ 73) (KK 67, Bar 69)
		6.4	Ge(Li)	Nat-Pb		(KK 73)
		20	Ge(Li)		Nat-Pb, ^{208}Pb	(Luc+ 72)

variable-energy methods (Axe+ 63, KK 67, FH 62b, Swa 73a). In ^{206}Pb and ^{209}Bi, and to a lesser extent in ^{208}Pb, the level densities are sufficiently high that several levels λ are included within the monochromator-beam energy spread. However, application of Eq. (3.4) to deduce $\vec{f}$, even in ^{206}Pb and ^{209}Bi, is scarcely warranted because, for nuclides this close to the ^{208}Pb closed shell, $\vec{f}$, $\varrho(E_\gamma - E_{\gamma'})$, and S (Eq. 3.4) cannot be relied upon to give representative statistical averages. Therefore, strength functions corresponding to $\bar{\sigma}_{\gamma\gamma}$ measurements have been extracted only in the special cases where branching ratios and level densities are also obtained directly from the measurements. In particular Swann's (Swa 73a) measurements with a broad-incident-beam, high-resolution-detector technique permit crude estimates of the strength function at low energies in ^{206}Pb. By observing inelastic and elastic scattering from individual resonances and making angular distribution measurements, he was able to deduce the width of the ground-state transitions and the multipole type. From his results for several neighboring resonances, we have obtained rough values for $\bar{\Gamma}^J_{\gamma 0\lambda}$ and $\varrho_J(E_\lambda)$, and hence $\vec{f}$ using Eq. (2.1). Similar estimates of $\vec{f}$ were made for the peak cross sections, $\sigma_{\gamma\gamma}$, in ^{208}Pb at 5.5 and 7.3 MeV (Fig. 2) for which the branching ratios are known (KK 73) to be unity. The results are shown in Fig. 15.

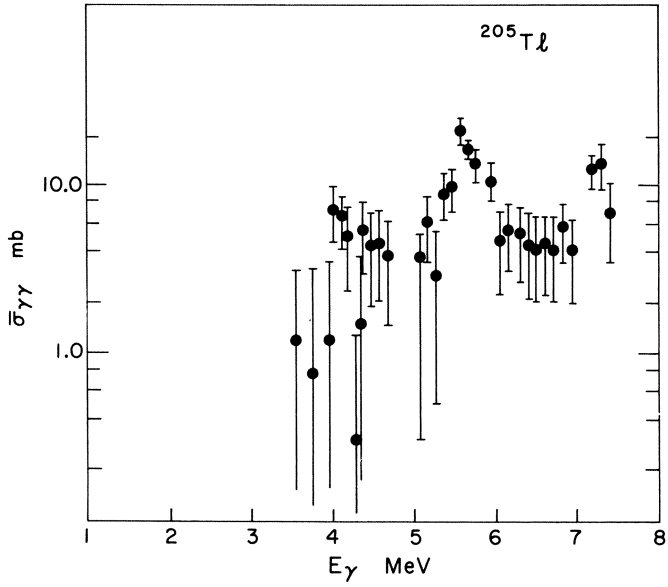

Fig. 5. The elastic scattering cross section $\bar{\sigma}_{\gamma\gamma}$ of ^{205}Tl (Ear+ 73).

In ^{205}Tl rather better statistical behavior of the levels is found and for this nuclide the elastic scattering cross section (Fig. 5) has been used (Ear+ 73) to obtain $\vec{f}$ with the aid of Eq. (3.4). Because the cross section is unknown below 3.5 MeV, values of $\vec{f}$ for that region were taken to be the same as those of ^{204}Tl. The final curve for $\vec{f}$ is shown in Sec. 4.1, Fig. 16. A similar procedure is used to obtain $\vec{f}$ for ^{197}Au (Fig. 18).

3.1.3. Photoexcitation Measurements Giving $\vec{f}$

Gamma-decay strength functions $\vec{f}$ may be obtained from spectral distributions of the inelastically scattered γ-radiation (MW 69). The information obtained from such reactions is similar to that obtained from neutron-capture γ-ray spectra. Individual γ-ray k-values (Sec. 1) can be deduced and $\vec{f}$ can in principle be extracted by the spectrum fitting method discussed in the next section. Although this method has not been widely applied, the information obtained is complementary to that obtained by (n, γ) reactions since stable nuclei are not always accessible through the (n, γ) reaction.

3.2. Spectrum Fitting Method

The γ-ray strength function $\vec{f}$ may be obtained by calculating the shape of the spectral distribution with different trial strength functions until good agreement is achieved with the observed shape (Lon 73). This is the only approach that can be used to deduce $\vec{f}$ from γ-ray spectra for which no information is available enabling the primary spectrum to be separated from the secondary and subsequent radiations. Different versions of this method have been used earlier by several groups (e.g., GDP 60, Tro 61, Sta 64, Brz+ 71). In heavier nuclei the high-energy part of the γ-ray spectrum from the decay of levels excited by s- and p-wave neutron capture is dominated by $E1$ and $M1$ radiation (Secs. 3.4, 4.2.2). We therefore make the simplifying assumption that only dipole γ-emission is important at all energies. However, no attempt is made to separate $\vec{f}_{E1}$ and $\vec{f}_{M1}$ and the empirical strength function deduced is thus a mixture of both. For the sake of brevity the XL subscript will henceforth be dropped. This assumption, that all radiation is of dipole type, probably leads to serious errors in the deduced strength function at low energies in some nuclei, e.g., in the collective region, in which the predominant mode of decay between low-lying excited states is quadrupole radiation. However, a correction for higher multipole decay would be difficult to formulate in most cases because of ignorance of the

level-structure and γ-decay details above all but the lowest few states. Because of these uncertainties, energies below $\sim$2 MeV are ignored in comparing observed and fitted spectral distributions.

3.2.1. Derivation

The strength function $\overleftarrow{f}$ is related to the absolute average primary γ-ray spectral distribution per unit population, $\nu_{i\lambda}(E_\gamma)$, as discussed in Sec. 2.3 by

$$\nu_{i\lambda}(E_\gamma)\,\Delta E_\gamma = 3\,\frac{E_\gamma{}^3\overleftarrow{f}(E_\gamma)\varrho_0(E_\lambda - E_\gamma)\,\Delta E_\gamma}{\bar{\Gamma}_{\gamma T\lambda}\,\varrho_0(E_\lambda)} \tag{3.5}$$

where, for simplicity, we assume a constant spin-cutoff parameter and that the functional form of $\overleftarrow{f}$ is independent of E_λ and J. The average total radiative width is usually known for the resonance region just above the neutron threshold and substituting this in Eq. (3.5) one obtains $\overleftarrow{f}$ in absolute units provided $\nu_{i\lambda}$ is in absolute units. For excitation regions where $\Gamma_{\gamma T\lambda}$ is not known, it may be calculated from the expression

$$\Gamma_{\gamma T\lambda} = 3\int_0^{E_\lambda} \overleftarrow{f}(E_\gamma)E_\gamma{}^3\,\frac{\varrho_0(E_\lambda - E_\gamma)}{\varrho_0(E_\lambda)}\,dE_\gamma \tag{3.6}$$

To calculate the γ-ray spectral distributions one divides the region between the ground state and the initial excitation energy, E_λ, into n intervals, each of width ΔE. Let P_m be the population probability of interval m at excitation $E_m = m\Delta E$. Then

$$P_m = \int_{E_m}^{E_\lambda} \nu_{m\mu}(E_\mu - E_m)P_\mu\,dE_\mu \tag{3.7}$$

For unit initial population ($P_\lambda = 1$), the total spectral distribution, $\nu_{t\lambda}(E_\gamma)$, of primary plus secondary and subsequent γ-rays from an initial excitation E_λ is

$$\nu_{t\lambda}(E_\gamma = E_m - E_i)\,\Delta E_\gamma = \Delta E_\gamma \int_0^{E_\lambda - E_\gamma} \nu_{im}(E_m - E_i)P_m\,dE_i \tag{3.8}$$

Within the framework of these calculations, a strength function which gives agreement between the observed and calculated $\nu_{t\lambda}(E_\gamma)$ is selected by trial. Uncertainties in the assumed level-density distributions and in the observed spectral distributions provide the main sources of uncertainty in the $\overleftarrow{f}$ deduced. We now discuss these in more detail.

3.2.2. Level-Density Distributions

Information on the energy dependence of the level-density distributions needed for these calculations must be obtained from other sources. Inadequacies of available level-density expressions were discussed in Sec. 2.3. In the absence of a universally reliable prescription for the energy dependence, it is necessary to make use of the available empirical data for each nucleus of interest. Immediately above the neutron threshold, level densities, for a few spins only, are known from neutron resonance spectroscopy. Up to 1–2 MeV above the ground state, level densities are known from (n, γ) and charged-particle reactions. In particular, spectrum average techniques used in (n, γ) spectroscopy (Sec. 3.4) are valuable in revealing all final states that can be fed by dipole transitions from the resonances (usually s-wave) excited. Between these two regions the level-density distributions must be obtained by a suitable interpolation.

3.2.3. Observed Spectral Distributions

Spectral distributions are obtained by unfolding the detector response function from the observed γ-ray spectra. This procedure introduces errors due to uncertainties in the response function and cumulative errors from repeated unfolding operations. In general, the magnitudes of these errors are difficult to assess. The spectra measured with magnetic Compton, magnetic pair, and NaI spectrometers are suitable for obtaining spectral distributions, because their response functions are fairly well known and, for the magnetic spectrometers, of simple, near-Gaussian shape. From spectra obtained with these instruments one obtains the complete γ-spectral distributions $\nu_{i\lambda}(E_\gamma)$ over the energy range covered. High-resolution Ge(Li) single-detector data, on the other hand, yield information on the resolved γ-rays only. Because of the form of the Ge(Li) detector response function (large Compton distribution with sharp total absorption and pair peaks), unfolding of a spectrum to extract unresolved γ-ray intensity is impractical. This difficulty is overcome if one uses a Ge(Li)–NaI coincidence arrangement in Compton-suppression or pair spectrometer modes (Ras+ 70).

The uncertainty in $\nu_{i\lambda}(E_\gamma)$ due to the Porter–Thomas fluctuations (PT 56) is

$$\Delta\nu_{i\lambda}(E_\gamma) = \nu_{i\lambda}(E_\gamma)\sqrt{2/m} \tag{3.9}$$

where m is the number of transitions in the γ-ray energy interval. In spectra from nuclei near closed shells, particularly in even–even or even–odd nuclei, there are, often, only a few primary transitions within 2–3 MeV of the upper

limit. Thus γ-ray spectra from the decay of individual excited levels at E_λ, as obtained for example in thermal neutron capture, provide $\nu_{i\lambda}(E_\gamma)$ with large errors $\Delta\nu_{i\lambda}(E_\gamma)$ for E_γ near E_λ. However, for several nuclei better average intensities are available at high energies from resonance-averaged neutron capture γ-ray measurements (Sec. 3.4). At lower γ-ray energies, at least in heavier nuclei, there are many transitions ($\sim$40 MeV^{-1} at $\sim$5 MeV in Au) and the uncertainty in $\nu_{i\lambda}(E_\gamma)$ from Porter–Thomas fluctuations is reduced.

3.2.4. Results

Thermal neutron-capture γ-ray spectra (Gro+ 69) measured with a magnetic Compton spectrometer by Groshev *et al.* (Gro+ 58) and magnetic pair spectrometer by Bartholomew and Kinsey (BK 53) were used by Lone (Lon 73) to deduce strength function for several elements. In order to

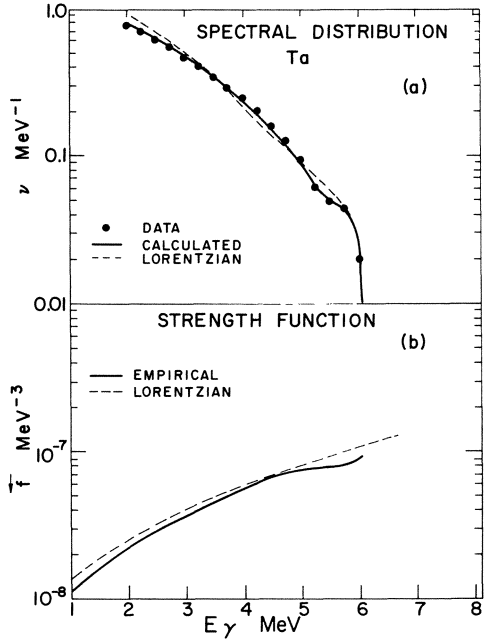

Fig. 6. Comparison of calculated and observed spectral distributions ν and $\tilde{f}$ for Ta. The points in (a) show the observed spectral distribution following thermal neutron capture (Gro+ 69) smoothed to remove fine-structure. The spectral distributions shown by the solid and broken curves were calculated from the empirical and Lorentzian strength functions, respectively, (b) with giant dipole resonance and level-density parameters given in Tables V and VI.

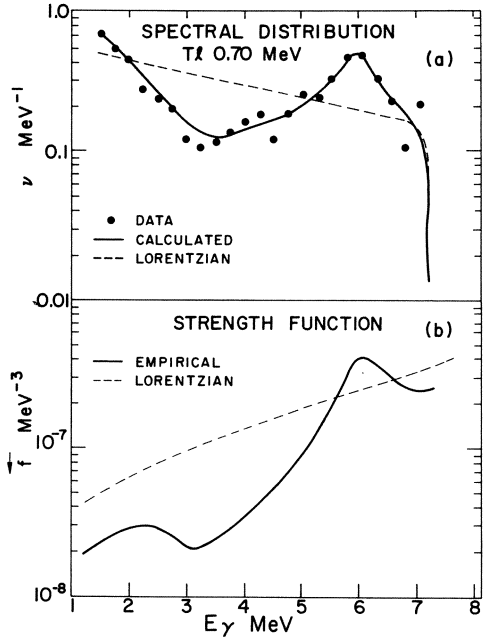

Fig. 7. Comparison of calculated and observed ν and $\bar{f}$ for Tl. The points in (a) show the observed spectral distribution (Ear+ 72b) following 0.7-MeV neutron capture in natural Tl. For other details see Fig. 6.

reduce Porter–Thomas fluctuations, the data were first smoothed by averaging over the γ-ray fine-structure and, for even–even and odd–even nuclei, the intensity information in the high-energy part of the spectrum was augmented by resonance neutron-capture data. For excitation energies above a lower limit E_t (approximately equal to the pairing energy gap) the constant temperature formula, Eq. (2.14), was used for spin-zero level-density distributions. The constants A and T were determined empirically from the known level densities at the neutron threshold and in the region 1–2 MeV above the ground state. Below E_t the known levels were adopted explicitly with their appropriate spins and parities. A similar analysis was also done for the fast-neutron-capture data of Earle *et al.* (Ear+ 72b).

A typical fit to the Ta thermal capture γ-ray spectrum is shown in Fig. 6a. The points give the smoothed measured spectrum (Gro+ 69). The broken and the solid curves are the fits obtained by using the strength function deduced from the giant dipole Lorentzian tail and by the spectrum fitting method, respectively. These strength functions are plotted in Fig. 6b. As a second example, in Fig. 7a, the points give the spectral distribution

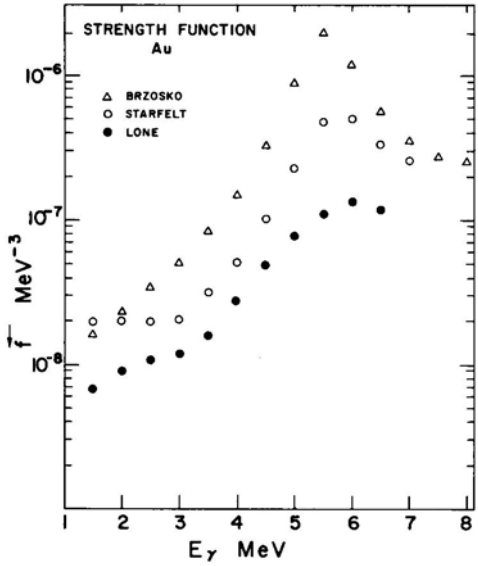

Fig. 8. A comparison of strength functions for Au based on the same spectral distribution showing the sensitivity to level-density parameters. Strength functions extracted with the constant temperature level-density formula with $T = 0.753$ and 0.6 MeV and with the Gilbert and Cameron formula (GC 65) are shown by solid circles (Lon 73), open circles (Sta 64) and triangles (Brz+ 71), respectively.

from 700-keV neutron capture in Tl (Ear+ 72b). The broken and solid curves show the spectra calculated with $\overleftarrow{f}$ obtained from the tail of the giant dipole resonance and with a trial $\overleftarrow{f}$, respectively. These strength functions are shown in Fig. 7b.

Starfelt (Sta 64) and Brzosko *et al.* (Brz+ 71) also used the spectrum fitting method to investigate $\overleftarrow{f}$ in medium weight and heavier nuclei. Both used a strength function of the form

$$\overleftarrow{f}(E_\gamma) \propto \left[\frac{\Gamma_1 e^{-a(E_\gamma - E_1)}}{E_1[(E_\gamma - E_1)^2 + \frac{1}{4}\Gamma_1^2]} + b\,\frac{\Gamma_2 e^{-a(E_\gamma - E_2)}}{E_2[(E_\gamma - E_2)^2 + \frac{1}{4}\Gamma_2^2]} \right] \quad (3.10)$$

where the first term is the expression proposed by Lane and Lynn (LL 60) for the giant dipole resonance, and the second term represents a superimposed pigmy resonance ($E_2 \sim 6$ MeV) whose strength is adjusted to give the observed spectral distribution and total radiation width. Starfelt imposes the further constraint that $\overleftarrow{f}$ be constant below 3 MeV. The strength functions for Au deduced by Lone (Lon 73), Starfelt (BS 70a) and Brzosko *et al.* (Brz+ 71) are shown in Fig. 8. The serious disagreement between these

deduced strength functions, particularly in absolute magnitude at ~6 MeV, is primarily due to the assumed level-density distributions. Starfelt used a constant temperature expression with $T = 0.6$ MeV. Brzosko *et al.* adopted the Gilbert and Cameron (GC 65) expression and parameters. In our recent evaluation (Lon 73), both of these distributions were found to be inadequate for predicting both the resonance level densities (Gol+ 66) and the density of levels below 2 MeV (Gro+ 69, LBT 72). Instead a constant temperature expression with $T = 0.753$ MeV which gives good agreement with these level densities was adopted.

3.3. Sequential Extraction Method

The separation of the primary spectrum from the total decay spectrum can be effected if the spectral distributions of secondary and all subsequent decay radiations are known. In the sequential extraction method, one begins with measured total spectra from each of a complete set of contiguous intervals in excitation energy populated in some experiments as illustrated in Fig. 9. By a procedure described in detail in an earlier paper (Bar+ 70) it is possible, for any interval λ, knowing the detector response function, to construct from the spectra of all lower intervals i the distribution of all secondary and subsequent decay radiation, and hence to unfold the primary

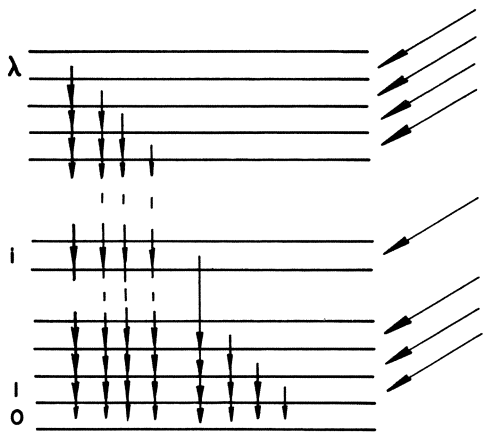

Fig. 9. Schematic showing population and γ-decay of levels in particle reactions. Each interval corresponds to an energy window applied to the coincident particle spectrum. From experiments in which the γ-rays in coincidence with each particle window are recorded, the γ-decay from each interval, comprising primary and all subsequent transitions, are known. From these data, knowing the detector response function, one can solve for the primary spectrum from each interval in sequence, beginning at the lowest.

spectrum $\nu_{i\lambda X1}(E_\gamma)$ for interval λ. It is assumed as in Sec. 3.2, that the cascade involves dipole transitions only. The primary spectrum so obtained can then be used in the same way to unfold the primary spectrum of interval $\lambda + 1$, and so on. It is a fundamental assumption of the method that the branching ratios for γ-decay from any excitation interval to lower intervals are independent of how the upper interval was populated. This implies the assumption that, on the average, the same distribution in the population of individual levels in each interval is obtained regardless of the mode of excitation or that, if these microscopic populations differ with the mode of excitation then, on the average, the branching ratios are independent of J or of other parameters distinguishing the levels. Once the individual primary spectra are available they can be used to deduce a relative strength function $\overleftarrow{f}_{X1}(E_\gamma)/\bar{\Gamma}_{\gamma T\lambda}$ with the aid of Eq. (2.13) and available level-density information. If $\bar{\Gamma}_{\gamma T\lambda}$ is known for any interval, as, for example, when E_λ overlaps the region of known resonances near the threshold, then the absolute value of $\overleftarrow{f}$ can be determined for the region $0 < E_\gamma < E_\lambda$.

The above procedure was followed in analyzing spectra from the ^{197}Au$(d, p\gamma)^{198}$Au and ^{181}Ta$(d, p\gamma)^{182}$Ta reactions at $E_d = 12$ MeV (Bar+ 70). The spectra were measured in coincidence with protons with energies falling within 24 contiguous windows, each 240 keV wide, corresponding to excitation intervals in the product nucleus between 0.8 MeV and the neutron separation energy. Relative strength functions from a selection of primary spectra obtained from the analysis are shown in Fig. 10. Within uncertainties introduced by finite counting statistics and the use of finite

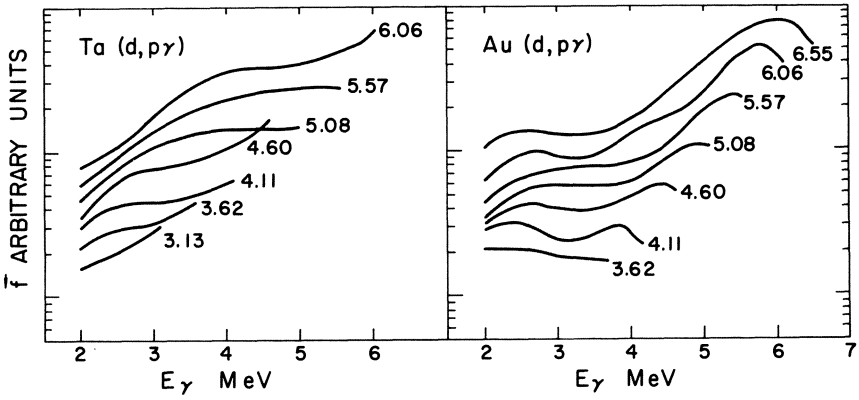

Fig. 10. Relative strength functions $\overleftarrow{f}_{i\lambda}$ for Ta and Au. The curves were obtained by the sequential extraction method from γ-ray spectra measured in the Ta$(d, p\gamma)$ and Au$(d, p\gamma)$ reactions (Bar+ 70). The numbers on the curves give E_λ in MeV.

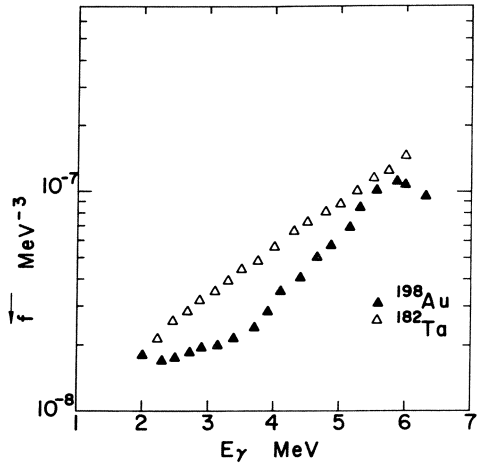

Fig. 11. Absolute strength functions for Au and Ta derived by the sequential extraction method from $(d, p\gamma)$ reactions in Au and Ta (Bar+ 70).

energy intervals in the analysis, these and all other strength functions obtained in the calculation have common functional forms for each target. The $\bar{f}$ obtained by normalizing and averaging these strength functions evaluated absolutely for the interval at the neutron threshold with the aid of Eq. (2.13) and with $\bar{\Gamma}_{\gamma T\lambda}$ and $\varrho(E_\lambda)$ estimated as in Sec. 3.2, are shown in Fig. 11.

The sequential extraction method has the distinct advantage of providing a complete strength function $\bar{f}$ to low energies by an unambiguous analytical procedure. However, the validity of the assumption that the branching ratios for decay from any interval are independent of the mode by which it was populated is open to some doubt and the justification of the method lies largely in its internal consistency and the agreement achieved with other methods. The internal consistency achieved in the application to the $(d, p\gamma)$ reaction (Bar+ 70) seems satisfactory as is the agreement between the results of this and other methods as shown in Sec. 4.1. It should be noted, however, that the distributions in J_i of levels in interval i when fed by γ-ray cascade cannot be greatly different from that when the interval is fed directly in the (d, p) reaction because only a small range of angular momentum transfers (the most probable l_n is $\sim$3) can occur at $E_d = 12$ MeV, and only one or two cascade steps are sufficient to account for most of the decay from any interval to the ground state. Therefore the assumption of independence of branching ratios on the mode by which the interval was populated seems plausible enough in this application. However, as

discussed in Sec. 4.2.3 when the same excitation interval is populated by different reactions, e.g., $(d, p)E_d = 12$ MeV and $(p, p')E_p = 18$ MeV, large differences in J-distributions, and possibly in other parameters, can result in significantly different spectral distributions.

The conclusion that the strength function $\overleftarrow{f}_{i\lambda}$ derived for each excitation interval λ are the same except for an unknown normalizing factor is important in the support it provides for the Brink hypothesis. But, as discussed in Sec. 2.2, it is not sufficient to establish its validity. For a complete test of the hypothesis it is necessary to establish that this common functional form of the $\overleftarrow{f}_{i\lambda}$ is also consistent with that of $\overrightarrow{f}_{0\lambda}$. This compatibility has not yet been checked in the same nucleus but partial tests will be discussed in Sec. 5.2.

3.4. High-Resolution Gamma-Ray Method

A fourth method of studying the γ-ray strength function involves detection of the individual high-energy primary γ-rays by high-resolution γ-ray spectroscopy with Porter–Thomas fluctuations reduced or eliminated by averaging the γ-ray intensities over many neighboring resonances. The observed average intensity for transitions, E_γ, to a particular final state i must be calibrated in absolute units (photons per initial excitation), whence the average partial radiation width, $\overline{\Gamma}_{\gamma i\lambda}$, can be found if the total radiation width is known. The strength function $\overleftarrow{f}_{i\lambda}$ at the energy E_γ then follows from Eq. (2.2). The method has so far been applied mostly to neutron-capture γ-ray spectra but it can also be applied to other reactions. The measurements of elastically and inelastically scattered γ-rays with good detector resolution (Swa 73a, KK 73) discussed in Sec. 3.1 fall into this class.

Two techniques can be employed to obtain the averaged spectra: (a) by measuring the γ-spectra with a Ge(Li) detector from many individual resonances selected by a high-resolution neutron time-of-flight spectrometer and then averaging over resonances the intensity for each γ-ray (Sam+ 68, Was+ 68, LEB 70), and (b) by measuring the average γ-ray spectra (All 68, BT 70) following bombardment with neutrons with energy spread large enough to span many resonances but small enough to avoid serious smearing of the γ-ray resolution. In the former method, absolute calibrations are made on the γ-rays prior to averaging while in the latter an absolute calibration is made on the observed average intensity. We shall call these (a) the high neutron resolution (HNR) and (b) the low neutron resolution (LNR) spectrum average techniques, respectively.

It should be noted that the averages obtained by the two methods are not necessarily the same. In the HNR method all individual intensities are weighted equally and $\bar{\Gamma}_{\gamma i\lambda}$ is obtained directly while in the LNR method (BT 70) the determination of $\bar{\Gamma}_{\gamma i\lambda}$ from the average intensity is, or may be, complicated. For a thin target the average intensity is proportional to $\overline{\Gamma_{n\lambda}\Gamma_{\gamma i\lambda}}$ which is related to $\bar{\Gamma}_{\gamma i\lambda}$ by

$$\overline{\Gamma_{n\lambda}\Gamma_{\gamma i\lambda}} = S\bar{\Gamma}_{n\lambda}\bar{\Gamma}_{\gamma i\lambda} \tag{3.11}$$

where S is the fluctuation factor discussed in Sec. 2.2. For a thick target, a more complex relationship applies (BT 70). In Eq. (3.11), if $\Gamma_{n\lambda}$ and $\Gamma_{\gamma i\lambda}$ are not correlated, one has $S = 1$ and the average absolute intensity is the same as for the HNR method. If, however, the widths are correlated, and assuming $\Gamma_{n\lambda}$ conforms to the Porter–Thomas distribution, S can have any value $1 < S \leq 3$ depending on the degree of correlation, and the average absolute intensity obtained by this method then exceeds that from the HNR method. There would appear now to be no strong evidence for $(\Gamma_{n\lambda}, \Gamma_{\gamma i\lambda})$ correlations in heavy elements (Chr 72). While future investigations may show that some correlating effects are definitely present, it will be assumed in this review that they are small and therefore that the average absolute intensities and hence the strength functions obtained by the HNR and LNR techniques are equivalent.

The HNR technique has the advantage that resonance capture effects can be cleanly separated from direct capture and other nonresonant background but it has the disadvantage that in most attempts to use it to date it has not been possible, because of limitations imposed by neutron intensity, to include enough resonances in the average to remove all Porter–Thomas fluctuations. At the present state of development of these techniques, better smoothing of fluctuations can be achieved with the LNR method, but that method is also limited to regions where level densities are high enough to provide a good statistical sample within the energy spread of the bombarding neutrons. In either method, additional smoothing of Porter–Thomas fluctuations can be achieved by extending the average over several neighboring γ-rays and ascribing the strength so obtained to the mean E_γ.

The HNR technique has been applied to many nuclei (see examples in Table III). In nuclides where final state spins and parities are already known, $E1$ and $M1$ γ-rays can be identified and information on the corresponding strength function obtained. Where the $J\pi$ are not known, it has been possible only to establish the distribution of intensities for "dipole" radiation. High-resolution, HNR, data are used to establish reliable intensity averages and estimates of the energy dependence of the relative

TABLE III

Relative Strength Functions from High-Resolution γ-Ray Methods

For each residual nucleus in the first column the energy range covered in the experiment and the number of γ-rays of $E1$, $M1$, or $E2$ type are shown in the next three columns. In the fifth column a smooth energy dependence is indicated by "Lorentzian" or n in E_γ^n and a peak structure by giving the energy of the peak in MeV. In the sixth column the technique, low neutron resolution (LNR) or high neutron resolution (HNR), is indicated and for the latter the number of resonances in the average are shown in brackets.

Residual nucleus	E_γ range, MeV	Multipole	No. of transitions	Energy dependence, n, or peak energy, MeV	Technique	Reference
^{239}U	3.3–4.1	$E1$	13	3.7	HNR(9)	(BT 72)
		$M1$	9	3.7		
	3.0–4.0	$E1$	9	3	HNR(23)	(Was+ 71)
	3.6–4.7	$M1$	4	3		
	4.0–4.8	$E2$	4	3		
^{206}Tl	4.5–6.5	$E1$	12	Peak ~5.5	HNR(2)	(Ear+ 72b)
	4.0–6.5	$M1(E2)$	12	Peak ~6		
^{198}Au	5.1–6.5	$E1$	79	5	LNR	(LBT 72)
		$M1$	3	5		
	4.78–6.51		97	Peak ~6	HNR(9)	(Was+ 68)
^{196}Pt	6.2–8.0	$E1$	8	Lorentzian	HNR(10)	(BT 67)
	6.0–8.0	$E1$	9	5	HNR(22)	(Sam+ 68)
^{182}Ta	4.8–6.0	$E1$	44	5	LNR	(HGR 71)
		$M1$	10	5		
		$E1$		5	LNR	(LBT 72)
			50		HNR(10)	(Was+ 69)
^{176}Lu	5.05–6.05		37		HNR(15)	(WC 70)

^{166}Ho	5.4–6.2	$E1$	22	Lorentzian	LNR	(BT 70)
	5.7–6.1	$E1$	9	7.2		
	5.7–6.2	$M1$	8	5		
^{158}Gd	5.6–7.9	$E1$	18	Lorentzian	LNR	(BT 70)
	6.1–7.0	$M1$	4	3		
^{156}Gd	6.25–8.5	$E1$	20	7.5		
	6.25–7.4	$M1$	7	3		
^{153}Sm	4.0–6.0	$E1$	24	7	LNR	(Smi+ 72)
		$M1$	13	5		
		$E2$	18	5		
^{151}Sm	4.0–6.0	$E1$	21	7		
		$M1$	16	5		
		$E2$	11	5		
^{150}Sm	5.4–7.7	$E1$	31	5	LNR	(BS 70b)
	5.6–7.0	$M1$	12	5		
^{148}Sm	5.5–7.6	$E1$	23	5		
	6.7–7.0	$M1$	4	5		
^{124}Sb	4.75–6.5	$E1$	14	5	HNR(4)	(LP 71)
		$M1$	17	3		
^{122}Sb	5.0–6.8	$E1$	11	5	HNR(12)	(LP 71)
		$M1$	15	3		
^{119,121}Sn	6.5–9.3	$M1$	12	Peak ~8.5	LNR	(BL 70)
^{116}In	5.5–6.6	$E1$	15	3	HNR(31)	(Ste+ 72)
		$M1$	12	Peak $E_\gamma \leq 5.5$		
^{106}Pd	6.5–7.5	$E1$	9	5	LNR	(BT 70)
	6.8–9.0	$M1$	14	Peak ~7.7		
^{104}Rh	4.1–7.0		145	3, Peak ~6	HNR(7)	(Rim+ 70)

intensity at the high-energy end of capture γ-ray spectral distributions for strength function determinations by the spectrum fitting method (Sec. 3.2). These data are separately identified in the strength functions plotted in Sec. 4.1.

The LNR technique has been developed and exploited most vigorously by the Argonne group (BT 70). In their technique the sample under study is surrounded by ^{10}B and placed in a region of high flux near the reactor core. The ^{10}B absorbs the thermal neutrons so that the neutron spectrum reaching the sample consists of the epithermal component which has a $1/E$ energy dependence. The neutron flux in the $1/E$ tail is such that resonance capture can be observed for s-wave and some p-wave resonances; there is no sharp cutoff but the effective energy spread of the neutrons responsible for most of the captures is about 2 keV beginning at thermal energies. This energy spread is sufficient to include a large number of resonances in most heavy elements of interest. By close examination of the γ-ray line-shape, which is broadened by the neutron energy spread, it is possible to establish whether or not a particular high-energy γ-ray is

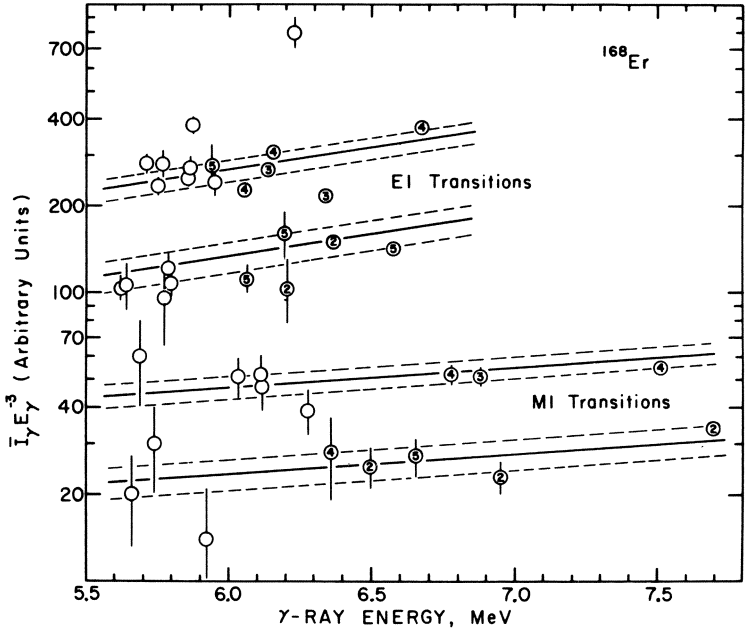

Fig. 12. Average reduced γ-ray intensities in ^{168}Er obtained by the low-neutron-resolution technique (BT 70). The upper two curves are for $E1$ γ-rays, the lower two for $M1$ γ-rays. Known final-state spins are shown in the circles. The estimated limits of uncertainty from Porter–Thomas fluctuations are shown by the broken lines.

emitted in a primary transition. Bollinger and Thomas (BT 70) have shown that the technique is useful in determining the multipolarity of the γ-rays and is also sensitive to the spins of the final states, specifically whether the final state spin J_i is $J_0 \pm \frac{1}{2}$ or $J_0 \pm \frac{3}{2}$, where J_0 is the target spin. The latter effect follows simply from counting the number of transition paths by which states of a particular J_i can be reached by primary transitions of a given multipolarity from the resonances excited by s-wave capture. Figure 12 for ^{168}Er (taken from BT 70) illustrates the quality of the results obtained with this technique. The figure shows the partial separation of γ-rays according to final state spins, 3 and 4 or 5 and 2 (the alternatives available for dipole transitions following s-wave capture on a $J_0 = \frac{7}{2}$ target), and according to γ-ray multipolarity. At energies below about 5.8 MeV in this target the energy resolution is not sufficient to resolve all γ-rays and the clear separation into bands disappears. Similar data have been obtained for a large number of other nuclei as shown in Table III.

Most published distributions such as Fig. 12 provide only relative strength function information, but with suitable calibration they can be compared with absolute strength function data or with the prediction of the Lorentzian shape (Bol 68). Absolute calibrations can be obtained by normalizing the total average intensity for several high-energy lines to the average for lines in the thermal-capture spectrum for which an absolute calibration is available. The validity of this procedure has been justified by Bollinger (BT 72).

The LNR technique has also been used by Allen and Bird (AB 68) to study the energy dependence of the γ-ray strength function in gold. In this work the broad neutron beam, extending between 10- and 60-keV neutron energy, is obtained from the Li(p, n) reaction by a time-of-flight technique. Although this type of neutron source provides some flexibility in the energy and width of the neutron beam available, it suffers from low beam intensity and from neutron background problems.

A promising technique for LNR average resonance measurements employs reactor neutrons filtered with a scandium filter (SM 68) or iron filter (CWG 73). The scandium device provides an external neutron beam with 800 eV full width at half maximum at 2 keV. It has been used by Greenwood and collaborators (GR 71, Gre+ 69, HGR 71) for the study of γ-ray spectra from a number of heavy nuclei including Ta, Hf, W, and Pb. A drawback of this method is that the 800-eV beam spread may sometimes be too narrow to encompass a sufficiently large number of resonances to completely smooth out Porter–Thomas fluctuations. There may also be intensity limitations compared to the ^{10}B filter method. Reduced intensities for Ta obtained with the scandium filter are shown in Fig. 13

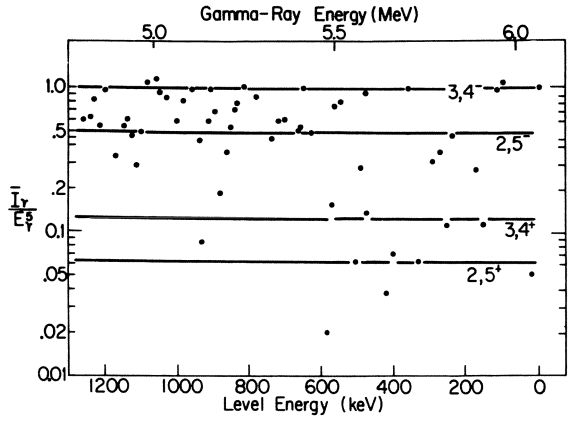

Fig. 13. Average reduced γ-ray intensities for ^{182}Ta obtained by the low-neutron-resolution technique (HGR 71). The upper two curves are for $E1$ transitions and the lower two for $M1$ transitions. Final-state spins and parities are indicated on each line.

(HGR 71). The iron filter device provides a 25-keV beam 4 keV wide (CWG 73).

The value of the average-resonance method lies in the facility it provides to examine the strengths of individual γ-rays, to test that they are primaries, and to distinguish between multipoles. In Table III, for example, one sees a clear indication that the spectra above 5 MeV are dominated by $E1$ radiation in nuclei at the heavy end of the table; the ratio of the number of $M1$ γ-rays to $E1$ γ-rays gradually grows with decreasing Z, becoming roughly unity at Sm and greater than unity, in general, for still lighter nuclei. A disadvantage, at the present state of the art, is the small energy range covered. In particular, below 5 MeV individual lines become difficult to resolve in most elements in Table III and the multipolarity and primary assignments become difficult to establish. The table shows that the energy dependence of the $E1$ radiation width is widely represented by any power between E_γ^3 and $E_\gamma^{7.5}$ with most cases conforming to the E_γ^5 dependence expected from the Lorentzian (Axe 62). The $M1$ dependence similarly varies widely with some evidence of peaking.

3.5. Comparison of Methods

Below the neutron separation energy, none of the four methods described in Secs. 3.1–3.4, at least insofar as it has been possible to exploit them to date, stands out as clearly superior for studying γ-ray strength functions. All have advantages and disadvantages and to a large degree

they complement one another. Above the separation energy most strength function information has been derived from photoexcitation data. The quantity measured in each method, and parameters needed for strength function extraction, are summarized in Table IV. Strength functions derived by the various methods are compared in Sec. 4.1.

The photoexcitation method is the only one providing $\vec{f}(E_\gamma)$. By suitable angular and polarization correlation measurements it is possible to distinguish $E1$, $M1$, and higher multipoles although these techniques have as yet been little used in this application. For a substantial region above the neutron threshold a measurement of $\bar{\sigma}_{\gamma n}$ gives a good approximation to the total absorption cross section, $\bar{\sigma}_{\gamma a}$, required for the calculation of $\vec{f}(E_\gamma)$, but for precise results one must correct for the total cross section for γ-emission, $\bar{\sigma}_{\gamma T}$, and, where applicable, for charged-particle emission cross sections. Below the neutron threshold, transmission measurements to obtain $\bar{\sigma}_{\gamma a}$ are difficult if not impossible because of competition from electron scattering and absorption processes. In this region one usually measures the elastic or, more precisely, in most cases a quasielastic cross section $\bar{\sigma}_{\gamma\gamma}$, from which one can estimate $\bar{\sigma}_{\gamma a}$. The latter estimate involves, among other things, the branching ratio for decay by the quasielastic channel, evaluation of which poses a serious difficulty for the method because it requires prior knowledge of the γ-decay strength function, $\overleftarrow{f}(E_\gamma)$. So far, the photoexcitation method has given much strength function information above the threshold but below the threshold it has yet to be applied extensively over the full range of targets and excitation energies of which it is capable.

The spectrum fitting method has the advantage that it can provide an empirical strength function for a wide energy range from near zero to the initial excitation energy used in the experiment. However, the strength function extracted depends strongly on the form of the level-density formula used in the calculation. Not only can uncertainties in $\varrho(E)$ affect the form of the strength function but also its absolute value. The absolute value is also affected by uncertainties in the value adopted for the average total radiation width, $\bar{\Gamma}_{\gamma T\lambda}$. A fundamental assumption used in the spectrum fitting method is that the same form, but not necessarily the same absolute magnitude, of strength function, $\overleftrightarrow{f}$, governs decay from each excitation interval. Strong support for this assumption is given by the sequential extraction method. It is also assumed that the spectral distribution contains only dipole radiation. A serious weakness of the spectrum fitting method is that it provides no means of uniquely separating multipoles so that the strength function obtained is a composite of the $E1$ and $M1$ strength

TABLE IV

Gamma-Ray Strength Function Parameters

For each method listed in column (1) are given the input experimental data (column 3), data required from other sources (column 4), and parameters derived (column 5).

Method	Section	Experimental data	External data	Derived parameters	Remarks
Photoexcitation	3.1				
(γ, n)		$\bar{\sigma}_{\gamma n}$	$\bar{\sigma}_{\gamma T}$, $\bar{\sigma}_{\gamma p}$, ---	$\vec{f}$, $E1/M1$	[a]
(γ, γ)		$\bar{\sigma}_{\gamma\gamma}$	$\bar{\Gamma}_{\gamma 0\lambda}/\bar{\Gamma}_{\gamma T\lambda}$, $\varrho(E_\lambda)$, S, $\bar{\Gamma}_{\gamma T\lambda}$	$\vec{f}$, $E1/M1$	[a]
Spectrum fitting	3.2	$\nu_{t\lambda}(E_\lambda = E_B)$	$\varrho(E)$, $\bar{\Gamma}_{\gamma T\lambda}$	$\vec{f}$	
Sequential extraction	3.3	$\nu_{t\lambda}(0 < E_\lambda < E_B)$	$\varrho(E)$, $\bar{\Gamma}_{\gamma T\lambda}$	$\vec{f}$	
High-resolution γ-ray	3.4	I_γ	$\varrho(E_\lambda)$, $\bar{\Gamma}_{\gamma T\lambda}$	$\vec{f}$, $E1/M1$, p	[b]

[a] Multipolarity identified by subsidiary polarization correlation measurements.
[b] Primary nature of radiation, p, verified from line-shapes and energy shifts in keV neutron capture.

functions. It can be assumed with some confidence that this empirical strength function conforms closely to the $E1$ strength function at high energies in the mass region $182 < A < 208$ but this assumption becomes less reliable toward lower energies and in certain other regions of the table where $M1$ radiation competes well with $E1$ radiation (Secs. 1, 4.2.2).

The sequential extraction method, like the spectrum fitting method, provides a complete strength function over the full energy range available to the experiment and like that method it depends strongly on level-density and total radiation-width information obtained externally. However, sequential extraction is the only method in which the form of $\overleftarrow{f}$ can be solved for directly, for all initial excitation energies, E_λ, a very valuable property. The same uncertainties, concerning the multipole content of the extracted strength function, apply as for the spectrum fitting method. An important assumption of the sequential extraction method is that the branching ratios for γ-decay from any excitation interval to lower intervals are the same whether the upper interval was populated by the initiating reaction or by γ-decay from higher intervals. This presupposes that the strength function is independent of spin (see Sec. 2.2) and other parameters of the levels involved, a supposition that is open to question and, hopefully, eventual verification.

The high-resolution γ-ray method is essentially the only method in which average reduced width of individual γ-rays can be studied; such studies are also possible in the photoexcitation method but, as yet, few measurements of this kind have been made. The method provides means for assigning multipole type and of testing whether γ-rays are primary or occur later in the cascade. Both the average reduced widths and multipole assignments become unreliable when γ-rays are not well-resolved. With detectors now available, this limits the method to the high-energy end of the spectrum; i.e., to ≥ 5 MeV approximately in (n, γ) experiments in most heavy elements. The method requires a knowledge of the level density and total radiation width at the initial excitation energy and also a calibration of the absolute intensity for at least one γ-ray in the spectrum. The last quantity has proved difficult to obtain directly.

4. PROPERTIES OF GAMMA-RAY STRENGTH FUNCTIONS

Basic data in the form of photoexcitation cross sections or neutron capture γ-ray spectra, necessary for the determination of γ-ray strength functions, are available for most heavy elements but the extraction of

strength functions is often thwarted, particularly below the neutron threshold, because a knowledge of branching ratios, multipolarities, or level densities is lacking. Because of the usually greater strength of $E1$ radiation as compared to $M1$ and higher multipoles (Secs. 1, 4.2.2) most of the data presented below have to do with the $E1$ strength function, much less with the $M1$ strength function, and little with higher multipoles. Indeed, in many examples it has not been possible to separate $E1$ from the other multipoles and the strength function must be understood as being mostly $E1$ with smaller but unknown contributions from other types of radiation. In a few examples (Sec. 4.2) the multipoles have been specifically identified.

Because of the above limitations we are unable to present a complete overview of the dependence of even the $E1$ strength function on E_γ and A. Nor will we attempt a complete review of all the fragmentary strength function information that can be extracted. Instead, we have selected some of the more complete examples. These show the degree of agreement between the various methods of Sec. 3 and also, in spite of the gaps in our knowledge, suffice to sketch the general overall trends of the strength function with E_γ and A and more importantly to show some of the detailed structure.

4.1. General Properties

In this section we show the overall energy dependence of the strength function as obtained by the various methods of Sec. 3. All available photoexcitation strength function data for a given target are plotted together on a diagram for $\vec{f}$ and similarly all available $\overleftarrow{f}$ data are plotted together. Where $\vec{f}$ and $\overleftarrow{f}$ strength functions are available for the same element, they are usually shown in adjacent diagrams in the same figure. In all figures, the strength function derived from the Lorentzian line is shown as a basis for comparison. The giant dipole resonance parameters used for the Lorentzian calculation are given in Table V. It is important to note that with few exceptions, the strength functions are absolute; no arbitrary normalizations have been applied.

In order to properly assess the agreement achieved among the various experimental strength functions and between these and the Lorentzian-based curves, one requires some appreciation of the uncertainties associated with each. Some general remarks on this question will be made here and particular remarks appropriate to individual determinations will be made in connection with the element by element review to follow.

All methods are, of course, susceptible to uncertainties from finite counting statistics and, in the high-resolution method in particular, there

TABLE V

Giant Dipole Resonance Parameters

For each nucleus in the first column, the giant dipole resonance width, the peak energy, and the peak cross section of the first component are shown in the next three columns. The width, the peak energy, and the peak cross section of the second component are shown in the fifth, sixth, and seventh columns.

Nucleus	Γ_{G1}, MeV	E_{G1}, MeV	σ_{0G1}, mb	Γ_{G2}, MeV	E_{G2}, MeV	σ_{0G2}, mb	Reference
^{238}U	2.90	10.96	301	4.52	14.04	369	(Ber+ 72)
Bi	4.8	13.8	537				(GL 57)
^{208}Pb	4.05	13.42	640				(Bei+ 69)
Tl	4.6	14.0	648				(GL 57)
Hg	4.5[a]	14.0[a]	405[b]				
Au	2.9	13.15	255	4.0	13.90	365	(FW 58)
Pt	4[a]	14.0[a]	446[b]				
Ir	4[a]	14.0[a]	443[b]				
Re	4[a]	14.0[a]	428[b]				
W	2.29	12.59	211	5.18	14.88	334	(Ber+ 69b)
Ta	1.94	12.59	171	4.98	15.13	265	(BBV 68)
Er	2.9	12.0	225	5.0	15.45	260	(Ber+ 69a)
Eu	2.75	12.33	155	5.83	15.79	222	(Ber+ 69b)
Sm	4.25	12.77	155	4.6	15.46	260	(Ber+ 69a)
Sb	4.5[a]	15.2[a]	254[a]				
^{119}Sn	4.81	15.54	253				(Ful+ 69)
^{117}Sn	5.02	15.66	254				(Ful+ 69)
In	5.24	15.63	266				(Ful+ 69)
Zr	4.0	16.65	211				(Lep+ 71)

[a] Interpolation.
[b] Sum rule.

may be an additional statistical uncertainty from Porter–Thomas fluctuations owing to averaging over too small a number of resonances. In all determinations where f can be extracted point by point from the original measurements, the vertical error bars shown in Figs. 15 to 25 will reflect these statistical uncertainties only. The horizontal bars show the energy

range of the γ-rays contributing to the average. In the spectrum fitting and sequential extraction methods, the statistical uncertainties tend to be reduced because the intervals, ΔE_i, over which spectra are averaged are relatively large (usually > 0.1 MeV). But more important, because of the iterative nature of these methods, realistic estimates of the statistical uncertainties are difficult to carry through. Therefore, for strength functions derived by these two methods error bars have been omitted.

Systematic errors are in general not indicated in the figures. In determinations of $\vec{f}$ from the photoneutron cross section, systematic errors may be introduced by failing to take proper account of competing photon scattering cross sections. In the methods of Secs. 3.2, 3.3, and 3.4, systematic

TABLE VI

Resonance and Level-Density Parameters

Product nucleus	E_B, MeV	$\bar{\Gamma}_{\gamma T\lambda}$, meV[a]	$\varrho_0(E_B)\times 10^4$ MeV^{-1} [b]	T, MeV	E_t, MeV
^{204}Tl	6.54	640.0 ± 70.0	0.078 ± 0.04	0.897	0.0
^{200}Hg	8.028	205.0 ± 11.0	0.4 ± 0.1	0.858	1.5
^{198}Au	6.5	125.2 ± 11.0	0.75 ± 0.1	0.753	0.0
^{196}Pt	7.92	110.8 ± 18.0	1.4 ± 0.3	0.717	1.5
^{192}Ir	6.14	73.9 ± 3.2	4.3 ± 0.6	0.575	0.0
^{187}Re	5.95	51.7 ± 5.4	1.8 ± 0.4	0.555	0.0
^{186}Re	6.23	54.3 ± 4.0	2.7 ± 0.4	0.556	0.0
^{187}W	5.25	64.0 ± 10.0	0.6 ± 0.3	0.629	0.0
^{183}W	6.5	60.0 ± 7.0	0.9 ± 0.2	0.637	0.0
^{182}Ta	6.06	55.7 ± 5.0	1.5 ± 0.2	0.582	0.0
^{168}Er	7.771	86.3 ± 0.8	1.8 ± 1.0	0.6	1.0
^{152}Eu	6.305	85.4 ± 7.0	15.0 ± 6.0	0.55	0.0
^{150}Sm	7.987	60.6 ± 2.0	3.3 ± 1.0	0.6	1.2
^{122}Sb	6.807	94.0 ± 13.0	0.63 ± 0.3		
^{116}In	6.784	74.0 ± 4.7	0.5 ± 0.2		

[a] Ref. (Gol+66).
[b] s-wave resonance density $\varrho_0 = \varrho/2(2J_0 + 1)$, where J_0 is the target spin, Ref. (Gol+66); for ^{187}Re Ref. (SNG 71).

errors of 10–50% may be introduced by adopting an incorrect value for $\bar{\Gamma}_{\gamma T\lambda}$ and in the method of Sec. 3.4 a further uncertainty of about the same size is associated with $\varrho_0(E_\lambda)$ (Gol+ 66). The level-density parameters and $\bar{\Gamma}_{\gamma T\lambda}$ are given in Table VI. By far the most important systematic error affecting strength functions obtained from photoexcitation below the neutron threshold and by the spectrum fitting and sequential extraction methods is introduced through the nuclear temperature, T, used for the level-density estimate, Eq. (2.14). The temperature is obtained from known level densities at the neutron threshold and from the region below ~2 MeV. The latter density is least certain and, in general, available estimates provide only a lower limit. At high γ-ray energies, $E_\gamma \geq 4.5$ MeV, the error in $\vec{f}$ arising from a systematic error in T may be estimated from

$$\Delta \vec{f} \approx -E_\gamma \vec{f} \frac{\Delta T}{T^2} \tag{4.1}$$

For example, in Au for which we derive $T = 0.753$ MeV, a 20% decrease in T increases $\vec{f}$ at 6 MeV by a factor of ~3. This strong dependence of $\vec{f}$ on T is shown graphically in Fig. 8, Sec. 3.2. Thus for $\vec{f}$ obtained by methods of Secs. 3.2 and 3.3, for which no error bars are shown, the systematic uncertainty far exceeds any possible statistical errors.

Uncertainties in Γ_G, E_G, and σ_{0G} entering the Lorentzian prediction for f through Eqs. (2.5), (2.7), and (2.8), introduce uncertainties in the absolute value of the Lorentzian prediction sometimes by as much as a factor of 2. Therefore failure to achieve agreement in absolute magnitude between the Lorentzian curves and the experimentally determined strength functions is much less significant than departures in functional form.

4.1.1. Nuclei with $Z \geq 82$

(a) ^{238}U, ^{232}Th. The strength functions $\vec{f}$ for ^{238}U and ^{232}Th have been calculated from $\bar{\sigma}_{\gamma n}$ and $\bar{\sigma}_{\gamma f}$ measurements (Ber+ 72) as described in Sec. 3.1. The results above 8 MeV in ^{238}U are shown in Fig. 14 where they are plotted with the results of Knowles and Mafra (KM 73) below that energy. The relatively low values of $\vec{f}$ near threshold may not be significant because, in this region where $\bar{\sigma}_{\gamma n}$ varies rapidly with energy, systematic errors in the correction for beam spread may be appreciably larger than the statistical error bars shown on the points. The overall agreement with the Lorentzian-based curve is good. Similar good agreement is found in ^{232}Th (Ber+ 72, MKG 72).

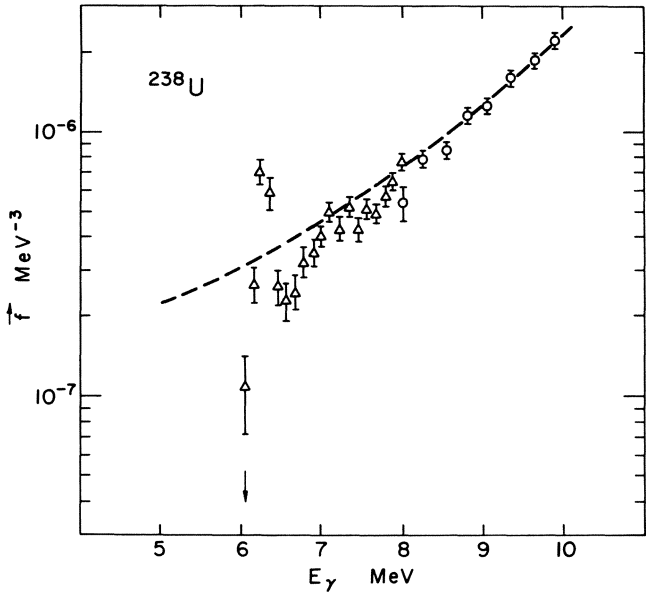

Fig. 14. The strength function $\vec{f}$ for ^{238}U. The △ and ○ points are from the $\bar{\sigma}_{\gamma a}$ measurements (KM 73) and (Ber+ 72), respectively, shown in Fig. 3. The broken line is derived from the Lorentzian curve fitted to the giant dipole resonance with constants given in Table V. The arrow indicates the (γ, n) threshold.

(*b*) *Pb, Bi.* Strength functions $\vec{f}$ for ^{206}Pb, ^{207}Pb, ^{208}Pb, and ^{209}Bi have been calculated from the $\bar{\sigma}_{\gamma n}$ and $\bar{\sigma}_{\gamma\gamma}$ measurements as described in Sec. 3.1. The open circles and triangles in Fig. 15 are from the $\bar{\sigma}_{\gamma n}$ measurements of Fuller and Hayward (FH 62b) and Beil *et al.* (Bei+ 69), respectively. The open square at 7.6 MeV in ^{208}Pb is obtained by averaging the ground-state radiation widths of $J = 1^-$ resonances from the $\bar{\sigma}_{\gamma n}$ measurements by Bowman *et al.* (Bow+ 70). The level spacing used, $D = 0.04$ MeV, is obtained from the (n, γ) measurements of Allen and Macklin (AM 71) assuming that half of the observed $J = 1$ resonances are 1^-. The closed squares and circles are $\vec{f}$ calculated from the photoelastic scattering cross sections of Swann (Swa 73a) and Khan and Knowles (KK 67), respectively. Only a limited number of points are obtained below the neutron separation energy because strength functions calculated from $\bar{\sigma}_{\gamma\gamma}$ are limited to those few measurements discussed in Sec. 3.1 for which branching ratios and level densities are known. The parity of the levels have not been measured. Above the neutron separation energy the smoothed empirical strength function is in good agreement with that derived from the Lorentzian.

4.1.2. Nuclei with $73 \leq Z < 82$

Strength functions for nuclei in this mass range have been obtained from all the methods discussed in Sec. 3. The $M1$ contribution for γ-ray energies >4.5 MeV following s-wave neutron capture is believed to be small (Secs. 3.4 and 4.2.2) and therefore the empirical strength functions are essentially f_{E1} in this region. Below 4.5 MeV the multipole purity of the strength function is less certain.

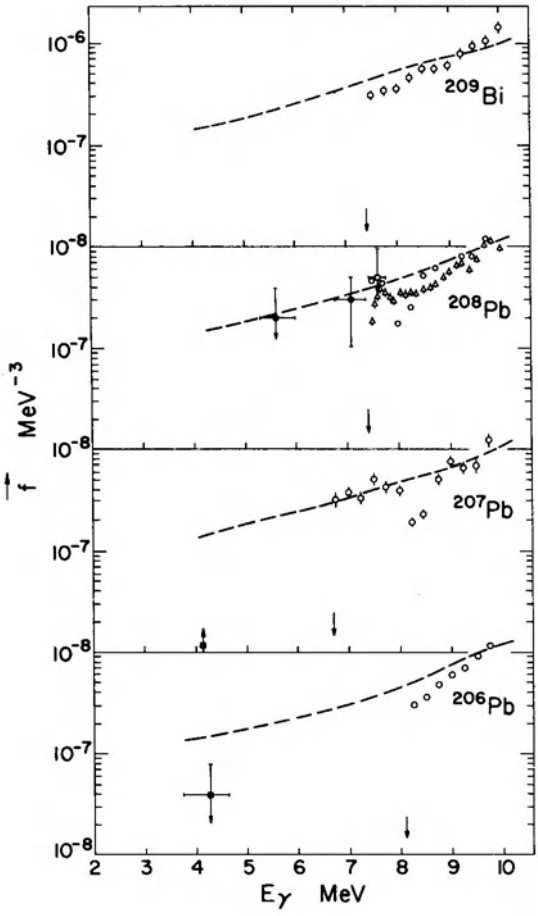

Fig. 15. Strength functions $\vec{f}$ for ^{209}Bi, ^{208}Pb, ^{207}Pb, and ^{206}Pb. Above the neutron separation energies, shown by arrows, the points are calculated from $\bar{\sigma}_{\gamma n}$ measurements, some of which, ○ (FH 62b), △ (Bei+ 69) and □ (Bow+ 70) are shown in Fig. 2. The data points ● in ^{208}Pb and ■ in ^{207,206}Pb are from $\bar{\sigma}_{\gamma\gamma}$ measurements (KK 67) and (Swa 73a) respectively. Other details are as in Fig. 14.

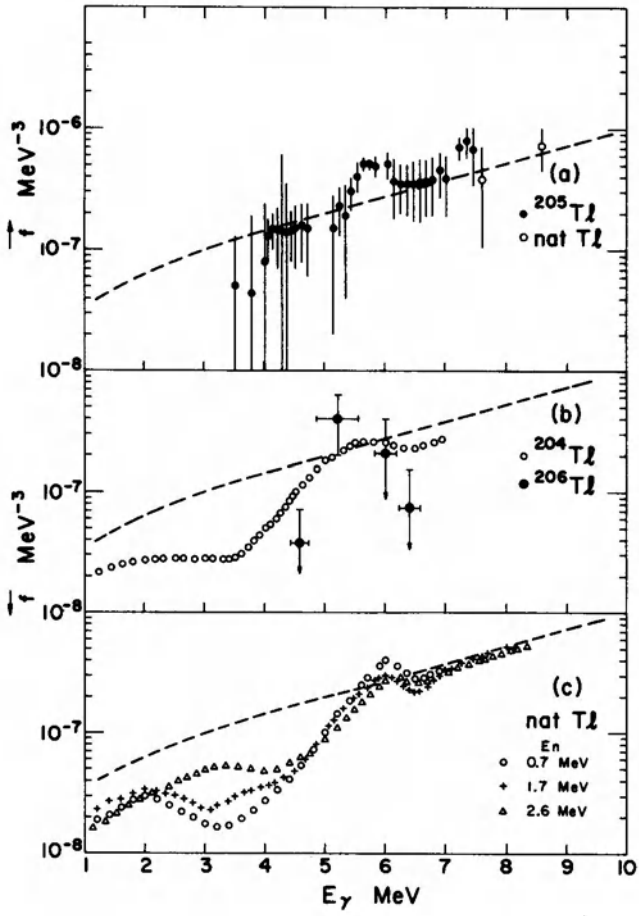

Fig. 16. Strength functions for Tl. (a) The solid circles show $\vec{f}$ in ^{205}Tl calculated from $\bar{\sigma}_{\gamma\gamma}$ (Ear+ 73) shown in Fig. 5 and the open circles from $\bar{\sigma}_{\gamma n}$ (GL 57). (b) The closed circles are from resonance (n, γ) data (Ear+ 72a) and the open circle from thermal (n, γ) data (BK 53). (c) The strength functions obtained from fast-neutron capture data (Ear+ 72b). The broken curves are derived from the Lorentzian.

(*a*) *Tl.* Strength functions for isotopes of Tl are shown in Figs. 16a, b, and c. The solid points in (a) give $\vec{f}$ for ^{205}Tl from the photoelastic scattering measurements (Ear+ 73). The open circles in (a) are values of $\vec{f}$ for natural Tl (70% ^{205}Tl) from photoneutron cross sections (GL 57).

Strength functions $\vec{f}$ from neutron-capture reactions are shown in (b) and (c). The open circles in (b) show $\vec{f}$ for ^{204}Tl obtained by the spectrum fitting method from thermal neutron capture γ-ray data (BK 53) and the

solid circles are obtained by the high-resolution γ-ray method from individual γ-ray transitions in ^{206}Tl following resonance neutron capture in ^{205}Tl (Ear+ 72a). In (c) three strength functions obtained by fitting the spectral distribution following ~0.7 MeV (○), ~1.7 MeV (+), and ~2.6 MeV (△) neutron capture in natural Tl are shown. For $E_\gamma > 4$ MeV these have similar form. However, below 4 MeV, the shape of $\vec{f}$ is found to depend on the excitation energy.

Relative to $\vec{f}$ derived from the Lorentzian tail, the strength functions in all three isotopes and for both photoexcitation and capture reactions show a marked irregularity, i.e., a small resonancelike structure at ~6 MeV and a pronounced dip below 5 MeV (see Sec. 4.2.2). When uncertainties in f arising from uncertainties in level-density parameters and, in the Lorentzian curve, from uncertainties in giant dipole resonance parameters are allowed for, the absolute magnitudes of the strength function and the Lorentzian above 6 MeV are not significantly different.

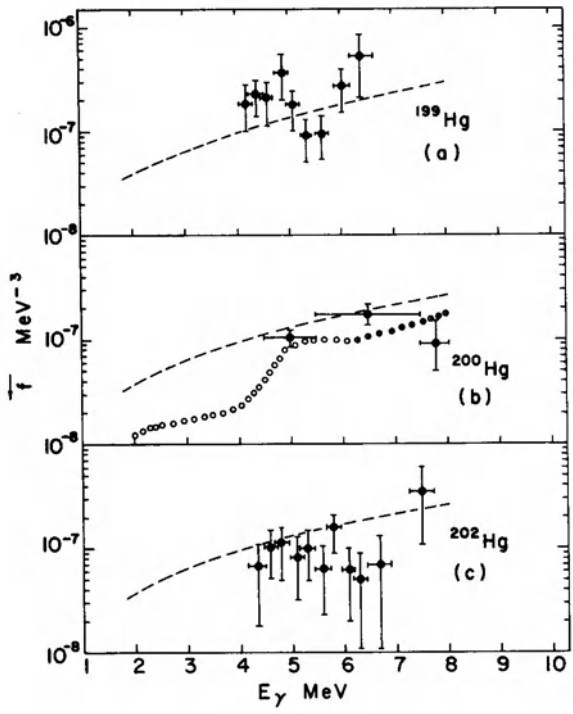

Fig. 17. Strength functions for Hg. The solid circles in a, b, and c are from resonance (n, γ) data (LEB 73). In (b) the open and half-filled circles are from (n, γ) thermal (Gro+ 69) and resonance data (LEB 73), respectively.

(*b*) *Hg.* The strength functions for ^{199}Hg, ^{200}Hg, and ^{202}Hg are shown in Fig. 17a, b, and c. The solid points are obtained by averaging the high-resolution γ-ray absolute intensities, from neutron capture in resonances (LEB 73), over the energy interval shown by the horizontal bars. The open circles in (b) are strength functions for ^{200}Hg obtained by spectrum fitting the γ-ray distributions from thermal neutron capture (Gro+ 69). The energy dependence of the strength function shown by half-filled circles was obtained from epithermal neutron capture (LEB 73). The general shape of this strength function (open circles) is the same as in the Tl isotopes, i.e., there is a dip with respect to the Lorentzian below 5 MeV. Unfortunately, the data for both ^{199}Hg and ^{202}Hg are neither extensive nor precise enough to confirm this trend. The maximum (scarcely prominent enough to be called a pigmy resonance) seems to be at $\sim$5 MeV, somewhat lower in energy than in Tl.

(*c*) *Au.* Strength functions for isotopes of gold above 4.8 MeV have been extracted by each of the four methods discussed in Sec. 3. Thus their mutual consistency can be tested.

The strength function $\vec{f}$ for ^{197}Au shown by solid points in Fig. 18a has been deduced from $\bar{\sigma}_{\gamma\gamma}$ measurements (Bar 69) as described in Sec. 3.1. Above the (γ, n) threshold (8.1 MeV) $\vec{f}$ obtained from $\bar{\sigma}_{\gamma n}$ measurements is shown by open circles (FW 58) and triangles (Ful+ 62). The $\vec{f}$ for ^{198}Au, shown by the open circles in (b) and (c), was extracted by the spectrum fitting method from γ-ray distributions obtained from capture of thermal neutrons (Gro+ 69) and $\sim$2.6 MeV neutrons (Ear+ 72b), respectively. The solid triangles in (b) show $\vec{f}$ obtained by the sequential extraction method (Bar+ 70) and the solid circles by the high-resolution γ-ray method from individual γ-ray intensities following capture of neutrons from a $\sim$2 keV broad beam (LBT 72). Each of the solid circles was obtained by further averaging over γ-rays in a 250-keV-wide interval.

In the region of overlap, $E_\gamma > 4.8$ MeV, the strength functions obtained from all four methods are consistent. At 6 MeV the absolute magnitude of $\vec{f}$ is consistent with the Lorentzian tail (broken curve), however, below 5 MeV the empirical strength functions depart significantly below the Lorentzian.

There is a shallow maximum or pigmy resonance peaking at $\sim$6 MeV in ^{197}Au and ^{198}Au.

(*d*) *Pt, Ir, Re, W.* The strength functions for these elements shown by open circles in Figs. 19a-d were deduced by fitting spectral distributions of γ-rays following thermal neutron capture in the natural elements (Gro+

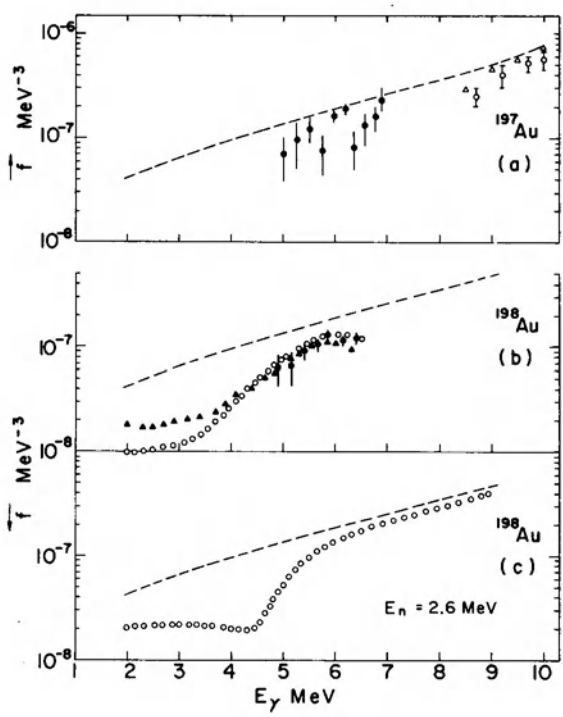

Fig. 18. Strength functions for Au. (a) The solid circles are from $\bar{\sigma}_{\gamma\gamma}$ (Bar 69), points above 8 MeV are from $\sigma_{\gamma n}$, ○ (FW 58) and △ (Ful+ 62). (b) The points ○, ▲, and ● are from the spectrum fitting method—thermal (n, γ) data (Gro+ 69), the sequential extraction method—$(d, p\gamma)$ data (Bar+ 70) and the high-resolution method (LBT 72). (c) Open circles $\vec{f}$ from spectrum fitting method. Other details are as in Fig. 14.

69). For the even–even ^{196}Pt nucleus the energy dependence of $\vec{f}$ in the 6.2- to 7.9-MeV region (half-filled circles) was obtained from the relative intensities of the average partial radiation widths observed by Bollinger and Thomas (BT 67). The solid point for ^{196}Pt was obtained by averaging partial radiation widths of 9 γ-rays between 6.0 and 7.9 MeV observed from twenty-two $J = 1^-$ resonances (Sam+ 68).

The solid point for ^{188}Re was obtained by averaging reduced partial widths of 53 γ-rays in the region $4.8 < E_\gamma < 5.9$ MeV following thermal neutron capture (She+ 72).

The solid point in W was obtained from intensities of 7.302- and 7.413-MeV γ-rays in ^{184}W following 2-keV neutron capture (GR 71). The level spacing $D = 28.7$ eV for resonances of spin 1 was used. In the energy

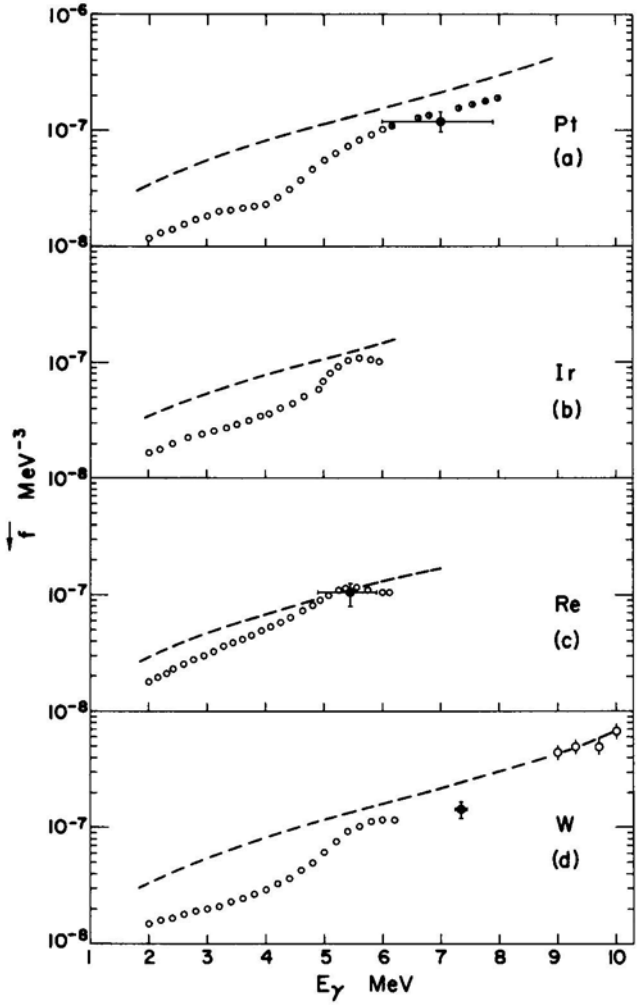

Fig. 19. Strength functions for Pt, Ir, Re, and W. The open circles in (a) to (d) below 8 MeV are from fitting of spectra from thermal neutron capture (Gro+ 69) In (a) the energy dependence of $\bar{f}$ shown by half-filled circles was obtained from (BT 67 see text). The solid points are from high-resolution method, Pt (Sam+ 68), Re (She+ 72) and W (GR 71). In (d) the open circles above 8 MeV are from $\bar{\sigma}_{\gamma n}$ (Ber+ 69b). Broken curves are from Lorentzians.

range 9 to 10 MeV the strength functions $\vec{f}$ for natural W have been obtained from $\bar{\sigma}_{\gamma n}$ (Ber+ 69b).

The strength functions in these elements also show features similar to those in Hg, Au, and Tl, i.e., relative to the Lorentzian tail, there is a dip in the empirical strength function below 5 MeV and a hint of a pigmy resonance in Ir and Re.

(*e*) *Ta.* The consistency of form of the strength function $\vec{f}$ obtained by the different methods discussed in Sec. 3 can also be demonstrated for Ta. The strength functions for ^{182}Ta shown by the open circles in Fig. 20a and by open circles and triangles in Fig. 20b were obtained by fitting spectral distributions of γ-rays following capture of thermal neutrons (Gro+ 69) and neutrons of 0.7 and 2.6 MeV (Ear+ 72b), respectively. Above 6.2 MeV the strength function shown by the open triangles has an uncertainty of about a factor of 2 owing to poor precision of the data in this energy region. The strength function, given by solid triangles in Fig. 20a, was obtained from $(d, p\gamma)$ measurements using the sequential extraction method (Bar+ 70) and the solid points with error bars are obtained from the individual γ-ray intensities following capture of a ~2-keV-broad beam of neutrons (LBT 72). In order to reduce the Porter–Thomas fluctuations at each point,

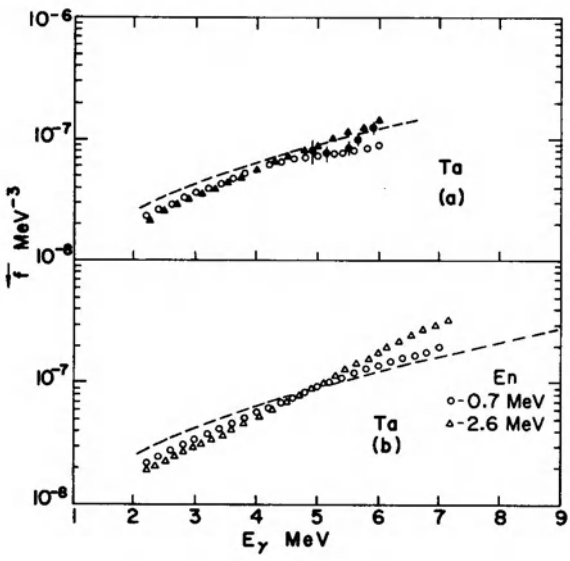

Fig. 20. Strength functions for Ta. (a) The points ○, ▲, and ● have the same meaning as in Fig. 18b. (b) The points ○ and △ are obtained by the spectrum fitting method from fast-neutron capture data (Ear+ 72b).

additional averaging was carried out over all γ-rays in a 250-keV interval. The strength functions obtained from the different methods are consistent within the uncertainties inherent in each method.

In overall form the empirical strength function for Ta is very similar to the Lorentzian tail of the giant dipole resonance with no sign of a pigmy resonance.

4.1.3. Nuclei with $55 < Z < 73$

Strength functions $\vec{f}$ above the neutron separation energy can be obtained from $\bar{\sigma}_{\gamma n}$ measurements in natural isotopes of many nuclei in this region. These cross sections, in the energy range from the neutron threshold to well above the giant dipole resonances, have been measured for example in Ba, La, Ce, Pr (Bei+ 71), Ce, Sm, Eu, Er, Lu (Ber+ 69a), Eu, Gd, Ho (Ber+ 69b), and Tb (BBV 68). However, below the neutron threshold there is little or no information from which values of $\vec{f}$ can be obtained.

Strength functions $\vec{f}$ can be obtained from the spectrum fitting method, however, because of the presence of both $E1$ and $M1$ radiation in the spectra, the empirical strength functions extracted lose much of their significance. In Fig. 21a, b, and c, $\vec{f}$ obtained from $\bar{\sigma}_{\gamma n}$ are shown by open circles, above 8 MeV for natural samples of Er (Ber+ 69a), Eu (Ber+ 69b) and Sm (Ber+ 69a), respectively. The open circles below 8 MeV are obtained by the spectrum fitting method from the thermal neutron capture spectra (Gro+ 69). The solid points in (a) show $\vec{f}_{E1}$ obtained from average neutron capture data (BT 70), as discussed in Sec. 3.4. The absolute normalization was obtained by comparing the average reduced intensities with those observed in thermal capture (Ras+ 69). The uncertainties arising from this calibration are shown by the error bars. In (b) the solid points are obtained by averaging individual γ-ray intensities (without regard to multipole type) from thermal capture (SH 68). In (c) the solid points are from the relative intensities of $E1$ γ-rays following average neutron capture (BS 70). The absolute normalization was obtained as in Er.

In Er and Eu the Lorentzian is in good agreement with the data. In Sm there is an apparent discrepancy which, in view of inherent uncertainties, may not be significant.

The strength functions from different methods for any one element are consistent among themselves and follow the general form of the Lorentzian curve.

The functional form of $\vec{f}_{E1}$ for ^{156,158}Gd (BT 70) is compared with the Lorentzian in Fig. 22. The solid curve which is the best fit through the data points deviates slightly ($\sim$20% at 7.5 MeV) from the Lorentzian. Between

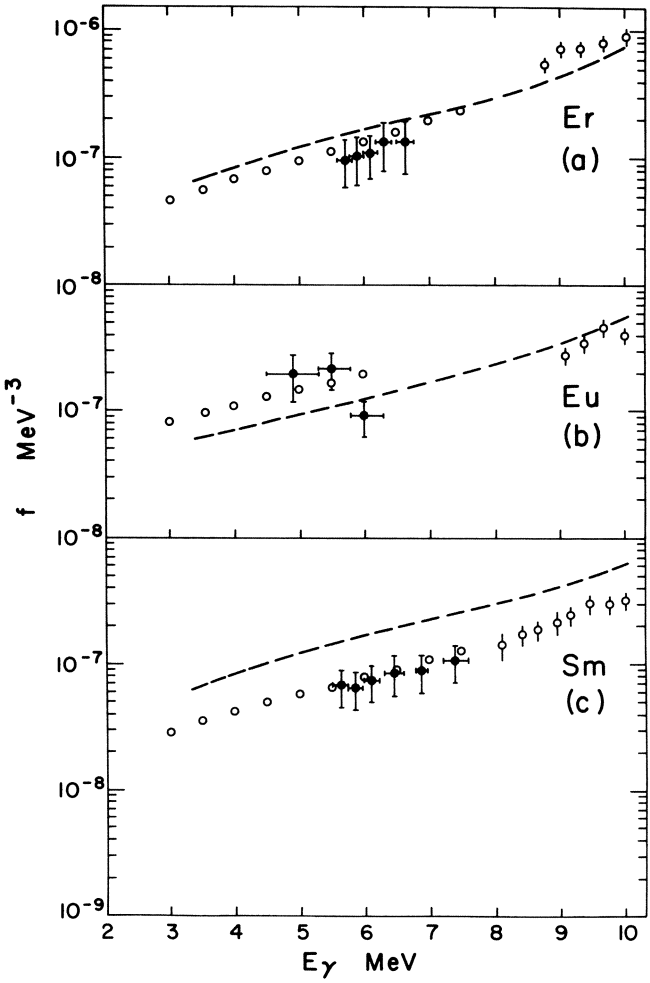

Fig. 21. Strength functions for Er, Sm, and Eu. The open circles above 8 MeV are from $\bar{\sigma}_{\gamma n}$, Er and Sm (Ber+ 69a) and Eu (Ber+ 69b). Below 8 MeV the open circles are obtained by the spectrum fitting method from thermal capture data (Gro+ 68, 69). The solid circles are obtained by the high-resolution method from (a) (BT 70), (b) (SH 68), and (c) (BS 70). The broken curves are from the Lorentzian.

7.5 and 8 MeV the empirical $\overleftarrow{f}_{E1}$ appears steeper than that derived from the Lorentzian.

Similar local deviations from the Lorentzian have been observed in other nuclei in this mass range (see Table III). Several $M1$ transitions have been identified in the spectra from average resonance capture.

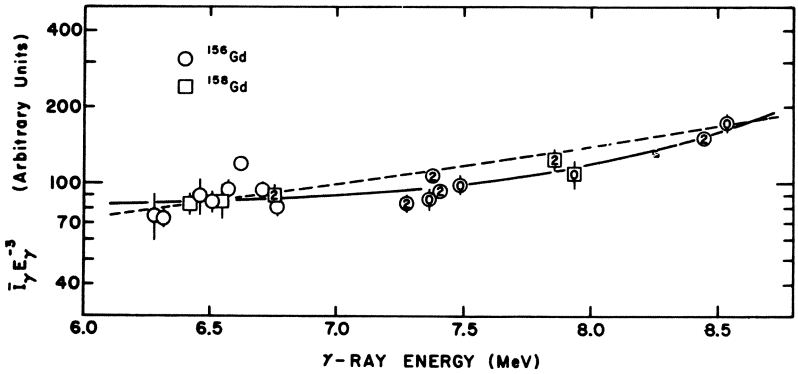

Fig. 22. The relative strength function for ^{156,158}Gd (BT 70). The numbers within some of the points are the spins of final states. The solid line is the best fit through the points and the broken line is derived from the Lorentzian.

4.1.4. Nuclei with $40 < Z \leq 55$

The γ-ray spectral distributions from (n, γ) and $(d, p\gamma)$ reactions in Cs, I, and Sb (see Sec. 4.2.2) contain a bump similar to those for nuclei near Pb. Because of the difficulty in obtaining reliable estimates of level densities both near the neutron threshold (because of unidentified p-wave resonances) and at lower excitation energies, we have not attempted to extract $\overleftarrow{f}$ by the spectrum fitting method. However, Starfelt (Sta 64), using both Newton's level-density formula (New 56) and the constant temperature level-density formula, had concluded that $\overleftarrow{f}$ in Cs exhibits a small peak at ~5.5 MeV. Brzosko *et al.* (Brz+ 71), using the Gilbert and Cameron (GC 65) level-density formula, have also extracted strength functions from spectral distributions observed in (p, γ) and (n, γ) reactions. They conclude that "echo-resonances" in $\overleftarrow{f}$ at 7, 8, 6.8, 6.5, and 6 MeV are required to fit the data in Ag, In, Sb, I, and Cs, respectively. Unfortunately, as discussed in Secs. 2.3 and 3.2, the Gilbert and Cameron formula does not give reliable estimates of level densities and therefore the strength of these echo resonances would appear to require further verification when better level densities are available.

In Fig. 23, $\overleftarrow{f}_{E1}$ and $\overleftarrow{f}_{M1}$ for ^{122}Sb obtained from the resonance neutron capture data of Lottin and Paya (LP 71) are shown. The basis for the identification of $E1$ and $M1$ transitions used by these authors is the separation of the average γ-ray intensities into two groups (see Sec. 3.4). The ratio $\overleftarrow{f}_{E1}/\overleftarrow{f}_{M1}$ is about 3. Similar conclusions were drawn by Bhat *et al.* (Bha+ 70).

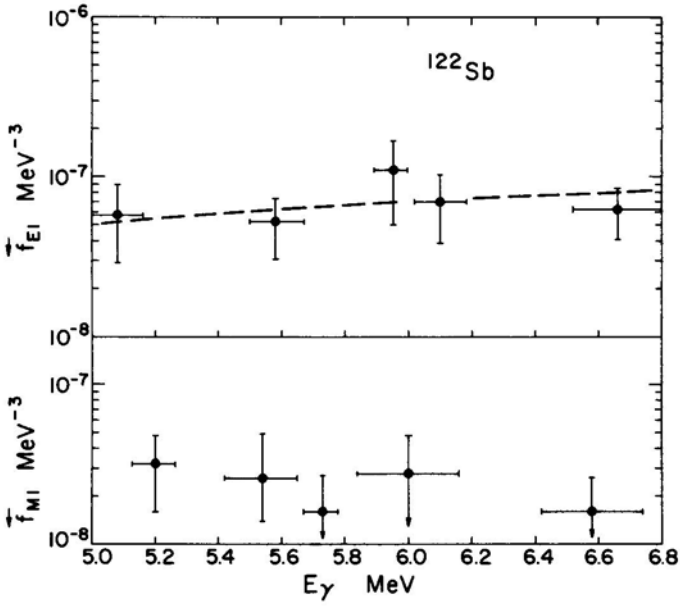

Fig. 23. Strength functions for ^{122}Sb. The points are from the neutron-resonance capture data (LP 71). The broken curve is from the Lorentzian.

The large uncertainty in the data preclude any investigation of a structure in $\overleftarrow{f}$.

The form of $\overleftarrow{f}_{M1}$ derived from the average neutron capture γ-rays in Sn isotopes (Bol 70) is shown in Fig. 24. There is a suggestion of a peak at ~8.5 MeV. In Fig. 25 $\overleftarrow{f}_{E1}$ and $\overleftarrow{f}_{M1}$ for ^{116}In from neutron capture in seven

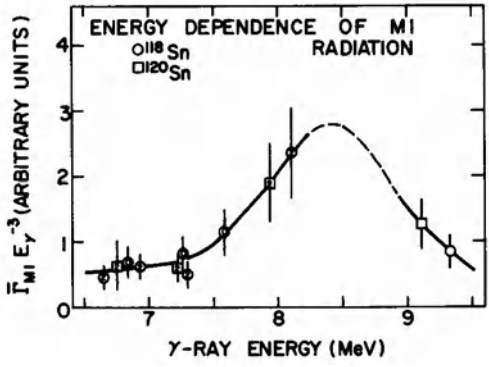

Fig. 24. The relative $M1$ strength function for ^{118,120}Sn (Bol 70). The numbers within the points refer to the final state spins, and the solid curve represents a best fit through the points. The broken curve is interpolated.

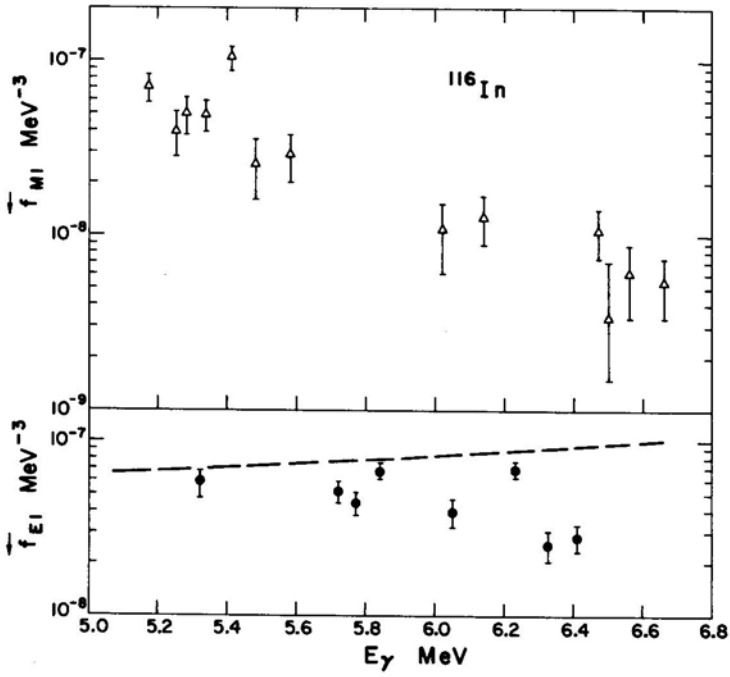

Fig. 25. The $M1$ and $E1$ strength functions for ^{116}In. The points are from neutron resonance capture (LEB 70). The broken curve is from the Lorentzian.

resonances (LEB 70) are shown. The $E1$ and $M1$ γ-rays were identified from the known spins and parities of final states. The $\overleftarrow{f}_{E1}$ is almost constant, however, $\overleftarrow{f}_{M1}$ shows an energy dependence apparently peaking below 5.4 MeV. Stefanon *et al.* (Ste+ 72) also investigated γ-rays above 5.4 MeV from 31 resonances in ^{115}In; their data confirm the above trends in f. Although the apparent peaks in $\overleftarrow{f}_{M1}$ in In and Sn are at different energies, it is interesting to note that transitions in these peaks feed states $\sim$1.5 MeV above the ground state in both cases.

The general form of (dipole) strength functions in ^{90}Zr and Sn is presented in the next section (see Figs. 26-28) in connection with discussions of substructure. While the original measurements (AMS 70, Win+ 70) included no determination of multipolarity, these curves are similar in overall form and absolute magnitude to those derived from the Lorentzian. Although this is consistent with the presence, if not a preponderance, of $E1$ transitions it cannot be construed as evidence that the substructure peaks are $E1$.

4.2. Detailed Properties

From the general shapes of the γ-ray strength functions described in Sec. 4.1 it is clear that they are not always smoothly varying but may possess more or less prominent irregularities or gross-substructure involving many transitions and, sometimes, extending over a range of nuclei. Single-line (microstructure) effects which, by definition, deserve no attention in a treatment concerned with average behavior are in general smoothed out in these curves. However, at closed shells, particularly in ^{208}Pb, the average approach is scarcely appropriate even at 5–8 MeV and some attention to individual transitions is essential for an adequate appreciation of the overall trends of the substructure.

Much experimental effort has been expended in investigating the nature and origin of the strength function irregularities or, more precisely, of the γ-ray structures to which they give rise in the observed spectra. Chronologically, it was in such experiments (e.g., LS 65) that the spectral irregularities were originally demonstrated to arise from the strength function and not some other parameter such as the level density. The justification of the spectrum fitting and sequential extraction methods, in which uniformly varying statistical level densities are assumed and irregularly varying strength functions are derived, depends in part on prior knowledge established by these experiments.

In this section we review the results of some of the more important experiments revealing substructure. Since some irregularities show up more clearly in one type of reaction than in others, it will be convenient to subdivide the discussion by the reactions used. We will also, for directness of presentation, frequently discuss the irregularities as properties of the spectra rather than of the underlying strength functions.

4.2.1. Photoexcitation Reactions, Local Substructure

Gross structure has been observed in the photoabsorption cross section of a number of nuclei above the neutron separation energy. In all cases, averaging is over many resonances so that the major irregularities in strength are not attributable to statistical fluctuations. We now discuss the evidence for some of these substructures and their significance.

(*a*) *^{90}Zr, Sn.* Substructure appears in the photon strength functions $\vec{f}$ of ^{90}Zr and Sn, Figs. 26 and 27, respectively, which we have obtained by applying Eq. (2.5) to the total photon cross section reported by Axel *et al.* (AMS 70). The 70-keV γ-beam resolution used in these measurements

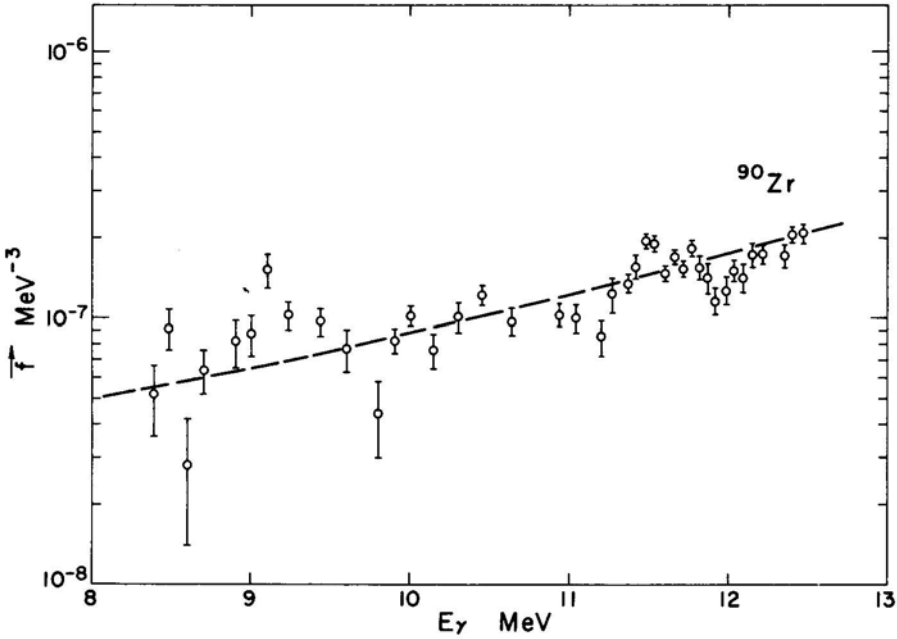

Fig. 26. The strength function $\bar{f}$ for ^{90}Zr. The points are calculated from $\bar{\sigma}_{\gamma a}$ (AMS 70). In estimating $\bar{\sigma}_{\gamma a}$ it was assumed that the elastic photon scattering above 8.68 MeV was due to ^{90}Zr only. The broken curve is derived from the Lorentzian.

is sufficient to average over many resonances. In ^{90}Zr, below the effective (γ, p) threshold at 10.6 MeV, only photon elastic and inelastic scattering contribute to the cross section; the neutron threshold is at 12 MeV. Above 10.6 MeV, $\sigma_{\gamma p}$ must be taken into account in estimating the photon strength function. For this estimate the $\bar{\sigma}_{\gamma p}$ were obtained (AMS 70) by detailed balance from (p, γ) measurements in ^{89}Y (ORR 66, ORW 67, Mas+ 69). Of particular interest is the substructure in ^{90}Zr between 11.2 and 11.8 MeV, since this structure has been inferred previously from (p, γ) measurements (ORR 66). As emphasized by Axel *et al.* (AMS 70) the increase in the photon interaction near 11.5 MeV cannot be ascribed to the photoproton cross section alone but is the combined result of $\sigma_{\gamma T}$ and $\sigma_{\gamma p}$.

It is pointed out by Axel *et al.* (AMS 70) that the strength shown in Fig. 27 involves only the even isotopes of Sn because in the odd isotopes neutron emission is allowed, and dominates over photoemission. Prominent substructure has also been observed in the photon strength functions of ^{119}Sn and ^{117}Sn in measurements of the ground-state photoneutron cross section $\bar{\sigma}_{\gamma n_0}$ near 7.8 MeV by Winhold *et al.* (Win+ 70; see however, JS 73).

These are shown in Fig. 28 along with the extrapolated Lorentzian line (Ful+69). The peaks have widths of several hundred keV and include many individual levels. Because photon emission is relatively weak, $\bar{\sigma}_{\gamma n_0}$ provides a good approximation to $\bar{\sigma}_{\gamma a}$ and gives a good measure of $\vec{f}$. The authors point out that the decrease in $\sigma_{\gamma n_0}$ above 7.8 MeV in ^{119}Sn might be due to p-wave neutron emission but that explanation cannot account for the corresponding decrease in ^{117}Sn where the threshold is higher. They compare these results with the quasielastic scattering data of Axel *et al.* (AMS 70) for natural Sn near 8 MeV (see Fig. 27) and conclude that since the widths and general shapes are similar, all the isotopes of Sn, even as well as odd, must exhibit this characteristic structure near 8 MeV.

(*b*) ^{209}*Bi*, $^{206-208}$*Pb*. Fluctuations of the elastic cross section $\bar{\sigma}_{\gamma\gamma}$ and strength function $\vec{f}$ in ^{208}Pb and neighboring nuclei, shown in Figs. 2 and 15, cannot be identified for certain as either gross substructure or statistical fluctuations because the level spacing is large and the statistical

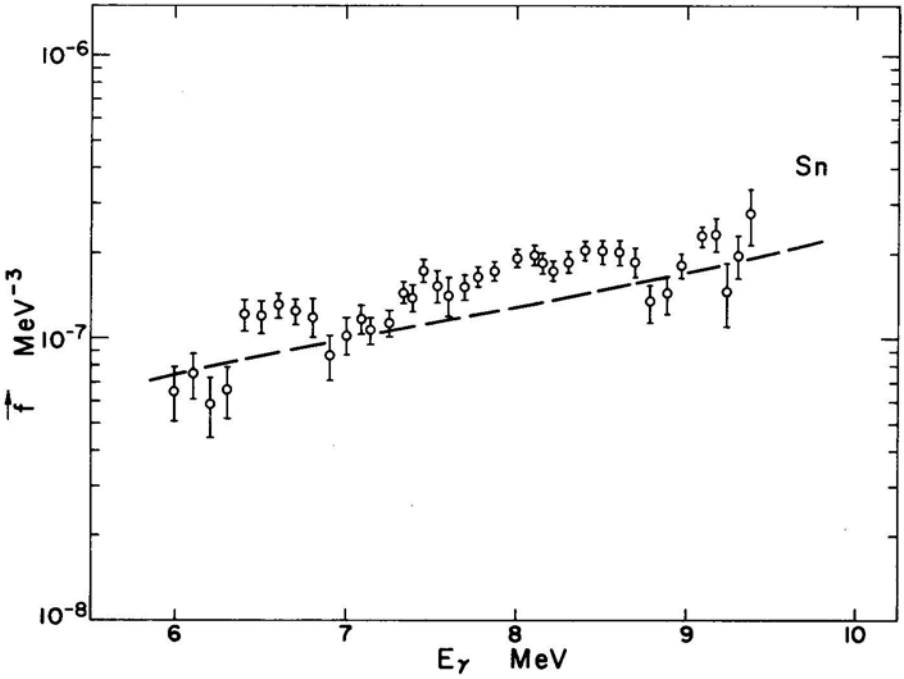

Fig. 27. The strength function $\vec{f}$ for Sn. The points are calculated from $\bar{\sigma}_{\gamma a}$ (AMS 70). In estimating $\bar{\sigma}_{\gamma a}$ it was assumed that only those isotopes contribute which have photoneutron thresholds above E_γ, that these isotopes have equal cross sections, and that photon partial widths follow a Porter–Thomas distribution.

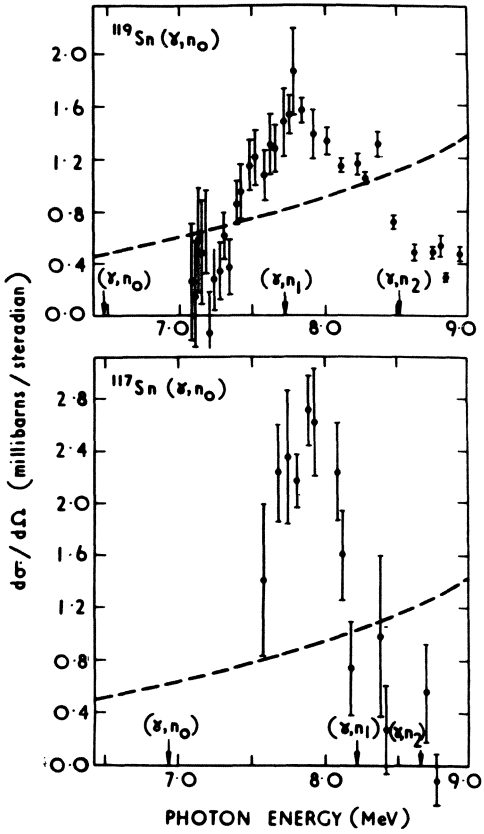

Fig. 28. Differential cross section measurements for ^{119}Sn(γ, n_0) and ^{117}Sn(γ, n_0) (Win+ 70).

sample size small. For example, the strength function below 7 MeV in ^{208}Pb (Fig. 15), obtained by averaging the few available individual transitions shows, within the wide limits of uncertainty, no evidence of substructure. On the other hand, $\bar{\sigma}_{\gamma\gamma}$ for ^{206}Pb and ^{209}Bi, obtained with moderate resolution (Fig. 2) shows considerable fluctuations which may represent a real substructure, especially if many transitions are involved in each peak. Perhaps a more definite substructure effect is indicated by the low values of $\bar{f}$ relative to the Lorentzian in ^{206}Pb and ^{207}Pb at 4.2 MeV in Fig. 15 and by the complete absence of dipole photoabsorption below 5.0 MeV in ^{208}Pb (Swa 73a). This is undoubtedly just a continuation of the step effect in f at ~4.5 MeV in elements between Tl and W (Figs. 16–19). This effect is discussed further in Sec. 4.2.2. A concentration of $M1$ strength is evident in the threshold photoneutron cross section and angular distribution

measurements on ^{208}Pb by Bowman *et al.* (Bow+ 70) and Toohey and Jackson (TJ 72). Bowman *et al.* report seven 1^+ states in ^{208}Pb between 7.5 and 8.5 MeV which combine to give a total $M1$ width of 52 eV. These measurements are only partly supported by Toohey and Jackson who conclude, because of uncertainty in identifying the outgoing neutrons as p or s-plus-d wave, that only two of the seven can be unambiguously assigned 1^+. For the same reason, some of the peaks between 602 and 846 keV, assigned by Bowman *et al.* (Bow+ 70) are probably not $M1$. Toohey and Jackson set a minimum integrated width of 20 eV for the $M1$ strength detected.

According to the shell model, the strength of the $M1$ excitation in ^{208}Pb is mostly contributed by spin flips from $i_{13/2}$ to $i_{11/2}$ for neutrons and from $h_{11/2}$ to $h_{9/2}$ for protons. If the $i_{13/2}$ and $h_{11/2}$ orbits contain more than one particle (Coh 71), the $M1$ strength can be enhanced to several times the single-particle value. Weiss (Wei 70) estimates a total $M1$ width of 100 eV, of which 43 eV is for the $i_{13/2}$ neutrons and 57 eV for the $h_{11/2}$ protons. However, spin-dependent forces between the excited particles and the residual nucleus can cause polarization effects (BM 69, page 388) which can reduce the single-particle magnetic moments by two and thus the $M1$ radiation widths by 4. With polarization included then, the total $M1$ strength can be between 25 and 50 eV. Thus the observed total width 20–50 eV could account for any amount between all the strength to less than half. Polarization, as well as reducing the strength, can cause a splitting in its distribution (GGS 66). Thus an $M1$ strength of 20 eV between 7.5 and 8.5 MeV might be accompanied by a like amount at lower energy. In the ^{208}Pb(e, e') reaction, $M1$ peaks at 7.9 MeV, $\Gamma_{\gamma 0} = 43$ eV and 6.2 MeV, $\Gamma_{\gamma 0} = 11$ eV have been observed (Fag+ 73). In the ^{208}Pb(γ, γ) reaction an $M1$ transition at 7.20 MeV, $\Gamma_{\gamma 0} = 0.8$ eV has been identified (MSW 70). A considerable amount of additional strength is known to be present (KK 67, KK 73, Sec. 5.3). Any one of these transitions, if $M1$, together with the $M1$ strength already observed would account for all $M1$ strength predicted by shell-model calculations.

Concentrations of $M1$ strength in ^{206,207}Pb (Bow+ 70) and of $E2$ strength in ^{207}Pb (Bow+ 70) and ^{208}Pb (Bus+ 72) are also reported.

(*c*) ^{238}U. A further example of substructure is that shown at 6.2 MeV in the photon strength function $\vec{f}$ of ^{238}U (KM 73) (Fig. 14). The peak, ~300 keV wide, is located at the fission threshold, just above the neutron separation energy, and is prominent in both the photoneutron and photofission cross sections. Angular distribution measurements of the fission

yield show the 6.2 MeV peak to have a $\sin^2\theta$ distribution, θ being the angle between the fission fragment direction and the incident beam direction. In the theory of fission discussed by Albertson and Forkman (AF 65) low-energy states with $J\pi = 1^{\pm}$ near the fission threshold can be described by exit channel quantum numbers $K = 0$ and $K = 1$ and should display photofission angular distributions $\sin^2\theta$ and $2 - \sin^2\theta$, respectively (KM 73). On this basis one associates the prominent peak at 6.2 MeV with the $K = 0$ exit channel and the underlying continuum with the $K = 1$ exit channel (KKC 70). However, this interpretation of fission yield substructure in terms of exit channels does not account for the corresponding substructure in the γ-ray strength function which concerns the entrance channel. A possible explanation is that photoabsorption over the 300-keV-wide energy interval containing the substructure takes place through at least two channels of comparable strength, each involving levels of spin $J = 1$. The most natural interpretation for these two channels is that they correspond to electric and magnetic dipole photoabsorption, the electric dipole absorption being associated with the substructure and the magnetic dipole with the underlying continuum.

4.2.2. Nucleon Transfer Reactions, 5.5-MeV Radiation

An oustanding feature common to many of the strength functions in Figs. 15–19 (Bi to W) is the irregularity below $\sim$6 MeV. This takes the form of a small "pigmy" resonance at 5.5 MeV in some nuclei, and a more or less abrupt decrease below 5 MeV in all nuclei in the range $182 < A \leq 206$. This feature gives rise to a bump $\sim$1 MeV wide at $\sim$5.5 MeV in the γ-ray spectra from (n, γ), $(d, p\gamma)$, and (γ, γ') reactions which was originally referred to as the "anomalous" bump (see historical remarks, Sec. 1). A similar but weaker bump is found in spectra from the region $108 \leq A \leq 134$ and evidence for a similar effect in (p, γ) reactions has been reported (Brz+ 71).

In this section we review experiments contributing to the understanding of the 5.5-MeV bump and relate the results to properties of the strength function. The fast neutron capture and $(d, p\gamma)$ reactions together provide a means of studying the 5.5-MeV bump over a wide range of excitation energy from $\sim$5 MeV, where some evidence of the effect begins to appear, to $\sim$4 MeV above the neutron separation energy, above which the effect becomes progressively obscured by the more intense γ-rays from the $(n, n'\gamma)$ reaction. Because of low energy resolution, (one is generally restricted to the use of NaI detectors by available γ-ray intensities in fast-

neutron capture and in $(d, p\gamma)$ particle–gamma coincidence measurements) detailed information about γ-rays comprising the bump is generally not obtained in those reactions. Fortunately, thermal and resonance neutron capture γ-ray spectra can be studied with high-resolution spectrometers and some information on the properties of individual γ-rays in the bump can be obtained. However, such measurements are limited to a narrow region of excitation energy, at most 100 keV wide, above the neutron separation energy. Examples of resolved lines in the bump from resonance capture in ^{205}Tl are shown in Fig. 29 (Ear+ 72a).

(*a*) *Origin of the 5.5-MeV Radiation.* The experimental results which we shall now discuss show that the 5.5-MeV bump γ-rays are primary, that they are emitted in the decay of resonances of the compound nucleus, and that the bump is not a consequence of local level-density irregularities but must be, as portrayed in Sec. 4.1, a strength function effect.

The 5.5-MeV bump has been shown to consist of primary radiation by application of the Ritz combination principle to neutron capture γ-rays aided by knowledge of the level scheme gained from other reactions. This has been particularly successful in fitting thermal neutron capture γ-rays from the bump region in ^{203}Tl$(n, \gamma)^{204}$Tl and ^{205}Tl$(n, \gamma)^{206}$Tl (Wei+ 69) and in ^{197}Au$(n, \gamma)^{198}$Au (Joh+ 66), and resonance neutron capture γ-rays in ^{205}Tl$(n, \gamma)^{206}$Tl (Ear+ 72a). Other examples of decay-scheme-fitting in the $182 < A \leq 206$ mass region have been compiled (Gro+ 69). In an elaboration of this approach, γ-ray coincidence measurements have been used to show that at least 45% of the bump γ-rays in the ^{199}Hg$(n, \gamma)^{200}$Hg thermal neutron capture spectrum are primaries (Bar+ 67). A still more convincing confirmation of the primary nature of the bump γ-rays is obtained in resonance neutron capture where it has been possible to show in several instances that the energies of bump γ-rays obey $E_\gamma = E_{\gamma 0} + E_n$, where $E_{\gamma 0}$ is the γ-ray energy corresponding to thermal capture. Similar shifts in E_γ or distortions of the resonance-averaged γ-ray line-shape obtained with the LNR technique (Sec. 3.4) can be used to establish primary assignment. By such methods the predominance of primary radiation has been demonstrated above ~5 MeV in Au (AB 68, LBT 72) and above ~4.7 MeV in Ta (HGR 71, LBT 72).

That the 5.5-MeV-bump γ-rays are emitted in γ-decay from resonances is evident (ELB 69) from many results, such as illustrated by the 2.800- and 3.048-keV resonances in Fig. 29, in which the fine-structure intensities fluctuate strongly from one resonance to the next while the overall bump shape is preserved. Were the bump a nonresonant, direct-capture effect,

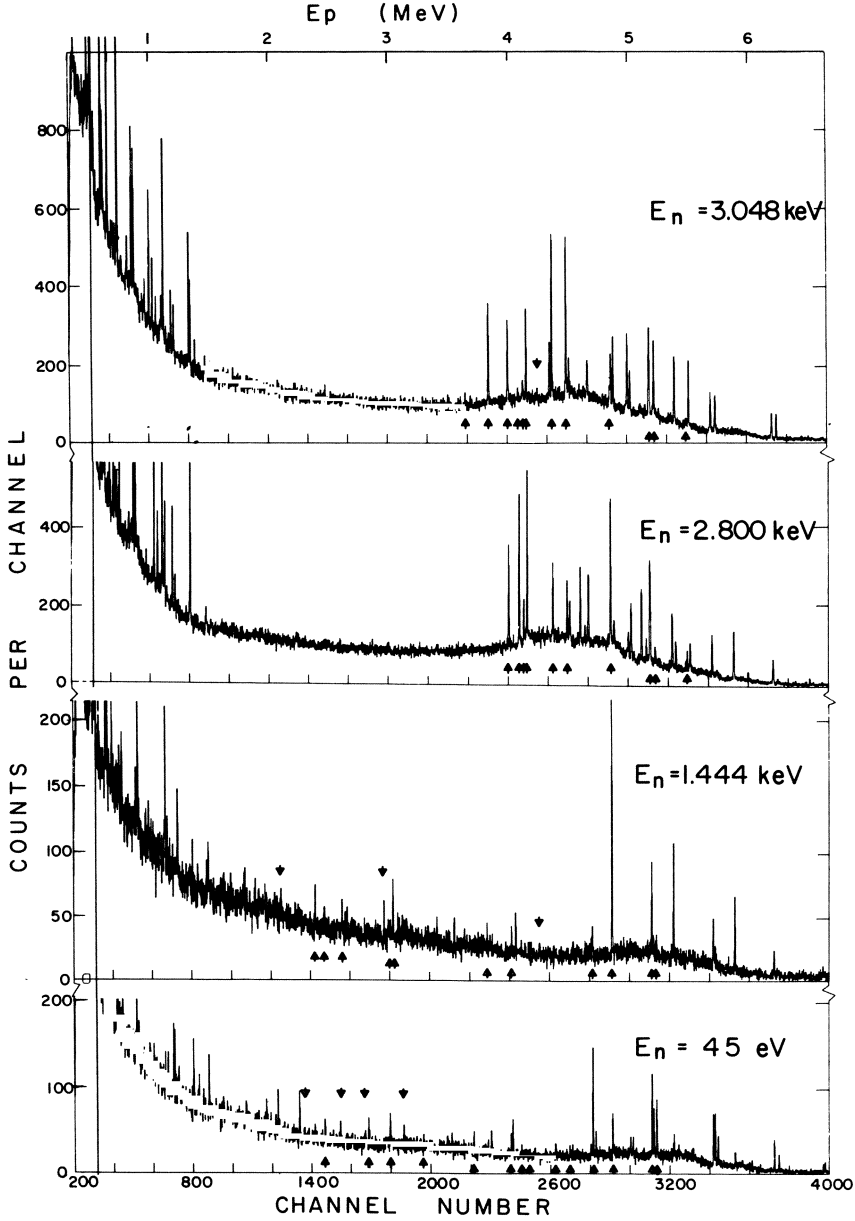

Fig. 29. High-resolution Ge(Li) spectra from neutron capture at neutron energies E_n in four resonances in the $^{205}Tl(n, \gamma)^{206}Tl$ reaction (Ear + 72a). The upper two are s-wave and the lower two p-wave resonances. Arrows under the curves indicate second-escape peaks of γ-rays known to be primaries. Arrows above the curves indicate γ-rays which may be either primaries or secondaries. The scale E_p gives the second-escape peak energy.

a uniform intensity pattern would persist over this narrow region of E_n. Furthermore, the partial capture cross section for production of the bump radiation in resonances is orders of magnitude larger than the prediction (LL 60) of $\sim$0.1 b for direct capture near lead.

Evidence that the 5.5-MeV bump radiation does not arise in primary transitions to a special group of levels at $(E_\lambda - 5.5)$ MeV was first given by Bergqvist *et al.* (BS 62, LS 65). As mentioned in Sec. 1, these authors showed that the center of gravity of the bump in Au does not change with E_λ for neutron bombarding energies, E_n, in the range $0 < E \leq 4$ MeV.* Similar effects are shown in Fig. 30 (Ear+ 72b) which displays γ-ray spectra observed in fast capture in Tl with $0.7 \leq E_n \leq 2.6$ MeV. The same invariance of the center of gravity of the bump with E_λ is shown in the region below E_B by the series of γ-ray spectra from ^{197}Au$(d, p\gamma)^{198}$Au (Fig. 31) (Bar+ 70). Clearly, with the final state E_i fed by the bump ranging over $0 < E_i < \sim 5$ MeV, as it does in the fast-neutron capture and $(d, p\gamma)$ experiments in Au, the possibility of involvement of special levels in a narrow region of excitation energy is eliminated. From Eq. (2.10) the most likely remaining variable able to account for the bump is then $\overleftarrow{f}_{XL}$. Closer inspection, however, shows that explanations involving nonuniform level densities and smooth, Lorentzian-like, strength functions cannot be so easily dismissed because, as E_λ increases both in the $(d, p\gamma)$ and fast-neutron capture reactions, the angular momentum transferred increases and the distribution of J for levels E_λ changes. The resonance-averaged primary spectrum is thus in reality given by $\sum_J \nu^J_{i\lambda XL}$ and it is conceivable that nonuniform distributions of levels in spin or parity at $(E_\lambda - 5.5)$ MeV might be matched with the changing J-distributions as E_λ increases to provide a 5.5-MeV bump, even with a smooth Lorentzian-type strength function. However, our attempts to reproduce the observed spectra by calculation from the known J-distribution and with plausible assumptions for the nonuniform spin and parity distributions at $(E_\lambda - 5.5)$ MeV and assuming a Lorentzian-type $\overleftarrow{f}$ have not met with success. Therefore, the simpler explanation involving an irregular $\overleftarrow{f}$ is preferred. This is also sup-

* In a recent study (Jai 72) of resonance neutron capture in Au, it is claimed that an intense cluster of γ-rays at $\sim$6.25 MeV following capture with thermal and 4.9-eV neutrons does not persist in capture in the range $80 < E_n < 830$ eV and therefore that this radiation must result from Porter–Thomas fluctuations. This confirms earlier conclusions (BS 62, Was+ 68), about the four γ-rays in this group; however, it does not support the suggestion (Jaï 72) that the entire bump in Au, which comprises some 100 γ-rays between 4 and 6.5 MeV and persists over several MeV of excitation energy, has a similar explanation.

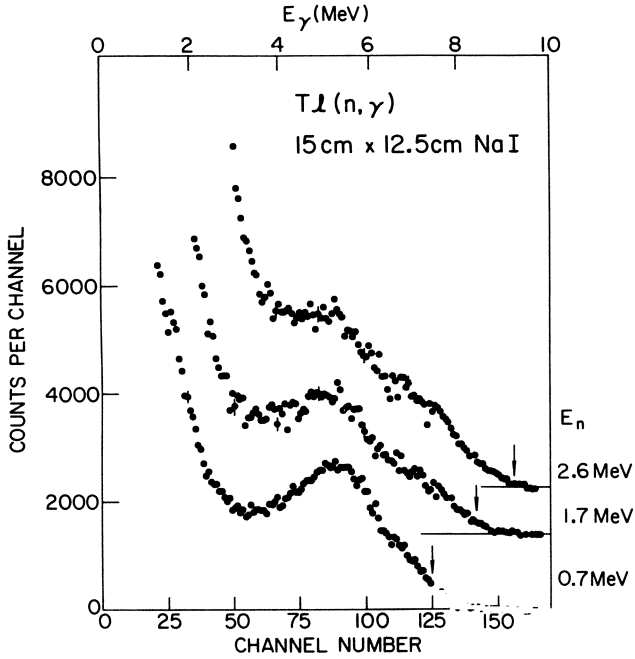

Fig. 30. Background-subtracted NaI spectra from neutron capture in natural Tl (Ear+ 72b). Neutron energies, E_n, are indicated at the right of each curve. The upper energy-limit for each spectrum is shown by an arrow. The sharp increase in counts at low energies is caused by the intense γ-rays from the $(n, n'\gamma)$ reaction.

ported, of course, by the available results for the photoexcitation strength function, $\vec{f}$, which show evidence of the pigmy resonance in Figs. 16 and 18 and some evidence for the step below ~4.5 MeV in Figs. 15 and 16.

Most of the above discussion has been concerned with the bump in the region $182 < A \leq 206$. In the lighter region $108 \leq A \leq 134$, the bump is weaker and uncertainties in $\varrho(E)$ greater. In the latter region, it has not been possible to ascribe the bump to the strength function with the same confidence, but the behavior of the observed spectra with E_λ (LS 65, Bar+ 70, see also Fig. 33) suggests that essentially the same phenomena are at work.

(*b*) *Properties of the 5.5-MeV Radiation.* We here discuss experiments that show that the bump γ-rays are largely of $E1$ type and we review the dependence of the detailed shape of the bump on Z, N, and E_λ.

The well-known fact that the high-energy $E1$ radiation ($E_\gamma > \sim 4.5$ MeV) is generally stronger than $M1$ radiation, except in isolated cases or limited regions of A (see Sec. 1), provides no guide to the multipole type predominating in the 5.5-MeV bump. Indeed, it is quite plausible to suppose (Sta 64) that this feature is a manifestation of a collective $M1$ giant resonance (Mot 60). However, as we now show, all evidence, at least in the $182 < A \leq 206$ region, points to $E1$ radiation.

In ^{206}Tl, the energies, parities, and some spins of the states $E_i < 2$ MeV fed by bump γ-rays in the ^{205}Tl(n, γ) reaction have been well studied (LD 70). On the basis of this information it is possible to conclude (Ear+ 71)

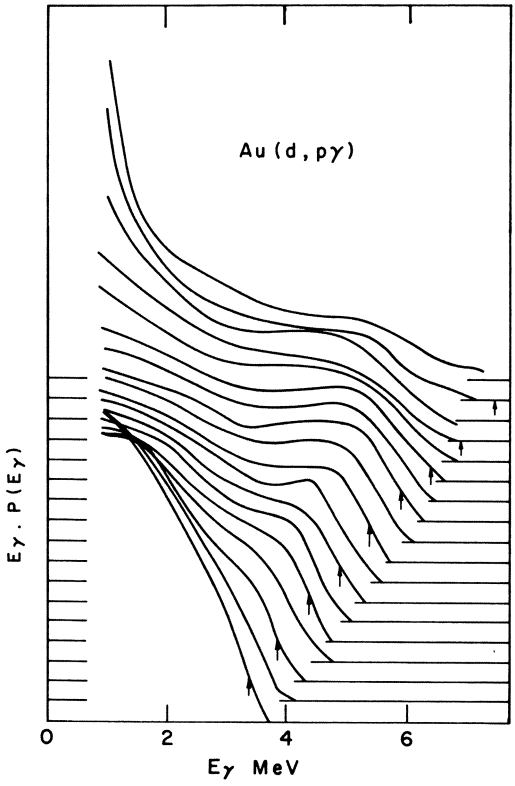

Fig. 31. Background-subtracted, smoothed, NaI spectra normalized to equal area, from the ^{197}Au$(d, p\gamma)^{198}$Au reaction (Bar+ 70). Curves are plotted as a function of channnel energy. The ordinate is counts per channel times channel energy. Each spectrum was obtained in coincidence with a proton energy window $\sim$ 0.24 MeV wide as indicated in Fig. 9. The upper energy limits of various spectra are indicated by arrows; the neutron separation energy is $\sim$ 6.5 MeV.

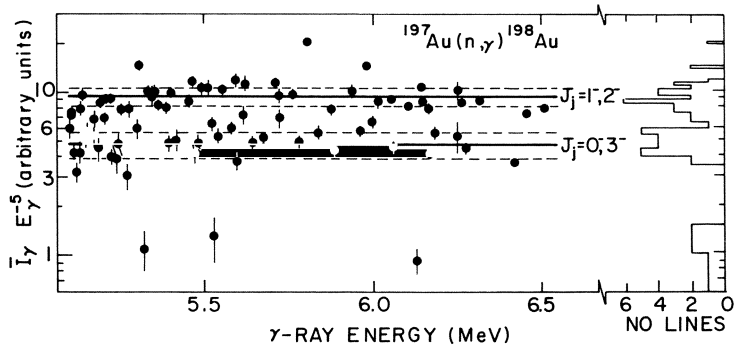

Fig. 32. Average reduced γ-ray intensities for ^{198}Au obtained by the low-neutron-resolution method (LBT 72). See Fig. 12 for further explanation of curves. The histogram on the right shows the distribution of points on the intensity scale.

that all of the strong-bump γ-rays from the s-wave resonances $E_n = 2.800$ and 3.048 keV in Fig. 29 are of $E1$ type. The γ-rays feeding the same levels following p-wave capture for resonances at $E_n = 45$ eV and 1.444 keV in the same figure, are by the same arguments $M1$ and show a less pronounced bump (see also Ear+ 72a).

In ^{200}Hg at least 85% of the γ-rays above ~4.5 MeV following thermal neutron capture in ^{199}Hg have been shown to be $E1$ by coincidence and polarization correlation measurements (Bar+ 67, BGE 67).

In ^{198}Au (LBT 72), Fig. 32, and Ta (HGR 71), Fig. 13, the LNR high-resolution γ-ray technique (Sec. 3.4) has been used to identify $E1$ and $M1$ radiation in the bump. In both cases a predominance of $E1$ radiation was found. Similar conclusions have been reached by this technique in other nuclei (Table III) and also, on the basis of the known spins and parities of the states involved, in Re (She+ 72).

In the mass region $108 \leq A \leq 134$, the γ-ray assignments are, in general, less certain. However, Lottin and Paya (LP 71) have shown that in ^{122,124}Sb the γ-rays between 5 and 6.8 MeV are equally distributed between $M1$ and $E1$ type. Similar results are found in ^{116}In and ^{106}Pd (see Table III).

The progressive diminution of the irregularity in f with decreasing Z between Pb and Ta in Figs. 15–20 is shown rather more dramatically by the sequence of smoothed γ-ray spectra for the $(d, p\gamma)$ reaction Fig. 33a, c and the (n, γ) reaction Fig. 33b, d (Bar+ 70). All curves correspond to $E_\lambda \simeq E_B$. This mass dependence of the 5.5-MeV radiation is presented quantitatively for the $182 \leq A \leq 208$ region in Fig. 34. Part (a) of this figure shows the integrated strength between 1 and 6 MeV for both the experimental $\bar{f}$ and the Lorentzian-based curve. This shows that the strength

in this energy region is roughly half that predicted from the giant dipole tail. The total ground-state radiation width for levels of a particular J of γ-rays comprising the 5.5-MeV bump, as given by the sum between 4 and 6 MeV, is shown in Fig. 34b. This quantity, as typified by the value of $\sim$25 eV for Au, is considerably less than previous estimates, $\sim$90 eV (BS 70), because of readjustments incorporating more realistic level densities (see Sec. 3.2, Fig. 8). In Fig. 34c we present a measure of the irregularity as percent deviation of the energy-weighted strength function from the Lorentzian cross section. To obtain these points, the energy-weighted spectrum-fitted strength functions (Figs. 16-20) were shifted until equal deviations occurred above and below the smooth Lorentzian, and the integrated

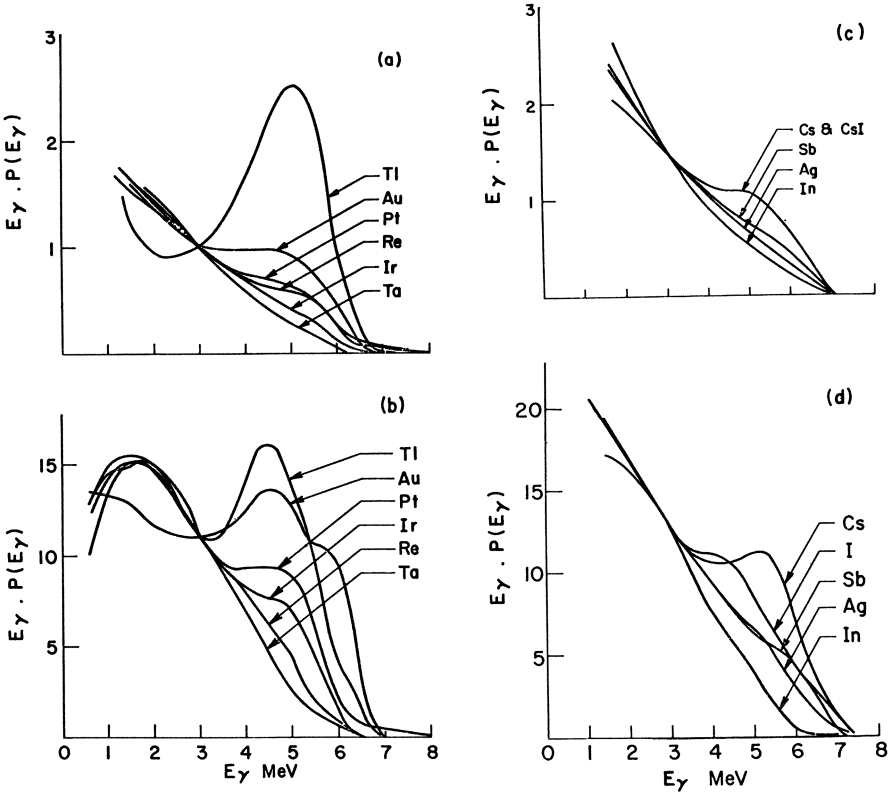

Fig. 33. Spectral shapes from $(d, p\gamma)$ and (n, γ) reactions. Background-subtracted, smoothed, NaI spectra are arbitrarily normalized at 3 MeV for (a), (c), the $(d, p\gamma)$ reaction and (b), (d) the (n, γ) reaction with thermal neutrons, for the target elements shown. The abscissa and ordinate are channel energy and counts per channel times channel energy, respectively.

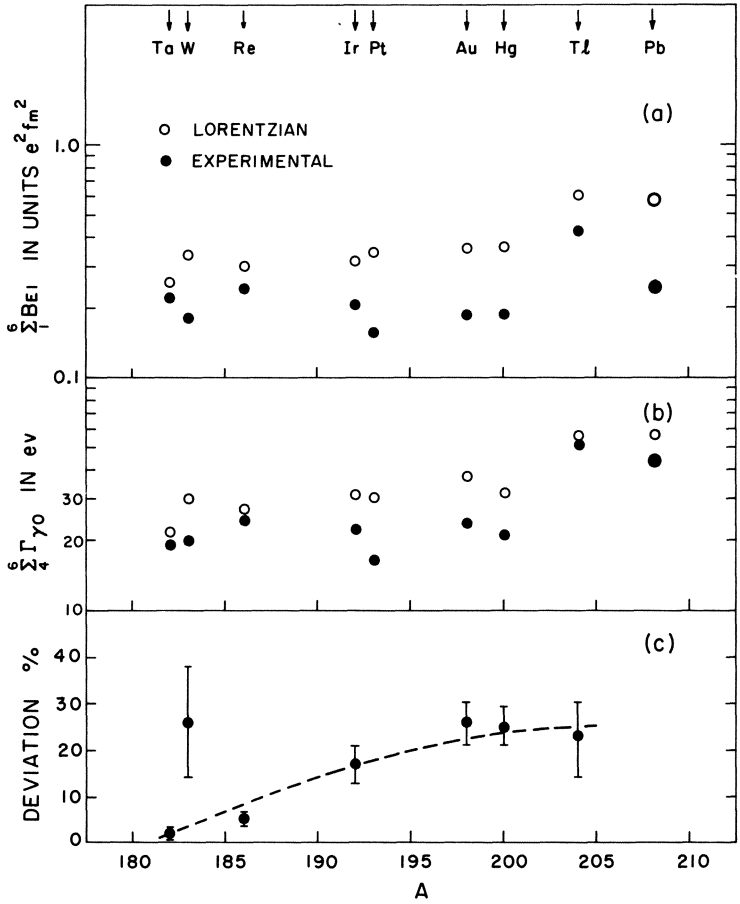

Fig. 34. Assessment of the dipole strength below 6 MeV in nuclei Ta to Pb. (a) The sum of $E1$ reduced widths of levels of a particular J between 1 and 6 MeV in e^2fm^2 units. The $B_{E1}(e^2fm^2)$ per unit excitation energy interval (BM 69, p. 382), averaged over all possible spin combinations, is equal to $0.956 \times 10^6 f_{E1}$ (MeV^{-3}). (b) Total ground-state γ-ray width of levels of a particular J in the γ-ray bump region, 4–6 MeV. (c) Percent deviation of the observed energy-weighted strength function from that derived from the Lorentzian. Target elements are identified at the top of the figure.

deviation below the crossover energy was computed. The error bars represent uncertainties from Porter–Thomas fluctuations. Apart from tungsten, for which the fluctuations are large, all points fall near a smooth curve increasing with A. In ^{208}Pb itself (Fig. 15), Porter–Thomas fluctuations prevent a meaningful estimate of the deviation but, from Fig. 34a and b, it would appear that the behavior in Pb represents a normal continuation

of that in the lighter nuclei. This conclusion is at variance with an earlier impression that in spite of the apparent close connection of the irregularity with the ^{208}Pb closed shell, ^{208}Pb itself presented a glaring anomaly. That notion was engendered partly by the absence of a strong bump at 5.5 MeV in the thermal neutron (n, γ) spectrum from natural Pb (Gro+ 69) and in $(d, p\gamma)$ spectra above the neutron threshold (Bar+ 70), but more by the seemingly low value of $\sum_4^6 \Gamma_{\gamma 0}$ of only $\sim$40 eV from photoexcitation experiments in ^{208}Pb as compared to the once current higher values, $\sim$200 eV, for all levels which decay to the ground state by $E1$ radiation in Au and neighboring nuclei (BS 70).

Inspection of Figs. 16–19 shows that within the errors, no consistent variation of the position or magnitude of the strength function irregularity can be associated with even or odd values of N.

Some differences in the shapes of the strength functions with E_λ ($E_\lambda = E_B + E_n$) are evident in the curves of Fig. 16c and Fig. 20b, and between the curves of Figs. 18b and c. Similarly, below the threshold, some differences in functional form are shown by the curves of Fig. 10. It is not clear, in view of the large possibilities for systematic error (Sec. 4.1) whether any of these trends represent a real dependence of f on E_λ. The most significant trend is perhaps the smoothing of the irregularity with increasing E_λ in Tl (Fig. 16). But even this is not supported by a similar trend in Ta (Fig. 20). Therefore it seems prudent to conclude that more careful measurements are needed before any dependence on E_λ can be inferred with confidence.

4.2.3. Other Reactions

In this section we consider several experiments whose results cannot yet be completely reconciled with the essentially consistent, though fragmentary, picture of strength functions derived from studies with (γ, γ), (n, γ) and $(d, p\gamma)$ reactions presented in Secs. 4.2.1 and 4.2.2. The experiments in question involve $(n, n'\gamma)$, $(p, p'\gamma)$ and $(\mu^-, xn\gamma)$ reactions in which the observed γ-ray spectra in general fail to show the 5.5-MeV bump seen in the other reactions. A typical example of this effect in the $182 \leq A \leq 208$ range is provided by the γ-ray spectrum observed by Bergqvist *et al.* (Ber+ 66a) following 7.5-MeV neutron bombarding of Au (Fig. 35). The γ-ray spectrum from the (n, γ) reaction with 0.3-MeV neutrons shown in the same figure exhibits the usual bump at $\sim$5.5 MeV while the $(n, n'\gamma)$ spectrum shows no sign of it.

It is a weakness of most $(n, n'\gamma)$ measurements that it has not been possible, because of insufficient intensity, to isolate narrow intervals in

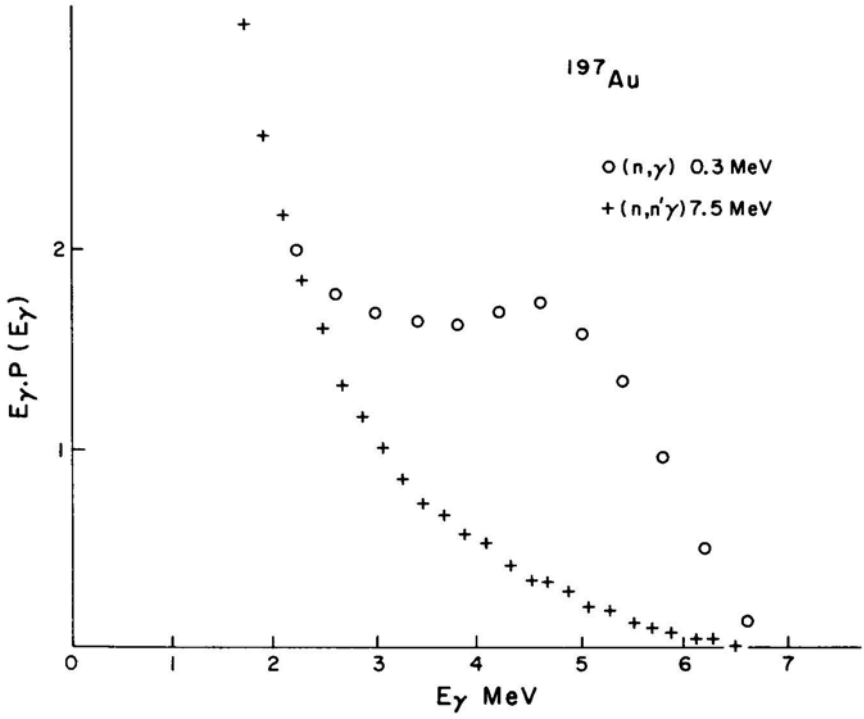

Fig. 35. Comparison of NaI spectra from the (n, γ) and $(n, n'\gamma)$ reactions on ^{197}Au. The abscissa and ordinate are channel energy and counts per channel times channel energy, respectively (Ber+ 66a).

excitation energy by imposing energy selection on the inelastic neutrons. In the absence of this energy gating, the γ-ray spectrum observed is the sum over the spectra from all energetically possible excitations weighted according to the partial cross section for excitations of those regions. This need not necessarily obscure the 5.5-MeV radiation, since this radiation is emitted essentially independently of E_λ, but details of the γ-ray spectrum are likely to be smeared compared to what would be obtained if spectra in coincidence with neutrons in a narrow energy band could be measured. This lack of energy definition on the outgoing particle, so difficult to avoid in $(n, n'\gamma)$ experiments, may be overcome in the $(p, p'\gamma)$ reaction where energy gating is easier. However, it has been shown (Lon+ 72) in the ^{195}Pt$(p, p'\gamma)$ reaction with the energy of the p' particles well-defined by suitable energy windows, that there is still no evidence for the 5.5-MeV bump in the coincident γ-ray spectra. We have found the results, shown on the right-hand side of Fig. 36, to be common to Tl, Au, and other targets

in the $182 < A < 206$ mass range. Figure 36 also shows for comparison, spectra from the ^{194}Pt$(d, p\gamma)^{195}$Pt reaction in which the same regions of excitation in ^{195}Pt are gated. These clearly show the presence of a 5.5-MeV bump. From these results we conclude that the absence of the bump in the $(n, n'\gamma)$ experiments (Fig. 35) is probably real, i.e., not simply a consequence of the absence of gating on the inelastic neutrons.

A further difference noted in γ-ray spectra from the $(n, n'\gamma)$ reaction as compared to the reactions considered earlier is the presence of a 4.1-MeV radiation in the γ-spectra from targets near lead. This effect has been observed in Pb$(n, n'\gamma)$ (Ber+ 66a), ^{206}Pb$(n, n'\gamma)$ (Ber 70), ^{208}Pb$(n, n'\gamma)$ (Ber+ 66b, NMH 70) and ^{209}Bi$(n, n'\gamma)$ (Ber+ 66a). Figure 37 shows an example of the results in ^{206}Pb$(n, n'\gamma)$ where the effect is particularly pronounced. It is well established from high-resolution γ-ray data in ^{208}Pb$(n, n'\gamma)$ that the 4.1-MeV γ-ray is a secondary emitted in the decay of the 4.07-MeV 2+ state (NMH 70), a conclusion supported by the observation of a strong neutron group feeding that level (Ber+ 66b, Ste+ 65). It seems likely that the same interpretation should apply to the other spectra where this radia-

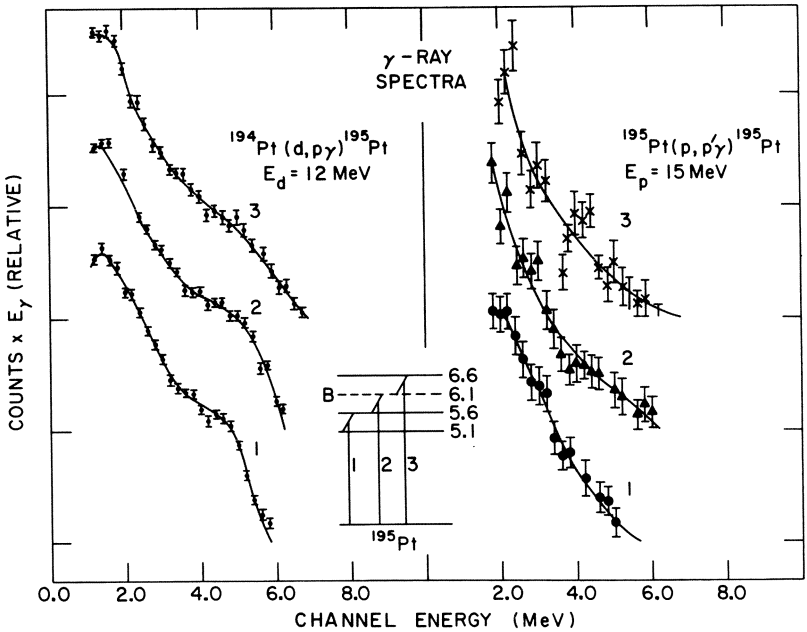

Fig. 36. Comparison of NaI γ-ray spectra from the ^{194}Pt$(d, p\gamma)^{195}$Pt and ^{195}Pt$(p, p'\gamma)$ ^{195}Pt reactions (Lon+ 72). The final state energy intervals are indicated in the inset decay scheme. The broken line, B, indicates the neutron separation energy in ^{195}Pt. The abscissa and ordinate are channel energy and counts per channel times channel energy, respectively.

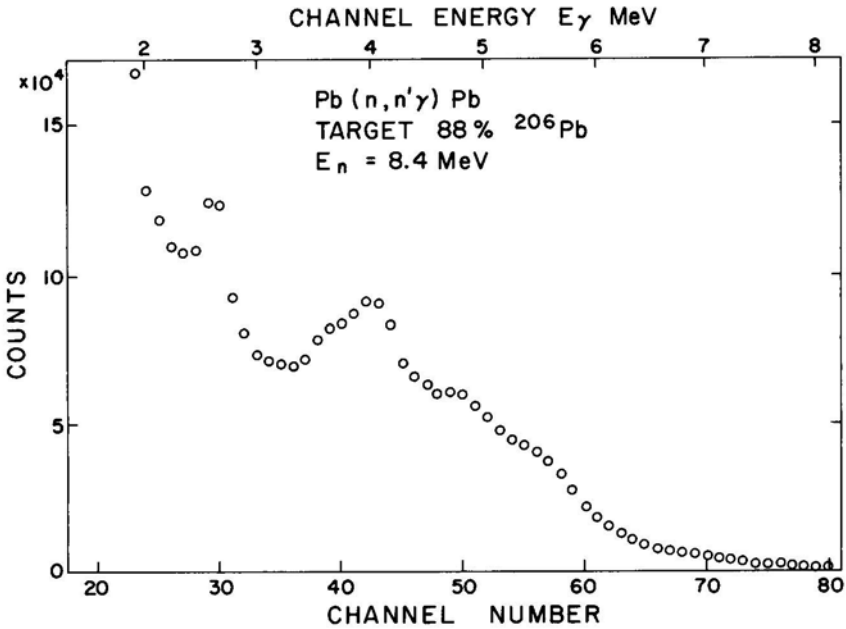

Fig. 37. NaI spectrum of γ-rays from the Pb(n, $n'\gamma$)Pb reaction (Ber 70).

tion is seen. Therefore this 4.1-MeV radiation is, in a sense, extraneous to the present topic of strength functions which concerns the primary decay spectrum.

Another type of reaction in which the overall spectrum shape near 5.5 MeV can be investigated is the (μ^-, $xn\gamma$) reaction. Gamma-ray spectra following this reaction have been studied in Bi, ^{208}Pb, radiogenic Pb, Au, Ag, and Zr targets (EB 71). These spectra are complicated by formation of several product nuclei in each reaction, corresponding to the emission of zero, one, two, etc., neutrons, and by a wide (and largely unknown) energy distribution in the final nucleus prior to γ-emission. Nevertheless, the γ-ray spectra are of interest because as in the (n, $n'\gamma$) spectra, there is no 5.5-MeV bump and, for Bi, radiogenic Pb, and Au targets, a γ-ray or group of γ-rays centered at $\sim$4.1 MeV is clearly evident (Fig. 38).

In an attempt to explain the absence of the 5.5-MeV reaction in the (n, $n'\gamma$) experiments, three alternatives have been considered (Ber+ 66a):

a. An isotope effect. The (n, $n'\gamma$) reaction excites the target of mass A while the (n, γ) reaction excites the final nucleus $A + 1$.
b. An angular momentum effect. The (n, γ) reaction involves relatively

low l-values, ≤ 3 for $E_n < 4$ MeV, while the $(n, n'\gamma)$ reaction at $E_n \sim 8$ MeV can in general involve much higher l-transfers.

c. A reaction mechanism effect. For example, the (n, γ) reaction might involve excitation of only a few valence nucleons while the $(n, n'\gamma)$ reaction might involve primarily collective core excitations.

Alternative (a) was ruled out by Bergqvist and co-workers (Ber+ 66a) from examination of spectra from natural targets containing both even and odd isotopes. It is now even more effectively ruled out by observations (Sec. 4.2.2) that the 5.5-MeV bump, when present, is independent of N and by the evidence of Fig. 35 which shows the bump in $(d, p\gamma)$ but not in $(p, p'\gamma)$ for the same N.

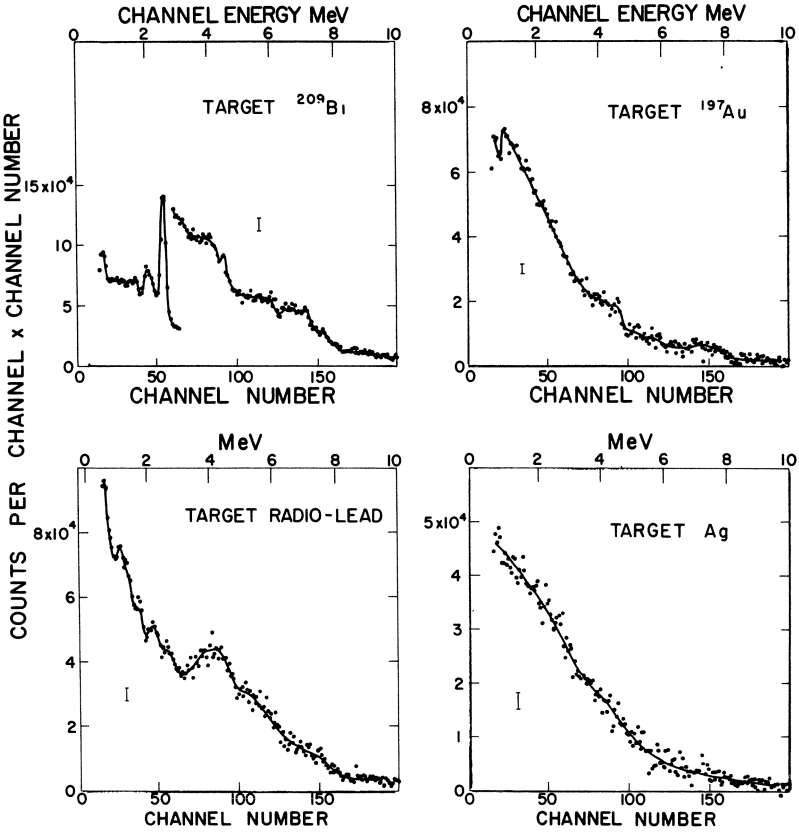

Fig. 38. Background-subtracted NaI spectra of γ-rays from the $(\mu^-, xn\gamma)$ reaction (EB 71). The radiolead target contained 88% ^{206}Pb, 9% ^{207}Pb, and 3% ^{208}Pb. Vertical arrow bars near each curve are representative of uncertainties from counting statistics.

Under alternative (b) it is necessary to postulate a scarcity of high-spin states at $E_\lambda - 5.5$ MeV that can be fed by dipole transitions from the high-spin levels in which the nucleus is left at E_λ following emission of the n' neutron. Thus for $E_n = 7.5$ MeV as in Fig. 35, assuming the peak of the distribution of inelastic neutrons occurs at $\sim$1 MeV, we expect the residual nucleus to be excited to roughly 6.5 MeV and subsequent 5.5-MeV γ-emission to feed states near 1 MeV. At the latter energy, because of the spin-cutoff effect, there may be very few states of high J and hence few γ-rays near 5.5 MeV could appear, regardless of the form of $\bar{f}$. In considering this possibility Bergqvist *et al.* (Ber+ 66a) noted that, while the initial J-distribution at E_λ after inelastic scattering by 7.5-MeV neutrons would, on the basis of Hauser–Feshbach calculations, be expected to be wider than that following fast-neutron capture, about one third of the states would nevertheless have the same J. They further surmised that if the absence of the 5.5-MeV bump was caused by a shortage of high-spin states at $\sim$1 MeV, inelastic scattering at a higher bombarding energy should give a γ-ray spectrum more similar to that from neutron capture. To test this, they increased E_n to 8 MeV but again observed no bump. They therefore rejected alternative (b) in favor of (c). Recently, we have made a calculation of the spectral distribution assuming an energy-dependent spin-cutoff as discussed in Sec. 2.3. The results for $E_\lambda = 6$ MeV, given in Fig. 39, show that while a bump is obtained for low J, it does disappear progressively as J increases. Similar results are obtained at 8 MeV. Thus we conclude that alternative (b) cannot be ruled out. A somewhat similar conclusion was reached by Brzosko *et al.* (Brz+ 69).

To explore alternative (c), we note that it implies that two more-or-less independent types of levels must coexist in the resonance region, those favored in neutron transfer and those favored in inelastic scattering and μ^--capture, and that these two types of levels must be associated with different strength functions, $\bar{f}$. The difference between the two classes might again be simply a matter of the average J. However, unlike (b) where the level distribution with J is suspect, here we assume that $\bar{f}$ is J-dependent. Alternatively, some other parameter could give rise to different γ-decay strength functions.

In one attempt to shed more light on this possibility (Bar+ 69, Bar 69), the ^{207}Pb$(p, p'\gamma)^{207}$Pb reaction was studied at bombarding energies exciting, in ^{208}Bi, isobaric analog resonances (IAR) of various well-localized (MKB 67) neutron particle–hole states in ^{208}Pb. It was recognized that inelastic proton emission from these IAR's would lead to states in ^{207}Pb with large components in their wavefunctions corresponding to configurations in

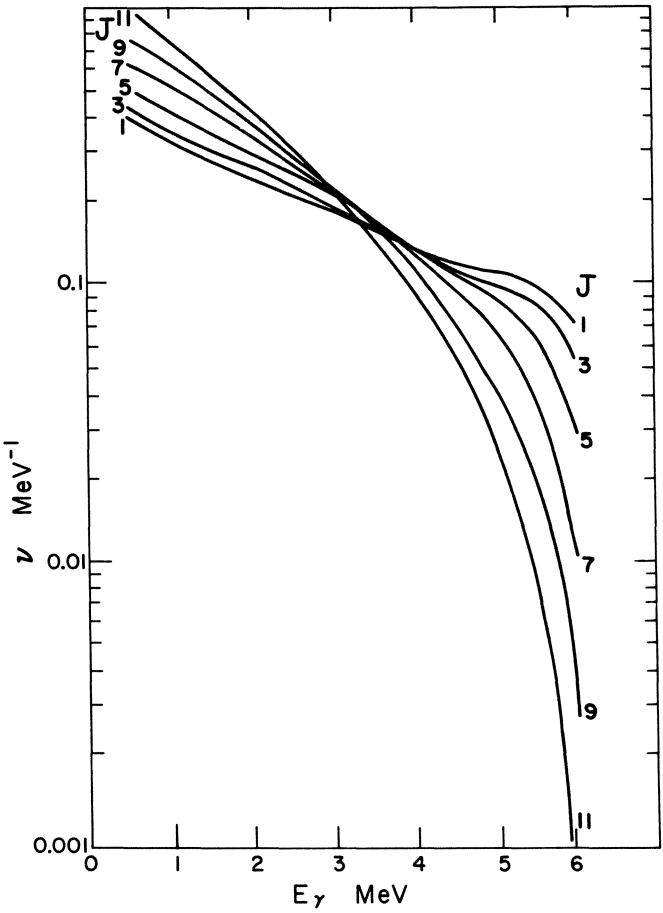

Fig. 39. Gamma-ray spectral distributions calculated with an energy dependent spin-cutoff parameter $\sigma(E) = \sigma(E_0)(E/E_0)^{1/4}$. Each curve is identified with spin J of the initially excited state.

which the particle–hole in question was coupled to a second neutron hole, forming a one-particle–two-hole state. Since many of the latter states would be precisely the type that might be expected to be excited strongly as doorway states in neutron-transfer reactions in ^{206}Pb, it was felt that the observation of a 5.5-MeV bump in ^{207}Pb$(p, p'\gamma)^{207}$Pb via the IAR that was similar in size and shape to that found in the ^{206}Pb$(d, p\gamma)^{207}$Pb reaction would be evidence at least of a simple doorway mechanism in the neutron transfer reaction. However, at the same time, to support alternative (c), it would be necessary to find *no* bump at off-IAR bombarding energies in

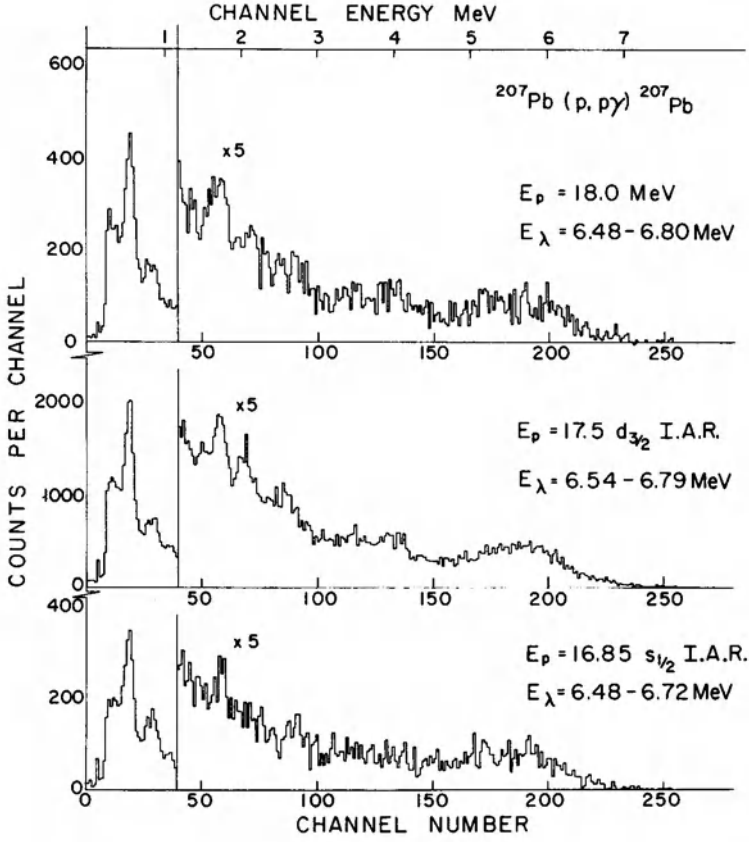

Fig. 40. Background-subtracted NaI spectra of γ-rays from the ^{207}Pb$(p, p'\gamma)^{207}$Pb reaction. Proton bombarding energies are indicated by E_p, and the excitation energy intervals in the residual nucleus by E_λ. The uppermost curve represents excitation in ^{208}Bi above the particle–hole IAR region. The lower two curves represent the excitation of isobaric analog resonances (IAR) corresponding to the $d_{3/2}p_{1/2}^{-1}$ and $s_{1/2}p_{1/2}^{-1}$ neutron particle–hole states in ^{208}Pb.

accordance with the usual $(p, p'\gamma)$ spectra as in Fig. 36 or with the $(n, n'\gamma)$ spectra. The results, presented in Fig. 40, show that a 5.5-MeV bump *does* appear in spectra following bombardment at the $s_{1/2}p_{1/2}^{-1}$ and $d_{3/2}p_{1/2}^{-1}$ isobaric analog resonances but an equally strong bump also occurs with bombardment at $E_p = 18$ MeV, well above the IAR region. Hence no definitive support for alternative (c) can be claimed.

In another attempt to explore alternative (c), differences in $\bar{\Gamma}_n$ were sought for levels just above threshold in ^{195}Pt excited by ^{194}Pt(d, p) and

^{195}Pt(p, p') reactions (Lon+ 72). It was hypothesized that if alternative (c) were true, then the type of resonance favored in neutron transfer might on the average tend to have larger neutron widths than those participating in inelastic scattering and this property might be correlated with the differences in γ-ray spectra. It was found, however, that while the $\bar{\Gamma}_n$ associated with the (d, p) reaction were indeed larger by a factor of about 6 than those associated with the (p, p') reaction, these results and the differences in γ-spectra in Fig. 36 could be accounted for by the dissimilarities in J-distributions and it was therefore not necessary to seek further differences between the resonances favored in the two types of reaction.

In summary, it would appear that while alternative (c) is not ruled out, it is not necessary to assume anything more complicated than (b). It can be said in favor of (c), however, that it is well known in the lighter elements and at low excitations in heavy elements, that (d, p) reactions favor shell-model type states while scattering reactions tend to excite collective states. It might be assumed therefore that some tendency in this direction persists into the resonance region and indeed the presence of the 4.1-MeV radiation suggests that higher collective band members may also be strongly excited. On the other hand, this picture of more or less distinct types of resonance is contrary to the extreme statistical model of the compound nucleus; it would violate the Porter–Thomas distribution, for example. Much firmer evidence would therefore be required to establish such a radical departure (Lan 72b).

5. DISCUSSION

5.1. General

From diverse fragments of information, obtained from several experimental methods, it has been possible to gain a rough overview of the absolute strength function for $E1$ radiation and, less completely, for $M1$ radiation, in the range $2 < E_\gamma < 10$ MeV as a function of A in heavy elements. Almost no information is available on higher multipoles. Except for the limited range $\sim 5 < E_\gamma < \sim 8$ MeV in some elements, separation of $E1$ and $M1$ strength functions has not been achieved. Outside this range it is necessary either to make do with a composite (all multipoles) strength function or to assume from known systematics that $E1$ radiation will, on the average, be somewhat stronger than $M1$ and therefore tentatively adopt the composite strength function as purely $E1$.

In elements where several isotopes have been examined, the strength functions are found to be roughly similar in form and magnitude from isotope to isotope. In Ta, Au, and Tl, where measurements have been made as a function of initial excitation energy, E_λ, the decay strength function, $\overleftarrow{f}_{i\lambda}$, maintains roughly the same functional form in the range $\sim 3.5 < E_\lambda < E_B + 4$ MeV.

5.2. Compatibility of Strength Functions

Agreement among the three methods yielding $\overleftarrow{f}$ is, within the errors, satisfactory. In the two low-resolution γ-ray methods, spectrum fitting and sequential extraction, both the functional form and absolute magnitude of $\overleftarrow{f}$ depend crucially on the form and scale of the level-density function used. Good agreement between these methods and the high-resolution γ-ray method for $E_\gamma > 5$ MeV occurs largely because the most accurate estimates of the level densities at low energies, $E_i < (E_B - 5$ MeV), are obtained as a byproduct of the latter method. Failure to detect *all* the levels of required spin and parity at low excitation energies has been a source of error in earlier level-density determinations from other reactions. On the other hand, good agreement between the spectrum fitting and sequential extraction methods in the range $E_\lambda < 5$ MeV, where they stand alone as the only methods giving $\overleftarrow{f}$, does not necessarily indicate good absolute reliability for either method because in the excitation energy region concerned, $(E_B - 5 \text{ MeV}) < E_\lambda < E_B$, both methods make use of level densities obtained by interpolation.

The present studies present an opportunity to compare the photoexcitation strength function and the γ-decay strength function. Within the limited energy ranges in the two examples, Au and Tl, wherein energy overlap of $\overleftarrow{f}$ and $\overrightarrow{f}$ occurs (albeit in neighboring isotopes) there are, within the errors, no significant differences in form or magnitude between these strength functions. Most noticeable is the tendency of $\overrightarrow{f}$ in Tl (Fig. 16a) not to follow the sharp decrease with decreasing E_γ below 5 MeV shown by $\overleftarrow{f}$ in Figs. 16b and c. This may be merely a statistical fluctuation or possibly the result of a systematic error introduced in the measurements or analyses of either $\overrightarrow{f}$ or $\overleftarrow{f}$. On the other hand, it may be real, e.g., it may be a true isotopic difference or, as suggested by the cross section (Fig. 5) it may be a local substructure effect that the spectrum fitting and sequential extraction methods for $\overleftarrow{f}$ do not resolve.

For a valid test of the Brink hypothesis it is necessary, as pointed out in Sec. 2.2, to establish that $\overrightarrow{f}_{0\lambda}$ and all the $\overleftarrow{f}_{i\lambda}$ have the same functional form

in the same nucleus. The necessary data for a complete test are not at hand but a comparison of $\vec{f}_{0\lambda}$ for ^{197}Au with the internally compatible $\overleftarrow{f}_{i\lambda}$ from sequential extraction in ^{198}Au (Fig. 18) shows reasonable consistency in the small range, 5–6.5 MeV, where they overlap. Fair compatibility between $\overleftarrow{f}_{i\lambda}$ for a limited range of E_λ above the neutron threshold in ^{204,206}Tl and $\vec{f}_{0\lambda}$ for ^{205}Tl is also shown in Fig. 16 but the necessary demonstration of common form for the $\overleftarrow{f}_{i\lambda}$ for all E_λ is lacking in this case. However, these partial tests, together with the partial demonstration by Rosensweig (Ros 68) using ^{196}Pt resonance-average γ-ray data, support the Brink hypothesis as a good working hypothesis in heavy elements. It is unclear over what range of E_λ this hypothesis might remain even approximately true. There are some suggestions of a gradual, but consistent, smoothing of $\overleftarrow{f}_{i\lambda}$ with increasing E_n in Tl (Fig. 16) but, as discussed earlier, these differences are scarcely significant in view of the possible systematic errors.

5.3. *E*1 Strength Function

In most elements far from closed shells, f_{E1} is in fair agreement in form and magnitude with that predicted from the Lorentzian both above and below the neutron threshold. In elements between Ta and Pb, f_{E1} usually falls below the Lorentzian curve for $E_\gamma < 6$ MeV (Fig. 34). Near closed shells there are strong irregularities in f_{E1}. In extreme cases, e.g., Tl (Fig. 16) there is a small but definite pigmy resonance at $\sim$5.5 MeV, but more markedly in all nuclei in the range $182 \leq A \leq 208$ there is rapid decrease of strength for $E_\gamma < 4.5$ MeV as compared to the Lorentzian. The 5.5-MeV bump in the γ-ray spectra from these elements is more a result of this sharp step than of any pigmy resonance that may or may not be present. Other evidence for coarse substructure is found near the 82-neutron and 50-proton closed shells. Thus, while the E_γ^5-law (Axe 62) provides a reasonably good approximation to the energy dependence for $E1$ radiation in the range $5.5 < E_\gamma < 8$ MeV in most nuclei, it should not be regarded as an appropriate standard for intensity comparison below 5.5 MeV, as has been a frequent practice in the recent literature.

Because of the proximity to closed shells of elements exhibiting the 5.5-MeV γ-ray bump, attempts to explain that effect have all naturally assumed a part to be played by shell structure. It has also seemed appropriate to invoke simple models of the capture mechanism which might be valid near closed shells. It was early established (LL 60) from a consideration of the partial capture cross sections involved, that the 5.5-MeV bump in elements near Pb cannot be a result of direct capture or of channel, i.e.,

valency (Lyn 68, p. 236) capture. It was natural therefore to consider (Bar+ 70) that the next most complicated process, viz., doorway capture, might be responsible. In this process, one pictures the incoming nucleon undergoing a two-body interaction exciting a nucleon from the core to some higher orbit while itself dropping to a bound orbit thereby forming a two-particle–one-hole ($2p1h$) "doorway state" (BF 63). Near closed shells the particle–hole (ph) excitation would for most, but not all, orbitals of interest introduce a parity change. In nuclides near ^{208}Pb many of the unperturbed ph energies for neutrons cluster near 5.5 MeV; those for protons somewhat higher. Hence γ-decay of the doorway state which would occur by ph annihilation might be expected to give rise to the 5.5-MeV $E1$ radiation. Furthermore, because the second excited particle might occupy any unfilled orbit consistent with the energy balance and selection rules, a mechanism is provided for the 5.5-MeV radiation to be emitted over a a wide range of E_λ, as observed. In a real nucleus the $2p1h$ state would of course be mixed with other states near the same energy. What is needed to complete this picture is a mechanism providing significant $E1$ strength at 5.5 MeV or, in other words, enabling these simple configurations to dominate over all others in the transition matrix elements.

This problem has been addressed by Lane (Lan 71), who found a promising clue in a certain zero-range ph calculation of Pal, Soper, and Stamp (PSS 64). This calculation indicated that in ^{208}Pb the $s_{1/2}p_{1/2}^{-1}$ neutron ph state would be uncoupled from the other ph states in the process by which most of the $E1$ strength is pushed up into the giant resonance. This suggested that the $s_{1/2}p_{1/2}^{-1}$ particle–hole could act as the required doorway in neutron-transfer reactions. Furthermore, the estimates of Pal *et al.* ascribed a total ground-state width, $\Sigma\Gamma_{\gamma 0} \simeq 200$ eV, to states near 5.5 MeV with large $s_{1/2}p_{1/2}^{-1}$ components. This width was in good agreement with estimates (BS 70) for the total ground-state width in the pigmy resonance in Au.

Recent developments suggest that the doorway picture, at least in so simple a form, may not provide an appropriate basis for describing the 5.5-MeV phenomenon. The evidence is as follows:

(*a*) *Re-evaluated ground-state width*: Present strength functions show between 4 and 6 MeV, for levels of a particular spin J that $\Sigma\Gamma_{\gamma 0} \simeq 25$ eV (Fig. 34) instead of $\sim$90 eV in Au and not so much a bunching of strength at 5.5 MeV as a dip below that energy. (Sec. 4.2.2).

(*b*) *Experimental test for* $2p1h$ *states*: An attempt to show that ph annihilation in $2p1h$ configurations was instrumental in 5.5-MeV γ-emission, by selectively exciting such configurations through isobaric analog resonances in the ^{207}Pb$(p, p'\gamma)^{207}$Pb reaction was inconclusive (Sec. 4.2.3).

(*c*) *Recent particle–hole calculations*: A recent study of *ph* calculations with finite-range forces in ^{208}Pb by Khanna and Harvey (KH 73) shows that the $s_{1/2}p_{1/2}^{-1}$ neutron particle–hole state is not uncoupled from other, *ph* configurations as a general rule. The lowest state, which appears at ~4.5 MeV in these calculations, does carry a significant fraction (~1.5%) of the total $B(E1 : 0^+ \rightarrow 1^-)$ strength while states in the next ~2.5 MeV above it carry essentially none. This lowest state thus provides the basis for a small pigmy resonance. However, although composed of 83% neutron *ph* structures, this state appears "collective" insofar as none of its *ph* components contributes an intensity ≥15%. The calculations predict a second grouping of $E1$ strength between 7 and 8 MeV. The distribution of $E1$ strength predicted is shown in Fig. 41 where it is compared with the measurements of Knowles (KK 73). The agreement in integrated strength below 7.4 MeV is satisfactory. Other *ph* calculations (KBB 70, Per 70) give somewhat similar results. The calculations (KH 73) also show that

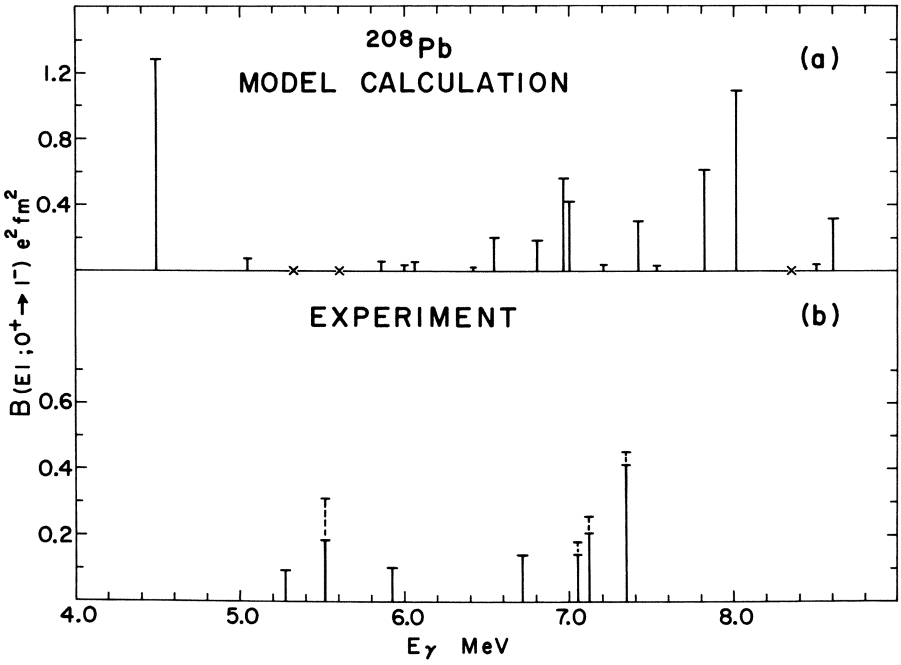

Fig. 41. Theoretical and experimental values of $B(E1;\ 0^+ \rightarrow 1^-)$ in ^{208}Pb. (a) Model calculations (KH 73) with realistic single-particle energies and Gaussian interaction with Gillet admixture. The spurious center-of-mass state is projected out and lies at zero energy. The crosses indicate dipole states with negligible strength. (b) $B(E1;\ 0^+ \rightarrow 1^-)$ calculated from the measured widths in ^{208}Pb(γ, γ). The dashed bars show the limits of precision, caused mainly by uncertainties in corrections for self-absorption (KK 73).

the $s_{1/2}p_{1/2}^{-1}$ neutron *ph*-states have their largest intensities ($\sim$20%) in states that carry little $E1$ strength, a result also, at least qualitatively, in accord with observations (Ear+ 70). The $s_{1/2}p_{1/2}^{-1}$ and $d_{3/2}p_{1/2}^{-1}$ fragments moreover are not well localized but are distributed over several MeV above the lowest state (KH 73).

On the basis of the Khanna–Harvey calculations one must conclude that there is no single *ph* doorway to account for the bump radiation at 5.5 MeV and that, because of the wide spreading, a description in terms of multiple doorways is probably not appropriate. The pigmy resonance at $\sim$4.5 MeV and the second clumping at $\sim$7.5 MeV appear in the calculations to arise from the difference of $\sim$2 MeV between the mean unperturbed energies of neutron-*ph* and proton-*ph* states. The step in the strength function at $\sim$4.5 MeV appears to arise simply because the redistribution of the $E1$ strength under the residual particle–hole interaction leaves a finite amount distributed downward from the giant resonance to roughly the energy of the lowest unperturbed *ph* state, where there is an abrupt decrease to zero strength for lower excitation energies. As A decreases below ^{208}Pb this sharp break becomes progressively more diffuse causing a gradual diminishing of the 5.5-MeV bump with decreasing A. A similar step effect is to be expected near other closed shells or wherever shell structure introduces a similar parity gap in the unperturbed $E1$ *ph* energies.

The Brink hypothesis is consistent with the above particle–hole description insofar as it is possible to couple the *ph* states of the Khanna–Harvey calculations to any excited state of the core thereby displacing the whole distribution upward in excitation energy.

The above arguments against the appropriateness of the doorway formalism in accounting for the 5.5-MeV bump say nothing, of course, about its suitability for describing other phenomena. Indeed, evidence for doorway states in neutron scattering (New 72) and in photoexcitation reactions (BBB 71) above the neutron threshold in ^{208}Pb seems unassailable. Also the success of the valency model near $A = 100$ (Mug 72) is evidence for a nonstatistical behavior closely related to doorway states (Lan 72a).

5.4. *M*1 Strength Function

The information on the energy dependence of the $M1$ strength is more fragmentary than that for $E1$ radiation. Predictions of the peaking of $M1$ strength (Mot 60, Bri 63, SE 69) have not been very specific about the energies at which maximum strength should be found in different A. The

experimental evidence suggests peaking of $M1$ strength between 7.5 and 8.5 MeV in ^{208}Pb (Bow+ 70), Ba and Sn (Bol 70), at 7.7 MeV in ^{106}Pd (BT 70) and $\leq$5.5 MeV in ^{116}In (LEB 70). In many other nuclei, resonance-averaged measurements show an E_γ^5 energy dependence for $M1$ parallel to $E1$ radiation over the narrow range 5-8 MeV approximately. The last result is rather unexpected, since no theory predicts an $M1$ giant resonance coincident with the tail of the $E1$ giant dipole. Much more data are required before $M1$ strengths can be understood in detail.

6. CONCLUSION

Results now available on absolute γ-ray strength functions show roughly their overall energy dependence and some details of substructure. Strength function information promises to be important for the detailed understanding of the giant resonance, in particular, how giant collective effects may be described in terms of the shell model or other microscopic models. For example, it can provide the higher moments of the dipole distribution, hence more stringent tests of the distribution of the small fragments of $E1$ strength among states in the giant dipole tail in ^{208}Pb. It can also test possible theories describing how these distributions are modified as a function of A. The investigation of shell effects in the resonance region, aided by detailed studies of high-energy γ-decay, may also contribute new insight into how the transition (Sol 72) can be made from a statistical description of the compound nucleus to the more physical models appropriate at low excitation energies. Many of the available experimental techniques for strength function measurement have been but little used and much remains to be done in extending their range and accuracy.

ACKNOWLEDGMENTS

The authors acknowledge help and advice on theoretical questions generously given by J. M. Blair, F. C. Khanna, and M. Harvey during preparation of this review and by A. M. Lane throughout the experimental work from this laboratory herein reported. They wish to thank I. Bergqvist and L. M. Bollinger for permission to display some of their results prior to publication. They are grateful to Mrs. A. Cipriani for typing the manuscript, and to W. F. Mills for technical assistance in its preparation.

REFERENCES

AB 68 B. J. Allen and J. R. Bird, *Phys. Letters* **27B**:494 (1968).

AF 65 E. Albertson and B. Forkman, *Nucl. Phys.* **70**:209 (1965).

All+ 64 R. G. Allas, S. S. Hanna, L. Meyer-Schützmeister, and R. E. Segel, *Nucl. Phys.* **58**:122 (1964).

All 68 B. J. Allen, *Nucl. Phys.* **A111**:1 (1968).

AM 71 B. J. Allen and R. L. Macklin, in: *Proceedings of the Third Neutron Cross Section and Technological Conference, Knoxville, Tennessee,* 1970, University of Tennessee, Knoxville (1971), p. 764.

AMS 70 P. Axel, K. Min, and D. C. Sutton, *Phys. Rev.* **C2**:689 (*1970*).

Axe 62 P. Axel, *Phys. Rev.* **126**:671 (1962).

Axe 63 P. Axel, *Phys. Letters* **4**:320 (1963).

Axe+ 63 P. Axel, K. Min, N. Stein, and D. C. Sutton, *Phys. Rev. Letters* **10**:299 (1963).

Axe 68 P. Axel, in: *Proceedings of International Symposium on Nuclear Structure, Dubna, 1968,* IAEA Vienna (1968), p. 299.

BBV 68 R. Bergère, H. Beil, and A. Veyssiere, *Nucl. Phys.* **A121**:463 (1968).

BK 53 G. A. Bartholomew and B. B. Kinsey, *Can. J. Phys.* **31**:1051 (1953).

Bar+ 57 G. A. Bartholomew, P. J. Campion, J. W. Knowles, and G. Manning, in: *Proceedings of the International Conference on Neutron Interactions with the Nucleus, New York 1957,* U.S. Atomic Energy Commission Technical Information Service, Oak Ridge, Tenn., Report TID-7547 (1957), p. 252.

Bar 61 G. A. Bartholomew, *Ann. Rev. Nucl. Sci.* **11**:259 (1961).

Bar 62 G. A. Bartholomew, in: *Proceedings of Conference on Electromagnetic Lifetimes and Properties of Nuclear States, Gatlinburg 1961,* Nuclear Science Series Report Number 37, National Academy of Sciences—National Research Council, Washington D.C. (1962), p. 209.

Bar+ 67 G. A. Bartholomew, S. I. H. Naqvi, M. R. Gunye, and E. D. Earle, *Can. J. Phys.* **45**:1517 (1967).

Bar 69 G. A. Bartholomew, in: *Proceedings of the International Symposium on Neutron Capture Gamma-Ray Spectroscopy, Studsvik, 1969,* IAEA, Vienna (1969), p. 553.

Bar+ 69 G. A. Bartholomew, E. D. Earle, A. J. Ferguson, and M. A. Lone, *Bull. Am. Phys. Soc.* **14**:590 (1969).

Bar+ 70 G. A. Bartholomew, I. Bergqvist, E. D. Earle, and A. J. Ferguson, *Can. J. Phys.* **48**:687 (1970).

BBB 71 R. J. Baglan, C. D. Bowman, and B. L. Berman, *Phys. Rev.* **C3**:2475 (1971).

Bei+ 69 H. Beil, R. Bergère, P. Carlos, and A. Veyssière, *Comp. rendus* **269B**:216 (1969).

Bei+ 71 H. Beil, R. Bergère, P. Carlos, A. Leprêtre, A. Veyssière, and A. Parlag, *Nucl. Phys.* **A172**:426 (1971).

Ben+ 66 G. Ben-David, B. Arad, J. Balderman, and Y. Schlesinger, *Phys. Rev.* **146**: 852 (1966).

Ber+ 66a I. Bergqvist, B. Lundberg, L. Nilsson, and N. Starfelt, *Nucl. Phys.* **80**:198 (1966).

Ber+ 66b I. Bergqvist, B. Lundberg, L. Nilsson, and N. Starfelt, in: *Proceedings of the International Conference on the Study of Nuclear Structure with Neutrons, Antwerp, 1965* (M. Neve de Mevergnies, P. Van Assche, and J. Vervier, eds.), North Holland Publishing Co., Amsterdam (1966), p. 504.

Ber 70 I. Bergqvist, private communication (1970).

Ber+ 69a R. Bergère, H. Beil, P. Carlos, and A. Veyssière, *Nucl. Phys.* **A113**:417 (1969).

Ber+ 69b B. L. Berman, M. A. Kelly, R. L. Bramblett, J. T. Caldwell, H. S. Davis, and S. C. Fultz, *Phys. Rev.* **185**:1576 (1969).

Ber+ 72 R. Bergère, H. Beil, P. Carlos, A. Veyssière, and A. Leprêtre, in: *Proceedings of the International Conference on Nuclear Structure Studies Using Electron Scattering and Photoreaction, Sendai 1972* (K. Shoda and H. Ui, eds.) (supplement to Research Report of Laboratory of Nuclear Science Tohoku University, Vol. 5, 1972, Tomizawa, Sendai, Japan) (1972) p. 273, and private communication.

Bet 36 H. A. Bethe, *Phys. Rev.* **50**:332 (1936).

BF 63 C. Block and H. Feshbach, *Ann. Phys.* **53**:47 (1963).

BGE 67 G. A. Bartholomew, M. R. Gunye, and E. D. Earle, *Can. J. Phys.* **45**:2063 (1967).

Bha+ 70 M. R. Bhat, R. E. Chrien, D. I. Garber, and O. A. Wasson, *Phys. Rev.* **C2**: 1115 (1970).

Blo 72 C. Bloch, in: *Statistical Properties of Nuclei* (J. B. Garg, ed.), Plenum Press, New York (1972), p. 379.

BM 69 A. Bohr, and B. R. Mottelson, in: *Nuclear Structure*, Benjamin, New York (1969), Vol. 1.

Bol 68 L. M. Bollinger, in: *Proceedings of International Symposium on Nuclear Structure, Dubna, 1968*, IAEA Vienna (1968), p. 317.

Bol 70 L. M. Bollinger, in: *Proceedings of the International Meeting on Perspectives of Neutron Spectroscopy, Dubna, 1970*, AED-CONF.-70-364-002, ZAED Zentralstelle für Atomkernenergie-Dokumentation, Kernforschungszentrum Karlsruhe.

Bow+ 70 C. D. Bowman, R. J. Baglan, B. L. Berman, and T. W. Phillips, *Phys. Rev. Letters* **25**:1302 (1970).

Bri 55 D. M. Brink, Doctoral Thesis, Oxford University (1955).

Bri 63 D. M. Brink, in: *Proceedings of the International Conference on Nuclear Physics with Reactor Neutrons, Argonne 1963* (F. E. Throw, ed.), ANL 6797 (1963), p. 194.

Brz+ 69 J. S. Brzosko, E. Gierlik, A. Soltan, and Z. Wilhelmi, *Can. J. Phys.* **47**:2849 (1969).

Brz+ 71 J. S. Brzosko, E. Gierlik, A. Soltan Jr., Z. Szeflinski, and Z. Wilhelmi, *Acta Phys. Polon.* **B2**:489 (1971).

BS 62 I. Bergqvist and N. Starfelt, *Nucl. Phys.* **39**:353 (1962).

BS 70a I. Bergqvist and N. Starfelt, *Prog. Nucl. Phys.* **11**:1 (1970).

BS 70b B. J. Buss and R. K. Smither, *Phys. Rev.* **C2**:1513 (1970).

BSB 66 B. L. Berman, G. S. Sidhu, and C. D. Bowman, *Phys. Rev. Letters* **17**:761 (1966).

BST 63 W. Bertozzi, C. P. Sargent, and W. Turchinetz, *Phys. Letters* **6**:108 (1963).

BT 67 L. M. Bollinger and G. E. Thomas, *Phys. Rev. Letters* **18**:1143 (1967).

BT 70 L. M. Bollinger and G. E. Thomas, *Phys. Rev.* **C2**:1951 (1970).

BT 72 L. M. Bollinger and G. E. Thomas, *Phys. Rev.* **C6**:1322 (1972).

Bus+ 72 F. R. Buskirk, H. D. Graf, R. Pitthan, H. Theissen, O. Titze, and T. Watcher, *Phys. Letters* **42B**:194 (1972).

BW 52 J. M. Blatt and V. F. Weisskopf, *Theoretical Nuclear Physics*, John Wiley and Sons, New York (1952).

Cam 59 A. G. W. Cameron, *Can. J. Phys.* **37**:322 (1959).

Car 62 R. J. Carpenter, Argonne National Laboratory report ANL-6589 (1962).

Chr 72 R. E. Chrien, in: *Proceedings of the International Conference on Nuclear Structure Study with Neutrons, Budapest, 1972*, to be published.

Coh 71 B. L. Cohen, *Concepts of Nuclear Physics*, McGraw-Hill Inc., New York (1971) p. 84.

CWG 73 R. E. Chrien, O. A. Wasson, and R. G. Greenwood, *Bull. Am. Phys. Soc.* **18**:59 (1973).

DG 65 M. Danos and W. Greiner, *Phys. Rev.* **B138**:876 (1965).

DS 68 A. M. Demidov and N. Shadiev, *Akad. Nauk SSSR* **32**:111 (1968).

dST 63 A. de Shalit and I. Talmi, *Nuclear Shell Theory*, Academic Press, New York (1963).

EB 71 E. D. Earle and G. A. Bartholomew, *Nucl. Phys.* **A176**:363 (1971).

Ear+ 70 E. D. Earle, A. J. Ferguson, G. van Middelkoop, G. A. Bartholomew, and I. Bergqvist, *Phys. Letters* **32B**:471 (1970).

Ear+ 71 E. D. Earle, G. A. Bartholomew, M. A. Lone, B. J. Allen, J. A. Harvey, and G. G. Slaughter, *Bull. Am. Phys. Soc.* **16**:496 (1971).

Ear+ 72a E. D. Earle, M. A. Lone, G. A. Bartholomew, B. J. Allen, G. G. Slaughter, and J. A. Harvey, in: *Statistical Properties of Nuclei* (J. B. Garg, ed.), Plenum Press, New York (1972), p. 263.

Ear+ 72b E. D. Earle, M. A. Lone, G. A. Bartholomew, W. J. McDonald, K. H. Bray, G. A. Moss, and G. C. Nielson, in: *Contributions to Conference on Nuclear Structure Study with Neutrons, Budapest, 1972*, Central Research Institute of Physics, Budapest (1972), p. 262.

Ear+ 73 E. D. Earle, J. W. Knowles, M. A. Lone, and G. A. Bartholomew, *Contributions to the XXIII National Conference on Nuclear Spectroscopy and Structure of the Atomic Nucleus, Tbilisi, U.S.S.R. 1973*, and to be published.

ELB 69 E. D. Earle, M. A. Lone, and G. A. Bartholomew, *Bull. Am. Phys. Soc.* **14**:515 (1969).

Eri 60 T. Ericson, *Adv. Phys.* **9**:425 (1960).

Fag+ 73 L. W. Fagg, W. L. Bendel, E. C. Jones, N. Ensslin, and F. E. Cecil, *Contribution to Proceedings of International Conference on Nuclear Physics Munich, 1973*, to be published.

FC 72 J. B. French and F. C. Chang, *Statistical Properties of Nuclei* (J. B. Garg, ed.), Plenum Press, New York (1972), p. 405.

FGC 70 E. G. Fuller, H. M. Gerstenberg and T. M. Collins, *Photonuclear Data Index, January 1965 through January 1970, Special Publication 322* (1970), U.S. Government Printing Office, Washington D.C. 20402.

FH 56 E. G. Fuller and E. Hayward, *Phys. Rev.* **101**:692 (1956).

FH 62a E. G. Fuller and E. Hayward, *Nucl. Phys.* **33**:431 (1962).

FH 62b E. G. Fuller and E. Hayward, *Nuclear Reactions* (P. M. Endt and P. B. Smith, eds.), Vol. II, North Holland, Amsterdam (1962), p. 113.

Fir 70 F. W. K. Firk, *Ann. Rev. Nucl. Sci.* **20**:39 (1970).

Ful+ 62 S. C. Fultz, R. L. Bramblett, J. T. Caldwell, and N. A. Kerr, *Phys. Rev.* **127**:1273 (1962).

FW 58 E. G. Fuller and M. S. Weiss, *Phys. Rev.* **112**:560 (1958).

Ful+ 69 S. C. Fultz, B. L. Berman, J. T. Caldwell, R. L. Bramblett, and M. A. Kelly, *Phys. Rev.* **186**:1255 (1969).

GC 65 A. Gilbert and A. G. W. Cameron, *Can. J. Phys.* **43**:1446 (1965).

GDP 60 L. V. Groshev, A. M. Demidov, and V. I. Pelekhov, *Nucl. Phys.* **16**:645 (1960); V. M. Strutinski, L. V. Groshev, and M. K. Akimova, *Nucl. Phys.* **16**:657 (1960).

GF 67 H. M. Gerstenberg and E. G. Fuller, *National Bureau of Standards, Technical Note 416*, United States Department of Commerce, Government Printing Office, Washington, D.C. 20402 (1967).

GGS 66 V. Gillet, A. M. Green, and E. A. Sanderson, *Nucl. Phys.* **88**:321 (1966).

GL 57 B. I. Gavrilov and L. E. Lazareva, *Soviet Physics JETP* **3**:871 (1957).

Gol+ 66 M. D. Goldberg, S. F. Mughabghab, S. N. Purohit, B. A. Magurno, and V. M. May, Brookhaven National Laboratory Report, *BNL 325 Supplement 2*, Volumes IIB and IIC (Physics TID-4500) (1966).

GR 71 R. C. Greenwood and C. N. Reich, *Trans. Am. Nucl. Soc.* **14**:905 (1971).

Gre+ 69 R. C. Greenwood, R. A. Harlan, R. G. Helmer, and C. W. Reich, in: *Proceedings of the International Symposium on Neutron Capture Gamma-Ray Spectroscopy, Studsvik, 1969*, IAEA, Vienna (1969), p. 607.

Gro 55 L. V. Groshev, *Dokl. Akad. Nauk SSSR* **100**:651 (1955).

Gro+ 58 L. V. Groshev, A. M. Demidov, V. N. Lutsenko, and. V. I. Pelekhov, in: *Proceedings of the 2nd International Conference on the Peaceful Uses of Atomic Energy, Geneva*, (1958), Vol. 15, p. 138.

Gro+ 68 L. V. Groshev, A. M. Demidov, V. I. Pelekhov, L. L. Sokolovskii, I. V. Kurchatov, G. A. Bartholomew, A. Doveika, K. M. Eastwood, and S. Monaro, *Nuclear Data Tables A5, No. 1, 2* (1968).

Gro+ 69 L. V. Groshev, A. M. Demidov, V. I. Pelekhov, L. L. Sokolovskii, G. A. Bartholomew, A. Doveika, K. M. Eastwood, and S. Monaro, *Nuclear Data Tables A5, No. 3*, **4**:243 (1969).

Han 73 P. G. Hansen, in: *Advances in Nuclear Physics, Vol. 7* (M. Baranger and E. Vogt, eds.), Plenum Press, New York (1973), p. 159.

Hay 65 E. Hayward, in: *Nuclear Structure and Electromagnetic Interactions, Scottish Universities, Summer School 1964* (N. MacDonald, ed.), Oliver and Boyd Press (1965), p. 141.

HG 69 M. Hillman and J. R. Grover, *Phys. Rev.* **185**:1303 (1969).

HGR 71 R. G. Helmer, R. C. Greenwood, and C. W. Reich, *Nucl. Phys.* **A168**:449 (1971).

HKW 72 O. Hausser, F. C. Khanna, and D. Ward, *Nucl. Phys.* **A194**:113 (1972).

HSM 65 J. A. Harvey, G. G. Slaughter, and M. J. Martin, Oak Ridge National Laboratory report ORNL-p-1353 (1965).

Hui+ 62 J. R. Huizenga, K. M. Clarke, J. E. Gindler, and R. Vandenbosch, *Nucl. Phys.* **34**:439 (1962).

Hui 72 J. R. Huizenga, in: *Statistical Properties of Nuclei* (J. B. Garg, ed.), Plenum Press, New York (1972), p. 425.

Jac 67 R. Jackiw, *Phys. Rev.* **157**:1220 (1967).

Jai 72 A. P. Jain, *Phys. Letters* **42B**:419 (1972).

JK 51 J. D. Jackson and B. B. Kinsey, *Phys. Rev.* **82**:345 (1951).

Joh+ 66 L. V. Johnson, L. B. Hughes, T. J. Kennett, and W. V. Prestwich, *Nucl. Phys.* **84**:113 (1966).

JS 71 H. E. Jackson and E. N. Strait, *Phys. Rev.* **C4**:1314 (1971).

JS 73 H. E. Jackson and E. N. Strait, *Bull. Am. Phys. Soc.* **18**:592 (1973).

KA 66 J. W. Knowles and N. M. Ahmed, Atomic Energy of Canada Limited report AECL-2535 (1966).

KBB 70 T. T. S. Kuo, J. Blomqvist, and G. E. Brown, *Phys. Letters* **31B**:93 (1970).

KH 73 F. C. Khanna and M. Harvey, *Contribution to Proceedings of International Conference on Photonuclear Reactions and Applications, Asilomar, California, 1973*, CONF 730301, Ernest O. Lawrence Livermore Laboratory, U. of California (1973), p. 2E-12, and private communication (1973).

Kin 55 B. B. Kinsey, in: *Beta and Gamma Ray Spectroscopy* (K. Siegbahn, ed.), North Holland, Amsterdam (1955), p. 795.

KK 67 A. M. Khan and J. W. Knowles, *Bull. Am. Phys. Soc.* **12**:538 (1967).

KK 73 J. W. Knowles and A. M. Khan, to be published (1973).

KKC 70 J. W. Knowles, A. M. Khan, and W. G. Cross, in: *XX Annual National Conference on Nuclear Spectroscopy and Structure of the Atomic Nucleus, Leningrad, U.S.S.R. 1970*; *Izv. Akad. Nauk SSSR* (*ser. fiz.*) **34**:1627 (1970).

KM 73 J. W. Knowles and O. Y. Mafra, to be published (1973).

Kno 70 J. W. Knowles, *Bull. Can. Assn. of Physicists* **26**:78 (1970).

Lan 71 A. M. Lane, *Ann. Phys.* (*N.Y.*) **63**:171 (1971).

Lan 72a A. M. Lane, in: *Statistical Properties of Nuclei* (J. B. Garg, ed.), Plenum Press, New York (1972), p. 271.

Lan 72b A. M. Lane, private communication (1972).

LB 50 J. S. Levinger and H. A. Bethe, *Phys. Rev.* **78**:115 (1950).

LBE 72 M. A. Lone, G. A. Bartholomew and E. D. Earle, Atomic Energy of Canada Limited Physics Division Progress Report, AECL 4257 (1972) p. 42.

LBT 72 G. D. Loper, L. M. Bollinger, and G. E. Thomas, *Bull. Am. Phys. Soc.* **17**: 580 (1972); Argonne National Laboratory Progress Report, ANL 7971 (1972), and private communication from L. M. Bollinger (1972).

LD 70 M. B. Lewis and W. W. Daehnick, *Phys. Rev.* **C1**:1577 (1970).

LEB 70 M. A. Lone, E. D. Earle, and G. A. Bartholomew, *Nucl. Phys.* **A156**:113 (1970).

LEB 73 M. A. Lone, E. D. Earle, and G. A. Bartholomew, to be submitted to *Nucl. Phys.* (1973).

Lep+ 71 A. Leprêtre, H. Beil, R. Bergère, P. Carlos, A. Veyssière, and M. Sugawara, *Nucl. Phys.* **A175**:609 (1971).

LL 60 A. M. Lane and J. E. Lynn, *Nucl. Phys.* **17**:563 and 586 (1960).

Lon+ 72 M. A. Lone, G. A. Bartholomew, E. D. Earle, and A. J. Ferguson, *Contributions to Conference on Nuclear Structure Study with Neutrons, Budapest, 1972*, Central Research Institute of Physics, Budapest (1972), p. 264.

Lon 73 M. A. Lone, Atomic Energy of Canada Limited report AECL-4372, to be published.

Lon+ 73 M. A. Lone, G. A. Bartholomew, E. D. Earle, A. J. Ferguson, and J. W. Knowles, *Contribution to Proceedings of International Conference on Photonuclear Reactions and Applications, Asilomar, California, 1973*, CONF 730301, Ernest O. Lawrence Livermore Laboratory, University of California (1973), p. 2E-11.

LP 71 A. Lottin and D. Paya, *J. de Phys.* **32**:849 (1971).

LS 65 B. Lundberg and N. Starfelt, *Nucl. Phys.* **67**:321 (1965).

Luc+ 72 R. Lucas, R. Babinet, J. Fagot, and H. Nifenecker, *Contributions to Conference*

on Nuclear Structure Study with Neutrons, Budapest, 1972, Central Research Institute of Physics, Budapest (1972), p. 36.

Lyn 68 J. E. Lynn, *The Theory of Neutron Resonance Reactions*, Clarendon Press, Oxford (1968).

Mar 69 M. Maruyama, *Nucl. Phys.* **A131**:145 (1969).

Mas+ 69 W. M. Mason, G. Kernel, J. L. Blackand, and N. W. Tanner, *Nucl. Phys.* **A135**, 193 (1969).

MKB 67 C. F. Moore, J. G. Kulleck, and P. von Brentano, *Phys. Rev.* **164**:1559 (1967).

MKG 72 O. Y. Mafra, S. Kuniyoshi, and J. Goldemberg, *Nucl. Phys.* **A186**:110 (1972).

Mot 60 B. R. Mottelson, *Proceedings of the International Conference on Nuclear Structure, Kingston 1960* (D. A. Bromley and E. W. Vogt, eds.), University of Toronto Press, Toronto (1960), p. 525.

MSW 70 R. Moreh, S. Shlomo, and A. Wolf, *Phys. Rev.* **C2**:1144 (1970).

Mug 72 S. F. Mughabghab, in: *Proceedings of the Conference on Nuclear Structure Study with Neutrons, Budapest, 1972*, to be published.

MW 69 R. Moreh and A. Wolf, *Phys. Rev.* **182**:1236 (1969).

New 56 T. D. Newton, *Can. J. Phys.* **34**:804 (1956).

New 72 H. W. Newson, in: *Statistical Properties of Nuclei* (J. B. Garg, ed.), Plenum Press, New York (1972), p. 309.

NH 54 R. Nathans and J. Halpern, *Phys. Rev.* **93**:437 (1954).

NMH 70 D. O. Nellis, I. L. Morgan, and E. L. Hudspeth, *Bull. Am. Phys. Soc.* **15**: 807 (1970), and private communication from D. O. Nellis (1970).

ORR 66 E. Obst, F. Rauch, and E. Rossle, *Phys. Letters* **21**:50 (1966).

ORW 67 E. Obst, F. Rauch, and H. G. Wahsweiler, *Nucl. Phys.* **A103**:17 (1967).

OTA 62 J. S. O'Connell, P. A. Tipler, and P. Axel, *Phys. Rev.* **126**:228 (1962).

Per 66 C. F. Perdrisat, *Rev. Modern Phys.* **38**:41 (1966).

Per 70 S. M. Perez, *Phys. Letters* **33B**:317 (1970).

PSS 64 M. K. Pal, J. M. Soper, and A. P. Stamp, United Kingdom Atomic Energy Research Establishment report T. P. 148 (1964).

PT 56 C. E. Porter and R. G. Thomas, *Phys. Rev.* **104**:483 (1956).

PW 71 R. Pitthan and T. H. Walcher, *Phys. Letters* **36B**:563 (1971).

Ras+ 69 N. C. Rasmussen, Y. Hukai, T. Inouye, and V. J. Orphan, Massachusetts Institute of Technology report MIT NE-85 (1969).

Ras+ 70 N. C. Rasmussen, V. J. Orphan, T. L. Harper, J. Cunningham, and S. A. Ali, Gulf General Atomic Inc., report DSA 2570 (1970).

Rim+ 70 K. Rimawi, J. B. Garge, R. E. Chrien, and R. G. Graves, *Phys. Rev.* **C2**:1973 (1970).

RM 60 K. Reibel and A. K. Mann, *Phys. Rev.* **118**:701 (1960).

Ros 68 N. Rosensweig, *Nucl. Phys.* **A118**:650 (1968).

Sam+ 68 C. Samour, H. E. Jackson, J. Julien, A. Bloch, J. M. Kuchly, C. Lopata, and J. Morgenstern, *Nucl. Phys.* **A121**:65 (1968).

SE 69 C. S. Shapiro and G. T. Emery, *Phys. Rev. Letters* **23**:244 (1969).

SG 65 P. H. Stelson and L. Grodzins, *Nuclear Data* **A1**:1 (1965).

SH 68 E. B. Shera and D. W. Hafemeister, private communication (1968), and see (Gro+ 68).

She+ 72 E. B. Shera, U. Gruber, B. P. K. Maier, H. R. Koch, O. W. B. Schult, R. G. Lanier, N. Onishi, and R. K. Sheline, *Phys. Rev.* **C6**:537 (1972).

SHR 66 S. J. Skorka, J. Hertel, and T. W. Retz-Schmidt, *Nuclear Data* **A2**:347 (1966).

SM 68 O. D. Simpson and L. G. Miller, *Nucl. Instr. and Meth.* **61**:245 (1968).

Smi+ 72 R. K. Smither, D. J. Bus, D. L. Bushnell, and G. E. Thomas, *Bull. Am. Phys. Soc.* **17**:28 (1972).

SNG 71 A. Stolovy, A. I. Namenson, and T. F. Godlove, *Phys. Rev.* **C4**:1466 (1971).

Sol 72 V. G. Soloviev, *Sov. J. Nucl. Phys.* **15**:410 (1972).

Sta 64 N. Starfelt, *Nucl. Phys.* **53**:397 (1964).

Ste+ 65 P. H. Stelson, R. L. Robinson, H. J. Kim, J. Rapaport, and G. R. Satchlu, *Nucl. Phys.* **68**:97 (1965).

Ste+ 72 M. Stefanon, F. Corvi, C. Coceva, and P. Giacobbe, *Contributions to Conference on Nuclear Structure Study with Neutrons, Budapest, 1972*, Central Research Institute of Physics, Budapest (1972), p. 74.

Swa 73a C. P. Swann, *Contribution to Proceedings of International Conference on Photonuclear Reactions and Applications, Asilomar, California 1973*, CONF 730301, Ernest O. Lawrence Livermore Laboratory, University of California (1973) p. 2E-13, and private communication.

Swa 73b C. P. Swann, *Nucl. Phys.* **A201**:534 (1973).

TJ 72 R. E. Toohey and H. E. Jackson, *Phys. Rev.* **C6**:1440 (1972).

Tro 61 E. S. Troubetzkoy, *Phys. Rev.* **122**:212 (1961).

UVL 66 J. Urbanec, J. Vrzal, and J. Liptak, in: *Proceedings of the International Conference on the Study of Nuclear Structure with Neutrons, Antwerp, 1965* (M. Nève de Mévergnies, P. Van Assche, and J. Vervier, eds.), North Holland Publishing Co., Amsterdam (1966), p. 535.

Was+ 68 O. A. Wasson, R. E. Chrien, M. R. Bhat, M. A. Lone, and M. Beer, *Phys. Rev.* **173**:1170 (1968).

Was+ 69 O. A. Wasson, R. E. Chrien, M. A. Lone, M. R. Bhat, and M. Beer, *Nucl. Phys.* **A132**:161 (1969).

Was+ 71 O. A. Wasson, R. E. Chrien, G. G. Slaughter, and J. A. Harvey, *Phys. Rev.* **C4**:900 (1971).

WC 70 O. A. Wasson and R. E. Chrien, *Phys. Rev.* **C2**:675 (1970).

Wei 70 M. S. Weiss, private communication in (Bow+ 70).

Wei+ 69 C. Weitkamp, J. A. Harvey, G. G. Slaughter, and E. C. Campbell, in: *Proceedings of International Symposium on Neutron Capture Gamma-Ray Spectroscopy, Studsvik, 1969*, IAEA, Vienna (1969), p. 421.

Win+ 70 E. J. Winhold, E. M. Bowey, D. B. Gayther, and B. H. Patrick, *Phys. Letters* **32B**:607 (1970).

Wol+ 72 A. Wolf, R. Moreh, A. Nof, O. Shahal, and J. Tanenbaum, *Phys. Rev.* **C6**: 2276 (1972).

INDEX

A

Anomalous bump (*see also* Pygmy resonance), 232, 294–311
  vs. pygmy resonance, 233
Anti-analog state, 167, 203
Antisymmetrization operator, 82
Atom–photon model, 3
Autoionization, 8, 33
Average cross section theory, 85

B

Beta decay
  gross theory of, 178, 193, 198, 201, 212
  statistical behavior of, 180
Beta-delayed fission, 202
Beta strength function, 159–228
  β^-, 201, 211
  β^+, 201
  cut-off, 193, 214, 219
  definition, 161
  delayed proton emission, 184
  electron capture, 201
  fluctuations, 180, 219
  one-parameter, 195
  properties of, 172
  statistical properties of, 212
Beta transitions
  allowed, 161, 163
  allowed unhindered, 169, 186
  and isobaric analog state, 172
  collective, 163, 171, 172, 179
  effective coupling constants for, 163
  electron capture, 173
  first forbidden, 163, 164
  forbidden, 161, 171
  hindrance phenomena for, 165, 171
  nonunique, 171
Beta transitions *(cont'd)*
  pure Fermi, 166
  second forbidden, 163
  unique forbidden, 171
Black-nucleus model (*see also* Uniform model), 20, 24, 238
Bohr picture, 10, 19
Breit–Wigner resonance, 19, 74, 138
Bremsstrahlung monochromator, 250
Brink hypothesis, 231, 241, 250, 312, 316
Brueckner theory, 21, 214

C

Charge-dependent forces, 97, 99
Charge monopole operator, 97, 99
Charge monopole oscillation, 100, 102, 119
Classical damped oscillator, 239
Cloudy-crystal-ball model (*see* Optical model)
Collective beta transitions, 163, 171, 172, 179
Compound elastic scattering, 88
Compound nucleus, 2, 19, 205, 216, 219
Compton monochromator, 247, 250
Compton spectrometer, 255
Configuration states, 121
Core polarization, 163, 168, 169
Coulomb displacement energy, 98, 123, 177
  of analog states, 126
  of shell-model states, 142
  of single-particle states, 139
Coulomb energy
  first-order, 116
  second-order, 117
Coulomb force
  effective one-body, 98–101, 117, 146, 149
  scalar, 98, 101

Coulomb force *(cont'd)*
shell-model sum rules for, 153
tensor, 98, 101
two-body, 101
two-body vs. one-body, 118, 147
vector, 98, 101
Coulomb mixing, 97–158
basic approximations for, 101
effect of correlations, 152
manifestations, 98
of oscillator orbitals, 155

D
Damping width (*see* Line broadening)
Decay width
of doorway state, 10
of unbound state, 13
Delayed neutron emission, 212
spectrum, 211
Delayed proton emission, 183, 206
spectrum, 209, 210
Direct capture, 55
Direct inelastic scattering, 29
Doorway states
channel decay, 10
compound decay, 10
energy, 39, 80
fission, 57
giant dipole, 51
inelastic electron scattering, 55
isobaric analog, 42, 51
lifetime of, 10
linewidth of, 8, 35, 39, 86
neutron elastic scattering, 89
optical model strength and, 33
partial width correlations of, 61
particle-hole, 2
photon strength function of, 54
pygmy resonance, 2
strong mixing of, 15
theoretical framework for, 77–90
vibrational, 40
vs. intermediate structure, 74
weak mixing, 12, 14

E
Echo resonance, 286
Effective charge, 163
Effective coupling constant, 163, 219
Effective mass, 112
Electron capture, 173
Ericson fluctuations, 51, 68, 72, 74, 180
Exponential decay law, 7

F
ft values, 161
Fermi coupling constant, 164
Fermi function, 164
Fermi gas, 177, 242
Fermi golden rule, 6
Fermi interaction, 164
Fermi resonance, 179
Fermi surface, 173, 177
diffuse, 175
Fermi transitions
allowed, 163
collective, 167
experimental data for, 115
of isobaric analog state, 165
superallowed, 98, 113
Fine structure of
beta strength function, 208
doorway–hallway systems, 82–84
gamma strength function, 290
intermediate structure, 79
isobaric analog state, 45
muon capture, 216
Fission doorway state, 9, 57
and fine structure, 59
and second minimum, 57
Fluctuations of beta strength, 180, 219
Form factor of isobaric monopole, 56
Frivolous model, 24

G
Gamma strength function, 175, 191, 218, 229–324
definition, 229
excitation vs. decay, 237
high resolution method, 262, 270
irregularities, 289
nomenclature, 235
parameters of, 270
photoexcitation method, 244, 269
properties of, 271
sequential extraction method, 259, 270
spectrum fitting method, 253, 269

Gamow–Teller interaction, 164
Gamow–Teller operator, 168
Gamow–Teller resonance width, 177, 179, 203
Gamow–Teller transitions, 176
  collective, 168
  mirror, 99, 163
Gap energy, 197, 219
Gap parameter, 174
Giant dipole resonance, 51, 90, 273
  shape, 231, 258
  width, 53, 138, 218
Giant-resonance model
  beta decay, 169
  nucleons, 24, 33
Goldhaber–Teller model, 53
Griffin's model, 64
Gross theory of beta decay, 178, 193, 198, 201, 212

H
Hamada–Johnston force, 109
Hartree–Fock calculation, 111
Hauser–Feshbach calculation, 308
Hierarchy of states, 2, 28
Hindrance phenomena, 165, 171
Hydrodynamical model, 100, 111

I
Independent-particle model (*see also* Shell model), 21, 27
Inelastic electron scattering, 55
Intermediate coupling model, 24
Intermediate structure (*see also* Doorway state)
  and fission, 57
  and neutron cross sections, 71, 73
  and neutron evaporation spectra, 64
  correlation coefficients for, 76
  criteria for, 73
  definition, 2
  Ericson fluctuations of, 68
  for heavy-ions, 90
  theoretical framework for, 77–90
  vs. doorways, 74
Isobaric analog state, 9, 42–51, 101, 167, 308
  and Fermi transitions, 165, 172
Isobaric analog state *(cont'd)*
  and Gamow–Teller resonance, 203
  fine structure, 45
  first-order shift, 126
  isospin impurities, 98, 112
  level shift, 48, 123
  line width, 44, 48, 98, 126, 130, 137, 143–145, 204
  pseudo-first-order shift, 126
  second-order shift, 130, 132
  strength function, 127
  substructure, 50
Isobaric mass formula, 98, 115
  observed coefficients, 122
Isospin impurities, 98, 110
  for different models, 111
  of isobaric analog states, 112
Isospin selection rule, 166

K
K-matrix, 11, 12, 81, 82
Kapur–Peierls theory, 20

L
Lee model, 8
Level density, 67, 242, 255
  of Gilbert and Cameron, 73, 213, 243, 259, 286
  of Newton, 213, 286
  parameters for, 274
  spin cut-off factor for, 242
Level shift
  Coulomb (*see* Coulomb displacement energy)
  effect of correlations, 128
  first-order, 126
  of isobaric analog state, 48, 123
  second-order, 130, 132
Level spacing, 3
  and shell effects, 37
  of doorway states, 35
  Wigner law for, 69–72, 180
Levinson's theorem, 27
Line broadening
  and delayed-particle emission, 203
  atom–photon model, 8
  for natural decay, 9
  for optical model, 138

Line broadening *(cont'd)*
of doorway states, 8, 35, 86
of fission doorways, 60
of Gamow–Teller resonance, 177
of giant dipole state, 53
of isobaric analog state, 44, 98, 126, 130, 137, 143, 145, 204
of single-particle state, 24, 138
of two-particle levels, 220
theory, 77–90
Line shape (*see also* Line broadening)
Gaussian, 177, 194
Lorentzian, 5, 10, 12, 25, 81, 177, 194, 231, 232, 246, 257, 267–271, 275–279, 283–288, 291, 297, 302, 313
non-Lorentzian, 15
of charge monopole mode, 100
of classical damped oscillator, 239
of giant dipole resonance, 231, 239
Lorentzian (*see* Line shape)

M
magnetic pair spectrometer, 255
Mass monopole mode, 119
Maxwellian energy distribution, 65
Mean free path, 30
Microgiant resonance (*see also* Pygmy resonance), 38
Mixing parameter, 14
Muon capture
allowed, 214
and neutron emission, 216
blocking of, 214
direct, 214
gross theory for, 215
particle multiplicities for, 215
Primakoff formula for, 214
strength function for, 162, 175, 220
vs. electron capture, 213

N
Neutron drip line, 185
Neutron evaporation spectra, 64, 90
Neutron strength function, 32
Nilsson quantum numbers, 199
Nolen–Schiffer anomaly, 98, 128, 135, 146
and level shift, 135
Nucleon–nucleus scattering, 27

O
Optical model, 2, 20, 24
and fluctuating strength, 33
and Pauli principle, 23
and spreading width, 138
compound elastic scattering for, 88
foundation for, 22
mean free path for, 30
microscopic description of, 30
shape elastic scattering for, 88
strength function for, 22, 31, 90
transmission functions for, 72, 211
Oscillator orbitals, 155
Oscillator shell model, 106, 110, 117

P
Pairing effects, 173, 178
Pairing theory, 174
Partial width correlation, 61, 66, 90, 234
Particle-hole excitations, 162
Photoabsorption cross sections, 238
Photon emission, 8
Porter–Thomas distribution, 61, 70, 72, 181, 182, 213, 229, 240, 241, 255–257, 263, 273, 283, 297, 302, 311
Potential scattering resonances, 17, 28
Precompound emission, 29
Precompound excitation, 29
Primakoff formula, 216
Proton capture, 52
Pygmy resonance, 62, 175, 195, 210, 211, 219, 233, 258, 280, 284, 294, 313, 314, 316

Q
Quasiparticle states, 175

R
R-matrix, 13, 24, 123
Ramsauer effect, 25
Rapid neutron capture, 202, 220
Reduced beta transition probability, 161
Resonance reactions
and atom–photon model, 3
and compound nucleus, 17
and potential scattering, 17
Breit–Wigner formula for, 17, 19, 74, 138
channel projection theory for, 17

Resonance reactions *(cont'd)*
Dirac theory for, 77
effective interaction theory for, 77
Kapur–Peierls theory for, 20, 77
parameters of, 274
shell-model theory for, 77–90
Wigner–Eisenbud theory for, 77
Ritz combination principle, 295
Rodberg's criteria, 74
Rosenfeld force, 109, 138

S
S-matrix, 11, 82
unitarity of, 87
Second moment, 25
Serber force, 138
Shape elastic scattering, 88
Shell model
and pairing effects, 173
and reaction theory, 77–90
extended, 30
oscillator, 106, 110, 117
Saxon–Woods, 118, 139
with correlations, 106, 111, 119, 132, 134, 198
Slow-neutron cross sections, 18
Spectral distribution, 241, 254
Spreading width (*see* Line broadening)
Statistical rate function *f*, 161, 164
Strength function of
analog state, 123
beta decay, 159, 172, 178
black nucleus, 24
charge monopole state, 102, 104, 137
Fermi transitions, 169
first forbidden transitions, 169
gamma rays, 175, 191, 218, 229–324
Gamow–Teller transitions, 169
giant dipole resonance, 54, 218, 229
magnetic dipole transitions, 54
muon capture, 162, 175, 220
optical model, 22, 31, 33, 176
p-wave neutrons, 160, 161
s-wave neutrons, 32, 160
single-particle state, 176, 177
Subthreshold fission, 57, 90
Sum rules
and correlations, 145
and Coulomb mixing, 97–158
and line spreading, 15
dipole vs. monopole, 109
for separate isospins, 104
of electric dipole, 239
of shell model, 153
Super heavy element synthesis, 202

T
T-matrix, 11, 12
poles and residues of, 14
Tamm–Dancoff method, 103, 106, 108
Temperature, 66, 259, 275
Thermal neutron capture, 230, 256
Thomas–Ehrmann shift, 139
Threshold photonuclear technique, 248
Time translation operator, 6
Total absorption spectrometry, 188
Total radiative width, 242
Transmission functions, 72, 211

U
Uniform model, 24, 116, 134, 148, 154, 238

V
Vibrational doorways, 40

W
Weisskopf unit, 231, 232
Wigner distribution law, 69, 70, 72, 180
Wigner single-particle limit, 61
Wigner supermultiplets, 168, 169, 177, 214, 219

Z
Zeldes mass formula, 200